frontiers | Research Topics

Insights in extreme microbiology: 2021

Edited by
Andreas Teske and Virginia P. Edgcomb

Published in
Frontiers in Microbiology

ISSN 1664-8714
ISBN 978-2-83251-357-6
DOI 10.3389/978-2-83251-357-6

About Frontiers

Frontiers is more than just an open access publisher of scholarly articles: it is a pioneering approach to the world of academia, radically improving the way scholarly research is managed. The grand vision of Frontiers is a world where all people have an equal opportunity to seek, share and generate knowledge. Frontiers provides immediate and permanent online open access to all its publications, but this alone is not enough to realize our grand goals.

Frontiers journal series

The Frontiers journal series is a multi-tier and interdisciplinary set of open-access, online journals, promising a paradigm shift from the current review, selection and dissemination processes in academic publishing. All Frontiers journals are driven by researchers for researchers; therefore, they constitute a service to the scholarly community. At the same time, the *Frontiers journal series* operates on a revolutionary invention, the tiered publishing system, initially addressing specific communities of scholars, and gradually climbing up to broader public understanding, thus serving the interests of the lay society, too.

Dedication to quality

Each Frontiers article is a landmark of the highest quality, thanks to genuinely collaborative interactions between authors and review editors, who include some of the world's best academicians. Research must be certified by peers before entering a stream of knowledge that may eventually reach the public - and shape society; therefore, Frontiers only applies the most rigorous and unbiased reviews. Frontiers revolutionizes research publishing by freely delivering the most outstanding research, evaluated with no bias from both the academic and social point of view. By applying the most advanced information technologies, Frontiers is catapulting scholarly publishing into a new generation.

What are Frontiers Research Topics?

Frontiers Research Topics are very popular trademarks of the *Frontiers journals series*: they are collections of at least ten articles, all centered on a particular subject. With their unique mix of varied contributions from Original Research to Review Articles, Frontiers Research Topics unify the most influential researchers, the latest key findings and historical advances in a hot research area.

Find out more on how to host your own Frontiers Research Topic or contribute to one as an author by contacting the Frontiers editorial office: frontiersin.org/about/contact

Insights in extreme microbiology: 2021

Topic editors

Andreas Teske — University of North Carolina at Chapel Hill, United States

Virginia P. Edgcomb — Woods Hole Oceanographic Institution, United States

Citation

Teske, A., Edgcomb, V. P., eds. (2023). *Insights in extreme microbiology: 2021*. Lausanne: Frontiers Media SA. doi: 10.3389/978-2-83251-357-6

The authors declare that the research was conducted in the absence of any commercial or financial relationships that could be construed as a potential conflict of interest.

Table of contents

05 Editorial: Insights in extreme microbiology: 2021
Andreas P. Teske and Virginia P. Edgcomb

08 Biological Sulfate Reduction in Deep Subseafloor Sediment of Guaymas Basin
Toshiki Nagakura, Florian Schubert, Dirk Wagner, Jens Kallmeyer and IODP Exp. 385 Shipboard Scientific Party

20 Novel Cesium Resistance Mechanism of Alkaliphilic Bacterium Isolated From Jumping Spider Ground Extract
Takahiro Koretsune, Yoshiki Ishida, Yuri Kaneda, Eri Ishiuchi, Miyu Teshima, Nanami Marubashi, Katsuya Satoh and Masahiro Ito

34 Microbial Hydrocarbon Degradation in Guaymas Basin—Exploring the Roles and Potential Interactions of Fungi and Sulfate-Reducing Bacteria
Virginia P. Edgcomb, Andreas P. Teske and Paraskevi Mara

50 A Novel NADP-Dependent Formate Dehydrogenase From the Hyperthermophilic Archaeon *Thermococcus onnurineus* NA1
Ji-in Yang, Seong Hyuk Lee, Ji-Young Ryu, Hyun Sook Lee and Sung Gyun Kang

62 Proteomic Signatures of Microbial Adaptation to the Highest Ultraviolet-Irradiation on Earth: Lessons From a Soil Actinobacterium
Federico Zannier, Luciano R. Portero, Thierry Douki, Wolfgang Gärtner, María E. Farías and Virginia H. Albarracín

80 Cryptic Methane-Cycling by Methanogens During Multi-Year Incubation of Estuarine Sediment
Richard T. Kevorkian, Katie Sipes, Rachel Winstead, Raegan Paul and Karen G. Lloyd

93 Differences in Bioenergetic Metabolism of Obligately Alkaliphilic *Bacillaceae* Under High pH Depend on the Aeration Conditions
Toshitaka Goto, Shinichi Ogami, Kazuaki Yoshimume and Isao Yumoto

110 Approaches to Unmask Functioning of the Uncultured Microbial Majority From Extreme Habitats on the Seafloor
Stefanie Böhnke and Mirjam Perner

119 Diversity of Microbial Eukaryotes Along the West Antarctic Peninsula in Austral Spring
Jean-David Grattepanche, Wade H. Jeffrey, Rebecca J. Gast and Robert W. Sanders

134 Characterizing the Piezosphere: The Effects of Decompression on Microbial Growth Dynamics
Anaïs Cario, Gina C. Oliver and Karyn L. Rogers

146 High-Pressure Microfluidics for Ultra-Fast Microbial Phenotyping
Anaïs Cario, Marina Larzillière, Olivier Nguyen, Karine Alain and Samuel Marre

161 Metagenomics Reveals Dominant Unusual Sulfur Oxidizers Inhabiting Active Hydrothermal Chimneys From the Southwest Indian Ridge
Yong Wang, Hong-Yu Bi, Hua-Guan Chen, Peng-Fei Zheng, Ying-Li Zhou and Jiang-Tao Li

174 Advances in Defining Ecosystem Functions of the Terrestrial Subsurface Biosphere
D'Arcy R. Meyer-Dombard and Judy Malas

193 Multiple Adaptive Strategies of Himalayan *Iodobacter* sp. PCH194 to High-Altitude Stresses
Vijay Kumar, Prakriti Kashyap, Subhash Kumar, Vikas Thakur, Sanjay Kumar and Dharam Singh

209 Unexpected diversity found within benthic microbial mats at hydrothermal springs in Crater Lake, Oregon
Amanda Stromecki, Laura Murray, Heather Fullerton and Craig L. Moyer

frontiers | Frontiers in Microbiology

TYPE Editorial
PUBLISHED 04 January 2023
DOI 10.3389/fmicb.2022.1119051

OPEN ACCESS

EDITED AND REVIEWED BY
Philippe M. Oger,
UMR5240 Microbiologie, Adaptation et Pathogenie (MAP), France

*CORRESPONDENCE
Andreas P. Teske
✉ teske@email.unc.edu

SPECIALTY SECTION
This article was submitted to Extreme Microbiology, a section of the journal Frontiers in Microbiology

RECEIVED 08 December 2022
ACCEPTED 15 December 2022
PUBLISHED 04 January 2023

CITATION
Teske AP and Edgcomb VP (2023) Editorial: Insights in extreme microbiology: 2021.
Front. Microbiol. 13:1119051.
doi: 10.3389/fmicb.2022.1119051

Editorial: Insights in extreme microbiology: 2021

Andreas P. Teske[1]* and Virginia P. Edgcomb[2]

[1]Department of Marine Sciences, University of North Carolina at Chapel Hill, Chapel Hill, NC, United States, [2]Department of Geology and Geophysics, Woods Hole Oceanographic Institution, Woods Hole, MA, United States

KEYWORDS

insights 2021, Research Topic, editorial, extreme microbiology, diversity

Editorial on the Research Topic
Insights in extreme microbiology: 2021

This Research Topic has turned into an experiment. Without prescribing a specific research area, and in doing so, giving carte blanche to the associate and review editors of the Extreme Microbiology section, we wondered who would respond, and what kinds of papers would be submitted? Now it is time to wrap up the experiment and to take stock. Research teams from eight countries (USA, Japan, China, India, South Korea, Germany, France, Argentina) published fifteen articles, eight of these by female first authors and/or senior authors. Three author teams have taken the opportunity to write synthesis papers and to formulate current and future perspectives on hydrothermal vent and subsurface microbiology. While the contributions to this special topic reflect the wide-ranging endeavors and the extensive scientific expertise of our associate and review editors, some shared themes are emerging. Hydrothermal vent microbiology emerges as one of the best-represented fields and accounts for seven articles; recognizably related themes are taken up by a review on the deep terrestrial subsurface. Five physiological studies explore individual protein function or complex gene expression responses in obligate or facultative extremophiles, and two studies explore spatially or temporally changing marine microbial assemblages. Without further ado, here is the harvest of the year 2021.

In their hypothesis and theory article, Edgcomb et al. discuss the potential roles of hydrocarbon-degrading fungi and sulfate-reducing bacteria, and the possibility that they may interact in the hydrocarbon-rich hydrothermal sediments of Guaymas Basin to degrade specific hydrocarbons. While numerous lineages of alkane- and aromatics-degrading bacteria and fungi coexist in this habitat, the study of their interactions, for example in sequential or syntrophic hydrocarbon degradation, is just beginning.

The massive sediments of Guaymas Basin were recently probed by deep drilling during IODP Expedition 385. In surveying the activity of sulfate-reducing bacteria in diverse locations across Guaymas Basin, Nagakura et al. find activity peaks linked to hydrothermal influence and steep thermal gradients at the off-axis hydrothermal Ringvent site, where sulfate-reducing activity exceeds even levels at cold seep locations.

The microbial communities of hydrothermal vent sites are increasingly targeted with a complex network of *in-situ* and *ex-situ* analyses, stable isotope probing, geochemical and microbial process studies, (meta)genomic sequencing, and functional annotation of uncultured microbial lineages, and biogeochemical rate measurements and modeling. As discussed by Böhnke and Perner, these multipronged strategies are aiming for a holistic understanding of hydrothermal vent ecosystem function, a goal that becomes increasingly realistic.

Numerous hydrothermal vent locations remain poorly studied, in particular those in the remote reaches of the Southern Indian Ocean. Metagenomic analyses of hydrothermal chimneys of the Southwest Indian Ridge have uncovered novel types of sulfur-oxidizing bacterial communities where members of the gammaproteobacterial *Ectothiorhodospiraceae* predominate. Based on the discovery of bacteriophytochrome-encoding genes in some members of the Thiohalomonadales from this location, Wang et al. speculate on their potential for absorbing infrared radiation.

Hydrothermal locations do not have to be marine. In their sequence-based study of benthic mat communities at hydrothermal springs in Crater Lake (Oregon), Stromecki et al. find chemosynthetic bacteria that thrive by aerobic oxidation of iron, sulfur and nitrite; anaerobic pathways including arsenic reduction and denitrification; carbon fixation relies on the reverse TCA and the reverse pentose phosphate cycles. The importance of iron oxidation, and the prevalence of iron-oxidizing bacteria (*Gallionella*, Zetaproteobacteria) links these freshwater hydrothermal communities to iron-rich hydrothermal communities at Loihi seamount, and separates them from the vast majority of marine hydrothermal sites.

The cultivation and physiological study of extremophilic bacteria from deep-sea hydrothermal vents has always been hampered by the impossibility or at least difficulty of recreating hydrothermal vent conditions in the laboratory. Cario, Larzillière et al. introduce a miniaturized high-pressure microfluidic device that allows testing the temperature and pressure responses of deep-sea hyperthermophiles without depressurization, and they demonstrate this methodology with the barophilic model strain *Thermococcus barophilus* and the hydrogenotroph *Methanothermococcus thermolithotrophicus*. In a related study Cario, Oliver et al. compare survival and growth of a mesophilic deep-subsurface sulfate-reducing bacterium (*Desulfovibrio*) and a hyperthermophilic deep-sea archaeum (*Archaeoglobus*) under isobaric high-pressure cultivation, and under cyclic high-pressure cultivation followed by decompression. They note that sample decompression impacts growth negatively for both test organisms; since this effect becomes more severe under non-optimized pressure conditions. Depressurization selects against the enrichment and isolation of piezophiles. This difficulty can be circumvented using isobaric enrichment and culture methods, such as microfluidic devices with multiple cultivation chambers lined up along adjustable thermal and chemical gradients.

Terrestrial subsurface microbiology has developed as a sister field to marine deep subsurface and hydrothermal vent research; both fields share themes of rock-hosted energy and carbon sources that sustain subsurface microbial life independently from the surface biosphere. Meyer-Dombard and Malas survey recent progress in the study of microbial life and microbial ecosystems in deep rock laboratories, mines and boreholes, and introduce numerous case studies where microbial communities are sustained by iron and sulfur in deep basalt crust, or by hydrogen-generating serpentinization reactions. At the confluence of cracks in the rock, water and energy sources, microbial life is never far.

Physiological studies of extremophilic microorganisms constitute the next major group of papers in this special topic, represented by three articles. The hyperthermophilic archaeum *Thermococcus onnurineus* relies on formate dehydrogenase gene fdh2 for formate-dependent growth and mediation of NAD^+-dependent formate oxidation. By purifying and testing the function of formate dehydrogenase gene fdh3, Yang et al. show that this hydrogenase mediates electron transfer between formate and NADPH or ferredoxin, indicating redox-dependent finetuning of formate dehydrogenase activity.

An alkaliphilic *Microbacterium* strain with unusually high tolerance to the toxic alkali metal cesium (1.2 mM, almost twice the previously known limit of 0.7 mM), isolated from jumping spider ground extract, contained a novel low-affinity Cs^+/proton antiporter that removed Cs^+ from the cytoplasm. Koretsune et al. discuss the potential of this cesium-resistant bacterium and its antiporter as a bioremediation tool for purification of water contaminated with cesium radionuclides.

In a bioenergetic study of the obligate alkaliphile *Evansella clarkia*, a member of the Bacillaceae, Goto et al. demonstrate a new strategy to overcome the limitations of high extracellular pH for chemiosmotic energy generation. The predominant membrane-bound cytochrome C contains an extra asparagine-rich segment between the membrane anchor and the main body of the protein which appears to form a H^+ network that accumulates protons on the outer membrane surface. Thus, *E. clarkii* constructs a proton capacitator that ensures sufficient transmembrane proton flux and energy generation even under low-oxygen, high-pH conditions.

Two studies highlight the complex physiological adaptations of bacteria to high altitude habitats, where microbes have to contend with cold and dry conditions, and high UV exposure. Zannier et al. investigate the impact of extreme UV irradiation on the proteome of a *Nesterenkonia* strain, revealing its oxidative stress response, DNA damage repair, and reallocation strategies for metabolic energy that allow this actinobacterium to survive chronic UV stress in the Andean high plateau; the resulting network of physiological responses has been termed the "UV-resistome". In a study by Kumar et al., high-altitude stress

conditions (desiccation, extreme temperature fluctuations, UV exposure) also impact the lifestyle of a *Iodobacter* strain from a Himalayan lake; the bacterium is responding with custom-tailored survival strategies, including synthesis of antifreeze proteins and protective pigment formation.

Although Eukaryotes do not inhabit the same environmental extremes as bacteria and archaea, they do occur in abundance and in great diversity in some extreme habitats, for example in the polar oceans. Grattepanche et al. provide an example from the Antarctic ocean, a survey of eukaryotic phyto- and zooplankton along the Western Antarctic Peninsula in southern spring. Diatoms dominated the phytoplankton, and phototrophy was generally the dominant trophic mode. Toward the south, mixotrophic, phagotrophic and parasitic communities increased, and in the southernmost station nanoplankton predators dominated. Climate change will likely shift this phototrophic-heterotrophic community gradient further south.

We conclude this Research Topic with a paper by Kevorkian et al. on methane cycle dynamics at the marine methane-sulfate interface. Depending on the availability of electron donors and acceptors, methanogenesis and anaerobic methane oxidation intersect at this interface, where both processes appear to be mediated by ANME-1 archaea. In long-term incubations that transition from sulfate reduction to methanogenesis, ANME-1 archaea are selected against, methane is cycled at low sulfate concentrations for several months, followed by steady growth of sulfate reducers along with methanogens after sulfate is depleted. These results indicate a complex network of changing interactions between sulfate-reducing bacteria and methanogens.

To summarize, "*Insights in extreme microbiology 2021*" showcases not only the diversity of themes and contributors but also the different research scales in Extreme Microbiology, from individual proteins and enzymes to global microbial ecosystems. Of course, fifteen papers are just a start, and some readers may already miss their favorite topics, for example acidophiles, halophiles, or Astrobiology. To broaden the scope and to provide further opportunities, we note that the "*Insights in extreme microbiology 2022*" Research Topic is open for manuscript submission at the time of writing.

Author contributions

AT and VE wrote and edited the editorial. Both authors contributed to the article and approved the submitted version.

Acknowledgments

We acknowledge the engaged and hard-working associate and review editors who are essential for the current and future development of Frontiers in Microbiology.

Conflict of interest

The authors declare that the research was conducted in the absence of any commercial or financial relationships that could be construed as a potential conflict of interest.

Publisher's note

frontiers in Microbiology

ORIGINAL RESEARCH
published: 03 March 2022
doi: 10.3389/fmicb.2022.845250

Biological Sulfate Reduction in Deep Subseafloor Sediment of Guaymas Basin

Toshiki Nagakura[1†], Florian Schubert[1†], Dirk Wagner[1,2], Jens Kallmeyer[1] and IODP Exp. 385 Shipboard Scientific Party*

[1]*GFZ German Research Centre for Geosciences, Section 3.7 Geomicrobiology, Potsdam, Germany,* [2]*Institute of Geosciences, University of Potsdam, Potsdam, Germany*

Sulfate reduction is the quantitatively most important process to degrade organic matter in anoxic marine sediment and has been studied intensively in a variety of settings. Guaymas Basin, a young marginal ocean basin, offers the unique opportunity to study sulfate reduction in an environment characterized by organic-rich sediment, high sedimentation rates, and high geothermal gradients (100–958°C km^{-1}). We measured sulfate reduction rates (SRR) in samples taken during the International Ocean Discovery Program (IODP) Expedition 385 using incubation experiments with radiolabeled $^{35}SO_4^{2-}$ carried out at *in situ* pressure and temperature. The highest SRR (387 nmol cm^{-3} d^{-1}) was recorded in near-surface sediments from Site U1548C, which had the steepest geothermal gradient (958°C km^{-1}). At this site, SRR were generally over an order of magnitude higher than at similar depths at other sites (e.g., 387–157 nmol cm^{-3} d^{-1} at 1.9 mbsf from Site U1548C vs. 46–1.0 nmol cm^{-3} d^{-1} at 2.1 mbsf from Site U1552B). Site U1546D is characterized by a sill intrusion, but it had already reached thermal equilibrium and SRR were in the same range as nearby Site U1545C, which is minimally affected by sills. The wide temperature range observed at each drill site suggests major shifts in microbial community composition with very different temperature optima but awaits confirmation by molecular biological analyses. At the transition between the mesophilic and thermophilic range around 40°C–60°C, sulfate-reducing activity appears to be decreased, particularly in more oligotrophic settings, but shows a slight recovery at higher temperatures.

Keywords: sulfate reduction, subsurface life, deep biosphere, thermophiles, Guaymas Basin

OPEN ACCESS

Edited by:
Andreas Teske, University of North Carolina at Chapel Hill, United States

Reviewed by:
Doug LaRowe, University of Southern California, United States
Alexey Kamyshny, Ben-Gurion University of the Negev, Israel

***Correspondence:**
Jens Kallmeyer
kallm@gfz-potsdam.de

†These authors have contributed equally to this work

Specialty section:
This article was submitted to Extreme Microbiology, a section of the journal Frontiers in Microbiology

Received: *29 December 2021*
Accepted: *01 February 2022*
Published: *03 March 2022*

Citation:
Nagakura T, Schubert F, Wagner D, Kallmeyer J and IODP Exp. 385 Shipboard Scientific Party (2022) Biological Sulfate Reduction in Deep Subseafloor Sediment of Guaymas Basin. Front. Microbiol. 13:845250. doi: 10.3389/fmicb.2022.845250

INTRODUCTION

As early as the late 19th century microorganisms were anecdotally reported from surficial deep-sea sediment (Fischer, 1894). In the following decades, several studies mentioned the existence of bacteria in marine sediment (e.g., Rittenberg, 1940; ZoBell, 1952). In their seminal study, Morita and ZoBell (1955) showed the existence of viable microorganisms in abyssal clays from the central Pacific down to several meters depth below the seafloor, but evidence for widespread microbial colonization of deep subseafloor sediment down to hundreds of meters was only presented several decades later (Parkes et al., 1994). While Whelan et al. (1985) showed clear indications of metabolic activity at greater depths based on radiotracer measurements, the presence of an

abundant and metabolically active microbial community was only proven at the beginning of the 21st century (Schippers et al., 2005).

In subseafloor sediment, the decrease of microbial abundance with depth is mostly the result of decreasing nutrient availability, whereas increasing temperature and pressure only have a minor effect (Jørgensen, 1982; Middelburg, 1989; Møller et al., 2018; Heuer et al., 2020). However, upon deeper burial, the sediment eventually enters the zone of catagenesis. For sediment from Nankai Trough with mostly terrestrially derived organic matter Horsfield et al. (2006) showed that at temperatures above 60°C, the recalcitrant organic matter such as kerogen is thermally cracked, leading to the production of short-chain organic molecules, which can be utilized *in situ* by microorganisms.

Sulfate-reducing microorganisms (SRM) play a vital role in biogeochemical cycling of sulfur and carbon and therefore are key players in the regulation of global climate (Pester et al., 2012). Sulfate is reduced to hydrogen sulfide which, particularly in marine sediment, further reacts with other ions and organic matter and forms a variety of reduced organic and inorganic sulfur species. The sum of reduced inorganic sulfur species ($\Sigma H_2S + FeS + FeS_2 + S^0$) is also called Total Reduced Inorganic Sulfur (TRIS; Howarth, 1979; Howarth and Teal, 1979; Howarth and Giblin, 1983).

Sulfate concentrations are high near the sediment–water interface due to downward diffusion of sulfate from the overlying water column. With increasing depth sulfate concentration decreases as the rate of sulfate consumption exceeds the downward flux. There are two pathways of microbial sulfate reduction:

1. Organoclastic sulfate reduction: $2CH_2O + SO_4^{2-} = 2HCO_3^- + H_2S$
2. Methanotrophic sulfate reduction: $CH_4 + SO_4^{2-} = HCO_3^- + HS^- + H_2O$

Sulfate-reducing microorganisms can metabolize various carbon substrates, such as fatty acids (Widdel, 1980; Widdel and Pfennig, 1981), aromatic compounds (Widdel, 1980), sugars (Sass et al., 2002), amino acids (Baena et al., 1998), and, in a consortium with archaea, methane (Boetius et al., 2000). The selection of a specific metabolic pathway is based on the availability of substrates. In near-surface sediments, volatile fatty acids (VFAs) are produced by fermentation of macromolecular organic matter. Due to preferential degradation of easily degradable organic matter, the reactivity of the remaining bulk organic matter decreases with increasing burial depth (Middelburg, 1989), leading to lower production rates of VFAs and hence lower sulfate reduction rates (SRR; Hoehler and Jørgensen, 2013).

Methanogenesis is the final step in the degradation of organic matter, once all other electron acceptors with a higher energy yield have been depleted (Froelich et al., 1979). The upward diffusing methane eventually reaches depths where sulfate is still available, the so-called sulfate–methane transition zone (SMTZ) in which sulfate and methane coexist. In the SMTZ, methanotrophic sulfate reduction (i.e., anaerobic oxidation of methane, AOM) takes place. Although the concentration of sulfate is extremely low below the SMTZ, sulfate still exists due to the downwards diffusion of sulfide and re-oxidation to sulfate by reactive iron species. Thus, biological sulfate reduction can occur slowly below the SMTZ (Holmkvist et al., 2011).

With recent improvements in drilling techniques, exploration of the subseafloor biosphere ventured into great depths with correspondingly decreased microbial abundance and metabolic activity (Hoehler and Jørgensen, 2013; Ciobanu et al., 2014; Heuer et al., 2020). The low turnover rates encountered in the deep subsurface require highly sensitive quantification techniques. Since the first measurement of SRR with ^{35}S-radiotracer by Sorokin (1962), the method was improved several times to make it more user friendly, accurate, and sensitive (Howarth and Giblin, 1983; Canfield et al., 1986; Fossing and Jørgensen, 1989; Hsieh and Yang, 1989; Kallmeyer et al., 2004; Røy et al., 2014).

Microbial sulfate reduction occurs over almost the entire known temperature range of life, including the hyperthermophilic range > 80°C (Weber and Jørgensen, 2002). Even at temperatures exceeding 100°C sulfate reduction has been detected (Jørgensen et al., 1992; Elsgaard et al., 1994). High SRR were recorded near hydrothermal vents where a high flux of readily bioavailable low molecular weight carbon compounds fuel high per-cell activity of the SRM, which is necessary to maintain cellular integrity under extreme temperature conditions (Weber and Jørgensen, 2002).

Guaymas Basin, located in the Gulf of California, Mexico, is a young marginal ocean basin of approximately 1,100 km long and 200 km wide that connects to the eastern Pacific Ocean (**Figure 1**). The high sedimentation rates of >1 mm year^{-1} result in the mainly biociliceous fine-grained sediment containing abundant organic matter of both marine and terrestrial origin (van Andel, 1964; Curray et al., 1979; Teske et al., 2020). Since thick sediments are covering the active seafloor spreading there are hydrothermal vents on the seafloor and frequent basaltic sill intrusions into the sediment. Geothermal gradients in the subsurface of Guaymas Basin are reaching up to 1,000°C km^{-1} (Teske et al., 2020). Due to this peculiar geological setting, the bioavailability of organic substrates is expected to not follow the expected decrease as in non-hydrothermal sediments. One of the main objectives of the International Ocean Discovery Program (IODP) Expedition 385 (Guaymas Basin Tectonics and Biosphere) was the investigation of microbial communities and activity in the deep subseafloor biosphere of Guaymas Basin. Detailed drill site descriptions are given by Teske et al. (2020, 2021) (**Table 1**). Sites U1545C and U1546D have a similar stratigraphy since the distance between these two sites is only about 1.1 km. However, while the sediment at Site U1545C reveals an undisturbed sedimentary profile, the sediment in Site U1546D was intruded by a sill around 350–430 m below seafloor (mbsf), thus these two sites offer a chance to study the impact of sill intrusion on sedimentary biogeochemical cycling.

Sites U1547B and U1548C are located inside and outside of a ringvent (circular hydrothermal mound), respectively. Around these sampling sites, sills intruded into the sediment at relatively shallow depths; *ca.* 150 mbsf at Site U1547B and *ca.* 65 mbsf at Site U1548C. This hydrothermally active area was chosen to study the effects of extremely steep geothermal temperature gradients (958°C km^{-1} at Site U1548C) on biological processes.

Site U1551B is the only site from the southeast region of Guaymas Basin. Sediment at this site is of predominantly terrestrial region. Site U1552B is located close to cold methane seeps and gas hydrates were recovered.

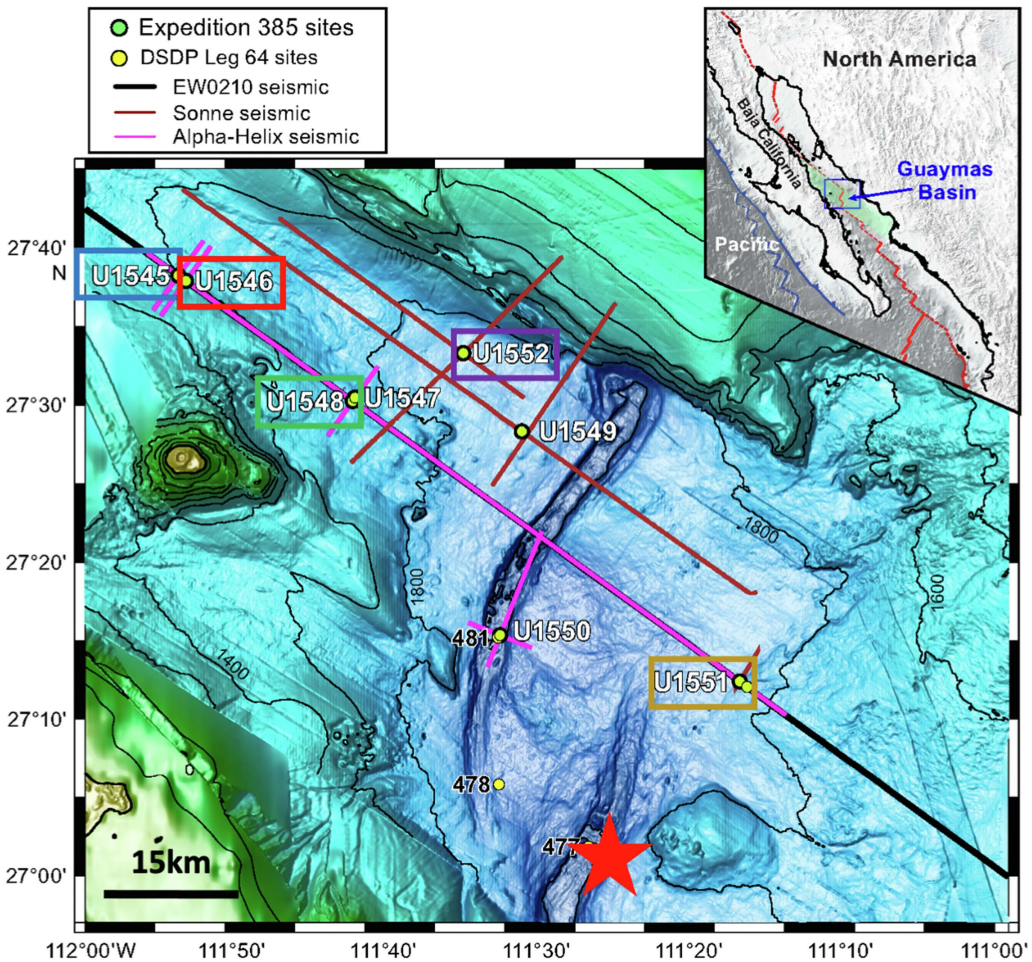

FIGURE 1 | Sampling sites in Guaymas Basin. Image adapted from Teske et al. (2020). Colored boxed indicate sampling sites where SRR could be measured. The color scheme is used for data plotted in **Figures 2–4**. The red line in the insert map is the boundary between the North American and Pacific tectonic plates. The red star in the map indicates the sampling site of Elsgaard et al. (1994).

Although SRR were measured previously in Guaymas Basin, the studies focused only on the top 40 cm sediment (Jørgensen et al., 1992; Elsgaard et al., 1994; Weber and Jørgensen, 2002), thus the rates and distribution of microbial sulfate reduction in the deep subseafloor and thermal effect on microbial sulfate reduction are still unclear. We investigated microbial sulfate reduction down to 326 mbsf in subsurface sediment of Guaymas Basin, using ^{35}S radiotracer incubations in the laboratory at approximate *in situ* temperature and pressure.

MATERIALS AND METHODS

Sampling

Core samples were collected from eight drill sites during IODP Exp. 385 (Guaymas Basin Tectonics and Biosphere) from 16 September 2019 to 16 November 2019 (Teske et al., 2020). **Figure 1** provides an overview of the sampling area of Exp. 385; detailed information about the sampling sites is given in **Table 1**. An advanced piston corer (APC)[1] can recover soft sediments without disturbing and the half-length APC (HLAPC)[2] is employed for firm sediments that are not suitable to use APC. Both coring systems are dedicated to recovering high-quality samples with minimal contamination from drilling fluid, which is a prerequisite for any geomicrobiological or biogeochemical analyses (Kallmeyer, 2017; IODP Tech. Note). Concentrations of pore water methane and sulfate as well as TOC were carried out on board according to established IODP protocols.[3] Data were taken from the IODP database.[4]

Subsampling, Storage, and Sample Processing

Immediately after retrieval of the core, whole round core (WRC) segments were cut off and capped. The WRC was then brought

[1]https://rosetta.iodp.tamu.edu/A/TechDoc/5682?encoding=UTF-8
[2]https://rosetta.iodp.tamu.edu/A/TechDoc/7146?encoding=UTF-8
[3]http://www-odp.tamu.edu/publications/pubs_tn.htm
[4]https://web.iodp.tamu.edu/OVERVIEW/

TABLE 1 | Summary of drill sites of International Ocean Discovery Program (IODP) Exp. 385 (Teske et al., 2020, 2021) from which samples were used for this study.

Site and Hole	Latitude and Longitude	Temperature gradient (°C km^{-1})	Seafloor depth (mbsl)	Number and depth range of samples	Site description
U1545C	27°38.2420'N 111°53.3290'W	225	1,595	21, 2.0–325.8 mbsf	About 52 km northwest of the western axial graben of the northern Guaymas Basin spreading segment, sediment strata are not disturbed by the intruding sill, 1.1 km distance to Site U1546D, mainly diatom ooze and clay.
U1546D	27°37.8943'N 111°52.7812'W	221	1,586	18, 2.1–292.4 mbsf	About 51 km northwest of the western axial graben, disturbed sedimentary layer due to the sill intrusion at approx. 350–430 mbsf, mainly diatom ooze and diatom clay.
U1548C	27°30.2698'N 111°40.8476'W	958	1,737	7, 1.9–59.8 mbsf	About 27 km northwest of the western axial graben, located at the outside of the active hydrothermal ringvent, mainly diatom ooze.
U1551B	27°12.3832'N 111°13.1841'W	100	1,844	5, 1.4–35.6 mbsf	About 29 km southeast of the western axial graben, the only sampling site from the southeastern region of Guaymas Basin among the eight sampling sites, and predominantly terrestrial silt and sand.
U1552B	27°33.2885'N 111°32.9640'W	262	1,841	5, 2.1–48.0 mbsf	About 20 km northwest of the western axial graben, cold seep seafloor, gas hydrate rich site, diatom/silty clay, and sandy silt.

mbsl stands for meter below sea level and mbsf stands for meter below seafloor. See ***Supplementary Table S1*** *for a list of all SRR data.*

into the ship's lab, put into gas-tight aluminum foil bags flushed with N_2 gas, and stored at *ca.* 4°C shipboard, in transit, and until use in the home lab. Unfortunately, due to a technical malfunction on board the drill ship, some samples were stored in an oxic atmosphere for several weeks. Samples from Site U1547B were compromised by the extended exposure to oxygen and no reliable SRR measurements could be conducted. Samples from sites U1549B and U1550B also suffered from the exposure to oxygen albeit for much shorter duration. SRR measurement of samples from sites U1549B and U1550B was partially successful but the quality of the data remained inconclusive. The SRR data for these sites, therefore, were also discarded. For this study, we used only SRR measurements from uncompromised samples from sites U1545C, U1546D, U1548C, U1551B, and U1552B.

Preparation of Media

The seawater media for the SRR measurement were prepared as follows, based on Morono et al. (2017): 0.2 g KH_2PO_4, 0.25 g NH_4Cl, 25 g NaCl, 0.5 g $MgCl_2 \times 6H_2O$, 0.5 g KCl, and 0.15 g $CaCl_2 \times 2H_2O$, were mixed with 1 L of ultrapure water (UPW). About 3 ml of 0.1% resazurin was added to the media and autoclaved. About 5 ml of Na_2S solution (0.12 g Na_2S in 10 ml UPW) and 5 ml of $NaHCO_3$ solution (0.84 g $NaHCO_3$ in 10 ml UPW) were added to the media after autoclaving. The media were bubbled with N_2/CO_2 gas for at least 2 h. After cooling, it was stored in pre-combusted crimp bottles with N_2 gas until use within a few days. For all samples from sites U1545C and U1546D, 0.71 g Na_2SO_4 was also added to set the sulfate concentration to 5 mM. For samples from sites U1548C, U1551B, and U1552B, we approximated the *in situ* porewater sulfate concentration by adding a separately prepared sterile 1 M Na_2SO_4 stock solution to those samples.

Control Samples

Killed controls (KC) and media controls (MC) were also prepared and incubated, alongside with the regular samples. For KC, 20% of zinc acetate was added to the sample instead of medium to stop all microbial activity. MC consisted of only the sterile medium and no sediment.

Incubation of Samples

All experiments were carried out at the GFZ German Research Centre for Geosciences, Potsdam, Germany. Inside an anaerobic

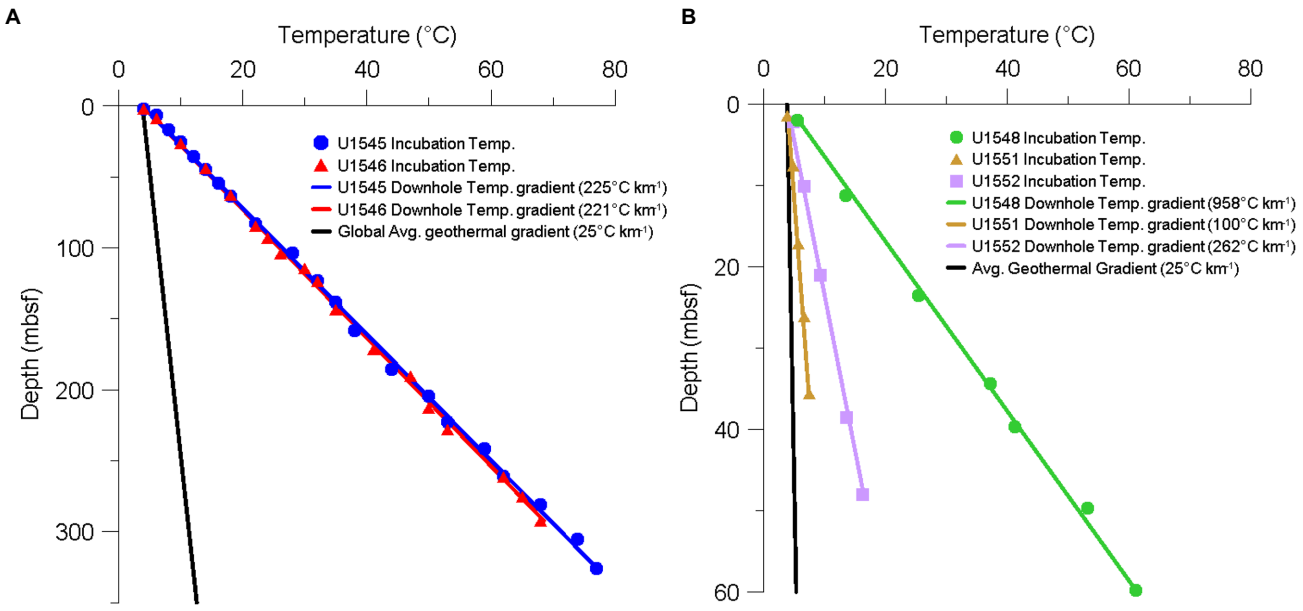

FIGURE 2 | Temperature gradients of the different sampling sites of IODP Exp. 385. **(A)** Downhole temperature gradients of sites U1545 (blue line) and U1546 (red line) measured *in situ*. Blue circles and red triangles show sampling depth and incubation temperature of each sample from sites U1545C and U1546D, respectively. **(B)** Downhole temperature gradients of sites U1548 (green line), U1551 (brown line), and U1552 (purple line) measured *in situ*. Green circles, brown triangles, and purple squares show sampling depth and incubation temperature of each sample from sites U1548C, U1551B, and U1552B, respectively. The black lines in both figures show the average global geothermal gradient of 25°C km^{-1}. Note the different depth scales on the two graphs.

glove box, 10 g of sample were weighed and put into pre-combusted glass vials. Medium was added and the vial was closed with a black butyl rubber stopper and crimped. To allow for more flexibility of the stopper and improved pressure transmission and hence avoiding breakage of the glass vial upon pressurization or depressurization, we cut off the bottom *ca.* 5 mm of the stopper. Particularly, at low temperatures, we found that the flexibility of the stoppers was severely reduced, leading to broken vials. We therefore stuck a 3 ml syringe with a cut-off plunger, containing 0.5 ml of medium into each vial (Nauhaus et al., 2002). The syringe can accommodate volume changes irrespective of incubation temperature. The samples were pre-incubated at 4°C overnight at ambient pressure. Then, 5 MBq of $^{35}SO_4^{2-}$ were injected into each sample, KC, and MC. Afterward, all vials were put into high-pressure cylinders, which were then placed in a high-pressure thermal gradient block (HPTGB) similar to the design of Kallmeyer et al. (2003). The HPTGB system consists of a thermally insulated aluminum block of 150 cm × 20 cm × 20 cm with three rows of 15 slots each, each slot is holding a stainless-steel high-pressure vessel. Temperature can be adjusted at the two ends of the block, allowing for a thermal gradient of ΔT_{max} 107°C, and minimum and maximum temperatures of −5 and 155°C, respectively. Pressure is created by high-pressure liquid chromatography pumps (Sykam, Fürstenfeldbruck, Germany), running at a constant flow rate against a back-pressure regulator (Swagelok, Germany) to prevent pressure fluctuations during thermal equilibration of the samples. The cylinders were pressurized to an approximate *in situ* pressure of 25 MPa and incubation ran for 10 days. **Figure 2** shows the incubation temperature of each sample, together with the downhole temperature gradient. All samples were incubated within ±2°C of their respective *in situ* temperature. Incubation was terminated by depressurization of the high-pressure cylinder, followed by removal of the crimp vial from the pressure cylinder, opening of the vial, and quantitative transfer of its contents into a 50 ml centrifuge tube preloaded with 5 ml of 20% zinc acetate solution to terminate microbial activity. Remaining sediment pieces were flushed out with 10 ml of 20% zinc acetate solution to transfer all of the incubated sediment into the centrifuge tube. All samples were stored at −20°C until analysis.

Distillation of the Samples

We used a slightly modified version of the cold chromium distillation of Kallmeyer et al. (2004) to liberate the reduced sulfur species from the sediment. After thawing the samples, they were centrifuged for 10 min at 2,500 × *g*. For quantification of total radioactivity (a_{TOT}), we mixed 50 µl of the supernatant with 4 ml of scintillation cocktail (Rotiszint® eco plus LSC-Universalcocktail, Carl Roth, Karlsruhe, Germany). The rest of the supernatant was carefully decanted off. The sediment pellet was then quantitatively transferred to the distillation flask and mixed with 15 ml N, N-dimethylformamide (DMF), technical grade. To ensure complete mixing of the sediment with the chemicals, a magnetic stir bar was added to the reaction flask. The flask was connected to a constant stream of nitrogen gas (approximately 5–10 bubbles per second) in order to maintain strictly anaerobic conditions during the

distillation. After 10 min of bubbling, the DMF-sediment suspension with N_2 gas, 8 ml of 6 M hydrochloric acid (HCl), and 15 ml of 1 M chromium (II) chloride solution were added to the flask *via* a reagent port. The chemicals will convert all reduced sulfur species (TRIS) to H_2S, which is driven out of solution by the stream of nitrogen gas. The produced gas is then led from the flask through a Poly-Ether-Ether-Ketone (PEEK) tube to the citrate trap filled with 7 ml of a buffered citric acid solution (19.3 g citric acid, 4 g NaOH in 1 l H_2O, and pH 4) to trap any aerosols potentially containing unreacted $^{35}SO_4^{2-}$ radiotracer but let all H_2S pass. Finally, the gas is led to a trap containing 7 ml of 5% (w/v) zinc acetate. To prevent overflowing of the zinc acetate trap, a few drops of silicon-based antifoam are added. After 2 h of distillation, the contents of the zinc acetate trap, containing the produced $H_2{}^{35}S$ are quantitatively transferred into a 20 ml plastic scintillation vial and mixed with 8 ml scintillation cocktail for quantification of radioactivity by scintillation counting. Each round of distillations also included one distillation blank (DB) containing just a few drops of non-radioactive zinc sulfide carrier and the distillation chemicals mentioned above. The DB was used to detect potential carry-over between distillation runs and therefore tracks the cleanliness of the distillation equipment. Counter blanks (CB) containing just 5% zinc acetate and scintillation cocktail in the same ratios as the samples, are added to each run of the scintillation counter. Counter blanks are required to quantify the background activity, i.e., all signals not associated with radioactivity. We use a HIDEX 600 SL Liquid Scintillation Counter (HIDEX Oy, Finland) with Guard Scintillator. Before the vials are put into the counter, they are vortexed, and the surface of the vial is wiped with 70% ethanol in order to remove any potential contamination on the vial's surface. Since the samples recovered during the expedition were incubated as slurries with additional medium, the total incubation conditions deviate considerably from *in situ* conditions. The measured rates should therefore be considered "potential" SRR (pSRR).

Calculation of Sulfate Reduction Rates and Minimum Quantification Limit and Minimum Detection Limit of SRR

The formula of Jørgensen (1978) for calculation of SRR based on radioisotope incubations was designed for whole core incubations, not slurries with added medium. We therefore use a revised version:

$$\mathrm{SRR} = \left(\left[\mathrm{SO_4}^{2-}\right]_{\mathrm{PW}} \times \mathrm{P_{SED}} \times \mathrm{V_{SED}} + \left[\mathrm{SO_4}^{2-}\right]_{\mathrm{MEDIA}} \times \mathrm{V_{MEDIA}}\right) / \mathrm{V_{SED}} \times \mathrm{a_{TRIS}} / \mathrm{a_{TOT}} \times 1 / \mathrm{t} \times 1.06 \times 1{,}000{,}000$$

where SRR is calculated in pmol cm^{-3} d^{-1}, $[SO_4^{2-}]_{PW}$ is the sulfate concentration (μmol cm^{-3}) of the sediment porewater, P_{SED} is the porosity of the sediment, V_{SED} is the volume of the sediment (cm^3), $[SO_4^{2-}]_{MEDIA}$ is the sulfate concentration (μmol cm^{-3}) of the media, V_{MEDIA} is the volume of the media (cm^3), a_{TRIS} is the radioactivity found in the TRIS fraction, a_{TOT} is total radioactivity used, t is incubation time (d), 1.06 is the correction factor for the expected isotopic fractionation (Jørgensen, 1978), and 1,000,000 is the factor to convert to pmol (Kallmeyer et al., 2004).

Any analytical method, in our case liquid scintillation counting (LSC), has an inherent background and uncertainty. The background (or blank) is a signal to which several factors contribute, but all of them are neither associated with radioactive decay nor with biological turnover of tracer. Ultra-low turnover rates require work at the absolute limit of detection, which in turn requires a strict separation of the background signal and "real" turnover. For assessment of turnover, we use the definitions of minimum quantification limit (MQL) and minimum detection limit (MDL) of Kaiser (1970):

$$\mathrm{MDL} = \text{mean value of blanks}$$
$$\mathrm{MQL} = \mathrm{MDL} + k \times \sigma b$$

Where k is the coverage factor associated with the level of confidence, b is the blank and σb is the SD of the background. Both mean value and SD were calculated for all control samples (KC and MC) and blanks (DB and CB), which were processed and measured together with the samples. A coverage factor of $k = 3$ is chosen to represent a level of confidence of 95% as recommended by Kaiser (1970) and Currie (1968) for one-tailed probabilities, i.e., false positives will only occur above MDL and not below.

The only parameter where the MQL and MDL become relevant is a_{TRIS}, due to the extremely low microbial activity in our samples. As we were using 5 MBq per sample, a_{TOT} is always well above the detection limit. Values of $a_{TOT} < \mathrm{MDL}$ are discarded, for values $\mathrm{MDL} < a_{TOT} < \mathrm{MQL}$ and $a_{TOT} > \mathrm{MQL}$, we calculate a SRR. SRR calculated from values $a_{TOT} > \mathrm{MQL}$ represent actual turnover measurements and exclude false positives with a level of confidence of 95%, whereas SRR calculated from values $\mathrm{MDL} < a_{TOT} < \mathrm{MQL}$ are rates that could be detected but cannot be distinguished from the inherent background of LSC with a sufficient level of confidence. Those rates are plotted as well, but with different symbols. The calculated SRR depends on sulfate concentration and the a_{TRIS}/a_{TOT} ratio, therefore the MQL is different for each sample.

RESULTS

Sulfate Reduction Rates at Sites U1545C and U1546D

The SRR for sites U1545C and U1546D are shown in **Figures 3A–D**. For sites U1545C and U1546D, the original objective in terms of microbiology was to elucidate the impact of sill intrusion on microbial activity at sites with similar sediment composition, TOC content (scattering between 1 and 2.5%) and stratigraphy but different sill intrusion histories. During the expedition downhole, temperature measurements indicated that the sill located at Site U1546D had reached thermal equilibrium with the surrounding sediment (Teske et al., 2021), so there is no local heating effect at present. Both sites have relatively high SRR near the seafloor, with maxima of 5.1 and 48.5 nmol cm^{-3} d^{-1} and with minima above MQL of 0.2 and 0.4 pmol cm^{-3} d^{-1} for sites U1545C and U1546D, respectively (**Figures 3A,B**). Sulfate-reducing activity was detectable down to about 300 mbsf at both sites. From the sediment surface down to about 100 mbsf, SRR at Site U1546D are higher than at Site U1545C. From *ca.*

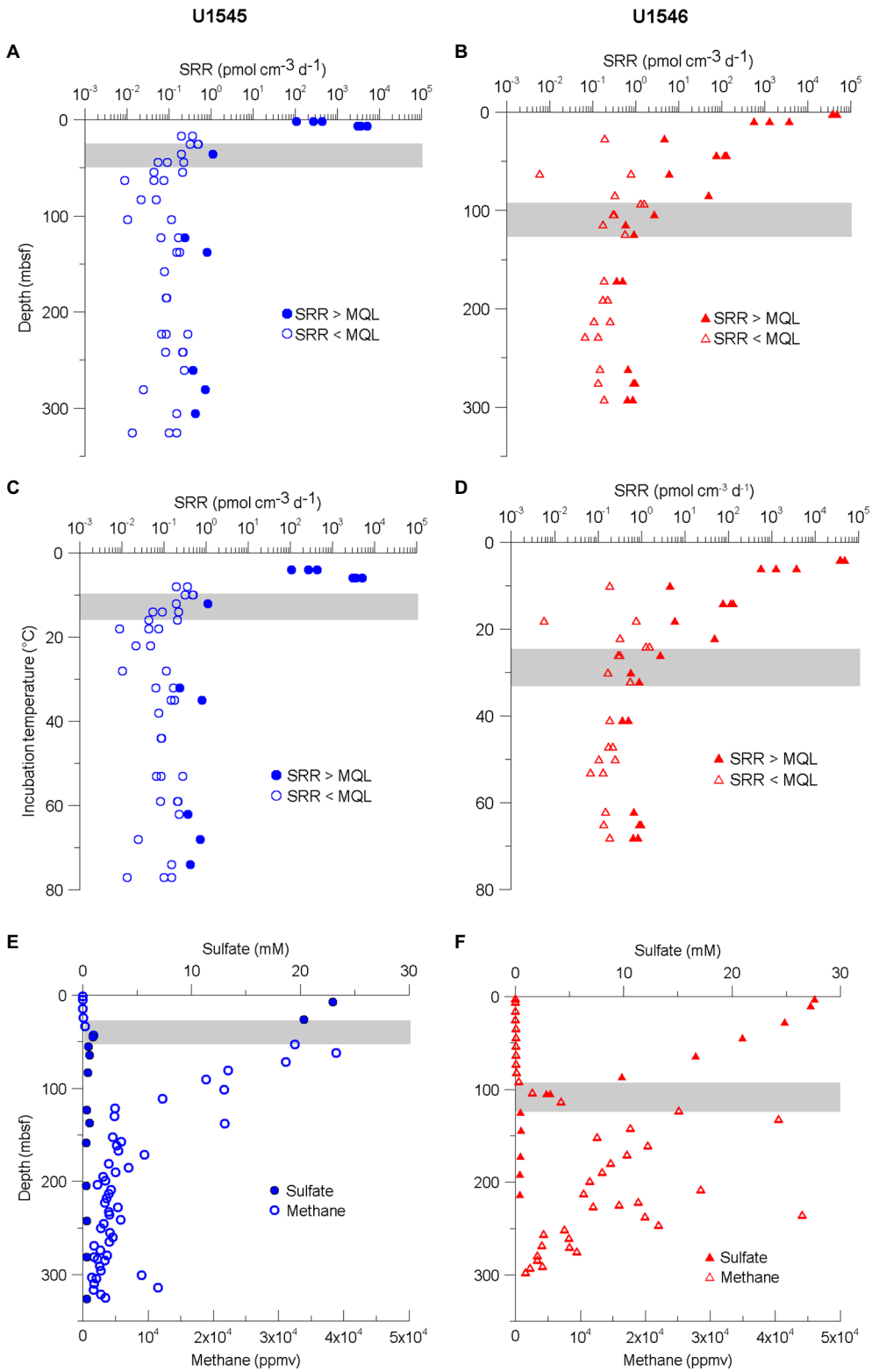

FIGURE 3 | (A,B) Sulfate reduction rates (SRR) for sites U1545C (blue circles) and U1546D (red triangles) plotted against sampled depth. Closed symbols indicate measurements SRR > MQL and open symbols MDL < SRR < MQL. See the definitions of MQL and MDL in the "Materials and Methods" section. **(C,D)** SRR for same sites plotted against incubation temperature. **(E,F)** Concentrations of sulfate and methane. The data were obtained from the Laboratory Information Management System (LIMS) report. Gray bar indicates Sulfate–Methane Transition Zone (SMTZ).

10 mbsf, SRR drop by several orders of magnitude with depth at Site U1545C, while at Site U1546D SRR decrease more gradually. Below 10 mbsf at Site U1545C and 100 mbsf at Site U1546D, we could detect SRR around 300 fmol cm^{-3} d^{-1} and many samples fell below our minimum detection limit. The depths at which SRR fall to near background rates coincide with the respective depths of the SMTZ, which are located around 40 mbsf at Site U1545C and around 110 mbsf at Site U1546D (**Figures 3E,F**). SRM show metabolic activity over a temperature range from 4 to 74°C (**Figures 3C,D**), thus the SRM inhabiting the subsurface of Guaymas Basin range from psychrophiles to thermophiles. Interestingly, at both sites, there is a depth interval in which all SRR measurements fell below MQL. At Site U1545C, the SRR < MQL interval reaches from 158.1 mbsf (38°C) to 241.6 mbsf (59°C), whereas at Site U1546D the interval is between 190.7 mbsf (47°C) and 228.4 mbsf (53°C). Above 60°C, in the thermophilic range, SRR start to increase again at both sites (**Figures 3C,D**).

Sulfate Reduction Rates at Sites U1548C, U1551B, and U1552B

The highest SRR value at sites U1548C, U1551B, and U1552B, 387 nmol cm^{-3} d^{-1}, was measured in a sample from 1.9 mbsf at Site U1548C (**Figure 4A**), which exhibits the highest geothermal gradient (958°C km^{-1}) among the eight expedition sites. The deepest sample (59.8 mbsf) at this site was located 10 m above a sill and revealed SRR of 4.8–68 pmol cm^{-3} d^{-1} at 61°C (**Figures 4A,D**). All SRR measurements from Site U1548C were above the MQL.

For sites U1551B and U1552B, SRR in near-surface samples are one to two orders of magnitude lower than that at Site U1548C, revealing maximum values of 34.2 and 46.1 nmol cm^{-3} d^{-1}, respectively (**Figures 4B,C**). The temperature ranges of samples retrieved from these two sites are between 3.9 and 7.4°C at Site U1551B and between 4.8 and 16.2°C at Site U1552B but SRR above the MQL could only be detected in samples with temperatures of up to 6.6°C (0.2 pmol cm^{-3} d^{-1}) and 9.2°C (0.1 pmol cm^{-3} d^{-1}; **Figures 4E,F**).

Owing to technical problems with our scintillation counter, we were not able to use the blank measurements (KC, MC, DB, and CB) from the U1548C samples. In order to calculate the MQL, which is crucially important to assess the SRR data, we used blank measurements (KC, MC, DB, and CB) from the Site U1547B samples.

A list of all SRR measurements is provided in the **Supplementary Table S1**.

DISCUSSION

Sulfate-Reducing Activity in Deep Subsurface Sediment of Guaymas Basin

We quantified SRR in subsurface sediments from several sites at Guaymas Basin, covering a wide range of geothermal gradients and depositional settings. One aspect of the IODP Exp. 385 was investigating the microbial community in this unique subseafloor environment. Ocean Drilling Program (ODP) Leg 201 was the first ocean drilling project dedicated to the study of subseafloor life. Several sites in the eastern Pacific Ocean and Peru margin were drilled to gain knowledge about the environmental conditions in deep marine subsurface sediments (D'Hondt et al., 2004; Jørgensen et al., 2006). Compared to ODP Leg 201 Site 1226 in the tropical Pacific Ocean (Parkes et al., 2005), SRR are generally higher in Guaymas Basin, particularly, near the seafloor. At depths of tens and hundreds meters below seafloor, SRR are in about the same range (**Figure 5**). Various reasons contribute to higher turnover rates in Guaymas Basin: firstly, Guaymas Basin sediment is characterized by a generally higher content of organic matter than sediments from open ocean sites (near seafloor samples at sites U1545C and U1546D have >3.5 wt% TOC, whereas at Site 1226 TOC concentrations are <1%). Secondly, the steep geothermal gradients lead to increased availability of organic substrates generated through thermal cracking of otherwise unavailable macromolecular organic matter (Horsfield et al., 2006) at comparatively shallow depths. A third potential factor appears to be local heating around sills to further elevate microbial activity, at least temporarily.

Compared to the data of Elsgaard et al. (1994), who quantified SRR in the upper 40 cm of hydrothermal sediment from the southern trough of Guaymas Basin (**Figure 1**), near-seafloor samples from our study revealed similar or higher SRR. The higher SRR could be a result of incubation of our samples at approximate *in situ* pressure (25 MPa), whereas Elsgaard et al. (1994) carried out all experiments at atmospheric pressure. Using slurries of surface sediment from Guaymas Basin, Kallmeyer et al. (2003) showed that SRR increased by almost an order of magnitude when the incubation was carried out at *in situ* pressure (*ca.* 25 MPa) instead of atmospheric pressure. Interestingly, when applying even higher pressure (45 MPa) SRR increased even further, but the increase in SRR when raising the pressure from 25 to 45 MPa was not as pronounced as for the pressure increase from 0.1 to 25 MPa.

Sulfate concentration in the media used for all samples from sites U1545C and U1546D was set to 5 mM, which is lower than *in situ* porewater sulfate concentrations of near-surface samples and higher for the deep samples. Although the sulfate concentration of the deep samples was increased, SRR of most of the deep samples were below MQL, which we interpret as either electron donor (organic substrate) limitation or a generally very small or metabolically slow SRM community that could not adapt to elevated sulfate levels within the 10 days incubation time.

Abiological sulfate reduction, also termed thermochemical sulfate reduction (TSR), is assumed to occur only at temperatures well over 100°C (Jørgensen et al., 1992; Machel, 2001) and turnover rates are much slower than biological sulfate reduction, we thus assume that SRR measured in our study are exclusively caused by microbial activity.

Effect of Sill Intrusion on the Microbial Sulfate-Reducing Activity

Although a thick sill was predicted from seismic data and observed at Site U1546D, the expected higher geothermal

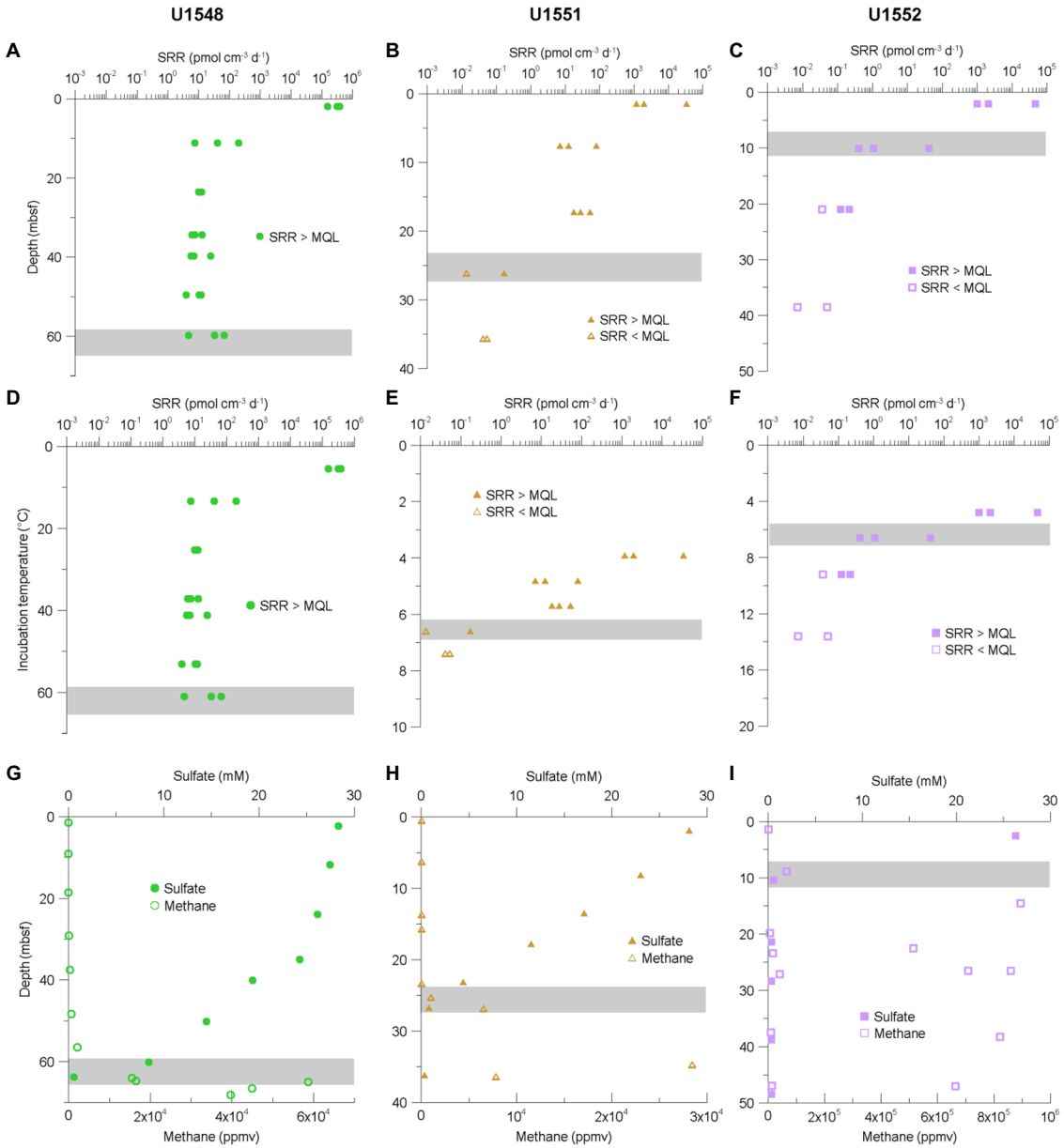

FIGURE 4 | (A–C) SRR for sites U1548C (green circles), U1551B (brown triangles), and U1552B (purple squares) plotted against sampled depth. **(D–F)** SRR for same sites plotted against incubation temperature. **(G–I)** Concentrations of sulfate and methane. The data were obtained from the Laboratory Information Management System (LIMS) report. Gray bar indicates Sulfate–Methane Transition Zone (SMTZ). Note the different scales on the graphs.

gradient was not observed, with current geothermal gradients at sites U1545C and U1546D being almost identical. This indicates that the sill at Site U1546D has reached thermal equilibrium with its surrounding sediment. The decrease of SRR with depth was steeper at Site U1545C than at Site U1546D and follows the respective decrease in sulfate concentration and thus, the position of the SMTZ, which is much shallower at Site U1545C than at Site U1546D (**Figures 3E,F**). It appears that presently sulfate availability exerts a much stronger control on SRR than past heating of the sediment. Another possible explanation for the deeper SMTZ at Site U1546D would be that due to past heating of the sediment, the remaining organic matter is more recalcitrant than at site U1545C, and therefore SRM are less active so sulfate can penetrate deeper into the sediment. Detailed organic geochemical analyses of the release potential for short-chain organic compounds (Glombitza et al., 2009) could provide insight into this matter.

Heating apparently has a positive effect on microbial activity. At Site U1548C, which has an extremely steep geothermal gradient of 958°C km^{-1} SRR are much higher than at all other sites. We acknowledge that sulfate concentrations during incubations of samples from Site U1545C and Site U1546D were all set to 5 mM and therefore deviate more strongly from porewater

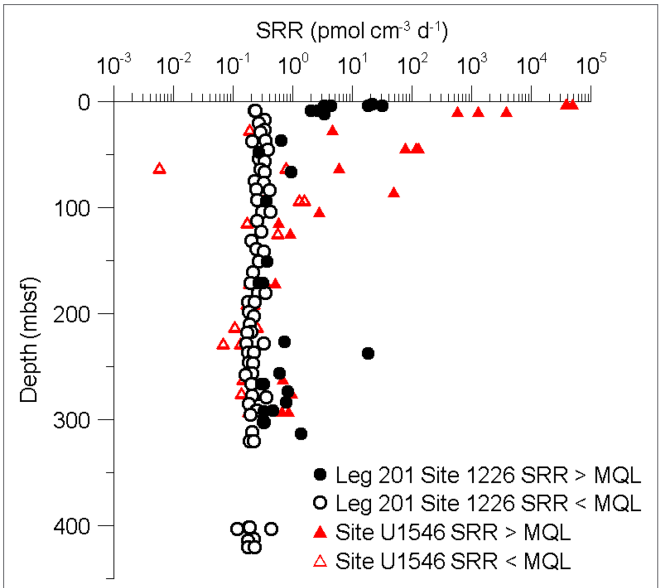

FIGURE 5 | Comparison of SRR in subsurface sediments from the tropical eastern Pacific Ocean (ODP Leg 201, Site 1,226) and Site U1546D.

concentrations than for samples from other sites, where we set the sulfate concentration individually to approximate *in situ* values (**Figures 4G–I**). Still, these deviations cannot explain differences in rates over several orders of magnitude between the sites, while still maintaining SRR vs. depth profiles that appear to be closely controlled by porewater sulfate concentration, even when incubation conditions differ considerably from *in situ* conditions.

Site U1548C suggests that heating does have a positive effect on microbial activity. However, the comparison between sites U1545C and U1546D shows that heating caused by sill intrusion at Site U1546D is only temporary. For a more detailed understanding of the influence of sill intrusion and local heating on subsurface microbiology, it would be necessary to recover a suite of sediment samples affected by the entire emplacement and cooling history of sills, plus their non-intruded counterparts for comparison.

Effect of Temperature on SRR

The drill cores from both sites U1545C and U1546D cover intervals with an *in situ* temperature between *ca.* 40 and 60°C in which all SRR measurements are below MQL (**Figures 3C,D**). This temperature is close to the shift between mesophiles (15°C–45°C) and thermophiles (45°C–80°C). In non-hydrothermal subseafloor sediment samples from Nankai Trough (IODP Exp. 370), Heuer et al. (2020) also observed a decrease in cell density in sediment around 50°C and an increase of endospores, which they interpreted as a shift in community composition. It appears that the decrease in SRR over the mesophilic to thermophilic temperature transition is not restricted to a specific site or hydrothermal/non-hydrothermal environment. Using slurries of surficial Guaymas Basin sediment, Elsgaard et al. (1994) could quantify SRR between *ca.* 40 and 60°C, but for samples without addition of short-chain fatty acids this temperature interval also represents a local minimum of activity. They also showed that addition of carbon sources not only caused a general increase in SRR, but also a shift of the temperature optimum from almost 70°C to <60°C. In our experiments, we did not add any carbon sources to the incubation and the results (**Figures 3C,D**) show a similar SRR-temperature profile as the data of Elsgaard et al. (1994) for the non-amended slurries, with a local minimum around 40°C–60°C, followed by an increase and local maximum around 65°C.

At sites U1551B and U1552B sulfate-reducing activity is strictly limited to the psychrophilic temperature range as the respective deepest samples from these sampling sites (7.4 and 16.2°C) reveal SRR that are already below the MQL. At least for Site 1552B, these samples roughly fall into a temperature range that marks the shift between psychrophiles (0°C–20°C) and mesophiles (15°C–45°C). At Site U1551B, the temperature range is especially limited and SRR can only be observed up to 6.6°C. The sediment at this site was more influenced by terrigenous sources than at the other sites drilled in Guaymas Basin during Exp. 385 and the thermal gradient is the lowest among the five sampling sites used in this study (Teske et al., 2020). A more detailed characterization of the organic matter is still lacking, so we can only assume that the sedimentary organic material is already more recalcitrant at the time of deposition, causing a more rapid decrease in substrate availability and hence, microbial activity. Additionally, thermal cracking starts at greater depth due to the comparatively lower geothermal gradient, pushing the potential source of substrates for subsurface life even deeper.

Site U1548C, which has the steepest geothermal gradient of all eight sites drilled during Exp. 385 (958°C km^{-1}) forms a stark contrast, in that all measured SRR are above the MQL. SRM are neither limited by electron acceptors, as sulfate concentrations are high throughout the core, nor by electron donors. There is abundant sedimentary organic matter (4.2 wt% of TOC at 2.5 mbsf) and thermal cracking of kerogen due to the onset of catagenesis (60°C) around 60 mbsf might become quantitatively significant in the SMTZ, leading to a supply of both methane and other short-chain organic compounds. However, the temperature at which catagenesis starts and/or becomes quantitatively important depends on the composition of the sedimentary organic matter. As we do not have such information for the IODP Exp. 385 drill cores, we can only assume that the temperature will be roughly in the same range as in Nankai Trough (Horsfield et al., 2006). The ample supply of electron donors is also reflected in the comparatively high SRR throughout the entire core and the lack of a drop in SRR at the mesophilic-thermophilic transition. Elsgaard et al. (1994) also showed in their slurry experiments that carbon addition not only leads to higher SRR, but also less variation in SRR with temperature.

Given the low cell abundances in parts of the cores recovered by Exp. 385 (Morono et al., 2017, pers. comm.) investigations of microbial community structure in these samples is challenging. Thus, our interpretations of changes

sulfate reducer community await confirmation by molecular biological analyses.

CONCLUSION

We measured SRR in deep subseafloor sediment from several sites in Guaymas Basin which were expected to have high microbial activity and abundance compared to other non-hydrothermal subsurface sediments due to their high content of bioavailable organic matter. Sulfate-reducing activity in Guaymas Basin was detected down to nearly 300 mbsf but at most sites only with low turnover rates of approximately 0.5 pmol cm^{-3} d^{-1}. By contrast, SRR near the seafloor are much higher, reaching 10 to 100s of nmol cm^{-3} d^{-1}. The highest SRR of 387 nm cm^{-3} d^{-1} was found at Site U1548C, where the sediment is very organic-rich and the geothermal gradient is roughly 1,000°C km^{-1}, supposedly leading to thermal cracking of organic matter already at shallow depth. The wide range of the current temperatures in these drill cores requires microbial communities with different temperature optima, ranging from psychrophiles over mesophiles to thermophiles. There is some indication that heating of the sediment leads to elevated microbial activity, but it appears that this effect is only temporarily and ceases once the temperature has decreased again.

DATA AVAILABILITY STATEMENT

The original contributions presented in the study are included in the article/**Supplementary Material**; further inquiries can be directed to the corresponding author.

AUTHOR CONTRIBUTIONS

TN, FS, and JK designed study and analyzed data. FS collected samples. TN carried out the experiments. TN wrote manuscript with input from all coauthors. All authors contributed to the article and approved the submitted version.

FUNDING

TN and FS are funded through DFG grants to JK (grant # 670521 and 651694).

ACKNOWLEDGMENTS

The authors would like to thank the crew of IODP Exp. 385 (Guaymas Basin Tectonics and Biosphere) for providing samples and data. Kathleen M. Marsaglia, Armelle Riboulleau, Florian Neumann, Ji-Hoon Kim, Virginia P. Edgcomb, Lucie C. Pastor, Toshiro Yamanaka, Christophe Y. Galerne, Yuki Morono, Tobias W. Höfig, and Andreas P. Teske provided comments on an earlier version of the manuscript.

SUPPLEMENTARY MATERIAL

The Supplementary Material for this article can be found online at: https://www.frontiersin.org/articles/10.3389/fmicb.2022.845250/full#supplementary-material

Supplementary Table S1 | List of all sulfate reduction rate measurements.

REFERENCES

Baena, S., Fardeau, M. L., Labat, M., Ollivier, B., Garcia, J. L., and Patel, B. K. C. (1998). Desulfovibrio aminophilus sp. nov., a novel amino acid degrading and sulfate reducing bacterium from an anaerobic dairy wastewater lagoon. *Syst. Appl. Microbiol.* 21, 498–504. doi: 10.1016/S0723-2020(98)80061-1

Boetius, A., Ravenschlag, K., Schubert, C. J., Rickert, D., Widdel, F., Gieseke, A., et al. (2000). A marine microbial consortium apparently mediating anaerobic oxidation of methane. *Nature* 407, 623–626. doi: 10.1038/35036572

Canfield, D. E., Raiswell, R., Westrich, J. T., Reaves, C. M., and Berner, R. A. (1986). The use of chromium reduction in the analysis of reduced inorganic sulfur in sediments and shales. *Chem. Geol.* 54, 149–155. doi: 10.1016/0009-2541(86)90078-1

Ciobanu, M.-C., Burgaud, G., Dufresne, A., Breuker, A., Rédou, V., Ben Maamar, S., et al. (2014). Microorganisms persist at record depths in the subseafloor of the Canterbury Basin. *ISME J.* 8, 1370–1380. doi: 10.1038/ismej.2013.250

Curray, J. R., Moore, D., Aguayo, E., Aubry, M., Einsele, G., Fornari, D., et al. (1979). Leg 64 seeks evidence on development of basins. *Geotimes* 24, 18–20.

Currie, L. A. (1968). Limits for qualitative detection and quantitative determination. Application to radiochemistry. *Anal. Chem.* 40, 586–593. doi: 10.1021/ac60259a007

D'Hondt, S., Jørgensen, B. B., Miller, D. J., Batzke, A., Blake, R., Cragg, B. A., et al. (2004). Distributions of microbial activities in deep subseafloor sediments. *Science* 306, 2216–2221. doi: 10.1126/science.1101155

Elsgaard, L., Isaksen, M. F., Jørgensen, B. B., Alayse, A.-M., and Jannasch, H. W. (1994). Microbial sulfate reduction in deep-sea sediments at the Guaymas Basin hydrothermal vent area: influence of temperature and substrates. *Geochim. Cosmochim. Acta* 58, 3335–3343. doi: 10.1016/0016-7037(94)90089-2

Fischer, B. (1894). *Die Bakterien des Meeres nach den Untersuchungen der Plankton-Expedition unter gleichzeitiger Berücksichtigung einiger älterer und neuerer Untersuchungen Ergebnisse der Plankton-Expedition*, (Kiel and Leipzig: Lipsius and Tischer) 1–83.

Fossing, H., and Jørgensen, B. B. (1989). Measurement of bacterial sulfate reduction in sediments: evaluation of a single-step chromium reduction method. *Biogeochemistry* 8, 205–222.

Froelich, P. N., Klinkhammer, G. P., Bender, M. L., Luedtke, N. A., Heath, G. R., Cullen, D., et al. (1979). Early oxidation of organic matter in pelagic sediments of the eastern equatorial Atlantic: suboxic diagenesis. *Geochim. Cosmochim. Acta* 43, 1075–1090. doi: 10.1016/0016-7037(79)90095-4

Glombitza, C., Mangelsdorf, K., and Horsfield, B. (2009). A novel procedure to detect low molecular weight compounds released by alkaline ester cleavage from low maturity coals to assess its feedstock potential for deep microbial life. *Org. Geochem.* 40, 175–183. doi: 10.1016/j.orggeochem.2008.11.003

Heuer, V. B., Inagaki, F., Morono, Y., Kubo, Y., Spivack, A. J., Viehweger, B., et al. (2020). Temperature limits to deep subseafloor life in the Nankai trough subduction zone. *Science* 370, 1230–1234. doi: 10.1126/science.abd7934

Hoehler, T. M., and Jørgensen, B. B. (2013). Microbial life under extreme energy limitation. *Nat. Rev. Microbiol.* 11, 83–94. doi: 10.1038/nrmicro2939

Holmkvist, L., Ferdelman, T. G., and Jørgensen, B. B. (2011). A cryptic sulfur cycle driven by iron in the methane zone of marine sediment (Aarhus Bay,

Denmark). *Geochim. Cosmochim. Acta* 75, 3581–3599. doi: 10.1016/j.gca.2011.03.033

Horsfield, B., Schenk, H. J., Zink, K., Ondrak, R., Dieckmann, V., Kallmeyer, J., et al. (2006). Living microbial ecosystems within the active zone of catagenesis: implications for feeding the deep biosphere. *Earth Planet. Sci. Lett.* 246, 55–69. doi: 10.1016/j.epsl.2006.03.040

Howarth, R. W. (1979). Pyrite: its rapid formation in a salt marsh and its importance in ecosystem metabolism. *Science* 203, 49–51. doi: 10.1126/science.203.4375.49

Howarth, R. W., and Giblin, A. (1983). Sulfate reduction in the salt marshes at Sapelo Island, Georgia1. *Limnol. Oceanogr.* 28, 70–82. doi: 10.4319/lo.1983.28.1.0070

Howarth, R. W., and Teal, J. M. (1979). Sulfate reduction in a New England salt marsh. *Limnol. Oceanogr.* 24, 999–1013. doi: 10.4319/lo.1979.24.6.0999

Hsieh, Y. P., and Yang, C. H. (1989). Diffusion methods for the determination of reduced inorganic sulfur species in sediments. *Limnol. Oceanogr.* 34, 1126–1130. doi: 10.4319/lo.1989.34.6.1126

Jørgensen, B. B. (1978). A comparison of methods for the quantification of bacterial sulfate reduction in coastal marine sediments. *Geomicrobiol J.* 1, 11–27. doi: 10.1080/01490457809377721

Jørgensen, B. B. (1982). Mineralization of organic matter in the sea bed—the role of sulphate reduction. *Nature* 296, 643–645. doi: 10.1038/296643a0

Jørgensen, B. B., d'Hondt, S. L., and Miller, D. J. (2006). "Leg 201 Synthesis: Controls on Microbial Communities in Deeply Buried Sediments." in *Proceedings of the Ocean Drilling Program, Scientific Results, The Program*.

Jørgensen, B. B., Isaksen, M. F., and Jannasch, H. W. (1992). Bacterial sulfate reduction above 100°C in Deep-Sea hydrothermal vent sediments. *Science* 258, 1756–1757. doi: 10.1126/science.258.5089.1756

Kaiser, H. (1970). Report for analytical chemists. II. Quantitation in elemental analysis. *Anal. Chem.* 42, 26A–59A.

Kallmeyer, J. (2017). "Chapter three—contamination control for scientific drilling operations," in *Advances in Applied Microbiology*. *Vol. 98*. eds. S. Sariaslani and G. M. Gadd (Cambridge, San Diego, London, Oxford: Academic Press), 61–91.

Kallmeyer, J., Ferdelman, T. G., Jansen, K.-H., and Jørgensen, B. B. (2003). A high-pressure thermal gradient block for investigating microbial activity in multiple deep-sea samples. *J. Microbiol. Methods* 55, 165–172. doi: 10.1016/S0167-7012(03)00138-6

Kallmeyer, J., Ferdelman, T. G., Weber, A., Fossing, H., and Jørgensen, B. B. (2004). A cold chromium distillation procedure for radiolabeled sulfide applied to sulfate reduction measurements. *Limnol. Oceanogr. Methods* 2, 171–180. doi: 10.4319/lom.2004.2.171

Machel, H. G. (2001). Bacterial and thermochemical sulfate reduction in diagenetic settings—old and new insights. *Sediment. Geol.* 140, 143–175. doi: 10.1016/S0037-0738(00)00176-7

Middelburg, J. J. (1989). A simple rate model for organic matter decomposition in marine sediments. *Geochim. Cosmochim. Acta* 53, 1577–1581. doi: 10.1016/0016-7037(89)90239-1

Møller, M. H., Glombitza, C., Lever, M. A., Deng, L., Morono, Y., Inagaki, F., et al. (2018). D:L-amino acid modeling reveals fast microbial turnover of days to months in the subsurface hydrothermal sediment of Guaymas Basin. *Front. Microbiol.* 9:967. doi: 10.3389/fmicb.2018.00967

Morita, R. Y., and ZoBell, C. E. (1955). Occurrence of bacteria in pelagic sediments collected during the mid-Pacific expedition. *Deep-Sea Res.* 3, 66–73. doi: 10.1016/0146-6313(55)90036-8

Morono, Y., Inagaki, F., Heuer, V., Kubo, Y., Maeda, L., Bowden, S., et al. (2017). "Expedition 370 methods." in *Proceedings of the International Ocean Discovery Program 370*.

Nauhaus, K., Boetius, A., Krüger, M., and Widdel, F. (2002). In vitro demonstration of anaerobic oxidation of methane coupled to sulphate reduction in sediment from a marine gas hydrate area. *Environ. Microbiol.* 4, 296–305. doi: 10.1046/j.1462-2920.2002.00299.x

Parkes, R. J., Cragg, B. A., Bale, S. J., Getlifff, J. M., Goodman, K., Rochelle, P. A., et al. (1994). Deep bacterial biosphere in Pacific Ocean sediments. *Nature* 371, 410–413. doi: 10.1038/371410a0

Parkes, R. J., Webster, G., Cragg, B. A., Weightman, A. J., Newberry, C. J., Ferdelman, T. G., et al. (2005). Deep sub-seafloor prokaryotes stimulated at interfaces over geological time. *Nature* 436, 390–394. doi: 10.1038/nature03796

Pester, M., Knorr, K.-H., Friedrich, M., Wagner, M., and Loy, A. (2012). Sulfate-reducing microorganisms in wetlands—fameless actors in carbon cycling and climate change. *Front. Microbiol.* 3:72. doi: 10.3389/fmicb.2012.00072

Rittenberg, S. C. (1940). Bacteriological analysis of some long cores of marine sediments. *J. Mar. Res.* 3, 191–201.

Røy, H., Weber, H. S., Tarpgaard, I. H., Ferdelman, T. G., and Jørgensen, B. B. (2014). Determination of dissimilatory sulfate reduction rates in marine sediment via radioactive 35S tracer. *Limnol. Oceanogr. Methods* 12, 196–211. doi: 10.4319/lom.2014.12.196

Sass, A., Rütters, H., Cypionka, H., and Sass, H. (2002). Desulfobulbus mediterraneus sp. nov., a sulfate-reducing bacterium growing on mono- and disaccharides. *Arch. Microbiol.* 177, 468–474. doi: 10.1007/s00203-002-0415-5

Schippers, A., Neretin, L. N., Kallmeyer, J., Ferdelman, T. G., Cragg, B. A., John Parkes, R., et al. (2005). Prokaryotic cells of the deep sub-seafloor biosphere identified as living bacteria. *Nature* 433, 861–864. doi: 10.1038/nature03302

Sorokin, Y. I. (1962). Experimental investigation of bacterial sulfate reduction in the Black Sea using S 35. *Microbiology* 31, 329–335.

Teske, A. P., Lizarralde, D., and Höfig, T. W. (2020). "International Ocean Discovery Program Expedition 385 Preliminary Report."

Teske, A., Lizarralde, D., Höfig, T., Aiello, I., Ash, J., Bojanova, D., et al. (2021). "Expedition 385 summary." in Guaymas Basin Tectonics and Biosphere. Teske, A., Lizarralde, D., Höfig, TW and the Expedition 385.

Van Andel, T. H. (1964). "Recent Marine Sediments of Gulf of California: PART 2."

Weber, A., and Jørgensen, B. B. (2002). Bacterial sulfate reduction in hydrothermal sediments of the Guaymas basin, gulf of California, Mexico. *Deep-Sea Res. I Oceanogr. Res. Pap.* 49, 827–841. doi: 10.1016/S0967-0637(01)00079-6

Whelan, J. K., Oremland, R., Tarafa, M., Smith, R., Howarth, R., and Lee, C. (1985). "Evidence for sulfatereducing and methane producing microorganisms in sediments from sites 618, 619, and 622," in *Initial reports of the deep sea drilling project*. eds. A. H. Bouma, J. M. Coleman and A. W. Meyer (Washington, DC: US Printing Office), 767–775.

Widdel, F. (1980). "Anaerober Abbau von Fettsäuren und Benzoesäure durch neu isolierte Arten sulfat-reduzierender Bakterien." PhD Thesis. Germany: Georg-August-Universität Göttingen.

Widdel, F., and Pfennig, N. (1981). Studies on dissimilatory sulfate-reducing bacteria that decompose fatty acids. *Arch. Microbiol.* 129, 395–400. doi: 10.1007/BF00406470

ZoBell, C. E. (1952). Bacterial life at the bottom of the Philippine trench. *Science* 115, 507–508. doi: 10.1126/science.115.2993.507

Conflict of Interest: The authors declare that the research was conducted in the absence of any commercial or financial relationships that could be construed as a potential conflict of interest.

frontiers in Microbiology

ORIGINAL RESEARCH
published: 08 March 2022
doi: 10.3389/fmicb.2022.841821

Novel Cesium Resistance Mechanism of Alkaliphilic Bacterium Isolated From Jumping Spider Ground Extract

*Takahiro Koretsune[1], Yoshiki Ishida[1], Yuri Kaneda[2], Eri Ishiuchi[2], Miyu Teshima[2], Nanami Marubashi[2], Katsuya Satoh[3] and Masahiro Ito[1,2,4,5]**

[1]Graduate School of Life Sciences, Toyo University, Oura-gun, Japan, [2]Faculty of Life Sciences, Toyo University, Oura-gun, Japan, [3]Department of Radiation-Applied Biology Research, Takasaki Advanced Radiation Research Institute, Quantum Beam Science Research Directorate, National Institutes for Quantum Science and Technology, Takasaki, Japan, [4]Bio-Nano Electronics Research Center, Toyo University, Kawagoe, Japan, [5]Bio-Resilience Research Project (BRRP), Toyo University, Oura-gun, Japan

OPEN ACCESS

Edited by:
Andreas Teske, University of North Carolina at Chapel Hill, United States

Reviewed by:
Isao Yumoto, National Institute of Advanced Industrial Science and Technology (AIST), Japan
Peter Pristas, Pavol Jozef Šafárik University in Košice, Slovakia

***Correspondence:**
Masahiro Ito
masahiro.ito@toyo.jp

Specialty section:
This article was submitted to Extreme Microbiology, a section of the journal Frontiers in Microbiology

Received: *22 December 2021*
Accepted: *31 January 2022*
Published: *08 March 2022*

Citation:
Koretsune T, Ishida Y, Kaneda Y, Ishiuchi E, Teshima M, Marubashi N, Satoh K and Ito M (2022) Novel Cesium Resistance Mechanism of Alkaliphilic Bacterium Isolated From Jumping Spider Ground Extract. Front. Microbiol. 13:841821. doi: 10.3389/fmicb.2022.841821

The radionuclide isotopes (^{134}Cs and ^{137}Cs) of Cesium (Cs), an alkali metal, are attracting attention as major causes of radioactive contamination. Although Cs^+ is harmful to the growth of plants and bacteria, alkaliphilic bacterium *Microbacterium* sp. TS-1, isolated from a jumping spider, showed growth even in the presence of 1.2 M CsCl. The maximum concentration of Cs^+ that microorganisms can withstand has been reported to be 700 mM till date, suggesting that the strain TS-1 is resistant to a high concentration of Cs ions. Multiple reports of cesium ion-resistant bacteria have been reported, but the detailed mechanism has not yet been elucidated. We obtained Cs ion-sensitive mutants and their revertant mutants from strain TS-1 and identified a Cs ion resistance-related gene, *MTS1_00475*, by performing SNP analysis of the whole-genome sequence data. When exposed to more than 200 mM Cs^+ concentration, the intracellular Cs^+ concentration was constantly lowered by MTS1_00475, which encodes the novel low-affinity Cs^+/H^+ antiporter. This study is the first to clarify the mechanism of cesium resistance in unexplained cesium-resistant microorganisms. By clarifying the new cesium resistance mechanism, it can be expected to be used as a bioremediation tool for treating radioactive Cs^+ contaminated water.

Keywords: cesium-resistant microorganisms, *Microbacterium*, alkaliphilic, mutant, whole-genome sequencing

INTRODUCTION

Cesium (Cs) is an alkali metal, and ^{134}Cs and ^{137}Cs are radioactive isotopes. Radioactive ^{137}Cs is produced from nuclear power generation waste and has attracted considerable attention as a major causative agent of radioactive contamination (Buesseler et al., 2012). The physicochemical properties of Cs^+ are similar to those of potassium ions (K^+; Avery, 1995). Studies have reported that Cs^+ uptake into cells *via* the K^+ uptake system is localized in the cell membrane of plants and bacteria and high concentrations of Cs^+ are toxic (Perkins and Gadd, 1995; Hampton et al., 2004), because of decreased intracellular K^+ concentration due to the influx of Cs^+ into

the cell (Bossemeyer et al., 1989; Jung et al., 2001). Since intracellular K^+ plays an important role in various physiological functions, such as maintenance of intracellular osmotic pressure (Jung et al., 2001), formation of membrane potential, and regulation of enzyme activity, when Cs^+ influx and intracellular K^+ are insufficient (Bossemeyer et al., 1989; Jung et al., 2001). In *Escherichia coli*, as it lacks a Cs^+ efflux system, Cs^+ influx into cells occurs through the Kup system, the main K^+ uptake system (Bossemeyer et al., 1989), resulting in an increased intracellular Cs^+ concentration. In contrast, K^+ is extracellularly effluxed by the K^+ efflux system resulting in only K^+ excretion from inside the cell and accumulation of Cs^+ inside the cell. The decrease in intracellular K^+ concentration inhibited the growth of *E. coli* (Bossemeyer et al., 1989). In addition, the expression of the *kdpFABC* operon, which encodes a high-affinity K^+ uptake system, is induced to compensate for the decrease in intracellular K^+ concentration (Jung et al., 2001).

Several Cs^+-resistant microorganisms have been reported (Bossemeyer et al., 1989; Buesseler et al., 2012; Kato et al., 2016; Swer et al., 2016). *Rhodococcus qingshengii* CS98 and *Arthrobacter* sp. KMSZP6, a cesium-accumulating bacterium, is used for bioremediation in radioactive Cs^+-contaminated environments (Takei et al., 2014; Swer et al., 2016). Other reported Cs^+-resistant bacteria, *Flavobacterium* sp. 200CS-4 (Kato et al., 2016), *Serratia* sp. Cs60-2 (Dekker et al., 2014), *Yersinia* sp. Cs67-2 (Dekker et al., 2014), and *Bacillus* sp. C-700 (Zhang et al., 2021) showed CsCl resistance at 200, 300, 500, and 700 mM, respectively. *Flavobacterium* sp. 200CS-4 was isolated from forest soil in Hokkaido, and the intracellular Cs^+ concentration was lower than that of the outer environment (Kato et al., 2016). However, the underlying mechanism has not yet been clarified. *Serratia* sp. Cs60-2 and *Yersinia* sp. Cs67-2 have been isolated from the nuclear fuel reservoir in Cambria, United States, and both have Cs^+ resistance not found in related species (Dekker et al., 2014). Therefore, these bacteria possess Cs^+ resistance properties; however, the mechanism has not been clarified. *Arthrobacter* sp. KMSZP6 was isolated from an untouched uranium deposit in India, and when exposed to a Cs^+-containing solution, it accumulated Cs^+ in the cells, and its dry weight became approximately three times that of the bacterium before Cs^+ treatment (Swer et al., 2016). Therefore, *Arthrobacter* sp. KMSZP6 can be used for bioremediation, such as decontaminating Cs^+-contaminated water; however, Cs^+ accumulation and the Cs^+ resistance mechanisms in cells have not been clarified. *Bacillus* sp. Cs-700 was isolated from sediments in the South China Sea, and related species were identified by 16S rRNA analysis and whole-genome analysis, but the Cs^+ resistance mechanism is unknown (Zhang et al., 2021). As described above, although multiple Cs^+-resistant bacteria have been reported, the Cs^+ resistance mechanism and proteins involved have not been clarified and identified, respectively.

In 2012, we isolated the *Microbacterium* sp. TS-1 (referred to as TS-1) from jumping spiders (Fujinami et al., 2013). Strain TS-1 is a facultative alkaliphilic bacterium with a growth pH range of 6.0–10.0 and an optimum growth pH range of 8.0–9.0. Strain TS-1 was closely related to *Microbacterium arborescens* based on 16S ribosomal DNA phylogenetic analysis. The whole-genome sequence of strain TS-1 was completed in 2013 and registered in the DNA Data Bank of Japan (DDBJ) (accession number for the genomic information of the TS-1 strain is BASQ01000000). In this study, strain TS-1 was a high-concentration Cs^+-resistant bacterium that could withstand up to 1.2 M CsCl. Therefore, strain TS-1 is expected to exhibit a unique Cs^+ resistance mechanism. Two major hypotheses regarding the Cs^+ resistance mechanism of strain TS-1 have been developed. The first is the mechanism that keeps the intracellular Cs^+ concentration low by effluxing the intracellular Cs^+ extracellularly by membrane transporters. The second mechanism is that the protein that adsorbs Cs^+ influx into the cell exists and reduces the free Cs^+.

In this study, to verify our hypothesis of the Cs^+ resistance mechanism of strain TS-1, we first obtained Cs^+-sensitive mutants by chemical treatment with ethyl methanesulfonate (EMS). Several Cs^+-resistant revertant strains were isolated from each Cs^+-sensitive mutant by spontaneous mutagenesis. Subsequently, whole-genome sequence analysis of the mutants was performed using a next-generation sequencer. Finally, the mutation sites of the Cs^+-sensitive mutants and their revertant mutants were comparatively analyzed to identify the Cs^+ resistance-related gene candidates. We believe that our findings will significantly improve the understanding of the mechanisms of bacterial adaptation to cesium ions.

MATERIALS AND METHODS

Bacterial Strains and Plasmids

The bacterial strains and plasmids used in the present study are listed in **Table 1**, and the primers used in our investigation are available upon request. The wild-type strain was alkaliphilic *Microbacterium* sp. TS-1, with its whole-genome previously sequenced (Fujinami et al., 2013).

Growth Media and Conditions

Escherichia coli and *Bacillus subtilis* strains were grown at 37°C in Luria-Bertani (LB) medium (BD Difco™, New Jersey, United States) and 30 mM Tris medium (Imazawa et al., 2016). *Escherichia coli* strains, Mach1™ (Thermo Fisher) and KNabc (three major Na^+/H^+ antiporters-deficient; Nozaki et al., 1998) strains were used for routine genetic manipulations and antiport assay, respectively. The *E. coli* KNabc transformants were grown in LBK medium (10 g tryptone; 5 g yeast extract; 6 g KCl, pH 7.5). *Microbacterium* sp. TS-1 (alkaliphilic in nature) and *Alkalihalobacillus pseudofirmus* OF4 (formerly, *Bacillus pseudofirmus* OF4; Patel and Gupta, 2020) were grown at 37°C in neutral complex medium (NC medium) and 30 mM Tris medium (Tris medium). The Tris medium contained 3.63 g Tris base, 1.47 g citric acid monohydrate, 0.5 g yeast extract, 9 g glucose, 1% (v/v) trace elements (Cohen-Bazire et al., 1957) per liter of deionized water (Imazawa et al., 2016). The pH was adjusted to 8 and 9 using 1 M N-methyl-D-glucamine. The pH was adjusted to 7 using 5 N H_2SO_4. Tris medium was used for the resistance test evaluation of monovalent cations because the carry-in of cations can be underestimated. The

TABLE 1 | Bacterial strains and plasmids used in this study.

Strains	Genotype	References
Microbacterium sp. TS-1	Wild type	Fujinami et al., 2013
Mut3	Cs^+-sensitive mutant from TS-1	This study
Mut3R	Cs^+-resistant revertant from Mut3	This study
Mut4	Cs^+-sensitive mutant from TS-1	This study
Mut4R	Cs^+-resistant revertant from Mut4	This study
Mut6	Cs^+-sensitive mutant from TS-1	This study
Mut6R	Cs^+-resistant revertant from Mut6	This study
Mut8	Cs^+-sensitive mutant from TS-1	This study
Mut8R	Cs^+-resistant revertant from Mut8	This study
Mut9	Cs^+-sensitive mutant from TS-1	This study
Mut9R	Cs^+-resistant revertant from Mut9	This study
Escherichia coli		
W3110	F^- *IN(rrnD-rrnE1) rph-1*	*E. coli* Genetic Stock Center
KNabc	*ΔnhaA*, *ΔnhaB*, *ΔchaA*, Kan^+, Ery^+, Cam^+, *supE*, *hsd*, *Δ5thi*, *Δ*(*lac-proAB*)/F′, [*traD36*, *proAB*$^+$, *lacLq*, *lacZ*, ΔM15]	Nozaki et al., 1998
Mach1™	F^-, [φ80*lacZ*ΔM15], Δ*lacX74*, *hsd*R,(r_K-, m_K^+), Δ*rec*A1398, *end*A1, *ton*A	Thermo Fisher
Bacillus subtilis		
BR151MA	*lys3 tripC2* (wild type)	Grundy et al., 1994
Alkalihalobacillus pseudofirmus OF4	Wild type	Guffanti et al., 1986
Plasmid		
pBAD24	Cloning expression vector, P_{BAD} promoter, Ap^R	Guzman et al., 1995
pBAD-00475	pBAD24 + MST1-00475 (*E. coli* codon-optimized sequence)	This study

NC medium contained 15.5 g K_2HPO_4, 4.5 g KH_2PO_4, 0.05 g $MgSO_4{\cdot}7H_2O$, 0.34 g citric acid, 5 g peptone, 2 g yeast extract, 5 g glucose, and 11.7 g NaCl per liter of deionized water (Aono et al., 1999). The final pH was adjusted to the desired value by adding KOH or H_2SO_4 as needed (Fujinami et al., 2011). These media were solidified by adding 1.5% (w/v) agar when necessary. The medium was supplemented with kanamycin (25 μg/ml) or ampicillin (100 μg/ml) when antibiotics were required for growth selection. Cells were grown at 37°C with shaking and monitored by measuring the optical density at 600 nm (OD_{600}) using a spectrophotometer.

Growth Analysis of Cs-Resistant TS-1 Strain

Strain TS-1 was grown in Tris medium (pH 8) containing various CsCl concentrations. *Escherichia coli* W3110 and *B. subtilis* BR151MA were used as control strains. A similar experiment was performed using NC medium (pH 8). *Alkalihalobacillus pseudofirmus* OF4 (OF4) was used as a control for the alkaliphilic bacterium. Single colonies of strains TS-1, *E. coli*, *B. subtilis*, and OF4 were inoculated into CsCl-free precultures and reciprocally shake-cultured at 200 rpm for 16 h at 30°C. Test medium (2 ml) was placed in each 14 ml culture tube, and the preculture was inoculated to an OD_{600} of 0.01. The culture was reciprocally shaken at 200 rpm for 24 h at 30°C. The OD_{600} of each culture was measured, and the Cs^+ resistance of each strain was evaluated. Three independent experiments were performed.

Intracellular Cs^+ Concentration of *Escherichia coli* and Strain TS-1

The method for preparing the sample was based on the method of Ito et al. (1997). *Escherichia coli* W3110 and strain TS-1 in the late log phase of growth in LB medium at 30°C were harvested by centrifugation (3,000 × *g*, 4°C, 10 min), resuspended in LB medium containing several concentrations of CsCl, then cultured at 30°C at 200 rpm for 1 h. Cells were harvested by centrifugation (3,000 *g*, 4°C, 10 min), washed in 300 mM sucrose twice, and then resuspended in 2 ml 5% TCA (w/v) solution, treated at 100°C for 10 min, and then centrifuged (3,000 × *g*, 4°C, 10 min). One milliliter of the supernatant was collected and Cs^+ concentration was measured. An atomic absorption spectroscope iCE3400 (Thermo Fisher Scientific, Massachusetts, United States) was used for the measurement.

Examination of Optimum Conditions for Chemical Mutation Treatment by EMS of Strain TS-1

A single colony of strain TS-1 grown on a complex agar plate (pH 8.0) was inoculated into 2 ml NC medium (pH 8.0) and reciprocally shaken at 200 rpm for 18 h at 30°C. Then, 50 μl of the culture was inoculated into four 24φ test tubes containing 5 ml NC medium (pH 8.0), and reciprocating shaking culture was performed at 200 rpm until the OD_{600} reached 0.6 at 30°C. Then, the whole culture medium was centrifuged at 9,100 × *g* for 5 min at 4°C. The supernatant was removed, and the cell pellet was resuspended in 5 ml ice-cold 200 mM phosphate buffer (pH 7.0); subsequently, 100 μl, 150 μl, or 200 μl undiluted ethyl methanesulfonate (EMS) (Sigma-Aldrich, United States) was added. No EMS was added to the remaining test tubes. EMS treatment was performed by shaking at 200 rpm for 2 h at 30°C. Sampling was performed in each test tube over time. After the treatment, the whole amount was dispensed into a 15 ml Falcon centrifuge tube and centrifuged at 9,100 × *g* for 5 min at 4°C. After removing the supernatant, the cell pellets were resuspended of in 5 ml ice-cold 200 mM phosphate buffer (pH 7.0) and centrifuged at 9,100 × *g* for 5 min at 4°C. After performing this washing step twice, the supernatant was removed, and the cell pellet was suspended in 5 ml ice-cold 200 mM phosphate buffer (pH 7.0). Each suspension was diluted 10-fold with ice-cold 200 mM phosphate buffer (pH 7.0). This operation was repeated, and the suspension was serially diluted 10^7 times;

each 100 µl dilution sample was plated on NC agar medium (pH 8.0) and incubated at 30°C for 2 days. Two days later, the viable colony count on the plate was calculated to determine the survival rate. The following formula was used to calculate the survival rate:

$$\text{Survival rate}(\%) = \left[\begin{array}{l}\text{Viable cell count at the start of}\\ \text{chemical mutagenesis /}\\ \text{Viable cell count 2 h after}\\ \text{chemical mutagenesis}\end{array}\right] \times 100.$$

Isolation of Cs⁺-Sensitive Mutants by Chemical Mutation Treatment and Replica Plating Method

The strain TS-1 was cultured by the method described above, the supernatant was removed, the cell pellets were suspended in 5 ml ice-cold 200 mM phosphate buffer (pH 7.0), and 150 µl of the EMS undiluted solution was added. In addition, mutagen treatment was performed by shaking at 200 rpm for 2 h at 30°C. After the treatment, the whole sample was dispensed into a 15 ml Falcon centrifuge tube and centrifuged at 9,100 × *g* for 5 min at 4°C. The supernatant was removed, and the cell pellet was washed thrice with 5 ml ice-cold 200 mM phosphate buffer (pH 7.0). After washing, the supernatant was removed, and the cell pellet was resuspended in 5 ml NC medium; the entire suspension was transferred to a 24φ test tube and reciprocally shaken at 200 rpm for 18 h at 30°C. After culturing, the whole amount was transferred to a 15 ml Falcon centrifuge tube and centrifuged at 9,100 × *g* for 5 min at 4°C. The supernatant was removed, and the cell pellet suspended in 5 ml ice-cold 200 mM phosphate buffer containing 20% glycerol, 100 µl was poured into 1.5 ml tubes, the rest was stored at −80°C. The poured suspension was diluted 10-fold with ice-cold 200 mM phosphate buffer (pH 7.0), which was further diluted 10-fold with 200 mM phosphate buffer (pH 7.0). This operation was repeated, and the suspension was serially diluted 10^7 times and plated (100 µl each) on 25 NC agar plates and cultured at 30°C for 2 days. Two days later, the colonies were independently transferred from the colony-formed plate onto an NC agar plate containing 100, 200, and 300 mM CsCl by the replica plating method, and incubated at 30°C for 2 days. After culturing, each plate was compared to identify the one in which colony formation was absent with or without CsCl, and four types of composites containing 100 and 200 mM of CsCl in addition to the NC agar medium. Strains exhibiting reproducible Cs⁺ sensitivity were designated candidate Cs⁺-sensitive mutants, and each strain was stored.

Isolation of Cs⁺-Resistant Revertants From Cs⁺-Sensitive Mutants

Single colony isolation was performed for the isolated Cs⁺-sensitive mutants on NC agar medium (pH 8). The colonies were inoculated into 2 ml NC medium (pH 8.0) and reciprocally shake-cultured at 200 rpm at 30°C for 18 h. The culture (100 µl) was independently plated on NC agar medium (pH 8) containing 200 mM or 400 mM CsCl to obtain spontaneous mutants whose cesium resistance was restored. The same culture diluted 10^7-fold with 200 mM phosphate buffer (pH 7) was plated onto an NC agar plate (pH 8.0) for measuring the viable cell count of the culture. Each plate was incubated at 30°C for 2 days. The number of colonies formed on the plate was counted, the viable cell count and the reversion mutation rate were calculated, and the Cs⁺-resistant revertants were isolated.

Cs⁺ Resistance Growth Test of Cs⁺-Sensitive Mutants and Cs⁺-Resistant Revertant Mutants

Each TS-1 mutant was isolated from a single colony growing on an NC agar plate (pH 8.0). Each mutant strain colony was inoculated into a 14 ml culture tube containing 2 ml NC medium (pH 8.0) and reciprocally shake-cultured at 200 rpm at 30°C for 18 h. The culture broth was used as the preculture broth. Two milliliters of test medium were placed in each 14 ml culture tube, and 10 µl of the preculture was inoculated into each tube. The culture was reciprocally shaken at 200 rpm at 30°C for 16 h. The OD_{600} of each culture was measured, and the Cs⁺ resistance of each strain was evaluated. Three independent experiments were performed.

Preparation of Chromosomal DNA From TS-1 Mutants

Mut3, Mut3R, and Mut4 mutants isolated from single colonies were inoculated into 2 ml NC medium (pH 8.0) and reciprocally shake-cultured at 30°C and 200 rpm for 18 h. Five hundred microliters of preculture was inoculated into 4.5 ml NC medium (pH 8.0) in a 24φ test tube and reciprocally shake-cultured at 30°C and 200 rpm for 4 h. Then, the whole culture medium was centrifuged at 9,100 × *g* for 5 min at 4°C and the supernatant was removed. Chromosomal DNA was prepared according to the operation manual of the DNeasy Blood & Tissue Kit (QIAGEN, Japan).

Comparative Analysis of Whole-Genome Sequencing Data

Whole-genome sequencing was performed on chromosomal DNA by Eurofins Genomics K.K using the next-generation sequencer HiSeq X 2 × 150 bp (Illumina, United States). The whole-genome sequence of each mutant strain was subjected to SNP analysis, and the mutation site was extracted. The variant call was analyzed using the following method: variant call: using samtools (ver. 1.6), bases different from the reference were extracted from the mapping results. Filtering: a variant that uses vcfutils.pl. from bcftools (ver. 1.6) and meets the default settings of the called variants. Genes with different mutation sites were selected as candidate Cs⁺ resistance-related genes. The selected Cs⁺ resistance-related candidate gene was identified from the annotation results of the TS-1 strain genome sequence, and it was investigated whether the mutation caused the non-synonymous substitution of amino acids. In addition, mutations were found in genes that overlapped between Cs⁺-sensitive mutant strains, and those in which reverse mutations were found in both revertant mutant strains were selected as promising candidates for Cs⁺ resistance-related genes. Nucleotide sequence data reported are available

in the DDBJ Sequenced Read Archive under the accession numbers DRR328004-DRR32806.

Artificial Synthetic Gene

To express MTS1_00475 in *E. coli*, the *MTS1_00475* gene was optimized for *E. coli* codons using GENEius.[1] Eurofins Genomics (Tokyo, Japan) artificially synthesized each identified gene. The gene sequence was registered in the DNA Data Bank of Japan (DDBJ). The accession number for the *MTS1_00475* gene is LC654691.

Alignment of the Cesium Resistance-Related Genes With Homologous Proteins of Several Bacterial Species

The amino acid sequences of the cesium resistance-related candidate genes and several homologs were obtained using the BLASTp algorithm at NCBI.[2] The selected amino acid residues in the alignment were analyzed using MAFFT ver. 7[3] (Katoh et al., 2002, 2019). Tree View[4] was used to create a molecular phylogenetic tree of cesium resistance-related genes and their homologs using the neighbor-joining method (NJ method). From the amino acid sequence of the cesium resistance-related genes, each protein structure was inferred using TMHMM 2.0.[5]

Construction of Plasmids for Expression of Optimized *Escherichia coli* Codons for *MTS1_00475*

The artificially synthesized DNA fragment of the *MTS1_00475* gene optimized for *E. coli* codons was double digested with restriction enzymes *Bsp*HI and *Xba*I, and pBAD24 double digested with *Nco*I and *Xba*I was ligated with T4 DNA ligase. pBAD24 is an arabinose-inducible expression vector (Guzman et al., 1994). The reaction solution was transformed into *E. coli* Mach1 competent cells. The appropriate amount was spread onto LB agar medium containing 100 μg/ml ampicillin and statically cultured overnight at 37°C. The plasmid was obtained and designated as pBAD-00475.

Cs^+ Growth Test of *Escherichia coli* KNabc Transformants

Single colonies of *E. coli* strains KNabc/pBAD24 and KNabc/pBAD-00475 were inoculated into 2 ml LBK medium (pH 7.5) at a final concentration of 100 μg/ml ampicillin and 25 μg/ml kanamycin and reciprocally shake-cultured at 37°C and 200 rpm. The culture broth was used as the preculture broth and 2 ml LBK medium (+0.1% arabinose), and various concentrations (50 mM, 100 mM, 150 mM) of CsCl with a final concentration of 100 μg/ml ampicillin and 25 μg/ml kanamycin were inoculated with 10 μl of the preculture. The culture was reciprocally shaken at 37°C and 200 rpm for 16 h. The OD_{600} of each culture was measured, and the Cs^+ resistance of each strain was evaluated. Three independent experiments were performed.

Membrane Preparations From *Escherichia coli* Transformants

Everted membrane vesicles from *E. coli* KNabc transformants were prepared using a standard procedure (Morino et al., 2008). Briefly, 400 ml LBK medium (+0.1% arabinose) was inoculated with a final concentration of 100 μg/ml ampicillin and 25 μg/ml kanamycin, and 1 ml preculture was grown at 37°C and 200 rpm for 16 h. Cells were harvested and then washed with TCDG buffer (10 mM Tris–HCl, pH 8.0; 5 mM $MgCl_2$; 10% glycerol; 140 mM choline chloride; 1 mM D-dithiothreitol). Subsequently, the cell suspension was passed through a French press (10,000 psi). After centrifugation at 4°C and 9,100 × *g* for 10 min, the membrane fraction was collected by ultracentrifugation at 14°C and 49,000 × *g* for 60 min and then suspended in fresh TCDG buffer. The membrane fraction was stored at −80°C. Protein content was determined by the Lowry method using lysozyme as a standard (Lowry et al., 1951).

Cation/H^+ Antiport Activity in the Everted Membrane Vesicles

Escherichia coli KNabc membrane vesicles (66 μg protein) were diluted in 2 ml assay buffer [10 mM bis-tris phosphonate (BTP)-Cl, 5 mM $MgCl_2$, 100 mM choline Cl, pH 7.0, 7.5, 8.0, and 8.5] supplemented with 1 μM acridine orange. The assay was initiated by adding succinate to a final concentration of 2.5 mM. After steady-state fluorescence quenching was reached, the cation was added. Finally, 1 mM NH_4Cl was added to the assay buffer to abolish ΔpH and establish a baseline. Using the baseline, % dequenching, a decrease in the succinate-dependent ΔpH due to cation addition was calculated by tracing the fluorescent changes. The % dequenching from empty vector control vesicles was subtracted from every value from *E. coli* KNabc/pBAD-00475 vesicles. The concentration of cations yielding half-maximal dequenching has been validated as a good estimate of the apparent K_m of cation/H^+ antiporters (Swartz et al., 2007). Measurements were conducted using a Hitachi High-Technologies model F-4500 fluorescence spectrophotometer (excitation wavelength: 420 nm, fluorescence wavelength: 500 nm, slit width: 10 nm).

RESULTS

Cs^+ Resistance Growth Test of Strain TS-1

The growth of strain TS-1 on Tris medium (pH 8) was compared to that of *E. coli* and *B. subtilis* at several CsCl concentrations (**Figure 1A**). *Escherichia coli* and *B. subtilis* grew in a medium containing up to 50 mM CsCl, but the TS-1 strain grew up to1200 mM CsCl. The growth of the strain TS-1 in NC medium (pH 8.0) was compared to that of the strain OF4 at several CsCl concentrations (**Figure 1B**). Strain OF4 showed growth inhibition in the medium containing 50 mM M CsCl, but strain TS-1 was able to grow in media containing up to 600 mM CsCl.

[1]https://www.geneius.de/GENEius/
[2]https://blast.ncbi.nlm.nih.gov/Blast.cgi?PAGE=Proteins
[3]https://mafft.cbrc.jp/alignment/server/
[4]https://code.google.com/archive/p/treeviewx
[5]https://services.healthtech.dtu.dk/service.php?TMHMM-2.0

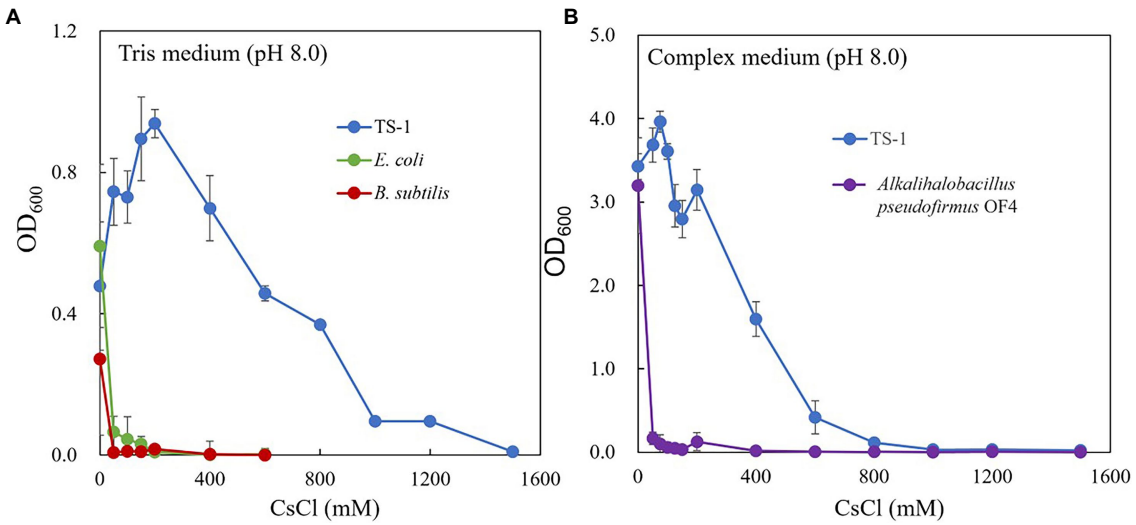

FIGURE 1 | Cs^+ resistance growth test of strain TS-1. The growth of strain TS-1 on Tris medium (pH 8) was compared to that of *Escherichia coli* and *Bacillus subtilis* at several CsCl concentrations **(A)**. The growth of strain TS-1 on a NC medium (pH 8.0) was compared to that of strain OF4 at several CsCl concentrations **(B)**. Reciprocally shaking culture was performed at 30°C at 200 rpm for 24 h, and the OD_{600} was measured. Three independent experiments were performed. Error bars indicate SD.

Intracellular Cs^+ Concentration of *Escherichia coli* and Strain TS-1

The results are shown in **Figure 2**. *Escherichia coli* increased the intracellular Cs^+ concentration in correlation with CsCl added to the medium, however, strain TS-1 kept the intracellular Cs^+ concentration low even when exposed to CsCl of 200 mM or more. Cs^+-resistant strain *Flavobacterium* sp. 200CS-4 was isolated from forest soil in Hokkaido, and it was clarified by measuring the intracellular Cs^+ concentration that the intracellular Cs^+ concentration was kept lower than that in the environment (Kato et al., 2016). However, the mechanism of intracellular Cs^+ excretion has not been clarified.

Determination of Chemical Mutagenesis Treatment Conditions by EMS of TS-1 Strain

Chemical mutagenesis treatment with different EMS concentrations against strain TS-1 was performed for 120 min to determine the survival rate. The survival rate was 106% when EMS was not administered. In contrast, when EMS was added at a final concentration of 2% (v/v), 3% (v/v), and 4% (v/v), the survival rate changed to 71%, 32%, and 0% (**Figure 3**). Since the general conditions for chemical mutagenesis treatment were set so that the survival rate was 10%–50%, in the subsequent chemical mutagenesis treatment, experiments were conducted under 3% (v/v) EMS treatment conditions for 2 h.

Isolation of Cs^+-Sensitive Mutant Strains by Chemical Mutagenesis Treatment and Replica Plating Method

After performing chemical mutagenesis with 3% (v/v) EMS for 2 h, the cells were cultured until the early stationary phase, spread on plates, and incubated at 30°C for 2 days. Approximately 50,000 colonies were duplicated by the replica plating method, and five candidate mutant strains (Mut3, Mut4, Mut6, Mut8, and Mut9) sensitive to 200 mM Cs^+ were isolated (**Supplementary Figure S1**). Strains Mut3, Mut4, and Mut9 did not grow in the medium containing 100 mM CsCl, and Mut6 and Mut8 showed tiny colonies in the medium containing 200 mM CsCl.

Isolation of Cs^+ Resistance-Revertant Strains From Each Cs^+-Sensitive Mutant Strain

The reversion mutation rates of each Cs^+-sensitive mutant strain were calculated. The reversion mutation rates of strains Mut3, Mut4, Mut6, Mut8, and Mut9 were 5.4×10^{-10}, 2.0×10^{-10}, 1.2×10^{-8}, 2.5×10^{-8}, and 9.2×10^{-9}, respectively. In general, the reversion mutation rates are stable at 1.0×10^{-8} or less and are unstable at 1.0×10^{-6} or more, and all five mutant strains were phenotypically considered stable.

Growth tests for CsCl were performed for each mutant strain, and the results are shown in **Figure 4**. All cesium ion-sensitive mutants showed decreased growth compared to the wild type. Each reverted strain regained the same level of cesium resistance as the wild-type strain, except for Mut3R and Mut9R strains, both of which did not recover as much cesium ion resistance as the wild type. However, they recovered resistance to cesium ions compared to the growth of each sensitive mutant.

Comparative Analysis of Whole-Genome Analysis Results by Next-Generation Sequencing

Whole-genome sequence analysis of strains Mut3 and Mut4, which are Cs^+-sensitive mutants obtained in the early stage

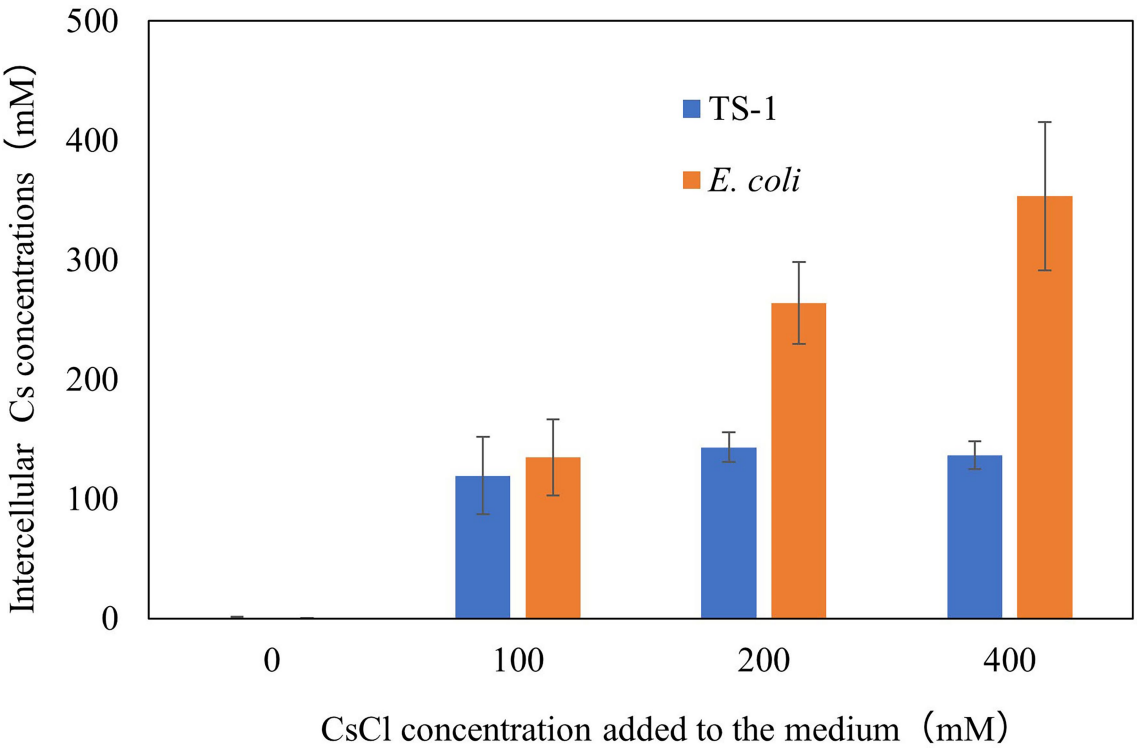

FIGURE 2 | Intracellular Cs^+ concentration of *E. coli* and strain TS-1 at several CsCl conditions. The details of the experiment are described in the Materials and Methods section. The error bars show the SD for two independent experiments.

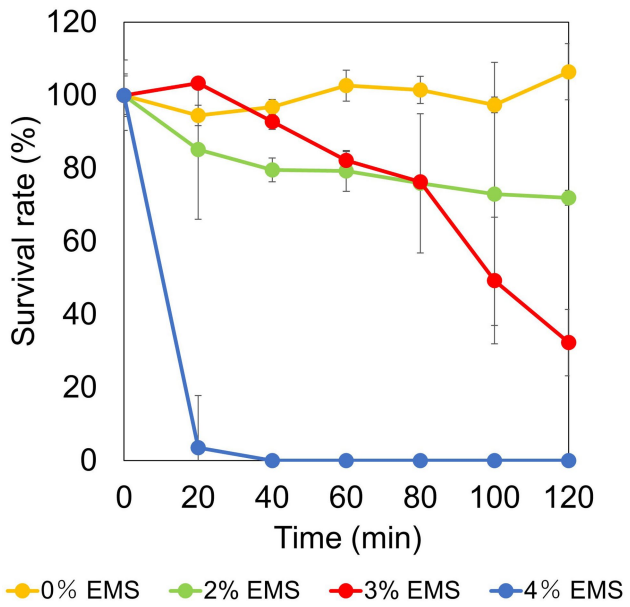

FIGURE 3 | Examination of conditions for chemical mutation treatment by ethyl methanesulfonate (EMS) in strain TS-1. The figure shows the change in survival rate depending on the EMS concentration when the strain TS-1 was subjected to chemical mutation treatment for 120 min. The vertical axis shows the survival rate obtained from the viable cell count, the horizontal axis shows the EMS concentration used for the chemical mutation treatment, and the error bar shows the SD for three independent experiments.

of this project, revealed 145 and 31 mutations, respectively. A common gene encodes a putative permease of the major facilitator superfamily (referred to as MTS1_00475). In addition, a comparison of the genome sequences of strains Mut3 and the revertant mutant Mut3R confirmed that Mut3R had a reversion mutation (Mut3: Q59* → Mut3R: *59Q) on the gene sequence of MTS1_00475. The nucleotide sequence of MTS1_00475 in the revertant was performed. The mutation site (Mut4: W253 Stop codon) in strain Mut4 exhibited intergenic suppression (Stop codon253R) in strain Mut4R. Mutations for strains Mut6, Mut8, and Mut9, isolated after strains Mut3 and Mut4, were also identified in *MTS1_00475* by analyzing the *MTS1_00475* region nucleotide sequences. In addition, the analysis of the nucleotide sequences of the *MTS1_00475* region for strains Mut6R, Mut8R, and Mut9R confirmed that the mutant site had reverted to the wild type and that intergenic suppression had occurred for Mut8R and Mut9R. The details of the mutant strains are summarized in **Table 2**.

Bioinformatics Analysis of MTS1_00475

Multiple sequence alignment of MTS1_00475 and its homologous proteins revealed that MTS1_00475 is widely distributed in the genus *Microbacterium* (**Figure 5**). In addition, MTS1_00475 showed 99% homology with the major facilitator superfamily (MFS) transporter of *Microbacterium* sp. Ru50 and *Microbacterium paludicola*. Furthermore, homologs were also identified for the MFS transporter of *Rhodococcus*

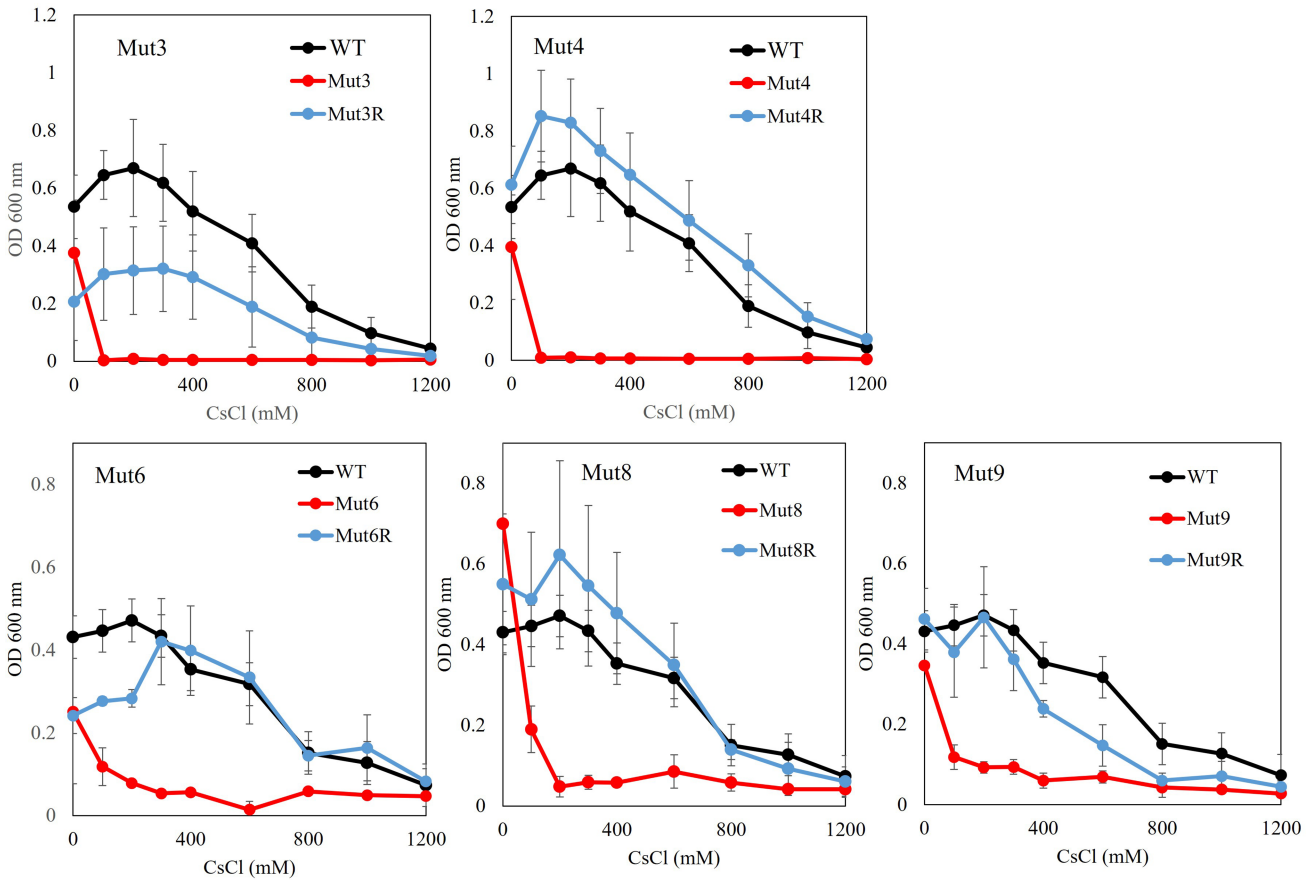

FIGURE 4 | Test to evaluate the Cs^+ resistance growth of each Cs^+-sensitive mutant and its revertant mutants. Colonies of each mutant isolated from a single colony were inoculated into 2 ml NC medium (pH 8.0) and reciprocally shake incubated at 200 rpm at 30°C for 18 h. Ten microliters of the preculture were inoculated into 2 ml Tris medium (pH 8.0) with various concentrations of CsCl (100–1,200 mM) and reciprocally shaken at 30°C at 200 rpm for 18 h, and the OD_{600} was measured. Error bars show the SD of three independent experiments.

sp. 06-1477-1B, *Zhihengliuella* sp. ISTPL4, and *Agromyces aureus*, and their amino acid identities were 73%, 72%, and 69%, respectively. A molecular phylogenetic tree based on these results is shown in **Figure 5**. The locations of the homologues of MTS1_00475 of the 13 isolated strains used to create the phylogenetic tree were investigated. The following bacteria and associated locations were identified: three bacteria related to plants (root spheres of plants, potato leaves, and a symptomatic Veronica plant; Morohoshi et al., 2011; Corretto et al., 2016; Savory et al., 2017); two bacteria isolated from the aquatic environment (marine animals like *Dictyopodium moseleyi* and salt lakes; Kageyama et al., 2007; Mishra et al., 2018); five bacteria derived from soil (Collins et al., 1983; Park et al., 2006; Kinegam et al., 2007; Zhang et al., 2010); one bacterium isolated from subsurface sediments (Brown et al., 2012); one bacterium isolated from oil reservoirs (Schippers et al., 2005); one bacterium isolated from Corn steep liquor (Yokota et al., 1993). *Microbacterium* spp. which harbor a protein with high homology to MTS1_00475 were obtained from the soil.

MTS1_00475 was predicted to be a 14-transmembrane protein based on protein structure prediction using TMHMM-2.0. A schematic of the predicted secondary structure is shown in **Figure 6**.

Measurement of Cs^+/H^+ Antiport Activity by Fluorescence Quenching Using Everted Membrane Vesicles

We prepared everted membrane vesicles from KNabc/pBAD-00475 and KNabc/pBAD24 and then measured the Cs^+/H^+ antiporter activity (**Figure 7**). The vesicle sample of KNabc/pBAD-00475 showed no Cs^+/H^+ antiport activity in buffers at pH 7.0, 7.5, and Cs^+/H^+ antiport activity was measured between pH 8.0 and 9.0. This enzyme was the most active pH 8.5 buffer and showed 44.6% Cs^+/H^+ antiporter activity. In addition, the Cs^+/H^+ antiport activity was observed when Cs^+ concentration changed in the buffer solution of pH 8.0–9.0. The apparent K_m value for Cs^+ was calculated from the Lineweaver–Burk plot equation and was found to be 250 mM, 370 mM, and 410 mM for pH 8.0, 8.5, and 9.0, respectively (**Figure 7**), indicating that MTS1_00475 is a low-affinity Cs^+/H^+ antiporter. When the antiport activity

at pH 8.0 in other monovalent cations was also measured, the apparent K_m value in Na^+, K^+, and Rb^+ was 1.7, 0.9, and 3.4 mM, respectively (**Supplementary Figure S2**). These data showed that MTS1_00475 is a membrane protein that transports not only Cs^+ but also monovalent cations, such as Na^+, K^+, and Rb^+.

TABLE 2 | The reversion mutation rates of each Cs^+-sensitive mutant strain proteins encoded by genes with revertant mutations in each revertant mutant.

Mutants	The frequency of Cs^+-resistant revertant strains	Amino acid mutation site (Cs^+-sensitive mutant → revertant mutant)	Accession number
Mut3R	5.4×10^{-10}	**MTS1_00475**	BASQ01000001.1
		(Permease of the major facilitator superfamily)	505359–506906 (minus strand)
		(Q59* → *59Q) (true reversion)	
		MTS1-02327	BASQ01000001.1
		50S ribosomal protein L16	2480985–2481404 (minus strand)
		(T122I → I122T) (true reversion)	
Mut4R	2.0×10^{-10}	**MTS1_00475**	BASQ01000001.1
		(W253* → *253R) (Intragenic suppression)	505359–506906 (minus strand)
Mut6R	1.2×10^{-8}	**MTS1_00475**	BASQ01000001.1
		(G164D → D164G) (true reversion)	505359–506906 (minus strand)
MutR8R	2.5×10^{-8}	**MTS1_00475**	BASQ01000001.1
		(W19* → *19Y) (Intragenic suppression)	505359–506906 (minus strand)
Mut9R	9.2×10^{-9}	**MTS1_00475**	BASQ01000001.1
		(W177* → *177R) (Intragenic suppression)	505359–506906 (minus strand)

Cs^+ Resistance Growth Test of *Escherichia coli* KNabc/pBAD-00475

To confirm whether the Cs^+ resistance of *E. coli* KNabc expressing MST1_00475 was improved, a Cs^+ resistance growth test was conducted. **Figure 8** shows the results of OD_{600} after independently culturing *E. coli* KNabc expressing MST1_00475 in a medium with different CsCl concentrations for 16 h. KNabc/pBAD-00475 and KNabc/pBAD24 (negative control) showed no growth in the presence of 100 mM CsCl. The expression of MTS1_00475 confirmed no improvement in Cs^+ resistance. This result may be related to the low affinity of MTS1_00475 Cs^+/H^+ antiport activity.

DISCUSSION

High Concentration Cesium Ion Resistance Strain TS-1

In recent years, there have been multiple reports of high-concentration cesium-resistant bacteria. Still, there have been no reports on the mechanism underlying the cesium ion resistance of these bacteria (Bossemeyer et al., 1989; Buesseler et al., 2012; Kato et al., 2016; Swer et al., 2016). *Bacillus* sp. C-700 is most CsCl-resistant bacterium, although strain C-700 did not show growth in a previous study (Zhang et al., 2021). We report that *Microbacterium* sp. strain TS-1, isolated from jumping spider ground extract, can grow in Tris medium (pH 8) containing 1,200 mM CsCl. Under the same growth conditions, *E. coli* and *B. subtilis* showed growth inhibition in the presence of 50 mM CsCl (**Figure 1A**). Therefore, owing to its resistance to high concentrations of cesium ions, strain TS-1 was expected to harbor unique Cs^+ resistance mechanisms.

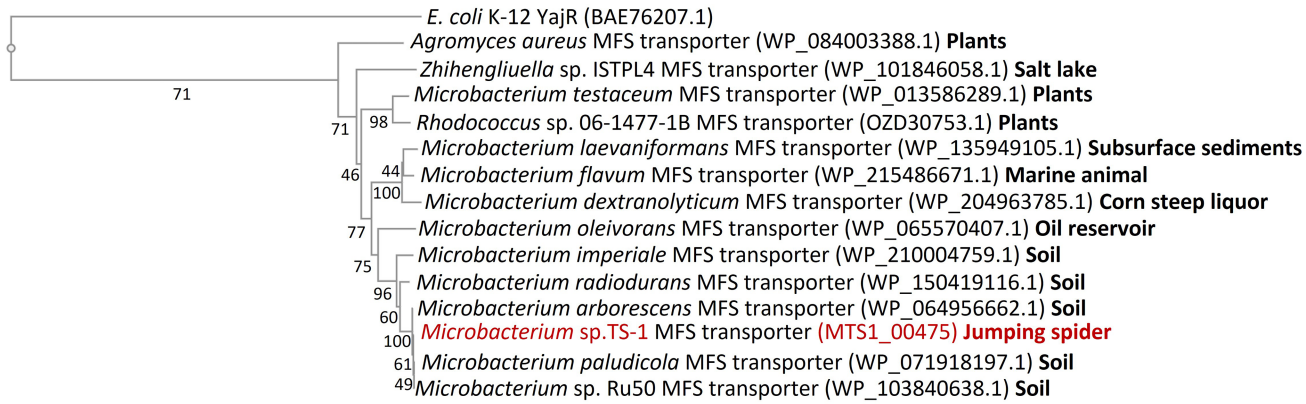

FIGURE 5 | Molecular phylogenetic tree analysis of MTS1_00475. A molecular phylogenetic tree was constructed based on multiple sequence alignment with the homolog of MTS1_00475. The details are described in the Materials and Methods section. MTS1_00475 from *Microbacterium* sp. TS-1 is shown in red. YajR from the major facilitator superfamily (MFS) of transporters of *E. coli* K-12 was used as an outgroup. The number between branches indicates the bootstrap value. The number after the bacterium indicates the GenBank accession number. The locations of isolation of the 13 strains harboring the MTS1_00475 homologs used to create the phylogenetic tree are shown in bold after each accession number.

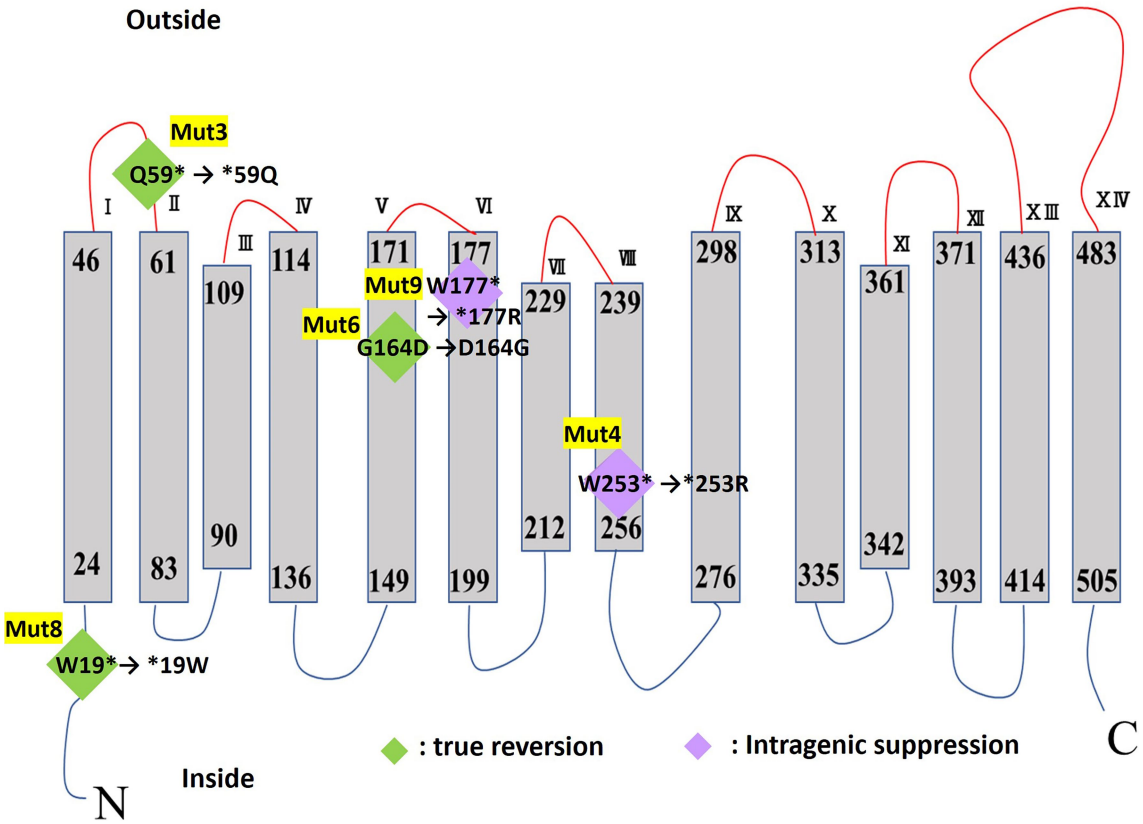

FIGURE 6 | TMHMM transmembrane model of MTS1_00475. The mutation site of each Cs^+-sensitive mutant strain is shown in diamonds. True reversion is shown in green diamonds, and in purple diamonds, intergenic suppression for mutations in the Cs^+-resistant revertant mutant strain. The asterisk indicates a stop codon.

Isolation of Cesium Ion-Sensitive Strains and Their Revertants, and Identification of Cesium Resistance Genes by Whole-Genome Sequence Analysis

Five Cs^+-sensitive mutants (Mut3, Mut4, Mut6, Mut8, and Mut9) were isolated through EMS treatment and by using the replica method of strain TS-1 (**Supplementary Figure S1**). A growth test of the Cs^+ resistance phenotype of each Cs^+-sensitive mutant and its revertant strain showed different results (**Figure 4**). In addition, the reversion mutation rate of each Cs^+-sensitive mutant strain ranged from 1.2×10^{-8} to 5.4×10^{-10}. In general, the reversion mutation rates are stable at 1.0×10^{-8} or less and are unstable at 1.0×10^{-6} or more, and all five mutant strains were phenotypically considered stable.

Compared with the wild type, strain Mut3 was observed to exhibit decreased growth, even in the absence of CsCl. In addition, strain Mut3 exhibited completely inhibited growth upon adding 100 mM CsCl to the medium. As with strain Mut3, strain Mut3R decreased growth, even in the absence of CsCl due to mutations in genes other than Cs^+ resistance-related genes. The growth of Mut3R was inhibited by adding 800 mM Cs^+ and Cs^+ resistance of strain Mut3R was a partial recovery compared with the Cs^+ resistance of the wild-type strain. Comparing and analyzing the mutation sites of strains Mut3 and Mut3R using the whole-genome sequence data, a mutation site difference of the MTS1_00475 gene region was observed. Therefore, MTS1_00475 was selected as a candidate for the Cs^+ resistance-related genes.

There are two possibilities for the growth phenotypes of Mut3 and Mut3R. There are other Cs^+ resistance-related genes where mutations may have occurred. For example, microorganisms are known to have large and diverse Cation/proton antiporters complementing adaptation to the external environment (Krulwich et al., 2009). Therefore, it is possible that strain TS-1 also has multiple Cs^+-resistance mechanisms. Second, Cs^+ resistance also decreased due to mutations in growth-related genes. From the Cs^+ resistance growth test results, the growth of strain Mut3R reduced even without Cs^+. Several studies have reported that mutations in the energy production system decrease growth and resistance to cations. A study by Hasim et al. (2018) reported that gene mutations in the energy-producing system that synthesize phosphatidylserine and phosphatidylethanolamine in *Candida albicans* reduced growth and resistance to farnesol. A study by Hamilton et al. (2002) also reported that the vacuolar H^+-ATPase gene mutations of *Saccharomyces cerevisiae* showed poor growth and Na^+ resistance. These suggest that strain Mut3R may also have gene mutations of the energy production system, resulting in decreased growth and Cs^+ resistance. From the results of next-generation sequence analysis, 145 mutations

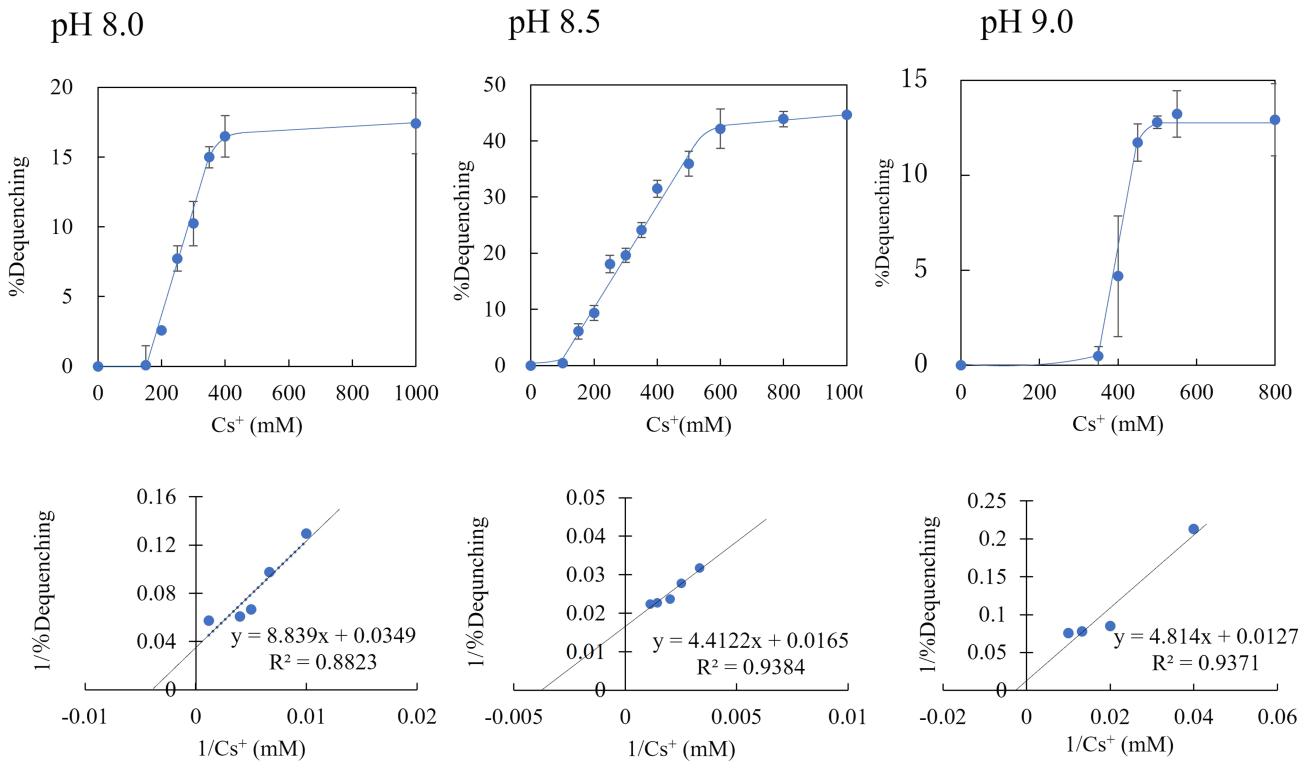

FIGURE 7 | Cs^+/H^+ antiport activity of everted membrane vesicle from strain KNabc/pBAD-00475 at pH 8.0, 8.5, and 9.0. The Cs^+/H^+ antiport activity of everted membrane vesicles from strain KNabc/pBAD-00475 in each pH buffer was shown when various concentrations of Cs_2SO_4 were added. The details are described in the Materials and Methods section. The vertical axis shows antiport activity (% Dequenching), and the horizontal axis shows the Cs^+ concentration. Error bars show the standard deviation of three independent experiments. In addition, each Lineweaver-Burk plot diagram is shown.

were found in the strain Mut3. Therefore, revertant mutants with restored growth and Cs^+ resistance will be obtained in future studies, and the reverted gene identified for further Cs^+ resistance-related and gene candidates.

Mut4 grew at the same level as the wild strain in the absence of Cs^+. However, growth was inhibited by the addition of 100 mM Cs^+. Mut4R showed almost the same level of growth as the wild type, with or without Cs^+. Therefore, this phenotype suggested that the revertant mutation site of Mut4R encodes a gene that is critical for Cs^+ resistance. When the MTS1_00475 gene region of Mut4 and Mut4R strains were compared, it was confirmed that the mutation in MTS1_00475 was restored [W253*(stop codon)→*253R] by intragenic suppression. This result strongly suggests that MTS1_00475 is a Cs^+ resistance-related gene. The mutation sites identified in Mut3 and Mut4 strains were 145 and 31, respectively. As strain Mut4 had fewer mutations than strain Mut3, this may have contributed to the recovery of the mutant Mut4R phenotype to a level that is almost the same as that of the wild type.

In this study, MTS1_00475 was identified as a Cs^+ resistance-related protein by multiple Cs^+-sensitive mutants and their revertant mutants. Strains Mut3 and Mut4 were first isolated, and the same gene mutations were identified in other Cs^+-sensitive mutants (Mut6, Mut8, Mut9; **Table 2**).

When the MTS1_00475 gene region of strain Mut9R was compared, it was confirmed that the mutation of MTS1_00475 was restored (W177*→*177R) by intragenic suppression. This may be why Mut9R did not exhibit restored growth in response to high concentrations of CsCl, that is, to the same level as the wild type (**Figure 4**). Therefore, to discover novel genes related to Cs^+ resistance, it is important to isolate a Cs^+-sensitive mutant with a mutation other than the MTS1_00475 gene.

We will try to obtain MTS1_00475 by changing the screening medium in the future. However, since a mutation in MTS1_00475 isolates so many Cs^+-sensitive strains, it is suggested that MTS1_00475 is a dominant Cs^+ resistance mechanism.

Functional Analysis of Cs^+ Resistance-Related Gene Candidate MTS1_00475

Prediction of protein structure using TMHMM revealed that MTS1_00475 is a 14-transmembrane protein (**Figure 6**). The MTS1_00475 mutations in Mut3, Mut4, Mut8, and Mut9 were all mutated to the stop codon inserted in the first half of the MTS1_00475. As a result, MTS1_00475 did not function and showed Cs^+ sensitivity. In addition, the strain Mut4R exhibited intragenic suppression of MTS1_00475-Trp253Arg. Nevertheless, Cs^+ resistance was comparable to that of the wild type suggesting that this site did not significantly affect the function of MTS1_00475.

In the Cs^+ resistance growth test, when the *MTS1_00475* gene was expressed in *E. coli*, no improvement in Cs^+ resistance

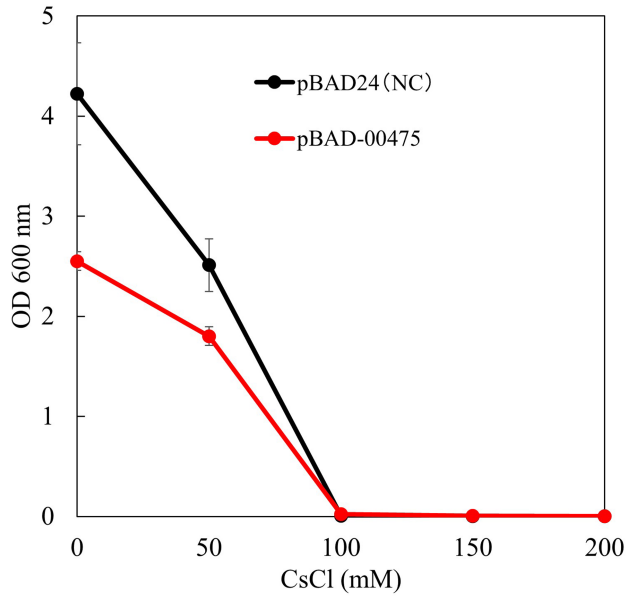

FIGURE 8 | Test to evaluate the Cs^+ resistance growth of strain KNabc/pBAD-00475. The turbidity of each concentration of CsCl when strain KNabc/pBAD-00475 in LBK medium was cultured for 16 h. Error bars show the standard deviation of three independent experiments. As the negative control, KNabc/pBAD24 was used.

was observed. However, the Cs^+/H^+ antiport activity of MTS1_00475 was measured under high Cs^+ conditions by producing everted membrane vesicles. In a previous report of K^+/H^+ antiporter activity using the right-side-out membrane of alkaliphilic *Bacillus* sp. No. 66, Rb^+, and Cs^+ were active as substrates (Kitada et al., 1997). However, no protein with Cs^+/H^+ antiporter activity has been reported. Therefore, MTS1_00475 was the first protein with Cs^+/H^+ antiporter (CshA) (MTS1_00475 is hereafter referred to as CshA).

As a future task, it is expected that the substrate affinity of CshA for Cs^+ will be improved by introducing random mutations into the *cshA* gene using error-prone PCR.

Expression of a heterologous Na^+/H^+ antiporter gene in the *E. coli* strain KNabc lacking the three major Na^+/H^+ antiporter genes improve the cells Na^+ resistance (Southworth et al., 2001; Liu et al., 2005; Morino et al., 2008). However, the expression of CshA did not improve Cs^+ resistance in *E. coli*, probably due to the low affinity for Cs^+ and sensitivity of *E. coli* to 100 mM CsCl. Subsequently, a host will confirm the improvement in Cs^+ resistance by CshA with high Cs^+ resistance. In addition, Cs^+ resistance of the host will be improved by introducing a mutation into the *CshA* gene to produce a mutated CshA with a high affinity for Cs^+.

It is inferred that the Cs^+ resistance mechanism in strain TS-1 involves the consistent reduction of the intracellular Cs^+ concentration by CshA in such a manner that the interior of the cell is not exposed to high concentrations of Cs^+.

As a further functional analysis of CshA, the antiport activity of monovalent cations other than Cs^+ was measured, and antiport activity against Na^+, K^+, and Rb^+ other than Cs^+ was observed (**Supplementary Figure S2**). As the apparent K_m value for these cations was approximately 1 mM, CshA was found to have a high affinity for Cs^+. Strain TS-1 has seven genes annotated as Na^+ (K^+)/H^+ antiporters, one belonged to the NhaA family (MST1_02247), one belonged to the NhaD-type Na^+/H^+ antiporter (MTS1_00585), two belonged to the NhaP-type Na^+ (K^+)/H^+ antiporter (MTS1_01618, MTS1_03246), and three belonging to the CPA3 family (multi-subunit Na^+/H^+ antiporter) (MTS1_01874–MTS1_01879, MTS1_02182–MTS1_02187, MTS1_02374–MTS1_02381). These major Na^+ (K^+)/H^+ antiporters are involved in Na^+ and K^+ homeostasis. Several microorganisms have multiple Na^+ (K^+)/H^+ antiporters to adapt to different environments (Krulwich et al., 2009); however, there are no reports of antiporters belonging to these families with Cs^+/H^+ antiport activity. In addition, CshA was mainly identified in *Microbacterium* spp., isolated from various environments, such as dairy goods, oral cavities, and human clinical specimens (Tsuzukibashi et al., 2015). Phylogenetic tree analysis revealed that the source of bacteria harboring homologs having high homology with MTS1_00475 was the soil. As the strain TS-1 is a bacterium isolated from jumping spiders, it is suggested that strain TS-1 is closely related to the bacterium isolated from terrestrial soil. The physiological mechanisms by virtue of which *Microbacterium* sp. TS-1 has a high Cs^+ resistance is still unknown.

Strain TS-1 is an alkaliphilic bacterium isolated from a ground jumping spider. Alkaliphilic bacteria were isolated from the posterior intestine of termites (Thongaram et al., 2005), beetle larvae intestines (Aizawa et al., 2010), and human feces (Vedder, 1934). The gut portion of termites that feed on soil generally contains large amounts of potassium ions, and their pH is highly alkaline (Bignell et al., 1983; Brune and Kuhl, 1996). Gut alkalinity promotes the solubilization and uptake of soil organic matter (Thongaram et al., 2003). In general, alkaliphilic bacteria isolated from soil require Na^+ for growth. However, bacteria isolated from the above-described species require Na^+ or K^+ for growth (Horikoshi, 1991; Ito et al., 2011). If strain TS-1 acquired high-concentration Cs^+ resistance in the process of growing in the special environment of the jumping spider, it would be interesting to elucidate the acquisition mechanism.

CONCLUSION

We clarified the mechanism by which, in strain TS-1, intracellular Cs^+ concentration is reduced by excreting Cs^+ that has flowed into the cell at a high concentration to the outside of the cell by CshA. There have been no reports in the past that the homolog of MTS1_00475 has Cs^+/H^+ antiport activity. In addition, since this protein is widely conserved in bacteria belonging to the genus *Microbacterium*, it is a protein specific to this genus.

We obtained another Cs^+-sensitive mutant from strain TS-1, and the existence of another Cs^+ resistance mechanism was expected. There have been reports of isolation of high Cs^+-resistant bacteria, but there are no reports that elucidate the mechanism of their Cs^+ resistance. Therefore, this study is the first to elucidate the mechanisms of Cs^+ resistance.

As a prospect, it is conceivable to express CshA in everted membrane vesicles and recover Cs^+ in the membrane vesicles

as a bioremediation tool, for example, for treating radioactive Cs^+ contaminated water. CshA is a low-affinity Cs^+/H^+ antiporter. Therefore, by introducing mutations into CshA, it is necessary to produce a CshA mutant protein with a high affinity for Cs^+. In the future, it will be necessary to establish a method for employing CshA in radioactive Cs^+ recovery technology.

DATA AVAILABILITY STATEMENT

The datasets presented in this study can be found in online repositories. The names of the repository/repositories and accession number(s) can be found in the article/ **Supplementary Material**.

AUTHOR CONTRIBUTIONS

MI: designed the research. TK, YI, YK, EI, MT, NM, KS, and MI: conducted the research. TK, YI, and MI: analyzed the data. MI: wrote the paper. All authors contributed to the article and approved the submitted version.

FUNDING

This work was supported by a grant for the Toyo University Top Priority Research Promotion Program and the Toyo University intellectual property practical application promotion program.

ACKNOWLEDGMENTS

We would like to thank Editage (www.editage.com) for English language editing.

SUPPLEMENTARY MATERIAL

The Supplementary Material for this article can be found online at: https://www.frontiersin.org/articles/10.3389/fmicb.2022.841821/full#supplementary-material

REFERENCES

Aizawa, T., Urai, M., Iwabuchi, N., Nakajima, M., and Sunairi, M. (2010). *Bacillus trypoxylicola* sp. nov., xylanase-producing alkaliphilic bacteria isolated from the guts of Japanese horned beetle larvae (*Trypoxylus dichotomus septentrionalis*). *Int. J. Syst. Evol. Microbiol.* 60, 61–66. doi: 10.1099/ijs.0.005843-0

Aono, R., Ito, M., and Machida, T. (1999). Contribution of the cell wall component teichuronopeptide to pH homeostasis and alkaliphily in the alkaliphile *Bacillus lentus* C-125. *J. Bacteriol.* 181, 6600–6606. doi: 10.1128/JB.181.21.6600-6606.1999

Avery, S. V. (1995). Caesium accumulation by microorganisms: uptake mechanisms, cation competition, compartmentalization and toxicity. *J. Ind. Microbiol.* 14, 76–84. doi: 10.1007/BF01569888

Bignell, D. E., Oskarsson, H., Anderson, J. M., Ineson, P., and Wood, T. G. (1983). Structure, microbial associations and function of the so-called "mixed segment" of the gut in two soil-feeding termites, *Procubitermes aburiensis* and *Cubitermes severus* (Termitidae, Termitinae). *J. Zool.* 201, 445–480. doi: 10.1111/j.1469-7998.1983.tb05070.x

Bossemeyer, D., Schlosser, A., and Bakker, E. P. (1989). Specific cesium transport via the *Escherichia coli* Kup (TrkD) K^+ uptake system. *J. Bacteriol.* 171, 2219–2221. doi: 10.1128/jb.171.4.2219-2221.1989

Brown, S. D., Palumbo, A. V., Panikov, N., Ariyawansa, T., Klingeman, D. M., Johnson, C. M., et al. (2012). Draft genome sequence for *Microbacterium laevaniformans* strain OR221, a bacterium tolerant to metals, nitrate, and low pH. *J. Bacteriol.* 194, 3279–3280. doi: 10.1128/JB.00474-12

Brune, A., and Kuhl, M. (1996). pH profiles of the extremely alkaline hindguts of soil-feeding termites (Isoptera: Termitidae) determined with microelectrodes. *J. Insect Physiol.* 42, 1121–1127. doi: 10.1016/S0022-1910(96)00036-4

Buesseler, K. O., Jayne, S. R., Fisher, N. S., Rypina, I., Baumann, H., Baumann, Z., et al. (2012). Fukushima-derived radionuclides in the ocean and biota off Japan. *Proc. Natl. Acad. Sci. U. S. A.* 109, 5984–5988. doi: 10.1073/pnas.1120794109

Cohen-Bazire, G., Sistrom, W. R., and Stanier, R. Y. (1957). Kinetic studies of pigment synthesis by non-sulfur purple bacteria. *J. Cell. Comp. Physiol.* 49, 25–68. doi: 10.1002/jcp.1030490104

Collins, M. D., Jones, D., and Kroppenstedt, R. M. (1983). Reclassification of *Brevibacterium imperiale* (Steinhaus) and "*Corynebacterium laevaniformans*" (Dias and Bhat) in a redefined genus *Microbacterium* (Orla-Jensen), as *Microbacterium imperiale* comb. nov. and *Microbacterium laevaniformans* nom. rev.; comb. nov. *Syst. Appl. Microbiol.* 4, 65–78. doi: 10.1016/S0723-2020(83)80034-4

Corretto, E., Antonielli, L., Sessitsch, A., Compant, S., Gorfer, M., Kuffner, M., et al. (2016). *Agromyces aureus* sp. nov., isolated from the rhizosphere of *Salix caprea* L. grown in a heavy-metal-contaminated soil. *Int. J. Syst. Evol. Microbiol.* 66, 3749–3754. doi: 10.1099/ijsem.0.001260

Dekker, L., Osborne, T. H., and Santini, J. M. (2014). Isolation and identification of cobalt- and caesium-resistant bacteria from a nuclear fuel storage pond. *FEMS Microbiol. Lett.* 359, 81–84. doi: 10.1111/1574-6968.12562

Fujinami, S., Sato, T., and Ito, M. (2011). The relationship between a coiled morphology and Mbl in alkaliphilic *Bacillus halodurans* C-125 at neutral pH values. *Extremophiles* 15, 587–596. doi: 10.1007/s00792-011-0389-9

Fujinami, S., Takeda, K., Onodera, T., Satoh, K., Sano, M., Narumi, I., et al. (2013). Draft genome sequence of sodium-independent alkaliphilic *Microbacterium* sp. strain TS-1. *Genome Announc.* 1, e01043–e01113. doi: 10.1128/genomeA.01043-13

Grundy, F. J., Turinsky, A. J., and Henkin, T. M. (1994). Catabolite regulation of *Bacillus subtilis* acetate and acetoin utilization genes by CcpA. *J. Bacteriol.* 176, 4527–4533. doi: 10.1128/jb.176.15.4527-4533.1994

Guffanti, A. A., Finkelthal, O., Hicks, D. B., Falk, L., Sidhu, A., Garro, A., et al. (1986). Isolation and characterization of new facultatively alkalophilic strains of *Bacillus* species. *J. Bacteriol.* 167, 766–773. doi: 10.1128/jb.167.3.766-773.1986

Guzman, L. M., Belin, D., Carson, M. J., and Beckwith, J. (1995). Tight regulation, modulation, and high-level expression by vectors containing the arabinose PBAD promoter. *J. Bacteriol.* 177, 4121–4130. doi: 10.1128/jb.177.14.4121-4130.1995

Guzman, C. A., Piatti, G., Walker, M. J., Guardati, M. C., and Pruzzo, C. (1994). A novel *Escherichia coli* expression-export vector containing alkaline phosphatase as an insertional inactivation screening system. *Gene* 148, 171–172. doi: 10.1016/0378-1119(94)90254-2

Hamilton, C. A., Taylor, G. J., and Good, A. G. (2002). Vacuolar H^+-ATPase, but not mitochondrial F_1F_0-ATPase, is required for NaCl tolerance in *Saccharomyces cerevisiae*. *FEMS Microbiol. Lett.* 208, 227–232. doi: 10.1111/j.1574-6968.2002.tb11086.x

Hampton, C. R., Bowen, H. C., Broadley, M. R., Hammond, J. P., Mead, A., Payne, K. A., et al. (2004). Cesium toxicity in *Arabidopsis*. *Plant Physiol.* 136, 3824–3837. doi: 10.1104/pp.104.046672

Hasim, S., Vaughn, E. N., Donohoe, D., Gordon, D. M., Pfiffner, S., and Reynolds, T. B. (2018). Influence of phosphatidylserine and phosphatidyletha nolamine on farnesol tolerance in *Candida albicans*. *Yeast* 35, 343–351. doi: 10.1002/yea.3297

Horikoshi, K. (1991). Microorganisms in Alkaline Environments. New York: VCH Publishers Inc., 38-46.

Imazawa, R., Takahashi, Y., Aoki, W., Sano, M., and Ito, M. (2016). A novel type bacterial flagellar motor that can use divalent cations as a coupling ion. *Sci. Rep.* 6:19773. doi: 10.1038/srep19773

Ito, M., Cooperberg, B., and Krulwich, T. A. (1997). Diverse genes of alkaliphilic *Bacillus firmus* OF4 that complement K^+-uptake-deficient *Escherichia coli* include an ftsH homologue. *Extremophiles* 1, 22–28. doi: 10.1007/s007920050011

Ito, M., Fujinami, S., and Terahara, N. (2011). "Bioenergetics: cell motility and chemotaxis of extreme alkaliphiles" in *Extremophiles Handbook*. ed. K. Horikoshi (Tokyo, Japan: Springer), 141–162.

Jung, K., Krabusch, M., and Altendorf, K. (2001). Cs^+ induces the *kdp* operon of *Escherichia coli* by lowering the intracellular K^+ concentration. *J. Bacteriol.* 183, 3800–3803. doi: 10.1128/JB.183.12.3800-3803.2001

Kageyama, A., Takahashi, Y., Matsuo, Y., Adachi, K., Kasai, H., Shizuri, Y., et al. (2007). *Microbacterium flavum* sp. nov. and *Microbacterium lacus* sp. nov., isolated from marine environments. *Actinomycetologica* 21, 53–58. doi: 10.3209/saj.SAJ210201

Kato, S., Goya, E., Tanaka, M., Kitagawa, W., Kikuchi, Y., Asano, K., et al. (2016). Enrichment and isolation of *Flavobacterium* strains with tolerance to high concentrations of cesium ion. *Sci. Rep.* 6:20041. doi: 10.1038/srep20041

Katoh, K., Misawa, K., Kuma, K., and Miyata, T. (2002). MAFFT: a novel method for rapid multiple sequence alignment based on fast Fourier transform. *Nucleic Acids Res.* 30, 3059–3066. doi: 10.1093/nar/gkf436

Katoh, K., Rozewicki, J., and Yamada, K. D. (2019). MAFFT online service: multiple sequence alignment, interactive sequence choice and visualization. *Brief. Bioinform.* 20, 1160–1166. doi: 10.1093/bib/bbx108

Kinegam, S., Tanasupawat, S., and Akaracharanya, A. (2007). Screening and identification of xylanase-producing bacteria from Thai soils. *J. Gen. Appl. Microbiol.* 53, 57–65. doi: 10.2323/jgam.53.57

Kitada, M., Morotomi, S., Horikoshi, K., and Kudo, T. (1997). K^+/H^+ antiporter in alkaliphilic *Bacillus* sp. no. 66 (JCM 9763). *Extremophiles* 1, 135–141. doi: 10.1007/s007920050026

Krulwich, T. A., Hicks, D. B., and Ito, M. (2009). Cation/proton antiporter complements of bacteria: why so large and diverse? *Mol. Microbiol.* 74, 257–260. doi: 10.1111/j.1365-2958.2009.06842.x

Liu, J., Xue, Y., Wang, Q., Wei, Y., Swartz, T. H., Hicks, D. B., et al. (2005). The activity profile of the NhaD-type $Na^+(Li^+)/H^+$ antiporter from the soda Lake Haloalkaliphile *Alkalimonas amylolytica* is adaptive for the extreme environment. *J. Bacteriol.* 187, 7589–7595. doi: 10.1128/JB.187.22.7589-7595.2005

Lowry, O. H., Rosebrough, N. J., Farr, A. L., and Randall, R. J. (1951). Protein measurement with the Folin phenol reagent. *J. Biol. Chem.* 193, 265–275. doi: 10.1016/S0021-9258(19)52451-6

Mishra, A., Jha, G., and Thakur, I. S. (2018). Draft genome sequence of *Zhihengliuella* sp. strain ISTPL4, a psychrotolerant and halotolerant bacterium isolated from Pangong Lake, India. *Genome Announc.* 6, e01533–17. doi: 10.1128/genomeA.01533-17

Morino, M., Natsui, S., Swartz, T. H., Krulwich, T. A., and Ito, M. (2008). Single gene deletions of mrpA to mrpG and mrpE point mutations affect activity of the Mrp Na+/H+ antiporter of alkaliphilic *Bacillus* and formation of hetero-oligomeric Mrp complexes. *J. Bacteriol.* 190, 4162–4172. doi: 10.1128/JB.00294-08

Morohoshi, T., Wang, W. Z., Someya, N., and Ikeda, T. (2011). Genome sequence of *Microbacterium testaceum* StLB037, an N-acylhomoserine lactone-degrading bacterium isolated from potato leaves. *J. Bacteriol.* 193, 2072–2073. doi: 10.1128/JB.00180-11

Nozaki, K., Kuroda, T., Mizushima, T., and Tsuchiya, T. (1998). A new Na^+/H^+ antiporter, NhaD, of *Vibrio parahaemolyticus*. *Biochim. Biophys. Acta* 1369, 213–220. doi: 10.1016/S0005-2736(97)00223-X

Park, H. Y., Kim, K. K., Jin, L., and Lee, S. T. (2006). *Microbacterium paludicola* sp. nov., a novel xylanolytic bacterium isolated from swamp forest. *Int. J. Syst. Evol. Microbiol.* 56, 535–539. doi: 10.1099/ijs.0.63945-0

Patel, S., and Gupta, R. S. (2020). A phylogenomic and comparative genomic framework for resolving the polyphyly of the genus *Bacillus*: proposal for six new genera of *Bacillus* species, *Peribacillus* gen. nov., *Cytobacillus* gen. nov., *Mesobacillus* gen. nov., *Neobacillus* gen. nov., *Metabacillus* gen. nov. and *Alkalihalobacillus* gen. nov. *Int. J. Syst. Evol. Microbiol.* 70, 406–438. doi: 10.1099/ijsem.0.003775

Perkins, J., and Gadd, G. M. (1995). The influence of pH and external K^+ concentration on caesium toxicity and accumulation in *Escherichia coli* and *Bacillus subtilis*. *J. Ind. Microbiol.* 14, 218–225. doi: 10.1007/BF01569931

Savory, E. A., Fuller, S. L., Weisberg, A. J., Thomas, W. J., Gordon, M. I., Stevens, D. M., et al. (2017). Evolutionary transitions between beneficial and phytopathogenic *Rhodococcus* challenge disease management. *eLife* 6:e30925. doi: 10.7554/eLife.30925

Schippers, A., Bosecker, K., Sproer, C., and Schumann, P. (2005). *Microbacterium oleivorans* sp. nov. and *Microbacterium hydrocarbonoxydans* sp. nov., novel crude-oil-degrading gram-positive bacteria. *Int. J. Syst. Evol. Microbiol.* 55, 655–660. doi: 10.1099/ijs.0.63305-0

Southworth, T. W., Guffanti, A. A., Moir, A., and Krulwich, T. A. (2001). GerN, an endospore germination protein of *Bacillus cereus*, is an Na^+/H^+-K^+antiporter. *J. Bacteriol.* 183, 5896–5903. doi: 10.1128/JB.183.20.5896-5903.2001

Swartz, T. H., Ito, M., Ohira, T., Natsui, S., Hicks, D. B., and Krulwich, T. A. (2007). Catalytic properties of *Staphylococcus aureus* and *Bacillus* members of the secondary cation/proton antiporter-3 (Mrp) family are revealed by an optimized assay in an *Escherichia coli* host. *J Bacteriol* 189, 3081–3090. doi: 10.1128/JB.00021-07

Swer, P. B., Joshi, S. R., and Acharya, C. (2016). Cesium and strontium tolerant *Arthrobacter* sp. strain KMSZP6 isolated from a pristine uranium ore deposit. *AMB Express* 6:69. doi: 10.1186/s13568-016-0247-3

Takei, T., Yamasaki, M., and Yoshida, M. (2014). Cesium accumulation of *Rhodococcus erythropolis* CS98 strain immobilized in hydrogel matrices. *J. Biosci. Bioeng.* 117, 497–500. doi: 10.1016/j.jbiosc.2013.09.013

Thongaram, T., Kosono, S., Ohkuma, M., Hongoh, Y., Kitada, M., Yoshinaka, T., et al. (2003). Gut of higher termites as a niche for alkaliphiles as shown by culture-based and culture-independent studies. *Microbes Environ.* 18, 152–159. doi: 10.1264/jsme2.18.152

Thongaram, T., Hongoh, Y., Kosono, S., Ohkuma, M., Trakulnaleamsai, S., Noparatnaraporn, N., et al. (2005). Comparison of bacterial communities in the alkaline gut segment among various species of higher termites. *Extremophiles* 9, 229–238. doi: 10.1007/s00792-005-0440-9

Tsuzukibashi, O., Uchibori, S., Kobayashi, T., Saito, M., Umezawa, K., Ohta, M., et al. (2015). A selective medium for the isolation of *Microbacterium* species in oral cavities. *J. Microbiol. Methods* 116, 60–65. doi: 10.1016/j.mimet.2015.06.016

Vedder, A. (1934). *Bacillus alcalophilus* n. sp.; benevens enkele ervaringen met sterk alcalische voedingsbodems *Anton. Leeuw.* 1, 143–147.

Yokota, A., Takeuchi, M., and Weiss, N. (1993). Proposal of two new species in the genus *Microbacterium*: *Microbacterium dextranolyticum* sp. nov. and *Microbacterium aurum* sp. nov. *Int. J. Syst. Bacteriol.* 43, 549–554. doi: 10.1099/00207713-43-3-549

Zhang, F., Guo, Y., Ji, J., Li, G., Zhang, H., and Yu, T. (2021). Complete genome sequence of a high cesium ion- tolerating bacterium *Bacillus* sp. Cs-700 isolated from the South China Sea sediment. *Mar. Genomics* 56:100810. doi: 10.1016/j.margen.2020.100810

Zhang, W., Zhu, H. H., Yuan, M., Yao, Q., Tang, R., Lin, M., et al. (2010). *Microbacterium radiodurans* sp. nov., a UV radiation-resistant bacterium isolated from soil. *Int. J. Syst. Evol. Microbiol.* 60, 2665–2670. doi: 10.1099/ijs.0.017400-0

Conflict of Interest: The authors declare that the research was conducted in the absence of any commercial or financial relationships that could be construed as a potential conflict of interest.

Publisher's Note: All claims expressed in this article are solely those of the authors and do not necessarily represent those of their affiliated organizations, or those of the publisher, the editors and the reviewers. Any product that may be evaluated in this article, or claim that may be made by its manufacturer, is not guaranteed or endorsed by the publisher.

frontiers in Microbiology

HYPOTHESIS AND THEORY
published: 09 March 2022
doi: 10.3389/fmicb.2022.831828

Microbial Hydrocarbon Degradation in Guaymas Basin—Exploring the Roles and Potential Interactions of Fungi and Sulfate-Reducing Bacteria

Virginia P. Edgcomb[1], Andreas P. Teske[2] and Paraskevi Mara[1]*

[1] Woods Hole Oceanographic Institution, Woods Hole, MA, United States, [2] Department of Earth, Marine and Environmental Sciences, University of North Carolina at Chapel Hill, Chapel Hill, NC, United States

Hydrocarbons are degraded by specialized types of bacteria, archaea, and fungi. Their occurrence in marine hydrocarbon seeps and sediments prompted a study of their role and their potential interactions, using the hydrocarbon-rich hydrothermal sediments of Guaymas Basin in the Gulf of California as a model system. This sedimented vent site is characterized by localized hydrothermal circulation that introduces seawater sulfate into methane- and hydrocarbon-rich sediments, and thus selects for diverse hydrocarbon-degrading communities of which methane, alkane- and aromatics-oxidizing sulfate-reducing bacteria and archaea have been especially well-studied. Current molecular and cultivation surveys are detecting diverse fungi in Guaymas Basin hydrothermal sediments, and draw attention to possible fungal-bacterial interactions. In this Hypothesis and Theory article, we report on background, recent results and outcomes, and underlying hypotheses that guide current experiments on this topic in the Edgcomb and Teske labs in 2021, and that we will revisit during our ongoing investigations of bacterial, archaeal, and fungal communities in the deep sedimentary subsurface of Guaymas Basin.

Keywords: hydrocarbon, fungi, sulfate-reducing bacteria, microbial interaction, Guaymas Basin

OPEN ACCESS

Edited by:
Jesse G. Dillon, California State University, Long Beach, United States

Reviewed by:
William J. Brazelton, The University of Utah, United States
Marco J. L. Coolen, Curtin University, Australia

****Correspondence:***
Virginia P. Edgcomb
vedgcomb@whoi.edu

Specialty section:
This article was submitted to Extreme Microbiology, a section of the journal Frontiers in Microbiology

Received: *08 December 2021*
Accepted: *04 February 2022*
Published: *09 March 2022*

Citation:
Edgcomb VP, Teske AP and Mara P (2022) Microbial Hydrocarbon Degradation in Guaymas Basin—Exploring the Roles and Potential Interactions of Fungi and Sulfate-Reducing Bacteria. Front. Microbiol. 13:831828. doi: 10.3389/fmicb.2022.831828

INTRODUCTION

Marine hydrocarbon seeps are common features of marine sediments worldwide that release complex and variable cocktails of hydrocarbon compounds depending on interactive physical, chemical, and microbial processes (e.g., Ruff et al., 2015; Levin et al., 2016). The origin and the microbial degradation of hydrocarbons have been studied extensively in the sedimented hydrothermal system of Guaymas Basin, a young spreading center in the central Gulf of California where hot basaltic sills intrude laterally into organic-rich seafloor sediments (Einsele et al., 1980). Within the thermal aureole, petroleum hydrocarbons are produced by pyrolysis of buried organic matter under high pressure and temperature (e.g., Kawka and Simoneit, 1994), and then migrate along hydrothermal flow paths to emerge at the seafloor in hydrocarbon-soaked sediment patches and mineral concretions (**Figure 1**). Gas chromatography Mass Spectrometry (GCMS) analyses show that the hydrothermal oils released in Guaymas Basin show compositional similarities to reservoir crude oil (Didyk and Simoneit, 1989), containing n-C_{12} to n-C_{38} alkanes, C_{27-36}

hopanes, steranes and diasteranes, and aromatic hydrocarbons [including various naphthalenes, methylnaphthalenes, phenanthrenes (including alkylated), fluoranthrene, and pyrene]. Lower concentrations of n-alkanes and aliphatic hydrocarbons and lower (<1) n-C_{17}/pristine and n-C_{18}/phytane ratios closer to the sediment surface are consistent with microbial biodegradation of those compounds (Bazylinski et al., 1988). Recent chemometric analysis of Guaymas Basin sediments has identified >5,000 hydrocarbon compounds that display systematic temperature-dependent trends, and complex spatial distribution patterns strongly affected by migration, biodegradation, water washing, and pyrolytic activity (Dalzell et al., 2021). These hydrocarbon-rich hydrothermal sediments provide excellent opportunities for investigating sedimentary microbial hydrocarbon biodegradation because seep sediment microbiota have been exposed to long-term selection pressure by hydrocarbon exposure.

Hydrocarbons differ in their susceptibility to microbial attack, with the most easily utilized compounds being linear alkanes followed by increasingly recalcitrant branched alkanes, small monoaromatic hydrocarbons such as benzene, toluene, ethylbenzene, and xylenes (BTEX), cyclic alkanes, and polyaromatic hydrocarbons (PAH) (Das and Chandran, 2011). Hydrocarbons are initially activated under aerobic conditions by addition of either one or both atoms of diatomic oxygen by monooxygenase and dioxygenase enzymes, after which the molecule is usually amenable to further degradation (Prince and Walters, 2007). Complex branching hinders initial oxidation and subsequent catabolism, likely since steric hindrance prevents access of hydrocarbon-oxidizing enzymes. Typically, the most readily-degraded compounds are the normal alkanes larger than hexane as well as benzene and substituted monoaromatics, followed by smaller unbranched and branched alkanes, monocycloalkanes, and at last polycyclic aromatics. Since less complex structures and molecules are more accessible and are preferentially attacked, the biodegradation stage of a particular hydrocarbon mixture can be assessed by comparing ratios of specific compounds and abundances of molecules with different structures (Prince and Walters, 2007).

The chemical inertness of hydrocarbons poses an energetic and mechanistic challenge for microbial metabolism because of the high energy requirements necessary for cleaving the apolar C-H bond (Rabus et al., 2016). Under oxic conditions, O_2-dependent oxygenase-catalyzed reactions add one or both atoms of diatomic oxygen using monooxygenase or dioxygenase enzymes, respectively. The initial C-H activation is essential for channeling hydrocarbons as substrates to catabolic routes and for making them amenable to further degradation (Prince and Walters, 2007). Under anaerobic conditions, there are a variety of intriguing biochemical reactions that can include Adenosin triphosphate (ATP)-dependent and ATP-independent mechanisms which can combine anaerobic hydrocarbon degradation with nitrate, sulfate or iron reduction, fermentation or syntrophic growth (Rabus et al., 2016). O_2-independent hydrocarbon degradation often involves enzymes (Moco-dependent homodimeric metalloenzymes) that resemble nitrate reductases in utilizing molybdenum as a co-factor (Rabus et al., 2016).

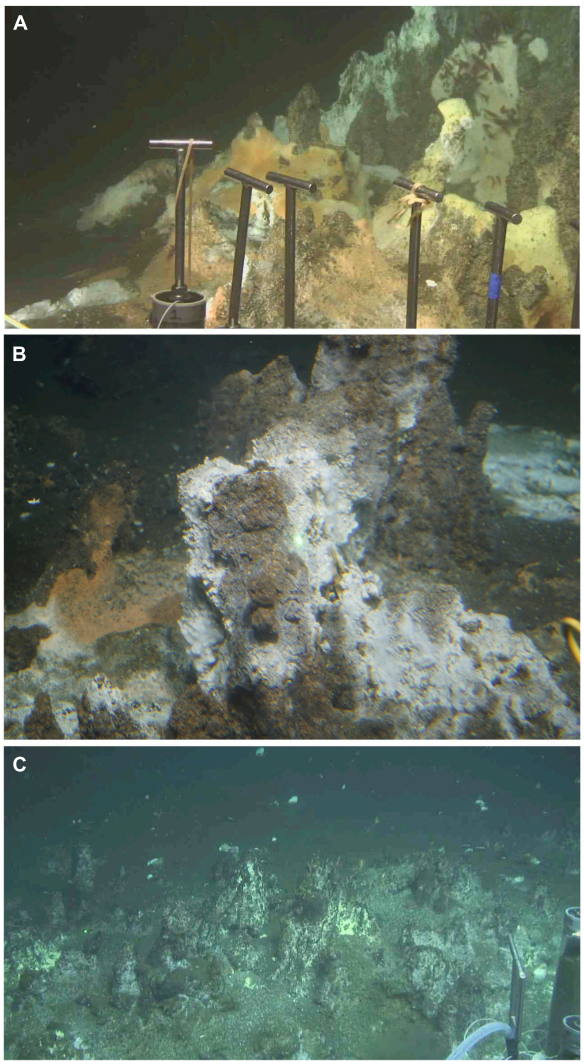

FIGURE 1 | Hydrocarbon-rich hydrothermal sites in Guaymas Basin. **(A)** Hydrocarbon-soaked concretions at the base of the "Rebecca's Roost" hydrothermal edifice (27°N00.70′/111°W24.23′). Nearby hydrocarbon-rich sediments were sampled by Deep-sea submersible *Alvin* in December 2016, and analyzed for geochemical properties and microbial community composition (Alvin core 4870-16, temperatures 31–52°C; Song et al., 2021 and Teske et al., 2021a). **(B)** Oil-soaked hydrothermal concretions, informally called "Ace chimney" (27°N00.671′/111°W24.262′), sampled in November 2018 during *Alvin* dives 4994 and 5000, yielding predominately Desulfobacterales in sulfate-reducing enrichments on mixed aromatic hydrocarbons (**Supplementary Figure 1** and **Supplementary Table 1**). **(C)** Oil-soaked concretions on the eastern approach to Rebecca's Roost (27°N00.686′/111°W24.379′), sampled in December 2016 during *Alvin* dive 4872, amended with mixed n-alkanes (C_6–C_{12}) and crude oil, and yielding enrichments of alkane-oxidizing sulfate-reducing bacteria (Desulfobacterales) at 30 and 55°C (Renxing et al., 2021). Photos by *Alvin* group, Woods Hole Oceanographic Institution.

Recalcitrance toward microbial degradation amplifies the ecosystem-level effects of PAHs, as they accumulate within the

food web. Due to their carcinogenic and mutagenic properties they can have significant toxicological effects on benthic organisms at concentrations of ≤1 mg-PAH/kg dry sediment (e.g., Long et al., 1995). PAHs can affect growth, maturity, and fecundity of metazoans (Bridges et al., 1994), impact immune systems (Tahir et al., 1993), and alter the structure of entire benthic communities (Nance, 1991). In humans, gut microbiota can metabolize persistent PAHs but produce toxic byproducts that affect the composition and metabolic activity of the gut microbiome (Claus et al., 2016). The cascading health impacts of hydrocarbon contamination lend particular urgency to microbial hydrocarbon degradation and bioremediation research.

CULTIVATION SURVEYS OF BACTERIAL AND ARCHAEAL HYDROCARBON DEGRADERS

The composition and activity of the hydrocarbon-degrading microbial community at a seep site or oil spill location depends on the availability of suitable electron acceptors (e.g., molecular oxygen, nitrate, sulfate, ferric iron, or carbon dioxide), nutrients (nitrogen, phosphorus, and trace metals), and the particular spectrum of aliphatic and aromatic hydrocarbons. Since sulfate concentrations in seawater and surficial benthic sediments are two or three orders of magnitude higher than nitrate or oxygen concentrations, sulfate-reducing bacteria are naturally ubiquitous in marine hydrocarbon seeps, and have evolved numerous lineages that oxidize aliphatic and aromatic hydrocarbons, either as specialists in utilizing specific carbon sources or as generalists who can utilize a wider substrate spectrum; collectively they are now perhaps the best-studied group of anaerobic hydrocarbon oxidizers (Davidova et al., 2018; Teske, 2019; Kleindienst and Knittel, 2020).

Model organisms for anaerobic hydrocarbon degradation have been obtained from the hydrothermal sediments of Guaymas Basin, a sedimented spreading center in the Gulf of California where sedimented organic matter is transformed to petroleum compounds under high temperature and pressure, resulting in hot gas and petroleum seepage with hydrothermal characteristics (Teske et al., 2014; Teske, 2020). The distinct microbial communities of Guaymas Basin (Teske et al., 2002) include naturally enriched hydrocarbon-degrading bacteria (Kleindienst et al., 2012) and archaea (Dombrowski et al., 2017, 2018). Their ubiquitous presence and activity in all but the hottest sediments of Guaymas Basin is revealed not only by sequencing surveys but also by selective ^{13}C-carbon enrichment in light alkanes, caused by preferential microbial oxidation of ^{12}C-carbon compounds (Dowell et al., 2016; Song et al., 2021).

Microbial habitat for aerobic hydrocarbon degradation is confined to surficial sediment, since oxygen penetrates only the upper millimeter of Guaymas Basin sediments, with occasional small pockets of oxygenated seawater reaching deeper in hydrothermal spots with active circulation (Winkel et al., 2014; Teske et al., 2016). So far, the spectrum of aerobic hydrocarbon-degrading bacterial isolates from Guaymas Basin is limited to phenanthrene-degrading aerobic isolates of *Cycloclasticus*, *Halomonas*, *Thalassospira*, and *Lutibacterium* within the Gammaproteobacteria (Gutierrez et al., 2015), aerobic isolates with a preference for aromatic organic acids (Goetz and Jannasch, 1993), and aerobic hexadecane- and naphthalene-utilizing bacteria (Bazylinski et al., 1989).

In contrast, anaerobic, sulfate-replete sediments are abundant in Guaymas Basin, and provide ample habitat for diverse sulfate-reducing hydrocarbon degraders with different substrate and temperature preferences. The spectrum of sulfate-reducing isolates and enrichments from this frequently sampled model site includes thermophiles, such as the decane-oxidizing bacterium *Desulfothermus naphthae* strain TD3 (Rüter et al., 1994), a propane-oxidizing bacterial enrichment dominated by *Desulfotomaculum* strain Propane60-GuB (Kniemeyer et al., 2007), and the thermophilic, hydrogenotrophic sulfate-reducing bacterium *Candidatus* Desulfofervidus auxilii that grows in syntrophic association with methane- and butane-oxidizing anaerobic archaea (Krukenberg et al., 2016). In stable isotope labeling experiments using butane and dodecane as carbon sources, dominant phylotypes were affiliated with the genera *Desulfosarcina*, *Desulfococcus*, and *Desulfonema* within the *Desulfobacteraceae* (Kleindienst et al., 2014), for example the mesophilic sulfate-reducing n-butane and propane oxidizer BuS5 from Guaymas Basin (Kniemeyer et al., 2007). Enrichments on benzene from Guaymas Basin sediments yielded sequences of the *Desulfobacteraceae* and of the *Desulfatiglans* lineage (Phelps et al., 1998), represented in pure culture by the ethylbenzene-oxidizing strain EbS7 (Kniemeyer et al., 2003).

In addition to Guaymas Basin, cold seep sediments of the Gulf of Mexico have been studied extensively for anaerobic hydrocarbon degradation (briefly reviewed in Teske, 2019), and turned out to harbor sulfate-reducing populations that oxidize alkanes and polycyclic aromatic compounds. For example, anaerobic degradation of hexadecane and phenanthrene coupled with sulfate reduction was studied and quantified using enriched consortia isolated from Gulf of Mexico seafloor sediments (Shin et al., 2019). The observed stoichiometric ratios for hexadecane and phenanthrene degradation (moles of carbon source degraded per mole of SO_4^{2-} reduced) matched the theoretical stoichiometric degradation ratios for hexadecane (12:1) and phenanthrene (8:1) when coupled to sulfate reduction (So and Young, 2001; Shin et al., 2019). Phenanthrene carboxylic acid was detected indicating active carboxylation, while metagenome-assembled genomes (MAGs) revealed that phenanthrene degradation is likely mediated by novel genera or families of sulfate-reducing bacteria along with their fermentative syntrophic partners (Shin et al., 2019).

Methane and short-chain alkanes are anaerobically activated by methyl- and alkyl-Coenzyme M reductase and stoichiometrically oxidized to CO_2 by archaeal enrichments and isolates from Guaymas Basin, such as the thermophilic methane-oxidizing (ANME-1) archaeal lineage (Holler et al., 2011; Wegener et al., 2015), the thermophilic propane- and butane-oxidizer *Candidatus Syntrophoarcheum* sp. (Laso-Pèirez et al., 2016), and the thermophilic ethane oxidizer *Candidatus* Ethanoperedens thermophilum (Hahn et al., 2020); the latter is a sister taxon to the mesophilic ethane oxidizer

Candidatus Argoarchaeum from cold seeps in the Gulf of Mexico (Chen et al., 2019). The thermophilic alkane-oxidizing archaea grow in syntrophic association with the thermophilic sulfate reducer *Candidatus* Desulfofervidus (Krukenberg et al., 2016).

In addition to terminal hydrocarbon oxidation to CO_2, anaerobic microbial degradation of aliphatic and aromatic hydrocarbons can be coupled to methane production (Siddique et al., 2007, 2011). There are at least two different—syntrophic and non-syntrophic—modes of mesophilic long-chain alkane degradation to methane: syntrophic hexadecane degradation to acetate and hydrogen is performed by the deltaproteobacterial genus *Syntrophus*, coupled to acetoclastic and hydrogenotrophic methanogenesis by *Methanosaeta*- and *Methanoculleus*-related strains (Zengler et al., 1999), and syntrophic degradation of long-chain alkanes (C_{28} to C_{50} paraffins) is performed by the deltaproteobacterial genus *Smithella* associated with acetoclastic and hydrogenotrophic methanogens (Tan et al., 2014; Wawrik et al., 2016). Non-syntrophic methanogenic alkane degradation of long-chain alkanes might be catalyzed by yet-uncultured archaea such as *Candidatus* Methanoliparia that possess both methyl- and alkyl-coenzyme M reductases (nickel-containing metalloenzymes) and produce methane by disproportionating acetate using methyl-coenzyme M reductase; the acetate is obtained *via* beta-oxidation of alkanes that are activated by alkyl-coenzyme M reductase (Borrel et al., 2019; Laso-Pérez et al., 2019).

MOLECULAR SURVEYS OF BACTERIAL AND ARCHAEAL HYDROCARBON DEGRADERS

Consistent with the phylogenetic placement of these largely deltaproteobacterial and methanomicrobial isolates and enrichments, global marker gene comparisons of hydrocarbon seep and non-seep deep-sea benthic communities have shown that members of the Deltaproteobacteria and Methanomicrobia are adapted to hydrocarbon seepage and dominate these habitats (Lloyd et al., 2010; Ruff et al., 2015). Using two case studies (Teske et al., 2019; Ramírez et al., 2021), we highlight the diversity of seep-adapted Deltaproteobacteria and Methanomicrobia by contrasting the deltaproteobacterial communities of hydrothermal hydrocarbon seep sediments in Guaymas Basin with nearby cold seafloor sediments. Small subunit ribosomal RNA (16S rRNA) gene amplicon surveys covered several types of warm and hot sediments in the hydrothermally active zone of Guaymas Basin (Ramírez et al., 2021) that were collected by push coring with the submersible *Alvin*. In contrast, off-axis shallow subsurface sediments (ca. 2–5 mbsf) were collected by piston coring outside the hydrothermal spreading center, from the northwestern flanking region of Guaymas Basin (Teske et al., 2019). Phylogenetic trees of deltaproteobacterial 16S rRNA gene sequences, obtained with near-identical primers that amplify the hypervariable V4-V5 region (Teske et al., 2019; Ramírez et al., 2021) allowed a direct comparison of hydrocarbon-degrading lineages and isolates from hot sediments of the hydrothermal spreading center and from off-axis sediments (**Figures 2**, **3**). The hydrothermal on-axis as well as the cold off-axis survey recovered members of the *Desulfobacteraceae*, a physiologically diverse family of sulfate reducers that completely oxidize low-molecular-weight substrates such as acetate, Low molecular weight (LMW)-organic acids, alkanes, and aromatics (Küver, 2014; Teske, 2019); this group is commonly the dominant sulfate-reducing group in marine sediments (Robador et al., 2016). However, members of the SEEP-SRB1 lineage, sulfate-reducing syntrophs of methane-oxidizing archaea at cool and temperate conditions (Knittel et al., 2003; Schreiber et al., 2010) were mostly found at the hydrothermally active methane-rich sites, and were barely detectable in the cold sediments. Members of the family-level *Desulfatiglans* lineage, containing isolates that oxidize substituted mono- and polycyclic aromatics (summarized in Teske et al., 2019), were found in both hydrothermal and cold sediments (**Figures 2**, **3**). *Desulfatiglans* phylotypes were detected as a dominant lineage even in surficial Guaymas Basin sediments that were sliced and analyzed in 2 mm intervals (Engelen et al., 2021). In addition, genome analyses indicate that Desulfatiglans-affiliated bacteria may play a role in reductive dehalogenation in marine subsurface sediments (Jochum et al., 2018).

The on- and off-axis sites share a lineage of predominantly deep subsurface clones, often annotated as members of the family Desulfoarculaceae (Davidova et al., 2016) in GenBank entries and phylogenetic analyses, but without significant bootstrap support for any phylogenetic relationship to cultured Desulfoarculaceae (Teske et al., 2019). While it is represented only by a single Amplicon sequence variant (ASV) in the hydrothermal on-axis sites (ASV 120; **Figure 2**), this uncultured lineage (termed "*marine subsurface lineage*" to distinguish it from proper Desulfoarculaceae) is the most frequently detected deltaproteobacterial lineage in off-axis subsurface sediments (**Figure 3**). It has been recovered frequently from deep-drilling surveys offshore Taiwan, the Shimokita peninsula of Japan, the Porcupine bight abyssal seafloor, and the Peru Margin and Peru Trench. A second lineage of independently branching deep subsurface clones is also annotated as a member of the Desulfoarculaceae, and occurs in the hot sediments (ASVs 219 and 251). The physiological capabilities of these misidentified "Desulfoarculaceae" remain unknown.

Several deltaproteobacterial lineages were only detected in the hydrothermal sediments (**Figure 2**): The *Desulfuromonadales* encompass sulfur-reducing, iron-reducing, and fermentative bacteria that commonly thrive on acetate and other LMW organic acids (Küver et al., 2005). The *Syntrophaceae* include sulfate-reducing but also fermentative bacteria that grow in syntrophic association with H_2/formate-utilizing bacterial partners (Küver, 2014). Uncultured lineages within the incompletely oxidizing family *Desulfobulbaceae* include the seep-associated lineages SEEP-SRB3 and SEEP-SRB4, and the mesophilic, sulfate-reducing, potentially alkane-oxidizing SEEP-SRB2 lineage (Kleindienst et al., 2012; Krukenberg et al., 2018). These lineages, originally described from cold seep sites (Knittel et al., 2003), occur predominantly in temperate (not hot) hydrothermal sediments (Ramírez et al., 2021). Two lineages, the *Thermodesulfobacteraceae* and the *Desulfofervidales*, are

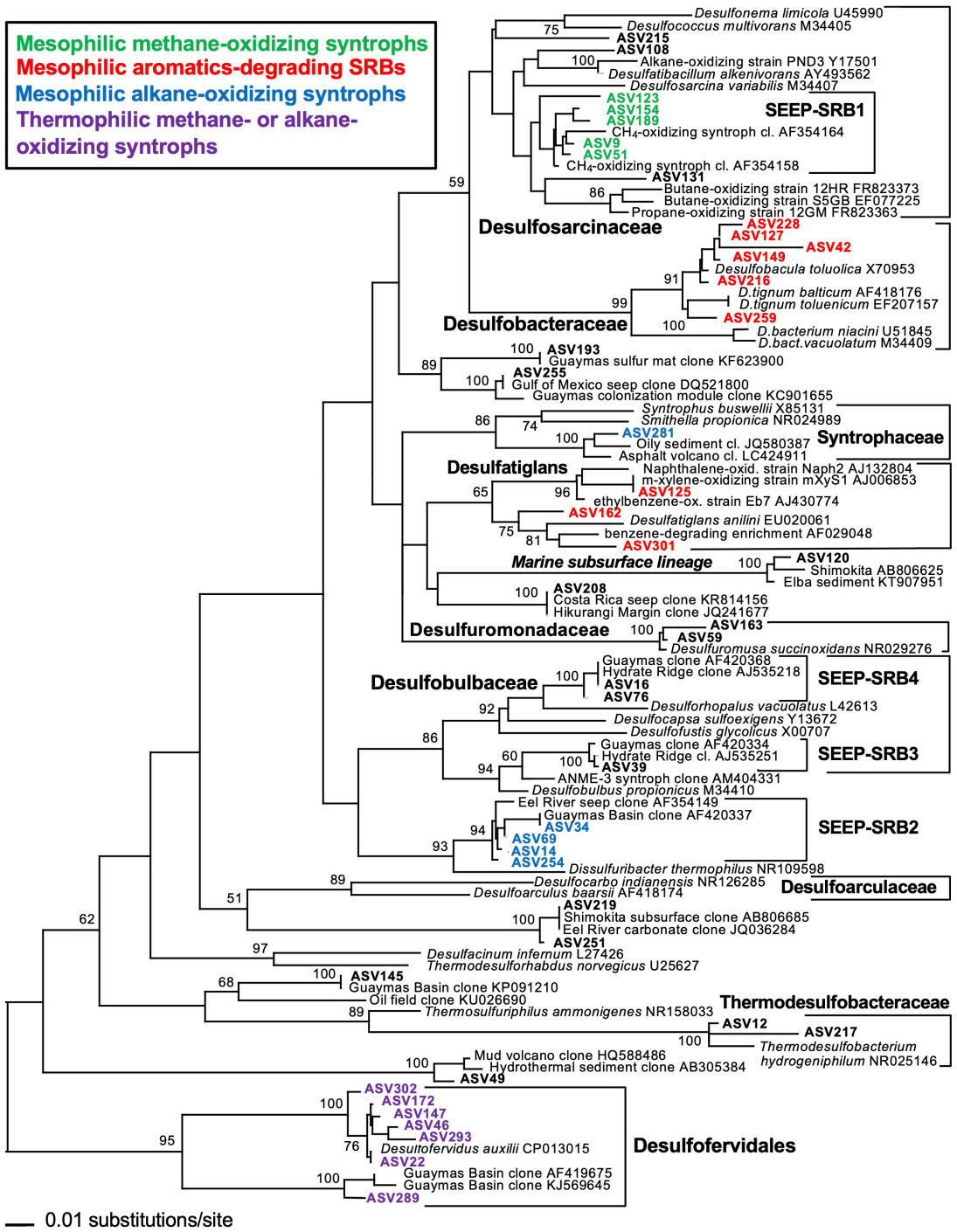

FIGURE 2 | 16S rRNA gene distance phylogeny of frequently occurring deltaproteobacterial ASV sequences according to Escherichia *coli* nucleotide positions 515–926 using forward primer 515F-Y and reverse primer 926R (Ramírez et al., 2021) in hydrothermal sediments of Guaymas Basin, southern axial valley. The branching pattern was checked by 1000 NJ Bootstrap iterations. The tree was rooted with the *Desulfofervidales* as outgroup. Modified by inferred substrate usage from Ramírez et al. (2021) (Supplements).

unequivocally linked to sulfate reduction at high temperatures. The *Thermodesulfobacteraceae* have temperature optima of 65–75°C and can grow lithoautotrophically with CO_2/H_2 or heterotrophically with LMW organic acids (Jeanthon et al., 2002). The *Desulfofervidales*, a deeply branching 16S rRNA lineage (McKay et al., 2016) that affiliate with the Deltaproteobacteria based on complete genome analyses (Waite et al., 2020), have a growth optimum of 50–60°C and form syntrophic consortia with

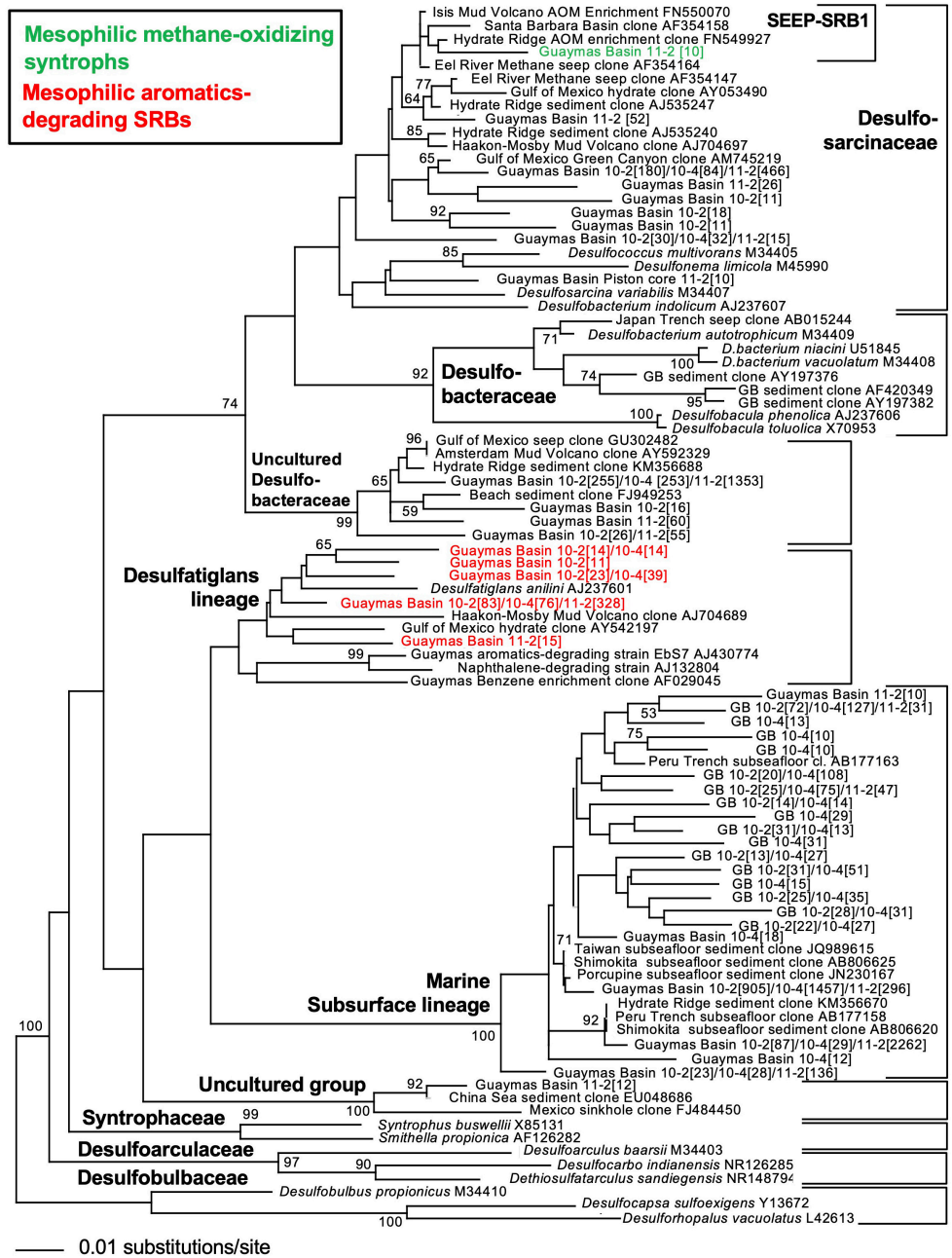

FIGURE 3 | 16S rRNA gene distance phylogeny of frequently occurring deltaproteobacterial ASV sequences according to *Escherichia coli* nucleotide positions 518–926 using forward primer 518F, and three versions of reverse primer 926R (Teske et al., 2019) in cold shallow subsurface sediments of Guaymas Basin, northwest of the axial valley. The taxon labels refer to number of sequences recovered from piston core 10 and 11 sediment subsections (10-2 = 1.24–1.29 mbsf; 10-4 = 3.73–3.78 mbsf; 11-2 = 1.15–1.20 mbsf). The branching pattern was checked by 1000 NJ Bootstrap iterations. Modified by inferred substrate usage, from Teske et al. (2019) (supplements).

methane and short-chain alkane-oxidizing thermophilic archaea (Laso-Peìrez et al., 2016; Hahn et al., 2020), but they can also thrive as free-living hydrogenotrophs (Krukenberg et al., 2016). Both thermophilic lineages, the *Thermodesulfobacteraceae* and *Desulfofervidales*, are found in increasing relative proportion in deeper and hotter sediments (Ramírez et al., 2021). In general, members of the *Desulfofervidales* belong to the most frequently found lineages in Guaymas Basin and appear consistently in these hydrothermal sediments (Dowell et al., 2016; McKay et al., 2016; Engelen et al., 2021).

To summarize, hydrothermal seep sediments of Guaymas Basin harbor a high diversity of hydrocarbon-degrading Deltaproteobacteria, which participate in hydrocarbon degradation either individually or in syntrophic association

with specialized archaea, whereas cold sediments from the same region contain a considerably more restricted range of Deltaproteobacteria. However, pure culture isolations and sequencing surveys cannot reveal whether these sulfate reducers might benefit from mutualistic interactions and whether they show enhanced activity in the presence of the second major group of hydrocarbon-degrading organisms that share the same sedimentary habitat, the Fungi.

THE POTENTIAL FOR DEEP-SEA HYDROCARBON-DEGRADING FUNGI

In contrast to bacterial and archaeal communities, unicellular microeukaryotes in deep-sea water columns and sediments are understudied, particularly in hydrothermal seep sediment habitats (Edgcomb et al., 2002). Microeukaryotes include protists and Fungi (filamentous fungi and yeasts), which are essential components of the marine microbial food web (Azam et al., 1983; Worden et al., 2015). The "mycoloop" concept suggests Ascomycetes and (to a lesser extent) Basidiomycete fungi participate in overlooked pathways salvaging substrates and energy, and thus shape aquatic and benthic ecosystems (Kagami et al., 2007, 2014). Fungi have even been posited to provide a source of energy to deep biosphere archaea and bacteria who could utilize hydrogen produced under anaerobic conditions by fungal hydrogenosome-based metabolism (Drake et al., 2017). Deep-sea seep fungi must be able to cope with elevated hydrostatic pressure and temperature. While evidence for piezophilic fungi is limited (Peng et al., 2021), some strains can tolerate pressures up to 40 MPa, and in some cases show sporulation and mycelial growth (Lorenz and Molitoris, 1997; Raghukumar and Raghukumar, 1998; Damare et al., 2006; Singh et al., 2010; Burgaud et al., 2015). Fungi can alter membrane and cell wall proteins as well as increase saturated fatty acid and ergosterol concentrations to maintain membrane fluidity and function when exposed to higher hydrostatic pressures (Fernandes et al., 2004; Iwahashi et al., 2005; Simonato et al., 2006). At hydrothermal sites like Guaymas Basin, sediment temperatures can quickly reach the upper known limit for fungi (62°C; Maheshwari et al., 2000), however, fungi appear to cope with *in situ* conditions in subsurface sediments where they have been investigated. For example, eukaryotic gene transcripts, including fungal gene transcripts, from subsurface Peru Margin and Canterbury Basin sediments (down to 159 and 350 mbsf, respectively; Orsi et al., 2013; Pachiadaki et al., 2016; Orsi, 2018) were assigned to cell growth and division, recycling of organic matter, cell-cell competition, and synthesis of antimicrobial secondary metabolites. Fungi secrete exoenzymes that break complex refractory carbohydrates in marine sediments (Orsi, 2018), and thus fungi can likely survive in deep-sea sediments and in nutrient-poor extreme environments (e.g., the lower oceanic crust) on refractory polysaccharides including peptidoglycan (Lomstein et al., 2009, 2012; Quemener et al., 2020), necromass of their microbial neighbors, and perhaps by activating carbon-starvation stress responses that include autolysis and utilization of polysaccharides from their own cell wall for survival (García-Lepe et al., 1997; Emri et al., 2005; Kim et al., 2011; Quemener et al., 2020).

Interestingly, fungi are thought to have a relatively high tolerance to hydrocarbons (Al-Nasrawi, 2012), and over 100 genera (Prince, 2005) are known to play important roles in the biodegradation of hydrocarbons in soils and sediments (e.g., Walker and Colwell, 1975; Hestbjerg et al., 2003; Šašek et al., 2003; Wiesche et al., 2003; Gesinde et al., 2008; Husaini et al., 2008; Obire and Anyanwu, 2009). Filamentous fungi such as *Cladosporium* (isolated from Guaymas Basin, **Table 1**) and *Aspergillus* are among those known to participate in aliphatic hydrocarbon degradation, and the genera *Cunninghamella, Penicillium, Fusarium*, *Mucor*, and *Aspergillus* are among those known to take part in degradation of aromatic hydrocarbons (Passarini et al., 2011; Al-Nasrawi, 2012 and references therein; Steliga, 2012). Culture-based studies have shown that the addition of different fungi increases the microbial degradation of aromatic hydrocarbons, such as benzene, toluene, ethylbenzene and xylene, and PAHs (i.e., Yadav and Reddy, 1993; Zheng and Obbard, 2001; Wattiau, 2002; Šašek et al., 2003; Wiesche et al., 2003; Steliga, 2008). While most filamentous fungi investigated to date are unable to fully mineralize aromatic hydrocarbons, fungi play a critical role in facilitating the degradation of more recalcitrant hydrocarbons in the environment by secreting extracellular enzymes that transform these compounds into intermediates that are increasingly susceptible to bacterial decomposition (Steliga, 2012).

Fungal communities utilize diverse enzymatic mechanisms to transform hydrocarbon structures. Saturated hydrocarbons (e.g., alkanes) are oxidized using cytochrome P450 monoxygenases, while unsaturated alkenes, alkynes, and alicyclics, are more recalcitrant, and fungi are considered to be able to partially oxidize them (Prenafeta-Boldú et al., 2018). Low and high-molecular weight PAHs can be degraded using a combination of enzymatic pathways including P450 monoxygenases as well as extracellular peroxidases and laccases produced by lignin-degrading fungi that can oxidize a broad range of aromatic hydrocarbons (Prenafeta-Boldú et al., 2018). Interestingly, fungal biodegradation often results in partially degraded hydrocarbon compounds that do not support further fungal growth, and might be more toxic than the parent substrates (Prenafeta-Boldú et al., 2018). Therefore, syntrophic growth of fungi with bacteria or archaea that can utilize the products of fungal hydrocarbon metabolism, or co-cultures that allow for sequential utilization of hydrocarbon compounds and degradation products within the same habitat, may be a win-win strategy for all microbiota involved in hydrocarbon degradation.

FUNGAL BIOSURFACTANTS AND HYDROCARBON DEGRADATION

The poor bioavailability of hydrocarbon constituent components is considered a major rate limiting factor in the hydrocarbon remediation process (Das et al., 2014). Biosurfactants act as surface-active amphiphilic compounds

TABLE 1 | | Sample site key for published fungal isolates from Guaymas Basin (Keeler et al., 2021; sampling key not reported therein).

Sample	Location	*In situ* temp.	Time of sampling	Water depth	Sediment depth	Isolates obtained	References for sampling site
El Puma piston core P03_4: cold seafloor sediment	Guaymas Basin NW flanking region 27°37.676/−111°52.574	3–4°C	October 17, 2014	1,611 m	276–281 cm	Redundant isolates	Teske et al., 2019; Ramírez et al., 2020
El Puma piston core P05_3: cold seep sediment	Sonora Margin/Guaymas Basin transition 27°38.765/−111°38.909	3–4°C	October 19, 2014	1,739 m	202–207 cm	GB_1 *Cladosporium* sp.; GB_10 *Xylaria feejeensis*	Parallel core P0_6: Teske et al., 2019; Ramírez et al., 2020
El Puma piston core P08_3: cold seafloor sediment	Sonora Margin slope 27°N40.342/−111°24.121	3–4°C	October 20, 2014	995 m	179–184 cm	GB_7 *Torulaspora delbrueckii*	This study
El Puma piston core P10_4: cold seafloor sediment	Guaymas Basin NW flanking region 27°30.519/−111°42.172	3–4°C	October 21, 2014	1,731 m	353–358 cm	GB_11 *Ramularia eucalypti*	Teske et al., 2019; Ramírez et al., 2020
Alvin push core 4862-4: hydrothermal sediment	Southern Guaymas Basin Mat Mound Massif	Ca. 40°C	December 13, 2016	2,000 m	26–28 cm	GB_5 *Engyodontium album*; GB_9 *Rhodotorula mucilaginosa*	Teske et al., 2021b
Alvin dive 4864 sample: hydrothermal silicate crusts	Off-axis Ringvent hydrothermal area 27°30.360/−111°40.870 27°30.380/−111°40.890 [ORP and Mound1 site]	Ca. 3–4°C	December 15, 2016	1,720 m	Seafloor	GB_8 *Cadophora* sp.	Escorcia-Ocampo et al., 2018; Teske et al., 2019
Alvin push core 4867-14, cold seep sediment	Off-axis Octopus Mound cold seep, Active site 27°28.150/−111°28.400	3°C	December 18, 2016	1,850 m	30–33 cm	GB_4 and GB_6, *Aureobasidium pullulans*; GB_12 *Dioszegia xingshanensis*	Teske et al., 2021b
Alvin push core 4868-12: hydrothermal sediment	Southern Guaymas Basin Mat Mound Massif 27°00.430/−111°24.520	Ca. 50°C at 20 cm	December 19, 2016	2,000 m	0–16 cm	Redundant isolates	Engelen et al., 2021; Teske et al., 2021b
Alvin push core 4871-10: hydrothermal sediment	Southern Guaymas Basin, Northern Towers area 27°02.680/−111°23.080	Ca. 60–70°C at 20 cm	December 23, 2016	1,995 m	Seafloor	GB_2 *Penicillium chrysogenum*; GB_3 *Cadophora malorum*	Teske et al., 2021b
Alvin push core 4872-13: hydrothermal sediment	Southern Guaymas Basin, Cathedral Hill area 27°00.680/−111°24.270	Ca. 40–50°C	December 24, 2016	2,000 m	19.5–52 cm	Redundant isolates	This study
Alvin dive 4872: hydrocarbon-rich mineral aggregate	Southern Guaymas Basin, Cathedral Hill area 27°00.700/−111°24.280	Ca. 3–50°C	December 24, 2016	2,000 m	Seafloor	Redundant isolates	This study

This table includes strains GB_9 Rhodotorula mucilaginosa, GB_4 and GB_6 Aureobasidium pullulans, GB_1 Cladosporium sp., and GB_8 Cadophora malorum that are used for long-term incubation experiments on polyaromatic hydrocarbons. Additional isolates that were not selected to represent the final 12 non-redundant isolates (Keeler et al., 2021) are listed as "redundant isolates".

with a hydrophobic and hydrophilic moiety interacting with phase boundaries in a heterogeneous system to solubilize organic compounds (Sen et al., 2017). Thus, in the presence of biosurfactants, the chemical inertness of hydrocarbon contaminants can be reduced, and microbial degradation can occur through improved solubilization (Banat et al., 2014). Surfactants are used to enhance bioremediation of accidental hydrocarbon releases, and in oil recovery. In contrast to chemical surfactants such as carboxylates, sulfonates, sulfates (Damare et al., 2012), biosurfactants have advantages such as lower toxicity and higher biodegradability (Shekhar et al., 2015). While bacterial biosurfactants are common, often produced by members of the genera *Pseudomonas, Acinetobacter,* and *Bacillus* (Soberón-Chávez and Maier, 2011), the importance of production of biosurfactants by yeasts and filamentous fungi is increasingly recognized; of total available biosurfactants 12% are from ascomycetes and 7% from basidiomycetes. Fungal biosurfactants are unique and include sophorolipids, mannosylerythritol lipids, cellobiose lipids, xylolipids, lipid polyols, and hydrophobins, all known to have a wide range of applications including in environmental remediation (da Silva et al., 2021 and references therein).

Known producers are affiliated to yeasts of the genera *Candida*, *Pseudozyma*, or *Rhodotorula* (Diniz Rufino et al., 2014; Sajna et al., 2015; Sen et al., 2017) and to filamentous fungi of the

genera *Cunninghamella*, *Fusarium*, *Phoma*, *Cladophialophora*, *Exophiala*, *Aspergillus*, and *Penicillium* (Silva et al., 2014; Lima et al., 2016). Biosurfactants also remain active under harsh conditions of temperature, pH, and salinity. As an example, biosurfactants produced by a yeast affiliated to the genus *Rhodotorula* exhibit high stability over a wide range of temperature (at 120°C for 30–120 min), salinity (2–10% NaCl), and pH (2–10) (Sen et al., 2017). Bacterial isolates from hydrocarbon-contaminated samples, such as *Pseudomonas* (Patowary et al., 2017) and *Halomonas* (Gutierrez et al., 2013) also synthesize biosurfactants while growing on crude oil components as carbon sources, thereby improving hydrocarbon degradation further by facilitating microbial access. Considering the plethora of microorganisms that produce biosurfactants (Cameotra and Makkar, 2010), and the existence of unique fungal biosurfactants, it is possible some Fungi play a critical role in facilitating the bioavailability of hydrocarbons to other microbial populations (i.e., to other Fungi or Bacteria) and by synthesizing biosurfactants.

FUNGAL ISOLATIONS AND FUNGAL DIVERSITY IN GUAYMAS BASIN

An in-depth investigation of Guaymas Fungi, their diversity, hydrocarbon-degrading capabilities, and abilities to enhance bacterial hydrocarbon degradation—for example, in a consortium of fungal and bacterial hydrocarbon degraders—is currently being conducted in the Edgcomb lab. The fungal project started with a sequencing survey that detected diverse fungal communities in Guaymas hydrothermal sediments using fungal ITS and 18S rRNA gene amplicons (Ramírez et al., 2021). Microeukaryotic signatures included previously described hydrocarbonoclastic fungal taxa (e.g., *Aureobasidium* sp., *Penicillium* sp., *Cladosporium* sp.), as well as basal fungi (e.g., chytrids) known to be degraders of recalcitrant carbon sources (Hassett et al., 2020; Ramírez et al., 2021). Fungal signatures in surficial sediment layers (0–30 cmbsf) of Guaymas Basin were dominated by chytrids (Ramírez et al., 2021); these zoosporic fungi are included among "fungal dark matter" due to unresolved biological questions regarding their life cycle and evolution, as well as their roles in the marine environment (Grossart et al., 2016; Naranjo-Ortiz and Gabaldo, 2019; Laundon and Cunliffe, 2021).

In parallel to the sequencing survey, an initial cultivation survey (Keeler et al., 2021) using hydrothermal and non-hydrothermal sediment inocula from Guaymas Basin yielded 12 distinct isolates of Ascomycota and Basidiomycota, after dereplication to account for redundant isolates (**Table 1**, **Figure 4**). Ten isolates showed growth based on optical density and light microscopy during 24 h of incubation at 25°C at *in situ* pressures in stainless steel pressure vessels (High Pressure Equipment Co., Erie, PA, United States). Interestingly, our isolate of the wide-spread marine yeast *Rhodotorula,* obtained from microbial-mat covered hydrothermal sediment in the Mat Mound Massif area (Teske et al., 2021a), maintained culture cell densities over 3 weeks in liquid medium with naphthalene substituted as the sole C source under reducing, anoxic conditions (100x *in situ* naphthalene concentration provided). To evaluate the role of fungi in hydrocarbon degradation, a deeper culturing effort was needed in order to obtain the broadest possible diversity of *in situ* fungi from different sites and depths. The Edgcomb lab is collaborating with Gaetan Burgaud at the University of Brest, France, to carry out high-throughput fungal culturing efforts. This collaboration has yielded ∼200 unique fungal isolates from subsurface Guaymas sediments, and all isolates in the collection are currently being tested for production of biosurfactants.

A persistent issue is that publications generally refer to aerobic hydrocarbon degradation by fungi, whereas anaerobic degradation is attributed to bacteria. For example, hexadecane is oxidized under aerobic conditions by fungi isolated from surficial marine sediments in the Gulf of Mexico (Velez et al., 2020), whereas anaerobic degradation of hexadecane in marine sediments is performed by sulfate-reducing bacteria (So and Young, 2001; Cravo-Laureau et al., 2005; Shin et al., 2019). As a possible interaction between fungi and sulfate-reducing bacteria, fermentative anaerobic fungi could supply sulfate-reducing bacteria with H_2 or acetate (Ivarsson et al., 2018), to provide sulfate-reducing microbial communities with a head start and to create suitably reducing conditions that allow anaerobic hexadecane degradation by sulfate-reducing bacteria. In the case of recalcitrant polyaromatics, such as the non-substituted 4-ring components pyrene and chrysene, the available evidence suggests that aerobic fungi initiate this process, whereas anaerobic degradation of polyaromatics, as far as known, is a slow-acting bacterial process. Multiple studies have shown that pyrene can be metabolized by fungi aerobically (Ravelet et al., 2000, 2001; da Silva et al., 2003). Chrysene is metabolized by some aerobic fungal strains producing napthoic acid (Hadibaratam et al., 2009), and is completely remineralized to CO_2 by co-cultures of fungi with bacteria in soils (Boonchan et al., 2000). Yet in anaerobic marine sediments exposed to long-term hydrocarbon pollution, chrysene and pyrene are slowly degraded under anaerobic, sulfate-reducing conditions, by 25 and 13% of the original concentration, respectively, after 11 months of incubation (Rothermich et al., 2002). Controls with the sulfate-reducing inhibitor molybdate did not show any polyaromatic degradation, leading to the conclusion that specifically sulfate-reducing bacteria were the key agents of chrysene and pyrene degradation (Rothermich et al., 2002). In pyrene-amended anoxic incubations with 10–20% (v/v) inoculum of contaminated sludge, a (non-sulfate-reducing) *Klebsiella* isolate degraded pyrene *via* the intermediate phenanthrene to substituted monoaromatic compounds (Li et al., 2018).

Given the well-documented potential for anaerobic degradation of long-chain alkanes and polycyclic aromatics in anoxic marine sediments, we speculate that highly recalcitrant hydrocarbons can be metabolized in multiple redox zones in Guaymas Basin, for example by aerobic cracking of polyaromatic rings in surficial sediments (Gutierrez et al., 2015), and also in the organic-rich sediments immediately underneath that host a diverse cohort of sulfate-reducing bacteria with different substrate preferences. Since sulfate reduction rate maxima are found consistently in the upper 4 cm of Guaymas Basin

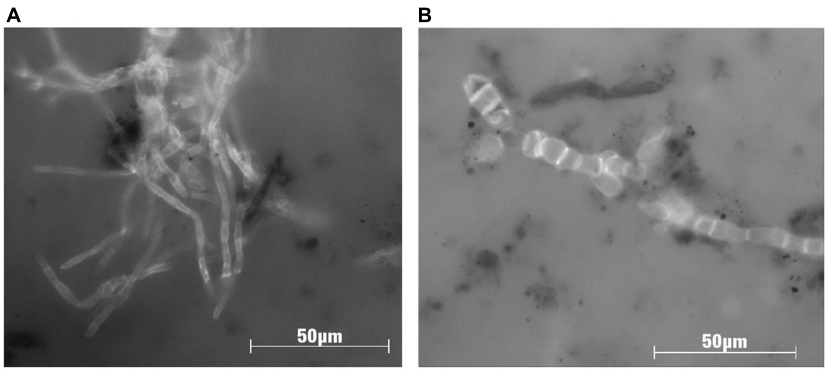

FIGURE 4 | Microphotographs of Guaymas Basin fungal strains imaged under fluorescence after calcofluor staining, which highlights the chitin cell walls of fungi. Strains were isolated from Guaymas Basin sediments (**Table 1**), and images were taken after 40 days of incubation with the polyaromatic substrate naphthalene (5 µg/ml) in co-culture with Desulfobacterales-dominated sulfate-reducing bacteria. Panel **(A)** shows growth of the filamentous ascomycete fungus *Cadophora malorum*, and panel **(B)** shows filamentous arrangement of cells of the yeast-like ascomycete fungus *Aureobasidium pullulans*.

sediments (Meyer et al., 2013), and oxygenated bubbles are circulating in hydrothermally active, sulfate-replete surficial sediments (Gundersen et al., 1992; Teske et al., 2016), aerobic and sulfate-reducing degradation processes could occur simultaneously, at least in close proximity to each other at the redox interface or on overlapping spatial scales in mixed communities that thrive in dynamic redox gradients (**Figure 5**). The active microbiota might involve aerobic as well as anaerobic fungi that share the surficial sediment habitat with similarly diverse bacteria.

Given the co-occurrence of fungi and sulfate-reducing bacteria in Guaymas Basin sediment (Ramírez et al., 2021), we are exploring the efficacy of co-cultures of fungal isolates and sulfate-reducing bacterial enrichments to degrade selected hydrocarbons. Under controlled lab conditions, fungal isolates are being used individually and in co-culture experiments with hydrocarbon-degrading sulfate-reducing bacterial enrichments (dominated by members of the Desulfobacterales, **Supplementary Figure 1** and **Supplementary Table 1**), but supplemented with short-term oxygen spikes, comparable to the impact of hydrothermal circulation and seawater inmixing into surficial Guaymas Basin sediments. As a first step, cultures of fungi alone, bacterial enrichments alone, and bacterial-fungal co-cultures are incubated with a mixture of aliphatic and polyaromatic hydrocarbons in sulfate-reducing media (Widdel and Bak, 1992). The Guaymas sediments that were used to initiate the bacterial enrichments had been conditioned by adding benzoate (0.5 mM) and acetate (2 mM), to start sulfate-reducing activity; benzoate is a successful substrate for bacterial isolations from Guaymas Basin under aerobic (Goetz and Jannasch, 1993) and sulfate-reducing conditions (Phelps et al., 1998). Once the fungal/SRB hydrocarbon incubations were established in stoppered serum bottles and sulfide production indicated robust sulfate-reducing activity, weekly injections of oxygen in low concentrations (∼5–10% headspace concentration) were added to some replicates to imitate the biogeochemical regime that can occur in Guaymas Basin hydrothermal sediments, where oxygenated seawater percolates through surficial anaerobic and sulfide-rich sediment and introduces oxygen "bubbles" into an otherwise anaerobic and sulfidic sediment (Teske et al., 2016). Under these conditions, some Guaymas Basin fungal isolates that were originally isolated aerobically can maintain their presence in the sulfate-reducing enrichment cultures, and coexist with mixed populations of sulfate-reducing bacteria. Incubations without oxygen additions and fungal inoculum are running in parallel, to serve as controls for purely anaerobic hydrocarbon-degrading activity by sulfate-reducing bacteria. The long-term incubation experiment is currently in its eighth month; in suitable intervals subsamples are collected and analyzed for microbial community composition and hydrocarbon degradation using 16S rRNA gene itag sequencing and two-dimensional gas chromatography (Ventura et al., 2012).

FUTURE DIRECTIONS

There is growing evidence that hydrocarbon biodegradation is an active process in Guaymas Basin sediments. Yet there are many avenues of investigation to pursue in order to obtain a more complete understanding of the roles played by diverse microorganisms in the utilization of hydrocarbons as an energy source. The recent International Ocean Discovery Program Expedition 385 (IODP X385) drilled hundreds of meters into the seafloor of Guaymas Basin at eight different sites (**Supplementary Figure 2**). The thickly sedimented northwestern spreading region with deeply emplaced sills is represented by sites 1545 and 1546 (Teske et al., 2018), Sites 1547 and 1548 are placed into the center and the periphery of the hydrothermal Ringvent site with a hot, shallow sill (Lizarralde et al., 2011; Soule et al., 2018; Teske et al., 2019), Site 1549 drills into the vicinity of a methane-rich cold seep, termed Central Seep (Geilert et al., 2018; Teske et al., 2021a), Site 1550 samples the northern axial trough of Guaymas Basin, Site 1551 represents the massive terrigenous sediments of the southeastern spreading region, and Site 1552 samples one of the numerous cold seep sites adjacent to the Sonora Margin (Portail et al., 2015; Teske et al., 2018). All Site reports

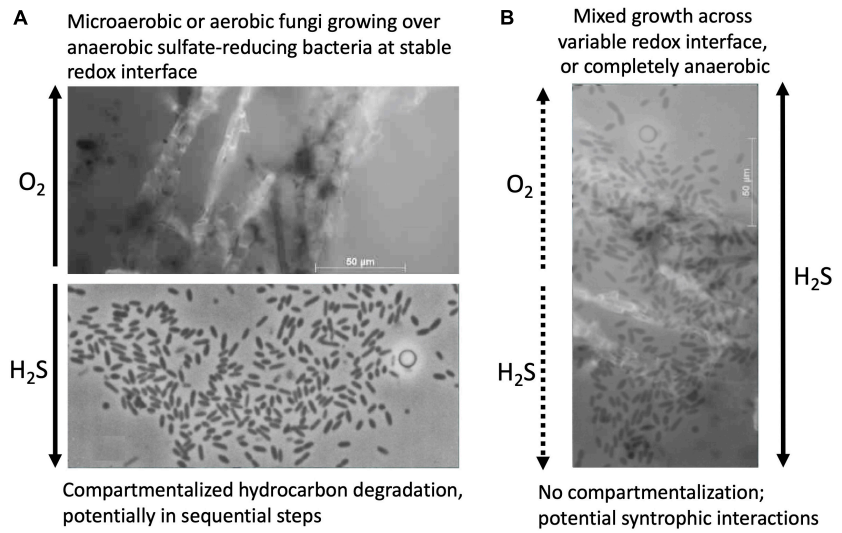

FIGURE 5 | Concept sketch for potential interactions of hydrocarbon-degrading fungi and sulfate-reducing bacteria in Guaymas Basin sediments. **(A)** Spatially separated, redox-stratified niches for aerobic hydrocarbon-degrading fungi and sulfate-reducing anaerobic bacteria, implying compartmentalized hydrocarbon degradation in distinct steps. **(B)** Co-occurrence and potential syntrophic associations of hydrocarbon-degrading fungi and sulfate-reducing bacteria in sediments with fluctuating redox gradients, or fully sulfidic conditions, visualized by superimposition of both microphotographs. The fungal isolate used for this sketch is *Cladosporium*_GB1 (**Table 1**) grown on naphthalene as sole carbon source; the bacterial image shows *Desulfothermus naphthae* strain TD3, a thermophilic hexadecane-degrading sulfate reducer from Guaymas Basin sediments (Rüter et al., 1994).

are available at http://iodp.tamu.edu/publications/proceedings.html. These deep subsurface sediments vary significantly in their thermal, biogeochemical, and microbial cell number profiles. Comparing sites where temperatures increase steeply above shallow, hot sills, and sites with more gradual temperature gradients offer a chance to systematically examine the influences of temperature and pressure. In-depth analyses of taxonomic diversity, genome content, and cell abundances along cores from these eight sites will inform on the distribution of deep biosphere microbiota (bacteria, archaea, and microbial fungi) in this hydrothermal setting along temperature, depth and substrate gradients. Correlation analyses, analyses of genomic potential in metagenomes and MAGs, and studies of cultured fungal isolates will reveal the likely nutritional sources (e.g., microbial necromass, buried organic material) that allow bacteria, archaea, and fungi to survive in this habitat.

Periodic historical magmatic sill intrusions, which have "baked" buried sediments surrounding each sill, invariably have had a major effect on the modern pool of available nutrients remaining in sediments in close proximity to buried sills (Teske et al., 2014). Current and future research will determine how these historic events shape the modern chemical composition of those sediments and whether microbiota are able to survive on remaining organic substrates. Analysis of the mRNA pool, proteome, and secretome isolated from samples along the depths drilled at each site are necessary to inform on the active fraction of the community and on microbial strategies for coping with increasing heat and the stresses of ever-scarcer nutrients with depth. The application of recently developed molecular methods such as bioorthogonal non-canonical amino acid tagging (BONCAT), RNA-SIP, and live/dead stains applied to isolated cells are needed to confirm results from interpretations of molecular data as to the fraction of the *in situ* community that is actively contributing to nutrient cycling in the deep subsurface Guaymas biosphere (Teske et al., 2021c). In the anoxic deep biosphere, we may discover diverse fungal-bacterial syntrophic interactions, that allow the syntrophic partners to survive by adapting to different sources of carbon and/or energy, and by cooperating in accessing substrates that individual taxa cannot access alone.

Finally, studies of enrichment cultures, cultured isolates, and co-cultures can provide critical information on whether interactions between microbial taxa enhance their ability to access otherwise refractory organic carbon substrates found in Guaymas Basin sediments, including diverse hydrocarbons. Promising isolates and enrichments could possibly be engineered to remediate and clean-up oil spills with minimal ecosystem disturbance. For example, experiments that prime indigenous soil bacteria capable of hydrocarbon degradation for oil bioremediation show that horizontally transferred gene vectors encoding genes for petroleum hydrocarbon degradation persist in indigenous populations only when under selection pressure, but disappear when the hydrocarbon source is removed (French et al., 2020).

Using new molecular assays and long-term enrichments, diverse fungal-bacterial syntrophic interactions might be discovered that allow these partners to survive in the anoxic deep biosphere by adapting to different carbon and energy sources, and by cooperating in accessing substrates that individual taxa cannot access alone. In this way, it will be possible to go beyond studies of individual fungal and sulfate-reducing species and their capabilities to oxidize hydrocarbon and low-molecular

weight organic compounds, and to explore the possibility that selected, fungi, fungal-bacteria co-cultures and syntrophic cultures enhance the accessibility of particular hydrocarbons through successive or simultaneous reactions.

DATA AVAILABILITY STATEMENT

The original contributions presented in the study are included in the article/**Supplementary Material**, further inquiries can be directed to the corresponding author.

AUTHOR CONTRIBUTIONS

VE led the fungal-bacterial interactions project and designed the experiments. PM performed the experiments. AT wrote the first draft of the manuscript. All authors commented and edited the manuscript in turn.

FUNDING

This project was supported by collaborative NSF Biological Oceanography grants OCE-1829903 and OCE-1829680 "Hydrothermal fungi in the Guaymas Basin Hydrocarbon Ecosystem" to VE and AT, and collaborative NSF Biological Oceanography grants OCE-2046799 and OCE-2048489 "IODP-enabled Insights into Fungi and Their Metabolic Interactions with Other Microorganisms in Deep Subsurface Hydrothermal Sediments" to VE and AT. PM was supported by OCE-2046799 and OCE-1829903. Sampling in Guaymas Basin was supported by collaborative NSF Biological Oceanography grant 1357238 "Collaborative Research: Microbial carbon cycling and its interaction with sulfur and nitrogen transformations in Guaymas Basin hydrothermal sediments" to AT.

ACKNOWLEDGMENTS

We thank the *Alvin* team on RV *Atlantis* and the piston coring team on RV *El Puma* for their dedication that made successful sampling in Guaymas Basin possible.

SUPPLEMENTARY MATERIAL

The Supplementary Material for this article can be found online at: https://www.frontiersin.org/articles/10.3389/fmicb.2022.831828/full#supplementary-material

REFERENCES

Al-Nasrawi, H. (2012). Biodegradation of crude oil by fungi isolated from the Gulf of Mexico. *J. Bioremed. Biodeg.* 2012:147. doi: 10.4172/2155-6199.1000147

Azam, F., Fenchel, T., Field, J. G., Gray, J. S., Meyer-Reil, L. A., and Thingstad, F. (1983). The ecological role of water column microbes in the sea. *Mar. Ecol. Prog. Ser.* 10, 257–263.

Banat, I. M., Satpute, S. K., Cameotra, S. S., Patil, R., and Nyayanit, N. V. (2014). Cost-effective technologies and renewable substrates for biosurfactant production. *Front. Microbiol.* 5:697.

Bazylinski, D. A., Farrington, J. W., and Jannasch, H. W. (1988). Hydrocarbons in surface sediments from a Guaymas Basin hydrothermal vent site. *Org. Geochem.* 12, 547–558. doi: 10.1016/0146-6380(88)90146-5

Bazylinski, D. A., Wirsen, C. O., and Jannasch, H. W. (1989). Microbial utilization of naturally occurring hydrocarbons at the Guaymas Basin hydrothermal vent site. *Appl. Environ. Microbiol.* 55, 2832–2836. doi: 10.1128/aem.55.11.2832-2836.1989

Boonchan, S., Britz, M. L., and Stanley, G. A. (2000). Degradation and mineralization of high-molecular- weight polycyclic aromatic hydrocarbons by defined fungal-bacterial cocultures. *Appl. Environ. Microbiol.* 66, 1007–1019. doi: 10.1128/AEM.66.3.1007-1019.2000

Borrel, G., Adam, P. S., McKay, L. J., Chen, L.-X., Sierra-Garcia, I. N., Sieber, C. M. K., et al. (2019). Wide diversity of methane and short-chain alkane metabolisms in uncultured archaea. *Nat. Microbiol.* 4, 603–613. doi: 10.1038/s41564-019-0363-3

Bridges, T. S., Levin, L. A., Cabrera, D., and Plaia, G. (1994). Effects of sediment amended with sewage, algae, or hydrocarbons on growth and reproduction in two opportunistic polychaetes. *J. Exp. Mar. Biol. Ecol.* 177, 99–119. doi: 10.1016/j.aquatox.2005.06.002

Burgaud, G., Thi Minh Hu, N., Arzur, D., Coton, M., Perrier-Cornet, J. M., Jebbar, M., et al. (2015). Effects of hydrostatic pressure on yeasts isolated from deep-sea hydrothermal vents. *Res. Microbiol.* 166, 700–709. doi: 10.1016/j.resmic.2015.07.005

Cameotra, S. S., and Makkar, R. S. (2010). Biosurfactant-enhanced bioremediation of hydrophobic pollutants. *Pure Appl. Chem.* 82, 97–116. doi: 10.1351/PAC-CON-09-02-10

Chen, S.-C., Musat, N., Lechtenfeld, O. J., Paschke, H., Schmidt, M., Said, N., et al. (2019). Anaerobic oxidation of ethane by archaea from a marine hydrocarbon seep. *Nature* 568, 108–111. doi: 10.1038/s41586-019-1063-0

Claus, S., Guillou, H., and Ellero-Simatos, S. (2016). The gut microbiota: a major player in the toxicity of environmental pollutants? *NPJ Biofilms Microbiom.* 2:16003. doi: 10.1038/npjbiofilms.2016.3

Cravo-Laureau, C., Grossi, V., Raphel, D., Matheron, R., and Hirschler-Rea, A. (2005). Anaerobic n- alkane metabolism by a sulfate-reducing bacterium, *Desulfatibacillum aliphaticivorans* strain CV2803T. *Appl. Environ. Microbiol.* 71, 3458–3467. doi: 10.1128/AEM.71.7.3458-3467.2005

da Silva, A. F., Banat, I. M., Giachini, A. J., and Robi, D. (2021). Fungal biosurfactants, from nature to biotechnological product: bioprospection, production and potential applications. *Bioprocess Biosyst. Eng.* 44, 2003–2034. doi: 10.1007/s00449-021-02597-5

da Silva, M., Cerniglia, C. E., Pothuluri, J. V., Canhos, V. P., and Esposito, E. (2003). Screening filamentous fungi isolated from estuarine sediments for the ability to oxidize polycyclic aromatic hydrocarbons. *World J. Microbiol. Biotech.* 19, 399–405.

Dalzell, C. J., Ventura, G. T., Walters, C. C., Nelson, R. K., Reddy, C. M., Seewald, J. S., et al. (2021). Hydrocarbon transformations in sediments from the Cathedral Hill hydrothermal vent complex at Guaymas Basin, Gulf of California – A chemometric study of shallow seep architecture. *Org. Geochem.* 152:104173. doi: 10.1016/j.orggeochem.2020.104173

Damare, S., Singh, P., and Raghukumar, S. (2012). Biotechnology of marine fungi. *Prog Mol Subcell Biol.* 53, 277–797. doi: 10.1007/978-3-642-23342-5_14

Damare, S. R., Raghukumar, C., and Raghukumar, S. (2006). Fungi in deep-sea sediments of the Central Indian Basin. *Deep-Sea Res.* 53, 14–27. doi: 10.1016/j.dsr.2005.09.005

Das, N., and Chandran, P. (2011). Microbial degradation of petroleu hydrocarbon contaminants: an overview. *Biotechnol. Res. Internat* 2011:941810. doi: 10.4061/2011/941810

Das, P., Yang, X. P., and Ma, L. Z. (2014). Analysis of biosurfactants from industrially viable *Pseudomonas* strain isolated from crude oil suggests how rhamnolipids congeners affect emulsification property and antimicrobial activity. *Front. Microbiol.* 5:696. doi: 10.3389/fmicb.2014.00696

Davidova, I. A., Marks, C. R., and Suflita, J. M. (2018). "Anaerobic Hydrocarbon-Degrading *Deltaproteobacteria*," in *Taxonomy, Genomics and Ecophysiology of Hydrocarbon-Degrading Microbes. Handbook of Hydrocarbon and Lipid Microbiology*, ed. T. McGenity (Cham: Springer), doi: 10.1007/978-3-319-60053-6_12-1

Davidova, I. A., Wawrik, B., Callaghan, A. V., Duncan, K., Marks, C. R., and Suflita, J. M. (2016). Dethiosulfatarculus *sandiegensis* gen. nov., sp. nov., isolated from a methanogenic paraffin-degrading enrichment culture and emended description of the family *Desulfarculaceae*. *Int. J. Syst. Evol. Microbiol.* 66, 1242–1248. doi: 10.1099/ijsem.0.000864

Didyk, B. M., and Simoneit, B. R. T. (1989). Hydrothermal oil of Guaymas Basin and implications for petroleum formation mechanisms. *Nature* 342, 65–69. doi: 10.1038/342065a0

Diniz Rufino, R., Moura de Luna, J., de Campos Takaki, G. M., and Asfora Sarubbo, L. (2014). Characterization and properties of the biosurfactant produced by *Candida lipolytica* UCP 0988. *Electron. J. Biotechnol.* 17:6.

Dombrowski, N., Seitz, K. W., Teske, A. P., and Baker, B. J. (2017). Genomic insights into potential interdependencies in microbial hydrocarbon and nutrient cycling in hydrothermal sediments. *Microbiome* 5:106. doi: 10.1186/s40168-017-0322-2

Dombrowski, N., Teske, A., and Baker, B. (2018). Extensive microbial metabolic diversity and redundancy in Guaymas Basin hydrothermal sediments. *Nat. Comm*. 9:4999. doi: 10.1038/s41467-018-07418-0

Dowell, F., Cardman, Z., Dasarathy, S., Kellermann, M. Y., McKay, L. J., MacGregor, B. J., et al. (2016). Microbial communities in methane and short alkane-rich hydrothermal sediments of Guaymas Basin. *Front. Microbiol* 7:17. doi: 10.3389/fmicb.2016.00017

Drake, H., Ivarsson, M., Bengtson, S., Heim, C., Siljeström, S., Whitehouse, M. J., et al. (2017). Anaerobic consortia of fungi and sulfate reducing bacteria in deep granite fractures. *Nature Comm.* 8:55. doi: 10.1038/s41467-017-00094-6

Edgcomb, V. D., Kysela, A., Teske, A., de Vera Gomez, A., and Sogin, M. L., (2002). Benthic eukaryotic diversity in the Guaymas Basin, a hydrothermal vent environment. *Proc. Natl. Acad. Sci.* USA 99, 7658–7662.

Einsele, G., Gieskes, J. M., Curray, J., Moore, D. M., Aguayo, E., Aubry, M.-P., et al. (1980). Intrusion of basaltic sills into highly porous sediments, and resulting hydrothermal activity. *Nature* 283, 441–445. doi: 10.1038/283441a0

Emri, T., Molnar, Z., and Pocsi, I. (2005). The appearances of autolytic and apoptotic markers are concomitant but differently regulated in carbon-starving *Aspergillus nidulans* cultures. *FEMS Microbiol. Lett*. 251, 297–303. doi: 10.1016/j.femsle.2005.08.015

Engelen, B., Nguyen, T., Heyerhoff, B., Kalenborn, S., Sydow, K., Tabai, H., et al. (2021). Microbial communities of hydrothermal Guaymas Basin surficial sediment profiled at 2 millimeter-scale resolution. *Front. Microbiol.* 12:710881. doi: 10.3389/fmicb.2021.710881

Escorcia-Ocampo, E., Gil-Bernal, F., Núñez-Useche, F., Canet, C., Teske, A., Antonio Rodriguez Diaz, A., et al. (2018). *New insights into authigenic and hydrothermal mineralization processes of the Guaymas Basin (Gulf of California)*. Boulder: Geological Society of America Annual Meeting.

Fernandes, P. M. B., Domitrovic, T., Kao, C. M., and Kurtenbach, E. (2004). Genomic expression pattern in *Saccharomyces cerevisiae* cells in response to high hydrostatic pressure. *FEBS Lett.* 556, 153–160. doi: 10.1016/s0014-5793(03)01396-6

French, K. E., Zhou, Z., and Terry, N. (2020). Horizontal 'gene drives' harness indigenous bacteria for bioremediation. *Sci. Rep.* 10:15091. doi: 10.1038/s41598-020-72138-9

García-Lepe, R., Nuero, O. M., Reyes, F., and Santamaría, F. (1997). Lipases in autolysed cultures of filamentous fungi. *Lett. Appl. Microbiol.* 25, 127–130. doi: 10.1046/j.1472-765x.1997.00187.x

Geilert, S., Hensen, C., Schmidt, M., Liebetrau, V., Scholz, F., Doll, M., et al. (2018). Transition from hydrothermal vents to cold seeps records timing of carbon release in the Guaymas Basin, Gulf of California. *Biogeosciences* 15, 5715–5731. doi: 10.5194/bg-15-5715-2018

Gesinde, A. F., Agbo, E. B., Agho, M. O., and Dike, E. F. C. (2008). Bioremediation of some Nigerian and Arabian crude oils by fungal isolates. *Int. J. Pure Appl. Sci.* 2, 37–44.

Goetz, F. E., and Jannasch, H. W. (1993). Aromatic hydrocarbon-degrading bacteria in the petroleum-rich sediments of Guaymas Basin hydrothermal vent site: Preference for aromatic carboxylic acids. *Geomicrobiol. J.* 11, 1–18. doi: 10.1080/01490459309377928

Grossart, H.-P., Wurzbacher, C., James, T. Y., and Kagami, M. (2016). Discovery of dark matter fungi in aquatic ecosystems demands a reappraisal of the phylogeny and ecology of zoosporic fungi. *Fungal Ecol.* 19, 28–38. doi: 10.1016/j.funeco.2015.06.004

Gundersen, J. K., Jørgensen, B. B., Larsen, E., and Jannasch, H. W. (1992). Mats of giant sulphur bacteria on deep-sea sediments due to fluctuating hydrothermal flow. *Nature* 360, 454–456. doi: 10.1038/360454a0

Gutierrez, T., Berry, D., Yang, T., Mishamandani, S., McKay, L. J., Teske, A., et al. (2013). Role of bacterial exopolymers in the fate of the oil released during the Deepwater Horizon oil spill. *PLoS One* 8:e67717. doi: 10.1371/journal.pone.0067717

Gutierrez, T., Biddle, J. F., Teske, A., and Aitken, M. D. (2015). Cultivation-dependent and cultivation-independent characterization of hydrocarbon-degrading bacteria in Guaymas Basin sediments. *Front. Microbiol.* 6:695. doi: 10.3389/fmicb.2015.00695

Hadibaratam, T., Tachibana, S., and Itoh, K. (2009). Biodegradation of chrysene, an aromatic hydrocarbon by *Polyporus* sp. S133 in liquid medium. *J. Hazard. Mater.* 164, 911–917. doi: 10.1016/j.jhazmat.2008.08.081

Hahn, C., Laso-Perez, R., Volcano, F., Vaziourakis, K. M., Stokke, R., Steen, I. H., et al. (2020). Candidatus Ethanoperedens", a thermophilic genus of Archaea mediating the anaerobic oxidation of ethane. *mBio* 11, e600–e620. doi: 10.1128/mBio.00600-20

Hassett, B. T., Vonnahme, T. R., Peng, X., Jones, E. B. G., and Heuze, C. (2020). Global diversity and geography of planktonic marine fungi. *Bot. Marina* 63, 121–139. doi: 10.1515/bot-2018-0113

Hestbjerg, H., Willumsen, P. A., Christensen, M., Andersen, O., and Jacobsen, C. S. (2003). Bioaugmentation of tar-contaminated soils under field conditions using *Pleurotus ostreatus* refuse from commercial mushroom production. *Environ. Toxicol. Chem*. 22, 692–698. doi: 10.1897/1551-5028(2003)022<0692:botcsu>2.0.co;2

Holler, T., Widdel, F., Knittel, K., Amann, R., Kellermann, M. Y., Hinrichs, K.-U., et al. (2011). Thermophilic anaerobic oxidation of methane by marine microbial consortia. *ISME J.* 5, 1946–1956. doi: 10.1038/ismej.2011.77

Husaini, A., Roslan, H. A., Hii, K. S. Y., and Ang, C. H. (2008). Biodegradation of aliphatic hydrocarbon by indigenous fungi isolated from used motor oil contaminated sites. *World J. Microb. Biot*. 24, 2789–2008. doi: 10.1007/s11274-008-9806-3

Ivarsson, M., Bengtson, S., Drake, H., and Warren, F. (2018). Fungi in deep subsurface environments. *Adv. Appl. Microbiol.* 102, 83–116. doi: 10.1016/bs.aambs.2017.11.001

Iwahashi, H., Odani, M., Ishidou, E., and Kitagawa, E. (2005). Adaptation of *Saccharomyces cerevisiae* to high hydrostatic pressure causing growth inhibition. *FEBS Lett*. 579, 2847–2852. doi: 10.1016/j.febslet.2005.03.100

Jeanthon, C., LHaridon, S., Cueff, V., Banta, A., Reysenbach, A. L., and Prieur, D. (2002). Thermodesulfobacterium *hydrogenophilum* sp. nov., a thermophilic, chemolithoautotrophic, sulfate-reducing bacterium isolated from a deep-sea hydrothermal vent at Guaymas Basin, and emendation of the genus *Thermodesulfobacterium*. *Int. J. Syst. Evol. Microbiol.* 52, 765–772. doi: 10.1099/00207713-52-3-765

Jochum, L. M., Schreiber, L., Marshall, I. P. G., Jørgensen, B. B., Schramm, A., and Kjeldsen, K. U. (2018). Single-cell genomics reveals a diverse metabolic potential of uncultivated *Desulfatiglans*-related Delta*proteobacteria* widely distributed in marine sediment. *Front. Microbiol.* 9:2038. doi: 10.3389/fmicb.2018.02038

Kagami, M., de Bruin, A., Ibelings, B. W., and Van Donk, E. (2007). Parasitic chytrids: their effects on phytoplankton communities and food-web dynamics. *Hydrobiologia* 578, 113–129. doi: 10.1007/s10750-006-0438-z

Kagami, M., Miki, T., and Takimoto, G. (2014). Mycoloop: chytrids in aquatic food webs. *Front. Microbiol.* 5:166. doi: 10.3389/fmicb.2014.00166

Kawka, O. E., and Simoneit, B. R. T. (1994). Hydrothermal pyrolysis of organic matter in Guaymas Basin: I. Comparison of hydrocarbon distributions in subsurface sediments and seabed petroleums. *Org. Geochem.* 22, 947–978. doi: 10.1016/0146-6380(94)90031-0

Keeler, E., Burgaud, G., Teske, A., Beaudoin, D., Mehiri, M., Dayras, M., et al. (2021). Deep-sea hydrothermal vent sediments reveal diverse fungi with antibacterial activities. *FEMS Microbiol. Ecol.* 97:103. doi: 10.1093/femsec/fiab103

Kim, Y., Islam, N., Moss, B. J., Nandakumar, M. P., and Marten, M. R. (2011). Autophagy induced by rapamycin and carbon-starvation have distinct proteome profiles in *Aspergillus nidulans*. *Biotechnol. Bioeng.* 108, 2705–2715. doi: 10.1002/bit.23223

Kleindienst, S., Herbst, F. A., Stagars, M., von Netzer, F., von Bergen, M., Seifert, J., et al. (2014). Diverse sulfate-reducing bacteria of the *Desulfosarcina/Desulfococcus* clade are the key alkane degraders at marine seeps. *ISME J.* 8, 2029–2044. doi: 10.1038/ismej.2014.51

Kleindienst, S., and Knittel, K. (2020). "Anaerobic Hydrocarbon-Degrading Sulfate-Reducing Bacteria at Marine Gas and Oil Seeps," in *Marine Hydrocarbon Seeps*. eds A. Teske and V. Carvalho (Cham: Springer), doi: 10.1007/978-3-030-34827-4_2

Kleindienst, S., Ramette, A., Amann, R., and Knittel, K. (2012). Distribution and in situ abundance of sulfate- reducing bacteria in diverse marine hydrocarbon seep sediments. *Environ. Microbiol.* 14, 2689–2710. doi: 10.1111/j.1462-2920.2012.02832.x

Kniemeyer, O., Fischer, T., Wilkes, H., Glockner, F. O., and Widdel, F. (2003). Anaerobic degradation of ethylbenzene by a new type of marine sulfate-reducing bacterium. *Appl. Environ. Microbiol.* 69, 760–768. doi: 10.1128/AEM.69.2.760-768.2003

Kniemeyer, O., Musat, F., Sievert, S. M., Knittel, K., Wilkes, H., Blumenberg, M., et al. (2007). Anaerobic oxidation of short-chain hydrocarbons by marine sulphate-reducing bacteria. *Nature* 449, 898–901. doi: 10.1038/nature06200

Knittel, K., Boetius, A., Lemke, A., Eilers, H., Lochte, K., Pfannkuche, O., et al. (2003). Activity, distribution, and diversity of sulfate reducers and other bacteria in sediments above gas hydrate (Cascadia Margin, OR). *Geomicrobiol. J.* 20, 269–294. doi: 10.1080/01490450303896

Krukenberg, V., Harding, K., Richter, M., Glockner, F.-O., Gruber-Vodicka, H. R., and Adam, B. (2016). *Candidatus* Desulfofervidus auxilii, a hydrogenotrophic sulfate-reducing bacterium involved in the thermophilic anaerobic oxidation of methane. *Environ. Microbiol* 18, 3073–3091. doi: 10.1111/1462-2920.13283

Krukenberg, V., Riedel, D., Gruber-Vodicka, H. R., Buttigieg, P. L., Tegetmeyer, H. E., Boetius, A., et al. (2018). Gene expression and ultrastructure of meso- and thermophilic methanotrophic consortia. *Environ. Microbiol.* 20, 1651–1666. doi: 10.1111/1462-2920.14077

Küver, J. (2014). "The family Syntrophaceae," in *The Prokaryotes*, eds E. Rosenberg, E. F. DeLong, S. Lory, E. Stackebrandt, and F. Thompson (Berlin: Springer), 281–288. doi: 10.1007/978-3-642-39044-9_269

Küver, J., Rainey, F. A., and Widdel, F. (2005). "Order V. Desulfuromonales ord. nov," in *Bergey's Manual of Systematic Bacteriology*, 2nd edn, (The *Proteobacteria*), Part C (The Alpha-, Beta-, Delta and Epsilon*proteobacteria*), eds D. J. Brenner, N. R. Krieg, J. T. Staley, and G. M. Garrity (New York: Springer), 1005–1006.

Laso-Pérez, R., Hahn, C., van Vliet, D. M., Tegetmeyer, H. E., Schubotz, F., and Smit, N. T. (2019). Anaerobic degradation of nonmethane alkanes by "Candidatus Methanoliparia" in hydrocarbon seeps of the Gulf of Mexico. *mBio* 10, e1814–e1819. doi: 10.1128/mBio.01814-19

Laso-Peìrez, R., Wegener, G., Knittel, K., Widdel, F., Harding, K. J., Krukenberg, V., et al. (2016). Thermophilic archaea activate butane via alkyl-coenzyme M formation. *Nature* 539, 396–401. doi: 10.1038/nature20152

Laundon, D., and Cunliffe, M. (2021). A call for a better understanding of aquatic chytrid biology. *Front. Fungal Biol.* 2:1–30. doi: 10.3389/ffunb.2021.708813

Levin, L. A., Baco, A. R., Bowden, D. A., Colaco, A., Cordes, E., Cunha, M. R., et al. (2016). Hydrothermal vents and methane seeps: rethinking the sphere of Influence. *Front. Mar. Sci.* 3:72. doi: 10.3389/fmars.2016.00072

Li, X., Zhang, X., Li, L., Lin, C., Dong, W., Zhang, X., et al. (2018). Anaerobic biodegradation of pyrene by *Klebsiella* sp. LZ6 and its proposed metabolic pathway. *Environ. Technol.* 7, 1–32. doi: 10.1080/09593330.2018.1556348

Lima, J. M. S., Pereira, J. O., Batista, I. H., Neto, P. D. Q. C., dos Santos, J. C., de Araújo, S. P., et al. (2016). Potential biosurfactant producing endophytic and epiphytic fungi, isolated from macrophytes in the Negro River in Manaus, Amazonas, Brazil. *Afr. J. Biotechnol.* 15, 1217–1223. doi: 10.5897/ajb2015.15131

Lizarralde, D., Soule, A., Seewald, J., and Proskurowski, G. (2011). Carbon release by off-axis magmatism in a young sedimented spreading centre. *Nat. Geo.* 4, 50–54. doi: 10.1038/ngeo1006

Lloyd, K. G., Albert, D., Biddle, J. F., Chanton, L., Pizarro, O., and Teske, A. (2010). Spatial structure and activity of sedimentary microbial communities underlying a *Beggiatoa* spp. mat in a Gulf of Mexico hydrocarbon seep. *PLoS One* 5:e8738. doi: 10.1371/journal.pone.0008738

Lomstein, B. A., Langerhuus, A. T., D'Hondt, S., Jørgensen, B. B., and Spivack, A. J. (2012). Endospore abundance, microbial growth and necromass turnover in deep sub-seafloor sediment. *Nature* 484, 101–104. doi: 10.1038/nature10905

Lomstein, B. A., Niggemann, J., Jørgensen, B. B., and Langerhuus, A. T. (2009). Accumulation of prokaryotic remains during organic matter diagenesis in surface sediments off Peru. *Limnol. Oceanogr.* 54, 1139–1151.

Long, E. R., MacDonald, D. D., Smith, S. J., and Calder, F. D. (1995). Incidence of adverse biological effects within ranges of chemical concentrations in marine and estuarine sediments. *Environ. Manag.* 19, 81–97. doi: 10.1007/bf02472006

Lorenz, R., and Molitoris, H. P. (1997). Cultivation of fungi under simulated deep-sea conditions. *Mycol. Res.* 11, 1355–1365. doi: 10.1080/21501203.2018.1541934

Maheshwari, R., Bharadwaj, G., and Bhat, M. K. (2000). Thermophilic fungi: their physiology and enzymes. *Microbiol. Molecul. Biol. Rev.* 64, 461–488. doi: 10.1128/MMBR.64.3.461-488.2000

McKay, L., Klokman, V., Mendlovitz, H., LaRowe, D., Zabel, M., Hoer, D., et al. (2016). Thermal and geochemical influences on microbial biogeography in the hydrothermal sediments of Guaymas Basin. *Environ. Microbiol. Rep.* 8, 150–161. doi: 10.1111/1758-2229.12365

Meyer, S., Wegener, G., Lloyd, K. G., Teske, A., Boetius, A., and Ramette, A. (2013). Microbial habitat connectivity across spatial scales and hydrothermal temperature gradients at Guaymas Basin. *Front. Microbiol.* 4:207. doi: 10.3389/fmicb.2013.00207

Nance, J. M. (1991). Effects of oil/gas field produced water on the macrobenthic community in a small gradient estuary. *Hydrobiol.* 220, 189–204. doi: 10.1007/bf00006575

Naranjo-Ortiz, M. A., and Gabaldo, N. T. (2019). Fungal evolution: diversity, taxonomy and phylogeny of the Fungi. *Biol. Rev. Camb. Philos. Soc.* 94, 2101–2137. doi: 10.1111/brv.12550

Obire, O., and Anyanwu, E. C. (2009). Impact of various concentrations of crude oil on fungal populations of soil. *Int. J. Environ. Sci. Technol.* 6, 211–218. doi: 10.1007/bf03327624

Orsi, W. (2018). Ecology and evolution of seafloor and subseafloor microbial communities. *Nat. Rev. Microbiol.* 16, 671–683. doi: 10.1038/s41579-018-0046-8

Orsi, W., Biddle, J., and Edgcomb, V. P. (2013). Deep sequencing of subseafloor eukaryotic rRNA reveals active fungi across marine subsurface provinces. *PLoS One* 8:e56335. doi: 10.1371/journal.pone.0056335

Pachiadaki, M. G., Rédou, V., Beaudoin, D. J., Burgaud, G., and Edgcomb, V. P. (2016). Fungal and prokaryotic activities in the marine subsurface biosphere at Peru Margin and Canterbury Basin inferred from RNA-Based analyses and microscopy. *Front. Microbiol.* 7:846. doi: 10.3389/fmicb.2016.00846

Passarini, M. R. Z., Rodrigues, M. V. N., da Silva, M., and Sette, L. D. (2011). Marine-derived filamentous fungi and their potential application for polycyclic aromatic hydrocarbon bioremediation. *Mar. Pollut. Bull.* 62, 364–370. doi: 10.1016/j.marpolbul.2010.10.003

Patowary, K., Patowary, R., Kalita, M. C., and Deka, S. (2017). Characterization of biosurfactant produced during degradation of hydrocarbons using crude oil as sole source of carbon. *Front. Microbiol.* 8:279. doi: 10.3389/fmicb.2017.00279

Peng, Q., Li, Y., Deng, L., Fang, J., and Yu, X. (2021). High hydrostatic pressure shapes the development and production of secondary metabolites of Mariana Trench sediment fungi. *Sci. Rep.* 11:11436. doi: 10.1038/s41598-021-90920-1

Phelps, C. D., Kerkhof, L. J., and Young, L. Y. (1998). Molecular characterization of a sulfate-reducing consortium which mineralizes benzene. *FEMS Microbiol. Ecol.* 27, 269–279. doi: 10.1111/j.1574-6941.2008.00536.x

Portail, M., Olu, K., Escobar-Briones, E., Caprais, J. C., Menot, L., Waeles, M., et al. (2015). Comparative study of vent and seep macrofaunal communities in the Guaymas Basin. *Biogeosciences* 12, 5455–5479. doi: 10.5194/bg-12-5455-2015

Prenafeta-Boldú, F. X., de Hoog, G. S., and Summerbell, R. C. (2018). "Fungal Communities in Hydrocarbon Degradation," in *Microbial Communities Utilizing Hydrocarbons and Lipids: Members, Metagenomics and Ecophysiology.*

Handbook of Hydrocarbon and Lipid Microbiology, ed. T. McGenity (Cham: Springer), doi: 10.1007/978-3-319-60063-5_8-1

Prince, R. C. (2005). "The microbiology of marine oil spill bioremediation," in *Petroleum Microbiology*, eds B. Oliver and M. Magot (Washington, D.C: ASM Press), 317–335. doi: 10.1128/9781555817589.ch16

Prince, R. C., and Walters, C. C. (2007). "Biodegradation of oil hydrocarbons and its implications for sorce identification," in *Oil Spill Environmental Forensics, Fingerprinting and Source Identification*, eds Z. Wang and S. A. Stout (Amsterdam: Elsevier), 349–379.

Quemener, M., Mara, P., Schubotz, F., Beaudoin, D., Li, W., Pachiadaki, M., et al. (2020). Meta−Omics highlights the diversity, activity and adaptations of fungi in deep oceanic crust. *Environ. Microbiol.* 22, 3950–3967. doi: 10.1111/1462-2920.15181

Rabus, R., Boll, M., Heider, J., Meckenstock, R. U., Buckel, W., Einsle, O., et al. (2016). Anaerobic microbial degradation of hydrocarbons: from enzymatic reactions to the environment. *J. Mol. Microbiol. Biotechnol.* 26, 5–28. doi: 10.1159/000443997

Raghukumar, C., and Raghukumar, S. (1998). Barotolerance of the fungi isolated from the deep-sea sediments. *Aquat. Microb. Ecol.* 15, 153–163. doi: 10.1128/jb.95.1.211-220.1968

Ramírez, G. A., McKay, L. J., Fields, M. W., Buckley, A., Mortera, C., Hensen, C., et al. (2020). The Guaymas Basin subseafloor sedimentary Archaeome reflects complex environmental histories. *iScience* 23:101459. doi: 10.1016/j.isci.2020.101459

Ramírez, G. A., Paraskevi, V. M., Sehein, T., Wegener, G., Chambers, C. R., Joye, S. B., et al. (2021). Environmental controls on bacterial, archaeal and fungal community structure in hydrothermal sediments of Guaymas Basin, Gulf of California. *PLoS One* 16:e0256321. doi: 10.1371/journal.pone.0256321

Ravelet, C., Grosset, C., Krivobok, S., Montuelle, B., and Alary, J. (2001). Pyrene degradation by two fungi in a freshwater sediment and evaluation of fungal biomass by ergosterol content. *Appl. Microbiol. Biotechnol.* 56, 803–808. doi: 10.1007/s002530100689

Ravelet, C., Krivobok, S., Sage, L., and Steiman, R. (2000). Biodegradation of pyrene by sediment fungi. *Chemosphere* 40, 557–563. doi: 10.1016/s0045-6535(99)00320-3

Renxing, L., Davidova, I. A., Teske, A., and Suflita, J. M. (2021). "Evidence for the anaerobic biodegradation of higher molecular weight hydrocarbons in the Guaymas Basin," in *The 18th International Biodeterioration and Biodegradation Symposium*, Amsterdam: Elsevier.

Robador, A., Muller, A. L., Sawicka, J. E., Berry, D., Hubert, C. R. J., Loy, A., et al. (2016). Activity and community structures of sulfate-reducing microorganisms in polar, temperate and tropical marine sediments. *ISME J.* 10, 796–809. doi: 10.1038/ismej.2015.157

Rothermich, M. M., Hayes, L. A., and Lovley, D. R. (2002). Anaerobic, sulfate-dependent degradation of polycyclic aromatic hydrocarbons in petroleum-contaminated harbor sediment. *Environ. Sci. Technol.* 36, 4811–4817. doi: 10.1021/es0200241

Ruff, E., Biddle, J. F., Teske, A., Knittel, K., Boetius, A., and Ramette, A. (2015). Global dispersion and local diversification of the methane seep microbiome. *Proc. Natl. Acad. Sci. USA* 112, 4015–4020. doi: 10.1073/pnas.1421865112

Rüter, P., Rabus, R., Wilkes, H., Aeckersberg, F., Rainey, F. A., Jannasch, H. W., et al. (1994). Anaerobic oxidation of hydrocarbons in crude oil by new types of sulphate-reducing bacteria. *Nature* 372, 455–458. doi: 10.1038/372455a0

Sajna, K. V., Sukumaran, R. K., Gottumukkala, L. D., and Pandey, A. (2015). Crude oil biodegradation aided by biosurfactants from *Pseudozyma* sp. NII 08165 or its culture broth. *Biores. Technol.* 191, 133–139.

Šašek, V., Cajthaml, T., and Bhatt, M. (2003). Use of fungal technology in soil remediation: A case study. *Water Air Soil Pollut.* 3, 5–14.

Schreiber, L., Holler, T., Knittel, K., Meyerdierks, A., and Amann, R. (2010). Identification of the dominant sulfate-reducing bacterial partner of anaerobic methanotrophs of the ANME-2 clade. *Environ. Microbiol.* 12, 2327–2340. doi: 10.1111/j.1462-2920.2010.02275.x

Sen, S., Borah, S. N., Bora, A., and Deka, S. (2017). Production, characterization, and antifungal activity of a biosurfactant produced by *Rhodotorula babjevae* YS3. *Micro. Cell Fact.* 16:95. doi: 10.1186/s12934-017-0711-z

Shekhar, S., Sundaramanickam, A., and Balasubramanian, T. (2015). Biosurfactant producing microbes and their potential applications: A review. *Crit. Rev. in Environ. Sci. Technol.* 45, 1522–1554. doi: 10.1080/10643389.2014.955631

Shin, B., Kim, M., Zengler, K., Chin, K. J., Overholt, W. A., Gieg, L. M., et al. (2019). Anaerobic degradation of hexadecane and phenanthrene coupled to sulfate reduction by enriched consortia from northern Gulf of Mexico seafloor sediment. *Sci. Rep.* 9:1239. doi: 10.1038/s41598-018-36567-x

Siddique, T., Fedorak, P. M., MacKinnon, M. D., and Foght, J. M. (2007). Metabolism of BTEX and naphtha compounds to methane in oil sands tailings. *Environ. Sci. Technol.* 41, 2350–2356. doi: 10.1021/es062852q

Siddique, T., Penner, T., Semple, K., and Foght, J. M. (2011). Anaerobic biodegradation of longer-chain n- alkanes coupled to methane production in oil sands tailings. *Environ. Sci. Technol.* 45, 5892–5899. doi: 10.1021/es200649t

Silva, R. F., Almeida, D. G., Rufino, R. D., Luna, J. M., Santos, V. A., and Sarubbo, L. A. (2014). Applications of Biosurfactants in the Petroleum Industry and the Remediation of Oil Spills. *Int. J. Mol. Sci.* 15, 12523–12542. doi: 10.3390/ijms150712523

Simonato, F., Campanaro, S., Lauro, F. M., Vezzi, A., D'Angelo, M., and Vitulo, N. (2006). Piezophilic adaptation: a genomic point of view. *J. Biotechnol.* 126, 11–25. doi: 10.1016/j.jbiotec.2006.03.038

Singh, P., Raghukumar, C., Verma, P., and Shouche, Y. (2010). Phylogenetic diversity of culturable fungi from the deep-sea sediments of the Central Indian Basin and their growth characteristics. *Fungal Diver.* 40, 89–102.

So, C. M., and Young, L. Y. (2001). Anaerobic biodegradation of alkanes by enriched consortia under four different reducing conditions. *Environ. Toxicol. Chem.* 20, 473–478. doi: 10.1002/etc.5620200303

Soberón-Chávez, G., and Maier, R. M. (2011). *Biosurfactants: a general overview. In Biosurfactants*. Berlin: Springer, 1–11.

Song, M., Schubotz, F., Kellermann, M. Y., Hansen, C. T., Bach, W., Teske, A., et al. (2021). Formation of ethane and propane via abiotic reductive conversion of acetic acid in hydrothermal sediments. *Proc. Natl. Acad. Sci. USA* 118:e2005219118. doi: 10.1073/pnas.2005219118

Soule, S. A., Seewald, J., Wankel, S., Michel, A., Beinart, R., Escobar Briones, E., et al. (2018). Exploration of the Northern Guaymas Basin. *Oceanography* 31, 39–41.

Steliga, T. (2008). Optimization research on biodegradation of hydrocarbon pollutions in weathering soil samples from manufactured gas plant (MGP). *Arch. Environ. Protect.* 34, 51–70.

Steliga, T. (2012). Role of Fungi in biodegradation of petroleum hydrocarbons in drill waste. *Pol. J. Environ. Stud.* 21, 471–479.

Tahir, A., Fletcher, T. C., Houlihan, D. F., and Secombes, C. J. (1993). Effect of short-term exposure to oil-contaminated sediments on the immune response of dab, *Limanda limanda* (L.). *Aquat. Toxicol.* 27, 71–82. doi: 10.1016/0166-445x(93)90048-6

Tan, B., Nesbø, C., and Foght, J. (2014). Re-analysis of omics data indicates *Smithella* may degrade alkanes by addition to fumarate under methanogenic conditions. *ISME J.* 8, 2353–2356. doi: 10.1038/ismej.2014.87

Teske, A. (2019). "Hydrocarbon-degrading anaerobic microbial communities in natural oil seeps," in *Microbial Communities Utilizing Hydrocarbons and Lipids: Members, Metagenomics and Ecophysiology, Handbook of Hydrocarbon and Lipid Microbiology*, ed. T. J. McGenity (Berlin: Springer), doi: 10.1007/978-3-319-60063-5_3-2

Teske, A. (2020). "Guaymas Basin, a hydrothermal hydrocarbon seep ecosystem," in *Marine Hydrocarbon Seeps - Microbiology and Biogeochemistry of a Global Marine Habitat*, eds A. Teske and V. Carvalho (Berlin: Springer), 43–68. doi: 10.1007/978-3-030-34827-4_3

Teske, A., Callaghan, A. V., and LaRowe, D. E. (2014). Biosphere frontiers of subsurface life in the sedimented hydrothermal system of Guaymas Basin. *Front. Microbiol.* 5:362. doi: 10.3389/fmicb.2014.00362

Teske, A., de Beer, D., McKay, L., Tivey, M. K., Biddle, J. F., Hoer, D., et al. (2016). The Guaymas Basin hiking guide to hydrothermal mounds, chimneys and microbial mats: complex seafloor expressions of subsurface hydrothermal circulation. *Front. Microbiol.* 7:75. doi: 10.3389/fmicb.2016.00075

Teske, A., Lizarralde, D., and Höfig, T. W. (2018). *Expedition 385 Scientific Prospectus: Guaymas Basin Tectonics and Biosphere*. College Station, TX: International Ocean Discovery Program. iodp.sp.385.2018 doi: 10.14379/

Teske, A., Lizarralde, D., Höfig, T. W., Aiello, I. W., Ash, J. L., Bojanova, D. P., et al. (2021b). "Expedition 385 summary. *In* Teske, A., Lizarralde, D., Höfig, T.W., and the Expedition 385 Scientists, *Guaymas Basin Tectonics and Biosphere*," in *Proceedings of the International Ocean Discovery Program, 385*, (College Station,

TX: International Ocean Discovery Program), doi: 10.14379/iodp.proc.385.101.2021

Teske, A., Lizarralde, D., Höfig, T. W., Aiello, I. W., Ash, J. L., Bojanova, D. P., et al. (2021c). "Expedition 385 methods," in *Guaymas Basin Tectonics and Biosphere*. Proceedings of the International Ocean Discovery Program, 385, eds A. Teske, D. Lizarralde, and T. W. Höfig (College Station, TX: International Ocean Discovery Program), doi: 10.14379/iodp.proc.385.102.2021

Teske, A., McKay, L. J., Ravelo, A. C., Aiello, I., Mortera, C., Núñez-Useche, F., et al. (2019). Characteristics and Evolution of sill-driven off-axis hydrothermalism in Guaymas Basin – the Ringvent site. *Sci. Rep.* 9:13847. doi: 10.1038/s41598-019-50200-5

Teske, A., Wegener, J. P., Chanton, D., White, B. J., MacGregor, D., Hoer, D., et al. (2021a). Microbial communities under distinct thermal and geochemical regimes in axial and off-axis sediments of Guaymas Basin. *Front. Microbiol.* 12:633649. doi: 10.3389/fmicb.2021.633649

Teske, A., Hinrichs, K.-U., Edgcomb, V., de Vera Gomez, A., Kysela, D., Sylva, S. P., et al. (2002). Microbial diversity in hydrothermal sediments in the Guaymas Basin: Evidence for anaerobic methanotrophic communities. *Appl. Environ. Microbiol.* 68, 1994–2007.

Velez, P., Gasca-Pineda, J., and Riquelma, M. (2020). Cultivable fungi from deep-sea oil reserves in the Gulf of Mexico: Genetic signatures in response to hydrocarbons. *Mar. Environ. Res.* 153:104816. doi: 10.1016/j.marenvres.2019.104816

Ventura, G. T., Simoneit, B. R. T., Nelson, R. K., and Reddy, C. M. (2012). The composition, origin and fate of complex mixtures in the maltene fractions of hydrothermal petroleum assayed by comprehensive two-dimensional gas chromatography. *Org. Geochem.* 45, 48–65. doi: 10.1016/j.orggeochem.2012.01.002

Waite, D. W., Chuvochina, M., Pelikan, C., Parks, D. H., Yilmaz, P., Wagner, M., et al. (2020). Proposal to reclassify the *proteobacteria*l classes Delta*proteobacteria* and Oligoflexia, and the phylum Thermodesulfobacteria into four phyla reflecting major functional capabilities. *Int. J. Syst. Evol. Microbiol.* 70, 5922–6016. doi: 10.1099/ijsem.0.004213

Walker, J. D., and Colwell, R. R. (1975). Degradation of hydrocarbons and mixed hydrocarbon substrate by microorganisms from Chesapeake Bay. *Progr. Water Technol.* 7, F83–F91. doi: 10.1139/m75-044

Wattiau, P. (2002). "Microbial aspects in bioremediation of polluted by polyaromatic hydrocarbons," in *Biotechnology for the Environment: Strategy and Fundamentals, Focus on Biotechnology*, eds S. N. Agathos and W. Reineke (Dordrecht: Springer), 69–89. doi: 10.1007/978-94-010-0357-5_5

Wawrik, B., Marks, C. R., Davidova, I. A., McInerney, M. J., Pruitt, S., Duncan, K. E., et al. (2016). Methanogenic paraffin degradation proceeds via the alkane addition to fumarate by *Smithella* spp. mediated by a syntrophic coupling with hydrogenotrophic methanogens. *Environ. Microbiol.* 18, 2604–2619. doi: 10.1111/1462-2920.13374

Wegener, G., Krukenberg, V., Riedel, D., Tegetmeyer, H. E., and Boetius, A. (2015). Intracellular wiring enables electron transfer between methanotrophic archaea and bacteria. *Nature* 526, 587–590. doi: 10.1038/nature15733

Widdel, F., and Bak, F. (1992). "Gram-negative mesophilic sulfate-reducing bacteria," in *The Prokaryotes*. Second edition, eds A. Balows, H. G. Trüper, M. Dworkin, W. Harder, and K. H. Schleifer (New York, NY: Springer), 3352–3378. doi: 10.1128/AEM.65.4.1516-1523.1999

Wiesche, C., Martens, R., and Zadrazil, F. (2003). The effect of interaction between white-root fungi and indigenous microorganisms on degradation of polycyclic aromatic hydrocarbons in soil. *Water Air Soil Pollut.:Focus* 3, 73–79. doi: 10.1023/A:1023944527951

Winkel, M., De Beer, D., Lavik, G., Peplies, J., and Mussmann, M. (2014). Close association of active nitrifyers with *Beggiatoa* mats covering deep-sea hydrothermal sediments. *Environ. Microbiol.* 16, 1612–1626. doi: 10.1111/1462-2920.12316

Worden, A. Z., Follows, M. J., Giovannoni, S. J., Wilkin, S., Zimmerman, A. E., and Keeling, P. J. (2015). Rethinking the marine carbon cycle: Factoring in the multifarious lifestyles of microbes. *Science* 347:1257594. doi: 10.1126/science.1257594

Yadav, J. S., and Reddy, C. A. (1993). Degradation of benzene, toluene, ethylbenzene, and xylenes (BTEX) by the lignin –degrading basidiomycete *Phanerochaete chrysosporium*. *Appl. Environ. Microbiol.* 53, 756–762. doi: 10.1128/aem.59.3.756-762.1993

Zengler, K., Richnow, H. H., Rossello-Mora, R., Michaelis, W., and Widdel, F. (1999). Methane formation from long-chain alkanes by anaerobic microorganisms. *Nature* 401, 266–269. doi: 10.1038/45777

Zheng, Z., and Obbard, J. P. (2001). Effect of non-ionic surfactants on elimination of polycyclic aromatic hydrocarbons (PAHs) in soil-slurry by *Phanerochaete chrysosporium*. *J. Chem. Technol. Biotechnol.* 76, 423–429. doi: 10.1002/jctb.396

Conflict of Interest: The authors declare that the research was conducted in the absence of any commercial or financial relationships that could be construed as a potential conflict of interest.

Publisher's Note: All claims expressed in this article are solely those of the authors and do not necessarily represent those of their affiliated organizations, or those of the publisher, the editors and the reviewers. Any product that may be evaluated in this article, or claim that may be made by its manufacturer, is not guaranteed or endorsed by the publisher.

frontiers in Microbiology

ORIGINAL RESEARCH
published: 15 March 2022
doi: 10.3389/fmicb.2022.844735

A Novel NADP-Dependent Formate Dehydrogenase From the Hyperthermophilic Archaeon *Thermococcus onnurineus* NA1

Ji-in Yang[1,2], Seong Hyuk Lee[1], Ji-Young Ryu[1†], Hyun Sook Lee[1,2] and Sung Gyun Kang[1,2]**

[1]Marine Biotechnology Research Centre, Korea Institute of Ocean Science and Technology, Busan, South Korea,
[2]Department of Marine Biotechnology, KIOST School, University of Science and Technology, Daejeon, South Korea

OPEN ACCESS

Edited by:
Andreas Teske,
University of North Carolina at Chapel Hill, United States

Reviewed by:
Volker Müller,
Goethe University Frankfurt, Germany
Baris Binay,
Gebze Technical University, Turkey

***Correspondence:**
Hyun Sook Lee
leeh522@kiost.ac.kr
Sung Gyun Kang
sgkang@kiost.ac.kr

†Present address:
Ji-Young Ryu,
Korean Agency for Technology and Standards, Eumseong, South Korea

Specialty section:
This article was submitted to Extreme Microbiology, a section of the journal Frontiers in Microbiology

Received: *28 December 2021*
Accepted: *03 February 2022*
Published: *15 March 2022*

Citation:
Yang J-i, Lee SH, Ryu J-Y, Lee HS and Kang SG (2022) A Novel NADP-Dependent Formate Dehydrogenase From the Hyperthermophilic Archaeon Thermococcus onnurineus NA1. Front. Microbiol. 13:844735. doi: 10.3389/fmicb.2022.844735

The genome of the hyperthermophilic archaeon *Thermococcus onnurineus* NA1 contains three copies of the formate dehydrogenase (FDH) gene, *fdh1*, *fdh2*, and *fdh3*. Previously, we reported that *fdh2*, clustered with genes encoding the multimeric membrane-bound hydrogenase and cation/proton antiporter, was essential for formate-dependent growth with H_2 production. However, the functionality of the other two FDH-coding genes has not yet been elucidated. Herein, we purified and characterized cytoplasmic Fdh3 to understand its functionality. The purified Fdh3 was identified to be composed of a tungsten-containing catalytic subunit (Fdh3A), an NAD(P)-binding protein (Fdh3B), and two Fe-S proteins (Fdh3G1 and Fdh3G2). Fdh3 oxidized formate with specific activities of 241.7 U/mg and 77.4 U/mg using methyl viologen and $NADP^+$ as electron acceptors, respectively. While most FDHs exhibited NAD^+-dependent formate oxidation activity, the Fdh3 of *T. onnurineus* NA1 showed a strong preference for $NADP^+$ over NAD^+ as a cofactor. The catalytic efficiency (k_{cat}/K_m) of Fdh3 for $NADP^+$ was measured to be 5,281 $mM^{-1}\,s^{-1}$, which is the highest among NADP-dependent FDHs known to date. Structural modeling suggested that Arg^{204} and Arg^{205} of Fdh3B may contribute to the stabilization of the 2′-phosphate of NADP(H). Fdh3 could also use ferredoxin as an electron acceptor to oxidize formate with a specific activity of 0.83 U/mg. Furthermore, Fdh3 showed CO_2 reduction activity using reduced ferredoxin or NADPH as an electron donor with a specific activity of 0.73 U/mg and 1.0 U/mg, respectively. These results suggest a functional role of Fdh3 in disposing of reducing equivalents by mediating electron transfer between formate and NAD(P)H or ferredoxin.

Keywords: formate dehydrogenase, formate oxidation, NAD(P) reduction, ferredoxin reduction, carbon dioxide reduction, *Thermococcus onnurineus* NA1

INTRODUCTION

Formate dehydrogenase (FDH), a ubiquitous enzyme in prokaryotes and eukaryotes, catalyzes the reversible oxidation of formate to carbon dioxide (CO_2). FDHs are highly diverse in metal contents, subunit composition, types of redox cofactors, and their physiological roles (Hartmann et al., 2015). FDHs can be divided into two main classes according to their metal content/structure and

catalytic strategy: metal-independent FDHs and metal-containing FDHs. The metal-containing FDH class is comprised of molybdenum or tungsten-containing enzyme families, mainly derived from bacteria and archaea, while metal-independent FDH class enzymes are more abundant in aerobic bacteria, yeasts, fungi, and plants (Maia et al., 2015). In contrast to metal-independent FDH, which mediates direct hydride transfer from formate to NAD^+, in metal-containing FDH, the transfer of proton and electrons is mediated by the metal center in the active site and there is no direct proton/electron transfer between formate and the electron acceptor (Maia et al., 2015, 2017). The active site of FDHs is conserved and consists of three amino acids, Cys (or SeCys)-His-Arg. Many of them are known to be oxygen-labile, and FDHs containing tungsten or SeCys are generally more sensitive to oxygen (Nielsen et al., 2019). However, there are exceptions to this trend. For example, FDH of *Methylobacterium extorquens* AM1 containing tungsten was found to be oxygen tolerant (Laukel et al., 2003). The mechanism of oxygen-induced loss of activity has not yet been investigated in detail.

Prokaryotic FDHs contribute to diverse formate metabolism. For example, a hydrogen-dependent carbon dioxide reductase (HDCR) complex containing FdhF has been demonstrated to generate formate as an energy metabolic intermediate in the acetogenic bacteria *Acetobacterium woodii* and *Thermoanaerobacter kivui* (Schuchmann and Müller, 2013; Schwarz et al., 2018; Müller, 2019). Likewise, FDH in *Clostridium autoethanogenum* and *Clostridium acidurici* forms a complex with electron-bifurcating hydrogenase to reduce CO_2 to formate as a biosynthetic precursor (Wang et al., 2013a,b). A variety of respiratory chains containing FDH benefit from formate oxidation coupled with the reduction of various terminal electron acceptors, such as nitrate, sulfate, polysulfide, fumarate, carbon dioxide, iron (Fe^{3+}), arsenate, oxygen, or even protons (Kim et al., 2010; Maia et al., 2015). In *Corynebacterium glutamicum*, FdhF oxidizes formate to CO_2 in the methanol oxidation pathway (Witthoff et al., 2013). A variety of bacteria possess a formate-hydrogen lyase composed of hydrogenase and FDH to detoxify formate as an end product during fermentation (Rittmann et al., 2015). Although the biochemical properties and physiological roles of FDHs are well studied in bacteria, research on FDHs in hyperthermophilic archaea is very limited.

On the other hand, FDHs are promising biocatalysts for the conversion of $NAD(P)^+$ to NAD(P)H for industrial applications. Many industrially interesting reactions catalyzed by oxidoreductases require NAD(P)H as a cofactor, and NADPH regeneration is a key issue since most biosynthetic reactions depend on NADPH, which is not feasible to add externally (Woodyer et al., 2005; Alpdagtas and Binay, 2020). Enzymatic NADPH regeneration methods have been developed by using glucose dehydrogenase, glucose-6-phosphate dehydrogenase, alcohol dehydrogenase, and FDH. One of the weaknesses of these enzymes is the accumulation of byproducts. For example, glucose dehydrogenase produces gluconolactone, glucose-6-phosphate dehydrogenase produces 6-phosphogluconolactone, and alcohol dehydrogenase produces aldehyde as a byproduct (Eckstein et al., 2004; Lee et al., 2007; Xu et al., 2021). The accumulation of nonvolatile byproducts requires additional separation processes that can affect cost (Wang et al., 2017). FDH has advantages over other enzymes in terms of low substrate cost and no byproduct accumulation. Therefore, many researchers have attempted protein engineering using FDHs to switch their substrate specificity from NAD^+ to $NADP^+$ or to discover novel enzymes which are naturally dependent to $NADP^+$ over NAD^+ (Wu et al., 2009; Alpdagtas et al., 2018).

Previously, we reported that the hyperthermophilic archaeon *Thermococcus onnurineus* NA1 was able to grow by formate oxidation coupled with H_2 production through the concerted activities of Fdh2 (TON_1563-TON_1564), Mfh2 hydrogenase (TON_1565-TON_1571), and Mnh2 Na^+/H^+ antiporter (TON_1574-TON_1580; Kim et al., 2010). Subsequently, we demonstrated that formate oxidation leads to H^+ translocation across the cytoplasmic membrane, driving Na^+ translocation to form a sodium motive force (Lim et al., 2014). The genome of *T. onnurineus* NA1 encodes two more copies of genes, *fdh1* (TON_0281) and *fdh3* (TON_0539), annotated as putative formate dehydrogenase catalytic subunits (Lee et al., 2008). While Fdh2 plays an essential role in formate-dependent growth, the physiological role of these FDHs has not been determined. A recent study suggested that the two gene clusters coding for a formate-hydrogen lyase and a putative formate dehydrogenase-NAD(P)H oxidoreductase may contribute to reducing equivalent disposal under specific conditions pressurized with H_2, which is near thermodynamic equilibrium (Guellec et al., 2021). However, the suggestion related to FDHs was mostly based on bioinformatic analysis and did not accompany any characterization of FDH at the molecular level. In this study, the functional role of Fdh3 in *T. onnurineus* NA1 was investigated by purifying the enzyme and identifying its biochemical properties.

MATERIALS AND METHODS

Strains, Medium, and Cultivation Conditions

The strains used in this study are summarized in **Table 1**. *T. onnurineus* NA1 strains were cultivated at 80°C in MM1 medium (Kim et al., 2013) containing 10 g yeast extract, 35 g NaCl, 0.7 g KCl, 3.9 g $MgSO_4$, 0.4 g $CaCl_2{\bullet}H_2O$, 0.3 g NH_4Cl, 0.15 g Na_2HPO_4, 0.03 g Na_2SiO_3, 0.5 g $NaHCO_3$, 0.5 g cysteine-HCl supplied with 1 ml of 100X trace element solution, 20 ml of 500X Fe-EDTA solution (Holden et al., 2001), 1 ml of vitamin solution (Wolin et al., 1963), and 1 ml of 5% (w/v) $Na_2S{\bullet}9H_2O$ solution per liter. For batch cultures using bioreactors, the medium was purged with argon gas (99.999%) for 1 h to maintain anaerobic conditions at 80°C as described previously (Kim et al., 2010). Then, 100% CO was continuously supplied through a microsparger at a flow rate of 50–100 $ml\,L^{-1}\ min^{-1}$ after inoculation of cells. The agitation speed was 400 rpm, and the working volume of the bioreactors was 5l. The pH was adjusted to 6.1–6.2 using 0.2 N NaOH dissolved in 3.5% NaCl solution.

For purification of a ferredoxin (TON_0317), the *Escherichia coli* Rosetta (DE3) strain harboring the plasmid pET-28a(+)*_fd0317* was cultivated in Luria-Bertani (LB) medium. When the cell density (OD_{600nm}) reached 0.6 under aerobic

TABLE 1 | Strains and their genotype.

Strain	Parent strain	Genotype	References
Thermococcus onnurineus NA1			Lee et al., 2008
156T	NA1	Previously described	Lee et al., 2016
DF01	NA1	*Δfdh1*[a]*Δfdh2*[b]*Δfdh3*[c]	This study
MF01	DF01	P_{0157}-hmg_{pfu}-*fdh3*[d]	This study
MF02	156T	P_{0157}-hmg_{pfu}-*fdh3A*	This study
Escherichia coli			
Rosetta		F- ompT*hsdSB*(rB-mB-)gal*dcm* (DE3) pRARE(CamR)	Novagen
RTN0317	Rosetta	carrying a plasmid pET-28a(+)-*fd0317*	This study

[a]*fdh1, TON_0266-TON_0282.*
[b]*fdh2, TON_1563-TON_1580.*
[c]*fdh3, TON_0539-TON_0542.*
[d]*fdh3, TON_0539-TON_0543.*

conditions, protein expression was induced by the addition of 1 mM isopropyl-β-D-1-thiogalactopyranoside (IPTG, Duksan, Ansan, South Korea) and incubated for 12 h under anaerobic conditions at 37°C.

Construction of Mutants

All mutants were made by applying the gene disruption system with slight modification (Matsumi et al., 2007; Kim et al., 2015). All recombinant plasmids used in this study were constructed by the sequence and ligation-independent cloning (SLIC) method (Jeong et al., 2012). Cells were transformed and incubated in the presence of 10 μM simvastatin as a selection marker. All mutants were isolated by single colony isolation. All primers used for introduction of mutations, gene disruption, and verification of constructs are given in **Supplementary Table 1**.

A parental strain (Δ*fdh1* Δ*fdh2* Δ*fdh3*) was constructed by deleting three gene clusters encoding formate dehydrogenases, *fdh1* (TON_0266-TON_0282), *fdh2* (TON_1563-TON_1580), and *fdh3* (TON_0539-TON_0542). The markerless deletion mutant was generated through homologous recombination and designated DF01 (**Table 1**). Then, an Fdh3 overexpression mutant, designated MF01, was made as follows: the *fdh3* gene cluster (TON_0539-TON_0543) modified with a strong promoter (P_{TN0157}) and the hmg_{pfu} cassette were integrated into the genome of the DF01 strain between TON_1126 and TON_1127 (Lee et al., 2015). The 3-hydroxy-3-methylglutaryl coenzyme A (HMG-CoA) reductase gene from *P. furiosus* is abbreviated hmg_{pfu}. The *fdh3* gene cluster (TON_0539-TON_0543) was amplified using the genomic DNA of *T. onnurineus* NA1 with pUC_TON0539_NHis_F and pUC_TON0543_R primers. The primer was designed to add a 6X-His tag at the N-terminus of TON_0539. The genotype of MF01 was confirmed by PCR (**Supplementary Figure 1A**).

The Fdh3A overexpression mutant was constructed using the 156T strain (Lee et al., 2016), in which the genomic region of the *fdh3* gene was deleted, as follows: The *fdh3A* gene (TON_0539) was amplified using the genomic DNA of *T. onnurineus* NA1 with pUCfdh3-Nhis-slic-F and pUCfdh3-Nhis-slic-R primers. The vector, modified with the addition of left and right arms for homologous recombination, was amplified with pUC-HMG-M-inv-F and pUC-HMG-M-inv-R primers and assembled with the *fdh3A* gene fragment. The *fdh3A* gene with an N-terminal 6X-His tag was integrated into the 156T genome between TON_1126 and TON_1127, resulting in strain MF02 (**Table 1**; **Supplementary Figure 1B**).

The *E. coli* mutant with the TON_0317 gene encoding ferredoxin was constructed as follows: the TON_0317 gene was amplified using the genomic DNA of *T. onnurineus* NA1 with pET_TON0317_F and pET_TON0317_R primers and then inserted into pET-28a(+; Novagen, Madison, WI, United States). The recombinant plasmid, designated pET-28a(+)_*fd0317*, was transformed into the *E. coli* Rosetta (DE3) pLysS strain (Stratagene, La Jolla, CA, United States), resulting in strain RTN0317 (**Table 1**).

Protein Purification

To purify Fdh3, strain MF01 was cultivated using a bioreactor supplied with CO gas, and the harvested cells were resuspended in buffer A (0.1 M Tris–HCl, pH 8.0, 150 mM NaCl, 19 mM KCl, and 10% glycerol) containing EDTA-free protease inhibitor cocktail (cOmplete™, Roche Diagnostics, Mannheim, Germany). Cells were disrupted by sonication and centrifuged (12,000 ×*g*, 40 min, 4°C) for removal of debris. The supernatant was loaded into TALON immobilized metal affinity chromatography (IMAC) resin (Clontech, Mountain View, United States) equilibrated with buffer A. After washing with buffer B (0.1 M Tris–HCl, pH 8.0, 150 mM NaCl, 19 mM KCl, 10% glycerol, and 10 mM imidazole), the Fdh3 protein was eluted with buffer C (0.1 M Tris–HCl, pH 8.0, 150 mM NaCl, 19 mM KCl, 10% glycerol, and 300 mM imidazole). The fractions eluted from TALON IMAC were analyzed by SDS–PAGE, and the fractions containing Fdh3A were applied to a size exclusion chromatography (SEC) column, Superose 6 increase 10/300 Gl (GE Healthcare, Chicago, IL, United States) equilibrated with buffer A. Then, the SEC column was eluted with buffer A at a flow rate of 0.5 ml min^{-1}, and the fractions with absorbance at 280 nm were analyzed by SDS–PAGE.

The Fdh3A protein was also purified for comparative analysis with Fdh3. Strain MF02 was cultivated using a 5-L bioreactor supplied with CO gas. Fdh3A protein was purified by one-step purification using TALON IMAC as described earlier. Ferredoxin Fd_{0317} was purified using TALON IMAC from RTN0317 cultivated under anaerobic conditions (**Table 2**). All purification procedures were performed in an anaerobic chamber. The concentration and purity of the protein were analyzed by protein assay dye reagent (Bio-Rad, Hercules, CA, United States) and SDS–PAGE, respectively. The purified Fd_{0317} was chemically reduced by treatment with a titanium (III)-citrate solution (Zehnder and Wuhrmann, 1976; Jones and Pickard, 1980) and oxidized by treatment with a diamide solution for 1 h at room temperature (Jung et al., 2020).

Metal Content Analysis

The metal content (W, Mo, Fe, and Se) of the protein was determined by inductively coupled plasma–mass spectrometry

TABLE 2 | Specific activities of purified Fdh3 from *Thermococcus onnurineus* NA1.

Electron donors	Electron acceptors	Specific activity (U/mg)
Formate	**MV^{2+}**	241.7 ± 37.9
Formate	**NAD^+**	11.2 ± 0.25
Formate	**$NADP^+$**	77.4 ± 3.5
Formate	**$Fd_{0317(ox)}$**	0.830 ± 0.065
NADPH	**BV^{2+}**	108.6 ± 2.4
NADPH	CO_2	1.00 ± 0.12
$Fd_{0317(red)}$	CO_2	0.728 ± 0.094

One unit is equivalent to the transfer of 2 μmol of electrons per minute. Specific activity was calculated by spectrophotometric detection of the compounds marked in bold.

(ICP–MS). Approximately 2 mg of protein was analyzed by an Agilent 7,700x (Agilent Technologies, Santa Clara, United States) at the KOPTRI Institute (Seoul, South Korea).

Biochemical Characterization of FDH

Formate-dependent methyl viologen (MV)-reducing activity was measured using 100 mM sodium formate and 2 mM MV dissolved in buffer D consisting of 0.1 M Tris–HCl (pH 8.5) and 10% glycerol and 2 mM DTT. A total of 2.4 μg of Fdh3 (or Fdh3A) was used for each reaction. The reduction of MV was monitored at 578 nm ($\varepsilon = 9.78\,mM^{-1}\ cm^{-1}$) by using a UV–VIS spectrophotometer (UV-2600, Shimadzu, Kyoto, Japan; Lovitt et al., 1988).

Formate-dependent $NAD(P)^+$-reducing activity was measured using 100 mM sodium formate and 2 mM $NAD(P)^+$ dissolved in buffer D. A total of 1.2 μg of Fdh3 was used for each reaction. The time-course absorbance change of NAD(P)H generation was measured at 340 nm ($\varepsilon = 6.22\,mM^{-1}\ cm^{-1}$; Elia et al., 2003). NADPH oxidation activity coupled with benzyl viologen (BV) as an electron acceptor was measured by absorbance change at 578 nm of BV.

Formate-dependent ferredoxin-reducing activity was measured using 100 mM sodium formate and 100 μM oxidized ferredoxin dissolved in buffer D. A total of 10 μg of Fdh3 was used for each reaction. The ferredoxin oxidation/reduction activity was measured based on the absorbance change at 425 nm ($\varepsilon = 13\,mM^{-1}\ cm^{-1}$ and $\varepsilon = 28.9\,mM^{-1}\ cm^{-1}$ for the reduced and oxidized forms, respectively; Aono et al., 1989; Nguyen et al., 2017).

Ferredoxin-dependent CO_2 reducing activity was measured using 100 μM reduced ferredoxin and 10 μg of Fdh3 in buffer D saturated with N_2:CO_2 (8:2) gas. NADPH-dependent CO_2 reducing activity was measured using 0.3 mM NADPH and 10 μg of Fdh3 in buffer D saturated with N_2:CO_2 (8:2) gas. The condition saturated with N_2 only was used as a control.

The specific activity of Fdh3 is defined in units (U) per milligram of protein. One unit is equivalent to 2 μmol of electrons per minute. All enzymatic assays were performed in triplicate under anaerobic conditions.

The temperature and pH optima of Fdh3 were determined by measuring formate oxidation activity using MV as an electron acceptor. For the optimal temperature, the activity was measured in the range of 40–95°C in 0.1 M Tris–HCl (pH 8.5). For optimal pH, the activity was measured in 0.1 M Tris–HCl (pH 7.0–9.0) or 0.1 M potassium phosphate (pH 6.0–8.0) at 80°C.

WESTERN BLOT ANALYSIS

Polyclonal antibodies of Fdh2 and Fdh3 were produced after immunization of rabbits with purified proteins by Ab Frontier Co., Ltd. (Seoul, South Korea). Western blot analysis was performed as described previously (Jung et al., 2020) and analyzed using clarity western ECL substrate (Bio-Rad, Hercules, CA, United States). Chemiluminescent signals were visualized using the ChemiDoc MP imaging system (Bio-Rad, Hercules, CA, United States).

RESULTS

Sequence Analysis of Fdh3

The genome of *T. onnurineus* NA1 encodes three copies of genes annotated as putative formate dehydrogenase catalytic subunits, TON_0281 (*fdh1*), TON_1563 (*fdh2*), and TON_0539 (*fdh3*; Lee et al., 2008). The *fdh3* gene is clustered with genes encoding formate transporter (TON_0538), formate dehydrogenase large subunit (TON_0539), three iron–sulfur (Fe-S) proteins (TON_0540, TON_0541, and TON_0543), and NAD(P) binding protein (TON_0542; **Figure 1A**). Previously, it was determined that these six genes are transcribed as one transcriptional unit (Cho et al., 2017).

The gene organization of the *fdh3* gene cluster is conserved in the genomes of many Thermococcales strains (**Figure 1B**). Compared with the *fdh* gene clusters from strains belonging to other phyla, the *fdh3* gene clusters from Thermococcales strains appear to be unique in clustering with several genes encoding Fe-S proteins (Nielsen et al., 2019). Based on the multiple sequence alignment of various FDHs, the catalytic residues of Fdh3 of *T. onnurineus* NA1 can be pinpointed as Cys^{133}-His^{134}-Arg^{324}, which are well conserved in *Escherichia coli*, *Rhodobacter capsulatus*, and *Desulfovibrio gigas* (**Figure 2A**). The structural model of TON_0539 was constructed in SWISS-MODEL[1] using *R. capsulatus* FdsA (PDB-ID: 6TGA; **Figures 2B,C**),[2] which is a subunit of the FDH complex FdsABGD, as a template (Radon et al., 2020). However, other subunits of Fdh3 of *T. onnurineus* NA1 could not be modeled using structures of *R. capsulatus* FDH or other FDHs as a template.

[1]http://swissmodel.expasy.org/
[2]https://www.rcsb.org/

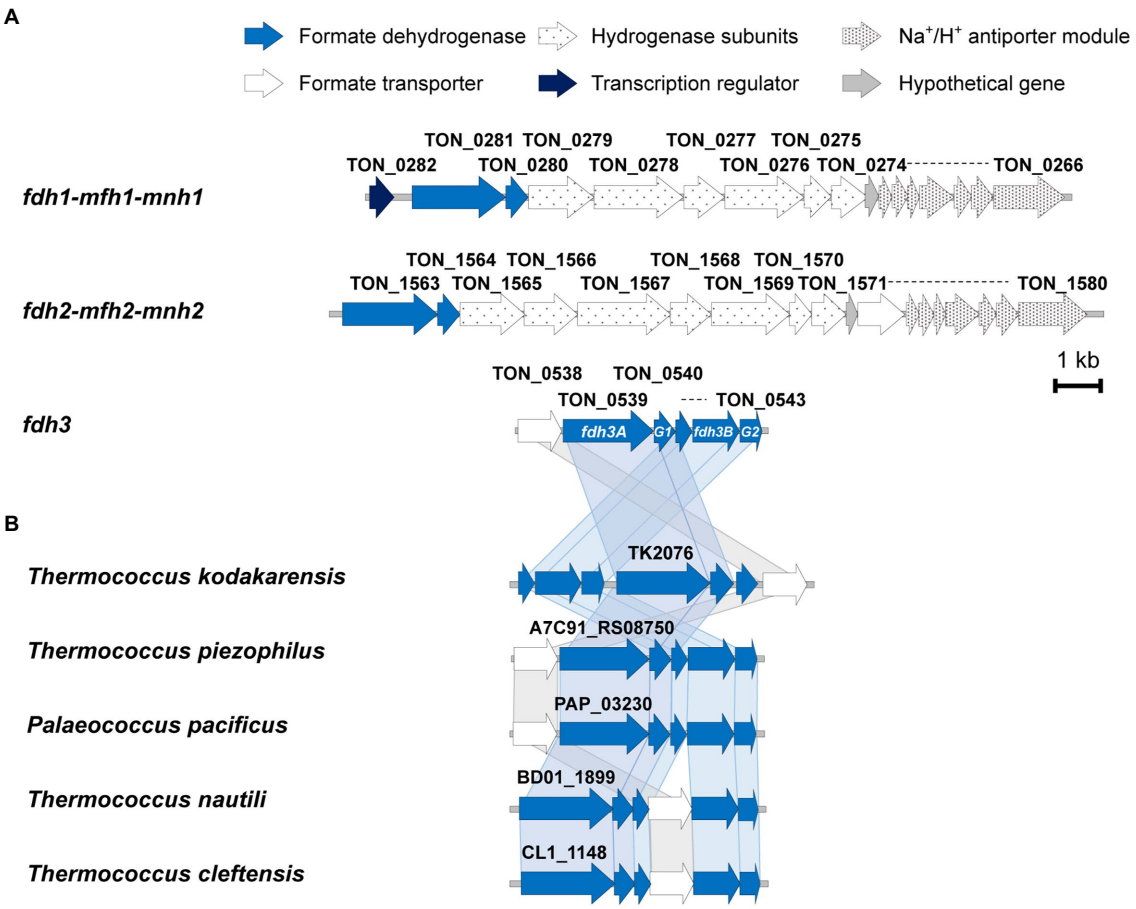

FIGURE 1 | (A) Three formate dehydrogenase gene clusters in *Thermococcus onnurineus* NA1. The *fdh3* gene cluster is composed of six genes, from TON_0538 to TON_0543, transcribed as an operon. On the other hand, the *fdh1* and *fdh2* gene clusters are composed of three modules: a formate dehydrogenase module, a membrane-associated hydrogenase module, and a Na^+/H^+ antiporter module. **(B)** Conservation of the *fdh3* gene cluster in five other Thermococcales species.

Motif analysis revealed that TON_0542 (*fdh3B*) was predicted to have a FAD binding motif, G-X-G-X-X-G (**Figure 2D**). However, the cofactor of TON_0542, a flavin-containing prosthetic group, has not been precisely identified. The structural model of TON_0542 was made in SWISS-MODEL using NADH-dependent ferredoxin $NADP^+$ oxidoreductase I (NfnI) (PDB-ID: 5JCA) of *Pyrococcus furiosus* as a template. Despite substantial differences in *P. furiosus* NfnI, the FAD and NADPH binding domains of TON_0542 could be predicted (**Supplementary Figure 3**). Two arginine residues, Arg^{204} and Arg^{205}, of TON_0542, which are known to contribute to the stabilization of the 2′-phosphate of NADP(H), are in close proximity to the NADP(H) binding pocket (Lubner et al., 2017). These Arg residues were conserved in Fdh3B homologs (**Figures 2D,E**).

Subunit Composition and Metal Content

To purify and characterize Fdh3, an *fdh3* overexpression mutant, designated MF01, was constructed on the Δ*fdh1*, Δ*fdh2*, and Δ*fdh3* backgrounds as described in the Materials and Methods (**Table 1**). MF01 was cultivated in a bioreactor under CO conditions, and MF01 cell lysate was subjected to TALON immobilized metal affinity chromatography (IMAC) and size exclusion chromatography (SEC). Most of the protein eluted as a single peak in SEC, which corresponds to an estimated molecular mass of 524 kDa by the calibration curve (**Figures 3A,B**). Proteins that passed TALON IMAC and subsequent SEC were separated into three major bands by SDS–PAGE (**Figure 3C**).

These three bands were identified by MALDI mass spectrometry as TON_0539 (Fdh3A, 76.5 kDa), TON_0542 (Fdh3B, 39.1 kDa), TON_0540 (Fdh3G1, 18.3 kDa), and TON_0543 (Fdh3G2, 18.7 kDa; **Supplementary Table 2**). The subunit Fdh3A:Fdh3B:Fdh3G1G2 molar ratio was estimated to be 1:1:4. The exact subunit composition of Fdh3 has not yet been determined. The other two proteins of the *fdh3* gene cluster (TON_0538 and TON_0541) were not detected in the protein sample of the major fraction. The putative formate transporter (TON_0538) was predicted to be an integral membrane protein. Therefore, this protein likely interacts with other subunits of Fdh3 but was not expected to be present in the soluble fraction proteins. The absence of a putative Fe-S protein (TON_0541) in the purified protein fraction

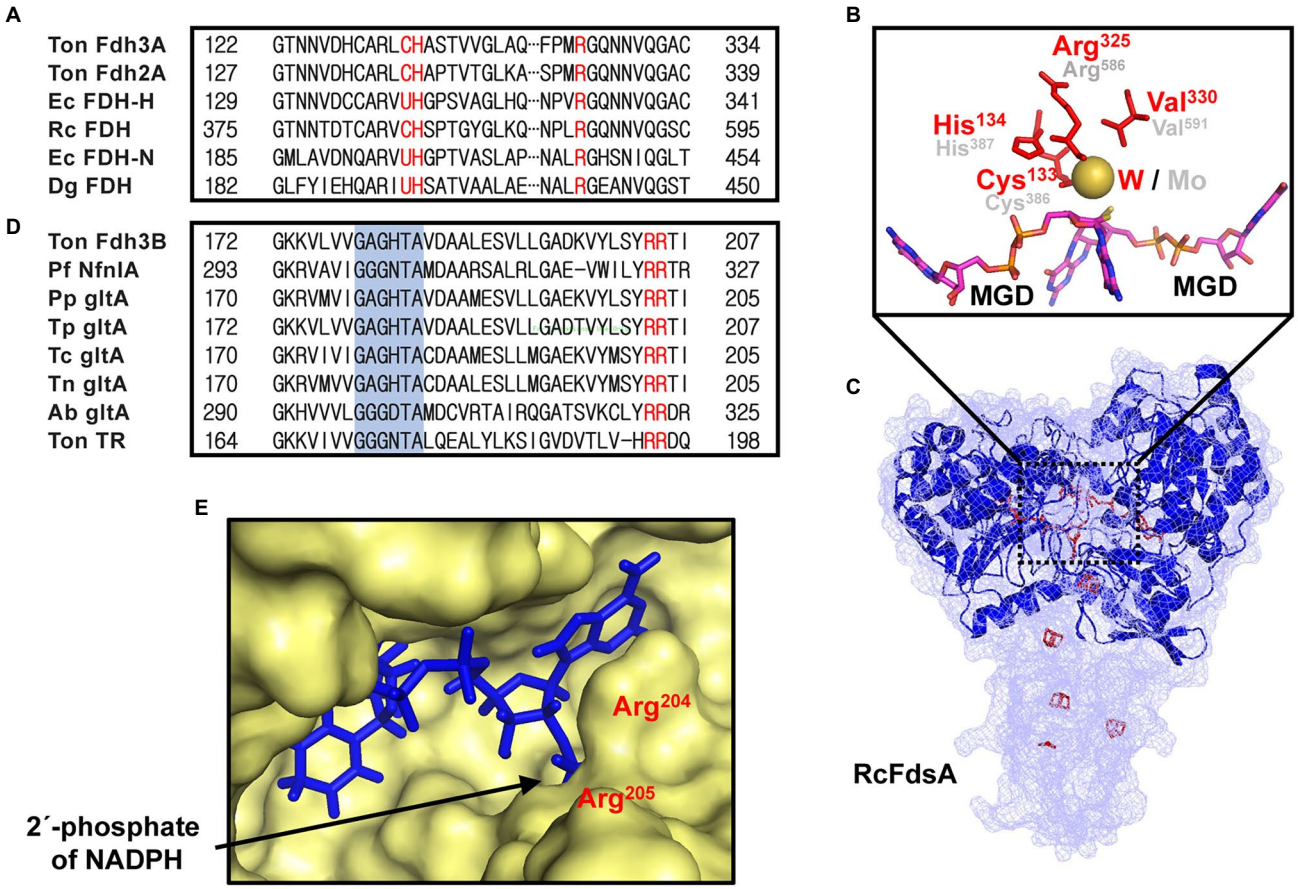

FIGURE 2 | Sequence-based analysis of Fdh3A and Fdh3B. **(A)** Multiple sequence analysis (MSA) of the Fdh3A homologs with the catalytic residues Cys^{133}-His^{134}-Arg^{325}, shown in red. **(B)** SWISS-MODEL of Fdh3A using the RcFDH cryo-EM structure as a template with the conserved residues around metal ions shown in red (Fdh3A) or gray (RcFDH). **(C)** Structure modeling of Fdh3A using SWISS-MODEL (blue ribbon) aligned with RcFdsA (mesh) (PDB-ID: 6TGA). Bis-MGD and Fe-S clusters of RcFdsA are marked in magenta and red, respectively. **(D)** MSA of homologs of Fdh3B with the FAD binding motif GXGXXG, shown in blue. **(E)** Fdh3B modeling using PfNfnI as a template with Arg^{204}-Arg^{205} residues surrounding the 2′-phosphate of NADP (H) shown in red. Ton, *Thermococcus onnurineus*; Ec, *Escherichia coli*; Rc, *Rhodobacter capsulatus*; Dg, *Desulfovibrio gigas*; Pf, *Pyrococcus furiosus*; Pp, *Palaeococcus pacificus*; Tp, *Thermococcsu piezophilus*; Tc, *Thermococcus cleftensis*; Tn, *Thermococcus nautili*; and Ab, *Azospirillum brasilense*.

suggests that it may not be tightly bound to the complex or may not interact with other subunits of the Fdh3 complex under the conditions tested in this study.

The metal content of purified Fdh3 was determined by ICP–MS analysis. Among the tested metals, specifically, molybdenum (Mo), tungsten (W), iron (Fe) and selenium (Se), W, and Fe were detected, but Mo and Se were not. Therefore, it can be concluded that Fdh3 contains W instead of Mo as an essential metal and cysteine instead of selenocysteine as a conserved amino acid in the active site. The content of W was calculated to be less than 10% of the molar fraction of the protein, and W and Fe quantification were not evaluated stoichiometrically.

Formate-Dependent NADP$^+$ Reducing Activity of Fdh3

Based on the molecular composition of the purified Fdh3, we hypothesized that electrons formed from formate oxidation by the catalytic subunit of Fdh3A could be transferred to the NAD(P)-binding domain of Fdh3B *via* the coordination of the Fe-S clusters in Fdh3G1 and Fdh3G2. This possibility was tested using either NAD$^+$ or NADP$^+$, and Fdh3 displayed the activity to oxidize formate while simultaneously reducing NAD(P)$^+$ to NAD(P)H (**Table 2**). The optimum temperature and pH conditions for the formate-dependent NADP$^+$-reducing activity of Fdh3 were determined to be 80°C and pH 8.5, respectively (**Figures 4A,B**). The specific activity of Fdh3 to reduce NAD$^+$ or NADP$^+$ was determined to be 11.2± 0.25 U/mg and 77.4±3.5 U/mg, respectively (**Table 2**). Fdh3A alone did not show NADP$^+$-reducing activity, indicating dependence on Fdh3B (**Figure 4C**; **Supplementary Figure 2A**). The specific activities of formate-dependent methyl viologen reduction of Fdh3 and Fdh3A were similar, so the possibility of malfunction of Fdh3A due to abnormal folding or damage during purification was excluded.

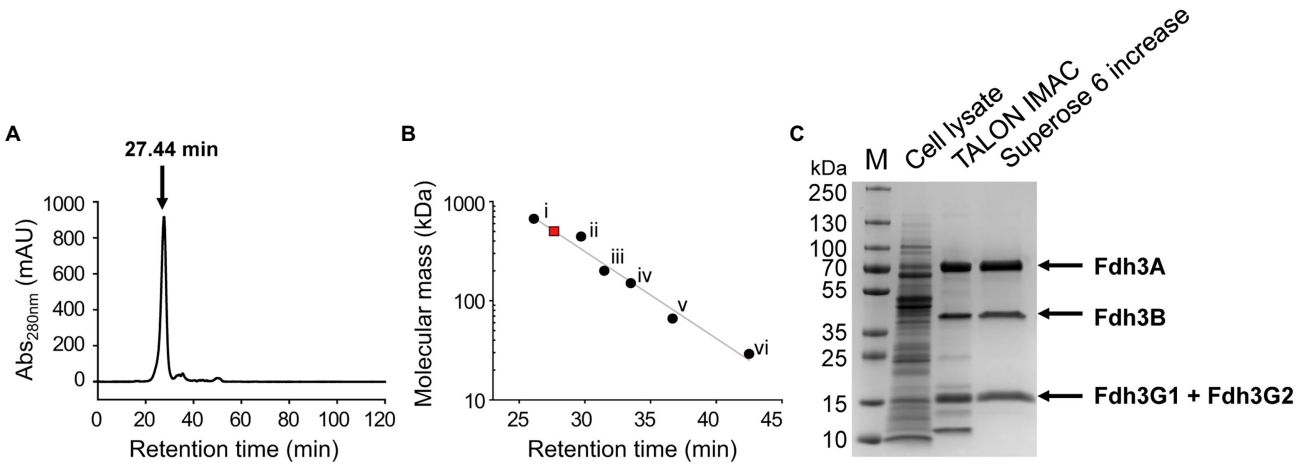

FIGURE 3 | Purification of Fdh3 proteins and SDS–PAGE analysis. **(A)** Elution profile of size exclusion chromatography. **(B)** Linear regression analysis between retention time and logarithm of molecular weight of protein standards ($r^2 = 0.975$). Protein standards were as follows: (i) thyroglobulin (669 kDa), (ii) apoferritin (443 kDa), (iii) β-amlyase (200 kDa), (iv) alcohol dehydrogenase (150 kDa), (v) albumin (66 kDa), and (vi) carbonic anhydrase (29 kDa). The Fdh3 complex corresponding to a molecular mass of 524 kDa is indicated by a red square. **(C)** SDS–PAGE of protein samples at each purification step. Ten micrograms of cell lysate and 5 μg of each of the protein samples from TALON IMAC and Superose 6 Increase were analyzed.

TABLE 3 | Comparison of catalytic efficiency (k_{cat}/K_m) values among NADP-dependent formate dehydrogenases.

k_{cat}/K_m value (mM^{-1} s^{-1})	Organism	References
17.9	*Mycolicibacterium vaccae*	Hoelsch et al., 2013
30	*Burkholderia stabilis*	Hatrongjit and Packdibamrung, 2010
56	*Candida methylica*	Özgün et al., 2016
5,281	*Thermococcus onnurineus* NA1	This study

The K_m and V_{max} of Fdh3 for formate were estimated to be 13.5 mM and 97.6 μmol/min/mg using $NADP^+$ as the electron acceptor. The K_m of Fdh3 for $NADP^+$ was estimated to be 0.040 mM, and the catalytic efficiency (k_{cat}/K_m) was calculated to be 5,281 mM^{-1} s^{-1}, which is the highest value among NADP-dependent FDHs known to date (**Table 3**).

Formate-Dependent Ferredoxin-Reducing Activity of Fdh3

The possibility of Fdh3 using ferredoxin as an electron carrier was investigated. Fd_{0317} (TON_0317), one of the ferredoxins of *T. onnurineus* NA1, can be purified from *E. coli* under anaerobic conditions and tested (**Supplementary Figure 2B**). As a result, Fdh3 could oxidize formate by coupling with Fd_{0317} with a specific activity of 0.830 ± 0.065 U/mg (**Table 2**).

We tested whether Fdh3A could reduce ferredoxin. The formate-dependent ferredoxin-reducing activities of Fdh3A and Fdh3 were determined to be 16.8 ± 0.3 mU/U and 17.9 ± 1.8 mU/U, respectively, based on the same methyl viologen activity (**Figure 4D**). The similar activity between Fdh3A and Fdh3 means that ferredoxin does not require other subunits for interaction with Fdh3A. However, it is difficult to declare that other subunits of Fdh3 are released from Fdh3A upon binding of ferredoxins or that the ferredoxin-reducing activity is certainly dependent on only the catalytic subunit in Fdh3.

CO_2 Reduction Activity of Fdh3

Since most FDHs mediate the reversible reaction of formate oxidation or CO_2 reduction, CO_2 reduction of Fdh3 was tested with NADPH or ferredoxin as an electron donor. The CO_2 reduction activities of Fdh3 coupled with Fd_{0317} and NADPH were determined to be 1.00 ± 0.12 U/mg and 0.728 ± 0.094 U/mg, respectively (**Table 2**). The formate-dependent Fd_{0317} reduction rate was similar to the Fd_{0317}-dependent CO_2 reduction rate (**Table 2**). However, the maximum CO_2 reduction rate could not be determined by the limit of ferredoxin supply.

To investigate any synergistic effect of the coexistence of electron acceptors, $NADPP^+$-reducing activity by formate oxidation was measured with or without Fd_{0317}. The results showed that the $NADPP^+$-reducing activity of Fdh3 was reduced rather than enhanced by the addition of Fd_{0317} (data not shown).

DISCUSSION

In this study, Fdh3 of *T. onnurineus* NA1 was purified and characterized to understand formate metabolism in the strain. The purified Fdh3 was presumed to be a heterotetrameric trimer distinct from the structure of other characterized FDHs.

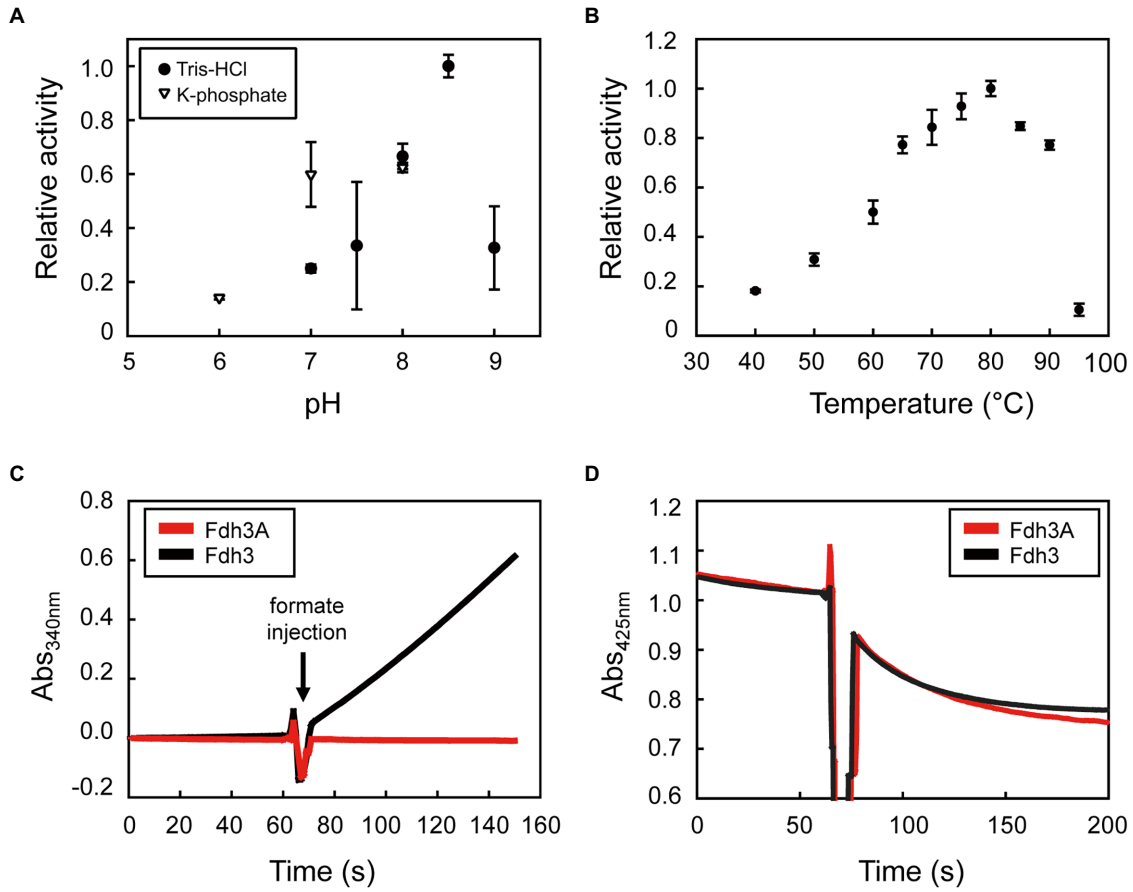

FIGURE 4 | Biochemical properties of Fdh3. **(A)** The pH dependence of Fdh3 determined by formate-dependent $NADP^+$-reducing activity in the pH 6.0–9.0 range in 100 mM potassium phosphate buffer (triangle) or 100 mM Tris–HCl (circle). **(B)** The temperature dependence of Fdh3 determined in the 40–95°C range in 100 mM Tris–HCl (pH 8.5) by measuring formate-dependent $NADP^+$-reducing activity. **(C)** Comparison of formate-dependent $NADP^+$-reducing activity between Fdh3 and Fdh3A. **(D)** Comparison of formate-dependent ferredoxin-reducing activity between Fdh3 and Fdh3A.

The subunit composition of FDH is known to be very diverse, and several FDHs with heterotetrameric structures have been reported (Hartmann et al., 2015). For example, the FDH of *Methylosinus trichosporium* OB3b is a heterotetrameric dimer, $(\alpha\beta\gamma\delta)_2$ (Jollie and Lipscomb, 1991). RcFDH from *R. capsulatus* was also identified as a heterotetrameric dimer, FdsABGD, where FdsD of FdsABGD was not part of FDH and was predicted to act as a chaperone for the insertion of bis-metal-binding pterin (molybdenum or tungsten) guanine dinucleotide (bis-MGD) into FdsA or a stabilizer of the quaternary structure of FdsA (Radon et al., 2020). No homolog of FdsD was detected in the *T. onnurineus* NA1 genome. Despite these examples, a heterotetrameric trimer composition is rare among FDHs. The purified Fdh3 contained only two Fe-S subunits, Fdh3G1 (TON_0540) and Fdh3G2 (TON_0543). Structure modeling of Fdh3G1 and Fdh3G2 using AlphaFold (Jumper et al., 2021) showed that the two subunits are highly similar (**Supplementary Figure 4**). The root-mean-square distance (RMSD) value between the two structures was calculated to be 0.608 Å. However, we cannot exclude the possibility that TON_0541 can associate with Fdh3 under certain conditions. The Fe-S cluster-rich nature of Fdh3 is interesting because Fe-S clusters may contribute to the electron relay between Fdh3A or Fdh3B and other protein(s), conferring other functional roles to Fdh3. Therefore, the study of the interaction between the Fdh3 subunits and the proteins of *T. onnurineus* NA1 expressed in various culture conditions will reveal novel enzymatic properties and *in vivo* functions. Comparative structural analysis with other FDHs can provide a spatial array of electron transfer centers in tetrameric or dimeric complexes, awaiting further study.

Purified Fdh3 could mediate NAD(P)- or ferredoxin-dependent formate oxidation and the reverse reaction. The absence of NAD(P)-dependent formate oxidation activity in Fdh3A suggests that the NAD(P)-dependent activity of Fdh3 is conserved by the catalytic subunit Fdh3A (TON_0539) and the $NAD(P)^+$ binding domain of Fdh3B (TON_0542). Moreover, Fdh3G1 (TON_0540) and Fdh3G2 (TON_0543) seemed likely to transfer electrons between the two subunits. Ferredoxin-dependent activity was detected in both Fdh3A and Fdh3.

The precise composition of the whole complex or spatial orientation of each subunit would help to elucidate the underlying mechanism of the biochemical properties.

T. onnurineus NA1 Fdh3 showed high k_{cat}/K_m value toward $NADP^+$, which can be attributed to the high optimum temperature and low K_m value toward $NADP^+$. Thermophilic FDH of *Moorella thermoacetica* has been reported and the optimum temperature was 70° and 80° for the electron acceptors NADP and MV, respectively (Andreesen and Ljungdahl 1974; Ljungdahl and Andreesen, 1978). The specific activity of formate oxidation using NADP as an electron acceptor was determined to be 34 U/mg for *M. thermoacetica* FDH and 77.4 U/mg for *T. onnurineus* NA1 Fdh3. k_{cat}/K_m value toward $NADP^+$ has not been determined for *M. thermoacetica* FDH. However, the specific mechanism of cofactor dependence and catalytic efficiency are still veiled. The K_m value of Fdh3 toward formate appeared high (13.5 mM). High K_m values toward formate have also been reported for other FDHs, such as *Moraxella* sp. strain C-1 (13 mM; Asano et al., 1988), *Komagataella pastoris* (15 mM; Allais et al., 1983), *Bacillus* sp. F1 (19.6 mM; Ding et al., 2011) and *Kloechkera* sp. No. 2201 (22 mM; Kato et al., 1974).

From a biotechnological perspective, the high conversion efficiency of Fdh3 toward NADPH offers an option for enzymatic NADPH regeneration. Glucose dehydrogenase (Weckbecker and Hummel, 2005), glucose-6-phosphate dehydrogenase (Lee et al., 2007), and alcohol dehydrogenase (Xu et al., 2021) are known to have significantly high conversion efficiency toward NADPH. Unlike the above mentioned enzymes, FDH is advantageous in that it produces only CO_2 without the accumulation of other byproducts. According to the structure modeling of Fdh3B, Arg^{204}-Arg^{205} residues in the putative NADPH binding pocket play an important role to stabilize the 2'-phosphate of NADP(H).

Fdh3 of *T. onnurineus* NA1 was shown to use ferredoxin as an electron carrier. Based on the Fdh3A data, the other subunits, Fdh3B, Fdh3G1, and Fdh3G2, did not seem essential for ferredoxin-dependent activity. The interaction between ferredoxin and FDH has been reported in *Thermococcus kodakarensis* (Burkhart et al., 2019). Fd-2 ferredoxin (TK1087) and FdhA (TK2076) were identified to interact by interactome analysis (Burkhart et al., 2019). Fd-2 and FdhA of *T. kodakarensis* share 88 and 57% identities with Fd_{0317} and Fdh3A of *T. onnurineus* NA1, respectively. We also tested formate oxidation or CO_2 reduction by Fdh3 using another ferredoxin, Fd_{1361}, of *T. onnurineus* NA1 and found highly unstable activity (data not shown). Fd_{1361} shares 73% identity with another Fd-1 ferredoxin (TK1694) of *T. kodakarensis*, of which no interaction with FdhA was observed in the interaction data (Burkhart et al., 2019).

Although ferredoxin-reducing activity was detected, it is not clear whether ferredoxin-dependent formate oxidation can occur *in vivo*. Since most ferredoxins are known to be in a reduced state under anaerobic biological conditions, assuming that the redox potential of ferredoxin is as low as −500 mV, ferredoxin-dependent CO_2 reduction is energetically more favorable than the opposite direction (Li and Elliott, 2016). The first reported ferredoxin-dependent FDH, also called CO_2 reductase, is from *Clostridium pasteurianum* (Scherer and Thauer, 1978). FDH consists of two subunits, FdhA (76 kDa) and FdhB (34 kDa), and was identified to reduce CO_2 to formate with reduced ferredoxin and oxidize formate using ferredoxin as an electron acceptor (Liu and Mortenson, 1984). Recently, it has been reported that ferredoxin reduced by carbon monoxide dehydrogenase can mediate CO_2 reduction by HDCR (Schuchmann and Müller, 2013). In addition to the purified enzyme assay, CO_2 reduction by HDCR using ferredoxin was also implicated in the resting cell assay in the wild-type strain and Δ*hydBA* and Δ*rnf* mutant strains of *A. woodii* (Schwarz et al., 2020). Comparative structural analysis between enzymes may provide a spatial array to elucidate the electron relay mechanism, which awaits further study.

A recent study suggested that gene clusters encoding formate hydrogenlyase or putative FDH-NAD(P)H oxidoreductase may contribute to reducing equivalent disposal under certain conditions with hydrogen pressure (Guellec et al., 2021). Previously, we showed that the *fdh2* gene cluster composed of Fdh2 (TON_1563-TON_1564), Mfh2 hydrogenase (TON_1565-TON_1571), and Mnh2 Na^+/H^+ antiporter (TON_1574-TON_1580) is essential for formate-dependent growth with a series of knockout experiments. Furthermore, the generation of osmotic electron potential and ATP was clearly demonstrated using resting cells in *T. onnurineus* NA1, experimentally demonstrating the role of Fdh2 in ATP generation (Kim et al., 2010; Lim et al., 2014). Even though the *fdh2* gene cluster is mainly responsible for formate oxidation coupled with hydrogen production, the catalytic subunit of Fdh2 may also mediate CO_2 reduction as well as formate oxidation under certain conditions, partly because most formate dehydrogenases mediate reversible reactions of formate oxidation or CO_2 reduction. This study demonstrated that reducing equivalents such as NAD(P)H and ferredoxin could be disposed of by Fdh3 (**Figure 5**). The contribution of Fdh3B (TON_0542) with $NAD(P)^+$ binding domain appears to be important in NAD(P)H disposal. The possibility of Fdh3B working with Fdh2 can be ruled out in two respects. First, the gene encoding Fdh3B was transcribed into a single operon with the fdh3 gene cluster (Cho et al., 2017), whose gene products form a stable complex. Second, we previously reported that the expression of the Fdh3 gene cluster was distinctive from that of the Fdh2 gene cluster in *T. onnurineus* NA1. Fdh3 was upregulated under sulfur-containing conditions, whereas Fdh2 was highly upregulated in the presence of CO or formate (Cho et al., 2017). Meanwhile, Western blotting analysis showed that Fdh3 and Fdh2 were expressed under different conditions (**Supplementary Figure 5**). At the protein level, Fdh3 was highly expressed when carbohydrates or CO was added and weakly expressed under sulfur-containing conditions. On the other hand, Fdh2 was highly expressed in pyruvate-containing medium followed by maltodextrin, formate and CO conditions.

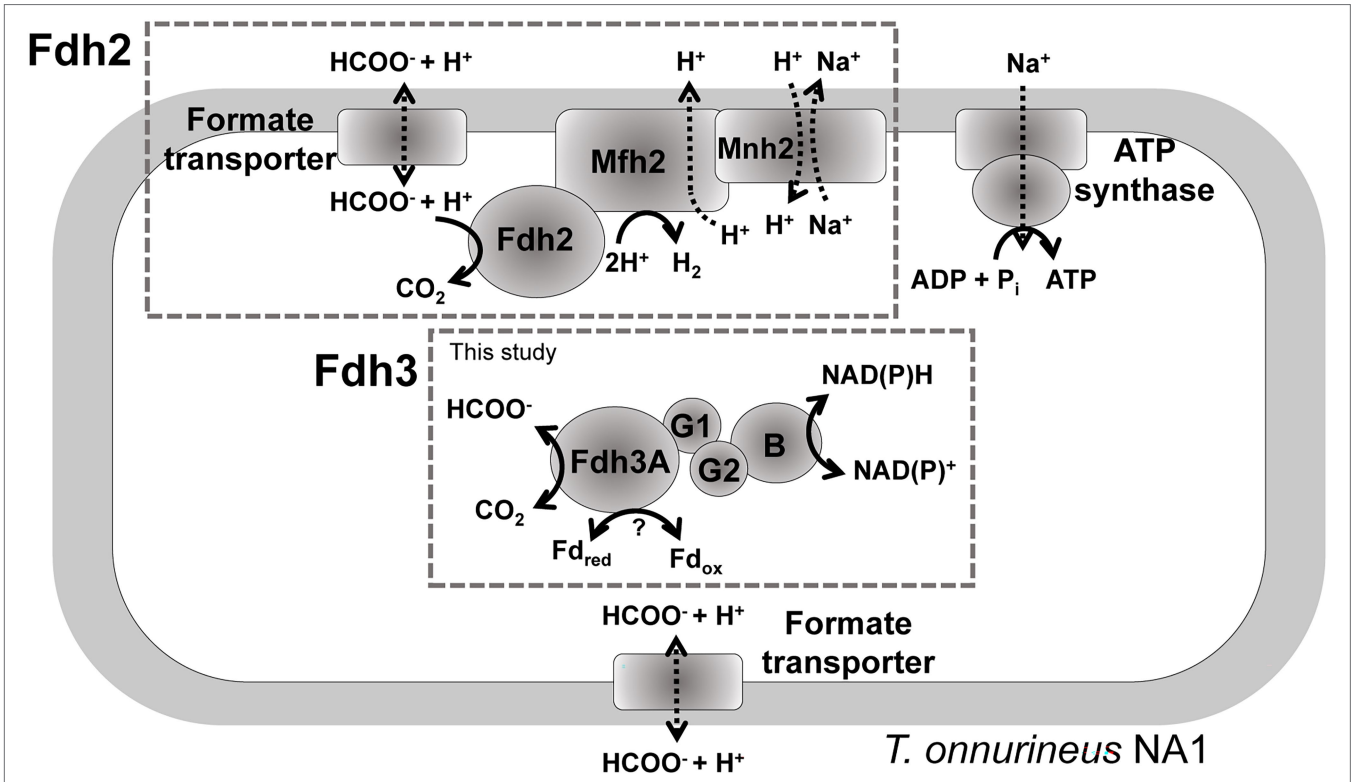

FIGURE 5 | A proposed model for the functional roles of Fdh2 and Fdh3. The schematic diagram does not represent the actual composition of each subunit of Fdh3.

Conclusively, purification and characterization of Fdh3 provided information on the functionality of the protein, suggesting a distinct role for FDH in hyperthermophilic archaea. Many questions remain, and further research will answer them.

DATA AVAILABILITY STATEMENT

The original contributions presented in the study are included in the article/**Supplementary Material**, further inquiries can be directed to the corresponding authors.

AUTHOR CONTRIBUTIONS

SK and HL designed the research. SL and J-YR carried out the experiments. J-iY interpreted the bioinformatic and experimental data analyses. J-iY, SK, and HL wrote the manuscript. All authors have read and approved the manuscript.

FUNDING

This study was funded by the KIOST In-House Program (grant number PE99922) and the Development of Biohydrogen Plant Operation Optimization System program of the Ministry of Oceans and Fisheries in the South Korea.

ACKNOWLEDGMENTS

The authors would like to thank Jae Kyu Lim, Young Jun An, and Hae-Chang Jung of Korea Institute of Ocean Science and Technology for their suggestions for this research.

SUPPLEMENTARY MATERIAL

The Supplementary Material for this article can be found online at: https://www.frontiersin.org/articles/10.3389/fmicb.2022.844735/full#supplementary-material

REFERENCES

Allais, J. J., Louktibi, A., and Baratti, K. (1983). Oxidation of methanol by the yeast *Pichia pastoris*. Purification and properties of the formate dehydrogenase. *Agric. Biol. Chem.* 47, 2547–2554. doi: 10.1271/bbb1961.47.2547

Alpdagtas, S., and Binay, B. (2020). Nadp⁺-dependent formate dehydrogenase: a review. *Biocatal. Biotransform.* 39, 260–268. doi: 10.1080/10242422.2020.1865933

Alpdagtas, S., Yücel, S., Kapkac, H. A., Liu, S., and Binay, B. (2018). Discovery of an acidic, thermostable and highly NADP⁺ dependent formate dehydrogenase from *Lactobacillus buchneri* NRRL B-30929. *Biotechnol. Lett.* 40, 1135–1147. doi: 10.1007/s10529-018-2568-6

Andreesen, J. R., and Ljungdahl, L. G. (1974). Nicotinamide adenine dinucleotide phosphate-dependent formate dehydrogenase from *Clostridium thermoaceticum*: purification and properties. *J. Bacteriol.* 120, 6–14. doi: 10.1128/jb.120.1.6-14.1974

Aono, S., Bryant, F. O., and Adams, M. W. (1989). A novel and remarkably thermostable ferredoxin from the hyperthermophilic archaebacterium *Pyrococcus furiosus*. *J. Bacteriol.* 171, 3433–3439. doi: 10.1128/jb.171.6.3433-3439.1989

Asano, Y., Sekigawa, T., Inukai, H., and Nakazawa, A. (1988). Purification and properties of formate dehydrogenase from *Moraxella* sp. strain C-1. *J. Bacteriol.* 170, 3189–3193. doi: 10.1128/jb.170.7.3189-3193.1988

Burkhart, B. W., Febvre, H. P., and Santangelo, T. J. (2019). Distinct physiological roles of the three ferredoxins encoded in the hyperthermophilic archaeon *Thermococcus kodakarensis*. *mBio* 10, e02807–e02818. doi: 10.1128/mBio.02807-18

Cho, S., Kim, M.-S., Jeong, Y., Lee, B.-R., Lee, J.-H., Kang, S. G., et al. (2017). Genome-wide primary transcriptome analysis of H_2-producing archaeon *Thermococcus onnurineus* NA1. *Sci. Rep.* 7:43044. doi: 10.1038/srep43044

Ding, H.-T., Liu, D.-F., Li, Z.-L., Du, Y.-Q., Xu, X.-H., and Zhao, Y.-H. (2011). Characterization of a thermally stable and organic solvent-adaptive NAD^+-dependent formate dehydrogenase from *Bacillus* sp. F1. *J. Appl. Microbiol.* 111, 1075–1085. doi: 10.1111/j.1365-2672.2011.05124.x

Eckstein, M., Daußmann, T., and Kragl, U. (2004). Recent developments in NAD(P)H regeneration for enzymatic reductions in one- and two-phase system. *Biocatal. Biotransformation* 22, 89–96. doi: 10.1080/10242420410001692769

Elia, A. C., Galarini, R., Taticchi, M. I., Dörr, A. J. M., and Mantilacci, L. (2003). Antioxidant responses and bioaccumulation in *Ictalurus melas* under mercury exposure. *Ecotoxicol. Environ. Saf.* 55, 162–167. doi: 10.1016/S0147-6513(02)00123-9

Guellec, S. L., Leroy, E., Courtine, D., Godfroy, A., and Roussel, E. G. (2021). H_2-dependent formate production by hyperthermophilic *Thermococcales*: an alternative to sulfur reduction for reducing-equivalents disposal. *ISME J.* 15, 3423–3436. doi: 10.1038/s41396-021-01020-x

Hartmann, T., Schwanhold, N., and Leimkühler, S. (2015). Assembly and catalysis of molybdenum or tungsten-containing formate dehydrogenases from bacteria. *Biochim. Biophys. Acta Proteins Proteomics* 1854, 1090–1100. doi: 10.1016/j.bbapap.2014.12.006

Hatrongjit, R., and Packdibamrung, K. (2010). A novel $NADP^+$-dependent formate dehydrogenase from Burkholderia stabilis 15516: screening, purification and characterization. *Enzym. Microb. Technol.* 46, 557–561. doi: 10.1016/j.enzmictec.2010.03.002

Hoelsch, K., Sührer, I., Heusel, M., and Weuster-Botz, D. (2013). Engineering of formate dehydrogenase: synergistic effect of mutations affecting cofactor specificity and chemical stability. *Appl. Microbiol. Biotechnol.* 97, 2473–2481. doi: 10.1007/s00253-012-4142-9

Holden, J. F., Takai, K., Summit, M., Bolton, S., Zyskowski, J., and Baross, J. A. (2001). Diversity among three novel groups of hyperthermophilic deep-sea *Thermococcus* species from three sites in the northeastern Pacific Ocean. *FEMS Microbiol. Ecol.* 36, 51–60. doi: 10.1111/j.1574-6941.2001.tb00825.x

Jeong, J.-Y., Yim, H.-S., Ryu, J.-Y., Lee, H. S., Lee, J.-H., Seen, D.-S., et al. (2012). One-step sequence- and ligation-independent cloning as a rapid and versatile cloning method for functional genomics studies. *Appl. Environ. Microbiol.* 78, 5440–5443. doi: 10.1128/AEM.00844-12

Jollie, D. R., and Lipscomb, J. D. (1991). Formate dehydrogenase from *Methylosinus trichosporium* OB3b: purification and spectroscopic characterization of the cofactors. *J. Biol. Chem.* 266, 21853–21863. doi: 10.1016/S0021-9258(18)54716-5

Jones, G. A., and Pickard, M. D. (1980). Effect of titanium (III) citrate as reducing agent on growth of rumen bacteria. *Appl. Environ. Microbiol.* 39, 1144–1147. doi: 10.1128/aem.39.6.1144-1147.1980

Jumper, J., Evans, R., Pritzel, A., Green, T., Figurnov, M., Ronneberger, O., et al. (2021). Highly accurate protein structure prediction with AlphaFold. *Nature* 596, 583–589. doi: 10.1038/s41586-021-03819-2

Jung, H.-C., Lim, J. K., Yang, T.-J., Kang, S. G., and Lee, H. S. (2020). Direct electron transfer between the FrhAGB-encoded hydrogenase and thioredoxin reductase in the nonmethanogenic archaeon *Thermococcus onnurineus* NA1. *Appl. Environ. Microbiol.* 86, 1–12. doi: 10.1128/AEM.02630-19

Kim, M. S., Bae, S. S., Kim, Y. J., Kim, T. W., Lim, J. K., Lee, S. H., et al. (2013). CO-dependent H_2 production by genetically engineered *Thermococcus onnurineus* NA1. *Appl. Environ. Microbiol.* 79, 2048–2053. doi: 10.1128/AEM.03298-12

Kim, Y. J., Lee, H. S., Kim, E. S., Bae, S. S., Lim, J. K., Matsumi, R., et al. (2010). Formate-driven growth coupled with H_2 production. *Nature* 467, 352–355. doi: 10.1038/nature09375

Kim, M.-S., Choi, A. R., Lee, S. H., Jung, H.-C., Bae, S. S., Yang, T.-J., et al. (2015). A novel CO-responsive transcriptional regulator and enhanced H_2 production by an engineered Thermococcus onnurineus NA1 strain. *Appl. Environ. Microbiol.* 81, 1708–1714. doi: 10.1128/AEM.03019-14

Kato, N., Kano, M., Tani, Y., and Ogata, K. (1974). Purification and characterization of formate dehydrogenase in a methanol-utilizing Yeast, Kloeckera sp. No. 2201. *Agr. Biol. Chem.* 38, 111–116. doi: 10.1080/00021369.1974.10861128

Laukel, M., Chistoserdova, L., Lidstrom, M. E., and Vorholt, J. A. (2003). The tungsten-containing formate dehydrogenase from *Methylobacterium extorquens* AM1: purification and properties. *Eur. J. Biochem.* 270, 325–333. doi: 10.1046/j.1432-1033.2003.03391.x

Ljungdahl, L. G., and Andreesen, J. R. (1978). Formate dehydrogenase, a selenium-tungsten enzyme from *Clostridium thermoaceticum*. *Meth. Enzymol.* 53, 360–372. doi: 10.1016/S0076-6879(78)53042-5

Lee, H. S., Kang, S. G., Bae, S. S., Lim, J. K., Cho, Y., Kim, Y. J., et al. (2008). The complete genome sequence of *Thermococcus onnurineus* NA1 reveals a mixed heterotrophic and carboxydotrophic metabolism. *J. Bacteriol.* 190, 7491–7499. doi: 10.1128/JB.00746-08

Lee, S. H., Kim, M.-S., Jung, H. C., Lee, J., Lee, J.-H., Lee, H. S., et al. (2015). Screening of a novel strong promoter by RNA sequencing and its application to H_2 production in a hyperthermophilic archaeon. *Appl. Microbiol. Biotechnol.* 99, 4085–4092. doi: 10.1007/s00253-015-6444-1

Lee, S. H., Kim, M. -S., Lee, J. -H., Kim, T. W., Bae, S. S., Lee, S. -M., et al. (2016). Adaptive engineering of a hyperthermophilic archaeon on CO and discovering the underlying mechanism by multi-omics analysis. *Sci. Rep.* 6:22896. doi: 10.1038/srep22896

Lee, W.-H., Park, J.-B., Park, K., Kim, M.-D., and Seo, J.-H. (2007). Enhanced production of ε-caprolactone by overexpression of NADPH-regenerating glucose 6-phosphate dehydrogenase in recombinant *Escherichia coli* harboring cyclohexanone monooxygenase gene. *Appl. Microb. Biotech.* 76, 329–338. doi: 10.1007/s00253-007-1016-7

Li, B., and Elliott, S. J. (2016). The catalytic bias of 2-oxoacid: ferredoxin oxidoreductase in CO_2: evolution and reduction through a ferredoxin-mediated electrocatalytic assay. *Electrochim. Acta* 199, 349–356. doi: 10.1016/j.electacta.2016.02.119

Lim, J. K., Mayer, F., Kang, S. G., and Müller, V. (2014). Energy conservation by oxidation of formate to carbon dioxide and hydrogen via a sodium ion current in a hyperthermophilic archaeon. *Proc. Natl. Acad. Sci. U. S. A.* 111, 11497–11502. doi: 10.1073/pnas.1407056111

Liu, C. L., and Mortenson, L. E. (1984). Formate dehydrogenase of *Clostridium pasteurianum*. *J. Bacteriol.* 159, 375–380. doi: 10.1128/JB.159.1.375-380.1984

Lovitt, R. W., Shen, G. J., and Zeikus, J. G. (1988). Ethanol production by thermophilic bacteria: biochemical basis for ethanol and hydrogen tolerance in *clostridium thermohydrosulfuricum*. *J. Bacteriol.* 170, 2809–2815. doi: 10.1128/jb.170.6.2809-2815.1988

Lubner, C. E., Jennings, D. P., Mulder, D. W., Schut, G. J., Zadvornyy, O. A., Hoben, J. P., et al. (2017). Mechanistic insights into energy conservation by flavin-based electron bifurcation. *Nat. Chem. Biol.* 13, 655–659. doi: 10.1038/nchembio.2348

Maia, L. B., Moura, J. J., and Moura, I. (2015). Molybdenum and tungsten-dependent formate dehydrogenases. *J. Biol. Inorg. Chem.* 20, 287–309. doi: 10.1007/s00775-014-1218-2

Maia, L. B., Moura, I., and Moura, J. J. G. (2017). Molybdenum and tungsten-containing formate dehydrogenases: aiming to inspire a catalyst for carbon dioxide utilization. *Inorg. Chim. Acta* 455, 350–363. doi: 10.1016/j.ica.2016.07.010

Matsumi, R., Manabe, K., Fukui, T., Atomi, H., and Imanaka, T. (2007). Disruption of a sugar transporter gene cluster in a hyperthermophilic archaeon using a host-marker system based on antibiotic resistance. *J. Bacteriol.* 189, 2683–2691. doi: 10.1128/JB.01692-06

Müller, V. (2019). FNew horizons in acetogenic conversion of one-carbon substrates and biological hydrogen storage. *Trends Biotechnol.* 37, 1344–1354. doi: 10.1016/j.tibtech.2019.05.008

Nguyen, D. M. N., Schut, G. J., Zadvornyy, O. A., Tokmina-Lukaszewska, M., Poudel, S., Lipscomb, G. L., et al. (2017). Two functionally distinct $NADP^+$-dependent ferredoxin oxidoreductases maintain the primary redox balance of *Pyrococcus furiosus*. *J. Biol. Chem.* 292, 14603–14616. doi: 10.1074/jbc.M117.794172

Nielsen, C. F., Lange, L., and Meyer, A. S. (2019). Classification and enzyme kinetics of formate dehydrogenases for biomanufacturing via CO_2 utilization. *Biotechnol. Adv.* 37:107408. doi: 10.1016/j.biotechadv.2019.06.007

Özgün, G. P., Ordu, E. B., Tütüncü, H. E., Yelboğa, E., Sessions, R. B., and Karagüler, N. G. (2016). Site saturation mutagenesis applications on *Candida methylica* formate dehydrogenase. *Scientifica*. 2016:4902450. doi: 10.1155/2016/4902450

Radon, C., Mittelstädt, G., Duffus, B. R., Bürger, J., Hartmann, T., Mielke, T., et al. (2020). Cryo-EM structures reveal intricate Fe-S cluster arrangement and charging in *Rhodobacter Capsulatus* formate dehydrogenase. *Nat. Commun.* 11:1912. doi: 10.1038/s41467-020-15614-0

Rittmann, S. K., Lee, H. S., Lim, J. K., Kim, T. W., Lee, J. H., and Kang, S. G. (2015). One-carbon substrate-based biohydrogen production: microbes, mechanism, and productivity. *Biotechnol. Adv.* 33, 165–177. doi: 10.1016/j.biotechadv.2014.11.004

Scherer, P. A., and Thauer, R. K. (1978). Purification and properties of reduced ferredoxin: CO_2 oxidoreductase from *clostridium pasteurianum*, a molybdenum iron-sulfur-protein. *Eur. J. Biochem.* 85, 125–135. doi: 10.1111/j.1432-1033.1978.tb12220.x

Schuchmann, K., and Müller, V. (2013). Direct and reversible hydrogenation of CO_2 to formate by a bacterial carbon dioxide reductase. *Science* 342, 1382–1385. doi: 10.1126/science.1244758

Schwarz, F. M., Schuchmann, K., and Müller, V. (2018). Hydrogenation of CO_2 at ambient pressure catalyzed by a highly active thermostable biocatalyst. *Biotechnol. Biofuels* 11:237. doi: 10.1186/s13068-018-1236-3

Schwarz, F. M., Ciurus, S., Jain, S., Baum, C., Wiechmann, A., Basen, M., et al. (2020). Revealing formate production from carbon monoxide in wild type and mutants of Rnf- and Ech-containing acetogens, *Acetobacterium woodii* and *Thermoanaerobacter kivui*. *Microb. Biotechnol.* 13, 2044–2056. doi: 10.1111/1751-7915.13663

Wang, S., Huang, H., Kahnt, J., Mueller, A. P., Kopke, M., and Thauer, R. K. (2013a). NADP-specific electron-bifurcating [FeFe]-hydrogenase in a functional complex with formate dehydrogenase in *Clostridium autoethanogenum* grown on CO. *J. Bacteriol.* 195, 4373–4386. doi: 10.1128/JB.00678-13

Wang, S., Huang, H., Kahnt, J., and Thauer, R. K. (2013b). *Clostridium acidurici* electron-bifurcating formate dehydrogenase. *Appl. Environ. Microbiol.* 79, 6176–6179. doi: 10.1128/AEM.02015-13

Wang, X., Saba, T., Yiu, H. H. P., Howe, R. F., Anderson, J. A., and Shi, J. (2017). Cofactor NAD(P)H regeneration inspired by heterogeneous pathways. *Chem* 2, 621–654. doi: 10.1016/j.chempr.2017.04.009

Weckbecker, A., and Hummel, W. (2005). "Glucose dehydrogenase for the regeneration of NADPH and NADH," in *Microbial Enzymes and Biotransformations*. *Vol. 17*. ed. J. L. Barredo (New Jersey: Humana Press), 225–238.

Witthoff, S., Muhlroth, A., Marienhagen, J., and Bott, M. (2013). C1 metabolism in *Corynebacterium glutamicum*: an endogenous pathway for oxidation of methanol to carbon dioxide. *Appl. Environ. Microbiol.* 79, 6974–6983. doi: 10.1128/AEM.02705-13

Wolin, E. A., Wolin, M. J., and Wolfe, R. S. (1963). Formation of methane by bacterial extracts. *J. Biol. Chem.* 238, 2882–2886. doi: 10.1016/S0021-9258(18)67912-8

Woodyer, R., Zhao, H. M., and van der Donk, W. A. (2005). Mechanistic investigation of a highly active phosphite dehydrogenase mutant and its application for NADPH regeneration. *FEBS J.* 272, 3816–3827. doi: 10.1111/j.1742-4658.2005.04788.x

Xu, J., Zhou, H., Yu, H., Deng, T., Wang, Z., Zhang, H., et al. (2021). Computational design of highly stable and soluble alcohol dehydrogenase for NADPH regeneration. *Bioresour. Bioprocess.* 8:12. doi: 10.1186/s40643-021-00362-w

Zehnder, A. J., and Wuhrmann, K. (1976). Titanium (III) citrate as a nontoxic oxidation-reduction buffering system for the culture of obligate anaerobes. *Science* 194, 1165–1166. doi: 10.1126/science.793008

Conflict of Interest: The authors declare that the research was conducted in the absence of any commercial or financial relationships that could be construed as a potential conflict of interest.

Publisher's Note: All claims expressed in this article are solely those of the authors and do not necessarily represent those of their affiliated organizations, or those of the publisher, the editors and the reviewers. Any product that may be evaluated in this article, or claim that may be made by its manufacturer, is not guaranteed or endorsed by the publisher.

frontiers in Microbiology

ORIGINAL RESEARCH
published: 15 March 2022
doi: 10.3389/fmicb.2022.791714

Proteomic Signatures of Microbial Adaptation to the Highest Ultraviolet-Irradiation on Earth: Lessons From a Soil Actinobacterium

*Federico Zannier[1,2], Luciano R. Portero[1,2], Thierry Douki[3], Wolfgang Gärtner[4], María E. Farías[1] and Virginia H. Albarracín[1,2,5]**

[1] Laboratorio de Microbiología Ultraestructural y Molecular, Centro Integral de Microscopía Electrónica, Facultad de Agronomía y Zootecnia, UNT y Centro Científico Tecnológico, CONICET NOASUR, San Miguel de Tucumán, Argentina, [2] Laboratorio de Investigaciones Microbiológicas de Lagunas Andinas, Planta Piloto de Procesos Industriales y Microbiológicos, Centro Científico Tecnológico, CONICET NOASUR, San Miguel de Tucumán, Argentina, [3] Université Grenoble Alpes, Commissariat a l'Energie Atomique et aux Energies Alternatives, Centre National de la Recherche Scientifique, Institut de Recherche Interdisciplinaire de Grenoble–Systèmes Moléculaires et nanoMatériaux p our l'Énergie et la Santé, Grenoble, France, [4] Institute of Analytical Chemistry, University of Leipzig, Leipzig, Germany, [5] Facultad de Ciencias Naturales e Instituto Miguel Lillo, Universidad Nacional de Tucumán, San Miguel de Tucumán, Argentina

OPEN ACCESS

Edited by:
Andreas Teske, University of North Carolina at Chapel Hill, United States

Reviewed by:
Aly Farag El Sheikha, Jiangxi Agricultural University, China
Santosh Kumar Karn, Sardar Bhagwan Singh University, India
Mak Saito, Woods Hole Oceanographic Institution, United States

***Correspondence:**
Virginia H. Albarracín
cime@tucuman-conicet.gov.ar

Specialty section:
This article was submitted to Extreme Microbiology, a section of the journal Frontiers in Microbiology

Received: *08 October 2021*
Accepted: *26 January 2022*
Published: *15 March 2022*

Citation:
Zannier F, Portero LR, Douki T, Gärtner W, Farías ME and Albarracín VH (2022) Proteomic Signatures of Microbial Adaptation to the Highest Ultraviolet-Irradiation on Earth: Lessons From a Soil Actinobacterium. Front. Microbiol. 13:791714. doi: 10.3389/fmicb.2022.791714

In the Central Andean region in South America, high-altitude ecosystems (3500–6000 masl) are distributed across Argentina, Chile, Bolivia, and Peru, in which poly-extremophilic microbes thrive under extreme environmental conditions. In particular, in the Puna region, total solar irradiation and UV incidence are the highest on Earth, thus, restraining the physiology of individual microorganisms and the composition of microbial communities. UV-resistance of microbial strains thriving in High-Altitude Andean Lakes was demonstrated and their mechanisms were partially characterized by genomic analysis, biochemical and physiological assays. Then, the existence of a network of physiological and molecular mechanisms triggered by ultraviolet light exposure was hypothesized and called "UV-resistome". It includes some or all of the following subsystems: (i) UV sensing and effective response regulators, (ii) UV-avoidance and shielding strategies, (iii) damage tolerance and oxidative stress response, (iv) energy management and metabolic resetting, and (v) DNA damage repair. Genes involved in the described UV-resistome were recently described in the genome of *Nesterenkonia* sp. Act20, an actinobacterium which showed survival to high UV-B doses as well as efficient photorepairing capability. The aim of this work was to use a proteomic approach together with photoproduct measurements to help dissecting the molecular events involved in the adaptive response of a model High-Altitude Andean Lakes (HAAL) extremophilic actinobacterium, *Nesterenkonia* sp. Act20, under artificial UV-B radiation. Our results demonstrate that UV-B exposure induced over-abundance of a

well-defined set of proteins while recovery treatments restored the proteomic profiles present before the UV-challenge. The proteins involved in this complex molecular network were categorized within the UV-resistome subsystems: damage tolerance and oxidative stress response, energy management and metabolic resetting, and DNA damage repair.

Keywords: *Nesterenkonia*, soil bacteria, Puna, proteomics, extremophiles, UV

INTRODUCTION

Free-living microorganisms endure physicochemical stochasticity of their environments, and due to their size and simplicity, they have relatively limited capabilities to adapt to or avoid the exposure of high levels of harmful environmental agents. Therefore, in unicellular organisms, genetic regulation plays a pivotal role in survival under stress conditions as it contributes to rescheduling gene expression and coordinating the synthesis of defense proteins, usually at the expense of expression of genes related to the cellular growth system. Changes in the concentration and activity of proteins encoded by these genes constitute the 'adaptive response' that, in turn, establishes a feedback circuit that modulates its intensity and duration, allowing the genetic system to restore the levels of expression before the onset of the stimulus or to adapt to the new environmental condition (Ramírez Santos et al., 2001; Aertsen and Michiels, 2004; Kaern et al., 2005). Thus, the adaptive response is a vital element for microorganisms that live in habitats with large physicochemical fluctuations allowing them to anticipate and acclimatize to harmful conditions (Thattai and Van Oudenaarden, 2004).

In the Central Andean region in South America, high-altitude ecosystems (3500–6000 masl) are distributed across Argentina, Chile, Bolivia, and Peru, in which poly-extremophilic microbes thrive under extreme environmental conditions (Albarracín et al., 2012, 2016; Orellana et al., 2018; Farías, 2020; Vignale et al., 2021). Previous studies demonstrated the high tolerance of these extremophiles to antibiotics, exposure to heavy metals and arsenic, dehydration, hypersalinity, and UV irradiation (Zenoff et al., 2006a,b; Albarracín et al., 2012, 2014; Dib et al., 2009; Flores et al., 2009; Belfiore et al., 2013; Kurth et al., 2015, 2017; Rascovan et al., 2016; Pérez et al., 2017; Rasuk et al., 2017; Ordoñez et al., 2018; Orellana et al., 2018; Portero et al., 2019; Zannier et al., 2019; Alonso-Reyes et al., 2020; Perez et al., 2020; Saona et al., 2021). Moreover, various underlying mechanisms and cellular processes were identified that indicate how these indigenous microbes cope with these multiple stress conditions, thus presenting an interesting side aspect of opening avenues of research for novel biotechnological applications.

In the Puna eco-region of the Andes between latitudes 8°S and 30°S, total solar irradiation and UV incidence are the highest on Earth (Liley and Mckenzie, 2006; Cabrol et al., 2009). UV measurements by climatologists and biologist exploring the Puna indicate that irradiance is 165% that of sea level with average UV-B values reaching 4 mW/m^2 while short UV wavelengths incidence (260–270 nm) peaks at 14.6 mW/m^2 on the ground (Liley and Mckenzie, 2006; Luccini et al., 2006; Cabrol et al., 2009, 2014). Also, both satellite-derived climatology as well as stations measurements register very high UV index and erythemal daily dose values with extreme monthly means above 18 and 10 kJ/m^2 in December–January, respectively (Luccini et al., 2006). Moreover, UV levels in the Puna are considerably higher than those for equivalent regions in the Northern Hemisphere (Luccini et al., 2006), setting strong limits to the physiology of individual microorganisms and the composition of microbial communities in this eco-region (Cabrol et al., 2004, 2009, 2014; Zenoff et al., 2006a,b; Escudero et al., 2007; Flores et al., 2009; Ordoñez et al., 2009; Albarracín et al., 2011; Rascovan et al., 2016; Pérez et al., 2017; Toneatti et al., 2017). There is extensive research on these poly-extremophiles focusing on the influence of UV irradiation on the molecular profiles and adaptive strategies of model microorganisms isolated from shallow lakes and soil across different sites in the Argentinean and Chilean Central Andes (Albarracín et al., 2011, 2015, 2016). Genomics and ultrastructural and physiological assays identified a number of UV-resistance mechanisms of bacterial and archaeal strains (Zenoff et al., 2006a,b; Albarracín et al., 2012, 2014, 2016; Flores et al., 2009; Kurth et al., 2015; Rasuk et al., 2017; Toneatti et al., 2017; Portero et al., 2019; Alonso-Reyes et al., 2020, 2021).

Andean microbes' high UV-resistance profile points to the existence of a network of physiological and molecular mechanisms triggered by ultraviolet light exposure. We called this the "UV-resistome" (Kurth et al., 2015; Portero et al., 2019; Alonso-Reyes et al., 2021) and it includes some or all of the following subsystems: (i) UV sensing and effective response regulators, (ii) UV-avoidance and shielding strategies, (iii) damage tolerance and oxidative stress response, (iv) energy management and metabolic resetting, and (v) DNA damage repair. Genes involved in the described UV-resistome were recently described in metagenomes (Kurth et al., 2017; Alonso-Reyes et al., 2020; Lamprecht-Grandío et al., 2020) as well as in many genomes from strains isolated from High-Altitude Andean Lakes (HAAL) including *Acinetobacter* sp. Ver3 (Kurth et al., 2015), *Salinivibrio* spp. (Gorriti et al., 2014), *Exiguobacterium* sp. S17 (Portero et al., 2019) and *Nesterenkonia* sp. Act20 (Alonso-Reyes et al., 2021). Among all these strains, we selected *Nesterenkonia* sp. Act20 as UV-resistant model strain to perform further assays. This selection is based on its superior UV-resistance profile (Rasuk et al., 2017; Portero et al., 2019) but also because of the high biotechnological potential of this actinobacterium. To our knowledge, there

are not in-depth studies on the molecular basis of UV-resistance in this genus.

The aim of this work is to dissect the adaptive response of *Nesterenkonia* sp. Act20 upon UV-B using a proteomic approach together with photoproduct measurement. The molecular events during the UV challenge and after photorepairing were included within hypothesized UV-resistome subsystems, including DNA repair. Our results demonstrate that UV-B exposure induced over-abundance of an exclusive set of proteins while recovery treatments restored the proteomic profiles present before the UV-challenge.

MATERIALS AND METHODS

Strains and Growth Conditions

Nesterenkonia sp. Act20 (strain Act20) belongs to the LIMLA extremophilic strain collection (Strain Number P156, PROIMI-CONICET). Axenic glycerol-freeze cultures were aerobically activated in a growth medium designed explicitly for this strain called "H medium" (i. e., Halophilic medium, 10 g NaCl, 3 g sodium citrate, pH 7–7.2) and cultured at 30°C with agitation (220 rpm) overnight. *Nesterenkonia halotolerans* DSM 15474 (strain DSM 15474), a close phylogenetic relative of strain Act20 but with a lower resistance profile to UV (Portero et al., 2019), was used as a control. This strain was grown under the same conditions as *Nesterenkonia* sp. Act20. Cultures of both strains were maintained in H agar (1.5%) for further inoculations.

Preparation of Cultures for Photoproduct Measurements and Proteomic Analysis

Nesterenkonia sp. Act20 and *N. halotolerans* cultures were exposed to the following experimental conditions as described previously (Portero et al., 2019); Cell suspensions in NaCl 0.9% (20 ml, OD_{600} ∼0.6), exposed to artificial UV-B irradiation (5.4 W/m^2 UV-B) for 20 min in quartz tubes (6.48 kJ/m^2) using a Vilber Lourmat VL-4 lamp (maximum intensity at 312 nm) [Irradiance was quantified with a radiometer (09811-56, Cole Parmer Instrument Company, Vernon Hills, IL, United States)]. This dose reduces the viability of the strain Act20 to 50% compared to unexposed cultures (Portero et al., 2019). UV-treated subsamples were set aside for protein analysis without recovery treatment. This treatment was named "UV." Subsequently, other UV-exposed subsamples were subjected to two parallel recovery treatments: named "photorecovery ("FR")" and "dark recovery ("DR") incubated under white light or in the dark for 120 min, respectively. On the other hand, a control treatment, named "total darkness" ("Dt")," consisted of placing the cell suspensions in quartz tubes coated with aluminum foil and kept in the dark during the UV exposure and recovery treatments. An additional control for photoproduct measurements was provided by the non-exposed cell cultures at time 0 (T0).

All suspensions were then centrifuged, washed with NaCl (0.9%) and resuspended in 0.1 M Tris-HCl buffer, pH 7. The samples were stored at −70°C until subsequent processing. The above-described protocol was carried out in triplicate, obtaining three independent biological replicates for each treatment.

Photoproduct Quantification

Ten milliliters of cell suspensions from the different treatments T0, Dt, UV, FR, and DR conditions were centrifuged at 3,000 × *g* for 10 min at 4°C. A cell suspension without exposure to any stimulus named T0 (initial time) was used as an additional control. Pellets were harvested and washed twice with distilled water. Total genomic DNA extraction was performed using a commercial genomic DNA kit (DNeasy Blood & Tissue Kit, Qiagen). Photoproducts were quantified using a pre-optimized procedure (Douki, 2013). After extraction, DNA was solubilized in an aqueous solution containing 0.1 mM desferrioxamine mesylate and then enzymatically hydrolyzed by incubation with nuclease P1, DNAase II, and phosphodiesterase II (2 h, 37°C, pH 6), followed by the second stage of digestion involving phosphodiesterase I and alkaline phosphatase (2 h, 37°C, pH 8). The digested DNA samples were injected into an Agilent 1100 Series HPLC system equipped with a reversed-phase ODB Uptisphere column (2 × 250 mm ID, particle size 5 μm, Interchim, Montluçon, France). The mobile phase (flow rate 0.2 ml/min) was an acetonitrile gradient (from 0 to 20%) in a 2 mM aqueous solution of triethylammonium acetate. The HPLC flow was split and funneled into an API 3000 electrospray triple quadrupole mass spectrometer operating in negative ionization mode. The pseudomolecular deprotonated ion of each photoproduct was collected and fragmented. Specific daughter ions of each photoproduct were quantified. Calibration curves were performed using proper reference compounds of varying concentrations. The results were expressed as the number of Photoproducts per 10^6 DNA bases (bpm). The standards for HPLC-ESI-MS/MS were synthesized according to a previously published procedure (Douki and Cadet, 2001). In summary, dinucleoside monophosphates were prepared by the triester synthesis. Cyclobutane pyrimidine dimers (CPDs) were obtained by photosensitized triplet energy transfer using acetophenone and UV-A treatment. Pyrimidine (6-4) pyrimidone photoproducts (6-4PPs) were prepared by photolysis with UV-C irradiation, and a subsequent UV-A irradiation of these latter compounds produced the Dewar valence isomers (for a detailed photoproduct type description see Ravanat et al., 2001). All photoproducts were HPLC purified. The four *cis*-syn CPDs were measured [i.e., thymine-thymine (TTCPD), thymine-cytosine (TCCPD), cytosine-thymine (CTCPD), and cytosine-cytosine sites (CCCPD)], with cytosine under its deaminated form uracil. 6-4PPs at thymine-thymine (TT64) and at thymine-cytosine (TC64) sites, together with their Dewar valence isomers (DEWTT and DEWTC, respectively), were also quantified.

The above-described protocol was carried out as four individual set-ups, obtaining four independent biological replicates for each treatment and each photoproduct category. Significant differences in photoproduct absolute concentrations and mean efficiency on photoproduct repair were analyzed through an ANOVA model and

TukeyHSD test. Photoproduct data are available in **Supplementary file 3**.

Protein Extraction Protocol

Once the necessary three replicates of each treatment were obtained, we performed the protein extraction protocol described by Belfiore et al. (2013). Pellets were washed with Tris buffer (25 mM), pH 7, EDTA (2 mM) and then resuspended with the same buffer composition supplemented with 5 μl of a reducing solution (DTT 200 mM, Tris 100 mM, pH 7.8). Intracellular proteins were obtained by breaking the cells with a French press and incubating for 1 h at room temperature to achieve complete denaturation. The protein concentration was measured using the Bradford assay. For every 50 μg of protein, 20 μl of reducing solution and 20 μl of alkylating solution (iodoacetamide, 200 mM, Tris, 100 mM, pH 7.8) were added to each sample. The mixture was allowed to incubate and centrifuged at 16,100 × *g* for 30 min (4°C). Then, the proteins were precipitated with 10% TCA and incubated overnight (−20°C). Samples were centrifuged (16,100 × *g*, 30 min, 4°C), and the protein pellets were washed twice by rinsing with 500 ml pre-chilled (−20°C) acetone. Once dried, the protein pellets were dissolved in ammonium bicarbonate (50 mM) and digested with trypsin at 37°C for an incubation period of 14–16 h. Finally, after digestion with trypsin, the concentration of peptides was determined, and the samples were stored at −80°C until further analysis through mass spectrometry (MS).

Protein Identification and Mass Spectrometry

Global proteomics ("Shotgun proteomics") was performed using the "bottom-up" method following Bonilla et al., 2020. For this purpose, the protein samples were digested with trypsin and then cleaned with Zip-Tip C18 to extract salts. Then, liquid chromatography was performed with nanoUHPLC Easy nLC 1000 (Thermo Scientific brand, model EASY-nLC 1000, Easy-Spray ColumnPepMap RSLC, P/N ES801) (Thermo Scientific) coupled to a mass spectrometer with Orbitrap technology, which allows a separation of the peptides obtained by tryptic digestion of the sample and subsequent identification. Sample ionization was carried out by nanoelectrospray (Thermo Scientific brand, model EASY-SPRAY. Spray voltage: 1.8 kV). The instrument was equipped with an HCD (High Collision Dissociation) cell and an Orbitrap analyzer yielding the identification of peptides simultaneously to their separation by chromatography. The parameters used during the mass spectrometry analysis were based in full MS (MS1) scan followed by MS/MS (MS2) scans (Data Dependent Acquisition or DDA) to identify + 1 or multiply charged precursor ions in the mass spectrometry data file. MS1 and MS2 peak ranges were 300–1,800 Da (resolution 70000) and 65–2,000 Da (resolution 17500), respectively. The analysis of the raw files delivered by the mass spectrometer was performed using the ProteomeDiscoverer version 2.1 search engine through SEQUEST HT, conducting peptide-to-spectrum mapping (PSMs) against the sequenced genome of *Nesterenkonia* sp. Act20. The following parameters were set for the search: carbamidomethyl (C) on cysteine was set as fixed; variable modifications included asparagine (N) and glutamine (Q) deamidation and methionine (M) oxidation. Only one missed cleavage was allowed; monoisotopic masses were counted; the precursor peptide mass tolerance was set at 10 ppm; fragment mass tolerance was 0.05 Da. The MS2 spectra were searched with Proteome Discoverer v2.1 using a 95% confidence interval (CI%) threshold ($P < 0.05$). The described protocol was carried out at CEQUIBIEM (by its Spanish acronym, "Centro de Estudios Químicos y Biológicos por Espectrometría de Masa"), University of Buenos Aires-Argentina. ProteomeDiscoverer results are available in **Supplementary file 1, sheet 1**. Proteomic mass spectrometry raw files have been deposited at the Mass Spectrometry Interactive Virtual Environment repository[1] with the dataset identifier MSV000088619.

Statistical Data Analysis

Data analysis was performed using the software Perseus v.1.6.2.3, Microsoft Excel, R v.3.6.1, and Cytoscape v.3.7.1 (Shannon et al., 2003; R Core Team, 2016; Tyanova et al., 2016). Proteins with only one valid value in each treatment, in only one treatment, or with missing values in all three replicates in each of the four treatments were filtered out, selecting proteins with at least two valid values in at least one treatment. Next, log2 transformation was performed and missing values (NaN, "Not a number") were imputed by the minimum detected values of the normal distribution of the whole dataset (Lazar et al., 2016) (Width = 0.5, Down shift = 1.8). Next, the abundance averages for each protein were compared between treatments through the *t*-test. Proteins were considered significantly regulated when (Witten and Tibshirani, 2007): (A) The *t*-test showed a value of significance $p < 0.05$, (B) the value of the difference between the log-scale averages of abundance (log2) was above or below the fold change (FC) 1 and −1 ($-1 < FC_{difference} < 1$), respectively (see note 1 in the **Supplementary file 2**). Treatments were compared against each other providing different information about the system under study (see section "Statistical Analysis of Proteomic Profiles Among Treatments").

Annotation and Bioinformatics Analysis

The sequenced genome of *Nesterenkonia* sp. Act20 has been deposited at DDBJ/ENA/GenBank under the accession JADPQH000000000 (Alonso-Reyes et al., 2021). The functional analysis of the identified proteins was performed using tools from the "KEGG" (Kyoto Encyclopedia of Genes and Genomes) and String databases (Szklarczyk et al., 2017) and exhaustive text mining.

RESULTS

DNA Repair Ability of *Nesterenkonia* sp. Strains

Ultraviolet-resistance was herein indirectly explored by assessing the level of DNA damage after UV and its repair in

[1]https://massive.ucsd.edu/

Act20 and DSM 15474 strains. DNA photoproducts were measured by HPLC-ESI-MS/MS in UV-exposed cells and in cultures subjected to recovery treatments in light (FR) and dark (DR), respectively. DNA photoproducts were also quantified in unexposed samples at the beginning (T0) of the experiment.

The sum of photoproducts of all categories accumulated within each treatment showed the damage/repair balance on DNA in both strains (**Figure 1A**). The maximum accumulation of photoproducts was found in cultures of the strain DSM 15474 exposed to the UV treatment (1228 bpm). In accordance with its higher UV-resistance profile (Portero et al., 2019; Alonso-Reyes et al., 2021), the strain Act20 accumulated 45% less DNA photoproducts (671 bpm) than the strain DSM 15474 (1228 bpm) under UV-exposure. Similar patterns were also detected under DR and FR treatments, in which the strain Act20 accumulated ca. 627 and ca. 515 photoproducts per million bases, that is ca. 41% fewer photoproduct accumulation compared to the strain DSM 15474 exposed to DR (ca. 1098 bpm) and FR (ca. 879 bpm), respectively (**Figure 1A**).

Ultraviolet irradiation increased the abundance of all types of photoproduct categories except Dewar isomers (**Figure 1B**). In both strains, and in all conditions tested, the main types of photoproduct produced were TCCPD and TC64 (**Figure 1A**). However, there were differences observed between strains. Compared to unexposed cells, UV treatment significantly increased the accumulation of TT64, TC64, TCCPD, TTCPD, CTCPD, and CCCPD photoproduct in the strain DSM 15474, while induced significant accumulation of TT64, TC64, TCCPD, and CCCPD in the strain Act20. Interestingly, FR significantly decreased the absolute abundances of TCCPD, TTCPD, CTCPD, and CCPD measured in the strain DSM 15474 while significantly reduced TCCPD in the strain Act20.

The mean efficiency to repair TT64, TC64, TCCPD, TTCPD, CTCPD, and CCCPD photoproducts under DR and FR were estimated for both strains (**Figure 1C**). Repair of photoproducts increased always under FR, although those differences were not always statistically significant. Thus, the strain Act20 repaired TCCPD and TTCPD significantly better under light (42.6% and 42.8%) than under dark conditions (11.8% and 0%). Likewise, the strain DMS 15474 repaired TTCPD more efficiently under light (59.8%) than in the dark (21%). Also, both strains improved their repair efficiency for TC64 and CCCPD in the light rather than in the dark, although these differences are not statistically significant. Surprisingly, in the strain Act20, CTCPD were better repaired under dark recovery while under light this activity is scarce or even not detected (**Figure 1C**). Since photolyases are the only light-driven enzymes capable of repairing DNA damaged nucleotides, the CPD and 6-4 photolyases detected in the genomes of both Act20 and DSM15474 strains (Alonso-Reyes et al., 2021) may be responsible for the observed decrease in photoproduct concentration under FR. Therefore, photolyases may contribute to protecting the integrity of the genome and as such they constitute active elements of the UV-resistome in both strains.

Panoramic Approach and Functional Orthology of Act20 Proteome

In order to explore the molecular basis of the superior UV-resistance profile of the strain Act20, we performed a proteomic study under four experimental conditions, Dt, UV, DR, and FR. Taking together the number of proteins with at least one valid value in at least one biological replicate of each treatment, a set of 1597 different proteins were detected, herein called the "experimental proteome (Ex.P)," that covers 59% of the predicted ORFs contained in the genome of the strain Act20 (Predicted proteome, Pred.P = 2689 ORFs). In this section, we performed a functional panoramic analysis of the proteomic profiles detected under each treatment based on detection limits of the mass spectrometry device. Thus, those proteins with missing values in the three samples of a treatment were considered as not present or deregulated under that condition. Contrary, the detection of proteins with at least one valid value in at least one sample of a treatment were considered as present in that treatment. Thus, by applied these criteria, there were 1476, 1521, 1546, and 1565 proteins listed in Dt, UV, DR, and FR proteomic datasets, respectively (**Table 1** and **Supplementary file 1, sheet 2**).

Metabolic pathway and functional modules are sets of proteins that functionally interacts, either by catalyzing steps in a series of ordered biochemical reactions to yield metabolites or by integrating protein complexes linked to specific tasks, in which each protein is necessary and usually must be present to ensure the activity of a cellular process. To assess the complete metabolic pathways and functional modules in which the list of proteins present in Pred.P, Ex.P, Dt, UV, DR, and FR datasets are involved, their amino acids sequences were BLAST against KEGG database. KEGG assigns a code (KO) to each recognized protein according to its function. Several proteins can share the same KO code, but each protein is assigned to only a single KO that reflects its functionality. The number of different proteins and different functionalities carry out by them, as well as the number of metabolic pathways and functional modules identified by KEGG in each dataset are summarized in **Table 1**. The lowest number of functionalities and complete metabolic pathways as well as functional modules were observed in Dt dataset (**Table 1**).

To further assess the influence of each treatment on the metabolism of *Nesterenkonia* sp. Act20, the number of proteins involved in the main nine categories of biomolecules was counted. There were no major variations between treatment datasets and, also, there were high percentages of proteins shared among them for each particular category (>90%), indicating a low degree of protein replacement induced by each experimental condition (**Figure 2A** and **Supplementary Table 1**). Thus, the influence of treatments on the metabolism of the strain Act20 is not dependent on the expression of large groups of proteins, but rather indicate that the high shared number of proteins constitute a protein repertoire essential to survival while the

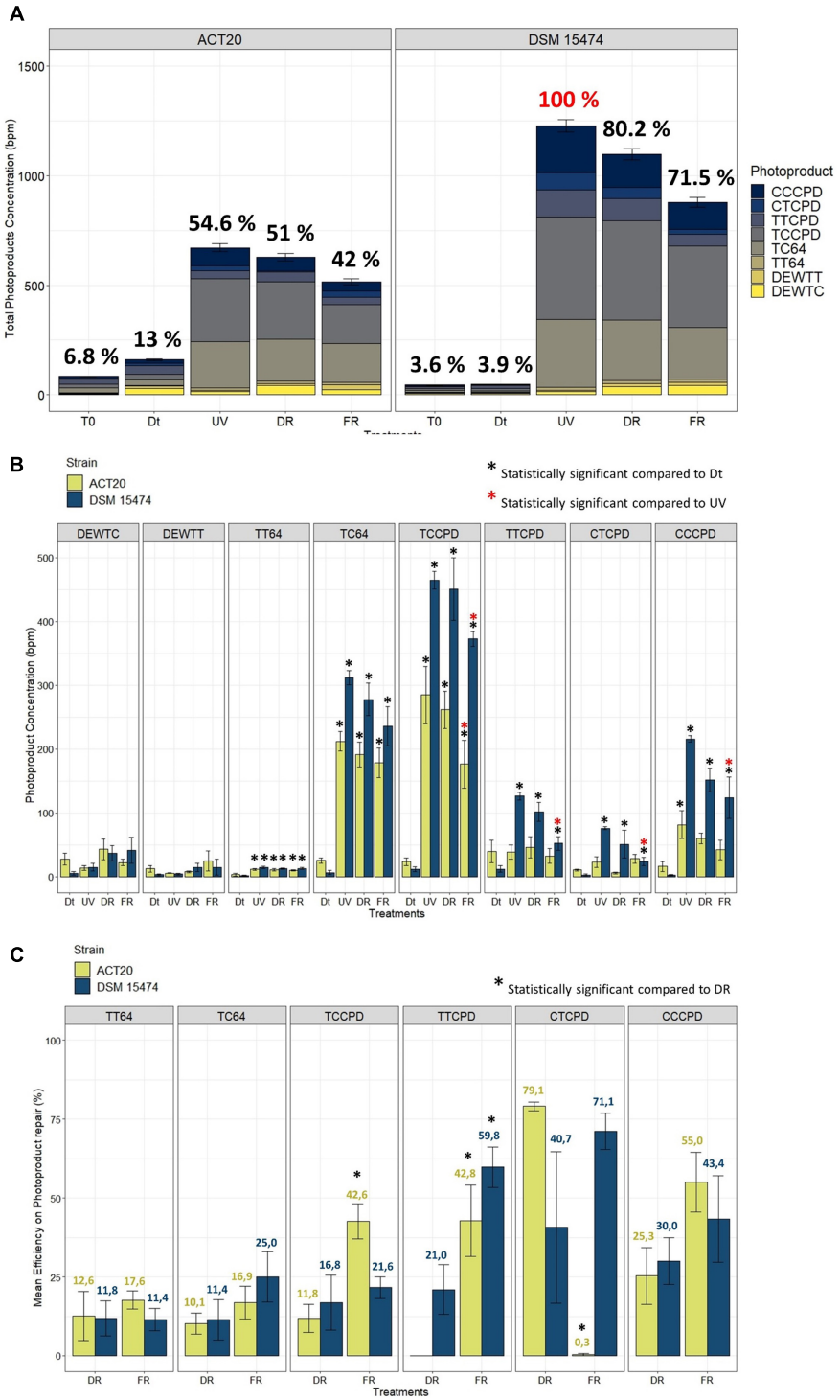

FIGURE 1 | (A) Stacked barplot showing the mean total concentration [as bases per million (bpm)] of photoproducts generated by each treatment and the contribution of each photoproduct category. Error bars means the standard deviation of the cumulative sum of photoproducts within each treatment. The 100% of photoproduct (in red) able to be produced under our experimental conditions was attributed to the condition with the highest photoproduct concentration found in the UV-treated cultures of DSM 15474. Relations to the 100% are shown as percentages in black. **(B)** Quantification of *cis*-syn cyclobutane pyrimidine dimers (TTCPD, TCCPD, CTCPD, and CCCPD), pyrimidine (6-4) pyrimidone photoproducts (TT64 and TC64), and Dewar valence isomers (DEWTT and DEWTC) plotted as the mean of their absolute concentration (bpm) achieved in each treatment (Dt, UV, DR, and FR). **(C)** Comparisons of the mean efficiency of DNA photoproduct repair between DR and FR treatments. *Nesterenkonia* sp. Act20 (yellow bars), *Nesterenkonia halotolerans* DSM 15474 (blue bars). Asterisks indicate statistically significant differences (see legends in the picture).

TABLE 1 | Summary of the number of proteins identified by mass spectrometry and the KEGG database for each conditions.

	Pred.P	Ex.P	Dt	UV	DR	FR
n° of proteins identified by MS	2689	1597	1476	1521	1546	1565
n° of proteins assigned to a KO	1381	1001	940	966	979	985
n° of different KO	1168	910	857	883	890	896
n° of pathways identified by KEGG server	155	150	149	150	150	150
n° of modules identified by KEGG server	38	37	33	37	37	36

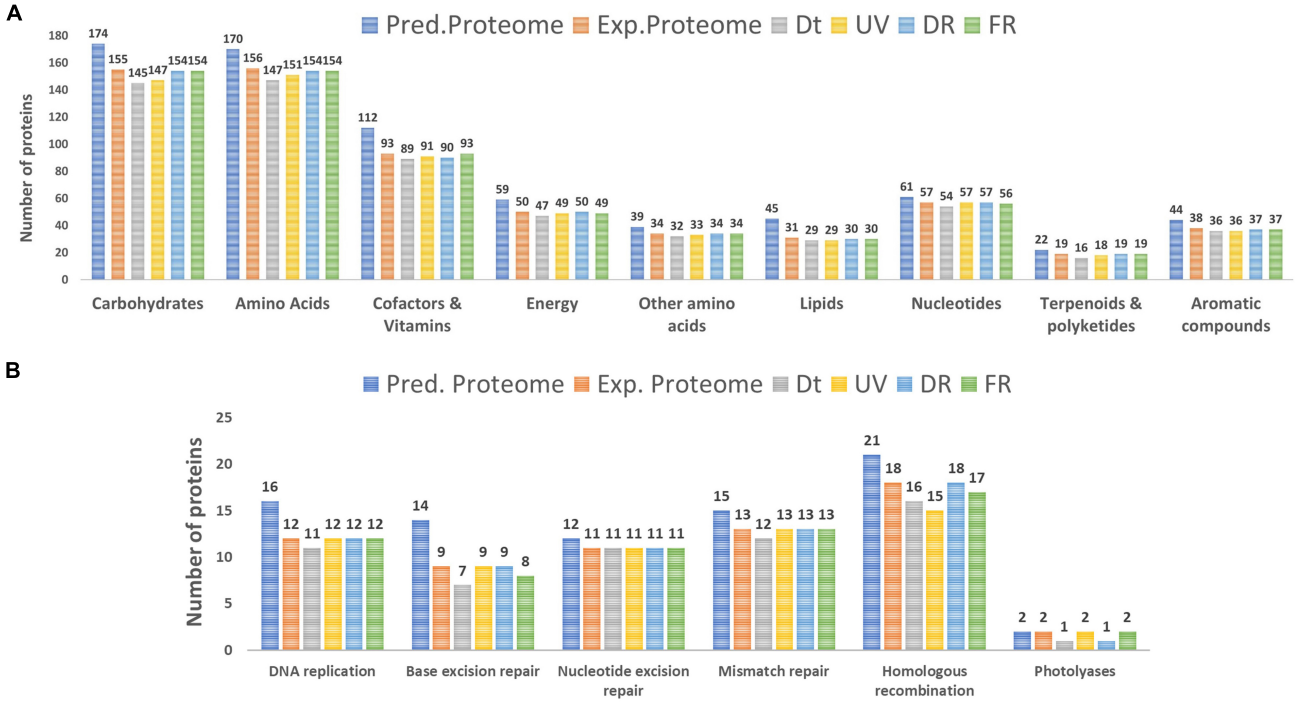

FIGURE 2 | (A) Number of proteins involved in the metabolism of the main categories of biomolecules identified in the predicted proteome (Pred.P), the experimental proteome (Exp.P), Dt, UV, DR, and FR datasets. **(B)** Number of proteins involved in the main categories of DNA repair mechanisms.

different treatments can only change a small proportion of this essential protein base. Moreover, the reconstruction of functional modules using the KEGG server showed that the non-oxidative phase of the pentose phosphate cycle and the biosynthesis of ornithine from glutamate could be interrupted in the Dt treatment due to the deregulation (non-detection) of specific proteins [i.e., ribulose-phosphate 3-epimerase (EC:5.1.3.1) (rpe) (see **Supplementary Figure 1** in **Supplementary file 2**), amino-acid *N*-acetyltransferase [EC:2.3.1.1] (ArgA), acetylornithine/*N*-succinyldiaminopimelate aminotransferase [EC:2.6.1.11 2.6.1.17] (ArgD)], as suggested by the mass spectrometer detection threshold (**Supplementary file 1,sheet 2**). In contrast, the set was proteins involved in these functional modules were detected in UV, DR, and FR protein datasets, respectively, suggesting that such metabolic processes could be influenced by UV exposure. Further, no proteins from the flagellum biosynthesis machinery were detected in Ex.P despite being encoded in the genome (Pred.P) (**Supplementary file 1**), which is consistent with the observation that no flagella were detected by electron microscopy in the strain Act20 with or without UV exposition (Alonso-Reyes et al., 2021). Also, specific pathways of carbohydrate metabolism involving the beta-*N*-acetylhexosaminidase [EC:3.2.1.52, (K01207)] (nagZ) protein could be affected by UV exposure as this protein was not detected in Dt but was detected in UV, DR, and FR (**Supplementary file 1**).

The DNA repair/metabolism subsystem of the hypothesized UV-resistome, including DNA replication, base excision repair, nucleotide excision repair, mismatch repair, homologous recombination and photolyases, was herein analyzed. In general, repairing treatments displayed more proteins for each of these repair functions than those in the control or the UV-treatment (**Figure 2B**). In fact, there was a probable variation in the number of proteins involved in homologous recombination among treatments. Remarkable, variations in the photolyase category agrees with the biological functionalities of these enzymes, as during the UV and FR treatments two types of photolyases, CPD as well as 6-4 photolyases, were expressed,

while in the control (Dt) or under DR only CPD photolyases were present as constitutive photorepairing proteins (**Figure 2B** and see **Supplementary file 1**).

Statistical Analysis of Proteomic Profiles

By filtering and imputing the entire dataset there were 1522 out of the 1597 proteins with sufficient valid values to be analyzed by statistical methods (Lazar et al., 2016) (see section "Statistical Data Analysis"). The average abundance values of each protein were compared between treatments by the *t*-test, and the statistical significance of the $FC_{difference}$ was estimated. The effect of artificial UV-B light exposure over the proteomic profile of the strain Act20 was determined mainly by comparing the UV treatment dataset against that of the Dt treatment (UV-Dt), although FR-UV and DR-UV comparisons were useful to interpret and to complete the UV-response model. Likewise, the effect of the photorecovery treatment was determined by comparing the abundance of proteins listed in FR dataset against Dt and UV (FR-Dt and FR-UV), and, in turn, by comparing each set of FR-upregulated proteins against UV-upregulated and UV-downregulated proteins (from UV-Dt). Also, DR-upregulated proteins taken from DR-Dt and DR-UV comparisons were added to the analysis in order to discriminate between FR-dependent and FR-independent effects on the proteomic profiles. Each particular comparison provides different information about the system under study (see **Figure 3**).

By applying the statistical criteria A and B (see section "Statistical Data Analysis"), there was a specific set of fourteen upregulated proteins induced by the UV challenge (**Figure 3A**). Of these, Fructokinase (EC 2.7.1.4) (FrK) remained upregulated after both recovery treatments, while Recombinase A (RecA), a DUF4229-domain-containing protein (DUF4229), and the HMP/thiamine import ATP-binding protein (YkoD) maintained significantly high levels of abundance during DR and FR, respectively (**Figure 3A**). Likewise, Lipoyl synthase [EC:2.8.1.8] (lipA) and the CarD N-terminal-like transcriptional regulator (CdnL) reached the highest abundance values during UV irradiation (**Figure 3B**), suggesting that they are relevant components of the UV-resistome of Act20 strain.

In contrast, 26 proteins were downregulated by UV exposure according to criteria A and B (**Figure 3C**). Among them, the abundance of the anti-sigma K factor (RskA), the Excinuclease C from UvrABC system (UvrC), 1,3-propanediol dehydrogenase (EC 1.1.1.202) (AdhP), Pyruvate carboxyl transferase (EC 6.4.1.1) (PC), glutathione-independent formaldehyde dehydrogenase [EC:1.2.1.46] (fdhA), the multiple sugar transport system ATP-binding protein (msmX), and an uncharacterized SRPBCC-domain-containing protein (SRPBCC') were decreased during UV but then significantly increased under both recovery treatments after UV exposure (**Figure 3C**), reaching mean abundance values non-significantly different to those achieved in Dt conditions (see **Supplementary file 1**). Due to their levels were restored under FR as well as DR conditions after UV, this suggest that their regulation is independent on FR.

Contrary, the SOS-response repressor and protease LexA (EC 3.4.21.88) (lexA), the Mn-containing catalase (Cat), a glutamate—cysteine ligase/carboxylate-amine ligase (gshA), an hypothetical protein which KO code is K09959 as well as three uncharacterized proteins related to the universal stress (pfam00582), the nucleoside-diphosphate-sugar epimerases (pfam01370), and the serine aminopeptidases (pfam12146) protein families, recovered their abundance dependent on FR as this does not occur under the DR treatment (**Figure 3C** and **Supplementary file 1**).

On the other hand, among the proteins that increased their abundance under FR after UV exposure, there are a well-defined set of twelve proteins whose levels seems to be specifically induced by the FR treatment (**Figure 3C**). Of these, the bifunctional enzyme 2-amino-4-hydroxy-6-hydroxymethyldihydropteridine pyrophosphokinase (EC 2.7.6.3) (SulD) involved in folate synthesis, a transcriptional regulator from TetR family (TetR), the methionine amino peptidase (map), reached abundance values that significantly exceed those achieved under Dt and UV (**Figure 3D**), suggesting that they might be central elements of cell recovery under FR. The same is true for the zinc-dependent aldehyde dehydrogenase (znADH) which reached higher abundance in FR than under Dt and UV, although is also induced under DR (**Figures 3C,D**).

Altogether, these results indicated that UV-exposure triggered the upregulation of fourteen main proteins. Also, suggest that once the UV challenge ceased, some UV-downregulated proteins restore their abundance levels independent as well as dependently on the photorecovery treatment (FR), reaching non-significantly different values than those achieved under Dt conditions.

Molecular Response Model Against Artificial Ultraviolet-B Radiation

In order to build a model of the molecular events involved in the response against UV, each of the main fourteen UV-upregulated proteins (**Figure 3A**) was functionally linked to a particular cellular process, when possible. Both the functions and biological implications of each protein were analyzed through extensive literature mining of homologous proteins using cured databases. In addition, to gain more evidence of the molecular events in which the proteins are involved, functionally related proteins (from UV-Dt comparison) with significant $FC_{difference}$ but below the imposed threshold were analyzed and taken into account for the model. Also, significantly UV upregulated proteins from FR-UV and DR-UV comparisons were added (**Figure 3B**). Finally, in order to interpret and complete the model, functionally related proteins encoded in the genome of strain Act20, but showing no significant UV-related changes in abundance were also added. Through this analysis it was interpreted that the fourteen co-expressed proteins could be functionally linked to the hypothesized UV-resistome subsystems (**Figure 4**).

A first functional module was associated to DNA repair and metabolic resetting. We observed that RecA was significantly upregulated by the UV effect (**Figure 3A**), but also, its associated protein, the ATP-dependent DNA helicase RecQ [EC:3.6.4.12] (RecQ), presented significant increases of their abundance in UV than in Dt (**Figure 4**), although the $FC_{difference}$ was lower

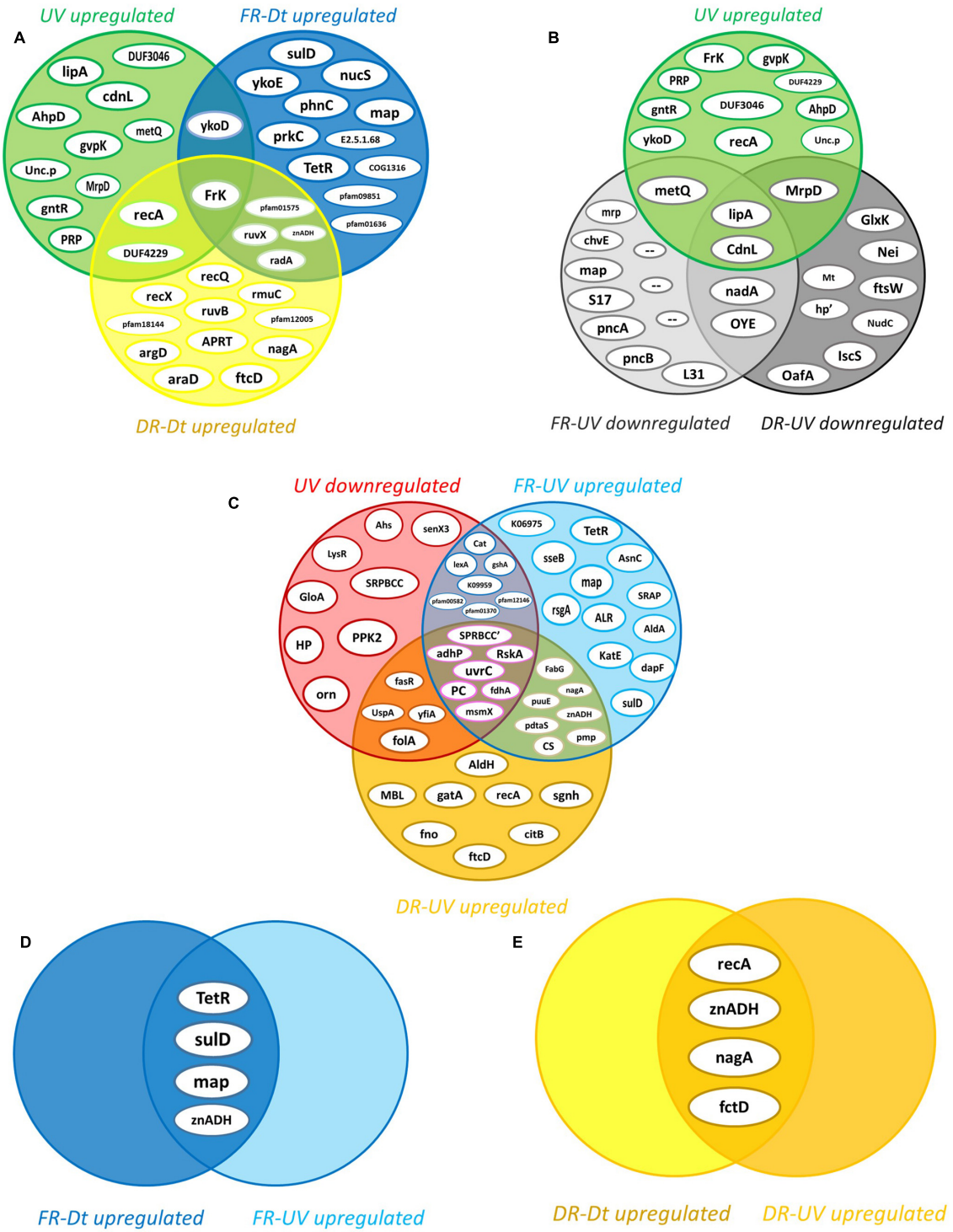

FIGURE 3 | Intersection analysis of proteins upregulated by the effect of each treatment. **(A)** Intersection of the 14 UV-upregulated proteins (from UV-Dt) versus (vs.) the set of FR- and DR-upregulated proteins (from FR-Dt and DR-Dt comparisons) highlights those UV-induced proteins that remains significantly upregulated throughout the recovery treatments. **(B)** Intersection of UV-upregulated proteins from UV-Dt comparison vs. UV-upregulated proteins from FR-UV and DR-UV comparison highlights the set of UV-induced proteins whose abundance levels are most strongly increased by UV exposure. **(C)** Intersection of UV-downregulated proteins (from UV-Dt comparison) vs. FR- and DR-upregulated proteins (from FR-UV and DR-UV comparison) highlights the set of proteins whose abundance decreased under UV but then restored their levels dependently or independently of FR treatment. **(D)** Intersection of FR-upregulated proteins from FR-Dt vs. FR-UV highlights the set of proteins whose abundances are strongly induced by FR as they reach higher levels of abundance in FR than in Dt and UV. **(E)** Intersection of DR-upregulated proteins from DR-Dt vs. DR-UV highlights the set of proteins whose abundances are strongly induced by DR as they reach higher levels of abundance in DR than in Dt and UV.

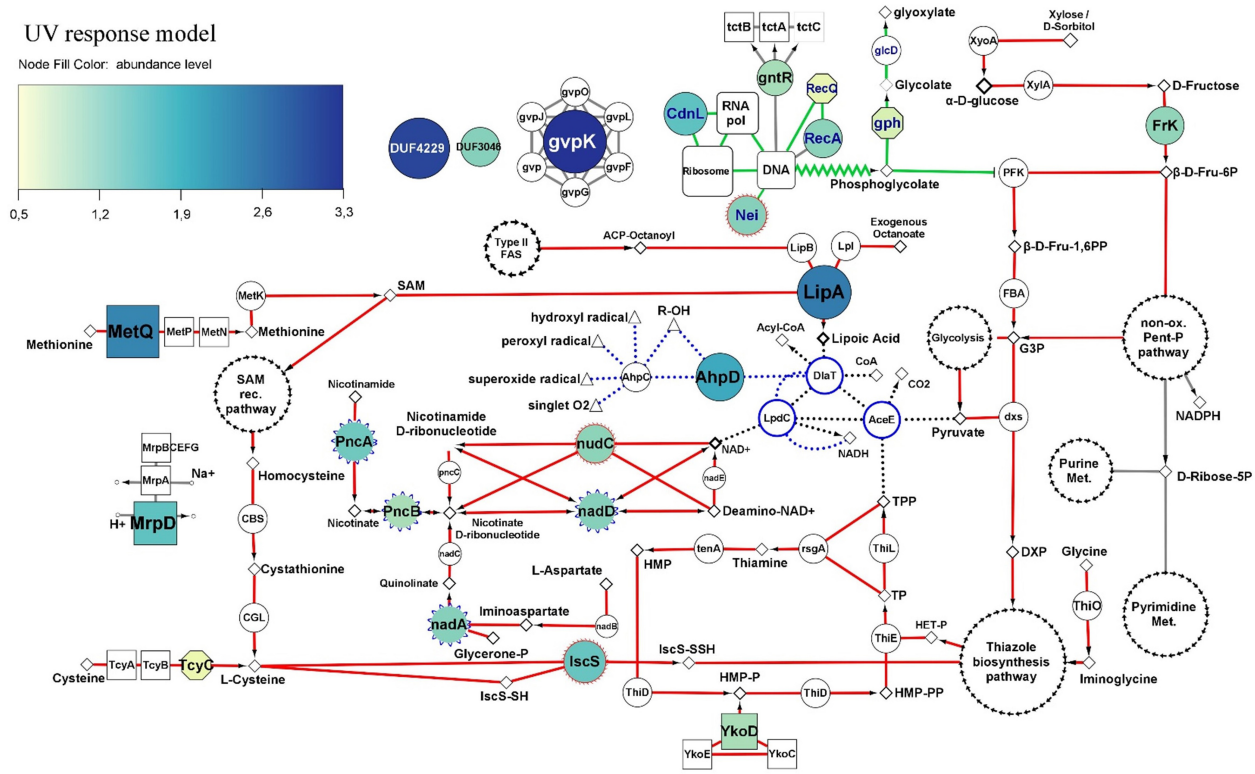

FIGURE 4 | Molecular UV-response model of Act20 strain. Nodes of the DNA repair and metabolic resetting functional module are highlighted with blue labels and green interactions (borders). Interactions of the functional module related to cofactor biosynthesis for the PDH complex are highlighted in red. PDH complex proteins and their interactions are highlighted with blue edges nodes and black punted borders. The antioxidant redox interactions between free radicals, and AhpC, AhpD, DlaT, and LpdC proteins are represented as blue punted borders. Additional interactions with less relationship to the mentioned functional modules are painted in gray. The color and size of nodes representing significant UV-upregulated proteins indicates their abundance levels (see color coding at the top left corner). Color-less nodes indicate functionally related proteins encoded in the genome of strain Act20, but showing no significant UV-related changes in abundance. The size of these color-less nodes are independent of their abundance levels. Rectangular nodes represent membrane transporters. Nodes with blue scalloped edges (e.g., nadD, in center) and nodes with red edges (e.g., IscS and nudC, center bottom), represent proteins taken from the FR-UV and DR-UV comparisons (**Figure 3B**), respectively. White nodes with separate black arrow edges represent metabolic pathways. Diamonds, triangles, and small circles nodes, represent substrates, free radicals and ions, respectively. Functional interactions among nodes are represented by borders: metabolic pathways/proteins–substrates interactions are represented by solid lines; metabolic pathways/proteins–products interactions are represented by arrows; truncated lines represent inhibitions; zig-zag lines represent DNA repair derivative products. This schema does not consider reversible reactions. All proteins are annotated in **Supplementary file 1, sheet 5**.

than the threshold (criterion B) (**Supplementary file 1** and **Supplementary Figure 4**). However, the comparison of the proteomic profiles achieved under the recovery treatments against the control condition also showed significant increases of other recombinant proteins (**Figure 3A** and **Supplementary Figure 4**). Among them, RecA, RecQ, and recombinant regulatory proteins that modulates RecA activity through direct physical interaction such as radA, recX, and rmuC, as well as proteins that promotes strand exchange reactions in homologous recombination such as the holliday junction DNA helicase RuvB [EC:3.6.4.12] (RuvB) and other putative holliday junction resolvase [EC:3.1.21.10] (RuvX) (**Figure 3A**), reached significantly higher abundance in DR than in Dt according to criteria A and B, as well as significant higher levels in FR but with slightly lower $FC_{difference}$ compared to DR, respectively (**Supplementary Figure 4**). Thus, this notable induction of recombinant proteins abundance observed in UV-treated cultures suggest high activity levels of RecA-dependent processes and homologous recombination, an error-free repair system of single strand gaps and double strand breaks on DNA (Smith and Wang, 1989; Kowalczykowski et al., 1994; Nickoloff and Hoekstra, 2001; Khan and Kuzminov, 2012; Kreuzer, 2013).

Also, the formamidopyrimidine-DNA glycosylase with endonuclease VIII activity [EC:4.2.99.18] (Nei), involved in excising pyrimidines damaged by mutagenic agents (Palmer et al., 1997), showed higher levels during UV exposure than after the dark recovery treatment (**Figure 3B**), suggesting that it may be involved in the UV response (**Figure 4**). Furthermore, another protein that gives indirect evidence about the repair of damaged DNA caused by UV-induced oxidative stress is the upregulation of phosphoglycolate phosphatase [EC:3.1.3.18] (gph), involved in the dissimilation of intracellular 2-phosphoglycolate formed during the repair of the 3′-phosphoglycolate ends in the DNA (Pellicer et al., 2003). Its abundance value was significantly increased in UV compared to Dt but with $FC_{difference}$ slightly

lower than the threshold (**Figure 4** and **Supplementary file 1**). This protein works together with glycolate oxidase [EC:1.1.3.15] (glcD) that reduce the glycolate yielded by gph to produce non-toxic glyoxylate and H_2O_2 which then can be removed by antioxidant enzymes (Pellicer et al., 2003). In addition, 2-phosphoglycolate is a potent inhibitor of 6-phosphofructokinase (EC 2.7.1.11) (PFK) impairing fructose-1,6-bisphosphate production (Seal and Rose, 1987; **Figure 4**).

Also, UV-induced metabolic resetting could be inferred due to the significant increase on CdnL abundance levels during UV exposure, as this protein has been linked to the global control of gene expression through a RNAP–protein interactions mechanism dependent on σA factor; its activity is vital and has been well characterized in Mycobacteriales (Stallings et al., 2009; Weiss et al., 2012; Srivastava et al., 2013; Garner et al., 2014, 2017; Kaur et al., 2014, 2018; Zhu et al., 2019) and Myxococcales (García-Moreno et al., 2010; Gallego-García et al., 2014; Bernal-Bernal et al., 2015) under different stress and virulence conditions. It is known that CdnL activates the transcription of rRNA and components of the transcription machinery (Garner et al., 2014, 2017). Although no measurements of ribosomal RNA levels were made in this study, the abundance of a set of ribosomal proteins, whose abundance are proportionally to rRNA expression levels (Garner et al., 2014, 2017), were significantly higher in the UV dataset compared to FR suggesting that ribosomal assembly and metabolic rates (Nomura, 1999; Casati, 2004) may be altered under UV exposure (**Supplementary Figure 2** in **Supplementary file 2**).

A second functional module induced by UV was linked to the antioxidant activity of the pyruvate dehydrogenase complex (PDH) and to proteins that we interpret, could act systematically to provide the necessary substrates for the synthesis of the cofactors required by PDH. In this sense, PDH are enormous protein complexes containing many copies of three proteins named E1 (AceE), E2 (DlaT), and E3 (LpdC) and three cofactors, lipoic acid (lipoate), thiamine pyrophosphate (TPP) and NAD+ (Rodionov et al., 2002, 2004, 2008; Cicchillo et al., 2004; Spalding and Prigge, 2010; McCarthy and Booker, 2017). In addition, PDH can be associated with adaptor proteins and act as a powerful antioxidant complex that can efficiently eradicate free radicals generated by UV radiation (Bryk et al., 2002; Jaeger et al., 2004; Spalding and Prigge, 2010; Lu and Holmgren, 2014; **Figure 4**).

Lipoyl synthase (lipA) was highly upregulated by UV. This key enzyme of the lipoate synthesis pathway catalyzes sulfur insertion in octanoylated-E2 subunits of PDH complexes to produce lipoylated proteins (Spalding and Prigge, 2010). It works together with the protein lipoyl(octanoyl) transferase [EC:2.3.1.181] (lipB) which transfers an octanoyl group from an octanoyl-acyl-carrier protein (octanoyl-ACP) produced through the type II fatty acid biosynthesis pathway, to the target apoprotein. Alternatively, octanoyl-E2 can be generated by the ATP-dependent ligation of free exogenous octanoate by the lipoate-protein ligase [EC:6.3.1.20] (Lpl). As lipA does not produce lipoate as a free acid (Spalding and Prigge, 2010), higher levels of lipA suggest greater levels of lipoylated-E2 subunits and in turn, suggest the involvement of lipoylated complexes such as PDH in the response against UV.

Following this line of evidence, there was also upregulation of proteins that seems to be linked to TPP biosynthesis through the supplying of substrates for hydroxymethylpyrimidine pyrophosphate (HMP-PP) and hydroxyethyl-thiazole phosphate (HET-P) synthesis (Rodionov et al., 2002). Because Act20 strain lacks an ortholog of a phosphomethylpyrimidine synthase [EC:4.1.99.17] (ThiC) to synthesize HMP-PP from intermediates of the purine biosynthesis pathway, exogenous HMP-P should be introduced into the cell through specific transporters complexes encoded by YkoCDE genes orthologs and then has to be phosphorylated by an hydroxymethylpyrimidine/phosphomethylpyrimidine kinase [EC:2.7.1.49 2.7.4.7] (ThiD) to yield HMP-PP (**Figure 4**). Results show that a homolog of the HMP/thiamine-import ATP-binding protein (YkoD) was significantly upregulated under the UV treatment, and also was the HMP/thiamine permease protein (YkoE) under FR after UV exposure (**Figure 3A**). Likewise, FR also showed high levels of YkoD but with lower $FC_{difference}$ (**Supplementary file 1**). The high levels reached by the YkoD and YkoE in UV-exposed cultures suggest that the YkoCDE complex could be involved in UV response, probably by supplying substrates for HMP-PP and for TPP biosynthesis (Rodionov et al., 2002).

On the other hand, Act20 strain encodes genes to synthesize HET-P via glycine, cysteine, and glycolysis metabolism derivatives, such as iminoglycine, a thiocarboxy-sulfur-carrier protein (ThiS-COSH), and 1-deoxy-D-xylulose-5-phosphate (DXP) (Rodionov et al., 2002). In this process, glycine oxidase [EC:1.4.3.19] (ThiO) enzymatically oxidize glycine to produce iminoglycine (**Figure 4** and **Supplementary Figure 3**). In turn, cysteine is use as SH groups donor to produce ThiS-COSH in a reaction catalyzed by cysteine desulfurase [EC:2.8.1.7] (iscS). Simultaneously, DXP is produced by coupling pyruvate and glyceraldehyde-3-phosphate by the enzyme 1-deoxy-D-xylulose-5-phosphate synthase (dxs). Then, iminoglycine, ThiS-COSH, and DXP are condensed by thiazole synthase [EC:2.8.1.10] (ThiG) to yield HET-P (Rodionov et al., 2002) (the condensation of these three compounds is represented as "thiazole biosynthesis pathway" in **Figure 4**) (see **Supplementary Figure S3** for a complete TPP biosynthesis pathway).

In this context, the significant UV-induced upregulation of the substrate-binding subunit of the D-methionine transport system (metQ) and iscS protein (**Figures 3A,B**), as well as the ATP-binding subunit of L-cystine transport system [EC:7.4.2.1] (tcyC) (**Supplementary file 1**), suggest that the availability of cysteine as a SH group donor may be enhanced in UV-exposed cultures by direct uptake via TycABC transporters, or indirectly via MetNPQ transporters which import methionine that can be transformed into cysteine through the reverse *trans*-sulfuration pathway (Rodionov et al., 2004). In this pathway, methionine is first converted into *S*-adenosylmethionine (SAM) by *S*-adenosylmethionine synthetase [EC:2.5.1.6] (metK), and then into homocysteine via the SAM recycling pathway (Rodionov et al., 2004; **Figure 4**). Subsequently, homocysteine is converted into L-cystathionine by cystathionine beta-synthase

[EC:4.2.1.22] (CBS) and then into cysteine by the action of a cystathionine gamma-lyase (CGL) (**Figure 4**; Rodionov et al., 2004). Act20 strain codes CBS and CGL genes in its genome clustered as an operon (**Supplementary file 1**).

Furthermore, the significant upregulation of Fructokinase (EC 2.7.1.4) (FrK) in UV-exposed cultures (**Figure 3A**), suggests that during UV-exposure intracellular fructose could be phosphorylated and converted into fructose-6-phosphate (Fruc-6P), a substrate of both glycolysis metabolism as well as the non-oxidative phase of the pentose phosphate pathway (**Figure 4** and **Supplementary Figure 1**; Kelker et al., 1970; Binet et al., 1998; Caescu et al., 2004). Next, 6-phosphofructokinase (EC 2.7.1.11) (PFK) could catalyze the phosphorylation of Fruc-6P to fructose-1,6-bisphosphate (Fru-1,6PP), the first committed step of glycolysis, which then could be converted into glyceraldehyde-3-phosphate (G3P) by the action of fructose-bisphosphate aldolase, class II [EC:4.1.2.13] (FBA). As glycolysis proceed, DXP could be produced by coupling pyruvate and G3P through the action of dxs, which get into the thiazole biosynthesis pathway together with iminoglycine and ThiS-COSH yielding HET-P in a reaction catalyzed by ThiG. In addition, pyruvate yielded through glycolysis is also a substrate of the PDH complex (Spalding and Prigge, 2010).

Lastly, thiamin monophosphate (TP) is formed by coupling HMP-PP and HET-P catalyzed by thiamine-phosphate pyrophosphorylase [EC:2.5.1.3] (ThiE). At the next step, TP is phosphorylated by thiamine-monophosphate kinase [EC:2.7.4.16] (ThiL) to form thiamine pyrophosphate, the cofactor of E1-subunits of the PDH complexes (Rodionov et al., 2002). Eventually, TP and TPP can be dephosphorylated by thiamine phosphate phosphatase [EC: 3.1.3.100] (rsgA) to yield thiamine that, in turn, can be reused by the thiaminase [EC:3.5.99.2] (TenA) to produce HMP which can then be reintroduced into the TPP biosynthesis cycle.

In addition, the second functional module includes UV upregulated proteins taken from FR-UV and DR-UV comparisons (**Figure 3C**) which are intimately linked to the *de novo* synthesis and regeneration pathways of NAD+ (Rodionov et al., 2008), a cofactor whose function is associated to several reactions, including the functioning of the PDH complex (Spalding and Prigge, 2010). These proteins were PncA, PncB, nadA, nadD, and nudC (see annotations in **Supplementary file 1**).

As mentioned, the PDH complex can act as an antioxidant by associating DlaT and LpdC proteins with two alkylhydroperoxide reductase peroxyredoxins, AhpC and AhpD. In this system, the oxidized (lipoamide) and reduced (dihydrolipoamide) forms of lipoic acid bounded to DlaT, comprise a redox couple that can effectively extinguish harmful free radicals such as hydroxyl radicals, peroxyl radicals, or superoxide radicals. Briefly, AhpC reduces free radicals and is regenerated by oxidation of AhpD. AhpD is then reduced by oxidation of the dihydrolipoamide linked to DlaT, which in turn is regenerated by LpdC in a NADH-dependent reaction. Thus, AhpC, AhpD, DlaT and LpdC function as redox partners, and also, AhpD acts as a bridge between AhpC and the PDH complex suggesting that an increase in its abundance may increase the antioxidant activity of the complex (**Figure 4**; for a more detailed mechanism see Bryk et al., 2002; Spalding and Prigge, 2010).

In addition, UV exposure induced a significant increase in the abundance of MrpD protein, which is fundamental in the assembly and functioning of a membrane complex involved in maintaining intracellular homeostasis through extrusion of sodium ions and intrusion of protons (Ito et al., 2017). Thus, this protein may be included in the above hypothesized subsystem of damage tolerance. Also, the abundance levels of gvpK protein [involved in gas vesicle biosynthesis (Pfeifer, 2012)], a GntR transcriptional regulator [probably involved in uptake of citrate and related compounds as suggested from the genomic context analysis (Winnen et al., 2003)], and two uncharacterized proteins with DUF4229 and DUF3046 domains, respectively, were significantly increased by UV effect (**Figures 3A**, **4**). Further work will be needed to characterize the exact functions of these proteins in the context of the UV-resistome.

Effects of the Photorecovery Treatment on Molecular Processes After Ultraviolet-B Irradiation

Upon UV-challenge, 26 proteins significantly decreased their abundance levels. In order to identify the cellular processes occurring once the UV stimulus has stopped and those stimulated by the photorecovery treatment, the proteins that decreased in abundance under UV irradiation and then restored their normal levels regardless of the recovery condition as well as those proteins that restored their levels by the effect of FR were studied (**Figures 3C**, **5**; see annotations in **Supplementary file 1**).

Ultraviolet exposure significantly reduced the abundance of the RskA protein, which acts as a repressor of the extracytoplasmic transcriptional factor SigK (ECF19 family) through physical interactions (Staroń et al., 2009; Huang et al., 2015). Then, RskA restored its abundance during FR and DR treatments, suggesting that SigK may coordinate the expression of genes involved in the response against UV-B radiation. UvrC endonuclease involved in nucleotide excision repair of bulky DNA damages such as photoproduct was significantly downregulated under UV, but was restored to its original levels during FR and DR treatments suggesting that the UvrABC base excision repair complex may be involved in the repair of DNA damage caused by UV radiation. Besides, adhP (EC:1.1.1.1), fdhA (EC: 1.2.1.46), Pyruvate carboxylase (PC), and msmX are involved in anaplerotic reactions that supply substrates for the tricarboxylic acid (TCA) cycle through the catabolism of carbohydrates such as alcohols, aldehydes and pyruvate (Gerstmeir et al., 2003; Tanaka et al., 2003; Sauer and Eikmanns, 2005; Arndt and Eikmanns, 2007; Arndt et al., 2008; Marçal et al., 2009) and showed noticeable changes upon UV treatment. Their abundances were significantly decreased under UV exposure and increased later during the recovery treatments, suggesting that energy metabolism and amino acid precursor production from the TCA cycle is truncated by UV irradiation.

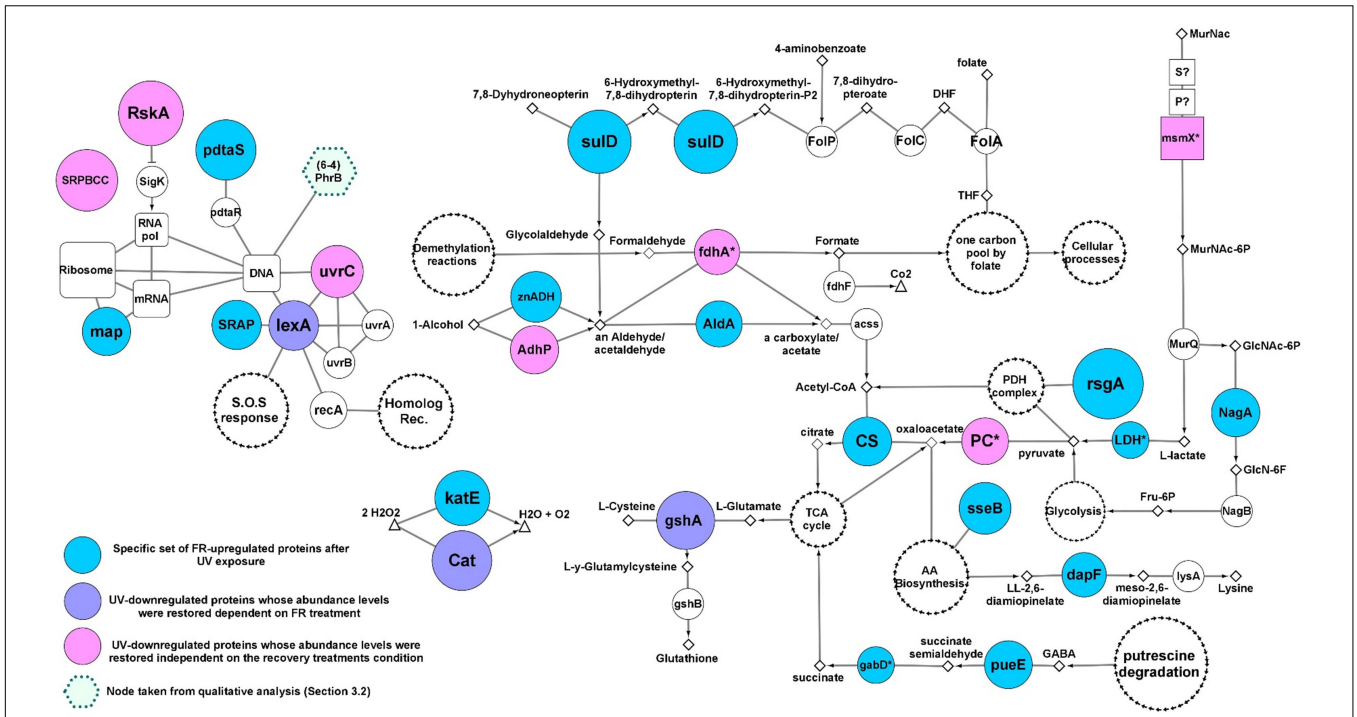

FIGURE 5 | Molecular events involved in FR- response (see **Figure 3C**). Colored nodes indicate proteins whose abundance were significantly increased after UV exposure independent or dependently on FR (see legends in the picture). The size of colored nodes indicates abundance levels. Color-less nodes represent functionally related proteins encoded in the genome of strain Act20, but showing no significant FR-related changes in abundance. The size of color-less nodes are independent of their abundance levels. Rectangular nodes represent membrane transporters. White nodes with separate black arrow edges represent metabolic pathways. Diamonds represent substrates. Functional interactions among nodes are represented by borders: metabolic pathways/proteins–substrates interactions are represented by solid lines; metabolic pathways/proteins–products interactions are represented by arrows. This schema does not consider reversible reactions. All proteins are annotated in **Supplementary file 1, sheet 5**.

The involvement of anaplerotic reactions in the recovery response was also supported by the upregulation of the zinc-dependent aldehyde dehydrogenase (znADH), the *Streptomyces aureofaciens* (AAD23400)-like aldehyde dehydrogenase (AldA), citrate synthase (CS), lactate dehydrogenase (LDH), gabD, and pueE proteins during FR treatment as well as AldH in DR (Sprušanský et al., 1999; Jaureguibeitia et al., 2007; Schneider and Reitzer, 2012; **Figure 5**).

Also, there was a restoration in abundance of both the catalase (Cat) belonging to the manganese cluster family and the glutamate-cysteine ligase gshA involved in thiol biosynthesis. In addition, an upregulation of a second catalase KatE belonging to the heme cluster family was found during FR (**Figures 3C**, **5**), suggesting a high antioxidant activity under this experimental condition, probably in response to an increase in the concentration of free radicals as a consequence of UV irradiation as well as the re-establishment of the metabolic rate.

Another protein that was found significantly increased in FR was the SOS response repressor lexA. In contrast, the RecA protein remains strongly overregulated in DR indicating that white light may be enhancing the repair of damaged DNA in agreement to the photoproduct repair assay (**Figure 1**). Furthermore, the lower abundance values of RecA, radA, and priA proteins in FR treated cultures relative to DR and the upregulation of DNA gyrases and DNA ligases compared to Dt (**Supplementary Figure 4**) are indicative of a temporarily more active state of DNA repair induced by FR. These results support the existence of an efficient photo-induced mechanism of DNA repair possibly involving photolyases as suggested by the qualitative analysis and the photoproduct quantification assay. This finding agrees well with the abundance profile and the biological implications of lexA and RecA proteins (Khan and Kuzminov, 2012; Kreuzer, 2013).

Finally, due to their significantly high abundance values, three unrelated proteins were added to the FR response model, SulD, map, and pdtaS (**Figure 5**). SulD is an essential enzyme involved in the synthesis of pterins such as folate, dihydrofolate and tetrahydrofolate which are essential for cell growth and repair (Garçon et al., 2006).

The methionine amino peptidase (map) participates in the transduction mechanism and protein biosynthesis by removing N-terminal methionine from nascent proteins. Finally, PdtaS is a recently discovered sensor in Actinobacteria whose function and biological implications are currently under discussion. It is proposed that it is involved in the control of amino acid biosynthesis, ribosomal protein levels, and amino acid transfer RNA biosynthesis in a c-di-GMP

dependent mechanism (Morth et al., 2005; Preu et al., 2012; Hariharan et al., 2019).

DISCUSSION

Our results confirm the high UV tolerance profile of *Nesterenkonia* sp. Act20 reported in previous works (Portero et al., 2019) and indicate photorecovery as critical strategy to ensure the viability of *Nesterenkonia* sp. cells exposed to high UV-B doses. Various physiological adaptations at the molecular level allow the organism to persist and survive in extreme environments (Thattai and Van Oudenaarden, 2004; Zenoff et al., 2006b; Albarracín et al., 2014; Portero et al., 2019).

The comparative proteomic assay of the strain Act20 revealed that proteins upregulated by UV-B exposure are part of three proposed UV-resistome subsystems: (i) damage tolerance and oxidative stress response; (ii) energy management and metabolic resetting; and (iii) DNA damage repair. Indeed, homologous recombination was shown to be the primary mechanism of DNA repair as suggested by the high levels of abundance of RecA and other recombinational proteins in UV exposed cultures (Kreuzer, 2013). While homolog recombination acts on single strand gaps and double strand breaks on DNA (secondary lesions), a point mutation (primary lesions) induced by UV irradiation can promote chromosomal fragmentation and single strand gaps when a replication fork advances across a primary lesion which then requires an efficient repair mechanism such as the RecA-dependent processes (Smith and Wang, 1989; Kowalczykowski, 2000; Morimatsu and Kowalczykowski, 2003; Khan and Kuzminov, 2012). Considering the protective mechanism against oxidative stress caused by UV exposure, the pyruvate dehydrogenase complex is the major system involved, as there was a significant increase in the abundance of proteins intimately related to its antioxidant activity and the production of the cofactors required for its function, mainly the lipA and AhpD proteins (Spalding and Prigge, 2010). Thus, despite the fact that at first glance ykoD, MetQ, tcyC, IscS, FrK, PncA, PncB, nadA, nadD, and nudC proteins seemed not to be related to the PDH complex, exhaustive literature mining and the and the review of curated databases indicate that these proteins might be linked to the supply of substrates for the production of cofactors such as thiamine pyrophosphate and NAD+ required by this complex (**Figure 4**). Equally, methionine imported by the MetQPN transporter is also necessary for the production of *S*-adenosylmethionine required by the lipoate synthase protein (LipA) which requires two equivalents of SAM to synthesize one equivalent of lipoic acid (Cicchillo et al., 2004), further linking also this set of proteins to the PDH complex. Likewise, it is also noteworthy to highlight the importance of the upregulation of Frk (EC:2.7.1.4) (Kelker et al., 1970; Binet et al., 1998; Caescu et al., 2004), as this protein accomplishes a dual function in the UV response model: it can supply substrates for thiamine pyrophosphate biosynthesis through the production of fructose-6P for glycolysis, and it is involved in the production of purine and pyrimidine metabolism intermediates through the non-oxidative phase of the pentose phosphate pathway (**Supplementary Figure 1**). In addition, intracellular fructose is the inducer of Frk expression (Kelker et al., 1970; Binet et al., 1998; Caescu et al., 2004). Since exogenous fructose is phosphorylated to fructose-1-phosphate when it enters the cell through the PTS FruAB II transport system, and that byproduct is neither a substrate or an inducer of Frk (ec 2.7.1.4) (Kelker et al., 1970; Binet et al., 1998; Caescu et al., 2004), the upregulation of Frk (EC:2.7.1.4) suggests that there is a consumption of intracellular fructose sources such as xylose or D-sorbitol (**Figure 4**). It should also be kept in mind that Frk remains abundant during recovery treatments. Thus, we consider that FrK (EC:2.7.1.4) is a key enzyme in the UV response, at least under oligotrophic conditions such as physiological solution and under the system tested here.

Upon exposure to UV radiation, the cell viability of Act20 cultures is recovered more efficiently under photorecovery treatment than in dark conditions. In accordance, the FR proteome overexpressed the SOS response repressor lexA, while RecA proteins remain highly abundant in DR-exposed cultures indicating that FR-exposed cultures were in a temporarily more advanced state of DNA repair than DR-cultures, since lexA and RecA proteins are intimately linked through a negative feedback circuit induced by the amount of damaged DNA (Kreuzer, 2013). This suggests the existence of an efficient photo-induced mechanism of DNA repair such as photolyases, as indicated by both the first analysis (in which there appears to be present a second type of photolyase under FR treatment, **Figure 2B**) and the photoproduct quantification assay in which there are significant reductions of photoproduct concentration in FR treatments (**Figure 1**). Replication events at DNA sites bearing cyclobutane pyrimidine dimers and pyrimidine (6-4) pyrimidone photoproduct can generate double strand breaks and single strand gaps in DNA (Smith and Wang, 1989; Kowalczykowski, 2000; Morimatsu and Kowalczykowski, 2003; Khan and Kuzminov, 2012). This induces the upregulation of RecA and other recombinational proteins, in turn triggering effective cleavage of lexA and thereby reducing its abundance. We reasoned that the stimulation of photolyase activity by the photorecovery treatment allows DNA lesions to be repaired before replication forks pass throughout these lesions, thus, preventing ssDNA gaps formation, chromosomal fragmentation, and RecA overexpression. In turn, decreased RecA abundance levels lead to the accumulation of lexA as occurs under FR conditions (Kowalczykowski et al., 1994; Nickoloff and Hoekstra, 2001; Kreuzer, 2013). Thus, photolyases seem to be critical elements of the UV-resistome of Act20 as they are the only light-driven enzymes detected in its genome capable of repairing damaged nucleotides in DNA. In addition, the substantial restoration of the RskA protein abundance levels after UV exposure and during recovery treatments suggests that the extra-cytoplasmic transcriptional factor sigK may coordinate the expression of stress response genes during UV irradiation (Staroń et al., 2009; Huang et al., 2015).

Finally, it is worth noting the remarkable similarity of Act20 molecular UV response mechanisms with those described for common nosocomial strains of the mycobacterial order in response to stress conditions such as the participation

of pyruvate dehydrogenase complex through lipA and AhpD proteins (Tian et al., 2005; Shi and Ehrt, 2006; Spalding and Prigge, 2010), the increased levels of CdnL (Stallings et al., 2009; Garner et al., 2014), and the involvement of the RskA-sigK molecular system (Staroń et al., 2009; Huang et al., 2015). Act20 showed also a remarkable similarity to proteins involved in the anaplerotic reaction of the TCA cycle machinery for the catabolism of aldehydes and alcohols compared to the industrial strain *Corynebacterium glutamicum* (Sprušanský et al., 1999; Jaureguibeitia et al., 2007; Schneider and Reitzer, 2012). Besides, the critical involvement of lipA protein in the UV irradiation response of Act20 suggests greater levels of lipoic acid production, probably due to an increased abundance of free radicals. This supports the idea that lipoate supplementation strategies can contribute to combat oxidative stress (Chen et al., 2014). These notes are of paramount importance in the context of the current interest in finding strains capable of carrying out biotechnological processes under extreme conditions.

CONCLUSION AND FUTURE PROSPECTS

High-Altitude Andean Lakes are natural photobiology laboratories for exploring and monitoring *in situ* interactions between solar irradiation and the dynamics of biodiversity. They also provide us with model strains to perform *in vitro* assays and test light and specially UV effects on microbial physiology. In this work, we have compared the UV-resistance profile of two *Nesterenkonia* strains, one isolated from the HAAL (Act20) and the other in another extreme setting such as a desert soil from China (*N. halotolerans*). Our results indicated the UV-resistance superior phenotype of Act20, a clear reflection of the environmental conditions prevailing in the Puna region. This phenotype was based mainly in the Act20 ability to cope with much more photoproduct accumulation in its DNA but also with more efficient repairing systems triggered by light (photolyases). Current work is heading toward the heterologous expression and structural/functional characterization of both, putative 6,4 and CPD photolyases detected in Act20 genome and experimental proteome.

Moreover, the herein presented research represents an advance in the knowledge on the integral molecular response to UV-B radiation in an environmental bacterium. Through a comparative analytical approach and photoproduct measurements, Act20 UV-resistome was dissected. Unlike previous reports that studied particular molecular mechanisms (e.g., photorepair or oxidative damage response) involved in the UV-C response of lab strains such as *E. coli* we have studied Act20 response to UV-B in an integral manner configuring a functional network of tightly related molecular events detonated upon the radiation challenge. Moreover, there were consistent differences with the molecular events occurring in both repair treatments -with and without light. Indeed, this proteomic versatility may be a reflection on their original changing environment and of utmost importance for survival in this ecosystem, the highest UV irradiated environment on Earth. To our knowledge, this is the first work to show the UV-induced gene expression in a *Nesterenkonia* strain.

Finally, this work opens an avenue for biotechnological applications. As previously exposed, UV resistant microbes present a myriad of strategies to overcome the harmful radiation. In these strategies, molecules of diverse chemistry are produced and constitute excellent microbial metabolic reserves (i.e., extremolytes) that have been widely explored for industrial significance; however, their therapeutic implications remain to be investigated. That is the case for HAAL indigenous extremophiles and specially for *Nesterenkonia* sp. Act20 that produce biomolecules (i.e., ectoine, photolyase, carotenoids) adapted to their unusual living conditions that may represent valuable sources of novel bioproducts. This topic is intriguing and needs further investigations for reaching concrete applications.

DATA AVAILABILITY STATEMENT

The datasets presented in this study can be found in online repositories. The names of the repository/repositories and accession number(s) can be found in the article/ **Supplementary Material**.

AUTHOR CONTRIBUTIONS

LP, FZ, and VA performed the experimental assays on DNA and protein manipulation. FZ performed the data analysis, interpretation and wrote the manuscript. VA designed and coordinated the research work and wrote the manuscript. TD performed the photoproduct measurements and subsequent analysis and wrote the manuscript. WG provided lab space, analyzed and interpreted data and wrote the manuscript. MF, WG, and VA obtained funding for the original project idea. MF performed sampling expeditions and provided strains for the present project. All authors contributed to the article and approved the submitted version.

FUNDING

This study was funded by Project CONICET PIP 2013-11220120100519CO, Project PICT 2013-2991, Project PICT-RAICES 2019-03216, Project PIUNT G603, Marie Curie FP7-People-2010-IIF EXTREMOPHIL (273831) in Germany and its return phase in Argentina (PIIFR-GA-2010-910831-EXTREMOPHIL).

SUPPLEMENTARY MATERIAL

The Supplementary Material for this article can be found online at: https://www.frontiersin.org/articles/10.3389/fmicb.2022.791714/full#supplementary-material

REFERENCES

Aertsen, A., and Michiels, C. W. (2004). Stress and how bacteria cope with death and survival. *Crit. Rev. Microbiol.* 30, 263–273. doi: 10.1080/10408410490884757

Albarracín, V. H., Dib, J. R., Ordoñez, O. F., and Farías, M. E. (2011). "A harsh life to indigenous proteobacteria at the andeanmountains: microbial diversity and resistance mechanisms towards extreme conditions," in *Proteobacteria: Phylogeny, Metabolic Diversity and Ecological Effects*, ed. M. L. Sezenna (Hauppauge, NY: Nova Science Publishers), 91–130.

Albarracín, V. H., Gärtner, W., and Farías, M. E. (2016). Forged under the sun: life and art of extremophiles from Andean Lakes. *Photochem. Photobiol.* 92, 14–28. doi: 10.1111/php.12555

Albarracín, V. H., Kraiselburd, I., Bamann, C., Wood, P. G., Bamberg, E., Farias, M. E., et al. (2016). Functional green-tuned proteorhodopsin from modern stromatolites. *PLoS One* 11:e0154962. doi: 10.1371/journal.pone.0154962

Albarracín, V. H., Kurth, D., Ordoñez, O. F., Belfiore, C., Luccini, E., Salum, G. M., et al. (2015). High-up: a remote reservoir of microbial extremophiles in central Andean Wetlands. *Front. Microbiol.* 6:1404. doi: 10.3389/fmicb.2015.01404

Albarracín, V. H., Pathak, G. P., Douki, T., Cadet, J., Borsarelli, C. D., Gärtner, W., et al. (2012). Extremophilic *Acinetobacter* strains from high-altitude lakes in Argentinean Puna: remarkable UV-B resistance and efficient DNA damage repair. *Orig. Life Evol. Biosph.* 42, 201–221. doi: 10.1007/s11084-012-9276-3

Albarracín, V. H., Simon, J., Pathak, G. P., Valle, L., Douki, T., Cadet, J., et al. (2014). First characterisation of a CPD-class I photolyase from a UV-resistant extremophile isolated from high-altitude Andean Lakes. *Photochem. Photobiol. Sci.* 13, 739–751. doi: 10.1039/c3pp50399b

Alonso-Reyes, D. G., Galván, F. S., Portero, L. R., Alvarado, N. N., Farías, M. E., Vazquez, M. P., et al. (2021). Genomic insights into an andean multiresistant soil actinobacterium of biotechnological interest. *World J. Microbiol. Biotechnol.* 37:166. doi: 10.1007/s11274-021-03129-9

Alonso-Reyes, D., Farias, M., and Albarracín, V. H. (2020). Uncovering cryptochrome/photolyase gene diversity in aquatic microbiomes exposed to diverse UV-B regimes. *Aquat. Microbial. Ecol.* 85, 141–154. doi: 10.3354/ame01947

Arndt, A., and Eikmanns, B. J. (2007). The alcohol dehydrogenase gene adhA in *Corynebacterium glutamicum* is subject to carbon catabolite repression. *J. Bacteriol.* 189, 7408–7416. doi: 10.1128/JB.00791-07

Arndt, A., Auchter, M., Ishige, T., Wendisch, V. F., and Eikmanns, B. J. (2008). Ethanol catabolism in *Corynebacterium glutamicum*. *J. Mol. Microbiol. Biotechnol.* 15, 222–233. doi: 10.1159/000107370

Belfiore, C., Ordoñez, O. F., and Farías, M. E. (2013). Proteomic approach of adaptive response to arsenic stress in *Exiguobacterium* sp. S17, an extremophile strain isolated from a high-altitude Andean Lake stromatolite. *Extremophiles* 17, 421–431. doi: 10.1007/s00792-013-0523-y

Bernal-Bernal, D., Gallego-García, A., García-Martínez, G., García-Heras, F., Jiménez, M. A., Padmanabhan, S., et al. (2015). Structure-function dissection of *Myxococcus xanthus* CarD N-terminal domain, a defining member of the CarD-CdnL-TRCF family of RNA polymerase interacting proteins. *PLoS One* 10:e0121322. doi: 10.1371/journal.pone.0121322

Binet, M. R. B., Rager, M. N., and Bouvet, O. M. M. (1998). Fructose and mannose metabolism in *Aeromonas hydrophila*: identification of transport systems and catabolic pathways. *Microbiology* 144, 1113–1121. doi: 10.1099/00221287-144-4-1113

Bonilla, J. O., Callegari, E. A., Estevéz, M. C., and Villegas, L. B. (2020). Intracellular proteomic analysis of *Streptomyces* sp. MC1 when exposed to Cr(VI) by gel-based and gel-free methods. *Curr. Microbiol.* 77, 62–70. doi: 10.1007/s00284-019-01790-w

Bryk, R., Lima, C. D., Erdjument-Bromage, H., Tempst, P., and Nathan, C. (2002). Metabolic enzymes of mycobacteria linked to antioxidant defense by a thioredoxin-like protein. *Science* 295, 1073–1077. doi: 10.1126/science.1067798

Cabrol, N. A., Feister, U., Häder, D.-P., Piazena, H., Grin, E. A., and Klein, A. (2014). Record solar UV irradiance in the tropical Andes. *Front. Environ. Sci.* 2:19. doi: 10.3389/fenvs.2014.00019

Cabrol, N. A., Grin, E. A., Bebout, L., Chong, G., Demergasso, C., Fleming, E., et al. (2009). "High lakes project – impact of climate variability and high uv flux on lake habitat: implications for early mars and present-day earth," in *Proceedings of the 40th Lunar and Planetary Science Conference, (Lunar and Planetary Science XL), held March 23-27, 2009*, The Woodlands, TX, 1141.

Cabrol, N. A., Grin, E. A., Hock, A., Kiss, A., Borics, G., Kiss, K., et al. (2004). "Investigating the impact of uv radiation on high-altitude shallow lake habitats, life diversity, and life survival strategies: clues for mars' past habitability potential?," in *Proceedings of the 35th Annual Lunar and Planetary Science Conference*, League City, TX, 1049.

Caescu, C. I., Vidal, O., Krzewinski, F., and Artenie, V. (2004). *Bifidobacterium longum* requires a fructokinase (Frk; ATP: D. *J. Bacteriol.* 186, 6515–6525. doi: 10.1128/JB.186.19.6515

Casati, P. (2004). Crosslinking of ribosomal proteins to RNA in maize ribosomes by UV-B and its effects on translation. *Plant Physiol.* 136, 3319–3332. doi: 10.1104/pp.104.047043

Chen, C., Han, X., Zou, X., Li, Y., Yang, L., Cao, K., et al. (2014). 4-Methylene-2-octyl-5-oxotetrahydrofuran-3-carboxylic acid (C75), an inhibitor of fatty-acid synthase, suppressesthe mitochondrial fatty acid synthesis pathway and impairs mitochondrial function. *J. Biol. Chem.* 289, 17184–17194. doi: 10.1074/jbc.M114.550806

Cicchillo, R. M., Iwig, D. F., Jones, A. D., Nesbitt, N. M., Baleanu-Gogonea, C., Souder, M. G., et al. (2004). Lipoyl synthase requires two equivalents of S-adenosyl-L-methionine to synthesize one equivalent of lipoic acid. *Biochemistry* 43, 6378–6386. doi: 10.1021/bi049528x

Dib, J., Weiss, A., Neumann, A., Ordoñez, O., Estévez, M. C., and Farías, M. E. (2009). Isolation of bacteria from remote high altitude Andean lakes able to grow in the presence of antibiotics. *Recent Patents Anti Infect. Drug Discov.* 4, 66–76. doi: 10.2174/157489109787236300

Douki, T. (2013). The variety of UV-induced pyrimidine dimeric photoproduct in DNA as shown by chromatographic quantification methods. *Photochem. Photobiol. Sci.* 12, 1286–1302. doi: 10.1039/c3pp25451h

Douki, T., and Cadet, J. (2001). Individual determination of the yield of the main UV-induced dimeric pyrimidine photoproduct in DNA suggests a high mutagenicity of CC photolesions. *Biochemistry* 40, 2495–2501. doi: 10.1021/bi0022543

Escudero, L., Chong, G., Demergasso, C., Farías, M. E., Cabrol, N. A., Grin, E., et al. (2007). "Investigating microbial diversity and UV radiation impact at the high-altitude Lake Aguas Calientes, Chile," in *Proceedings of the Instruments, Methods, and Missions for Astrobiology X, 6694(2007), 66940Z*, San Diego, CA. doi: 10.1117/12.736970

Farías, M. E. (2020). *Microbial Ecosystems in Central Andes Extreme environments : Biofilms, Microbial Mats, Microbialites and Endoevaporites*. Cham: Springer, doi: 10.1007/978-3-030-36192-1

Flores, M. R., Ordoñez, O. F., Maldonado, M. J., and Farías, M. E. (2009). Isolation of UV-B resistant bacteria from two high altitude Andean lakes (4,400 m) with saline and non saline conditions. *J. Gen. Appl. Microbiol.* 55, 447–458. doi: 10.2323/jgam.55.447

Gallego-García, A., Mirassou, Y., García-Moreno, D., Elías-Arnanz, M., Jiménez, M. A., and Padmanabhan, S. (2014). Structural insights into RNA polymerase recognition and essential function of *Myxococcus xanthus* CdnL. *PLoS One* 9:e108946. doi: 10.1371/journal.pone.0108946

García-Moreno, D., Abellón-Ruiz, J., García-Heras, F., Murillo, F. J., Padmanabhan, S., and Elías-Arnanz, M. (2010). CdnL, a member of the large CarD-like family of bacterial proteins, is vital for *Myxococcus xanthus* and differs functionally from the global transcriptional regulator CarD. *Nucleic Acids Res.* 38, 4586–4598. doi: 10.1093/nar/gkq214

Garçon, A., Levy, C., and Derrick, J. P. (2006). Crystal structure of the bifunctional dihydroneopterin aldolase/6-hydroxymethyl-7,8-dihydropterin pyrophosphokinase from *Streptococcus pneumoniae*. *J. Mol. Biol.* 360, 644–653. doi: 10.1016/j.jmb.2006.05.038

Garner, A. L., Rammohan, J., Huynh, J. P., Onder, L. M., Chen, J., Bae, B., et al. (2017). Effects of increasing the affinity of CarD for RNA polymerase on *Mycobacterium tuberculosis* growth, rRNA transcription, and virulence. *J. Bacteriol.* 199:e00698-16. doi: 10.1128/JB.00698-16

Garner, A. L., Weiss, L. A., Manzano, A. R., Galburt, E. A., and Stallings, C. L. (2014). CarD integrates three functional modules to promote efficient transcription, antibiotic tolerance, and pathogenesis in mycobacteria. *Mol. Microbiol.* 93, 682–697. doi: 10.1111/mmi.12681

Gerstmeir, R., Wendisch, V. F., Schnicke, S., Ruan, H., Farwick, M., Reinscheid, D., et al. (2003). Acetate metabolism and its regulation in *Corynebacterium glutamicum*. *J. Biotechnol.* 104, 99–122. doi: 10.1016/S0168-1656(03)00167-6

Gorriti, M. F., Dias, G. M., Chimetto, L. A., Trindade-Silva, A. E., Silva, B. S., Mesquita, M., et al. (2014). Genomic and phenotypic attributes of novel salinivibrios from stromatolites, sediment and water from a high altitude lake. *BMC Genomics* 15:473. doi: 10.1186/1471-2164-15-473

Hariharan, V. N., Thakur, C., Singh, A., Gopinathan, R., Singh, D. P., Sankhe, G., et al. (2019). The histidine kinase PdtaS is a cyclic di-GMP binding metabolic sensor that controls mycobacterial adaptation to nutrient deprivation. *bioRxiv* [Preprint]. doi: 10.1101/615575

Huang, X., Pinto, D., Fritz, G., and Mascher, T. (2015). Environmental sensing in Actinobacteria: a comprehensive survey on the signaling capacity of this phylum. *J. Bacteriol.* 197, 2517–2535. doi: 10.1128/JB.00176-15

Ito, M., Morino, M., and Krulwich, T. A. (2017). Mrp antiporters have important roles in diverse bacteria and archaea. *Front. Microbiol.* 8:2325. doi: 10.3389/fmicb.2017.02325

Jaeger, T., Budde, H., Flohé, L., Menge, U., Singh, M., Trujillo, M., et al. (2004). Multiple thioredoxin-mediated routes to detoxify hydroperoxides in Mycobacterium tuberculosis. *Arch. Biochem. Biophys.* 423, 182–191. doi: 10.1016/j.abb.2003.11.021

Jaureguibeitia, A., Saá, L., Llama, M. J., and Serra, J. L. (2007). Purification, characterization and cloning of aldehyde dehydrogenase from Rhodococcus erythropolis UPV-1. *Appl. Microbiol. Biotechnol.* 73, 1073–1086. doi: 10.1007/s00253-006-0558-4

Kaern, M., Elston, T. C., Blake, W. J., and Collins, J. J. (2005). Stochasticity in gene expression: from theories to phenotypes. *Nat. Rev. Genet.* 6, 451–464. doi: 10.1038/nrg1615

Kaur, G., Dutta, D., and Thakur, K. G. (2014). Crystal structure of *Mycobacterium tuberculosis* CarD, an essential RNA polymerase binding protein, reveals a quasidomain-swapped dimeric structural architecture. *Proteins Struct. Funct. Bioinform.* 82, 879–884. doi: 10.1002/prot.24419

Kaur, G., Kaundal, S., Kapoor, S., Grimes, J. M., Huiskonen, J. T., and Thakur, K. G. (2018). *Mycobacterium tuberculosis* CarD, an essential global transcriptional regulator forms amyloid-like fibrils. *Sci. Rep.* 8:10124. doi: 10.1038/s41598-018-28290-4

Kelker, N. E., Hanson, T. E., and Anderson, R. L. (1970). Alternate pathways of D-Fructose in *Aerobacter aerogenes*. *J. Biol. Chem.* 245, 2060–2065. doi: 10.1016/S0021-9258(18)63206-5

Khan, S. R., and Kuzminov, A. (2012). Replication forks stalled at ultraviolet lesions are rescued via RecA and RuvABC protein-catalyzed disintegration in *Escherichia coli*. *J. Biol. Chem.* 287, 6250–6265. doi: 10.1074/jbc.M111.322990

Kowalczykowski, S. C. (2000). Initiation of genetic recombination and recombination-dependent replication. *Trends Biochem. Sci.* 25, 156–165. doi: 10.1016/S0968-0004(00)01569-3

Kowalczykowski, S. C., Dixon, D. A., Eggleston, A. K., Lauder, S. D., and Rehrauer, W. M. (1994). Biochemistry of homologous recombination in *Escherichia coli*. *Microbiol. Rev.* 58, 401–465. doi: 10.1177/0898264309358764

Kreuzer, K. N. (2013). DNA damage responses in prokaryotes: replication forks. *Cold Spring Harb. Perspect. Biol.* 5:a012674. doi: 10.1101/cshperspect.a012674

Kurth, D., Amadio, A., Ordoñez, O. F., Albarracín, V. H., Gärtner, W., and Farías, M. E. (2017). Arsenic metabolism in high altitude modern stromatolites revealed by metagenomic analysis. *Sci. Rep.* 7:1024. doi: 10.1038/s41598-017-00896-0

Kurth, D., Belfiore, C., Gorriti, M. F., Cortez, N., Farias, M. E., and Albarracín, V. H. (2015). Genomic and proteomic evidence unravel the UV-resistome of the poly-extremophile *Acinetobacter* sp. Ver3. *Front. Microbiol.* 6:328. doi: 10.3389/fmicb.2015.00328

Lazar, C., Gatto, L., Ferro, M., Bruley, C., and Burger, T. (2016). Accounting for the multiple natures of missing values in label-free quantitative proteomics data sets to compare imputation strategies. *J. Proteome Res.* 15, 1116–1125. doi: 10.1021/acs.jproteome.5b00981

Liley, J. B., and Mckenzie, R. L. (2006). Where on Earth has the highest UV? *Natl. Inst. Water Atmos. Res.* 1, 36–37.

Lamprecht-Grandío, M., Cortesão, M., Mirete, S., De la Cámara, M. B., De Figueras, C. G., Pérez-Pantoja, D., et al. (2020). Novel genes involved in resistance to both ultraviolet radiation and perchlorate from the metagenomes of hypersaline environments. *Front. Microbiol.* 11:453. doi: 10.3389/fmicb.2020.00453

Lu, J., and Holmgren, A. (2014). The thioredoxin antioxidant system. *Free Radic. Biol. Med.* 66, 75–87. doi: 10.1016/j.freeradbiomed.2013.07.036

Luccini, E., Cede, A., Piacentini, R., Villanueva, C., and Canziani, P. (2006). Ultraviolet climatology over Argentina. *J. Geophys. Res. Atmos.* 111:D17312. doi: 10.1029/2005JD006580

Marçal, D., Rêgo, A. T., Carrondo, M. A., and Enguita, F. J. (2009). 1,3-Propanediol dehydrogenase from *Klebsiella pneumoniae*: decameric quaternary structure and possible subunit cooperativity. *J. Bacteriol.* 191, 1143–1151. doi: 10.1128/JB.01077-08

McCarthy, E. L., and Booker, S. J. (2017). Destruction and reformation of an iron-sulfur cluster during catalysis by lipoyl synthase. *Science* 358, 373–377. doi: 10.1126/science.aan4574

Morimatsu, K., and Kowalczykowski, S. C. (2003). RecFOR proteins load RecA protein onto gapped DNA to accelerate DNA strand exchange: a universal step of recombinational repair. *Mol. Cell* 11, 1337–1347. doi: 10.1016/S1097-2765(03)00188-6

Morth, J. P., Gosmann, S., Nowak, E., and Tucker, P. A. (2005). A novel two-component system found in *Mycobacterium tuberculosis*. *FEBS Lett.* 579, 4145–4148. doi: 10.1016/j.febslet.2005.06.043

Nickoloff, J. A., and Hoekstra, M. F. (2001). *DNA Damage and Repair. Issue Advances from Phage to Humans*, Vol. III. Berlin: Springer Science & Business Media. doi: 10.1038/nature01408

Nomura, M. (1999). Regulation of ribosome biosynthesis in *Escherichia coli* and *Saccharomyces cerevisiae*: diversity and common principles. *J. Bacteriol.* 181, 6857–6864. doi: 10.1128/JB.181.22.6857-6864.1999

Ordoñez, O. F., Flores, M. R., Dib, J. R., Paz, A., and Farías, M. E. (2009). Extremophile culture collection from Andean lakes: extreme pristine environments that host a wide diversity of microorganisms with tolerance to UV radiation. *Microb. Ecol.* 58, 461–473. doi: 10.1007/s00248-009-9527-7

Ordoñez, O. F., Rasuk, M. C., Soria, M. N., Contreras, M., and Farías, M. E. (2018). Haloarchaea from the Andean Puna: biological role in the energy metabolism of arsenic. *Microb. Ecol.* 76, 695–705. doi: 10.1007/s00248-018-1159-3

Orellana, R., Rojas, C., Seeger, M., Cumsille, A., Macaya, C., Dorochesi, F., et al. (2018). Living at the frontiers of life: extremophiles in Chile and their potential for bioremediation. *Front. Microbiol.* 9:2309. doi: 10.3389/fmicb.2018.02309

Palmer, C. M., Serafini, D. M., and Schellhorn, H. E. (1997). Near ultraviolet radiation (UVA and UVB) causes a formamidopyrimidineglycosylase-dependent increase in G to T transversions. *Photochem. Photobiol.* 65, 543–549. doi: 10.1111/j.1751-1097.1997.tb08602.x

Pellicer, M. T., Nun, M. F., and Baldoma, L. (2003). Role of 2-phosphoglycolate phosphatase of *Escherichia coli* in metabolism of the 2-phosphoglycolate formed in DNA Repair. *Microbiology* 185, 5815–5821. doi: 10.1128/JB.185.19.5815

Perez, M. F., Kurth, D., Farías, M. E., Soria, M. N., Castillo Villamizar, G. A., Poehlein, A., et al. (2020). First report on the plasmidome from a high-Altitude Lake of the Andean Puna. *Front. Microbiol.* 11:1343. doi: 10.3389/fmicb.2020.01343

Pérez, V., Hengst, M., Kurte, L., Dorador, C., Jeffrey, W. H., Wattiez, R., et al. (2017). Bacterial survival under extreme UV radiation: a comparative proteomics study of Rhodobacter sp., isolated from high altitude wetlands in Chile. *Front. Microbiol.* 8:1173. doi: 10.3389/fmicb.2017.01173

Pfeifer, F. (2012). Distribution, formation and regulation of gas vesicles. *Nat. Rev. Microbiol.* 10, 705–715. doi: 10.1038/nrmicro2834

Portero, L. R., Alonso-Reyes, D. G., Zannier, F., Vazquez, M. P., Farías, M. E., Gärtner, W., et al. (2019). Photolyases and cryptochromes in UV-resistant Bacteria from High-altitude Andean Lakes. *Photochem. Photobiol.* 95, 315–330. doi: 10.1111/php.13061

Preu, J., Panjikar, S., Morth, P., Jaiswal, R., Karunakar, P., and Tucker, P. A. (2012). The sensor region of the ubiquitous cytosolic sensor kinase, PdtaS, contains PAS and GAF domain sensing modules. *J. Struct. Biol.* 177, 498–505. doi: 10.1016/j.jsb.2011.11.012

R Core Team (2016). *R: A Language and Environment for Statistical Computing*. Vienna: R Foundation for Statistical Computing.

Ramírez Santos, J., Solís Guzmán, G., and Gómez Eichelmann, M. C. (2001). Regulación genética en la respuesta al estrés calórico en *Escherichia coli*. *Rev. Latinoam. Microbiol.* 43, 51–63.

Rascovan, N., Maldonado, J., Vazquez, M. P., and Farías, M. E. (2016). Metagenomic study of red biofilms from Diamante Lake reveals ancient arsenic bioenergetics in haloarchaea. *Int. Soc. Microb. Ecol.* 109, 299-309. doi: 10.1038/ismej.2015.109

Rasuk, M. C., Ferrer, G. M., Kurth, D., Portero, L. R., Farías, M. E., and Albarracín, V. H. (2017). UV-Resistant actinobacteria from high-altitude Andean Lakes: isolation, characterization and antagonistic activities. *Photochem. Photobiol.* 93, 865–880. doi: 10.1111/php.12759

Ravanat, J. L., Douki, T., and Cadet, J. (2001). Direct and indirect effects of UV radiation on DNA and its components. *J. Photochem. Photobiol. B Biol.* 63, 88–102. doi: 10.1016/S1011-1344(01)00206-8

Rodionov, D. A., De Ingeniis, J., Mancini, C., Cimadamore, F., Zhang, H., Osterman, A. L., et al. (2008). Transcriptional regulation of NAD metabolism in bacteria: NrtR family of Nudix-related regulators. *Nucleic Acids Res.* 36, 2047–2059. doi: 10.1093/nar/gkn047

Rodionov, D. A., Vitreschak, A. G., Mironov, A. A., and Gelfand, M. S. (2002). Comparative genomics of thiamin biosynthesis in procaryotes. New genes and regulatory mechanisms. *J. Biol. Chem.* 277, 48949–48959. doi: 10.1074/jbc.M208965200

Rodionov, D. A., Vitreschak, A. G., Mironov, A. A., and Gelfand, M. S. (2004). Comparative genomics of the methionine metabolism in Gram-positive bacteria: a variety of regulatory systems. *Nucleic Acids Res.* 32, 3340–3353. doi: 10.1093/nar/gkh659

Saona, L. A., Soria, M., Durán-Toro, V., Wörmer, L., Milucka, J., Castro-Nallar, E., et al. (2021). Phosphate-arsenic interactions in Halophilic Microorganisms of the microbial mat from Laguna Tebenquiche: from the microenvironment to the genomes. *Microb. Ecol.* 81, 941–953. doi: 10.1007/s00248-020-01673-9

Sauer, U., and Eikmanns, B. J. (2005). The PEP-pyruvate-oxaloacetate node as the switch point for carbon flux distribution in bacteria. *FEMS Microbiol. Rev.* 29, 765–794. doi: 10.1016/j.femsre.2004.11.002

Schneider, B. L., and Reitzer, L. (2012). Pathway and enzyme redundancy in putrescine catabolism in *Escherichia coli*. *J. Bacteriol.* 194, 4080–4088. doi: 10.1128/JB.05063-11

Seal, S. N., and Rose, Z. B. (1987). Characterization of a phosphoenzyme intermediate in the reaction of phosphoglycolate phosphatase. *J. Biol. Chem.* 262, 13496–13500. doi: 10.1016/s0021-9258(19)76454-0

Shannon, P., Markiel, A., Ozier, O., Baliga, N. S., Wang, J. T., Ramage, D., et al. (2003). Cytoscape: a software environment for integrated models of biomolecular interaction networks. *Genome Res.* 13:249. doi: 10.1101/gr.1239303

Shi, S., and Ehrt, S. (2006). Dihydrolipoamide acyltransferase is critical for. *Society* 74, 56–63. doi: 10.1128/IAI.74.1.56

Smith, K. C., and Wang, T. V. (1989). recA-dependent DNA repair processes. *BioEssays* 10, 12–16. doi: 10.1002/bies.950100104

Spalding, M. D., and Prigge, S. T. (2010). Lipoic acid metabolism in microbial pathogens. *Microbiol. Mol. Biol. Rev.* 74, 200–228. doi: 10.1128/mmbr.00008-10

Sprušanský, O., Homérová, D., Ševčíková, B., and Kormanec, J. (1999). Cloning of the putative aldehyde dehydrogenase, aldA, gene from *Streptomyces aureofaciens*. *Folia Microbiol.* 44, 491–502. doi: 10.1007/BF02816249

Srivastava, D. B., Leon, K., Osmundson, J., Garner, A. L., Weiss, L. A., Westblade, L. F., et al. (2013). Structure and function of CarD, an essential mycobacterial transcription factor. *Proc. Natl. Acad. Sci. U.S.A.* 110, 12619–12624. doi: 10.1073/pnas.1308270110

Stallings, C. L., Stephanou, N. C., Chu, L., Hochschild, A., Nickels, B. E., and Glickman, M. S. (2009). CarD is an essential regulator of rRNA transcription required for *Mycobacterium tuberculosis* persistence. *Cell* 138, 146–159. doi: 10.1016/j.cell.2009.04.041

Staroń, A., Sofia, H. J., Dietrich, S., Ulrich, L. E., Liesegang, H., and Mascher, T. (2009). The third pillar of bacterial signal transduction: classification of the extracytoplasmic function (ECF) σ factor protein family. *Mol. Microbiol.* 74, 557–581. doi: 10.1111/j.1365-2958.2009.06870.x

Szklarczyk, D., Morris, J. H., Cook, H., Kuhn, M., Wyder, S., Simonovic, M., et al. (2017). The STRING database in 2017: quality-controlled protein-protein association networks, made broadly accessible. *Nucleic Acids Res.* 45, D362–D368. doi: 10.1093/nar/gkw937

Tanaka, N., Kusakabe, Y., Ito, K., Yoshimoto, T., and Nakamura, K. T. (2003). Crystal structure of glutathione-independent formaldehyde dehydrogenase. *Chem. Biol. Interact.* 143–144, 211–218. doi: 10.1016/S0009-2797(02)00168-0

Thattai, M., and Van Oudenaarden, A. (2004). Stochastic gene expression in fluctuating environments. *Genetics* 167, 523–530. doi: 10.1534/genetics.167.1.523

Tian, J., Bryk, R., Shi, S., Erdjument-Bromage, H., Tempst, P., and Nathan, C. (2005). *Mycobacterium tuberculosis* appears to lack α-ketoglutarate dehydrogenase and encodes pyruvate dehydrogenase in widely separated genes. *Mol. Microbiol.* 57, 859–868. doi: 10.1111/j.1365-2958.2005.04741.x

Toneatti, D. M., Albarracín, V. H., Flores, M. R., Polerecky, L., and Farías, M. E. (2017). Stratified bacterial diversity along physico-chemical gradients in high-altitude modern stromatolites. *Front. Microbiol.* 8:646. doi: 10.3389/fmicb.2017.00646

Tyanova, S., Temu, T., Sinitcyn, P., Carlson, A., Hein, M. Y., Geiger, T., et al. (2016). The Perseus computational platform for comprehensive analysis of (prote)omics data. *Nat. Methods* 13, 731–740. doi: 10.1038/nmeth.3901

Vignale, F. A., Lencina, A. I., Stepanenko, T. M., Soria, M. N., Saona, L. A., Kurth, D., et al. (2021). Lithifying and non-lithifying microbial ecosystems in the wetlands and salt flats of the Central Andes. *Microb. Ecol.* 1–17. doi: 10.1007/s00248-021-01725-8

Weiss, L. A., Harrison, P. G., Nickels, B. E., Glickman, M. S., Campbell, E. A., Darst, S. A., et al. (2012). Interaction of CarD with RNA polymerase mediates *Mycobacterium tuberculosis* viability, rifampin resistance, and pathogenesis. *J. Bacteriol.* 194, 5621–5631. doi: 10.1128/jb.00879-12

Winnen, B., Hvorup, R. N., and Saier, M. H. (2003). The tripartite tricarboxylate transporter (TTT) family. *Res. Microbiol.* 154, 457–465. doi: 10.1016/S0923-2508(03)00126-8

Witten, D., and Tibshirani, R. (2007). A comparison of fold-change and the t-statistic for microarray data analysis. *Analysis* 1776, 58–85.

Zannier, F., Portero, L. R., Ordoñez, O. F., Martinez, L. J., Farías, M. E., and Albarracin, V. H. (2019). Polyextremophilic bacteria from high altitude Andean Lakes: arsenic resistance profiles and biofilm production. *Biomed. Res. Int.* 2019:1231975. doi: 10.1155/2019/1231975

Zenoff, V. F., Heredia, J., Ferrero, M., Siñeriz, F., and Farías, M. E. (2006a). Diverse UV-B resistance of culturable bacterial community from high-altitude wetland water. *Curr. Microbiol.* 52, 359–362. doi: 10.1007/s00284-005-0241-5

Zenoff, V. F., Siñeriz, F., and Farías, M. E. (2006b). Diverse responses to UV-B radiation and repair mechanisms of bacteria isolated from high-altitude aquatic environments. *Appl. Environ. Microbiol.* 72, 7857–7863. doi: 10.1128/AEM.01333-06

Zhu, D. X., Garner, A. L., Galburt, E. A., and Stallings, C. L. (2019). CarD contributes to diverse gene expression outcomes throughout the genome of *Mycobacterium tuberculosis*. *Proc. Natl. Acad. Sci. U.S.A.* 116, 13573–13581. doi: 10.1073/pnas.1900176116

Conflict of Interest: The authors declare that the research was conducted in the absence of any commercial or financial relationships that could be construed as a potential conflict of interest.

Publisher's Note: All claims expressed in this article are solely those of the authors and do not necessarily represent those of their affiliated organizations, or those of the publisher, the editors and the reviewers. Any product that may be evaluated in this article, or claim that may be made by its manufacturer, is not guaranteed or endorsed by the publisher.

frontiers in Microbiology

ORIGINAL RESEARCH
published: 17 March 2022
doi: 10.3389/fmicb.2022.847563

Cryptic Methane-Cycling by Methanogens During Multi-Year Incubation of Estuarine Sediment

*Richard T. Kevorkian, Katie Sipes, Rachel Winstead, Raegan Paul and Karen G. Lloyd**

Department of Microbiology, University of Tennessee, Knoxville, TN, United States

As marine sediments are buried, microbial communities transition from sulfate-reduction to methane-production after sulfate is depleted. When this biogenic methane diffuses into the overlying sulfate-rich sediments, it forms a sulfate-methane transition zone (SMTZ) because sulfate reducers deplete hydrogen concentrations and make hydrogenotrophic methanogenesis exergonic in the reverse direction, a process called the anaerobic oxidation of methane (AOM). Microbial participation in these processes is often inferred from geochemistry, genes, and gene expression changes with sediment depth, using sedimentation rates to convert depth to time. Less is known about how natural sediments transition through these geochemical states transition in real-time. We examined 16S rRNA gene amplicon libraries and metatranscriptomes in microcosms of anoxic sediment from the White Oak River estuary, NC, with three destructively sampled replicates with methane added (586-day incubations) and three re-sampled un-amended replicates (895-day incubations). Sulfate dropped to a low value (~0.3 mM) on similar days for both experiments (312 and 320 days, respectively), followed by a peak in hydrogen, intermittent increases in methane-cycling archaea starting on days 375 and 362 (mostly *Methanolinea* spp. and *Methanosaeta* spp., and *Methanococcoides* sp. ANME-3), and a methane peak 1 month later. However, methane $\delta^{13}C$ values only show net methanogenesis 6 months after methane-cycling archaea increase and 4 months after the methane peak, when sulfate is consistently below 0.1 mM and hydrogen increases to a stable 0.61 ± 0.13 nM (days 553–586, n = 9). Sulfate-reducing bacteria (mostly *Desulfatiglans* spp. and *Desulfosarcina* sp. SEEP-SRB1) increase in relative abundance only during this period of net methane production, suggesting syntrophy with methanogens in the absence of sulfate. The transition from sulfate reduction to methane production in marine sediments occurs through a prolonged period of methane-cycling by methanogens at low sulfate concentrations, and steady growth of sulfate reducers along with methanogens after sulfate is depleted.

Keywords: methane, methanogen, marine sediment, sulfate reducer, anaerobic oxidation of methane, sulfate methane transition zone

OPEN ACCESS

Edited by:
Virginia P. Edgcomb, Woods Hole Oceanographic Institution, United States

Reviewed by:
Guangchao Zhuang, Ocean University of China, China
Hiroyuki Imachi, Japan Agency for Marine-Earth Science and Technology (JAMSTEC), Japan

***Correspondence:**
Karen G. Lloyd
klloyd@utk.edu

Specialty section:
This article was submitted to Extreme Microbiology, a section of the journal Frontiers in Microbiology

Received: *02 January 2022*
Accepted: *07 February 2022*
Published: *17 March 2022*

Citation:
Kevorkian RT, Sipes K, Winstead R, Paul R and Lloyd KG (2022) Cryptic Methane-Cycling by Methanogens During Multi-Year Incubation of Estuarine Sediment. Front. Microbiol. 13:847563. doi: 10.3389/fmicb.2022.847563

INTRODUCTION

Marine sediments produce ~85 Tg/yr of the greenhouse gas methane, making them the third largest producer of methane on Earth (D'Hondt et al., 2002; Reeburgh, 2007; Bange et al., 2009; Bradley et al., 2020). However, only ~10 Tg/yr of this methane is emitted to the atmosphere, well behind emissions from rice paddies, wetlands, animals, landfills, biomass burning, and commercial gas

production (Reeburgh, 2007). This discrepancy is because most of the methane produced in marine sediments is consumed by sulfate-dependent anaerobic oxidation of methane (AOM) before it has a chance to escape to the atmosphere or overlying water. Most methanogenesis is microbial and derives its substrates from the products of organic matter fermentation below the depth of sulfate depletion (Reeve et al., 1997). Hydrogenotrophic methanogens use hydrogen and carbon dioxide, acetoclastic methanogens use acetate, and methylotrophic methanogens use methylated compounds (Reeve et al., 1997). This methane diffuses up through the sulfate/methane transition zone (SMTZ) where it is oxidized through reverse hydrogenotrophic methanogenesis, since sulfate reducers keep hydrogen concentrations low enough to make this process exergonic in the reverse direction (Hoehler et al., 1994, 1998; Reeburgh, 2007; Egger et al., 2018). This is distinct from the direct electron transfer and nanowire connections that have been observed for methane seeps operating at much higher rates of AOM and in the presence of high hydrogen concentrations (Alperin and Hoehler, 2010; Mcglynn et al., 2015; Wegener et al., 2015).

Much of what is known about the microbes that drive the transition from sulfate reduction to methanogenesis in marine sediments has been determined by coupling microbiological and geochemical measurements across sediment core depth gradients [e.g., (Leloup et al., 2009; Lloyd et al., 2011; Kevorkian et al., 2021)]. When rates of sediment accumulation and porewater advection are known, reaction transport models can be used to calculate microbial rates of methanogenesis, sulfate reduction, and AOM (Alperin et al., 1988). However, such studies are complicated by the fact that both AOM and methanogenesis occur simultaneously with sulfate reduction in the SMTZ, when measured by turnover of trace amounts of radioactively labeled substrates in sediments in Cape Lookout Bight, NC (Hoehler et al., 1994), Aarhus Bay, Denmark (Beulig et al., 2019), and Skagerrak, Denmark (Parkes et al., 2007; Knab et al., 2008). This methane-cycling is "cryptic" because methanogenesis and AOM both occur at the same sediment depth layers, even though the change in methane concentrations through the depth layers indicates net AOM within the SMTZ and net methanogenesis below it. Most near-equilibrium enzymatic processes will express some back reaction, like a leaky valve. However, the methanogenesis rates that occur simultaneously with AOM correlate with sulfate reduction rates and even exceed them at very low sulfate concentrations, making it unlikely that the methane-cycling is due to a back reaction of AOM (Beulig et al., 2019).

Some evidence supports the possibility that microbes can conserve energy from methane-cycling. Hydrogenotrophic methanogenesis can be reversed to AOM at low hydrogen concentrations, although it does not provide sufficient energy to sustain actively growing laboratory cultures (Valentine et al., 2000). Natural marine sediment communities, however, operate at orders of magnitude lower energy yields than laboratory cultures (Hoehler and Jørgensen, 2013), and for such communities, AOM provides sufficient energy (Martens and Berner, 1977; Iversen and Jorgensen, 1985). The ability to reverse between methanogenesis and AOM based on hydrogen concentrations has been observed in enrichments of uncultured ANME-1 archaea (Wegener et al., 2015), a clade that is common in marine sediments (Harrison et al., 2009; Lloyd et al., 2011; Underwood et al., 2016; Beulig et al., 2019; Kevorkian et al., 2021). ANME-1 are dominant and active in both in the SMTZ during net AOM and in the net methanogenic sediments below it, suggesting they catalyze either direction (Lloyd et al., 2011). Furthermore, subpopulations of ANME-1 have a heterogeneous distribution (Kevorkian et al., 2021) and substrate usage (House et al., 2009) within the SMTZ, suggesting that metabolic flexibility during methane-cycling may lead to the observed patchiness of their distribution and cellular $\delta^{13}C$ biomass values.

Together, these studies suggest that the transition from sulfate reduction to methanogenesis in marine sediments is more complex than a simple cessation of sulfate reduction at the bottom of the SMTZ, with a switch from only AOM above to only methanogenesis below. Long-term incubations on natural marine sediments allow these processes to be measured in real-time, linking microbes to the processes that occur while they grow, thus removing some of the uncertainty of downcore studies (Alperin et al., 1992; Timmers et al., 2015; Kevorkian et al., 2018). If the organic matter is sufficiently labile, natural quantities of sulfate can be consumed in just a few months, followed by net methane production (Alperin et al., 1992; Kevorkian et al., 2018). However, many marine sediments have less labile organic matter than that of the Cape Lookout Bight sediments used in these studies (Martens et al., 1998). Performing long-term incubations with less organic rich sediments may therefore slow the processes down and display these complex transitions in real-time.

We performed laboratory incubations of marine-influenced White Oak River estuary sediments, which are typical of non-methane-emitting methanogenic sediments. Here, all methane is removed via AOM in the SMTZ and the flux of organic matter is 7- to 30-fold lower than Cape Lookout Bight (Martens et al., 1998; Lloyd et al., 2011). We performed 3 replicate 586-day anoxic incubations of the top 3 cm of White Oak River (WOR) estuary sediment, with timepoints destroyed from 54 separate bottles, each of which had a single addition methane added to the headspace on day 44 (incubation WOR 5.17) to attempt to stimulate AOM while sulfate was available. In a separate experiment, we performed 3 replicates 895-day incubations of subsampled and unamended anoxic incubations of the top 3 cm of WOR sediments (incubation WOR 5.16). We tracked both the geochemistry (methane, sulfate, hydrogen for both incubations, and $\delta^{13}C$ of methane for the WOR 5.17 incubation) and microbial community composition (16S rRNA gene amplicon libraries for both and transcriptomics for WOR 5.16) to observe changes in the microbial community during the transition from sulfate reduction to methanogenesis.

MATERIALS AND METHODS

Sample Collection

Plunger cores were collected in May 2016 (WOR 5.16) and May 2017 (WOR 5.17) (multiple 30cm length cores) at the White Oak

River estuary station H (34 44.490' N, 77 07.44' W), in 1.5 m water depth. Using a plunger inserted from the bottom, the first three centimeters of sediment from each core was removed and mixed together in a sterile flask. For WOR 5.16, 1.5 L of the slurry was placed in three 2L Erlenmeyer flasks, similar to the method used in Kevorkian et al. (2018) (**Supplementary Figure 1A**). The flask was stoppered with a butyl stopper fitted with a wide-bore stopcock for sediment subsampling and gas sampling ports. For WOR 5.16, about 100 ml of sediment were autoclaved and incubated alongside the experiments under anoxic conditions as a negative control. For WOR 5.17, 20 ml of the slurry was added to 54 60 ml glass serum vials, plus two more with autoclaved sediments, and three more with autoclaved distilled water (**Supplementary Figure 1B**). All vials were stoppered with thick butyl rubber stoppers, crimp sealed, and the headspace was gassed with O_2-scrubbed ultra-high purity N_2 gas.

Sampling and Geochemical Measurements

Each of the three WOR5.16 flasks were fitted with a custom butyl rubber stopper with a hole drilled through the center to accommodate a wide bore (6 mm) glass and Teflon stopcock for the removal of samples. Two 18-gauge needles with stainless steel stopcocks were inserted into the stopper as well. Using the luer-lock fitting on the needles, ultra-high purity nitrogen gas (99.999%) that had been scrubbed of oxygen using heated copper fillings was flowed through the bottles using the second needle for the outflow to make the headspace anoxic. Then the flasks were let stand at constant room temperature (21.4°C), which is the temperature of the samples when they were taken, in the dark.

The WOR5.16 incubations were turned over once every month just before sampling. Prior to gas sampling, 2 ml of anoxic N_2 gas (99.999%) was used to blow the needle clear of sediment. Separate hydrogen and methane gas samples were collected in glass gastight Hamilton syringes using the steel needle ports in the custom stopper. About 32 ml of sediment was removed through the glass and Teflon stopcock using a sterile 60 ml plastic catheter tip syringe. After sampling, 30 ml of oxygen- and hydrogen-scrubbed N_2 was injected into the bottle to replace the lost volume.

The WOR5.17 incubation bottles were sampled destructively in triplicate on a monthly basis. The crimp seal and butyl stopper were removed after sampling the headspace for hydrogen, methane, and stable carbon isotopes. On day 44, 4 ml methane was added by syringe to the 40 ml headspace, which is 5.11 mM when equilibrated with porewater.

From both incubations, two 15 ml conical centrifuge tubes were filled and capped, one used for porewater analysis and the other frozen at −80°C for later molecular analysis. One ml of sediment was placed in a 2 ml screw cap tube with 3% paraformaldehyde. The 15 ml tube destined for porewater analysis was centrifuged at 5 000 × *g* for 5 min. A syringe was used to remove the supernatant not in contact with the air. The porewater was then filtered using a 0.2 μm syringe filter into 100 μl of 10% HCl to a final volume of 1 ml. Porewater sulfate concentrations were determined by ion chromatography (Dionex, Sunnyvale, CA, United States).

A total of 500 μl of headspace gas was injected into a Peak Performer 1 Reducing Compound Photometer (Peak Laboratories, Mountain View, CA, United States). Premixed hydrogen ppm lab bottles (Airgas, Radnor, PA, United States) were used as standards. Hydrogen was assumed to be equilibrated between headspace and porewater. Methane was determined by injecting 500 μl of gas from the headspace into an evacuated glass bottle to be later analyzed on a gas chromatograph with a flame ionization detector (Agilent, Santa Clara, CA, United States). Methane concentrations were not assumed to be equilibrated with the aqueous phase; therefore, concentrations are presented as headspace partial pressures. The formula for determining methane concentration was peak area of sample multiplied by the volume of the bottle headspace, which was divided by gas constant times temperature, porosity, volume of sediment.

To measure $\delta^{13}C$ values of methane, 4 ml of headspace from the vial used for methane measurements was removed via syringe and injected into a gas bag containing hydrocarbon free zero gas (Airgas, Radnor, PA, United States). This was then measured on a cavity ring down spectrometer using a small sample introduction module (Picarro, Santa Clara, CA, United States).

Cell Quantification

Total cell counts were determined by direct epifluorescence microscopy SYBRGold DNA stain (Invitrogen, Carlsbad, CA, United States). Sediments were sonicated at 20% power for 40 s to disaggregates cells from sediments and diluted 40-fold into PBS prior to filtration onto a 0.2 μm polycarbonate filter (Fisher Scientific, Waltham, MA, United States) and mounted onto a slide.

16S Ribosomal RNA Gene Amplicons

DNA was extracted from WOR5.16 frozen sediments using the Qiagen Powersoil Total DNA extraction kit. DNA was extracted from WOR5.17 frozen sediments using a protocol modified from Mills et al. (2008). DNA was extracted from each of the three separate bottles that were destroyed at each timepoint. Autoclaved sediment and water blanks were used as negative controls. The V4 region of each DNA extraction was amplified using primers 806r and 515f (Caporaso et al., 2012), as a universal primer pair for Bacteria and Archaea. Library preparations via Nextera kit and sequencing using an Illumina MiSeq were performed at the Center for Environmental Biotechnology at the University of Tennessee in Knoxville. At total of 22,477,189 reads were produced as a result of 2 Miseq sequencing runs.

Qiime2 was used to trim adaptors and make contigs of bidirectional sequences, denoised using Dada2, and generate Amplicon Sequence Variants (ASVs) at 99% similarity, and classify them with the Silva reference set 132 (Pruesse et al., 2007). Following quality control 16,632,317 (74%) of original reads surviving containing 72,445 unique sequences. Samples with fewer than 20,000 reads were removed from further analysis and ASV's appearing in fewer than three samples were also removed. All remaining samples were then scaled to even depth of the smallest sequence library size, which was 20,000

reads (McMurdie and Holmes, 2013). Sequences that identified as chloroplast, eukaryote, or failed to classify on the domain level were removed from further analysis. ASV's for WOR5.16 incubation were agglomerated to the species (97% similarity) level using the command taxa_glom() in the package phyloseq (McMurdie and Holmes, 2013) due to the sequences being produced using two separate Miseq runs.

Transcriptomics

RNA was extracted from WOR5.16 frozen sediments using the Qiagen RNA Powersoil kit. The concentration of total RNA was determined (**Supplementary Table 1**) using the Qubit®RNA Assay Kit (Life Technologies). 200–500 ng of total RNA was used to remove the DNA contamination using Baseline-ZERO™ DNase (Epicentre) following the manufacturer's instructions followed by purification using the RNA Clean & Concentrator columns (Zymo Research). DNA-free RNA samples were used for library preparation using the TruSeq™ RNA LT Sample Preparation Kit (Illumina) according to the manufacturer's instructions. Following the library preparation, the final concentration of all the libraries (**Supplementary Table 1**) were measured using the Qubit®dsDNA HS Assay Kit (Life Technologies), and the average library size was determined using the Agilent 2100 Bioanalyzer (Agilent Technologies). The libraries were then pooled in equimolar ratios of 2nM, and 5.5pM of the library pool was clustered using the cBot (Illumina) and sequenced paired end for 500 cycles using the HiSeq 2500 system (Illumina) at Mr. DNA (Shallowater, Texas).

Reads were trimmed using Trimmomatic in paired-end read mode with a minimum quality score of 25 and a maximum of 4 low-quality bases (122). There was an average of 3185420 (minimum = 616402, maximum = 7063586) RNA reads across the ten samples after quality filtering from 0 to 647 days of incubation. Transcriptomic reads were mapped to publicly available assembled metagenomic contigs from the same station in the White Oak River estuary sediments (PRJNA366356) using Bowtie version 2.3.5 with the "sensitive" end-to-end setting (123). Resulting files were converted to bam files using SAMtools version 1.9 and an anvi'o v5.3.0 database was created and each sample profiled against the metagenomic contigs using the anvi'o command anvi-profile and ORF determined by Prodigal (124–126). Gene coverage and detection files were exported using the anvi'o command anvi-export-gene-converage-and-detection, resulting in reads per kilobase per million (RPKM). ORFs were exported as amino acid sequences using anvi'o command anvi-get-aa-sequences-.

Gibbs Free Energy Calculations

The Gibbs Free Energy change (△G) associated with hydrogenotrophic methanogenesis, $2H_2 + CO_2 \rightarrow CH_4 + 2H_2O$, was calculated with the following equation:

$$\triangle G = \triangle G^{\circ} + RTln\frac{[CH_4]_{(aq)}}{[CO_2]_{(aq)}[H_2]_{(aq)}{}^4}$$

where, △G° is the standard state Gibbs Free Energy of -194.53 kJ/mol at 18°C, close to the incubation temperature of 21°C (Amend and Shock, 2001), R is the gas constant 0.0083145 kJ/molK, T is the incubation temperature of 21°C, and aqueous concentrations are used instead of the activities because uncharged constituents have activity coefficients close to 1. The concentration of CO_2 was estimated at 10 mM, the average sum CO_2 for the upper 35 cm of station H, White Oak River (Kelley et al., 1990) to provide a high estimate, providing as exergonic an estimate as possible for the △G of hydrogenotrophic methanogenesis in the final three timepoints.

Data Archiving

16S rRNA gene sequences and RNA transcripts can be found at the NCBI sequence read archive Bioproject PRJNA624356. Geochemistry and qPCR data can be found at www.bco-dmo.org with project number 649807.

RESULTS

WOR5.17 Incubation, Methane Added on Day 44, No Resampling

The WOR5.17 incubation was designed to minimize gas leaks and make subsampling easy by allowing each incubation vial to remain undisturbed until it was destroyed for a timepoint. Sediments from WOR5.17 were incubated in separate butyl-rubber-stoppered glass vials (**Figure 1** and **Supplementary Table 1**) and each remained sealed until it was destroyed for a timepoint. Sulfate decreases from an initial value of 10.8 ± 0.7 mM to 1.0 ± 1.5 mM on day 320, and does not change for the next 3.7 months (1.3 ± 1.4 mM, mean of 12 measurements during days 320–431; **Figure 1A**). Afterward, sulfate falls to 0.38 ± 0.36 mM for 2 months, averaged across all 9 measurements from days 461–524. Finally, sulfate decreases again to 0.08 ± 0.07 mM for 1 month, averaged across all 9 measurements from days 553–586. Aqueous methane concentrations are initially 0.014 ± 0.011 mM (**Figure 1B**). After the addition of 5.11 mM methane on day 44, methane decreases gradually to 0.02 ± 0.03 mM by day 200, likely from sulfate-dependent AOM, and then varies between 0.01 and 2.05 mM among replicates and timepoints over days 238 – 320. By day 363, methane drops to < 0.01 mM in all three replicates, increases to 4.51 ± 0.30 mM by day 396, and decreases in a variable way to a low point of 0.47 ± 0.02 mM on day 553, coinciding with the full depletion of sulfate to 0.08 ± 0.07 mM. Methane then increases to a final value of 1.83 ± 0.55 mM on day 586. The high variability of methane when sulfate is low but not absent (days 238–524) is not due to small changes in sulfate concentrations since methane and sulfate do not correlate over this time period (**Supplementary Figure 2**). Aqueous hydrogen concentrations are < 1.08 nM in the 18 measurements until day 238, when hydrogen increases to a maximum of 7.01 ± 2.58 nM on day 276, even though sulfate is still > 1 mM (**Figure 1C**). After this, hydrogen declines to an extremely low precise value of 0.30 ± 0.05 nM for 2 months, averaged across all 9 measurements between days 461–524, coinciding with the time that sulfate is stable at ∼0.3 mM. After this, when sulfate decreases to ∼0.07 mM, and methane increases, hydrogen rises slightly to 0.61 ± 0.13 nM for 1 month,

averaged across all 9 measurements between days 553–586. The methane added experimentally on day 45 had a δ^{13}C-CH_4 value of -34.9 ‰. The δ^{13}C-CH_4 values are depleted in the lighter isotope slightly at 111 and 323 days, each corresponding to a depletion of aqueous methane concentrations (**Figure 1E**). This is consistent with the presence of AOM due to kinetic preference for ^{12}C over ^{13}C, leaving the residual methane ^{13}C-enriched (Alperin et al., 1988; Jørgensen and Kasten, 2006; Holler et al., 2009). No large differences in δ^{13}C-CH_4 were observed until days 524–586 when δ^{13}C-CH_4 steadily declines to the lowest value at –79 ‰ on day 568. These values are indicative of the biogenic production of methane, resulting in enrichment of the lighter carbon isotope, ^{12}C (Whiticar, 1999). Total cellular abundance in WOR5.17 is $2.06 \times 10^8 \pm 1.14 \times 10^8$ cells/ml initially, increasing in abundance to $8.32 \times 10^8 \pm 2.34 \times 10^8$ cells/ml at 161 days, and then declining to $2.68 \times 10^8 \pm 8.64 \times 10^7$ cells/ml at 586 days followed by a slight increase until the end of the incubation (**Figure 1D**). At the end of the experiment, autoclaved sediment controls had 5.13 mM sulfate, 0.38 mM methane, 0.62 nM hydrogen, and methane δ^{13}C of –34.9. Sulfate and methane concentrations were below detection limit in the sterilized water controls.

The most abundant genera of the Methanomicrobia are, in order of abundance, *Methanolinea* sp., ANME-3, *Methanosaeta* sp., and uncultured Methanomicrobiaceae, and they all have similar abundance dynamics throughout the incubation (**Figure 2** and **Supplementary Figure 3**). Only two ASVs of ANME-1 are present at five timepoints with low relative abundances ($<1\times 10^{-5}$). For the first 363 days, Methanomicrobia are in very low abundance (sums ranging from 0 to 0.08% of total libraries), even though methane was added to the headspace on day 44 and methane concentrations increase and decrease during this time period. The Methanomicrobia increase slightly between days 363 - 431, varying between 0.03 to 0.10% when sulfate drops to ∼1.3 mM. Between days 461–524, Methanomicrobia increase again to a range of 0.02 to 0.32% while sulfate drops again to ∼0.3 mM. The only time interval over which Methanomicrobia are consistently high (0.20 ± 0.90%) is during the final three timepoints, when sulfate is fully depleted, methane is $>$ 0.45 mM, hydrogen is stable at 0.6 nM, and δ^{13}C-CH_4 indicates net methanogenesis.

Bacteria closely related to cultured sulfate reducing bacteria are represented by 1563 ASVs accounting for as much as 11% of the total sequence abundance (**Figure 3** and **Supplementary Figure 4**). The three most abundant ASVs are unclassified members of the family Desulfobulbaceae, which together account for ∼2% of total sequences. Classified and unclassified members of the family Desulfobulbaceae (242 ASVs) account for ∼3.5% of total sequences observed throughout the incubation. The Desulfobacteraceae/Sva0081 sediment group has 121 ASV's consistently accounting for ∼2–3% of sequence abundance. The genus *Desulfatiglans* in the Desulfarculales represent 1.5% of sequence abundance and 353 ASVs. Desulfobacteraceae/SEEP-SRB1, another putative SRB and partner with anaerobic methane oxidizers (Schreiber et al., 2010), accounts for ∼0.5% of total sequences and 141 unique ASVs. Syntrophobacteraceae, which also contain sulfate reducers, accounts for ∼3.5% of total sequences and 133 ASVs. The relative abundance of these groups does not change noticeably through day 524, with the exception of a decline in all three replicates on day 431, as sulfate decreases from ∼1.3 mM to ∼0.3 mM. Desulfobacteraceae, Desulfobulbaceae, and Syntrophobacteraceae increase in all three replicates in the last three timepoints when sulfate is fully depleted and methanogenesis begins to affect the carbon isotopes. Aerobic sulfur-oxidizing bacteria and aerobic methanotrophs are less than 0.3% of the amplicons and do not increase over time. Aerobic methane and sulfur oxidizers were also present, but in low abundance and with no clear changes with geochemistry (**Supplementary Figure 5**).

Bacteria comprise the majority of total amplicon sequences with a slight decrease over time, beginning at ∼78% and ending at ∼73% of sequences (**Supplementary Figure 6**). Proteobacteria are the most abundant bacterial phylum, accounting for approximately 38% of sequences throughout the incubation. Archaeal sequences represent ∼12% of total microbial abundance at the beginning of the incubation and ∼17% of abundance after 586 days (**Supplementary Figure 7**). Bathyarchaeaota (called Crenarchaeota in the Genome Taxonomy Database taxonomy, and Miscellaneous Crenarchaeotal Group and Marine Benthic Group C, previously) are the most abundant archaeal phylum in the WOR5.17 incubation and gradually increase over time from 5% of sequences to 8% of sequences after 586 days. Lokiarchaeia (also called Deep Sea Archaeal Group and Marine Benthic Group B) increase to 2% of sequences during the final methanogenic portion of the incubation. Thermoprofundales (also called Marine Benthic Group D, Deep Sea Hydrothermal Vent Euryarchaeota Group 1, and Izemarchaea) increase to 2% of sequences during the methane-cycling portion of the incubation and fall off during the methanogenic portion.

WOR5.16 Incubation, No Amendments, With Resampling

WOR5.16 lacks data for some timepoints due to the difficulty of pulling samples through the stopcock for subsampling. Sulfate concentrations decrease from 12.9 ± 0.2 mM to 0.3 mM by day 312 and remain at or below 1.61 mM until day 769, when they gradually increase to a final value of 7.5 ± 5.5 mM by day 895 (**Figure 4A** and **Supplementary Table 1**). Methane concentrations are $<$ 0.01 mM in 25 out of the 26 measurements in the first 124 days, show slightly higher variable concentrations in days 124 - 312 where few measurements were made, and peak on day 487 at 1.7 mM (**Figure 4B**). After this, methane drops to 0.07 ± 0.06 mM, averaged across all 22 datapoints available on days 570–895 except replicate 3 on day 769, which is 8.16 mM. The initial aqueous hydrogen concentration is 0.118 ± 0.401 nM and remains $<$ 1.0 nM until sulfate is depleted at day 312 (**Figure 4C**). Hydrogen rises to a maximum of 10.1 ± 0.36 nM on day 375, before declining and reaching a very low value of $0.19 \pm .03$ nM on day 895. Total cellular abundance is $2.64 \times 10^8 \pm 1.03 \times 10^8$ cells/ml initially, increases to $1.22 \times 10^9 \pm 2.00 \times 10^8$ cells/ml by 35 days, before decreasing to a final value of $1.94 \times 10^8 \pm 3.29 \times 10^7$ by day 895 (**Figure 4D**).

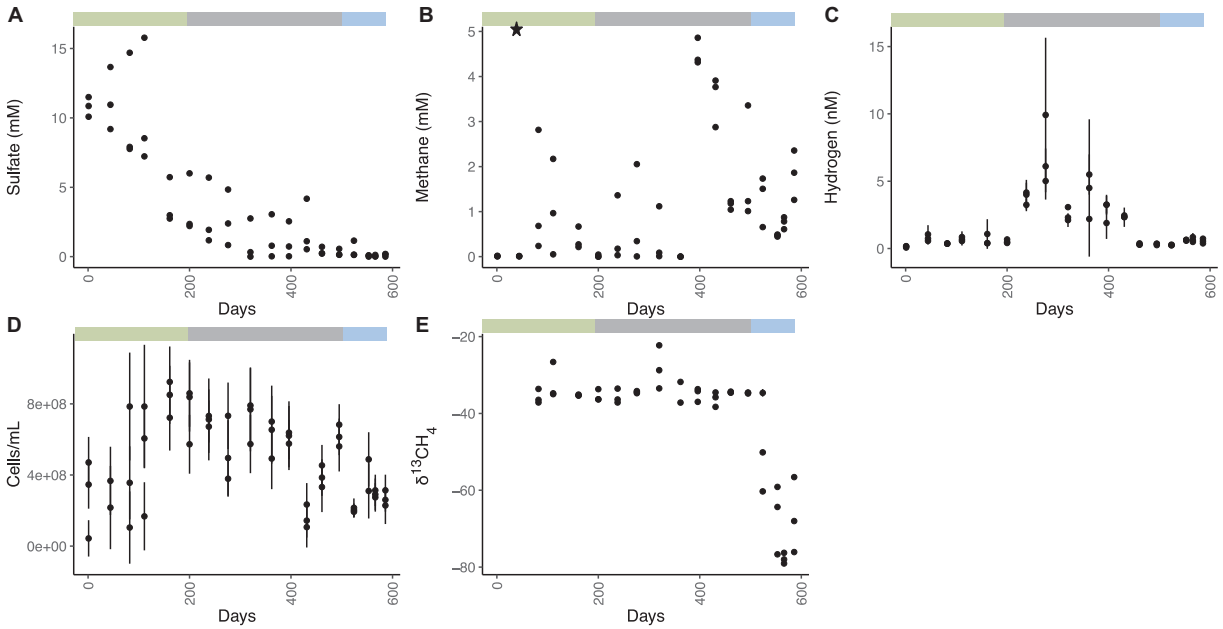

FIGURE 1 | Geochemistry for WOR 5.17 incubation, with **(A)** aqueous sulfate concentrations, **(B)** aqueous methane concentrations, with the star representing the time and concentration of methane added to all bottles, **(C)** aqueous hydrogen concentrations, **(D)** cell abundance, and **(E)** $\delta^{13}CH_4$. Error bars are one standard deviation from triplicate measurements from a single bottle, and are available only for methane, hydrogen, and cell abundance. Green bar shows the time period of sulfate reduction and AOM, gray bar shows the time period of methane cycling through methanogenesis and AOM, and the blue bar shows the time period of methanogenesis.

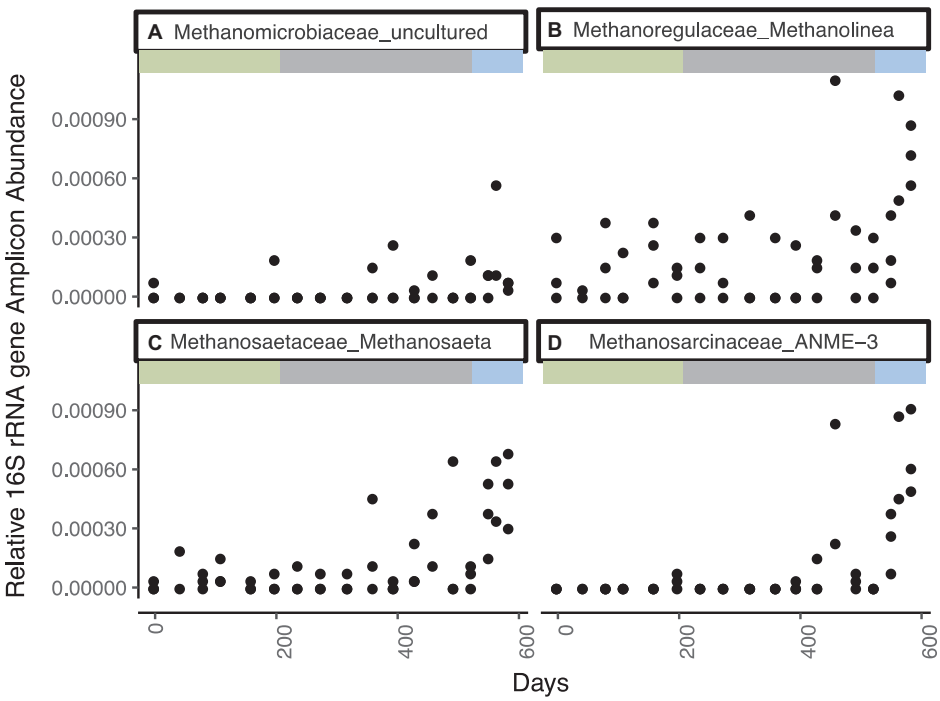

FIGURE 2 | Genera from the Methanomicrobia that increase in 16S rRNA gene amplicon abundance, divided by the total reads in each library, for WOR 5.17 incubation, with **(A)** Methanomicrobiaceae_uncultured, **(B)** Methanoregulaceae_Methanolinea, **(C)** Methanosaetaceae_Methanosaeta, and **(D)** Methanosarcinaceae_ANME-3.

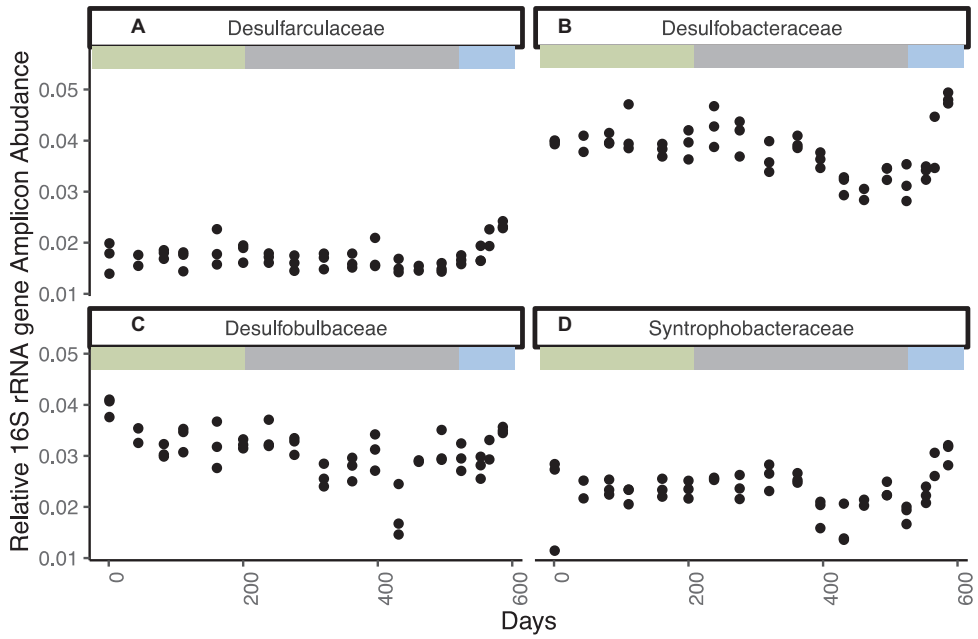

FIGURE 3 | Families with cultured sulfate reducers that increase in relative 16S rRNA gene amplicon abundance for WOR 5.17 incubation, with **(A)** Desulfarculaceae, **(B)** Desulfobacteraceae, **(C)** Desulfobulbaceae, and **(D)** Syntrophobacteraceae.

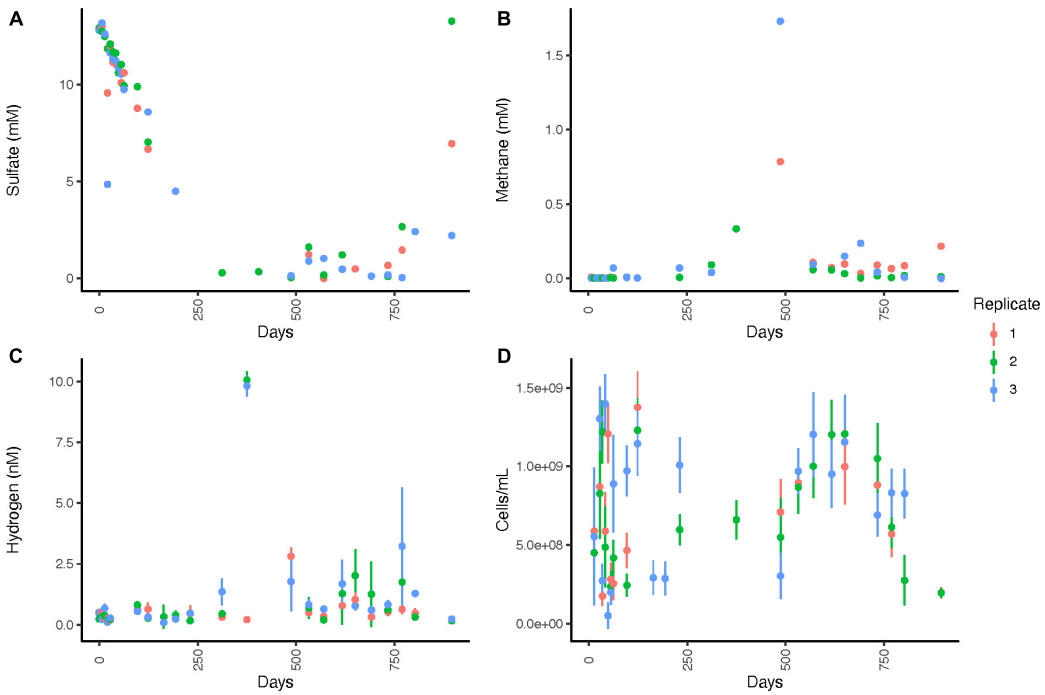

FIGURE 4 | Geochemistry for WOR 5.16 incubation, with **(A)** aqueous sulfate concentrations, **(B)** aqueous methane concentrations, **(C)** aqueous hydrogen concentrations, and **(D)** cell abundance. Error bars are one standard deviation from triplicate measurements from a single bottle, and are available only for methane, hydrogen, and cell abundance. No clear designations for time periods of sulfate reduction, AOM, or methanogenesis were made since it is unclear when oxygen began leaking into the system, $\delta^{13}CH_4$ was not measured for this incubation, and many datapoints were missing due to difficulty pulling sediments through the stopcock, so net processes were less clear than for WOR 5.17 and are therefore not listed. Note that timepoints were weekly for the first 63 days and then moved to longer intervals after that.

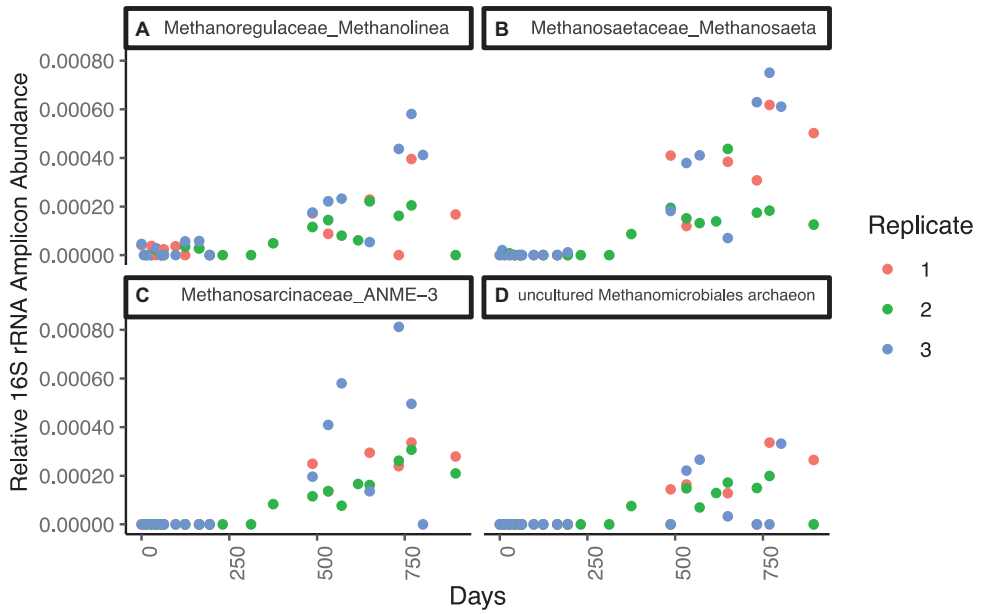

FIGURE 5 | Families from the Methanomicrobia that increase in relative 16S rRNA gene amplicon abundance for WOR 5.16 incubation, with **(A)** Methanoregulaceae_Methanolinea, **(B)** Methanosaetaceae_Methanosaeta, **(C)** Methanosarcinaceae_ANME-3, and **(D)** Methanomicrobiales_uncultured, which was only taxonomically classified at the order level.

The most abundant genera of the Methanomicrobia are, in order of amplicon abundance, *Methanosaeta* sp., ANME-3, and *Methanolinea* sp., and they all have similar abundance dynamics throughout the incubation (**Figure 5** and **Supplementary Figure 8**). Unclassified clades of Methanosarcinales and Methanomicrobiales are well-represented, with 33 ASVs. Five ASVs of ANME-1 are in negligible abundance (3 timepoints at or below 1.0×10^{-5}). All Methanomicrobia are in very low relative abundance (sums ranging from 0 to 0.01% of total libraries) for the first 312 days, while sulfate is present (**Figure 5**). After this, Methanomicrobia increase to $>$ 0.05% in all timepoints and replicates. Its relative abundance varies between 0.05 and 0.15% between days 312 and 895, and does not correlate to methane, sulfate, or hydrogen concentrations.

Evidence that oxygen leaked into the three incubation vessels comes from the increase in sulfate concentrations after 500 days. During this time, sulfate reducing bacteria, which are anaerobic, decline in relative abundance (**Supplementary Figure 9**). Aerobic sulfur oxidizers *Sulfurovum* sp. and *Sulfurimonas* sp. increase in relative abundance when sulfate increased at the end of the incubation (**Supplementary Figure 10**). Aerobic methanotrophs, *Methylmonaceae* sp. and *Methyloligellaceae* sp. also increase during this time (**Supplementary Figure 10**). Air contamination was likely during sampling since we could smell sulfide, and if sulfide gas was escaping into the air, then oxygenated air was getting into the bottles. This may have only affected the incubations toward the end of the experiment since during that time free sulfide may have become limited due to pyritization.

Total bacteria decrease from ∼92% of sequences initially to ∼89% after 895 days, with archaea making up the balance (**Supplementary Figure 11**). Proteobacteria is the most abundant bacterial phylum and accounts for approximately 40% of sequences throughout the timepoints. Bathyarchaeaota (called Crenarchaeota in the GTDB taxonomy) is consistently one of the most abundant archaeal clades in the WOR5.16 incubation and increases over time from 2% of sequences to ∼6% sequences after 895 days (**Supplementary Figure 12**).

mRNA transcripts mapping to 41 methane-cycling genes increase in abundance as sulfate approaches depletion at 312 days and peak shortly afterward at 375 days (**Figure 6**). This agrees with previous studies showing that the highest rate of methane production occurs prior to sulfate depletion (Beulig et al., 2018a). Transcripts for the gene encoding methyl coenzyme M reductase (*mcrA*), a key gene in methane production, were not detected. Transcripts mapped to only three genes in two time points in sulfur-cycling pathways, one of which was exclusive to dissimilatory sulfate reduction, adenylylsulfate reductase subunit A (*aprA*), at 375 days of incubation. Five transcripts mapped to genes related to nitrogen cycling metabolism across 3 samples. None of them were exclusive to energy generation and they included amino acid synthesis genes such as glutamine synthase (*glnA*) and glutamate dehydrogenase (*gdhA*). Transcripts mapped to 42 genes related to carbon fixation. These peak in expression at 194 days but remain actively expressed throughout the incubation. This suggests that microbes may be actively using other carbon pathways, such as the reductive citrate cycle and the reductive acetyl-CoA pathway, however, we cannot accurately distinguish between them since these genes are commonly shared with methanogenesis. Six mRNA transcripts associated with pyrimidine metabolism have the highest expression occurring after 375 days. Conversely, 13 purine metabolism associated genes are more evenly distributed

between 63 and 532 days. The expression of genes associated with DNA replication were not detected and only 4 genes associated with DNA mismatch repair were detected while the two highest expression levels are both on day 194; proliferating cell nuclear antigen and replication factor A1, respectively. The expression of only one gene, *motB*, associated with flagellar motility occurs at 124 days. No other genes recruited mRNA reads in more than two timepoints.

DISCUSSION

In both sets of triplicate WOR sediment incubations, methane production begins well before sulfate is depleted and oscillates between production and consumption, with variable increases in methanogenic groups. The highest concentrations of hydrogen and methane are reached during this period of methane cycling. It is only after sulfate is fully depleted that methane increases reliably, isotopes show net methanogenesis, and methanogenic groups increase consistently. This is the only time that sulfate reducing bacteria increase in abundance. A similar increase and decrease in methane right after sulfate depletion was also observed for CLB sediments, but it lasted only 18 days, vs 315 in our WOR incubations (Kevorkian et al., 2018). Reaction transport models suggest that lower organic matter fluxes in the WOR support slower microbial metabolic rates (Martens et al., 1998). Despite starting with 1–8 mM less sulfate than CLB, WOR sediments take much longer for sulfate to decrease to ∼1 mM and begin producing methane: 312–323 days in WOR sediments vs. 40 days (Alperin et al., 1992) and 68 days (Kevorkian et al., 2018) for CLB sediments, with all incubations at 21.5°C.

In our WOR incubations, once sulfate concentrations decrease to less than ∼5 mM after ∼200 days, all replicates in both incubations show a consistent pattern of a peak in hydrogen, followed by a peak in methane about 4 months later, and then consumption of that methane, all occurring in the 315 days before sulfate is fully depleted. Hydrogen increases at a rate of 0.09 nM H_2/day (WOR5.17, days 200-276, $n = 9$, $R^2 = 0.82$) suggesting that sulfate reducers lose thermodynamic control of hydrogen even though sulfate is still present (1–5 mM), possibly because, at these low concentrations of sulfate, diffusion limits the concentration of sulfate at the cell surfaces (Hoehler et al., 2001). The subsequent decrease in hydrogen is likely driven by hydrogenotrophic methanogens converting hydrogen to methane at a rate of 0.13 mM CH_4/day (WOR5.17, days 362–396, $n = 6$, $R^2 = 0.99$) even though sulfate concentrations are still 0–3 mM. At this time, methane-cycling archaea (designated here as archaea belonging to genera whose cultured members are methanogens, or that have been shown in previous studies to have full methanogenic genetic pathways) increase sporadically, and RNA expression of methane-cycling genes in the WOR5.16 incubation are present, suggests that methane-cycling occurs well before sulfate is depleted. However, during this time δ^{13}C-CH_4 shows no net AOM or methanogenesis. The subsequent decrease in methane at a rate of 0.05 mM CH_4/day (WOR5.17, days 396–461, $n = 9$, $R^2 = 0.89$) is not accompanied by any major changes in methane-cycling population or δ^{13}C-CH_4.

This 11.5-month period of overlap between methanogenesis, AOM, and sulfate reduction is likely not an artifact of sampling methods since it was observed in incubation 5.16, which was subsampled from the same bottles over time, and incubation 5.17 where bottles were incubated separately and destroyed for each timepoint. Diffusion limitation on the microscale likely creates heterogeneity in space and time in the hydrogen concentrations that cells experience, meaning that some cells oxidize methane while others produce it, or individual cells oscillate between production and oxidation of methane. It is also possible that cryptic sulfur cycling extended the length of this transition period and allows methane to cycle. In cryptic sulfur cycling, sulfide produced by sulfate reducing bacteria, is reoxidized by oxidized compounds such as ferric iron or barite dissolution (Borowski et al., 1996; Knab et al., 2008; Holmkvist et al., 2011; Xiao et al., 2017; Pellerin et al., 2018; Beulig et al., 2019). Radiotracer experiments in marine sediment columns have shown that when sulfate concentrations are low, the rate of reoxidation roughly balances the rate of depletion (Holmkvist et al., 2011; Pellerin et al., 2018; Jørgensen et al., 2019), which would explain why sulfate did not change much over this interval in WOR5.17. The cessation of sulfate reduction and commencement of steady methanogenesis around day 553, therefore, could have occurred because sulfide became fully mineral-bound so it was no longer available for reoxidation.

For the latter part of the incubations, we consider only the results from WOR5.17, since WOR5.16 shows evidence of oxygen contamination during these late stages. In the final 3 months of this methane- and sulfur-cycling period (days 461–553), the mean sulfate concentration drops to 0.08 ± 07 mM ($n = 9$) and hydrogen drops to the lowest and most stable value of the entire experiment (0.30 ± 0.05 nM, $n = 9$). Even though the sediment in all nine bottles sampled during this time period have been separated for a year and a half, they all reach this precise low hydrogen concentration during this same time interval. Methane concentrations and the relative abundance of 16S rRNA genes of methane-cycling archaea, on the other hand, are variable between individual bottles during this interval, with no trends.

It is not until sulfate is depleted to ∼0.07 mM (day 553) that δ^{13}C-CH_4 finally decreases to -80‰, showing evidence of net methanogenesis, and methane-cycling populations consistently increase in relative abundance in all bottles. During this month, methanogenesis rates are 0.04 mM/day (WOR5.17, $n = 9$, $R^2 = 0.79$). This rate is a third of the methanogenesis rate observed after the hydrogen peak during the time of methane- and sulfur-cycling, reflecting the slower methanogenesis rates at lower hydrogen concentrations. This suggests that the period of methane-cycling has stopped, and methane is mainly produced, not oxidized. These rates of methane production (both during methane-cycling and methane production) are much higher than rates inferred from reaction transport modeling at this site of 0.007 mM/day (Lloyd et al., 2011) and 0.002 mM/day (Martens et al., 1998). However, they are quite similar to *in situ* radiotracer rate measurements made in Aarhus Bay, Denmark (0.06 mM/day), suggesting that rates from reaction transport models may underestimate the real metabolic rates.

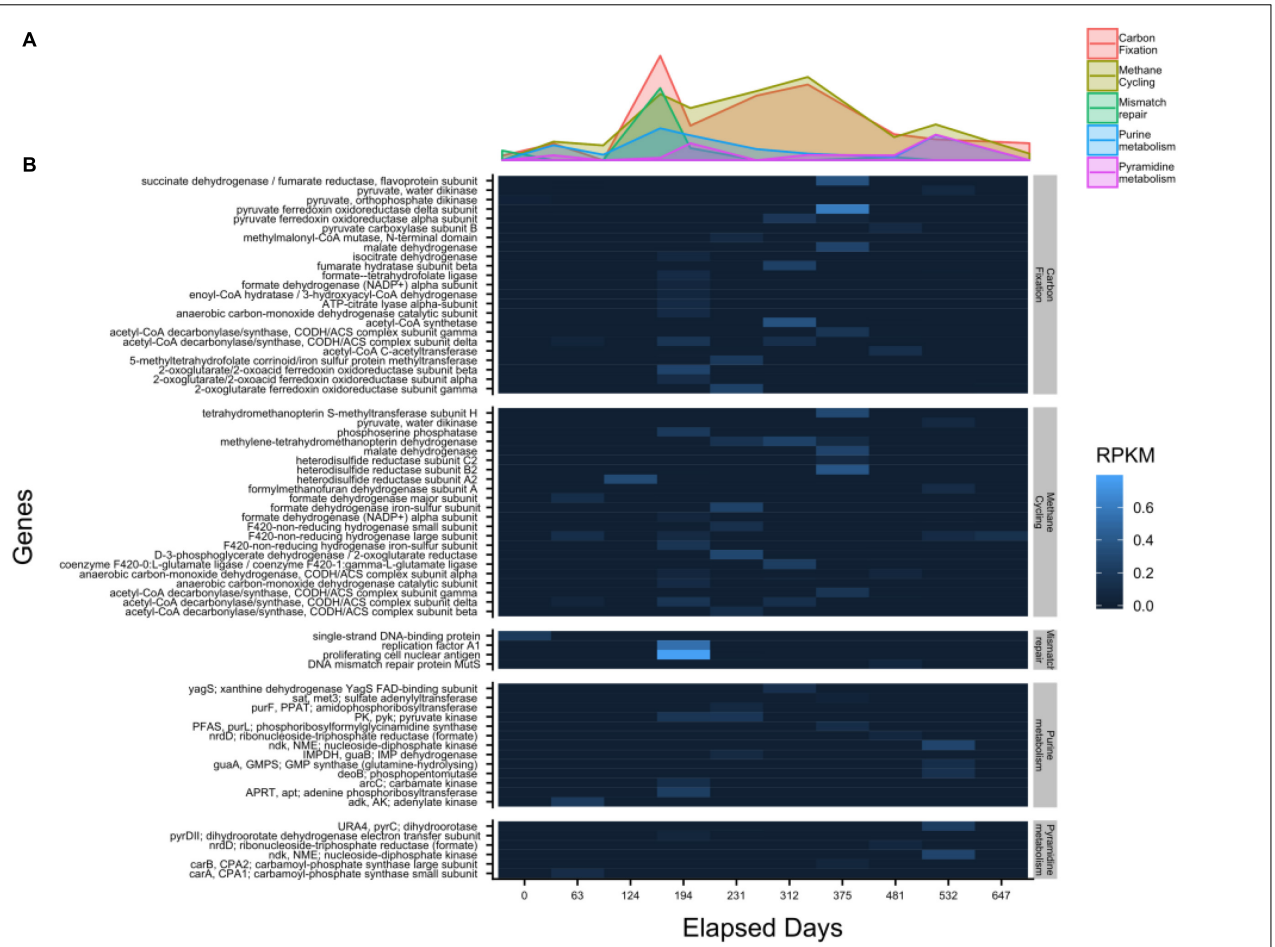

FIGURE 6 | Transcript abundances, shown by function in the WOR 5.16 incubation reveal the highest level of carbon fixation related gene expression occurs prior to sulfate depletion, with **(A)** the summed value of each pathway over time, and **(B)** the individual genes detected in each pathway. Heatmap color corresponding to RPKM (Reads Per Kilobase Mapped).

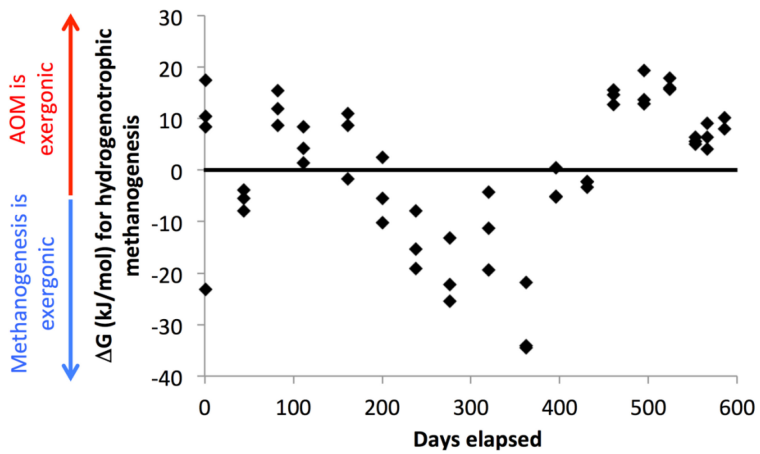

FIGURE 7 | Gibbs free energy associated with hydrogenotrophic methanogenesis in WOR 5.17 incubation, with positive values meaning that AOM through reverse methanogenesis is exergonic and negative values meaning that hydrogenotrophic methanogenesis is exergonic.

Throughout the methane-cycling and methanogenic phases of the incubations, the only methane-cycling archaea that increase belong to families whose only cultured relatives are hydrogenotrophic and aceotclastic methanogens, *Methanoregulaceae* (*Methanolinea* sp. and *Methanoregula* sp.), *Methanosarcinaceae* (*Methanosaeta* sp., ANME-3, and other uncultured genera), and *Methanomicrobiaceae* (uncultured genera). ANME-3 has been implicated as a methanotroph based on its presence in methane seeps performing AOM (Knittel et al., 2005; Parkes et al., 2007), and it is in the genus *Methanococcoides*, whose cultured relatives are all methanogens. These different clades of methane-cycling archaea have the same patterns of growth during these incubations, suggesting that they all benefit intermittently during the period of methane-cycling and then consistently during the period of methanogenesis. It is possible that each of these archaea is capable of reversing between methanogenesis and AOM, taking advantage of hydrogenotrophic methanogenesis or AOM, depending on which one is exergonic. Even members of the *Methanosarcinales*, whose cultured members are acetoclastic methanogens that do not use hydrogen directly, still require adequate hydrogen concentrations to respire since they "leak" hydrogen as a metabolic intermediate when they are in very low hydrogen concentrations (Finke et al., 2007).

These populations of methane-cycling archaea are very different than those found *in situ* at this site, which are almost entirely ANME-1 (Lloyd et al., 2011; Lazar et al., 2015; Kevorkian et al., 2021). The methane-cycling archaea growing in the WOR incubations are more similar to those that grow in CLB incubations, *Methanosarcinaceae* (*Methanosaeta* sp. and uncultured genera) and *Methanomicrobiaceae* (uncultured genera) (Kevorkian et al., 2018). ANME-1 are in very low abundance in WOR5.16 and WOR5.17, and do not increase in relative abundance during the incubations, even in WOR5.17 where the early addition of methane enabled AOM. The methane-cycling archaea in the WOR incubations may simply have grown faster than ANME-1, which has a doubling time of 7 months (Nauhaus et al., 2007). In fact, the addition of methane early in the incubations of WOR5.17 makes very little effect on the progress of sulfate reduction, or the microbial community at all, even though it is consumed via AOM. Here, sulfate concentrations are consistently high (>4 mM), which keeps hydrogen consistently low (<1 nM), making AOM using reverse methanogenesis exergonic (**Figure 7**). The fact that methane-cyclers do not grow when sulfate is > 5 mM and methane only decreases, grow intermittently when sulfate is 0–5 mM and methane and hydrogen are variable, and grow consistently when sulfate is ∼0 mM and methane only increases, suggests that methanogenesis may provide more energy for growth than AOM for these populations. This implies that they only grow during periods of methanogenesis, and simply meet maintenance energy needs during periods of AOM.

Curiously, after the final depletion in sulfate, when net methanogenesis becomes consistent, the small hydrogen concentration increase to 0.61 nM ± 0.13 ($n = 9$) is not sufficient to make hydrogenotrophic methanogenesis exergonic (**Figure 7**). It is possible, therefore, that other types of methanogenesis, such as acetoclastic or methylotrophic support methane production here, but this would not explain which terminal electron accepting process keeps hydrogen concentrations so low. Desulfarculaceae, Desulfobulbaceae, and Syntrophobacteraceae increase along with the methane-cycling archaea during this time, suggesting that a syntrophic relationship where these bacteria ferment organic matter and donate reduced compounds to methanogens may allow them to push close to their thermodynamic limits as has been predicted previously (Jackson and McInerney, 2002; D'Hondt et al., 2004; Wang et al., 2008, 2010) or to supplement their metabolism with direct electron transfer. This is the only time during the incubation that these sulfate reducing bacteria increase in relative abundance, even though sulfate reduction has been occurring through much of the incubation. The only other major clades that increase in relative abundance during the incubation are Bathyarchaeota, which increase steadily irrespective of geochemical shifts, and Lokiarchaeota and Thermoprofundales, which have not been found to contain methanogenic genes. Unlike the methanogens, the sulfate-reducing bacteria in the WOR5.16 and WOR5.17 incubations are from the same genera found *in situ* (Kevorkian et al., 2021): SEEP-SRB1, *Desulfatiglans* sp., and *Desulfobulbus* sp. This suggests that if the sulfate reducers form syntrophic relationships with methanogens, these relationships are not species specific. Syntrophy with the newly grown methanogens may open a new niche that the sulfate reducers are able to grow into, allowing them to finally be able to remove the last bit of sulfate. This offers an alternative explanation to the waning sulfide availability due to mineralization discussed above.

Our results agree with those inferred from down-core studies (Beulig et al., 2018b; Kevorkian et al., 2021) that the transition between sulfate reduction/AOM to methanogenesis in marine sediments goes through a substantial transitional period of methane-cycling. Here, sulfate concentrations are low and sediments shift between AOM and methanogenesis. This methane-cycling supports intermittent growth of methanogens including *Methanoregulaceae* (*Methanolinea* sp. and *Methanoregula* sp.), *Methanosarcinaceae* (*Methanosaeta* sp., ANME-3, and other uncultured genera), and *Methanomicrobiaceae* (uncultured genera), all of which begin to increase consistently in relative abundance when sulfate is finally depleted and methanogenesis becomes continuous. Since these are the only methane-cycling archaea present, and they all have the same relative abundance patterns, it is likely that they reverse between AOM and methanogenesis, depending on which process is exergonic. Reversals between AOM and methanogenesis have been observed for these clades previously although only methanogenesis has been shown to support growth for them (Valentine et al., 2000). Our results support that they grow only from methanogenesis, but they also perform AOM. Growth of these organisms under conditions of continuous methanogenesis in turn benefits sulfate reducing communities (Desulfarculaceae, Desulfobulbaceae, and Syntrophobacteraceae) that only grow after sulfate depletion, possibly due to syntrophy with methanogens.

DATA AVAILABILITY STATEMENT

16S rRNA gene sequences and RNA transcripts can be found at the NCBI sequence read archive Bioproject PRJNA624356. Geochemistry and qPCR data can be found at www.bco-dmo.org with project number 649807.

AUTHOR CONTRIBUTIONS

RK and KL conceived of the experiments, analyzed data, and wrote the manuscript. RK obtained samples and conducted the experiments. RW and RP made substantial data contributions. KS performed data analysis and visualization. KL advised other authors and obtained funding. All authors contributed to the article and approved the submitted version.

FUNDING

This work was funded by NASA Exobiology (NNX16AL59G), U.S. Department of Energy Office of Science, Office of Biological and Environmental Research (DE-SC0020369), and NSF Chemical Oceanography (OCE-1948720).

ACKNOWLEDGMENTS

We thank Brandi Barber, Andrew Steen, Jordan Bird, Lauren Mullen, Taylor Royalty, Katherine Fullerton, and Joy Buongiorno for assistance retrieving the sediment samples, Michael Piehler for the use of his laboratory at the UNC Institute of Marine Sciences, Frank Löffler for use of ion and flame ionized detector chromatographs, Robert Murdoch and the University of Tennessee Knoxville Bioinformatics Resource Center for computational resources, and Christopher G. Kevorkian and Alexandra Emmons for analytical assistance.

SUPPLEMENTARY MATERIAL

The Supplementary Material for this article can be found online at: https://www.frontiersin.org/articles/10.3389/fmicb.2022.847563/full#supplementary-material

REFERENCES

Alperin, M., and Hoehler, T. (2010). The ongoing mystery of sea-floor methane. *Science* 329, 188–289.

Alperin, M. J., Blair, N. E., Albert, D. B., Hoehler, T. M., and Martens, C. S. (1992). Factors that control the stable carbon isotopic composition of methane produced in an anoxic marine sediment. *Global Biogeochem. Cycles* 6, 271–291.

Alperin, M. J., Reeburgh, W. S., and Whiticar, M. J. (1988). Carbon and hydrogen isotope fractionation resulting from anaerobic methane oxidation. *Global Biogeochem. Cycles* 2, 279–288.

Amend, J. P., and Shock, E. L. (2001). Energetics of overall metabolic reactions of thermophilic and hyperthermophilic Archaea and Bacteria. *FEMS Microbiol. Rev.* 25, 175–243.

Bange, H. W., Bergmann, K., Hansen, H. P., Kock, A., Koppe, R., Malien, F., et al. (2009). Dissolved methane during hypoxic events at the Boknis Eck Time Series Station (Eckernförde Bay, SW Baltic Sea). *Biogeosci. Discuss.* 6, 11463–11477. doi: 10.5194/bgd-6-11463-2009

Beulig, F., Røy, H., Glombitza, C., and Jørgensen, B. B. (2018a). Control on rate and pathway of anaerobic organic carbon degradation in the seabed. *Proc. Natl. Acad. Sci.* 115, 367–372. doi: 10.1073/pnas.1715789115

Beulig, F., Røy, H., McGlynn, S. E., and Jørgensen, B. B. (2018b). Cryptic CH4 cycling in the sulfate-methane transition of marine sediments apparently mediated by ANME-1 archaea. *ISME J.* 2018:273. doi: 10.1038/s41396-018-0273-z

Beulig, F., Røy, H., McGlynn, S. E., and Jørgensen, B. B. (2019). Cryptic CH4 cycling in the sulfate-methane transition of marine sediments apparently mediated by ANME-1 archaea. *ISME J.* 13, 250–262.

Borowski, W. S., Paull, C. K., and Iii, W. U. (1996). gas hydrate Marine pore-water sulfate profiles indicate in situ methane flux from underlying gas hydrate. *Geology* 1996:655. doi: 10.1130/0091-7613-024-0655

Bradley, J. A., Arndt, S., Amend, J. P., Burwicz, E., Dale, A. W., Egger, M., et al. (2020). Widespread energy limitation to life in global subseafloor sediments. *Sci. Adv.* 6:eaba0697.

Caporaso, J. G., Lauber, C. L., Walters, W. A., Berg-Lyons, D., Huntley, J., Fierer, N., et al. (2012). Ultra-high-throughput microbial community analysis on the Illumina HiSeq and MiSeq platforms. *ISME J.* 2012, 1621–1624. doi: 10.1038/ismej.2012.8

D'Hondt, S., Jørgensen, B. B., Miller, D. J., Batzke, A., Blake, R., Cragg, B. A., et al. (2004). Distributions of microbial activities in deep subseafloor sediments. *Science* 306, 2216–2221.

D'Hondt, S., Rutherford, S., and Spivack, A. J. (2002). Metabolic activity of subsurface life in deep-sea sediments. *Science* 295, 2067–2070. doi: 10.1126/science.1064878

Egger, M., Riedinger, N., Mogollón, J. M., and Jørgensen, B. B. (2018). Global diffusive fluxes of methane in marine sediments. *Nat. Geosci.* 11, 421–425. doi: 10.1038/s41561-018-0122-8

Finke, N., Hoehler, T. M., and Jørgensen, B. B. (2007). Hydrogen "leakage" during methanogenesis from methanol and methylamine: implications for anaerobic carbon degradation pathways in aquatic sediments. *Environ. Microbiol.* 9, 1060–1071. doi: 10.1111/j.1462-2920.2007.01248.x

Harrison, B. K., Zhang, H., Berelson, W., and Orphan, V. J. (2009). Variations in archaeal and bacterial diversity associated with the sulfate-methane transition zone in continental margin sediments (Santa Barbara Basin, California). *Appl. Environ. Microbiol.* 75, 1487–1499. doi: 10.1128/AEM.01812-08

Hoehler, T. M., Alperin, M. J., Albert, D. B., and Martens, C. S. (1994). Field and laboratory studies of methane oxidation in an anoxic marine sediment: Evidence for a methanogen-sulfate reducer consortium. *Global Biogeochem. Cycles* 8, 451–463.

Hoehler, T. M., Alperin, M. J., Albert, D. B., and Martens, C. S. (1998). Thermodynamic control on hydrogen concentrations in anoxic sediments. *Geochim. Cosmochim. Acta* 621, 1745–1756.

Hoehler, T. M., Alperin, M. J., Albert, D. B., and Martens, C. S. (2001). Apparent minimum free energy requirements for methanogenic Archaea and sulfate-reducing bacteria in an anoxic marine sediment. *FEMS Microbiol. Ecol.* 38, 33–41.

Hoehler, T. M., and Jørgensen, B. B. (2013). Microbial life under extreme energy limitation. *Nat. Rev. Microbiol.* 11, 83–94. doi: 10.1038/nrmicro2939

Holler, T., Wegener, G., Knittel, K., Boetius, A., Brunner, B., Kuypers, M. M. M., et al. (2009). Substantial 13 C/ 12 C and D/H fractionation during anaerobic oxidation of methane by marine consortia enriched in vitro. *Environ. Microbiol. Rep.* 1, 370–376. doi: 10.1111/j.1758-2229.2009.00074.x

Holmkvist, L., Ferdelman, T. G., and Jørgensen, B. B. (2011). A cryptic sulfur cycle driven by iron in the methane zone of marine sediment (Aarhus Bay, Denmark). *Geochim. Cosmochim. Acta* 75, 3581–3599. doi: 10.1016/j.gca.2011.03.033

House, C. H., Orphan, V. J., Turk, K. A., Thomas, B., Pernthaler, A., Vrentas, J. M., et al. (2009). Extensive carbon isotopic heterogeneity among methane seep

microbiota. *Environ. Microbiol.* 11, 2207–2215. doi: 10.1111/j.1462-2920.2009.01934.x

Iversen, N., and Jorgensen, B. B. (1985). Anaerobic methane oxidation rates at the sulfate-methane transition in marine sediments from Kattegat and Skagerrak (Denmark). *Limnol. Oceanogr.* 1983, 944–955.

Jackson, B. E., and McInerney, M. J. (2002). Anaerobic microbial metabolism can proceed close to thermodynamic limits. *Nature* 415, 454–456. doi: 10.1038/415454a

Jørgensen, B. B., Findlay, A. J., and Pellerin, A. (2019). The Biogeochemical Sulfur Cycle of Marine Sediments. *Front. Microbiol.* 10:1–27. doi: 10.3389/fmicb.2019.00849

Jørgensen, B. B., and Kasten, S. (2006). "Sulfur cycling and methane oxidation," in *Marine Geochemistry*, eds H. Schulz and M. Zabel Berlin (Heidelberg: Springer), doi: 10.1007/3-540-32144-6

Kelley, C. A., Martens, C. S., and Chanton, J. P. (1990). Variations in sedimentary carbon remineralization rates in the White Oak River estuary, North Carolina. *Limnol. Oceanogr.* 35, 372–383. doi: 10.1093/acrefore/9780190846626.013.104

Kevorkian, R., Bird, J. T., Shumaker, A., and Lloyd, K. G. (2018). Estimating population turnover rates by relative quantification methods reveals microbial dynamics in marine sediment. *Appl. Environ. Microbiol.* 84, 1–16. doi: 10.1128/AEM.01443-17

Kevorkian, R. T., Callahan, S., Winstead, R., and Lloyd, K. G. (2021). ANME-1 archaea may drive methane accumulation and removal in estuarine sediments. *Environ. Microbiol. Rep.* 13, 185–194. doi: 10.1111/1758-2229.12926

Knab, N., Cragg, B., Borowski, C., Parkes, R., Pancost, R., and Jorgensen, B. (2008). Anaerobic oxidation of methane (AOM) in marine sediments from the Skagerrak (Denmark): I. Geochemical and microbiological analyses. *Geochim. Cosmochim. Acta* 72, 2868–2879. doi: 10.1016/j.gca.2008.03.016

Knittel, K., Lösekann, T., Boetius, A., Kort, R., and Amann, R. (2005). Diversity and distribution of methanotrophic archaea at cold seeps. *Appl. Envrion. Microbiol.* 71, 467–479. doi: 10.1128/AEM.71.1.467

Lazar, C. S., Biddle, J. F., Meador, T. B., Blair, N., Hinrichs, K. U., and Teske, A. P. (2015). Environmental controls on intragroup diversity of the uncultured benthic archaea of the miscellaneous Crenarchaeotal group lineage naturally enriched in anoxic sediments of the White Oak River estuary (North Carolina, USA). *Environ. Microbiol.* 17, 2228–2238. doi: 10.1111/1462-2920.12659

Leloup, J., Fossing, H., Kohls, K., Holmkvist, L., Borowski, C., and Jørgensen, B. B. (2009). Sulfate-reducing bacteria in marine sediment (Aarhus Bay, Denmark): abundance and diversity related to geochemical zonation. *Environ. Microbiol.* 11, 1278–1291. doi: 10.1111/j.1462-2920.2008.01855.x

Lloyd, K. G., Alperin, M. J., and Teske, A. (2011). Environmental evidence for net methane production and oxidation in putative ANaerobic MEthanotrophic (ANME) archaea. *Environ. Microbiol.* 13, 2548–2564. doi: 10.1111/j.1462-2920.2011.02526.x

Martens, C. S., Albert, D. B., and Alperin, M. J. (1998). Biogeochemical processes controlling methane in gassy coastal sediments - Part 1. A model coupling organic matter flux to gas production, oxidation and transport. *Cont. Shelf Res.* 18, 1741–1770.

Martens, S., and Berner, R. A. (1977). Interstitial water chemistry of anoxic Lbng Island Sound sediments. 1. Dissolved gases. *Limnol. Oceanogr.* 22, 10–25.

Mcglynn, S. E., Chadwick, G. L., Kempes, C. P., and Orphan, V. J. (2015). Single cell activity reveals direct electron transfer in methanotrophic consortia. *Nature* 526, 531–535. doi: 10.1038/nature15512

McMurdie, P. J., and Holmes, S. (2013). phyloseq: an r package for reproducible interactive analysis and graphics of microbiome census data. *PLoS One* 8:e61217. doi: 10.1371/journal.pone.0061217

Mills, H. J., Hunter, E., Humphrys, M., Kerkhof, L., McGuinness, L., Huettel, M., et al. (2008). Characterization of nitrifying, denitrifying, and overall bacterial communities in permeable marine sediments of the northeastern Gulf of Mexico. *Appl. Environ. Microbiol.* 74, 4440–4453. doi: 10.1128/AEM.02692-07

Nauhaus, K., Albrecht, M., Elvert, M., Boetius, A., and Widdel, F. (2007). In vitro cell growth of marine archaeal-bacterial consortia during anaerobic oxidation of methane with sulfate. *Environ. Microbiol.* 9, 187–196. doi: 10.1111/j.1462-2920.2006.01127.x

Parkes, R. J., Cragg, B. A., Banning, N., Brock, F., Webster, G., Fry, J. C., et al. (2007). Biogeochemistry and biodiversity of methane cycling in subsurface marine sediments (Skagerrak, Denmark). *Environ. Microbiol.* 2007:1237. doi: 10.1111/j.1462-2920.2006.01237.x

Pellerin, A., Antler, G., Røy, H., Findlay, A., Beulig, F., Scholze, C., et al. (2018). The sulfur cycle below the sulfate-methane transition of marine sediments. *Geochim. Cosmochim. Acta* 239, 74–89. doi: 10.1016/j.gca.2018.07.027

Pruesse, E., Quast, C., Knittel, K., Fuchs, B. M., Ludwig, W., Peplies, J., et al. (2007). SILVA: a comprehensive online resource for quality checked and aligned ribosomal RNA sequence data compatible with ARB. *Nucleic Acids Res.* 35, 7188–7196. doi: 10.1093/nar/gkm864

Reeburgh, W. S. (2007). Oceanic methane biogeochemistry. *System* 2007, 486–513.

Reeve, J. N., Nölling, J., Morgan, R. M., and Smith, D. R. (1997). Methanogenesis: Genes, genomes, and who's on first? *J. Bacteriol.* 179, 5975–5986.

Schreiber, L., Holler, T., Knittel, K., Meyerdierks, A., and Amann, R. (2010). Identification of the dominant sulfate-reducing bacterial partner of anaerobic methanotrophs of the ANME-2 clade. *Environ. Microbiol.* 12, 2327–2340. doi: 10.1111/j.1462-2920.2010.02275.x

Timmers, P. H. A., Gieteling, J., Widjaja-Greefkes, H. C. A., Plugge, C. M., Stams, A. J. M., Lens, P. N. L., et al. (2015). Growth of anaerobic methane-oxidizing archaea and sulfate-reducing bacteria in a high-pressure membrane capsule bioreactor. *Appl. Environ. Microbiol.* 81, 1286–1296. doi: 10.1128/AEM.03255-14

Underwood, S., Lapham, L., Teske, A., and Lloyd, K. G. (2016). Microbial community structure and methane-cycling activity of subsurface sediments at Mississippi Canyon 118 before the Deepwater Horizon disaster. *Deep. Res. Part II Top Stud. Oceanogr.* 129:11. doi: 10.1016/j.dsr2.2015.01.011

Valentine, D. L., Blanton, D. C., and Reeburgh, W. S. (2000). Hydrogen production by methanogens under low-hydrogen conditions. *Arch. Microbiol.* 2000, 415–421. doi: 10.1007/s002030000224

Wang, G., Spivack, A. J., and Hondt, S. D. (2010). Gibbs energies of reaction and microbial mutualism in anaerobic deep subseafloor sediments of ODP Site 1226. *Geochim. Cosmochim. Acta* 74, 3938–3947. doi: 10.1016/j.gca.2010.03.034

Wang, G., Spivack, A. J., Rutherford, S., Manor, U., and Hondt, S. D. (2008). Quantification of co-occurring reaction rates in deep subseafloor sediments. *Geochim. Cosmochim. Acta* 72, 3479–3488. doi: 10.1016/j.gca.2008.04.024

Wegener, G., Krukenberg, V., Riedel, D., Tegetmeyer, H. E., and Boetius, A. (2015). Intercellular wiring enables electron transfer between methanotrophic archaea and bacteria. *Nature* 526, 587–590. doi: 10.1038/nature15733

Whiticar, M. J. (1999). Carbon and hydrogen isotope systematics of bacterial formation and oxidation of methane. *Chem. Geol.* 161, 291–314.

Xiao, K. Q., Beulig, F., Kjeldsen, K. U., Jørgensen, B. B., and Risgaard-Petersen, N. (2017). Concurrent methane production and oxidation in surface sediment from Aarhus Bay, Denmark. *Front. Microbiol.* 8:1–12. doi: 10.3389/fmicb.2017.01198

Conflict of Interest: The authors declare that the research was conducted in the absence of any commercial or financial relationships that could be construed as a potential conflict of interest.

Publisher's Note: All claims expressed in this article are solely those of the authors and do not necessarily represent those of their affiliated organizations, or those of the publisher, the editors and the reviewers. Any product that may be evaluated in this article, or claim that may be made by its manufacturer, is not guaranteed or endorsed by the publisher.

frontiers in Microbiology

REVIEW
published: 18 March 2022
doi: 10.3389/fmicb.2022.842785

Differences in Bioenergetic Metabolism of Obligately Alkaliphilic *Bacillaceae* Under High pH Depend on the Aeration Conditions

*Toshitaka Goto[1,2], Shinichi Ogami[1,2], Kazuaki Yoshimume[3] and Isao Yumoto[1,2]**

[1] Bioproduction Research Institute, National Institute of Advanced Industrial Science and Technology (AIST), Sapporo, Japan, [2] Graduate School of Agriculture, Hokkaido University, Sapporo, Japan, [3] College of Industrial Technology, Nihon University, Narashino, Japan

Alkaliphilic *Bacillaceae* appear to produce ATP based on the H^+-based chemiosmotic theory. However, the bulk-based chemiosmotic theory cannot explain the ATP production in alkaliphilic bacteria because the H^+ concentration required for driving ATP synthesis through the ATPase does not occur under the alkaline conditions. Alkaliphilic bacteria produce ATP in an H^+-diluted environment by retaining scarce H^+ extruded by the respiratory chain on the outer surface of the membrane and increasing the potential of the H^+ for ATP production on the outer surface of the membrane using specific mechanisms of ATP production. Under high-aeration conditions, the high $\Delta\Psi$ (ca. -170 mV) of the obligate alkaliphilic *Evansella clarkii* retains H^+ at the outer surface of the membrane and increases the intensity of the protonmotive force (Δp) per H^+ across the membrane. One of the reasons for the production of high $\Delta\Psi$ is the Donnan potential, which arises owing to the induction of impermeable negative charges in the cytoplasm. The intensity of the potential is further enhanced in the alkaliphiles compared with neutralophiles because of the higher intracellular pH (ca. pH 8.1). However, the high $\Delta\Psi$ observed under high-aeration conditions decreased ($\sim$ -140 mV) under low-aeration conditions. *E. clarkii* produced 2.5–6.3-fold higher membrane bound cytochrome *c* in the content of the cell extract under low-aeration conditions than under high-aeration conditions. The predominant membrane-bound cytochrome *c* in the outer surface of the membrane possesses an extra Asn-rich segment between the membrane anchor and the main body of protein. This structure may influence the formation of an H^+-bond network that accumulates H^+ on the outer surface of the membrane. Following accumulation of the H^+-bond network producing cytochrome *c*, *E. clarkii* constructs an H^+ capacitor to overcome the energy limitation of low aeration at high pH conditions. *E. clarkii* produces more ATP than other neutralophilic bacteria by enhancing the efficacy per H^+ in ATP synthesis. In low H^+ environments, *E. clarkii* utilizes H^+ efficiently by taking advantage of its high $\Delta\Psi$ under high-aeration conditions, whereas under low-aeration conditions *E. clarkii* uses cytochrome *c* bound on its outer surface of the membrane as an H^+ capacitor.

Keywords: bioenergetic mechanism, membrane electrical potential, *Bacillaceae*, *Evansella clarkii*, Donnan effect, H^+ capacitor, cytochrome *c*, alkaliphilic

OPEN ACCESS

Edited by:
Andreas Teske, University of North Carolina at Chapel Hill, United States

Reviewed by:
Alfredo Cabrera-Orefice, Radboud University Nijmegen Medical Centre, Netherlands
Arthur Guffanti, AOL, United States

***Correspondence:**
Isao Yumoto
i.yumoto@aist.go.jp

Specialty section:
This article was submitted to Extreme Microbiology, a section of the journal Frontiers in Microbiology

Received: *24 December 2021*
Accepted: *22 February 2022*
Published: *18 March 2022*

Citation:
Goto T, Ogami S, Yoshimume K and Yumoto I (2022) Differences in Bioenergetic Metabolism of Obligately Alkaliphilic Bacillaceae Under High pH Depend on the Aeration Conditions. Front. Microbiol. 13:842785. doi: 10.3389/fmicb.2022.842785

INTRODUCTION

Extremophiles can thrive in extreme environments such as low or high temperatures, high or low pH, UV radiation and high salinity (Satyanarayana et al., 2005; Rampelotto, 2013). Such environmental adaptation mechanisms enable the species to exploit environments that are disadvantageous to the survival of other organisms in general, and to protect their biological systems from harsh environments. By studying the mechanisms of environmental adaptations of such microorganisms, it is possible to obtain an understanding of the mechanisms for sustaining life systems that could not be elucidated when studying organisms in ordinary environments. In other words, by observing the biological system from a different perspective, we may be able to understand the true meaning of the mechanism of the biological system. Environmental adaptation by microorganisms is achieved by the accumulation of slight modifications in their structural components and mechanisms while sharing basic life form principles with many other organisms. The factors related to environmental adaptation are related to each other. Therefore, a comprehensive perspective is necessary to understand the mechanism underlying environmental adaptation of microorganisms.

Reduction in intracellular pH and suppression of the pH difference between intracellular and extracellular spaces of less than 2 pH units is necessary for survival and adaptation of *Bacillaceae* in an alkaline environment. In addition, establishing a system that reduces the utilization of H^+ in various solute transportation systems will also be important for adapting to high pH. If complete ion transportation occurs using Na^+, it would not be necessary to enhance the efficiency of H^+ utilization. However, alkaliphilic *Bacillaceae* strains are thought to utilize both H^+ (e.g., ATP synthase) and Na^+ potentials (e.g., solute transport) for survival under H^+-deficient conditions (Dimroth and Cook, 2004). This is probably due to certain advantages of employing the respiratory chain system using H^+. While solute transportation and flagellar rotation are performed by Na^+/solute symporters, voltage-gated Na^+ channels (NavBP), and a Na^+-dependent flagellar motor stator (MotPS), the ATP production is performed by the H^+-based ATPase (Kitada et al., 1982; Ito et al., 2004a,b; Padan et al., 2005). The Na^+/H^+ antiporter, Mrp (Sha), plays an important role in sustaining the Na^+ cycle system in the cells of both *Alkalihalobacillus halodurans* C-125 and *Alkalihalobacillus pseudofirmus* OF4 (Hamamoto et al., 1994; Krulwich et al., 2001). The Na^+ efflux conducted by this antiporter is enhanced by activation of the respiratory chain in *A. halodurans* C-125, indicating that the antiporter plays a role in translating the H^+-based transmembrane potential (PMF) produced by the respiratory chain to the Na^+-based potential (SMF), which is concomitant with the necessity to increase the intracellular H^+ concentration. The protonmotive force (Δp) generated by the respiratory chain sustains not only ATP production, which is driven by the ATPase but also the Na^+ cycle system, which regulates cell homeostasis in *A. halodurans* C-125. To sustain the combination of energy production and solute transportation systems, H^+ and Na^+ should be localized in the vicinity of the membrane, and a large background membrane potential ($\Delta\Psi$) is necessary. It can be presumed that H^+ localizes to the respiratory system and the SMF is the predominant potential across the membrane.

Although there are certain variations depending on the species or strains, alkaliphilic *Bacillaceae* strains have acidic secondary cell walls. For example, *A. halodurans* C-125 possesses an acidic secondary cell wall consisting of teichuronopeptide and teichuronic acid (Aono and Horikoshi, 1983; Aono et al., 1993, 1995, 1999). These acidic components accompanied by high negative charge will attract H^+ around the cell surface and consequently delay the rapid loss of H^+ from the cell surface to the bulk high pH. In addition, the formation of the negatively charged secondary cell wall results in a lower pH inside of the cell wall than the extracellular pH (Tsujii, 2002). Slower growth was observed in a mutant deficient in the cell surface layer (S-layer) protein A (SlaA), especially when the Na^+ concentration was low in the medium of *A. pseudofirmus* OF4 (Gilmore et al., 2000). Similar to other secondary cell wall components in alkaliphilic *Bacillaceae* strains, SlpA is also an acidic component (pI = 4.36). It was considered that the abundance of SlpA attracts H^+ and expels OH^- on the cell surface. Thus, alkaliphilic *Bacillaceae* strains possess negatively charged cell wall components that protect intracellular metabolic activities by preventing equilibration with the harsh extracellular alkaline phase.

Alkaliphilic *Bacillaceae* strains mitigate alkaline environments by producing acid to avoid direct interactions with harsh environments. Many alkaliphilic *Bacillus* species have been reported to produce acid to reduce the ambient pH (Horikoshi, 2006; Hirota et al., 2013). Although acid production by bacteria is often a byproduct of carbohydrate metabolism, acid production by alkaliphilic *Bacillaceae* strains can often be observed even in media lacking carbohydrates. In such cases, acid may be produced by the deamination of amino acids by amino acid deaminases (Mano, 2020). Acid production may influence to the reduction of intracellular pH, as well as increase the availability of H^+ in the vicinity of the cell surface and outer surface of the membrane. In addition, cells produce acids as a group, and it can be presumed that acid production also alleviates the surrounding alkaline environments. Thus, acid production by alkaliphiles is considered an important factor for adaptation to high pH.

As described above, alkaliphilic bacteria comprise exquisite total adaptation mechanisms to mitigate harsh environments, which is one-thousandth of the normal H^+ concentration compared to neutral pH. However, ATP production through mechanisms that require a transmembrane pH gradient (outside < inside) is still difficult. In this review, we aimed to understand how alkaliphilic bacteria synthesize ATP, in alkaline environments by comparing the bioenergetic parameters in an obligate alkaliphilic bacterium (cannot grow in neutral pH), *Evansella clarkii*, a facultative alkaliphilic bacterium (can grow in both alkaline and neutral pH), *Sutcliffiella cohnii*, and a neutralophilic bacteria (can grow only in neutral pH), *Bacillus subtilis*, by changing the aeration conditions. Oxygen is the final electron acceptor in the aerobic respiratory chain. Therefore, the limitation

of oxygen will present an additional stress factor to the bacteria. By comparing the parameters related to energy production metabolism in alkaliphilic bacteria, we can understand the regulation of bioenergetic factors. Based on this observation, we will be able to understand the relationship between bioenergetic factors and adaptation mechanisms in the corresponding environment.

TAXONOMIC BACKGROUND OF ALKALIPHILIC *BACILLACEAE*

Alkaliphiles are defined as microorganisms, mostly bacteria, that exhibit higher growth intensity at pH $\geq$ 9. Since Vedder (1934) first isolated alkaliphilic *Bacillaceae*, *Bacillus alcalophilus* (*Alkalihalobacillus alcalophilus*), many alkaliphilic *Bacillaceae* strains have been isolated from various common environments such as garden soil, feces, and horse manure. Although it is strange that microorganisms adaptable to alkali conditions are isolated from mundane environments, this may indicate that it is not uncommon for ammonia production from plant or animal decays to temporarily flow into common environments. For example, following indigo fermentation originating from composted Chinese or Japanese indigo [*Persicaria tinctoria* (Aiton) Spach] used in China, Korea, and Japan, many alkaliphilic *Bacillaceae* species such as *Sutcliffiella* spp. (including *Sutcliffiella cohnii*), *Evansella* spp. (*including Evansella polygoni*), and *Amphibacillus* spp. have been isolated and detected using 16S rRNA gene-based next-generation sequence analyses (Lopes et al., 2021a,b; Tu et al., 2021). Another possible reason for the wide distribution of alkaliphiles in common environments is the existence of micro-alkaline environments, for example, in the intestines of termites. Using 16S rRNA gene clones derived from the contents of the intestine of termites [*Termes comis* (*Termitinae*)], many alkaliphilic *Bacillaceae* species, such as those belonging to *Sutcliffiella* spp. and *Alkalihalobacillus* spp., have been detected (Thongaram et al., 2003). Although many alkaliphilic *Bacillaceae* strains had been isolated until the mid-1990s, it was unclear whether alkaliphilic *Bacillaceae* involved numerous species because of the absence of studies based on their 16S rRNA gene sequences with reference to a gene sequence database. Since the determination of the 16S rRNA gene sequence and its application in bacterial taxonomic studies, the taxonomic position of alkaliphilic *Bacillaceae* has been elucidated, and the existence of many authorized species has been confirmed (Nielsen et al., 1994, 1995; Nogi et al., 2005). Although many identified alkaliphilic species were originally considered to belong to the genus *Bacillus*, their reclassification into several new genera has been proposed following the development of genomic analysis (Gupta et al., 2020; Patel and Gupta, 2020). The following strains were used for alkaline adaptation physiological studies were as follows: *Bacillus halodurans* C-125, *Bacillus alcalophilus*, *Bacillus firmus* RAB, and *Bacillus pseudofirmus* OF4, which were reclassified as the genus *Alkalihalobacillus*; *Bacillus cohnii* YN-2000, which was reclassified as the genus *Sutcliffiella*; and *Bacillus clarkii* DSM 8720^T and K24-1U, and *Bacillus polygoni*, which were reclassified as the genus *Evansella* (**Figure 1**).

MEMBRANE LIPIDS

Membrane lipid characteristics play an important role in conferring the bioenergetic features of bacteria owing to the respiratory components associated with the membrane. In addition, membrane lipids consistently define H^+ permeability across the membrane, and the head group of phospholipids influences the membrane surface charges. Furthermore, when the respiratory chain exhibits the function of an H^+ capacitor, it is possible that the H^+ retaining capacity may change depending on the properties of the membrane lipids. Clejan et al. (1986) performed a comparative study on the composition of total membrane lipids, neutral lipids, and polar lipids, in addition to fatty acids composition, in membrane lipids using neutralophilic *Bacillus subtilis*, two strains of obligate alkaliphiles (*Alkalihalobacillus pseudofirmus* RAB and *A. alcalophilus* ATCC 27647^T), and two strains of facultative alkaliphiles (*Alkalihalobacillus* sp. OF1 and *Alkalihalobacillus pseudofirmus* OF4). The total membrane lipids of obligate alkaliphiles are approximately 1.5-fold higher than those of neutralophilic *B. subtilis*, while those of facultative alkaliphiles are 1.1–1.4 times higher than those of neutralophilic *B. subtilis*. The ratio of neutral/polar lipids was higher in the two obligate alkaliphiles (approximately 82%) than that in *B. subtilis* (approximately 43%) and facultative alkaliphiles (33–54%). In facultative alkaliphiles the neutral lipid ratio was higher in cells grown at pH 7.5 than in those grown at pH 10.5. These results suggest that obligate alkaliphiles are fundamentally different from facultative alkaliphiles in their environmental adaptation strategies. All alkaliphiles contain appreciable amounts of squalene and C_{40} isoprenoids, whereas *B. subtilis* does not harbor them. Although the roles of squalene and C_{40} isoprenoids have not yet been clarified, these neutral lipids may play an important role in alkaline adaptation to alkaline environments. Among polar lipids phosphatidylglycerol (PG) content was higher in *B. subtilis* than in obligate and facultative alkaliphiles. Cardiolipin (CL) content was higher in obligate and facultative alkaliphiles than in *B. subtilis*. In facultative alkaliphiles, CL content was not always higher in the cells grown under an alkaline pH than in those grown under a neutral pH medium. Enomoto and Koyama (1999) examined polar lipid content using facultative alkaliphiles *Sutcliffiella cohnii* YN-2000 and *Exiguobacterium aurantiacum* BL77/1 grown at pH 7.5 and pH 10 each. The results showed that CL content was higher in cells grown at pH 10 in both the strains. Both CL and PG contents increased in the cells grown at pH 10 in strain BL77/1. They also estimated the negative ion capacity of the membrane and found that the negative surface charge was higher in the cells grown at pH 10 than in cells grown at pH 7.2 in both strains. Therefore, it was concluded that the increase in the negative surface charge of the cells grown at pH 10 was attributed to the increase in acidic phospholipids CL and PG. Clejan et al. (1986) reported that branched-chain fatty acids and unsaturated fatty acids are higher in obligate alkaliphiles than in facultative alkaliphiles. However, it has been reported that facultative alkaliphilic *S. cohnii* strains (YN-2000 and DSM 6307^T) exhibit much higher unsaturated

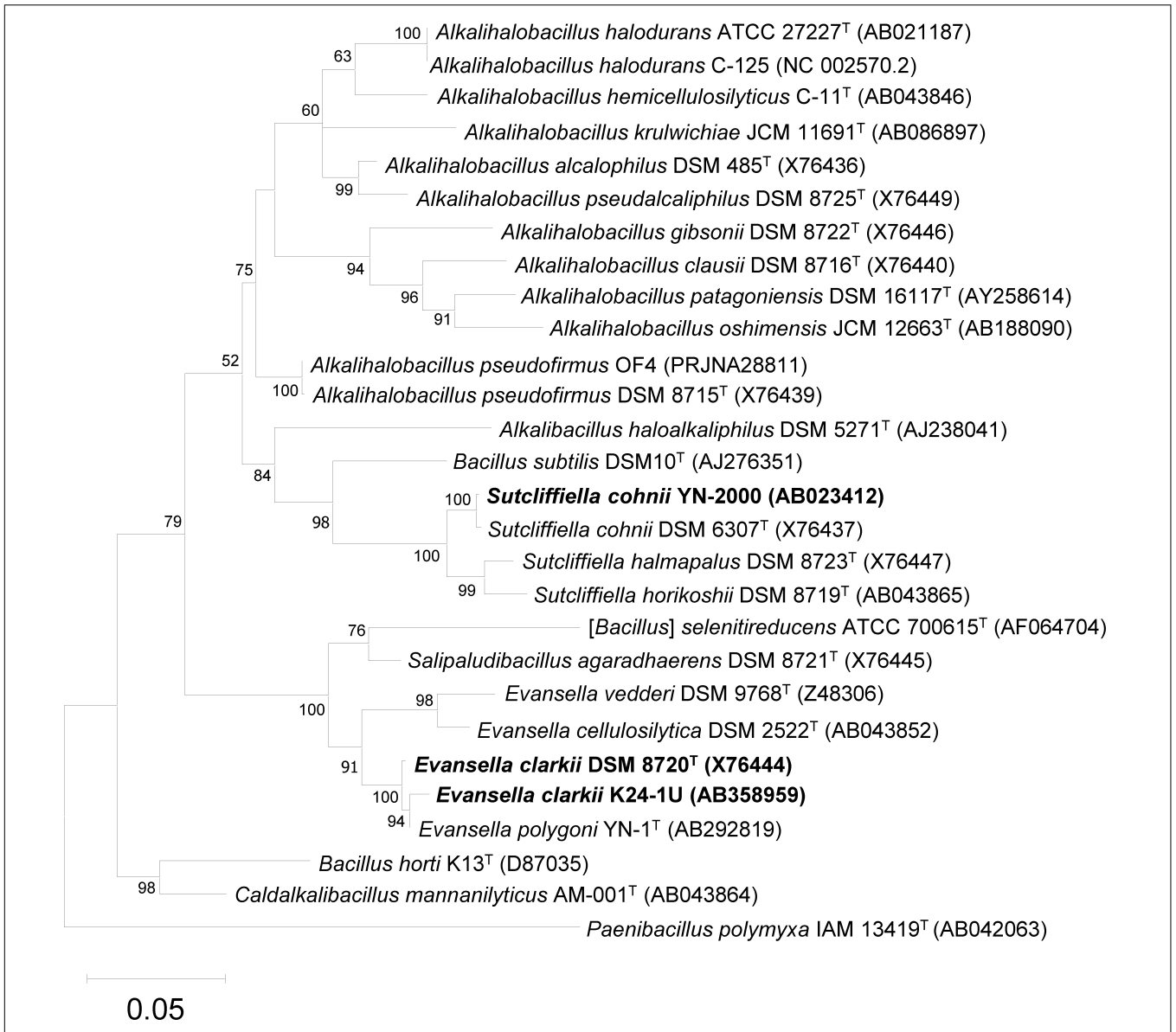

FIGURE 1 | Maximum-likelihood phylogenetic tree derived from 16S rRNA gene sequences of obligately alkaliphilic *Evansella clarkii* and other related alkaliphilic and neutralophilic *Bacillaceae*. General time reversible model (Nei and Kumar, 2000) was used as the evolutionary model. The tree with the highest log likelihood (-7837.68) is shown. Initial tree(s) for the heuristic search were obtained automatically by applying Neighbor-Join and BioNJ algorithms to a matrix of pairwise distances estimated using the maximum composite likelihood (MCL) approach, and then selecting the topology with a superior log likelihood value. A discrete gamma distribution was used to model evolutionary rate differences among sites [5 categories (+ G, parameter = 0.4765)]. The rate variation model allowed for some sites to be evolutionarily invariable [(+ I), 55.96% sites]. Phylogenetic positions of the obligately alkaliphilic *E. clarkii* DSM 8720^T and K24-1U, and the facultatively alkaliphilic *Sutcliffiella cohnii* YN-2000 are indicated in bold. The bootstrap values (> 50%) based on 1000 replications are shown at the branch node. *Paenibacillus polymyxa* IAM 13419^T was used as an outgroup. Bar, 0.05 substitution per nucleotide position. Evolutionary analyses were conducted in MEGA11 (Tamura et al., 2021).

fatty acid contents than obligate alkaliphilic *A. alcalophilus* JCM 5262^T. Unsaturated fatty acid content was lower in the cells grown at pH 10 than in those grown at pH 7 (Yumoto et al., 2000). The obligate alkaliphilic *Evansella polygoni* YN-1^T contains 22.1% unsaturated fatty acid within total fatty acids, whereas *Evansella clarkii* DSM 8720^T does not contain any unsaturated fatty acid (Aino et al., 2008). However, *E. clarkii* DSM 8720^T contains 92.5% branched chain fatty acids within total fatty acids. Since membrane lipids will change depending on the culture conditions, it is difficult to compare the result from different reports. The reported facts described above suggest that the strategies for alkaline adaptations of *Bacillaceae* differ depending on the strain. Therefore, it is important to understand the role of membrane lipids during environmental

adaptation to determine the interrelationships between other related factors.

VERTICALLY LOCALIZED BIOENERGETIC PARAMETERS IN MEMBRANE SURFACE

It has been considered that the protonmotive force (Δp), which drives F_1F_0-ATPase, consists of the following components: ΔpH (higher extracellular H^+) and the ΔΨ (larger intracellular negative charge) across the membrane (Mitchell, 1961).

$$\Delta p = \Delta\Psi - Z\Delta pH$$

$$Z = 2.3RT/F = \text{ca.}59\ \text{mV}(\text{at } 25^\circ\text{C}),$$

where R = gas constant (8.315 $J{\cdot}K^{-1}{\cdot}mol^{-1}$), T = absolute temperature (298 K = 25°C), and F = Faraday constant (96.485 $kJ{\cdot}mol^{-1}{\cdot}V^{-1}$).

In general, the bioenergetic parameters, ΔΨ and ΔpH, estimated in the bulk base are considered for application to the formula described above. One of the reasons for this is the difficulty in measuring the real ΔpH and ΔΨ in the vicinity of the outer surface of the membrane at the entrance of the F_1F_0-ATPase. However, in the case of alkaliphilic *Bacillaceae* strains, there are several specific factors affecting the membrane surface ΔΨ and ΔpH: (1) the estimated ΔΨ cannot account for the intensity of each H^+ for ATP production, (2) modified proteins located on the outer membrane surface may facilitate the transfer of H^+ on the outer surface of the membrane, and (3) the presence of phospholipids having negatively charged head groups on the outer surface of the membrane may create a localized low pH microlayer at the site.

Bioenergetic parameters and growth features have been estimated in facultative alkaliphilic *A. pseudofirmus* OF4 under pH-controlled culture conditions (Sturr et al., 1994). Strain OF4 exhibited a specific growth rate and measurable Δp (bulk-based) of 1.10 h^{-1} and -26 mV, respectively, at pH 10.6. On the other hand, the strain exhibited a specific growth rate and Δp of 0.77 h^{-1} and -140 mV, respectively at pH 7.5. Thus, the faster growth rate in pH 10.6 than that in pH 7.5 cannot account for using the measurable bioenergetic parameters. This discrepancy between the growth features and bioenergetic parameters can be observed in other alkaliphilic *Bacillaceae* strains. The facts described above indicate that bulk-based or measurable bioenergetic parameters cannot account for the growth of alkaliphilic *Bacillaceae* strains.

Although the contribution of the phospholipid head group to the accumulation of H^+ is expected to be high, we do not presently have data corresponding to obligate alkaliphilic *Evansella clarkii*. However, we found specific segments that may contribute to the H-bond network associated with the structure of membrane-bound cytochrome *c*. Here, enhanced efficiency in H^+ usage by reducing H^+ diffusion and the increasing H^+ concentration available for the ATP production in *E. clarkii* are discussed below.

CHARACTERISTICS OF CYTOCHROME *C* EXPRESSION FOLLOWING BACTERIAL ADAPTION TO DIFFERENT PH VALUES

It is known that cytochrome *c* is released from mitochondria when cells are stimulated to induce apoptosis. Thus, it is known that the function of cytochrome *c* is multifaceted. The primary role of cytochrome *c* as a component of the respiratory chain is to transfer electrons from the cytochrome bc_1 complex (complex III) to the cytochrome *c* oxidase (complex IV). Certain alkaliphilic bacteria, such as *S. chonii* and *E. clarkii*, are known to exhibit higher cytochrome *c* contents than neutralophilic *Bacillaceae*, such as *B. subtilis*. However, the specific functions related to the alkaline adaptation have not yet been clarified. To understand the molecular features of the intact protein, it is indispensable to consider the function of cytochrome *c*. Some of the cytochromes *c* from *Bacillaceae* strains have been reported to be in soluble forms due to the lacking of an N-terminal sequence associated with intrinsic protease activity (Yamaguchi et al., 1966; Miki and Okunuki, 1969a,b; Woolley, 1987; Davidson et al., 1988; Benini et al., 1998, 2000). Although the purification of a protein using a cocktail of protease inhibitors is promising, the inhibitors do not always inhibit protease activity adequately. Therefore, we attempted to purify intact membrane-bound cytochrome *c* from obligate alkaliphilic *E. clarkii*, which exhibited weak protease activity. Here, the molecular features of membrane-bound cytochromes *c* from neutralophilic *B. subtilis*, and facultative and obligate alkaliphiles are described. Comparison of cytochromes *c* derived from three categories of *Bacillaceae* (neutralophiles, facultative, and obligate alkaliphiles) revealed the peculiarities of cytochromes *c* obtained from obligate alkaliphiles.

Cytochrome *c* in Neutralophilic *Bacillus subtilis*

Since many *Bacillaceae* strains exhibit strong protease activity, it is difficult to purify intact cytochrome *c*. Although *Bacillaceae* strains should not have soluble cytochromes *c* due to the lack of the periplasmic space in the cell, several soluble cytochromes *c* have been purified. It has been reported that *B. subtilis* 168 possesses two types of membrane-binding cytochromes *c*-550 and *c*-551. Cytochrome *c*-551 has a molecular mass of 10 kDa and is composed of 92 amino acid residues, including 14 basic amino acid residues in its processed form, and binds to the membrane *via* a diacyl-glyceryl-cysteine moiety by modification of its N-terminal sequence (**Figure 2** and **Table 1**; Bengtsson et al., 1999). Cytochrome *c*-551 is the counterpart of cytochrome *c* to cytochrome *c*-550 in obligate alkaliphilic *E. clarkii*. The midpoint redox potential was considered to be > + 100 mV and its p*I* was 3.8. However, the function of cytochrome *c*-551 has not yet been elucidated. It is speculated that cytochrome *c*-551 is involved in the electron transfer between cytochrome bc_1 and cytochrome *c* oxidase. The phylogenetic position of cytochrome *c*-551 was similar to that of *Bacillus licheniformis* SCDB cytochrome *c* (**Figure 3**). Cytochrome *c*-550 has a molecular mass of 13 kDa and is composed of 120 amino acid residues with a membrane

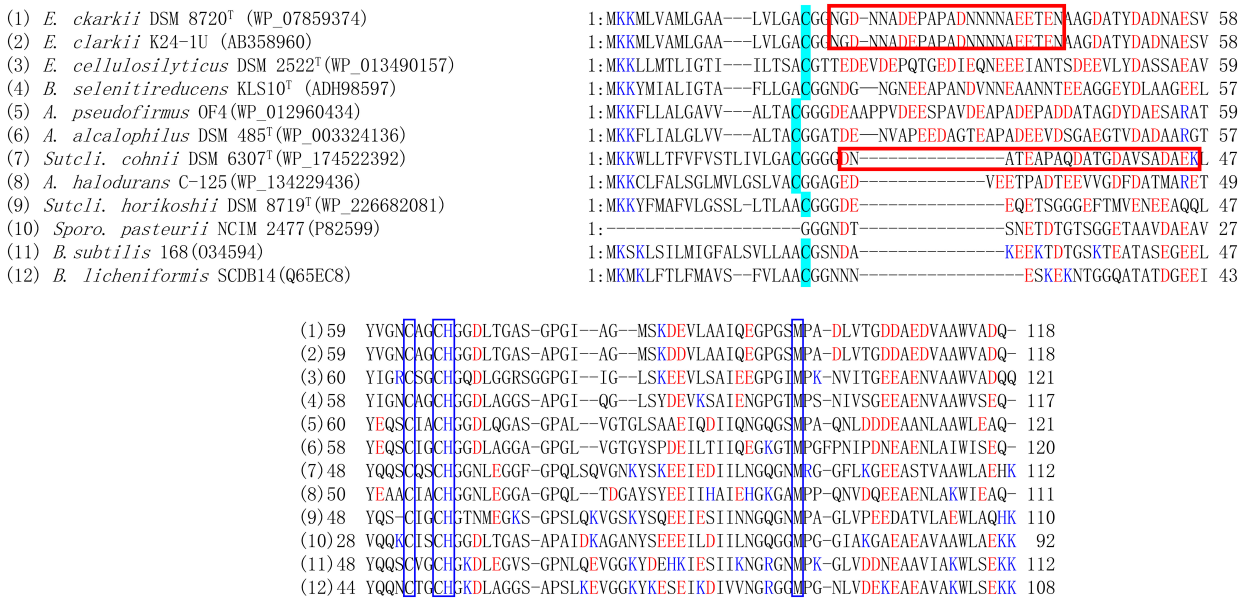

FIGURE 2 | Amino acid sequence alignment of membrane bound cytochrome *c*-550 from *Evansella clarkii* and other alkaliphilic and neutralophilic *Bacillaceae*. Asn (N)-rich segment, Asn $(N)^{21}$-Asn $(N)^{43}$ [Asn $(N)^{4}$-Asn $(N)^{26}$ in the processed protein base] in the *E. clarkii* cytochromes *c* is indicated by red box. The acid residue-abundant segment of Glu^{25}-Lys^{46} (Glu^{6}-Lys^{27} in the processed protein base) in *S. cohnii* DSM 6307^T is indicated by red box. N-terminal amino acid residue in processed cytochrome *c*, [Cys (C)] is indicated by blue marker. The blue boxed sequences are heme sequences representing heme-binding site and axical ligands (H and M). Acidic and basic residues are indicated by blue and red letters. Although *A. pseudofirmus* OF4 is a facultative alkaliphile, the species *A. pseudofirmus* and the presented cytochrome *c* sequence are classified in obligate alkaliphile. Although *Sporosarcina pasteurii* is an obligate alkaliphile, its cytochrome *c* sequence is similar to those in the facultative alkaliphilic strains.

anchor domain consisting of a single α-helical transmembrane segment of a hydrophobic polypeptide comprising 30 amino acid residues and a heme- containing main body protein comprising approximately 74 residues with a calculated p*I* of 5.4 (von Wachenfeldt and Hederstedt, 1990). The midpoint redox potential of cytochrome *c*-550 is + 178 mV (von Wachenfeldt and Hederstedt, 1993). The function of cytochrome *c*-550 is electron transfer from cytochrome b_6c to the cytochrome caa_3 terminal oxidase, and the main supercomplex formed by caa_3 oxidase, the b_6c complex, and cytochrome *c*-550 with ATP synthase has been isolated (García Montes de Oca et al., 2012).

Cytochromes *c* in Facultative Alkaliphilic *Sutcliffiella cohnii* YN-2000 and *Sporosarcina pasteurii* NCIM 2477

The abundance of membrane-bound cytochrome *c* was higher at pH 10 than that at pH 7 in facultative alkaliphilic *S. cohnii* YN-2000 (Yumoto et al., 1991). The elution profile of anion exchange chromatography loading of the solubilized membrane fraction by the detergent, Triton X-100 exhibited a larger amount of cytochrome *c*-553 in cells grown at pH 10 than in cells grown at pH 7 (Yumoto et al., 1991). Cytochrome *c*-553 has a molecular mass of 10.5 kDa by sodium dodecyl sulfate-polyacrylamide gel electrophoresis (SDS-PAGE) with a p*I* of 3.9 (**Table 1**). If cytochrome *c*-553 of strain YN-2000 is the same as that in *S. cohnii* DSM 6307^T, it consists of 93 amino acid residues including seven basic amino acid residues in the processed protein. The midpoint redox potential was + 87 mV in the pH range of 6–8. The native molecular mass, as determined by gel filtration, was 37 kDa. Therefore, it was suggested that cytochrome *c*-553 forms a tetramer in its native form in solution or in its original membrane-binding form.

The phylogenetic position of *S. cohnii* DSM 6307^T cytochrome *c* clustered with that of *Sporosarcina pasteurii* NCIM 2477 is shown in **Figure 3**. Cytochrome *c* oxidase in *S. cohnii* YN-2000, cytochrome aco_3, which is a different type from other *Bacillaceae* cytochrome *c* oxidases was purified and characterized (Qureshi et al., 1990). Cytochrome aco_3 reacts with cytochrome *c*-553, and the terminal enzymatic activity is greatly enhanced in the presence of poly-L-lysine, which accelerates interaction of two negatively charged molecules: cytochrome *c*-553 and cytochrome aco_3 (Yumoto et al., 1993).

The three-dimensional (3D) structure of cytochrome *c* in alkaliphilic *Bacillaceae* was first studied in *S. pasteurii* cytochrome *c*-553 (Benini et al., 2000). Cytochrome *c*-553 has a molecular mass of 9.6 kDa and consists of 92 amino acids having a midpoint redox potential of + 47 mV and a predicted p*I* of 3.96 (Benini et al., 1998). Most of the charges were localized on the opposite side of that exposed to the heme edge. This localization may be related to H^+ transfer on the outer surface of the membrane. The correlation between heme solvent accessibility and entropy suggests a direct link between the major determinant of the electrical potential (entropy) and a structural parameter (heme solvent exposure). The low midpoint redox potential of cytochrome *c* could be attributed to the decrease in reduction

TABLE 1 | Biochemical properties of membrane bound cytochromes *c* of obligate alkaliphilic *Evansella clarkii*, facultative alkaliphilic *Sutcliffiella cohnii*, and neutralophilic *Bacillus subtilis,* and *Geobacillus* PS3.

	***Evansella clarkii* cytochrome *c*-550[a]**	***Sutcliffiella cohnii* cytochrome *c*-553[b]**	***Bacillus subtilis* cytochrome *c*-551[c]**	***Geobacillus* PS3 cytochrome *c*-551[d]**
Number of amino acid residues[e]	101	93	92	93
Molecular mass in SDS-PAGE (kDa)	20, 17 (11.1)[I]	10.5 (9.7)	10 (11.0)	10.4 (10.4)
Molecular mass in gel-filtration (kDa)[f]	40 (44.4)[J]	37 (38.8)	ND[g]	33 (31.2)
Number of peak in analysis in Reverse-phase chromatography	3	ND	ND	1
Presence of Asn^4-Asn^{26} sequence[e]	Yes	No	No	No
Acidic and basic amino acid residues between 6th and 26th residues[e]	Acidic 6 or 7; basic 0	Acidic 6; basic 1	Acidic 8; basic 3	Acidic 5; basic 1
Number of basic residues[e]	2	7	14	12
Midpoint redox potential (mV)[h]	83	87	>100	225
p*I*	4.1	3.9	3.8	4.0
Absorption maxima at				
Oxidized form (nm)	408	411	409	409
Reduced form (nm)	415, 521, 550	417, 524, 553	416, 522, 551	416, 522, 551

[a] *The data obtained from Ogami et al. (2009) using E. clarkii K24-1U and whole genome sequence of E. clarkii DSM 8720^T (NZ_MTIV00000000.1) were considered.*
[b] *The data obtained from Yumoto et al. (1991) using S. cohnii YN-2000 and whole genome sequence of S. cohnii DSM 8720^T (NZ_CP018866.1) were considered.*
[c] *The data obtained from Bengtsson et al. (1999).*
[d] *The data obtained from Sone et al. (1989) and Fujiwara et al. (1993).*
[e] *Processed proteins were considered*
[f] *Values were subtracted from the molecular mass of Triton X-100.*
[g] *ND: No data.*
[h] *Values are estimated using redox titration.*
[I,J] *Theoretical value including of heme, anchor and N-terminal modification.*

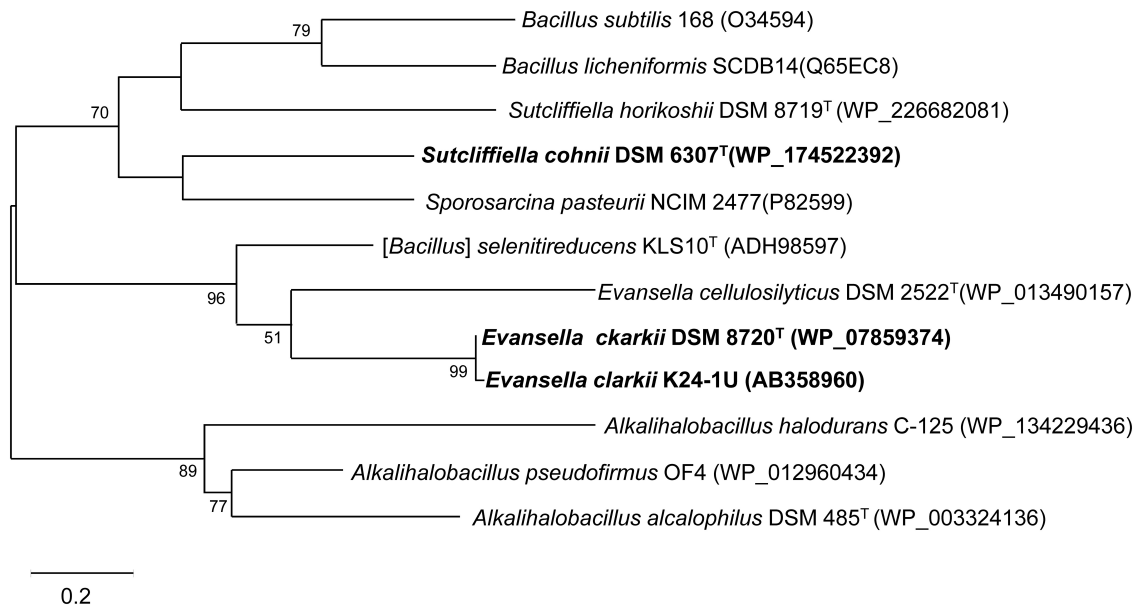

FIGURE 3 | Maximum-likelihood phylogenetic tree of membrane bound cytochromes *c* from *Evansella clarkii* and other alkaliphilic and neutralophilic *Bacillaceae*. The evolutionary history was inferred by using the Whelan and Goldman model (Whelan and Goldman, 2001). The tree with the highest log likelihood (-2371.51) is shown. The percentage of trees in which the associated taxa clustered together is shown next to the branches. Initial tree(s) for the heuristic search were obtained automatically by applying Neighbor-Join and BioNJ algorithms to a matrix of pairwise distances estimated using the JTT model, and then selecting the topology with a superior log likelihood value. A discrete Gamma distribution was used to model evolutionary rate differences among sites [5 categories (+ *G*, parameter = 1.7094)]. Phylogenetic positions of cytochromes *c* of obligately alkaliphilic *E. clarkii* are indicated in bold. Bar, 0.2 substitution per nucleotide position. Evolutionary analyses were conducted in MEGA11 (Tamura et al., 2021).

entropy caused by the extrusion of water molecules from the reduction of the hydration shell in this protein. This event affects solvent accessibility to the heme during its reduction. Thus, analysis of the 3D-structure revealed important structural characteristics that explain the low redox potential and retention of H^+ at the outer surface of the membrane of the cytochrome *c* in the alkaliphile.

Cytochromes *c* in Obligately Alkaliphilic *Alkalihalobacillus pseudofirmus* RAB and *Evansella clarkii* K24-1U

The first purified and characterized cytochrome *c* from an alkaliphilic *Bacillaceae* strain was cytochrome *c*-552 isolated from *A. pseudofirmus* RAB (Davidson et al., 1988). Cytochrome *c*-552 has a molecular mass of 16.5 kDa with an acidic p*I* of 3.4. The midpoint redox potential of this cytochrome is + 66 mV at pH 7, which decreases at pH > 8.3, depending on the pH increase. According to resonance Raman spectroscopy, this pH-dependent decrease in redox potential may be attributed to a switch in the sixth ligand of heme *c* from methionine to histidine when the oxidized cytochrome is reduced (Larsen et al., 1990). Cytochrome *c*-552 is autooxidizable and is purified in a soluble form. These characteristics may arise due to the partial digestion of cytochrome *c* by intrinsic proteinases during purification. Although most strains belong to the same species as *A. pseudofirmus* RAB are obligate alkaliphiles (Nielsen et al., 1995), whereas *A. pseudofirmus* OF4 is a facultative alkaliphile. If cytochrome *c*-552 in *A. pseudofirmus* RAB is the same as that in the corresponding cytochrome *c* in *A. pseudofirmus* OF4, cytochrome *c*-552 consists of 105 amino acid residues and exhibits the same branching with cytochrome *c* in obligate alkaliphilic *A. alcalophilus* DSM 485^T (**Figure 3**).

The cell extract of obligate alkaliphilic *E. clarkii* K24-1U exhibits higher cytochrome *c* content than that in neutralophilic *B. subtilis* under high-aeration conditions (4.5-fold). The cytochrome *c* abundance in *E. clarkii* K24-1U further increases under low-aeration conditions (6.3-fold) (Hijikata, 2004; Matsuno et al., 2018). Cytochrome *c*-550 purified from *E. clarkii* K24-1U, exhibited very weak protease activity (Ogami et al., 2009). Characterization of cytochrome *c*-550, determination of its gene sequence, and constricted recombinant expressing C18M anchorless mutant protein enables us to understand the molecular features in native and anchorless cytochrome *c* molecules. Native cytochrome *c*-550 and C18M cytochrome *c*-550 had molecular weights of 11,083–11,115 in the analysis of the separated fractions in HPCL and 10,543 by Matrix-assisted Laser Desorption/Ionization Time-of-Flight Mass Spectrometry (MALDI-TOF-MS) with an acidic p*I* of 4.1. The midpoint redox potential was + 83 mV in the redox titration (**Table 1**). The purified cytochrome *c*-550 exhibited two bands of 17 kDa and 20 kDa in SDS-PAGE. The native molecular mass determined by gel filtration was 40 kDa in both native and C18M cytochromes *c*. Therefore, it is suggested that cytochrome *c*-550 forms a tetramer in its native form in solution or in its original membrane-binding form. Cytochrome *c*-550 exhibited only one band of 23 kDa in blue native-PAGE for both native and C18M cytochromes *c*-550. These numbers of SDS-PAGE and blue native-PAGE of molecular mass correspond to the dimer based on the molecular mass of the minimum unit of molecular mass determined by MALDI-TOF-MS using fractions separated by HPLC and its gene sequence. These two bands in SDS-PAGE were shifted to 10 and 15 kDa in C18M cytochrome *c*-550. Therefore, the appearance of the two bands in SDS-PAGE was not attributed to the N-terminal modifications but to the internal specific sequence located near the N-terminal sequence of Asn^{21}-Asn^{43} because the specific sequence lacking *S. cohnii* YN-2000 tetrameric cytochrome *c* exhibited only one monomer band in SDS-PAGE (Yumoto et al., 1991). The above results suggested that the binding molecular mechanisms of dimeric and tetrameric (dimeric *plus* dimeric) forms are different.

The determined gene sequence of cytochrome *c*-550 revealed the hydrophobic N-terminal sequence Met^1-Ala^{17} as the signal peptide sequence (Ogami et al., 2009; **Figure 2**). In addition, MALDI-TOF-MS analysis using fractionated by HPLC of the native protein and fatty acid analysis of cytochrome *c* revealed the structure of the modified moiety of the protein. During the processing of mature cytochrome *c* production, expressed cytochrome *c*-550 is translocated to the extracellular side of the membrane by the signal peptide. After the signal peptide was dissociated from the main body protein, terminal Cys^{18} was modified by attaching diacylglycerol and acetyl moieties. Cytochrome *c*-550 binds to the fatty acid length of C_{15} in the internal moiety and different chain lengths of fatty acids, C_{15}, C_{16}, and C_{17} in the external moiety *via* glycerol-Cys^{18}. Molecular binding species are the major components of membrane fatty acids. Therefore, if the amount of cytochrome *c*-550 expressed fluctuates depending on the culture conditions, there will be a little influence on the fatty acid composition of the membrane.

The sulfate-reducing bacterium *Desulfovibrio gigas* possesses cytochrome c_3, which has four hemes per protein molecule (Coutinho and Xavier, 1994). It has been reported that cytochrome c_3 transfers H^+ *via* a cooperative H^+/e^- linkage (redox-Bohr effect) (Louro et al., 1997; Messias et al., 2006). These hemes exhibit different redox potentials by direct measurement on the electrode attached as self-assembled monolayers (SAMs) and by redox titration using mediators in a solution. This difference in redox potential in cytochrome *c* suggests changes in the redox potential depending on the distance between each heme (heme I–IV) and the electrode. Shorter distances between heme *c* and the electrode resulted in larger differences in the redox potential of the cytochrome *c* molecule between in solution status and the electrode-attached state of the cytochrome *c* molecule. These differences are attributed to the strength of the electric field (Coulomb force), which depends on the distance of each heme from the electrode (Rivas et al., 2005). The redox potential of cytochrome *c*-550 of *E. clarkii* measured by redox titration was + 83 mV (in a buffer solution) whereas that of cytochrome *c*-550 immobilized on the gold electrode using a SAMs of 2-amino-6-purinethiol was + 7 mV. These facts suggest that if the distances between the membrane surface and the main body cytochrome

c differ depending on the chain length of fatty acids (C_{15}, C_{16}, and C_{17}), the redox potential of heme *c* may change depending on their distance from the membrane surface. These electric field strength-dependent differences in redox potential may have an important role for H^+ transfer on the outer surface of the membrane in electron transfer-coupled H^+ transfer mechanisms.

The amino acid sequence of *E. clarkii* K24-1U cytochrome *c*-550 deduced from the determined gene sequence was very similar to that of cytochrome *c* in *E. clarkii* DSM 8720^T (only one residue difference among 118 residues) (**Figure 2**). We collected data on bioenergetic parameters, such as O_2 consumption and ATP production rates, in *E. clarkii* DSM 8720^T. Therefore, we can consider these bioenergetic data combined with the data for *E. clarkii* K24-1U cytochrome *c*-550. Multiple alignments of two strains of *E. clarkii* cytochrome *c* with other cytochromes *c* from obligate and the facultative alkaliphilic and the neutralophilic *Bacillaceae* strains were constructed (**Figure 2**). Cytochrome *c*-550 contains much fewer basic residues (only two, including His for axial ligand of the heme *c*) compared with cytochrome *c* from facultative alkaliphiles and neutralophiles. This scarcity of basic amino acids in the obligate alkaliphilic *Bacillaceae* may be related to the acidic nature of the molecule, which expels OH^- and attracts H^+ to protect the environment in the outer surface of the membrane. In the entire molecular structure, the particular part of the amino acid sequence of Asn_{21}-Asn_{43} in the cytochrome *c* of the two strains of *E. clarkii*, which consisted of eight Asn residues and six acidic amino acid residues in 23 residues (**Figure 2**). The corresponding amino acid sequence of Asn_{24}-Asn_{37} (Asn_7-Asn_{20} in the processed protein base) was observed neither in the facultative alkaliphilic nor the neutralophilic *Bacillaceae* strains. This means that obligate alkaliphiles express cytochromes *c*, which express an even more effective protein for the alkaline environment adaptation than the neutralophilic or the facultatively alkaliphilic *Bacillaceae*.

Theoretically, the Asn (N) residue could influence H^+-transfer. However, there have been few examples of the interpretation that accounts for the contribution of Asn in H^+ transfer due to the weak hydrogen binding of this individual residue. In the catalytic reaction of methyltetrahydrofolate (MTHF) and corrinoid-iron sulfur protein (CFeSP) methyltransferase (MeTr), the methyl group of CH_3-H_4folate in MTHF is transferred to cob (I) amide. This reaction requires electrophilic activation of the methyl group of MTHF, which involves H^+ transfer to the N5 group of the pterin ring of MTHF. This H^+ transfer reaction is possible by the extended H-bond network including Asn^{199}, Asp^{160}, and a water molecule (Doukov et al., 2007). Thus, although Asn exhibits weak hydrogen bonds, the overall effect of this cumulative H-bond network is significant in this series reactions. Considering the cooperation of Asn and other H^+ transferable acidic amino acid residues such as Asp or Glu, the amino acid sequence of Asn_{21}-Asn_{43} in the cytochrome *c* of *E. clarkii* strains produces a cumulative H-bond network in the corresponding region.

Based on the reported structure of membrane-bound cytochrome *c* in *Bacillus subtilis* (David et al., 2000), the Asn-rich segment, Asn_{21}-Asn_{43} (Asn_4-Asn_{26} in the processed protein base) in *E. clarkii* cytochrome *c* is presumed to be located in the α-helical domain between the membrane anchor and the main body cytochrome *c* molecule. Therefore, it is considered that this region is located between the outer surface of the membrane and the main body of cytochrome *c*. Based on the tetrameric structure of this cytochrome *c* molecule, the Asn-rich segment, Asn_{21}-Asn_{43}, further accumulated in the corresponding location. It can be presumed that this accumulated Asn-rich segment, contributing to the intense H-bond network, influences H^+ transfer on the outer surface of the membrane associated with the redox reaction of the main body of cytochrome *c*. The corresponding segment Asn_{23}-Asn_{37} (Asn_6-Asn_{20} in the processed protein base) was observed only in the obligate alkaliphilic *Bacillaceae* (**Figure 2**). If the corresponding region influences the H-bond network in the space between the main body cytochrome *c* molecule and the outer surface of the membrane, the segment of Glu_{25}-Lys_{46} (Glu_6-Lys_{27} in the processed protein base) in *S. cohnii* DSM 6307^T may also influence the H-bond network (**Figure 2**). The abundance ratio of acidic to basic amino acids was higher in the facultative alkaliphilic *Bacillaceae* than in the neutralophilic *Bacillaceae* (**Table 1** and **Figure 2**). A similar region found in membrane-bound cytochromes *c* in alkaliphilic *Bacillaceae* also contain other membrane-bound protein molecules, such as subunit II of *aco*$_3$-type or *caa*$_3$-type cytochrome *c* oxidase, which have abundant acidic residues and a few basic residues (Denda et al., 2001; Noor et al., 2014). This region is located in the external hydrophilic cytochrome *c*-binding domain of subunit II of the *aco*$_3$-type or *caa*$_3$-type cytochrome *c* oxidase. This shows that the H-bond network construction strategy, which is found in membrane-bound cytochrome *c*, is also found in the subunit structure of other protein molecules that have subunits containing cytochrome *c* segments. This configuration is probably connected to cytochrome *c*, which exhibits a low redox potential (< + 100 mV) (Orii et al., 1991). It can be predicted that the abundance of acidic amino acids, tetrameric structures, and low redox potentials are important for redox-coupled H^+ transfer on the outer membrane surface through the H-bond network.

BIOENERGETIC PARAMETERS IN OBLIGATELY ALKALIPHILIC *Evansella clarkii* DSM 8720^T

As described above alkaliphilic *Bacillaceae* exhibited higher cytochrome *c* content than that of neutralophilic *B. subtilis*. This higher content of cytochrome *c* in alkaliphiles increased further under low-aeration conditions in obligate alkaliphilic *E. clarkii* DSM 8720^T. High- and low-aeration conditions were generated in 2 L baffled Erlenmeyer flasks with shaking at 120 rpm (rotation) and shaking at 60 rpm (rotation), respectively. This difference in cytochrome *c* content depending on the aeration condition was larger in obligate alkaliphilic *E. clarkii* DSM 8720^T than that in facultative alkaliphilic *S. cohnii* YN-2000. Therefore, our aim was to understand the differences

in the energy production mechanisms between high- and low-aeration conditions by estimating the H^+ translocation rate and ATP production rate. In the present study, a comparison of the H^+ translocation rate and ATP production rate in three categories (neutralophiles, facultative and obligate alkaliphiles) of bacteria showed the peculiarities of cytochrome *c* isolated from obligate alkaliphiles. By estimation of the intensity per H^+ to produce ATP, we might understand the fundamental strategies of utilizing H^+ efficiently in obligate alkaliphiles. In addition, we will understand the relationship between the molecular features of cytochrome *c* and parameters related to ATP production.

Oxygen Consumption Rate

One of the alkaline adaptation mechanisms of alkaliphilic *Bacillaceae* is based on the enhancement of H^+ usage efficiency. This enhanced the efficacy of H^+ utilization in ATP synthesis and retention of H^+ in the vicinity of the outer surface of the membrane, compared to in neutralophilic *Bacillaceae*. In fact, it has been suggested that the number of H^+ translocated across the biological membrane from the intracellular side to the extracellular side by the respiratory chain in alkaliphilic *Bacillaceae* was significantly lower than that in neutralophilic *Bacillaceae* (Hirabayashi et al., 2012; Goto et al., 2016). The oxygen consumption rate based on the endogenous substrates of *B. subtilis* IAM 1026 (growth in high aeration, pH 7; O_2 consumption was measured at pH 7) was 0.50 ± 0.06 μmol $O_2 \cdot min^{-1} \cdot$mg cell $protein^{-1}$, while that of the obligate alkaliphilic *E. clarkii* DSM 8720^T [in high aeration, growth at pH 10; O_2 consumption was measured at pH 10) was 0.19 ± 0.04 μmol $O_2 \cdot min^{-1} \cdot$mg cell $protein^{-1}$ (**Table 2**). The low oxygen consumption value is comparable to the data obtained using *A. pseudofirmus* OF4 (0.21 μmol $O_2 \cdot min^{-1} \cdot$mg cell $protein^{-1}$ (based on indigenous substrates in the presence of Na^+)] (Guffanti et al., 1986). *A. alcalophilus* and *A. pseudofirmus* RAB exhibited the same O_2 consumption rate (0.49 μmol $O_2 \cdot min^{-1} \cdot$mg cell $protein^{-1}$) when L-malate is used as a substrate (Lewis et al., 1980). Therefore, the low oxygen consumption rate of *E. clarkii* DSM 8720^T may be attributed to the absence of the extracellular substrate. A low oxygen consumption rate compared to that of *B. subtilis* IAM 1026 under high aeration was also observed in facultative alkaliphilic *S. cohnii* YN-2000 (0.20 ± 0.07 μmol $O_2 \cdot min^{-1} \cdot$mg cell $protein^{-1}$; O_2 consumption was measured at pH 10) under high-aeration condition. These relatively low oxygen consumption rates, compared with *B. subtilis* under high-aeration conditions in obligate and facultative alkaliphiles, may be attributed to the hindered translocation of the positively charged H^+ by the respiratory chain *via* the attraction force of the intracellular negative charge due to the large $\Delta\Psi$. Thus, H^+ transfer coupled with electron transfer in the respiratory chain may be deterred. The reduction rate of heme *a* in cytochrome *c* oxidase in vesicles reportedly increases when $\Delta\Psi$ is abolished during steady-state respiration using cytochrome *c* (Gregory and Ferguson-Miller, 1989). This is probably due to the $\Delta\Psi$ influencing the electron transfer from cytochrome *c* to heme *a*. Although it is expected that $\Delta\Psi$ alters the redox potential of heme *a*, $\Delta\Psi$ potentially inhibits the electron transfer from the outer side of the membrane (cytochrome *c*) to the inner membrane heme *a* due to repulsion between negative charges (electron negative charge vs. inner membrane negative charge by $\Delta\Psi$). Therefore, the difficulties in H^+ transfer and electron transfer across the membrane under high $\Delta\Psi$ may produce a low oxygen consumption rate in high aeration in *E. clarkii* DSM 8720^T.

H^+/O Ratio

In the measurement of the H^+/O ratio in alkaliphiles and neutralophiles, each measured value was obtained by culturing and measuring at pH 10 and pH 7, respectively. Since *Bacillaceae* strains do not contain complex I, which translocates 4 H^+/O, the theoretical H^+/O ratio in the case of *Bacillaceae* strains is thought to be 4 H^+ from complex III plus 2 H^+ from complex IV, equal to 6 H^+. The H^+/O ratio of thermophilic *Bacillaceae* (*Geobacillus*) is 6–7 (Chichen et al., 1981; Sone and Fujiwara, 1991), while those in *B. subtilis*, *Bacillus megaterium*, and *Bacillus licheniformis* have been reported to be approximately 4 (Jones et al., 1975). In contrast, the H^+/O ratio in another *Bacillaceae*, *Brevibacillus brevis* was reported to be 5.01 ± 0.26 (Yaginuma et al., 1997). The variation in the H^+/O ratio depending on the *Bacillaceae* strain may be attributed to differences in the electron flow paths in the respiratory chain.

The H^+/O ratios under high- and low-aeration conditions in obligate alkaliphilic *E. clarkii* DSM 8720^T were 2.2 ± 0.2 and 0.6 ± 0.1, respectively (**Table 2**). These values were much lower than the theoretical values. The H^+/O ratios under high-aeration condition in facultative alkaliphilic *S. cohnii* YN-2000 and neutralophilic *B. subtilis* were 2.8 ± 0.8 and 4.9 ± 0.1, respectively (**Table 2**). The H^+/O ratio in the facultative alkaliphilic strain was higher than that in the obligate alkaliphilic strain, whereas the value was lower than that in the neutralophilic strain and the theoretical values. To date, it is unclear why the H^+/O ratios in alkaliphilic bacteria are much lower than the theoretical value. The possible reasons for these values might be due to the inhibition of translocation H^+ by the larger $\Delta\Psi$ compared with that in the neutralophiles or that the H^+ translocated by the respiratory chain may remain on the outer surface of the membrane. However, for measuring the H^+/O ratios, 0.15 μg/mL valinomycin and 0.85 mM KCl, which disrupt $\Delta\Psi$ across the membrane, were used. Therefore, it is difficult to determine whether the reason for the low H^+/O ratios in alkaliphiles can be attributed to $\Delta\Psi$ alone.

There is a possibility that the extremely low H^+/O ratio in obligate alkaliphilic *E. clarkii* DSM 8720^T is related to the Asn-rich distinct amino acid sequence in the membrane-bound cytochrome *c*, which may influence to the H-bond network probably related to the transfer of H^+ at the outer surface of the membrane. It is possible that this specific structure in *E. clarkii* cytochrome *c* spools up translocated H^+ *via* the respiratory chain on the outer surface of the membrane.

The H^+/O ratio was found to be 2.8 even under low-aeration conditions of *B. subtilis* (**Table 2**). Since the pumped H^+ was measured in bulk in the estimation of H^+/O, the measured values may be influenced by the activity of the respiratory chain. Thus, the H^+/O ratio may change depending on the cell activity. In addition, there is a possibility that the expressed respiratory

TABLE 2 | Summary for high aeration and low aeration in obligate alkaliphilic *Evansella clarkii*, facultative alkaliphilic *Sutcliffiella cohnii*, and neutralophilic *Bacillus subtilis**.

	Growth rate (μ_{max})[1]	Cytochrome *c* content (nmol · mg^{-1})[1]	$\Delta\psi$ (mV)[1,2]	Respiratory rate (μmol · O_2 min^{-1} mg^{-1})[2]	H^+/O[1]	Maximum ATP synthesis rate[2] (nmol · min^{-1} · mg^{-1})[2]
E. clarkii DSM8720^T Low aeration	0.36	0.89 ± 0.07	−135 ± 8	ND	0.6 ± 0.1 (6)[§]	ND
E. clarkii DSM 8720^T High aeration	0.42	0.36 ± 0.01	−192 ± 3	0.19 ± 0.04	2.2 ± 0.2 (6)	26.2 ± 1.7
S. cohnii YN-2000 High aeration	0.38	0.62 ± 0.01	−173 ± 5	0.20 ± 0.03	2.6 ± 0.3 (6)	9.6 ± 0.9
B. subtilis IAM 1026 Low aeration	0.26	0.18 ± 0.06	−133 ± 13	ND	2.8 ± 0.8 (6)	ND
B. subtilis IAM 1026 High aeration	0.55	0.21 ± 0.02	−121 ± 7	0.50 ± 0.06	4.9 ± 0.1 (6)	2.0 ± 0.6

**These data cited from [1]Goto (2006) and [2]Goto et al. (2016).*
[§]*The numbers in parentheses are based on the theoretically extruded H^+ in 1/2O_2 consumption by the respiratory chain.*

components may change depending on the culture conditions. Therefore, it is difficult to compare the values directly among the reported studies. Cyanide-insensitive Non-Proteinaceous Substance (NPS) with a molecular weight of 622 was found in the respiratory system of the obligate alkaliphilic *E. polygoni* YN-1^T (Higashibata et al., 1998). Thus, it can be predicted that NPS does not influence to H^+ translocation in the respiratory system. The terminal enzyme was a *caa*$_3$-type cytochrome *c* oxidase, constituting up to only 10% of the total oxygen reducing activity, while 90% of the respiratory activity was attributed to cyanide-insensitive NPS in strain YN-1^T. If the NPS is widely distributed in alkaliphilic *Bacillaceae*, it may lead to the reduction of the H^+/O ratio. NPS may prevent the production of excess energy during the later growth phase in the effective energy production systems of alkaliphiles.

H^+ Translocation Frequencies Based on the Obtained Data and Theoretical Ratio

Since the O_2 consumption rate is considered to be the turnover rate of the respiratory chain, by using the measured and theoretical H^+/O values, the amount of H^+ translocated by the respiratory chain when two electrons (e^-) reduce oxygen ($1/2O_2$) was estimated ($2e^- + 2H^+ + 1/2O_2 \rightarrow H_2O$) (**Table 2**). Based on the measured and theoretical H^+/O values, translocated H^+ by the respiratory chain is predicted to higher under low- aeration conditions than under high-aeration conditions in *E. clarkii* DSM 8720^T. This prediction could be attributed to the larger $\Delta\Psi$ in the high-aeration condition than that in the low-aeration condition, as described in the oxygen consumption rate section. Although the amount of translocated H^+, based on the measured H^+/O values, was lower in *E. clarkii* DSM 8720^T [0.84 (min^{-1}·mg protein^{-1})] than in *S. cohnii* YN-2000 (1.04) the translocated amounts of H^+ using theoretical H^+/O values were almost the same (*E. clarkii* DSM 8720^T, 2.28; *S. cohnii* YN-2000, 2.4). The number of translocated H^+ per $1/2O_2$ consumption in *E. clarkii* DSM 8720^T is lower than that in *B. subtilis* IAM 1026 (6.0, high aeration) on the basis of the theoretical value. Although the above comparison used the theoretical values, it is necessary to reconsider the reality of the measured H^+/O ratio in consideration of the actual contribution of the NPS, as described above.

If the measured values of H^+/O reflect the actual value of the number of H^+, it could mean that a very small number of H^+ were translocated by the respiratory chain compared to the theoretical values. In addition, the number of translocated H^+ in alkaliphiles was much lower than that in neutralophilic *B. subtilis*. The results described above are considered to indicate the physiological strategy of maintaining H^+ on the outer surface of the membrane as much as possible and operating the cell system in an environment lacking sufficient H^+ for ATP production and high $\Delta\Psi$ as a result of the physiological environmental adaptation at high pH. Therefore, although these estimated H^+/O values may be unrealistic, it is expected that the respiratory H^+ translocation rate of alkaliphilic bacteria is probably lower than that of neutral bacteria.

Efficiency of Respiratory Translocated H^+ for ATP Production

To understand the effect of H^+ translocated by the respiratory chain under high aeration conditions, the maximum ATP synthesis rates of obligate (i.e., *E. clarkii* DSM 8720^T) and facultative (i.e., *S. cohnii* YN-2000) alkaliphiles and neutralophile (i.e., *B. subtilis* IAM1026) were compared on the basis of the data described in **Table 2**. The ATP synthesis rates of *E. clarkii* DSM 8720^T were higher than those of *S. cohnii* YN-2000 and *B. subtilis* IAM 1026. This suggests that the intensity of H^+, which is translocated by the respiratory chain to drive ATP synthesis through the ATPase, is higher than that of other bacteria, while the number of H^+ retaining on the outer surface of the membrane is larger than in other bacteria under low aeration. This H^+ accumulation is attributed to the H^+-bond network producing cytochrome *c*. In addition, since *E. clarkii* DSM 8720^T

growth rate in low aeration conditions exhibits equivalent to *S. cohnii* in high aeration conditions and much higher than *B. subtilis* in low aeration conditions (**Table 2**), the H^+ potential in the vicinity of the outer surface of the membrane is expected to be much higher than that measured in the bulk base. This efficient H^+ usage may also be attributed to the H^+ capacitor strategy on the outer surface of the membrane (Matsuno et al., 2018). The increase of cytochrome *c*-550, which possesses a specific amino acid sequence between the main body protein and membrane-anchoring part facilitates the formation of an H^+ capacitor *via* the H-bond network. The H^+ capacitor strategy may also influence to the maximum ATP production rate per H^+ translocation by the respiratory chain. The predicted H^+ utilization strategy for ATP production in high and low aeration conditions in *E. clarkii* DSM 8720^T is illustrated in **Figure 4**. The maximum ATP production rate per H^+ translocated by the respiratory chain of *E. clarkii* DSM 8720^T under high-aeration conditions was 11.5 nmol ATP · translocated H^{+-1} (theoretical base), which is much higher than the 4.0 nmol ATP observed in *S. cohnii* YN-2000 and the neutralophilic *B. subtilis* IAM 1026 (0.33 nmol ATP · translocated H^{+-1}). Thus, H^+ efficiency under high-aeration conditions in *E. clarkii* is much higher than that in the *S. cohnii* and *B. subtilis*. This is attributed to the much higher $\Delta\Psi$ in *E. clarkii* than that in the other bacteria.

TRANSMEMBRANE ELECTRICAL POTENTIAL ($\Delta\Psi$)

It has been reported that the $\Delta\Psi$ in alkaliphilic *Bacillaceae* (ca. -180 to -210 mV) is larger than that in the neutralophilic *Bacillaceae* (ca. -130 mV) in the direction of ATP production (Yumoto, 2003; Goto et al., 2005). On the other hand, $\Delta\Psi$ in the acidophilic archaea, *Picrophilus oshimae* has a negative direction (ca, + 50 to + 100 mV) for ATP production (van de Vossenberg et al., 1998). These facts suggest that a large $\Delta\Psi$ in alkaliphilic *Bacillaceae* strains plays an important role in alkaline adaptation. The high intensity of H^+ translocated by the respiratory chain for ATP production under high aeration conditions in *E. clarkii* DSM 8720^T may be mainly attributed to $\Delta\Psi$. However, the observed $\Delta\Psi$ (**Table 2**) alone cannot explain the high ATP productivity in *E. clarkii* DSM 8720^T. A large $\Delta\Psi$ is considered indispensable for energy production in alkaliphilic *Bacillaceae*, and it may be difficult to produce it by intense reaction of the respiratory chain alone. Electron flow in the ordinary respiratory chain is coupled with H^+ extrusion from the intracellular space to the extracellular space. This H^+ extrusion across the membrane is hindered by a large $\Delta\Psi$, because H^+ has a positive charge. In addition, the electron flow from cytochrome *c*, which is located on the outer surface of the membrane, to prosthetic groups located on the inner membrane (e.g., cytochrome *a* in cytochrome *c* oxidase) is described above. Furthermore, it is considered that alkaliphilic *Bacillaceae* consume $\Delta\Psi$ to reduce intracellular pH. Therefore, we propose the use of the Donnan potential (Donnan, 1924; Ohshima and Ohki, 1985; Benarroch and Asally, 2020), which is a congenital factor that takes advantage of the disadvantageous environment that does not consume energy.

Contribution of $\Delta\Psi$ to Retain H^+ at the Outer Surface of the Membrane

H^+ extrusion in the bulk phase by the respiratory chain in *E. clarkii* K24-1U was observed to be very slow

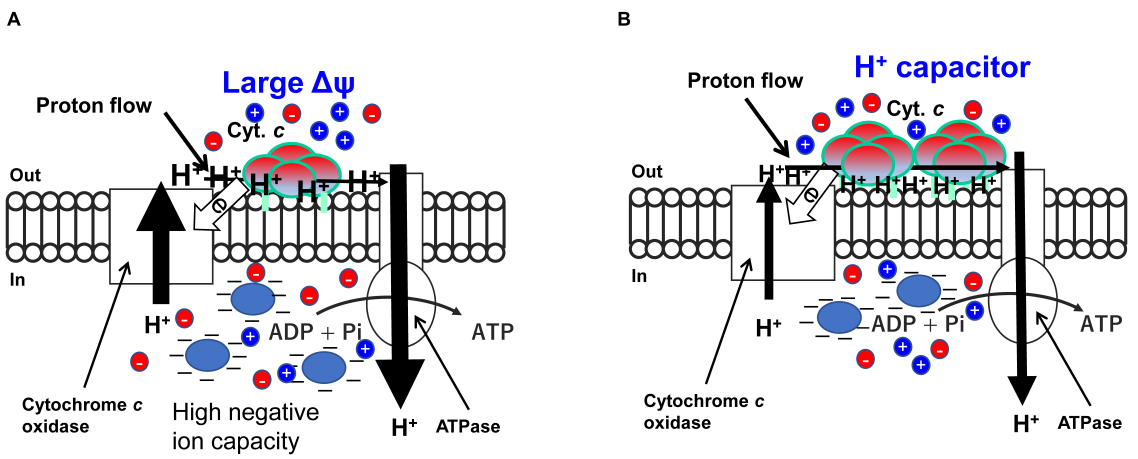

FIGURE 4 | High efficiency of H^+ located on the outer surface of the membrane based mainly on the $\Delta\Psi$ and hydrogen bond network produced by the membrane bound cytochrome *c* segment in high **(A)** and low **(B)** aeration conditions, respectively in obligately alkaliphilic *Evansella clarkii*. Although the rate of respiratory translocating H^+ is predicted to lower in high aeration **(A)**, efficiency per H^+ for production of ATP is higher in the high-aeration conditions compared with that of in low-aeration conditions **(B)**. This difference is attributed to the larger electrical potential ($\Delta\psi$) in high-aeration conditions than that in low-aeration conditions. The mechanism of the occurrence of the high $\Delta\psi$ may be attributed to a Donnan effect produced by membrane impermeable negatively charged substances (Blue ellipse) and heterogenous membrane permeable ions (red and blue circles). The high $\Delta\psi$ across the membrane may be a heavy burden for H^+ translocation by the respiratory chain. However, the translocated protons may have a large potential for ATP production. The membrane bound cytochrome *c* content is higher in low-aeration conditions than in high-aeration conditions. The specific segment near the N-terminal sequence [Asn $(N)^{21}$-Asn $(N)^{43}$; Asn $(N)^4$-Asn $(N)^{26}$ in the processed protein base] in the membrane bound cytochrome *c* produces an H^+-capacitor. The tetrameric structure and differences in the length of fatty acid anchors may have an important role for accumulation and transportation of H^+ on the outer surface of the membrane.

(Yoshimune et al., 2010). It appears that the H^+ extrusion into the bulk phase occurs after H^+ retention at sites in the vicinity of the outer surface of the membrane. Therefore, H^+, which is extruded by the respiratory chain, does not appear to be directly extruded into the bulk phase. However, the H^+, extruded by the respiratory chain the retained on the outer surface of the membrane is released into the bulk phase by the addition of valinomycin or ETH-157, which disrupts $\Delta\Psi$ (Yoshimune et al., 2010). Therefore, $\Delta\Psi$ prevents the release of H^+, which is translocated by the respiratory chain into the bulk phase. The rate of H^+ translocation in the presence of valinomycin in *E. clarkii* K24-1U was approximately 70% that in *B. subtilis* under the same experimental conditions. This suggests that the intrinsic H^+ translocation frequency was reduced by 70% in the alkaliphile as a strategy of reducing H^+ utilization frequency. Accumulation of H^+ at the outer surface of the membrane can also be demonstrated by addition of monensin, which is a Na^+/H^+ exchange reagent (Yoshimune et al., 2010). Monensin translocates H^+, previously located to the extracellular surface of the membrane, into the intracellular space, and Na^+ is located to the intracellular surface of the membrane. The transfer of H^+, which is extruded by the respiratory chain into the bulk phase is further retarded by the introduction of monensin, which translocates H^+ located extracellular surface, into intracellular space. These results indicate that $\Delta\Psi$ influences to the retardation of H^+ at the outer membrane surface in alkaliphilic *Bacillaceae*.

The much higher per H^+ efficiency for ATP production in *E. clarkii* DSM8720^T than in *B. subtilis* IAM 1026 may be attributed to the combination of the H^+ capacitor effect by cytochrome *c* and high $\Delta\Psi$ and a high $\Delta\Psi$ in the vicinity of the outer surface of the membrane. Although the contribution of the H^+ capacitor effect is unknown, it is difficult to account for the difference in H^+ efficiency for ATP production between *E. clarkii* DSM8720^T and *B. subtilis* IAM 1026 based on the difference in the estimated $\Delta\Psi$ values (**Table 2**). This may be attributed to either or both the reasons described below. Although $\Delta\Psi$ was estimated by substitutions of fluorescent changes in the reaction of respiration, it was calibrated by the diffusion potential produced by the different concentrations of K^+ between intra- and extra-cellular vesicles *plus* valinomycin. One possible reason for this is that the diffusion potential based on valinomycin *plus* K^+ was not reflected by the real $\Delta\Psi$ for H^+ across the membrane. It has been reported that the artificially imposed diffusion potential based on K^+ has an inferior effect compared to the equal intensity of $\Delta\Psi$ produced by the respiratory chain in *A. pseudofirmus* OF4 (Guffanti and Krulwich, 1994). Another reason is that the estimated $\Delta\Psi$ is different from the real values in the vicinity of the outer surface of the membrane. It seems reasonable to assume that the force attributed to $\Delta\Psi$ for H^+ would be larger for H^+ located closer to the outer surface of the membrane than H^+ located in the extracellular bulk phase.

Basis of Donnan Potential

Negative ion capacity was estimated in the cell extracts containing inside-out membrane vesicles of obligate alkaliphilic *E. clarkii* DSM 8720^T and facultative alkaliphilic *S. cohnii* YN-2000 grown at pH 10 and neutralophilic *B. subtilis* IAM 1026 grown at pH 7 under high-aeration conditions (Goto et al., 2016). The negative ion capacity of intracellular contents in the two strains of alkaliphiles increased with measured pH between pH 6 and pH 8, whereas that in *B. subtilis* IAM 1026 barely changes between pH 6 and pH 10. The negative ion capacity of *E. clarkii* DSM 8720^T and *S. cohnii* YN-2000 was 4.7-times and 4.1-times higher than that of *B. subtilis* IAM 1026 based on each corresponding intracellular pH. The intracellular materials obtained by two alkaliphiles grown under low-aeration conditions exhibited approximately 72% intensity of negative ion capacity than those under high-aeration conditions at the corresponding intracellular pH (Goto et al., 2016). The intensities of the intracellular negative-ion capacity and the corresponding measured $\Delta\Psi$ were correlated. Therefore, it is considered that the intracellular negative-ion capacity influences to $\Delta\Psi$, which is generated across the membrane. However, it is unclear whether the estimated negative ion capacity includes membrane-permeable ions. The high negative ion capacity in the alkaliphilic strains is probably attributed to the intracellular acidic substances, including proteins, at higher intracellular pH (ca. pH 8–8.2) than in the ordinary neutrophilic strains (pH 6–7). Protein p*I* distribution estimated using the genomes of alkaliphilic, neutralophilic, and acidophilic strains indicates a preference for acidic proteins (p*I* 4.01–5) in alkaliphiles (Lebre and Cowan, 2020).

Possible Effect of $\Delta\Psi$ to Membrane Bound Cytochrome *c*-550

Electron transfer-coupled H^+ transfer in horse heart cytochrome *c* was examined by SAMs cytochrome *c* attached to an Ag electrode produced at different distances connected to the different chain lengths (C_6–C_{16}) of ω-carboxyl alkanethiols (Murgida and Hildebrandt, 2001). Only in the case where the distance between cytochrome *c* and the electrode is short (C_2), a difference in the electron transfer rate of the H^+/D^+ effect is observed: 132 s^{-1} in H_2O_2 and 33 s^{-1} in D_2O. H^+/D^+ effect does not occur in cytochrome *c* in the solution. Therefore, these results suggest that the prerequisites for electron transfer coupled with H^+ transfer are (i) cytochrome *c* forms accumulated, such as a monolayer on the electrode, (ii) accumulated cytochrome probably should be lined up in the correct orientation, and (iii) cytochrome *c* is affected by Coulomb force from the electrode, which may correspond to $\Delta\Psi$ on the membrane surface. Considering the high ATP productivity in alkaliphilic *Bacillaceae*, it can be assumed that the actual $\Delta\Psi$ in the vicinity of the outer surface of the membrane is much higher than the estimated values. In addition, as described above, the redox potential of cytochrome *c*-550 immobilized on the gold electrode using SAMs was much lower than that in the redox titration. This suggests that Coulomb force from the electrode induces conformational changes around heme *c*, altering the redox potential (Murgida and Hildebrandt, 2004). Owing to this change in the redox potential of cytochrome *c*, the difference in the redox potential between cytochrome *c*-550 and the direct electron-accepting

prosthetic group in cytochrome *c* oxidase (i.e., heme *a*) becomes larger. This means that a very large redox potential gap [+ 7 mV → ca + 250 mV (e.g., heme *a*)] may be necessary to transfer electrons from cytochrome *c*, which is located on the outer surface of the membrane, to the inner prosthetic component (e.g., heme *a*), which is located on the inner membrane under high $\Delta\Psi$ and consists of strong intracellular negative charges. It is possible that this $\Delta\Psi$-dependent redox potential change mechanism regulates electron transfer in the respiratory chain depending on the intensity of the electric field on the outer surface of the membrane of *E. clarkii*.

The above-described are alkaliphilic *Bacillaceae* strains that utilize outer-surface-membrane-based $\Delta\Psi$ consisting of the Donnan potential, which is attributed to the high intracellular pH and the intracellular acidic substances, including proteins. In accordance with the large $\Delta\Psi$, the respiratory chain is modified to match the harsh conditions for electron flow from the extracellular side to the intracellular side and translocation of H^+ from the intracellular side to the extracellular side. The combination of enhanced $\Delta\Psi$ and specifically modified respiratory components in obligately alkaliphilic *E. clarkii*, and influenced the enhancement of respiratory extruded H^+ protection for ATP production. This system will make a limited amount of H^+ present in the harsh environment even more effective for utilization of H^+.

CONCLUSION AND PERSPECTIVE

The main sources of bacterial membrane potential consist of charge separations driven by heterogeneous permeable ions across the membrane (V_G) and membrane impermeable substances (V_D) (Benarroch and Asally, 2020). There is a possibility that charge separation driven by heterogeneous permeable ions across the membrane contributes to the total $\Delta\Psi$ (V_T). Constant investment of energy is necessary to maintain desirable charge separation across the membrane. This might be one of the reasons for the difference in ATP production rate between alkaliphiles and neutralophiles, which is not reflected in difference in growth intensity. Although the maximum ATP synthesis rates in alkaliphiles are approximately 5–13 times higher than that in *B. subtilis*, the growth rate of *B. subtilis* is higher than those of the alkaliphiles. To understand the breakdown of the overall energy balance of alkaliphilic bacteria, it is necessary to determine the intensity of each constituent factor, V_G, V_D, and the asymmetric surface potential on either side of the membrane produced by the differences in phospholipid head groups.

Based on the molecular features of membrane-bound cytochrome *c* in *E. clarkii*, it can be predicted that the segment near the N-terminus produces an H-bond network in the space between the main body cytochrome *c* molecule and the outer surface of the membrane. This configuration may lead to the formation of an H^+ capacitor on the outer membrane surface. The regulation of horizontal H^+ transfer on the outer membrane surface is thought to occur in conjunction with the redox reaction of cytochrome *c*. It can be predicted that the order of electron transfer in the tetramer depends on the distance of the molecule from the membrane. Inter-cytochrome *c* molecular horizontal electron transfer may regulate horizontal H^+ transfer on the outer membrane surface. Cytochromes *c* exhibit very low redox potentials and these potentials will further be decreased depending on the electric field on the outer surface of the membrane. Although the original electron acceptor of cytochrome *c* is cytochrome *c* oxidase, the low redox potentials may include other electron acceptors including NPS or redox centers in complex III. It is believed that a proper H^+ capacitor function will work with appropriate control of its functions. However, to clarify of the regulations, we must wait for future studies on these mechanisms.

As described above, a high $\Delta\Psi$ and an H^+ capacitor produced by the membrane-bound cytochrome *c* are the key points of energy acquisition under high- and low-aeration conditions, respectively (**Figure 4**). However, the rationales of each strategy in different environments have not yet been understood well. Therefore, we cannot explain the fundamental reasons why highly efficient ATP production can be possible under high aeration conditions although the turnover of the respiratory chain is not high. Since each bioenergetic factor is strongly related to one another (e.g., $\Delta\Psi$ vs. oxygen consumption rate), the fundamentals in each aeration condition can be determined in further studies.

Alkaliphilic bacteria exhibit a lower respiratory rate than neutralophilic *B. subtilis* under high aeration conditions. This could be explained by H^+ translocation from intracellular space to extracellular space under the presence of high $\Delta\Psi$ in alkaliphiles. On the contrary, under low aeration conditions, the voltage of the respiratory chain from NADH to O_2 drops, and H^+ cannot be translocated in the presence of high $\Delta\Psi$. Therefore, alkaliphiles decreased their $\Delta\Psi$, and take opt to accumulate H^+ *via* cytochrome *c*, which possesses a special segment producing an H-bond network on the outer surface of the membrane. It is considered that this accumulated H^+ exhibits attractive force toward the intracellular side of the membrane in the same way that a normal capacitor that stores electrons exhibits electrostatic attraction.

AUTHOR CONTRIBUTIONS

KY and IY designed this study. TG and SO collected the data. IY and TG performed calculations. IY wrote the manuscript. All authors approved the final version.

FUNDING

This work was supported by an internal grant from the National Institute of Advanced Industrial Science and Technology (AIST).

ACKNOWLEDGMENTS

We thank Editage (www.editage.com) for the English language editing.

REFERENCES

Aino, K., Hirota, K., Matsuno, T., Morita, N., Nodasaka, Y., Fujiwara, T., et al. (2008). *Bacillus polygoni* sp. nov., a moderately halophilic, non-motile obligate alkaliphile isolated from indigo balls. *Int. J. Syst. Evol. Microbiol.* 58, 120–124. doi: 10.1099/ijs.0.65193-0

Aono, R., and Horikoshi, K. (1983). Chemical composition of cell walls of alkalophilic strains of alkalophilic strains of *Bacillus*. *J. Gen. Microbiol.* 129, 1083–1087.

Aono, R., Ito, M., and Horikoshi, K. (1993). Occurrence of teichurono peptide in cell walls of group 2 alkaliphilic *Bacillus* sp. *J. Gen. Microbiol.* 139, 2738–2744.

Aono, R., Ito, M., Joblin, K. N., and Horikoshi, K. (1995). A high cell wall negative charge is necessary for the growth of alkaliphile *Bacillus lentus* C-125 at elevated pH. *Microbiology* 141, 2955–2964.

Aono, R., Ito, M., and Machida, T. (1999). Contribution of the cell wall component teichuronopeptide to pH homeostasis and alkaliphily in the alkaliphilic *Bacillus lentus* C-125. *J. Bacteriol.* 181, 6600–6606. doi: 10.1128/JB.181.21.6600-6606.1999

Benarroch, J. M., and Asally, M. (2020). The microbiologist's guide to membrane potential dynamics. *Trends Microbiol.* 28, 304–314. doi: 10.1016/j.tim.2019.12.008

Bengtsson, J., Rivolta, C., Hederstedt, L., and Karamata, D. (1999). *Bacillus subtilis* contains two small *c*-type cytochromes with homologous heme domains but different type of membrane anchors. *J. Biol. Chem.* 274, 26179–26184. doi: 10.1074/jbc.274.37.26179

Benini, S., Borsari, M., Ciurli, S., Dikiy, A., and Lamborghini, M. (1998). Modulation of *Bacillus pasteurii* cytochrome *c*553 reduction potential by structural and solution-parameters. *J. Biol. Inorg. Chem.* 3, 371–382.

Benini, S., González, A., Rypniewski, W. R., Wilson, K. S., Van Beeumen, J. J., and Ciurli, S. (2000). Crystal structure of oxidized *Bacillus pasteurii* cytochrome *c*553 at 0.97-Å resolution. *Biochemistry* 39, 13115–13126.

Chichen, E., Spode, J. A., and Jones, C. W. (1981). Respiration-linked proton translocation in the moderate thermophile of *Bacillus stearothermopilus*. *FEMS Microbiol. Lett.* 11, 181–185.

Clejan, S., Krulwich, T. A., Mondrus, K. R., and Seto-Yung, D. (1986). Membrane lipid composition of obligately and facultatively alkaliphilic strains of *Bacillus* spp. *J. Bacteriol.* 168, 334–340. doi: 10.1128/jb.168.1.334-340.1986

Coutinho, I. B., and Xavier, A. V. (1994). Inorganic microbial sulfur metabolism. *Methods Enzymol.* 234, 119–140.

David, P. S., Dutt, P. S., Wathen, B., Jia, Z., and Hill, B. C. (2000). Characterization of structural model of membrane bound cytochrome *c*-550 from *Bacillus subtilis*. *Arch. Biochem. Biophys.* 377, 22–30.

Davidson, M. W., Gray, K. A., Knaff, D. B., and Krulwich, T. A. (1988). Purification and characterization of two soluble cytochromes from the alkalophile *Bacillus firmus* RAB. *Biochim. Biophys. Acta.* 933, 470–477. doi: 10.1016/0005-2728(88)90082-5

Lopes, H. F. S.s Tu, Z., Sumi, H., and Yumoto, I. (2021a). Analysis of bacterial flora of indigo fermentation fluids utilizing composted indigo leaves (*sukumo*) and indigo extracted from plants (Ryukyu-ai and Indian indigo). *J. Biosci. Bioeng.* 132, 279–286. doi: 10.1016/j.jbiosc.2021.05.004

Lopes, H. F. S., Tu, Z., Sumi, H., Furukawa, H., and Yumoto, I. (2021b). *Indigofera tinctoria* leaf powder as a promising additive to improve indigo fermentation prepared with *sukumo* (composted *Polygonum tinctorium* leaves). *World J. Microbiol. Biotechnol.* 37:179. doi: 10.1007/s11274-021-03142-y

Denda, K., Oshima, A., and Fukumori, Y. (2001). Structural analyses of the deduced amino acid sequences of a novel type heme-copper terminal oxidase, cytochrome aco_3, from alkalophilic *Bacillus* YN-2000. *Can. J. Microbiol.* 47, 1075–1081.

Dimroth, P., and Cook, G. M. (2004). Bacterial Na^+- or H^+-coupled ATP synthases operating a low electrical potential. *Adv. Microb. Physiol.* 49, 175–218.

Donnan, F. G. (1924). The theory of membrane equilibria. *Chem. Rev.* 1, 73–90.

Doukov, T. I., Hemmi, H., Drenman, C. L., and Ragsdale, S. W. (2007). Structure and kinetic evidence for extended hydrogen-bonding network in catalysis of methyl group transfer. role of active site asparagine residue in activation of methyl transfer by methyltransferase. *J. Biol. Chem.* 282, 6609–6618. doi: 10.1074/jbc.M609828200

Enomoto, K., and Koyama, N. (1999). Effect of growth pH on the phospholipid contents of membranes from alkaliphilic bacteria. *Curr. Microbiol.* 39, 270–273. doi: 10.1007/s002849900458

Gilmore, R., Messner, P., Guffanti, A. A., Kent, R., Scheberl, A., Kendrick, N., et al. (2000). Two-dimensional gel electrophoresis of pH-dependent protein expression in facultatively alkaliphilic *Bacillus pseudofirmus* OF4 lead to characterization of an S-layer protein with a role in alkaliphily. *J. Bacteriol.* 182, 5969–5981. doi: 10.1128/JB.182.21.5969-5981.2000

García Montes de Oca, L. Y., Chagolla-Lopez, A., Gonzalez de la Vara, L., Cabellos-Avelar, T., Gomez-Lojero, C., and Gutierrez Cirlos, E. B. (2012). The composition of the *Bacillus subtilis* aerobic respiratory chain supercomplexes. *J. Bioenerg. Biomembr.* 44, 473–486.

Goto, T. (2006). *Functional Analyses of the Membrane Of Alkaliphilic Bacillus* spp. For Their Environmental Adaptations. [dissertation/Master's thesis]. Sapporo: Hokkaido University.

Goto, T., Hirabayashi, T., Morimoto, H., Yamazaki, K., Inoue, N., Matsuyama, H., et al. (2016). Contribution of intracellular negative ion capacity to donnan effect across the membrane in alkaliphilic *Bacillus* spp. *J. Bioeng. Biomembr.* 48, 87–96. doi: 10.1007/s10863-015-9641-9

Goto, T., Matsuno, T., Hishinuma-Narisawa, M., Yamazaki, K., Matsuyama, H., Inoue, N., et al. (2005). Cytochrome *c* and bioenergetic hypothetical model for alkaliphilic *Bacillus* spp. *J. Biosci. Bioeng.* 100, 365–379. doi: 10.1263/jbb.100.365

Gregory, L., and Ferguson-Miller, S. (1989). Independent control of respiration in cytochrome *c* oxidase vesicles by pH and electrical gradients. *Biochemistry* 28, 2655–2662. doi: 10.1021/bi00432a044

Guffanti, A. A., Finkelthal, O., Hicks, D. B., Falk, L., Sidhu, A., Garro, A., et al. (1986). Isolation and characterization of new facultatively alkalophilic strains of *Bacillus* species. *J. Bacteriol.* 167, 766–773. doi: 10.1128/jb.167.3.766-773.1986

Guffanti, A. A., and Krulwich, T. A. (1994). Oxidative phosphorylation by ADP + P_i-loaded membrane vesicles of alkaliphilic *Bacillus firmus* OF4. *J. Biol. Chem.* 269, 21576–21582.

Gupta, R., Patel, S., Saini, N., and Chen, S. (2020). Robust demarcation of 17 distinct *Bacillus* species clades, proposed as novel *Bacillaceae* genera, by phylogenomics and comparative genomic analysis: description of *Robertmurraya kyonggiensis* sp. nov. and proposal for an amended genus *Bacillus* limiting it only to the members of the subtilis and cereus clades of species. *Int. J. Syst. Evol. Microbiol.* 70, 5753–5798. doi: 10.1099/ijsem.0.004475

Hamamoto, T., Hashimoto, M., Hino, M., Kitada, M., Seto, Y., Kudo, T., et al. (1994). Characterization of a gene responsible for the Na^+/H^+ antiporter system of alkalophilic *Bacillus* species strain C-125. *Mol. Microbiol.* 14, 939–946. doi: 10.1111/j.1365-2958.1994.tb01329.x

Higashibata, A., Fujiwara, T., and Fukumori, Y. (1998). Studies on the respiratory system in alkaliphilic *Bacillus*; a proposed new respiratory mechanism. *Extremophiles* 2, 83–92. doi: 10.1007/s007920050004

Hijikata, S. (2004). *Purification and Characterization of Cytochrome c*-550 from obligate alkaliphilic *bacillus clarkii* K24-1U. [dissertation/Master's thesis]. Sapporo: Hokkaido University.

Hirabayashi, T., Goto, T., Morimoto, H., Yoshimune, K., Matsuyama, H., and Yumoto, I. (2012). Relationship between rates of respiratory proton extrusion and ATP synthesis in obligately alkaliphilic *Bacillus clarkii* DSM 8720^T. *J. Bioeng. Biomembr.* 44, 265–272. doi: 10.1007/s10863-012-9430-7

Hirota, K., Aino, K., and Yumoto, I. (2013). *Amphibacillus iburiensis* sp. nov., an alkaliphile that reduces an indigo dye. *Int. J. Syst. Evol. Microbiol.* 63, 4303–4308. doi: 10.1099/ijs.0.048009-0

Horikoshi, K. (2006). *Alkaliphiles*. New York, NY: Springer, 270.

Ito, M., Hicks, D. B., Henkin, T. M., Guffanti, A. A., Powers, B. D., Zvi, L., et al. (2004a). MotPS is the stator-force generator for motility of alkaliphilic *Bacillus*, and its homologue is a second functional Mot in *Bacillus subtilis*. *Mol. Microbiol.* 53, 1035–1049. doi: 10.1111/j.1365-2958.2004.04173.x

Ito, M., Xu, H. X., Guffanti, A. A., Wei, Y., Zvi, L., Clapham, D. E., et al. (2004b). The voltage-gated Na+ NavBP has a role in motility, chemotaxis, and pH homeostasis of an alkaliphilic *Bacillus*. *Proc. Natl. Acad. Sci. U.S.A* 101, 10566–10571. doi: 10.1073/pnas.0402692101

Jones, C. W., Brice, J. M., Downs, A. J., and Drozd, J. W. (1975). Bacterial respiration-linked proton translocation and its relationship to respiratory chain composition. *Eur. J. Biochem.* 52, 265–271.

Kitada, M., Guffanti, A. A., and Krulwich, T. A. (1982). Bioenergetic properties and viability of alkalophilic *Bacillus firmus* RAB as a function of pH and Na^+ contents of the incubation medium. *J. Bacteriol.* 152, 1096–1104. doi: 10.1128/jb.152.3.1096-1104.1982

Krulwich, T. A., Ito, M., and Guffanti, A. A. (2001). The Na^+-dependence of alkaliphily in *Bacillus*. *Biochim. Biophys. Acta.* 1501, 158–168.

Larsen, R. W., Chavez, M. D., Nunez, D. J., Davidson, M. W., Knaff, D. B., Krulwich, T. A., et al. (1990). Resonance raman investigation of a soluble cytochrome *c*522 from alkaliphilic *Bacillus firmus* RAB. *Arch. Biochem. Biophys.* 283, 266–270. doi: 10.1016/0003-9861(90)90641-b

Lebre, P. H., and Cowan, D. A. (2020). Genomics of Alkaliphiles. *Adv. Biochem. Eng. Biotechnol.* 172, 135–156.

Lewis, R. J., Belkina, S., and Krulwich, T. A. (1980). Alkalophiles have much higher cytochrome contents than conventional bacteria and then their own non-alkaliphilic mutant derivatives. *Biochem. Biophys. Res. Commun.* 95, 857–863. doi: 10.1016/0006-291x(80)90866-9

Louro, R. O., Catario, T., LaGall, J., and Xavier, A. V. (1997). Redox-Bohr effect in electron/proton energy transduction: cytochrome c_3 coupled to hydrogenase works as a 'proton thruster' in *Desulfivibrio vulgais*. *J. Biol. Inorg. Chem.* 2, 488–491.

Mano, G. (2020). Challenges and adaptation of life in alkaline habitats. *Adv. Biochem. Eng. Biotechnol.* 172, 85–134.

Matsuno, T., Goto, T., Ogami, S., Morimoto, H., Yamazaki, K., Inoue, N., et al. (2018). Formation of proton motive force under low-aeration alkaline conditions in alkaliphilic bacteria. *Front. Microbiol.* 9:2331. doi: 10.3389/fmicb.2018.02331

Messias, A. C., Aguiar, A. P., Brennan, L., Salgueiro, C. A., Saraiva, L. M., Xavier, A. V., et al. (2006). Solution structures of tetraheam ferricytochrome c_3 from *Desulfovibro vulgaris* (Hildenborough) and its K45Q mutant: the molecular basis of cooperativity. *Biochim. Biophys. Acta.* 1757, 143–153. doi: 10.1016/j.bbabio.2006.01.007

Miki, K., and Okunuki, K. (1969a). Cytochrome of *Bacillus subtilis* II. purification and spectral properties of cytochrome c-550 and c-554. *J. Biochem.* 66, 831–843. doi: 10.1093/oxfordjournals.jbchem.a129214

Miki, K., and Okunuki, K. (1969b). Cytochrome of *Bacillus subtilis* III. *J. Biochem.* 66, 845–854.

Mitchell, P. (1961). Coupling of phosphorylation to electron and hydrogen transfer by a chemi-osmotic type of mechanism. *Nature* 191, 144–148. doi: 10.1038/191144a0

Murgida, D. H., and Hildebrandt, P. (2001). Proton-coupled electron transfer of cytochrome *c*. *J. Am. Chem. Soc.* 123, 4062–4068.

Murgida, D. H., and Hildebrandt, P. (2004). Electron-transfer process of cytochrome *c* at interfaces. new insight by surface-enhanced resonance Raman spectroscopy. *Acc. Chem. Res.* 47, 854–861. doi: 10.1021/ar040043

Nei, M., and Kumar, S. (2000). *Molecular Evolution and Phylogenetics*. New York, NY: Oxford University Press.

Nielsen, P., Fritze, D., and Priest, F. G. (1995). Phenetic diversity of alkaliphilic *Bacillus* strains: proposal for nine new species. *Microbiology* 141, 1745–1761.

Nielsen, P., Rainey, F. A., Outtrup, H., Priest, F. G., and Fritze, D. (1994). Comparative 16S rDNA sequence analysis of some alkaliphilic bacilli and the establishment of sixth rRNA group within the genus *Bacillus*. *FEMS Microbiol. Lett.* 177, 61–66.

Nogi, Y., Takami, H., and Horikoshi, K. (2005). Characterization of alkaliphilic *Bacillus* strains used in industry: proposal of five novel species. *Int. J. Syst. Evol. Microbiol.* 55, 2309–2315. doi: 10.1099/ijs.0.63649-0

Noor, Y. M., Samsulrizal, N. H., Jema'on, N. A., Low, K. O., Ramili, A. N. M., Alias, N. I., et al. (2014). A comparative genomic analysis of the alkalitolerant soil bacterium *Bacillus lehensis* G1. *Gene* 545, 253–261. doi: 10.1016/j.gene.2014.05.012

Ohshima, H., and Ohki, S. (1985). Donnan potential and surface potential of a charged membrane. *Biophys. J.* 47, 673–678. doi: 10.1016/S0006-3495(85)83963-1

Ogami, S., Higikata, S., Tsukahara, T., Mie, Y., Matsuno, T., Morita, N., et al. (2009). A novel membrane-anchored cytochrome *c*-550 of alkaliphilc *Bacillus clarkii* K24-1U: expression, molecular features and properties of redox potential. *Extremophiles* 13, 491–504. doi: 10.1007/s00792-009-0234-6

Orii, Y., Yumoto, I., Fukumori, Y., and Yamanaka, T. (1991). Stopped-flow and rapid-scan studies of the redox behavior of cytochrome *aco* from faculataive alkalophilc *Bacillus*. *J. Biol. Chem.* 266, 14310–14316.

Padan, E., Bibi, E., Ito, M., and Krulwich, T. A. (2005). Alkaline pH homeostasis in bacteria: new insight. *Biochim. Biophys. Acta* 1717, 67–88.

Patel, S., and Gupta, R. S. (2020). A phylogenomic and comparative genomic framework for resolving the polyphyly of the genus *Bacillus*: proposal for six new genera of *Bacillus* species. peribacillus gen. nov., cytobacillus gen. nov., mesobacillus gen. nov., neobacillus gen. nov., metabacillus gen. nov. and alkalihalobacillus gen. nov. *Int. J. Syst. Evol. Microbiol.* 70, 406–438. doi: 10.1099/ijsem.0.003775

Qureshi, M. H., Yumoto, I., Fujiwara, T., Fukumori, Y., and Yamanaka, T. (1990). A novel *aco*-type cytochrome-*c* oxidase from a facultative alkalophilic *Bacillus*: purification, and some molecular and enzymatic features. *J. Biochem.* 107, 480–485. doi: 10.1093/oxfordjournals.jbchem.a123071

Rampelotto, P. H. (2013). Extremophiles and extreme environments. *Life* (Basel) 3, 482–485.

Rivas, L., Soares, C. M., Baptista, A. M., Simaan, J., Di Palo, R. E., Murgida, D. H., et al. (2005). Electric-field-induced redox potential shifts of tetraheme cytochrome c_3 immobilized on self-assembled monolayers: surface-enhanced resonance Raman spectroscopy and simulation studies. *Biophys. J.* 88, 4188–4199. doi: 10.1529/biophysj.104.057232

Satyanarayana, T., Raghukumar, C., and Sisinthy, S. (2005). Extremophilic microbes: diversity and perspectives. *Curr. Sci.* 89, 78–90.

Sone, N., and Fujiwara, Y. (1991). Effect of aeration during growth of *Bacillus stearothermophilus* on proton pumping activity and change of terminal oxidase. *J. Biochem.* 110, 1061–1021. doi: 10.1093/oxfordjournals.jbchem.a123671

Sturr, M. G., Guffanti, A. A., and Krulwich, T. A. (1994). Growth and bioenergetics of alkaliphilic *Bacillus firmus* OF4 in continuous culture at high pH. *J. Bacteriol.* 176, 3111–3116. doi: 10.1128/jb.176.11.3111-3116.1994

Tamura, K., Stecher, G., and Kumar, S. (2021). MEGA 11: molecular evolutionary genetics analysis Version 11. *Mol. Biol. Evol.* 38, 3022–3027. doi: 10.1093/molbev/msab120

Thongaram, T., Kosono, S., Ohkuma, M., Hongoh, Y., Kitada, M., Yoshinaka, T., et al. (2003). Gut of higher termites as a niche for alkaliphiles as shown by culture-based and culture-Independent studies. *Microbes. Environ.* 18, 152–159.

Tsujii, K. (2002). Donnan equilibria in microbial cell walls: a pH-homeostatic mechanism in alkaliphiles. *Coll. Surf. B Biointerfaces* 24, 247–251.

Tu, Z., Lopes, H. F. S., Narihiro, T., and Yumoto, I. (2021). The mechanism underlying of long-term stable indigo reduction state in indigo fermentation using *sukumo* (composted Polygonum tinctorium leaves). *Front. Microbiol.* 12:698674. doi: 10.3389/fmicb.2021.698674

van de Vossenberg, J. L. C. M., Driessen, A. J. M., Zilling, W., and Koning, W. N. (1998). Bioenergetic and cytoplasmic membrane stability of the extremely acidophilic, thermophilic archaeon Picrophilus oshimae. *Extremophiles* 2, 67–74. doi: 10.1007/s007920050044

Vedder, A. (1934). *Bacillus alcalophilus* n. sp.; benevens enkele ervaringen met sterk alcalische voedingsbodems. *Antonie Van Leeuwenhoek* 1, 47.

von Wachenfeldt, C., and Hederstedt, L. (1990). *Bacillus subtilis* 13-kilodalton cytochrome *c*-550 encoded by *cccA* consists of a membrane-anchor and a heme domain. *J. Biol. Chem.* 265, 13939–13948.

von Wachenfeldt, C., and Hederstedt, L. (1993). Physico-chemical characterisation of membrane-bound and water-soluble forms of *Bacillus subtilis* cytochrome *c*-550,". *Eur. J. Biochem.* 212, 499–509. doi: 10.1111/j.1432-1033.1993.tb17687.x

Whelan, S., and Goldman, N. (2001). A general empirical model of protein evolution derived from multiple protein families using a maximum-likelihood approach. *Mol. Biol. Evol.* 18, 691–699. doi: 10.1093/oxfordjournals.molbev.a003851

Woolley, K. J. (1987). The *c*-type cytochromes of the gram-positive bacterium *Bacillus licheniformis*. *Arch. Biochem. Biophys.* 254, 376–379.

Yamaguchi, T., Tamura, G., and Arima, K. (1966). A method for obtaining cytochrome *c* from *Bacillus megaterium*. *Biochim. Biophys. Acta* 124, 413–414.

Yaginuma, A., Tsukita, S., Sakamoto, J., and Sone, N. (1997). Characterization of two terminal oxidases in *Bacillus brevis* and efficiency of energy conservation of the respiratory chain. *J. Biochem.* 122, 969–976. doi: 10.1093/oxfordjournals.jbchem.a021859

Yoshimune, K., Morimoto, H., Hirano, Y., Sakamoto, J., Matsumoto, H., and Yumoto, I. (2010). The obligate alkaliphile *Bacillus clarkii* K24-1U retains

extruded protons at the beginning of respiration. *J. Bioeng. Biomembr.* 42, 111–116. doi: 10.1007/s10863-010-9278-7

Yumoto, I. (2003). Electron transport system in alkaliphilic Bacillus spp. *Recent* Res. *Dev. Bacteriol.* 1, 131–149. doi: 10.1263/jbb.100.365

Yumoto, I., Fukumori, Y., and Yamanaka, T. (1991). Purification and characterization of two membrane-bound *c*-type cytochromes from a facultative alkalophilic *Bacillus*. *J. Biochem.* 110, 267–273. doi: 10.1093/oxfordjournals.jbchem.a1235692

Yumoto, I., Takahashi, S., Kitagawa, T., Fukumori, Y., and Yamanaka, T. (1993). The molecular features and catalytic activity of Cu_A-containing aco_3-type cytochrome *c* oxidase from facultatively alkalophilic *Bacillus*. *J. Biochem.* 114, 88–95.

Yumoto, I., Yamazaki, K., Hishinuma, M., Nodasaka, Y., Inoue, N., and Kawasaki, K. (2000). Identification of facultative alkaliphilic *Bacillus* sp. YN-2000 and its fatty acid composition and cell-surface aspects depending on culture pH. *Extremophiles* 4, 285–290. doi: 10.1007/s007920070015

Conflict of Interest: The authors declare that the research was conducted in the absence of any commercial or financial relationships that could be construed as a potential conflict of interest.

Publisher's Note: All claims expressed in this article are solely those of the authors and do not necessarily represent those of their affiliated organizations, or those of the publisher, the editors and the reviewers. Any product that may be evaluated in this article, or claim that may be made by its manufacturer, is not guaranteed or endorsed by the publisher.

frontiers in Microbiology

MINI REVIEW
published: 29 March 2022
doi: 10.3389/fmicb.2022.845562

Approaches to Unmask Functioning of the Uncultured Microbial Majority From Extreme Habitats on the Seafloor

Stefanie Böhnke and Mirjam Perner**

Geomicrobiology, GEOMAR Helmholtz Centre for Ocean Research Kiel, Kiel, Germany

Researchers have recognized the potential of enzymes and metabolic pathways hidden among the unseen majority of Earth's microorganisms for decades now. Most of the microbes expected to colonize the seafloor and its subsurface are currently uncultured. Thus, their ability and contribution to element cycling remain enigmatic. Given that the seafloor covers ∼70% of our planet, this amounts to an uncalled potential of unrecognized metabolic properties and interconnections catalyzed by this microbial dark matter. Consequently, a tremendous black box awaits discovery of novel enzymes, catalytic abilities, and metabolic properties in one of the largest habitats on Earth. This mini review summarizes the current knowledge of cultivation-dependent and -independent techniques applied to seafloor habitats to unravel the role of the microbial dark matter. It highlights the great potential that combining microbiological and biogeochemical data from *in situ* experiments with molecular tools has for providing a holistic understanding of bio-geo-coupling in seafloor habitats and uses hydrothermal vent systems as a case example.

Keywords: hydrothermal vents, uncultured microbial majority, microbial dark matter, functional metagenomics, *in situ* technologies, activity-based screening, novel enzymes

OPEN ACCESS

Edited by:
Andreas Teske, University of North Carolina at Chapel Hill, United States

Reviewed by:
Ida Helene Steen, University of Bergen, Norway
Jason B. Sylvan, Texas A&M University, United States

****Correspondence:***
Stefanie Böhnke
sboehnke-brandt@geomar.de
Mirjam Perner
mperner@geomar.de

Specialty section:
This article was submitted to Extreme Microbiology, a section of the journal Frontiers in Microbiology

Received: *30 December 2021*
Accepted: *07 March 2022*
Published: *29 March 2022*

Citation:
Böhnke S and Perner M (2022) Approaches to Unmask Functioning of the Uncultured Microbial Majority From Extreme Habitats on the Seafloor. Front. Microbiol. 13:845562. doi: 10.3389/fmicb.2022.845562

INTRODUCTION

The ocean's seafloor covers ∼70% of our planet's surface and is vastly underexplored. Through its pivotal role for processing deposited material in marine sediments, the seafloor is critically involved in the extent to which carbon sequestration, nutrient recycling, carbonate dissolution and methane production occur (cf. Middelburg, 2018; LaRowe et al., 2020). Most of the seafloor is in the deep-sea and is hallmarked by hostile conditions, i.e., no light, high pressure, food scarcity, and is mostly characterized by comparatively low turnover rates (Middelburg et al., 1993). Although hydrothermal deep-sea vent ecosystems can be associated with even more extreme conditions, such as high temperatures or the presence of toxic compounds (Perner et al., 2014; McDermott et al., 2018), the emitted inorganic energy sources and chemosynthetic microbes capable of coping with local extreme conditions transform deep-sea hydrothermal vents into hot spots of activity. Venting is also a significant metal source to the ocean, with metal-organic complexation facilitating long-distance transport and potentially impacting primary production in the ocean's surface (Sander and Koschinsky, 2011; Resing et al., 2015; Fitzsimmons et al., 2017; Ardyna et al., 2019). Additionally, hydrothermal environments are relevant for providing bioactive trace metals (Li et al., 2014; Cohen et al., 2021) and organic carbon (Toner et al., 2009;

Bennett et al., 2015; Longnecker et al., 2018), and give insights into the origin of life and its limits (Martin et al., 2008).

Microbes make up most of the total biomass on Earth. However, the majority of prokaryotic cells resist cultivation and remain uncharacterized (Lloyd et al., 2018; Zamkovaya et al., 2021). It is estimated that this uncultured prokaryotic majority, often referred to as microbial dark matter, accounts for up to 91 and 96% of uncultured bacteria and 87 and 96% of uncultured archaea in marine sediments and hydrothermal vents, respectively (Lloyd et al., 2018). Sequencing of prokaryotic (meta)genomes has demonstrated that up to 40% of annotated genes cannot be allocated to a known or predicted function (Baric et al., 2016) and only as little as 16% of ocean metagenomic DNA encoding hypothetical proteins could be linked to proteins with an experimentally verified function (Sunagawa et al., 2015). One way to address this sequence-based limitation is the development of novel computational approaches like, e.g., the CSBFinder-S software. It allows identification of operon structures by inferring conserved synthetic blocks (CSBs), providing a functional context for unassignable enzymes (Svetlitsky et al., 2020).

So far, meta'omics has given us valuable insights into the taxonomic diversity, metabolic potential and gene expression patterns of microbial communities from extreme seafloor habitats (Fortunato and Huber, 2016 and references therein). Albeit, activity-based screening of metagenomic libraries is the only methodology that currently allows detection of entirely novel enzymes from known and unknown microbes for which homologies to known motifs lack and is a promising approach to overcome shortcomings associated with sequence-based strategies (Handelsman, 2004; Böhnke and Perner, 2014; Adam and Perner, 2018; Pushkarev et al., 2018). However, recombinant expression of metagenomic fragments in a surrogate host can be troublesome due to manifold reasons (divergent codon usage, translation, correct folding etc.), often leading to low hit rates that require high screening throughput which is the reason why functional metagenomic approaches might be very time-consuming and cost intensive (Perner et al., 2011b). Another way to study yet uncultured microbes is to perform the corresponding investigations directly in the natural habitat, i.e., *in situ*. Here, the main challenge is not only to further develop sensor technology and to optimize the collection and preservation of sample material, but also to provide technologies that synchronize *in situ* microbiological and geochemical investigations in space and time (**Figure 1**).

THE NOT YET CULTIVATED MICROBIAL MAJORITY AND ITS POTENTIAL FOR ELEMENT CYCLING AT HYDROTHERMAL VENT HABITATS

Deep-sea hydrothermal vent environments form along spreading ridges, where hot, highly reduced hydrothermal fluids mix with cold, oxygenated seawater, thereby creating steep thermal and chemical gradients. Chemosynthetic microorganisms exploit this thermodynamic disequilibrium by generating energy through redox reactions potentially fueling autotrophic carbon fixation. Since the discovery of hydrothermal vents (Ballard, 1977; Corliss et al., 1979), great cultivation efforts have been made to describe metabolic activities and physiological properties of respective microbes (reviewed in Dick, 2019). Cultivation is irreplaceable and includes (i) traditional and steadily improved techniques on liquid or solid media (cf. Reysenbach and Götz, 2001; Hansen and Perner, 2015; Zhang et al., 2018; Zeng et al., 2021 and references therein), (ii) gradient tube incubations (Emerson and Moyer, 1997), enrichments (iii) in bio-electrochemical systems (Pillot et al., 2018), (iv) on *in situ* enrichment carriers (Stokke et al., 2020), or (v) possibly–in the near future–even on synthetically grown hydrothermal vents (Barge and White, 2017; Martinez et al., 2019; Sanchez, 2021), and high-pressure laboratory techniques (Kato, 2011). Information from meta'omic data holds great promise to further improve the cultivation success by guiding the development of new cultivation technologies and strategies that are more responsive to the requirements of uncultured lineages (Gutleben et al., 2018). Once strains are in culture, the next step is the generation of a pure culture, but isolation of microbes is far from trivial. Strains often tend to grow in close co-culture with other strains and a variety of different isolation strategies include plating techniques (cf. Sass and Perner, 2020), role-tube isolations (cf. Zeng et al., 2013), dilution to extension approaches (cf. Adam et al., 2021), single cell separation micro tweezer technologies (Fröhlich and König, 2000; cf. Sass et al., 2020), flow cytometry (Ferrari et al., 2012), diffuse chamber incubation (Kaeberlein et al., 2002) etc. These approaches have resulted in the description of some hundred microbial species with hydrothermal origin (Jebbar et al., 2015). Nevertheless, sequence-based metagenome studies disclose a large discrepancy between microbes present in a certain environment and those that are cultivable (Rinke et al., 2013; Hug et al., 2016; Zamkovaya et al., 2021). With respect to hydrothermal systems and marine sediments, this corresponds to 4 and 9% cultured bacteria and 4 and 13% cultured archaea, respectively (Lloyd et al., 2018). Despite technical progress and relentless efforts, hydrothermal vents are still among the ecosystems with particularly high numbers of uncultivated representatives (Lloyd et al., 2018). Meta'omic studies of hydrothermal vent habitats suggest that the functional differences between closely related microbial species or strains are substantial (Hug et al., 2016; Dombrowski et al., 2017). This highlights an unprecedented potential for various new metabolic pathways and enzyme functions hidden among the non-cultured majority of hydrothermal vent microbes (Zamkovaya et al., 2021). In order to cope with the ever-increasing amount of sequence information and to prevent the gap between physiological and sequence-based information from widening, (high-throughput) approaches linking sequences with functions urgently need to be further developed and advanced.

METAGENOMICS: TOWARDS UNDERSTANDING THE METABOLIC MICROBIAL NETWORK

Metagenomics refers to the entire genetic information of a given ecosystem (Handelsman et al., 1998). The original

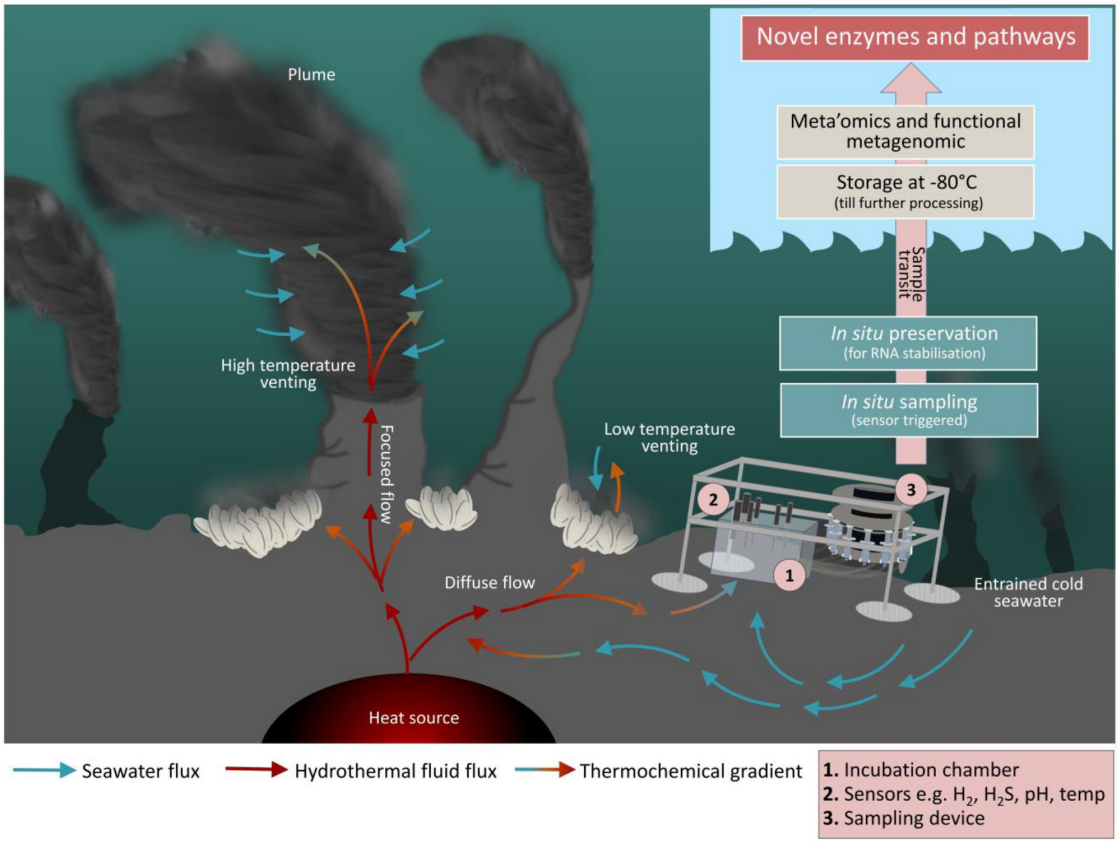

FIGURE 1 | Future perspective for hydrothermal vent *in situ* incubations. A mini chamber lander and the related work flow is shown next to a hydrothermal vent. The mini chamber is equipped with various sensors to measure the local environmental parameters like O_2, H_2, H_2S, pH, temperature, redox potential, and conductivity. Sampling may take place as a time series and/or controlled through the change in certain environmental parameters. Moreover, it is possible to simulate particular what-if scenarios as the syringe samplers may also function as injectors. This allows for manipulation of certain environmental conditions in the chamber as incubation proceeds. The subsamples collected during incubation are filtered and preserved *in situ* using appropriated fixation reagents. Finally, once on board, filters are stored at –80°C until further processing in the home laboratory. Mini chamber lander systems comparable to the here illustrated one have successfully been used to investigate benthic fluxes at the sediment-water interface zone of shallow waters or in the deep-sea (Thoms et al., 2018; Vonnahme et al., 2020; Kononets et al., 2021 and references therein). However, we are not aware of any published work that has reported data generated from the here presented approach where *in situ* incubation at hydrothermal vent environments with sensor-triggered sampling, *in situ* preservation, and subsequent microbiological analyses has been combined to elucidate interrelationships and interdependencies between abiotic factors and the biological world.

metagenomic approach was based on sequence- or function-based screening of metagenomic libraries that contained cloned environmental DNA (Lam et al., 2015). In 2004, the large marine whole genome shotgun sequencing project of the Sargasso Sea, provided, for the first time, a glimpse into the complex microbial community compositions of ocean habitats (Venter et al., 2004), pioneering future metagenome projects. The progress in next generation sequencing technologies has been rapid and together with bioinformatic tool development has allowed the subfields of metatranscriptomics and metaproteomics to further revolutionize meta'omic research (Simon and Daniel, 2011), as gene expression and protein profiles now enable insights into active metabolic processes and functional adaptations (Wilmes et al., 2015; Shakya et al., 2019). In this context, the term functional metagenomics has popped up frequently. This is rather misleading, as this term was originally used for function-based screening of metagenomic libraries seeking specific enzyme activities or valuable compounds (Handelsman, 2004). In the following we use the term functional metagenomics as it was initially coined.

However, high-throughput meta'omic approaches nowadays result in the rapid accumulation of DNA, RNA, and protein sequences, but current databases only allow the assignment of candidate functions based on homologs of already known motifs (Daniel, 2005). Thus, the vast majority of predicted enzyme functions have never been experimentally proven. Indeed, about one-third of the genes found in genomes of cultured and uncultured prokaryotes cannot even be assigned a predicted function due to the lack of homologies (Lloyd et al., 2018). One possible approach suited to verify if a predicted function is true is to clone and express targeted genes in a surrogate host (Yang et al., 2016; Danso et al., 2018; Oppermann et al., 2019). However, one major drawback of this strategy is that the original gene proximity and thus

relevant chaperones, transcriptional regulators and/or activators are missing, likely causing corresponding gene products to remain inactive (Böhnke and Perner, 2017). Although the use of large insert metagenomic libraries has the potential to counteract some of these challenges, problems with heterologous gene expression in the surrogate host, e.g., failed gene expression and incorrect post-transcriptional processing, remain one of the major limitations of functional metagenomic approaches (Perner et al., 2011b; Johnson et al., 2017). The use of custom expression strains, alternative vector systems, ionic liquids, or even *in vitro* recombinant transcription systems are promising techniques to mitigate these shortcomings (Lam et al., 2015; Kinfu et al., 2017; Mital et al., 2021).

Implementing a functional metagenomic approach requires two further major challenges to be overcome. First, there is the need to construct metagenomic libraries whereby isolation of high-quality environmental DNA is critical for successful cloning. The second major bottleneck is the often very time consuming and tedious establishments of high-throughput screening methods. A large range of biotechnologically motivated screening technologies for identifying novel biocatalysts or valuable biomolecules with industrial, commercial, clinical or bioremediational applications from uncultured microbes has identified proteases, oxidoreductases, esterases, amylases, phosphatases, chitinases, cellulases, glycosyltransferases, and decarboxylases (cf. Perner et al., 2011b; Rabausch et al., 2013; Berini et al., 2017; Johnson et al., 2017). However, functional metagenomic approaches with ecologically oriented objectives are extremely rare; although some enzymes discovered out of a biotechnological interest may also offer insights into ecologically relevant metabolic processes. Recently, one of the few purely ecologically and biogeochemically motivated functional screening approaches available targeted the distribution of active ribulose-1,5-bisphosphate carboxylases (RubisCO) at different hydrothermal vents (Böhnke and Perner, 2019). The study managed to place the identified RubisCOs (and respective uncultivated microbes) into an ecological context and demonstrated some possible RubisCO-protein interactions with neighboring gene products (Böhnke and Perner, 2017). As part of this work, some of the previously annotated "hypothetical proteins with unknown functions," could be assigned the probable role as RubisCO transcriptional regulators and post-translational activators or repressors.

Additionally, a second ecologically motivated function-based screen was developed that also targets RubisCO activity (Varaljay et al., 2016). Since Varaljay et al. (2016) used a different host-vector system, this heterologous complementation based functional metagenomic screen likely expands the spectrum of detectable active RubisCOs (Varaljay et al., 2016). Another ecologically and biogeochemically motivated functional metagenomic approach focused on hydrogenase activities (Adam and Perner, 2017). The screening detected three H_2-uptake expressing active metagenomic clones without any known hydrogenase-encoding genes or motifs on their DNA insert (Adam and Perner, 2018) suggesting novel hydrogenases. The discovery of heliorhodopsin, a globally abundant and widely distributed light-sensing rhodopsin, has also been enabled by functional metagenomics (Pushkarev et al., 2018). These studies highlight the tremendous diversity of currently unknown dark matter proteins and underline the urgent need for developing more novel screening methods for targeting specific enzymatic activities of unknown organisms. This methodology allows a window into the metabolic network of the uncultured microbes and their catalytic ability in biogeochemical cycling of key elements.

CURRENT CHALLENGES AND FUTURE PERSPECTIVES FOR *in situ* TECHNOLOGIES AT THE SEAFLOOR

Marine microbial communities hold a central role as drivers of major biogeochemical processes, impacting ecosystem functioning far beyond the oceans (Falkowski et al., 2008). Research into these microbial consortia and the processes they mediate is, however, often constrained by technical capabilities, as is particularly evident in deep-sea research (Fortunato et al., 2021). Thus, sampling hard accessible deep-sea environments is already a technical and logistical challenge, requiring the development of specialized underwater devices (Liang et al., 2021; Paulus, 2021). Over the past decades a variety of ocean deployable sampling instrumentation have been developed (McQuillan and Robidart, 2017). Yet, only a few of them are suited to retrieve samples from extreme deep-sea habitats and are able to withstand the high pressures and corrosive hot fluids (Reysenbach and Götz, 2001; Liang et al., 2021). Transporting the samples from the deep-sea through the water column to the research vessel laboratory poses further inherent limitations as the samples are exposed to physico-chemical changes (e.g., changes in pressure, temperature, light, pH, redox state etc.) altering the compositions and thus biasing subsequent analysis (Edgcomb et al., 2016). Chemical composition of sampled hydrothermal fluids can change dramatically if *in situ* pressure is not maintained, resulting in degassing and the loss of volatile species and distorting microbial activities and metabolic rates (McNichol et al., 2016). Gas-tight sampling devices are used to mitigate this effect and prevent outgassing (Seewald et al., 2002; Butterfield et al., 2004; Miyazaki et al., 2017; Wu et al., 2018; Garel et al., 2019; Wang et al., 2020). A long and often variable lag time during ascent may change redox reactions, introducing artifacts in subsequent analyses despite the usage of pressure maintaining sampling devices (Fortunato et al., 2021). Once on board, the samples are subjected to atmospheric pressure for *ex situ* filtration, likely causing cell lyses and release of RNA and DNA molecules (Edgcomb et al., 2016). Extracellular DNA and RNA from lysed cells can only partially be bound and recovered by filtration (Liang and Keeley, 2013), thereby losing parts of the unknown microbial community. Unpreserved biological material is also very labile and starts to degrade within minutes (RNA and proteins) or hours to days (cells and DNA), further biasing samples (Ottesen, 2016). Indeed, a comparative study of *in situ* and shipboard RNA stable isotope probing (RNA-SIP) experiments showed that microbial communities are significantly affected by the effects of depressurization and sample processing

delays, resulting in a shift of the community structure and metabolic function (Fortunato et al., 2021). *In situ* preservation is one approach that has successfully been used to overcome limitations associated with sample transit (Edgcomb et al., 2016; Fortunato et al., 2021). But devices designed for filtration and integrated subsequent preservation are still rare (reviewed in Ottesen, 2016). They include the Suspended Particulate Rosette V2 (SUPR-V2) System (Breier et al., 2014), the Biological Osmo Sampling System (BOSS) (Robidart et al., 2013), and the Fixation Filter Unit (FF3) (Taylor et al., 2015).

The more information on habitat specific physicochemical characteristics available, the more value can be deduced from generated meta'omic datasets. This is essential if aiming to understand the role of microbes for ocean ecosystem functioning. Deep-sea sensors are efficient tools for observing local geochemistry, allowing real-time monitoring of certain key chemical variables such as pH, dissolved H_2, H_2S, CH_4, CO_2, and dissolved inorganic nutrients (Luther et al., 2001; Moore et al., 2009; Petersen et al., 2011; Wankel et al., 2011; Perner et al., 2013; Daniel et al., 2020; Gros et al., 2021; Liang et al., 2021; Mowlem et al., 2021). However, technical limitations require that various chemical parameters still have to be determined *ex situ* (Mowlem et al., 2021). Although *in situ* filtration allows reduction of chemical alteration caused by precipitation and/or adsorption of some dissolved elements during transit from the seafloor to the ship's research laboratory, it is evident that the most representative data on deep-sea fluid chemistry would be provided by direct *in situ* measurements (Sievert and Vetriani, 2012; Cotte et al., 2015). Thus, future efforts must be directed toward further advancing existing sensors (more precision, robustness, serialization and standardization) and establishing novel sensor technologies.

Technological advances in the past decade have enabled the development of a limited set of samplers capable of performing *in situ* experiments directly in the deep-sea, pioneering future biogeochemical studies in deep-sea habitats. Respective devices have successfully been used to perform *in situ* tracer incubations (Edgcomb et al., 2016), RNA-SIP experiments (Fortunato et al., 2021), molecular analytical techniques (Scholin et al., 2017), and extraction of organic compounds (Grandy et al., 2020). This has impressively demonstrated that *in situ* experiments can provide a window into the seafloor microbial consortia, metabolic mechanisms and transformations. To obtain a more complete understanding of microbial community dynamics, functions and influences on ocean processes, microbiology and geochemistry must be sampled simultaneously. Automated mini chamber

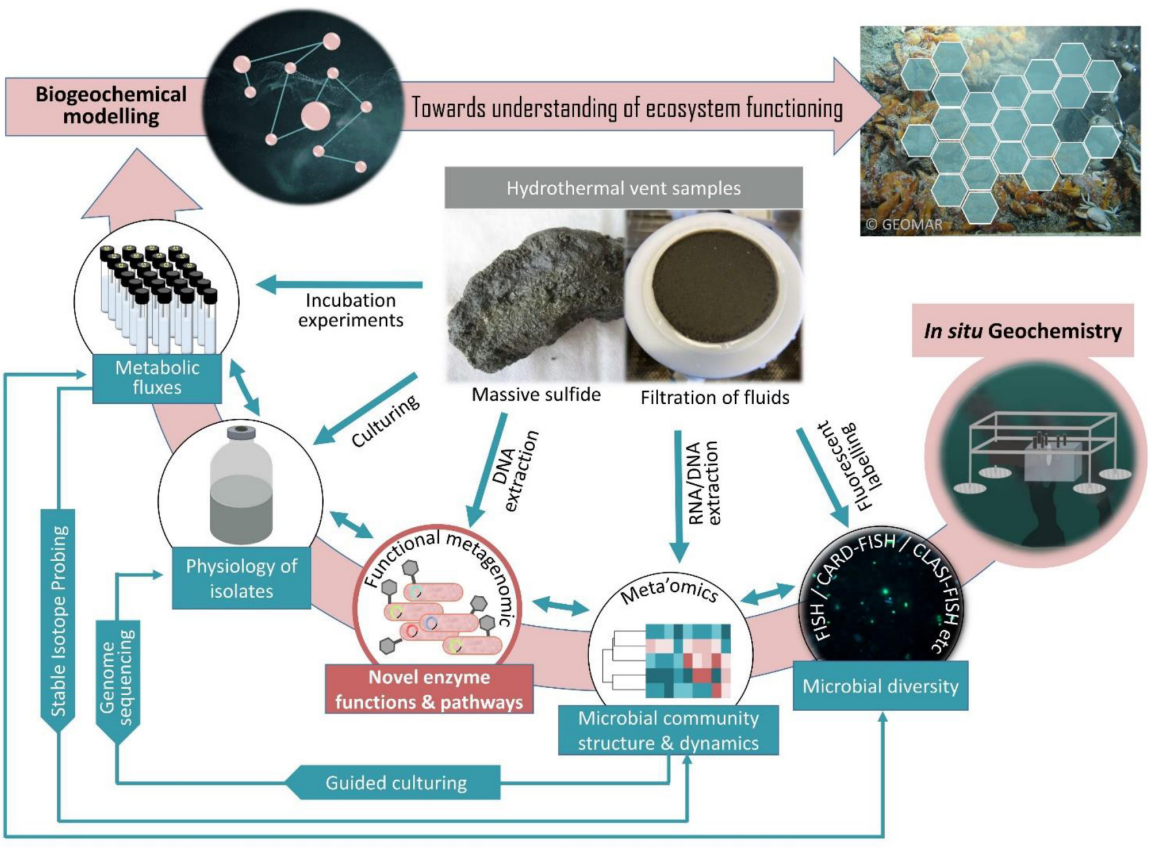

FIGURE 2 | A holistic approach to study the structure and function of microbial consortia in hydrothermal vents. The overview shows the approaches that should be considered and combined, if aiming at an omni-directional insight into hydrothermal vent ecosystem functioning, without neglecting the yet uncultivable majority of microorganisms.

lander systems have a great potential as they allow time series sampling in response to changes of environmental conditions, e.g., O_2, H_2S etc. (**Figure 1**). Furthermore, the possibility of injecting selected chemical compounds into the *in situ* incubation chamber could be used to simulate different what-if-scenarios. Thereby they can contribute to forecasting potential climate change impacts on the deep-sea microbes and the biogeochemical processes they mediate. Embedded in a holistic approach (**Figure 2**), *in situ* microbiological and biogeochemical analyses conducted in spatial and temporal proximity to each other can provide a more comprehensive picture of what features influence overall biogeochemical fluxes. This in turn improves the basis for building predictive models of how deep-sea microbial consortia contribute to global biogeochemical cycles.

Biogeochemical modeling is successfully used to determine (i) element flux rates of trace metals like, e.g., Fe, Mn, Ni, Cu, Co, Cd and Zn (reviewed in Homoky et al., 2016; cf. Somes et al., 2021), (ii) particulate organic material (POM) reactivity (reviewed in Lessin et al., 2018), (iii) thermodynamics (cf. Perner et al., 2011a) and (iv) energetics (cf. Böhnke et al., 2019), there by enhancing our theoretical and quantitative understanding of microbial and geochemical interactions (Dick, 2019). Only a few biogeochemical models have been established in recent years that allow the linkage between microbial biogeochemical rate measurements and meta'omic data, making key unknown physiological parameters, such as kinetic properties, transcription and translation rates, and mRNA and protein degradation rates recognizable (Reed et al., 2014; Louca et al., 2016). Such models have great potential and hold promise to unprecedented predictions about the role of ubiquitous microorganisms in mediating global element cycling.

CONCLUSION

The current understanding of the contribution of seafloor microbes to global biogeochemical cycles, metabolic fluxes and ecosystem functions is primarily aligned with what we known from culturable microbes. The cultured microbes, however, only represent a minor fraction of the total microbial vent community. This shows that our current understanding is vastly incomplete. Cultivation-independent approaches including *in situ* technologies, biogeochemical rate measurements, functional metagenomics, meta'omics, and biogeochemical modeling are promising tools that have already been used to effectively complement cultivation-dependent methods. Clearly, no single technology will provide full access to the vast potential of novel metabolic pathways hidden among the majority of uncultured microorganisms. The great challenge, but also the most promising approach for the future, can only lie in harnessing the strengths of available cultivation-dependent and cultivation-independent tools and smartly combining them in a holistic multidisciplinary approach. Here, continuing the development of existing *in situ* technologies and experimentation, but also the establishment of completely new ones, is of major importance and will significantly drive progress toward opening the window into previously inaccessible microbial physiologies of the microbial dark matter.

AUTHOR CONTRIBUTIONS

SB and MP wrote the manuscript. Both authors contributed to the article and approved the submitted version.

ACKNOWLEDGMENTS

We thank all colleagues and collaborators for their fruitful discussion on functional metagenomics and *in situ* experimentations. Furthermore, we greatly appreciate the help of the captains and crews of the research vessels and underwater vehicles for helping us to obtain our samples over the years.

REFERENCES

Adam, N., Han, Y., Laufer-Meiser, K., Bährle, R., Schwarz-Schampera, U., Schippers, A., et al. (2021). Deltaproteobacterium strain KaireiS1, a mesophilic, hydrogen-oxidizing and sulfate-reducing bacterium from an inactive deep-sea hydrothermal chimney. *Front. Microbiol.* 12:686276. doi: 10.3389/fmicb.2021.686276

Adam, N., and Perner, M. (2017). Activity-based screening of metagenomic libraries for hydrogenase enzymes. *Methods Mol. Biol.* 1539, 261–270.

Adam, N., and Perner, M. (2018). Novel hydrogenases from deep-sea hydrothermal vent metagenomes identified by a recently developed activity-based screen. *ISME J.* 12, 1225–1236. doi: 10.1038/s41396-017-0040-6

Ardyna, M., Lacour, L., Sergi, S., d'Ovidio, F., Sallee, J. B., Rembauville, M., et al. (2019). Hydrothermal vents trigger massive phytoplankton blooms in the Southern Ocean. *Nat. Commun.* 10:2451. doi: 10.1038/s41467-019-09973-6

Ballard, R. D. (1977). Notes on a major oceanographic find. *Oceanus* 20, 35–44.

Barge, L. M., and White, L. M. (2017). Experimentally testing hydrothermal vent origin of life on enceladus and other icy/ocean worlds. *Astrobiology* 17, 820–833. doi: 10.1089/ast.2016.1633

Baric, R. S., Crosson, S., Damania, B., Miller, S. I., and Rubin, E. J. (2016). Next-generation high-throughput functional annotation of microbial genomes. *mBio* 7, e1245–e1216. doi: 10.1128/mBio.01245-16

Bennett, S. A., Van Dover, C., Breier, J. A., and Coleman, M. (2015). Effect of depth and vent fluid composition on the carbon sources at two neighboring deep-sea hydrothermal vent fields (Mid-Cayman Rise). *Deep-Sea Res. Part I-Oceanogr. Res. Papers* 104, 122–133. doi: 10.1016/j.dsr.2015.06.005

Berini, F., Casciello, C., Marcone, G. L., and Marinelli, F. (2017). Metagenomics: novel enzymes from non-culturable microbes. *FEMS Microbiol. Lett.* 364:fnx211. doi: 10.1093/femsle/fnx211

Böhnke, S., and Perner, M. (2014). A function-based screen for seeking RubisCO active clones from metagenomes: novel enzymes influencing RubisCO activity. *ISME J.* 9, 735–745. doi: 10.1038/ismej.2014.163

Böhnke, S., and Perner, M. (2017). Unraveling RubisCO form I and form II regulation in an uncultured organism from a deep-sea hydrothermal vent via metagenomic and mutagenesis studies. *Front. Microbiol.* 8:1303. doi: 10.3389/fmicb.2017.01303

Böhnke, S., and Perner, M. (2019). Seeking active RubisCOs from the currently uncultured microbial majority colonizing deep-sea hydrothermal vent environments. *ISME J.* 13, 2475–2488. doi: 10.1038/s41396-019-0439-3

Böhnke, S., Sass, K., Gonnella, G., Diehl, A., Kleint, C., Bach, W., et al. (2019). Parameters governing the community structure and element turnover in Kermadec volcanic ash and hydrothermal fluids as monitored by inorganic electron donor consumption, autotrophic CO_2 fixation and 16S tags of the

transcriptome in incubation experiments. *Front. Microbiol.* 10:2296. doi: 10.3389/fmicb.2019.02296

Breier, J. A., Sheik, C. S., Gomez-Ibanez, D., Sayre-McCord, R. T., Sanger, R., Rauch, C., et al. (2014). A large volume particulate and water multi-sampler with *in situ* preservation for microbial and biogeochemical studies. *Deep-Sea Res. Part I-Oceanogr. Res. Papers* 94, 195–206. doi: 10.1016/j.dsr.2014.08.008

Butterfield, D. A., Roe, K. K., Lilley, M. D., Huber, J. A., Baross, J. A., Embley, R. W., et al. (2004). "Mixing, reaction and microbial activity in the sub-seafloor revealed by temporal and spatial variation in diffuse flow vents at axial volcano," in *The Subseafloor Biosphere at Mid-Ocean Ridges*, eds W. S. D. Wilcock, E. F. Delong, D. S. Kelley, J. A. Barass, and S. C. Cary (Washington, DC: AGU), 269–289. doi: 10.1029/144gm17

Cohen, N. R., Noble, A. E., Moran, D. M., McIlvin, M. R., Goepfert, T. J., Hawco, N. J., et al. (2021). Hydrothermal trace metal release and microbial metabolism in the northeastern Lau Basin of the South Pacific Ocean. *Biogeosciences* 18, 5397–5422. doi: 10.5194/bg-18-5397-2021

Corliss, J. B., Dymond, J., Gordon, L. I., Edmond, J. M., von Herzen, R. P., Ballard, R. D., et al. (1979). Submarine thermal springs on the Galápagos Rift. *Science* 203, 1073–1083. doi: 10.1126/science.203.4385.1073

Cotte, L., Waeles, M., Pernet-Coudrier, B., Sarradin, P. M., Cathalot, C., and Riso, R. D. (2015). A comparison of *in situ* vs. ex situ filtration methods on the assessment of dissolved and particulate metals at hydrothermal vents. *Deep-Sea Res. Part I* 105, 186–194. doi: 10.1016/j.dsr.2015.09.005

Daniel, A., Laës-Huon, A., Barus, C., Beaton, A. D., Blandfort, D., Guigues, N., et al. (2020). Toward a harmonization for using *in situ* nutrient sensors in the marine environment. *Front. Marin. Sci.* 6:773. doi: 10.3389/fmars.2019.00773

Daniel, R. (2005). The metagenomics of soil. *Nat. Rev. Microbiol.* 3, 470–478.

Danso, D., Schmeisser, C., Chow, J., Zimmermann, W., Wei, R., Leggewie, C., et al. (2018). New insights into the function and global distribution of polyethylene terephthalate (PET)-degrading Bacteria and enzymes in marine and terrestrial metagenomes. *Appl. Environ. Microbiol.* 84, e02773–17 doi: 10.1128/AEM.02773-17

Dick, G. J. (2019). The microbiomes of deep-sea hydrothermal vents: distributed globally, shaped locally. *Nat. Rev. Microbiol.* 17, 271–283. doi: 10.1038/s41579-019-0160-2

Dombrowski, N., Seitz, K. W., Teske, A. P., and Baker, B. J. (2017). Genomic insights into potential interdependencies in microbial hydrocarbon and nutrient cycling in hydrothermal sediments. *Microbiome* 5:106. doi: 10.1186/s40168-017-0322-2

Edgcomb, V. P., Taylor, C., Pachiadaki, M. G., Honjo, S., Engstrom, I., and Yakimov, M. (2016). Comparison of Niskin vs. *in situ* approaches for analysis of gene expression in deep Mediterranean Sea water samples. *Deep-Sea Res. Part II* 129, 213–222. doi: 10.1016/j.dsr2.2014.10.020

Emerson, D., and Moyer, C. (1997). Isolation and characterization of novel iron-oxidizing bacteria that grow at circumneutral pH. *Appl. Environ. Microbiol.* 63, 4784–4792. doi: 10.1128/aem.63.12.4784-4792.1997

Falkowski, P. G., Fenchel, T., and Delong, E. F. (2008). The microbial engines that drive Earth's biogeochemical cycles. *Science* 320, 1034–1039. doi: 10.1126/science.1153213

Ferrari, B. C., Winsley, T. J., Bergquist, P. L., and van Dorst, J. (2012). "Flow cytometry in environmental microbiology: A rapid approach for the isolation of single cells for advanced molecular biology analysis," in *Microbial Systems Biology: Methods and Protocols*, ed. A. Navid (New Jersey, NJ: Humana Press Inc), 3–26. doi: 10.1007/978-1-61779-827-6_1

Fitzsimmons, J. N., John, S. G., Marsay, C. M., Hoffman, C. L., Nicholas, S. L., Toner, B. M., et al. (2017). Iron persistence in a distal hydrothermal plume supported by dissolved-particulate exchange. *Nat. Geosci.* 10, 195–201. doi: 10.1038/ngeo2900

Fortunato, C. S., Butterfield, D. A., Larson, B., Lawrence-Slavas, N., Algar, C. K., Zeigler Allen, L., et al. (2021). Seafloor incubation experiment with deep-sea hydrothermal vent fluid reveals effect of pressure and lag time on autotrophic microbial communities. *Appl. Environ. Microbiol.* 87, e78–e21. doi: 10.1128/AEM.00078-21

Fortunato, C. S., and Huber, J. A. (2016). Coupled RNA-SIP and metatranscriptomics of active chemolithoautotrophic communities at a deep-sea hydrothermal vent. *ISME J.* 10, 1925–1938. doi: 10.1038/ismej.2015.258

Fröhlich, J., and König, H. (2000). New techniques for isolation of single prokaryotic cells. *FEMS Microbiol. Rev.* 24, 567–572. doi: 10.1111/j.1574-6976.2000.tb00558.x

Garel, M., Bonin, P., Martini, S., Guasco, S., Roumagnac, M., Bhairy, N., et al. (2019). Pressure-retaining sampler and high-pressure systems to study deep-sea microbes under *in situ* conditions. *Front. Microbiol.* 10:453. doi: 10.3389/fmicb.2019.00453

Grandy, J. J., Onat, B., Tunnicliffe, V., Butterfield, D. A., and Pawliszyn, J. (2020). Unique solid phase microextraction sampler reveals distinctive biogeochemical profiles among various deep-sea hydrothermal vents. *Sci. Rep.* 10:1360. doi: 10.1038/s41598-020-58418-4

Gros, J., Schmidt, M., Linke, P., Dötsch, S., Triest, J., Martínez-Cabanas, M., et al. (2021). Quantification of dissolved CO_2 plumes at the Goldeneye CO_2-release experiment. *Int. J. Greenhouse Gas Control* 109:103387. doi: 10.1016/j.ijggc.2021.103387

Gutleben, J., Chaib, De Mares, M., van Elsas, J. D., Smidt, H., Overmann, J., et al. (2018). The multi-omics promise in context: from sequence to microbial isolate. *Crit. Rev. Microbiol.* 44, 212–229. doi: 10.1080/1040841X.2017.1332003

Handelsman, J. (2004). Metagenomics: application of genomics to uncultured microorganisms. *Microbiol. Mol. Biol. Rev.* 68, 669–685. doi: 10.1128/MMBR.68.4.669-685.2004

Handelsman, J., Rondon, M. R., Brady, S. F., Clardy, J., and Goodman, R. M. (1998). Molecular biological access to the chemistry of unknown soil microbes: a new frontier for natural products. *Chem. Biol.* 5, R245–R249. doi: 10.1016/s1074-5521(98)90108-9

Hansen, M., and Perner, M. (2015). A novel hydrogen oxidizer amidst the sulfur-oxidizing Thiomicrospira lineage. *ISME J.* 9, 696–707. doi: 10.1038/ismej.2014.173

Homoky, W. B., Weber, T., Berelson, W. M., Conway, T. M., Henderson, G. M., van Hulten, M., et al. (2016). Quantifying trace element and isotope fluxes at the ocean-sediment boundary: a review. *Philos. Trans. Royal Soc. A* 374:20160246. doi: 10.1098/rsta.2016.0246

Hug, L. A., Baker, B. J., Anantharaman, K., Brown, C. T., Probst, A. J., Castelle, C. J., et al. (2016). A new view of the tree of life. *Nat. Microbiol.* 1:16048.

Jebbar, M., Franzetti, B., Girard, E., and Oger, P. (2015). Microbial diversity and adaptation to high hydrostatic pressure in deep-sea hydrothermal vents prokaryotes. *Extremophiles* 19, 721–740. doi: 10.1007/s00792-015-0760-3

Johnson, J., Jain, K., and Madamwar, D. (2017). "Functional metagenomics: exploring nature's gold mine," in *Current Developments in Biotechnology and Bioengineering*, eds P. Gunasekaran, S. Noronha, and A. Pandey (Amsterdam: Elsevier), 27–43.

Kaeberlein, T., Lewis, K., and Epstein, S. S. (2002). Isolating "uncultivable" microorganisms in pure culture in a simulated natural environment. *Science* 296, 1127–1129. doi: 10.1126/science.1070633

Kato, C. (2011). "Cultivation methods for piezophiles," in *Extremophiles Handbook*, ed. K. Horikoshi (Japan: Springer), 719–726. doi: 10.1007/978-4-431-53898-1_34

Kinfu, B. M., Jahnke, M., Janus, M., Besirlioglu, V., Roggenbuck, M., Meurer, R., et al. (2017). Recombinant RNA polymerase from Geobacillus sp. GHH01 as tool for rapid generation of metagenomic RNAs using *in vitro* technologies. *Biotechnol. Bioeng.* 114, 2739–2752. doi: 10.1002/bit.26436

Kononets, M., Tengberg, A., Nilsson, M., Ekeroth, N., Hylén, A., Robertson, E. K., et al. (2021). *In situ* incubations with the Gothenburg benthic chamber landers: applications and quality control. *J. Marin. Syst.* 214:103475. doi: 10.1016/j.jmarsys.2020.103475

Lam, K. N., Cheng, J., Engel, K., Neufeld, J. D., and Charles, T. C. (2015). Current and future resources for functional metagenomics. *Front. Microbiol.* 6:1196. doi: 10.3389/fmicb.2015.01196

LaRowe, D. E., Arndt, S., Bradley, J. A., Burwicz, E., Dale, A. W., and Amend, J. P. (2020). Organic carbon and microbial activity in marine sediments on a global scale throughout the Quaternary. *Geochimica Et Cosmochimica Acta* 286, 227–247. doi: 10.1016/j.gca.2020.07.017

Lessin, G., Artioli, Y., Almroth-Rosell, E., Blackford, J. C., Dale, A. W., Glud, R. N., et al. (2018). Modelling marine sediment biogeochemistry: current knowledge gaps, challenges, and some methodological advice for advancement. *Front. Marin. Sci.* 5:19. doi: 10.3389/fmars.2018.00019

Li, M., Toner, B. M., Baker, B. J., Breier, J. A., Sheik, C. S., and Dick, G. J. (2014). Microbial iron uptake as a mechanism for dispersing iron from deep-sea hydrothermal vents. *Nat. Commun.* 5:3192. doi: 10.1038/ncomms4192

Liang, J., Feng, J. C., Zhang, S., Cai, Y., Yang, Z., Ni, T., et al. (2021). Role of deep-sea equipment in promoting the forefront of studies on life in extreme environments. *iScience* 24:103299. doi: 10.1016/j.isci.2021.103299

Liang, Z. B., and Keeley, A. (2013). Filtration recovery of extracellular DNA from environmental water samples. *Environ. Sci. Technol.* 47, 9324–9331. doi: 10.1021/es401342b

Lloyd, K. G., Steen, A. D., Ladau, J., Yin, J., and Crosby, L. (2018). Phylogenetically novel uncultured microbial cells dominate earth microbiomes. *mSystems* 3, e55–e18. doi: 10.1128/mSystems.00055-18

Longnecker, K., Sievert, S. M., Sylva, S. P., Seewald, J. S., and Kujawinski, E. B. (2018). Dissolved organic carbon compounds in deep-sea hydrothermal vent fluids from the East Pacific Rise at 9°50′N. *Organ. Geochem.* 125, 41–49. doi: 10.1016/j.orggeochem.2018.08.004

Louca, S., Hawley, A. K., Katsev, S., Torres-Beltran, M., Bhatia, M. P., Kheirandish, S., et al. (2016). Integrating biogeochemistry with multiomic sequence information in a model oxygen minimum zone. *Proc. Natl. Acad. Sci. U.S.A.* 113, E5925–E5933. doi: 10.1073/pnas.1602897113

Luther, G. W., Rozan, T. F., Taillefert, M., Nuzzio, D. B., Di Meo, C., Shank, T. M., et al. (2001). Chemical speciation drives hydrothermal vent ecology. *Nature* 410, 813–816. doi: 10.1038/35071069

Martin, W., Baross, J., Kelley, D., and Russell, M. J. (2008). Hydrothermal vents and the origin of life. *Nat. Rev. Microbiol.* 6, 805–814.

Martinez, E., Vi, Dickson, J. D., Perl, S. M., and Barge, L. M. (2019). *Incorporating Microbes into Synthetic Deep-Sea Hydrothermal Vents*. (San Francisco, CA: American Geophysical Union, Fall Meeting).

McDermott, J. M., Sylva, S. P., Ono, S., German, C. R., and Seewald, J. S. (2018). Geochemistry of fluids from Earth's deepest ridge-crest hot-springs: Piccard hydrothermal field, Mid-Cayman Rise. *Geochimica Et Cosmochimica Acta* 228, 95–118. doi: 10.1016/j.gca.2018.01.021

McNichol, J., Sylva, S. P., Thomas, F., Taylor, C. D., Sievert, S. M., and Seewald, J. S. (2016). Assessing microbial processes in deep-sea hydrothermal systems by incubation at *in situ* temperature and pressure. *Deep-Sea Res. Part I* 115, 221–232. doi: 10.1016/j.dsr.2016.06.011

McQuillan, J. S., and Robidart, J. C. (2017). Molecular-biological sensing in aquatic environments: recent developments and emerging capabilities. *Curr. Opin. Biotechnol.* 45, 43–50. doi: 10.1016/j.copbio.2016.11.022

Middelburg, J. J. (2018). Reviews and syntheses: to the bottom of carbon processing at the seafloor. *Biogeosciences* 15, 413–427. doi: 10.5194/bg-15-413-2018

Middelburg, J. J., Vlug, T., and van der Nat, F. J. W. A. (1993). Organic matter mineralization in marine systems. *Glob. Planet. Change* 8, 47–58. doi: 10.1016/0921-8181(93)90062-s

Mital, S., Christie, G., and Dikicioglu, D. (2021). Recombinant expression of insoluble enzymes in *Escherichia coli*: a systematic review of experimental design and its manufacturing implications. *Microb. Cell Fact.* 20:208. doi: 10.1186/s12934-021-01698-w

Miyazaki, J., Makabe, A., Matsui, Y., Ebina, N., Tsutsumi, S., Ishibashi, J., et al. (2017). WHATS-3: an improved flow-through multi-bottle fluid sampler for deep-sea geofluid research. *Front. Earth Sci.* 5:45. doi: 10.3389/feart.2017.00045

Moore, T. S., Mullaugh, K. M., Holyoke, R. R., Madison, A. S., Yucel, M., and Luther, G. W. (2009). Marine chemical technology and sensors for marine waters: potentials and limits. *Annu. Rev. Marin. Sci.* 1, 91–115. doi: 10.1146/annurev.marine.010908.163817

Mowlem, M., Beaton, A., Pascal, R., Schaap, A., Loucaides, S., Monk, S., et al. (2021). Industry partnership: lab on chip chemical sensor technology for ocean observing. *Front. Marin. Sci.* 8:697611. doi: 10.3389/fmars.2021.697611

Oppermann, J., Fischer, P., Silapetere, A., Liepe, B., Rodriguez-Rozada, S., Flores-Uribe, J., et al. (2019). MerMAIDs: a family of metagenomically discovered marine anion-conducting and intensely desensitizing channelrhodopsins. *Nat. Commun.* 10:3315. doi: 10.1038/s41467-019-11322-6

Ottesen, E. A. (2016). Probing the living ocean with ecogenomic sensors. *Curr. Opin. Microbiol.* 31, 132–139. doi: 10.1016/j.mib.2016.03.012

Paulus, E. (2021). Shedding light on deep-sea biodiversity - a highly vulnerable habitat in the face of anthropogenic change. *Front. Marin. Sci.* 8:667048. doi: 10.3389/fmars.2021.667048

Perner, M., Gonnella, G., Hourdez, S., Böhnke, S., Kurtz, S., and Girguis, P. (2013). *In situ* chemistry and microbial community compositions in five deep-sea hydrothermal fluid samples from Irina II in the Logatchev field. *Environ. Microbiol.* 15, 1551–1560. doi: 10.1111/1462-2920.12038

Perner, M., Gonnella, G., Kurtz, S., and LaRoche, J. (2014). Handling temperature bursts reaching 464°C: different microbial strategies in the Sisters Peak hydrothermal chimney. *Appl. Environ. Microbiol.* 80, 4585–4598. doi: 10.1128/AEM.01460-14

Perner, M., Ilmberger, N., Köhler, H. U., Chow, J., and Streit, W. R. (2011b). "Emerging fields in functional metagenomics and its industrial relevance: overcoming limitations and redirecting the search for novel biocatalysts," in *Handbook of Moleculare Microbial Ecology II*, ed. F. J. De Bruijn (New Jersey, NJ: Wiley-Blackwell), 484–485.

Perner, M., Hentscher, M., Rychlik, N., Seifert, R., Strauss, H., and Bach, W. (2011a). Driving forces behind the biotope structures in two low-temperature hydrothermal venting sites on the southern Mid-Atlantic Ridge. *Environ. Microbiol. Rep.* 3, 727–737. doi: 10.1111/j.1758-2229.2011.00291.x

Petersen, J. M., Zielinski, F. U., Pape, T., Seifert, R., Moraru, C., Amann, R., et al. (2011). Hydrogen is an energy source for hydrothermal vent symbioses. *Nature* 476, 176–180. doi: 10.1038/nature10325

Pillot, G., Frouin, E., Pasero, E., Godfroy, A., Combet-Blanc, Y., Davidson, S., et al. (2018). Specific enrichment of hyperthermophilic electroactive *Archaea* from deep-sea hydrothermal vent on electrically conductive support. *Biores. Technol.* 259, 304–311. doi: 10.1016/j.biortech.2018.03.053

Pushkarev, A., Inoue, K., Larom, S., Flores-Uribe, J., Singh, M., Konno, M., et al. (2018). A distinct abundant group of microbial rhodopsins discovered using functional metagenomics. *Nature* 558, 595–599. doi: 10.1038/s41586-018-0225-9

Rabausch, U., Jürgensen, J., Ilmberger, N., Böhnke, S., Fischer, S., Schubach, B., et al. (2013). Functional screening of metagenome and genome libraries for detection of novel flavonoid-modifying enzymes. *Appl. Environ. Microbiol.* 79, 4551–4563. doi: 10.1128/AEM.01077-13

Reed, D. C., Algar, C. K., Huber, J. A., and Dick, G. J. (2014). Gene-centric approach to integrating environmental genomics and biogeochemical models. *Proc. Natl. Acad. Sci. U.S.A.* 111, 1879–1884. doi: 10.1073/pnas.1313713111

Resing, J. A., Sedwick, P. N., German, C. R., Jenkins, W. J., Moffett, J. W., Sohst, B. M., et al. (2015). Basin-scale transport of hydrothermal dissolved metals across the South Pacific Ocean. *Nature* 523, 200–203. doi: 10.1038/nature14577

Reysenbach, A.-L., and Götz, D. (2001). Methods for the study of hydrothermal vent microbes. *Methods Microbiol.* 30, 639–656. doi: 10.1016/s0580-9517(01)30066-1

Rinke, C., Schwientek, P., Sczyrba, A., Ivanova, N. N., Anderson, I. J., Cheng, J. F., et al. (2013). Insights into the phylogeny and coding potential of microbial dark matter. *Nature* 499, 431–437. doi: 10.1038/nature12352

Robidart, J., Callister, S. J., Song, P. F., Nicora, C. D., Wheat, C. G., and Girguis, P. R. (2013). Characterizing Microbial Community and Geochemical Dynamics at Hydrothermal Vents Using Osmotically Driven Continuous Fluid Samplers. *Environ. Sci. Technol.* 47, 4399–4407. doi: 10.1021/es3037302

Sanchez, A. M. (2021). Exploring habitability with artificial hydrothermal vents. *Nat. Rev. Earth Environ.* 2:590. doi: 10.1038/s43017-021-00206-3

Sander, S. G., and Koschinsky, A. (2011). Metal flux from hydrothermal vents increased by organic complexation. *Nat. Geosci.* 4, 145–150. doi: 10.1038/ngeo1088

Sass, K., Güllert, S., Streit, W. R., and Perner, M. (2020). A hydrogen-oxidizing bacterium enriched from the open ocean resembling a symbiont. *Environ. Microbiol. Rep.* 12, 396–405. doi: 10.1111/1758-2229.12847

Sass, K., and Perner, M. (2020). Characterization of two hydrogen-oxidizing *Hydrogenovibrio* strains from Kermadec Volcanic Island Arc hydrothermal vents. *Front. Marin. Sci.* 7:295. doi: 10.3389/fmars.2020.00295

Scholin, C. A., Birch, J., Jensen, S., Marin, R., Massion, E., Pargett, D., et al. (2017). The quest to develop ecogenomic sensores - a 25-year history of the Environmental Sample Processor (ESP) as a case study. *Oceanography* 30, 100–113. doi: 10.5670/oceanog.2017.427

Seewald, J. S., Doherty, K. W., Hammar, T. R., and Liberatore, S. P. (2002). A new gas-tight isobaric sampler for hydrothermal fluids. *Deep-Sea Res. Part I* 49, 189–196. doi: 10.1016/s0967-0637(01)00046-2

Shakya, M., Lo, C. C., and Chain, P. S. G. (2019). Advances and challenges in metatranscriptomic analysis. *Front. Gen.* 10:904. doi: 10.3389/fgene.2019.00904

Sievert, S. M., and Vetriani, C. (2012). Chemoautotrophy at deep-sea vents: past, present, and future. *Oceanography* 25, 218–233. doi: 10.5670/oceanog.2012.21

Simon, C., and Daniel, R. (2011). Metagenomic analyses: past and future trends. *Appl. Environ. Microbiol.* 77, 1153–1161. doi: 10.1128/AEM.02345-10

Somes, C. J., Dale, A. W., Wallmann, K., Scholz, F., Yao, W. X., Oschlies, A., et al. (2021). Constraining global marine iron sources and ligand-mediated scavenging Fluxes With GEOTRACES Dissolved Iron Measurements in an Ocean Biogeochemical Model. *Glob. Biogeochem. Cycles* 35:e2021GB006948.

Stokke, R., Reeves, E. P., Dahle, H., Fedøy, A. E., Viflot, T., Lie Onstad, S., et al. (2020). Tailoring hydrothermal vent biodiversity toward improved biodiscovery using a novel *In situ* enrichment strategy. *Front. Microbiol.* 11:249. doi: 10.3389/fmicb.2020.00249

Sunagawa, S., Coelho, L. P., Chaffron, S., Kultima, J. R., Labadie, K., Salazar, G., et al. (2015). Ocean plankton. Structure and function of the global ocean microbiome. *Science* 348:1261359. doi: 10.1126/science.1261359

Svetlitsky, D., Dagan, T., and Ziv-Ukelson, M. (2020). Discovery of multi-operon colinear syntenic blocks in microbial genomes. *Bioinformatics* 36, 21–29. doi: 10.1093/bioinformatics/btaa503

Taylor, C. D., Edgcomb, V. P., Doherty, K. W., Engstrom, I., Shanahan, T., Pachiadaki, M. G., et al. (2015). Fixation filter, device for the rapid *In situ* preservation of particulate samples. *Deep Sea Res. Part I* 96, 69–79. doi: 10.1016/j.dsr.2014.09.006

Thoms, F., Burmeister, C., Dippner, J. W., Gogina, M., Janas, U., Kendzierska, H., et al. (2018). Impact of macrofaunal communities on the coastal filter function in the Bay of Gdansk, Baltic Sea. *Front. Marin. Sci.* 5:201. doi: 10.3389/fmars.2018.00201

Toner, B. M., Fakra, S. C., Manganini, S. J., Santelli, C. M., Marcus, M. A., Moffett, J., et al. (2009). Preservation of iron(II) by carbon-rich matrices in a hydrothermal plume. *Nat. Geosci.* 2, 197–201. doi: 10.1038/ngeo433

Varaljay, V. A., Satagopan, S., North, J. A., Witte, B., Dourado, M. N., Anantharaman, K., et al. (2016). Functional metagenomic selection of RubisCO from uncultivated bacteria. *Environ. Microbiol.* 18, 1187–1199. doi: 10.1111/1462-2920.13138

Venter, J. C., Remington, K., Heidelberg, J. F., Halpern, A. L., Rusch, D., Eisen, J. A., et al. (2004). Environmental genome shotgun sequencing of the Sargasso Sea. *Science* 304, 66–74. doi: 10.1126/science.1093857

Vonnahme, T. R., Molari, M., Janssen, F., Wenzhofer, F., Haeckel, M., Titschack, J., et al. (2020). Effects of a deep-sea mining experiment on seafloor microbial communities and functions after 26 years. *Sci. Adv.* 6:eaaz5922.

Wang, S., Wu, S. J., Du, M. R., Yang, C. J., and Wang, X. (2020). A new serial sampler for collecting gas-tight samples from seafloor cold seeps and hydrothermal vents. *Deep Sea Res. Part I* 161:103282. doi: 10.1016/j.dsr.2020.103282

Wankel, S. D., Germanovich, L. N., Lilley, M. D., Genc, G., DiPerna, C. J., Bradley, A. S., et al. (2011). Influence of subsurface biosphere on geochemical fluxes from diffuse hydrothermal fluids. *Nat. Geosci.* 4, 461–468. doi: 10.1038/ngeo1183

Wilmes, P., Heintz-Buschart, A., and Bond, P. L. (2015). A decade of metaproteomics: where we stand and what the future holds. *Proteomics* 15, 3409–3417. doi: 10.1002/pmic.201500183

Wu, S. J., Wang, S., and Yang, C. J. (2018). Collection of gas-tight water samples from the bottom of the challenger deep. *J. Atmos. Ocean. Technol.* 35, 837–844. doi: 10.1175/jtech-d-17-0170.1

Yang, C., Xia, Y., Qu, H., Li, A. D., Liu, R., Wang, Y., et al. (2016). Discovery of new cellulases from the metagenome by a metagenomics-guided strategy. *Biotechnol. Biofuels* 9:138. doi: 10.1186/s13068-016-0557-3

Zamkovaya, T., Foster, J. S., de Crécy-Lagard, V., and Conesa, A. (2021). A network approach to elucidate and prioritize microbial dark matter in microbial communities. *ISME J.* 15, 228–244. doi: 10.1038/s41396-020-00777-x

Zeng, X., Alain, K., and Shao, Z. (2021). Microorganisms from deep-sea hydrothermal vents. *Marin. Life Sci. Technol.* 3, 204–230. doi: 10.1007/s42995-020-00086-4

Zeng, X., Zhang, X., Jiang, L., Alain, K., Jebbar, M., and Shao, Z. (2013). Palaeococcus pacificus sp. nov., an archaeon from deep-sea hydrothermal sediment. *Int. J. Syst. Evol. Microbiol.* 63, 2155–2159. doi: 10.1099/ijs.0.044487-0

Zhang, Z., Wu, Y., and Zhang, X.-H. (2018). Cultivation of microbes from the deep-sea environments. *Deep Sea Res. Part II* 155, 34–43. doi: 10.1016/j.dsr2.2017.07.008

Conflict of Interest: The authors declare that the research was conducted in the absence of any commercial or financial relationships that could be construed as a potential conflict of interest.

Publisher's Note: All claims expressed in this article are solely those of the authors and do not necessarily represent those of their affiliated organizations, or those of the publisher, the editors and the reviewers. Any product that may be evaluated in this article, or claim that may be made by its manufacturer, is not guaranteed or endorsed by the publisher.

frontiers | Frontiers in Microbiology

ORIGINAL RESEARCH
published: 16 May 2022
doi: 10.3389/fmicb.2022.844856

Diversity of Microbial Eukaryotes Along the West Antarctic Peninsula in Austral Spring

Jean-David Grattepanche[1], Wade H. Jeffrey[2], Rebecca J. Gast[3] and Robert W. Sanders[1]*

[1] Department of Biology, Temple University, Philadelphia, PA, United States, [2] Center for Environmental Diagnostics and Bioremediation, University of West Florida, Pensacola, FL, United States, [3] Department of Biology, Woods Hole Oceanographic Institution, Pensacola, MA, United States

During a cruise from October to November 2019, along the West Antarctic Peninsula, between 64.32 and 68.37°S, we assessed the diversity and composition of the active microbial eukaryotic community within three size fractions: micro- (> 20 μm), nano- (20–5 μm), and pico-size fractions (5–0.2 μm). The communities and the environmental parameters displayed latitudinal gradients, and we observed a strong similarity in the microbial eukaryotic communities as well as the environmental parameters between the sub-surface and the deep chlorophyll maximum (DCM) depths. Chlorophyll concentrations were low, and the mixed layer was shallow for most of the 17 stations sampled. The richness of the microplankton was higher in Marguerite Bay (our southernmost stations), compared to more northern stations, while the diversity for the nano- and pico-plankton was relatively stable across latitude. The microplankton communities were dominated by autotrophs, mostly diatoms, while mixotrophs (phototrophs-consuming bacteria and kleptoplastidic ciliates, mostly alveolates, and cryptophytes) were the most abundant and active members of the nano- and picoplankton communities. While phototrophy was the dominant trophic mode, heterotrophy (mixotrophy, phagotrophy, and parasitism) tended to increase southward. The samples from Marguerite Bay showed a distinct community with a high diversity of nanoplankton predators, including spirotrich ciliates, and dinoflagellates, while cryptophytes were observed elsewhere. Some lineages were significantly related—either positively or negatively—to ice coverage (e.g., positive for Pelagophyceae, negative for Spirotrichea) and temperature (e.g., positive for Cryptophyceae, negative for Spirotrichea). This suggests that climate changes will have a strong impact on the microbial eukaryotic community.

Keywords: picoplankton, nanoplankton, microplankton, Antarctic protists, high-throughput sequencing, RNA community

OPEN ACCESS

Edited by:
Andreas Teske, University of North Carolina at Chapel Hill, United States

Reviewed by:
Adrian Marchetti, University of North Carolina at Chapel Hill, United States
Thorsten Stoeck, University of Kaiserslautern, Germany

****Correspondence:***
Jean-David Grattepanche
jd.grattepanche@temple.edu

Specialty section:
This article was submitted to Extreme Microbiology, a section of the journal Frontiers in Microbiology

Received: *28 December 2021*
Accepted: *17 March 2022*
Published: *16 May 2022*

Citation:
Grattepanche J-D, Jeffrey WH, Gast RJ and Sanders RW (2022) Diversity of Microbial Eukaryotes Along the West Antarctic Peninsula in Austral Spring. Front. Microbiol. 13:844856. doi: 10.3389/fmicb.2022.844856

INTRODUCTION

The Southern Ocean, although connected to the other oceans, is separated from them by the polar front, which makes it a unique environment with many endemic species (Orsi et al., 1995). During the recent decades, the ice cover of Antarctica has changed dramatically due to climate change (Martinson et al., 2008; Comiso et al., 2017; Schofield et al., 2018; Clem et al., 2020), with a total

increase of 3°C since 1951 and an anthropogenic impact that is not yet clear (Whitehouse et al., 2008; Ducklow et al., 2012; Turner et al., 2016). These changes in ice cover resulted in a release of nutrients and modification of the salinity in the area (Moline et al., 2004), potentially impacting the Antarctic ecosystem, as well as influencing the global climate (Cavanagh et al., 2021; Lin et al., 2021). Within the Southern Ocean, the West Antarctic Peninsula (WAP) is in itself unique, as three circumpolar Antarctic marine ecosystems: the Permanently Open Ocean Zone, the Seasonal Ice Zone, and the Coastal and Continental Shelf Zone, converge (Tréguer and Jacques, 1992) and result in strong environmental gradients that may affect diversity.

Microbial eukaryotes (protists) have a pivotal role in aquatic food webs and, in the Southern Ocean, are an important link between nutrients, bacteria, and higher trophic levels, including krill, penguins, and whales (Hempel, 1985; Hopkins, 1985; Murphy et al., 2007; Saba et al., 2014). Moreover, they can be heterotrophs (nano- and microzooplankton), phototrophs (phytoplankton), and mixotrophs/"mixoplankton" (combining phagotrophy and phototrophy; Stoecker et al., 2016; Leles et al., 2018; Ward, 2019). While an increasing number of studies have looked at the composition of the protists in marine systems, some areas are still notably understudied, including the polar regions (de Vargas et al., 2015; Pernice et al., 2015; Lin et al., 2021).

Over the past several decades, the large-scale sequencing of ribosomal RNA genes from environmental samples has indicated that the diversity of microbial taxa is much higher than expected, with a large number of species forming what has been called the rare biosphere (Sogin et al., 2006). The rare biosphere represents a large diversity of lineages present in the system, which are mostly at low abundance. Many of the sequences observed by DNA and/or RNA sequences have been assigned to lineages such as the SAR clade (Stramenopila, Aveolata, and Rhizaria), which dominates the species richness in the oceans, but a fair number of sequences are still taxonomically unidentified because lineages are not characterized or present in any molecular database (de Vargas et al., 2015; Massana et al., 2015; Grattepanche et al., 2018).

The Antarctic Peninsula region has been significantly impacted by global climate change. In addition to warming ocean temperatures, the seasonal sea ice period has decreased by as much as 3 months (Vaughan et al., 2003; Martinson et al., 2008; Stammerjohn et al., 2012). The phytoplankton community shifts in this region have been attributed to effects of climate change (Montes-Hugo et al., 2009; Brown et al., 2019). Traditionally, diatoms dominated coastal Antarctic Peninsula phytoplankton communities (Schofield et al., 2017), but they are being replaced by a community composed of smaller phytoplankton, particularly cryptophytes (nanophytoplankton) and *Micromonas* (picophytoplankton; Irion et al., 2020; Brown et al., 2021; Trefault et al., 2021). Some cryptophytes and *Micromonas polaris* are phototrophic plankton that consume bacteria, possibly to supplement some lack of macro- and micronutrients (Gonzalez et al., 1993; McKie-Krisberg and Sanders, 2014; Anderson et al., 2018). These changes in the phytoplankton community will not only affect the nutrients available for competing phytoplankters but also for the rest of the food web, including krill and penguins that rely on the phytoplankton directly or indirectly as a food source (Ducklow et al., 2007; Montes-Hugo et al., 2009; Schofield et al., 2010).

Here, we assessed the composition of the active microbial eukaryotic community by targeting ribosomal RNA, with an emphasis on three size fractions—the pico (0.2–5 μm), the nano (5–20 μm), and the micro (>20 μm)—along the Antarctic peninsula as a baseline to understanding continuing climate change. We hypothesized that (1) the SAR lineage (Stramenopiles, Alveolata, and Rhizaria) would be the dominant lineage in the Southern Ocean in terms of diversity and activity, as elsewhere; (2) the community would show a distribution related to the latitude as already observed for some ciliate lineages (tintinnids; Dolan et al., 2016); and, (3) during our sampling season (late austral spring and early summer), the diatoms would be the dominant phytoplankter.

MATERIALS AND METHODS

During a cruise on the Nathaniel B. Palmer from November 6, 2019 to December 9, 2019 (NBP19-10), water samples were collected at the sub-surface (∼1-m depth) and at the deep chlorophyll maximum (DCM, ranging between 14- and 56-m depth) for 17 stations along the Antarctic peninsula (–64.54°; –62.37° to –68.05°; –68.30°; **Figure 1A**) using 12-L Niskin bottles mounted on a CTD rosette. At 3 stations, the surface was sampled with repeated bucket casts. We used bucket samples to find if there were distinct neustonic taxa that differed from the underlying water. Note that some stations were sampled at both the beginning and at the end of the cruise, so impact of time and geographical locations can be deciphered in our analyses.

Environmental Parameters

Conductivity, water temperature, depth, salinity, oxygen, fluorescence, beam transmission, irradiance (PAR), oxygen saturation, time, latitude, and longitude measurements were collected at all casts with a CTD Sea-Bird SBE 9–11 plus V5.1 g, with WET Labs ECO-AFL/FL and C-Star probes. For quantification of chlorophyll a, triplicate samples of 100–250 ml were filtered onto a 25-mm GF/F filter (Whatman, United Kingdom) and frozen at –80°C until extraction. Filters were later extracted in 90% acetone overnight at –20°C, and fluorescence was determined with a Model TD-700 fluorometer (Turner Designs, Sunnyvale, CA, United States). Ice coverage was estimated by the N. B. Palmer crew based on direct observations during the CTD casts; northern stations had free-floating ice floes, while southern stations had pack ice.

Dissolved inorganic nutrient analyses were performed on the filtrates from GF/F filters using colorimetric methods with an Autoanalyzer. For each dissolved organic nutrient, a standard curve was calculated to determine the concentration of the nutrients in each sample. Dissolved inorganic phosphate (DIP) was analyzed as in Parsons et al. (1984) using a composite reagent, containing molybdic acid, ascorbic acid, and trivalent antimony, turning blue in the presence of DIP. For the quantification of NH_4^+, the method described in

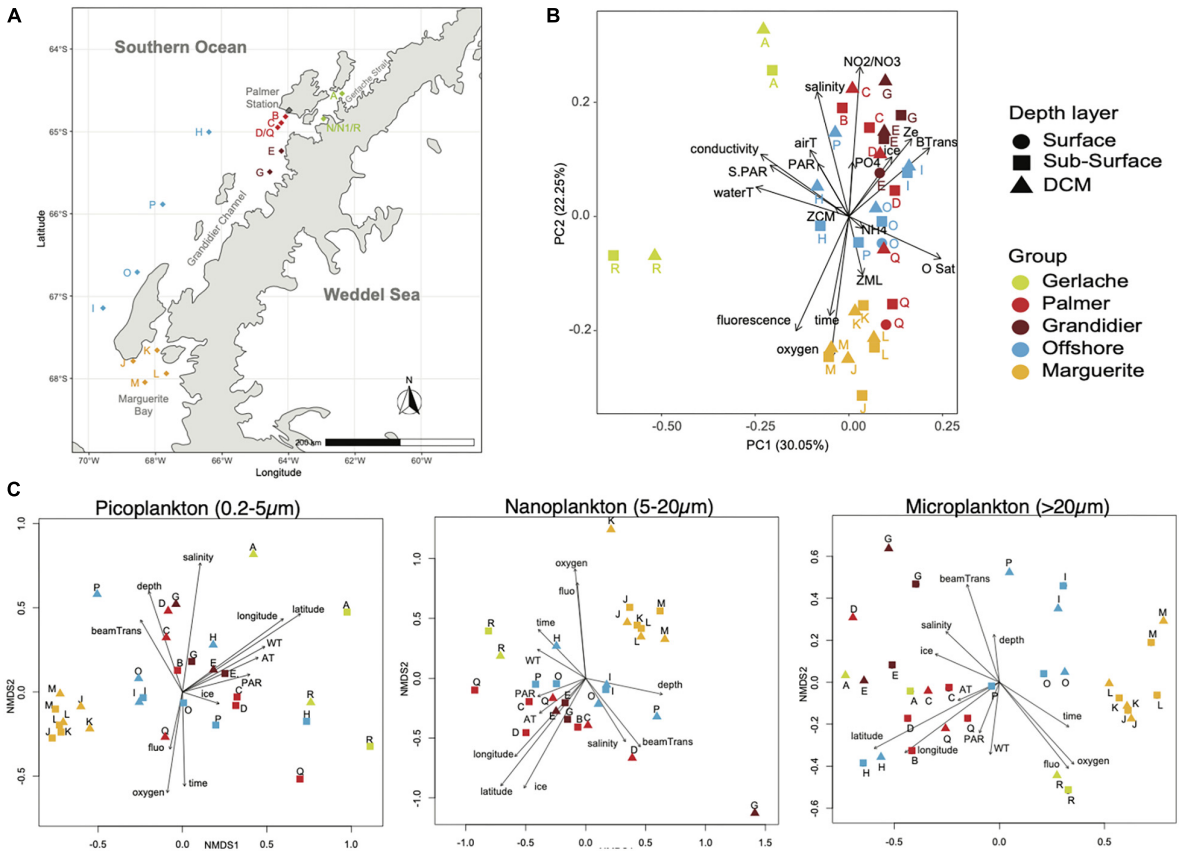

FIGURE 1 | Sample distribution: **(A)** A chart of stations sampled during the NBP19-10 cruise. **(B)** Principal component analysis of environmental parameters showing five groups of samples related to geographical location. **(C)** Non-metric multidimensional scaling analysis of micro-, nano-, and pico-plankton, showing a similar pattern as the environmental parameter PCA.

Holmes et al. (1999), which uses orthophthaldialdehyde (OPA) fluorescing in the presence of ammonium, was used. The concentration of NO^{3-} + NO^{2-} was determined using an acidic vanadium-(III)-solution and quantified by Griess–Ilosvay reaction, resulting in a purplish solution (Schnetger and Lehners, 2014). The sum of NH_4^+, NO^{3-}, and NO^{2-} is also reported as dissolved inorganic nitrogen (DIN).

Bacterial production was performed on water samples using ^{3}H-leucine (Smith and Azam, 1992). ^{3}H-leucine (120 Ci mmol^{-1}, Moravec Inc., Brea, CA) was added to six 1-ml samples in microfuge tubes to a final concentration of 10 nM. One sample was immediately killed with trichloroacetic acid (TCA) and served as the killed control. The samples were immediately capped, gently mixed, and incubated in the dark at *in situ* temperatures for 4 h. Incubations were terminated by the addition of TCA to a final concentration of 5%. The samples were processed using the microcentrifuge tube method of Smith and Azam (1992) and incorporation determined by liquid scintillation counting. Phytoplankton production was determined in 24-h incubations conducted at *in situ* temperature in deck incubators on the ship under 50% neutral density screens (Matrai et al., 1995). Six 16-ml seawater samples were placed in polyethylene bags (WhirlPak). ^{14}C-Bicarbonate (Moravec Inc., Brea, CA) was added to a final concentration of 2.0 μCi ml^{-1}. Three samples were then placed in opaque black plastic bags. The remaining three samples were placed inside a 50% neutral density screen envelope and all samples placed in a flowing seawater bath on the deck of the ship for 24 h. The samples were then retrieved, filtered onto 25-mm diameter GF/F filters, which were then rinsed with 10 ml of filtered seawater. The filters were then placed in liquid scintillation vials and acidified overnight after the addition of 100 μl of 20% HCl. Liquid scintillation cocktail (Ecolume) was added to each vial and fixed carbon determined by liquid scintillation counting.

Nucleic Acid Samples

For each layer (surface and DCM), 20 L of seawater was serially filtered through a 20-μm nylon mesh and a 47-mm diameter/5-μm porosity nitrocellulose filter, and then 3 L of this < 5-μm seawater was filtered on a 47-mm diameter/porosity of 0.22-μm nitrocellulose filters. This resulted in three size fractions: > 20 μm referred as microplankton; 5–20 μm as nanoplankton and 0.22–5 μm as picoplankton for simplifying the notation (the classic limit between nano- and picoplankton is set at 3 μm). The filters were transferred to 1.5-ml centrifuge tubes and stored at −80°C until extraction.

While both DNA and RNA were simultaneously extracted and purified using an all prep DNA/RNA kit (Qiagen, Germany), only RNA was used in this study. We decided to use RNA to assess the plankton community because (1) DNA can be misleading as cysts, and dead cells can still exhibit DNA, and there is the potential presence of eDNA; (2) RNA reveals the most active organisms and, potentially, the ones having the biggest ecological impact. The use of RNA in the present study has the advantage of avoiding the contamination by dead cells and other eDNA particles. The presence of rRNA is also related to the metabolic activity of the community. RNA and DNA can both, therefore, be problematic when attempting to relate RNA- or DNA-based marker genes with abundance of cells. By utilizing RNA, this study focuses primarily on the active members of the community. Other possible biases of RNA include faster degradation of RNA compared to DNA (Cristescu, 2019) and errors introduced during reverse transcription. Some studies showed that (1) diversity estimates using SSU rRNA tend to be lower than diversity estimate using the SSU rRNA gene (i.e., DNA; Lanzén et al., 2011), (2) DNA estimates can miss some taxa detected only by RNA (Baldrian et al., 2012), and (3) there is high similarity between rDNA and rRNA in terms of number of OTUs (Cordier et al., 2022) but with some variation in read numbers (Rachik et al., 2018). This study, as others that have defined community composition based solely on molecular molecules (DNA or RNA), should be confirmed using an integrative approach, combining microscopy and/or physiology to better understand the ecology of microbial eukaryotes (Caron and Hu, 2019; Keeling, 2019).

A portion of the RNA was reverse transcribed into cDNA using Superscript III and random hexamers (Invitrogen, CA, United States). Amplicon generation used the cDNA samples, the Q5 polymerase (New England Biolabs, MA, United States), and primers targeting the hypervariable region V4 of the eukaryotic small subunit ribosomal gene (TAReuk454FWD1: 5′-CCA GCA SCY GCG GTA ATT CC-3′, TAReukREV3: 5′-ACT TTC GTT CTT GAT YRA-3′; Stoeck et al., 2010) with adaptors for Illumina sequencing requested by the University of Rhode Island genomics and sequencing center in order to perform Illumina MiSeq sequencing (2 × 300 cycles). The biases of this primer set are described and discussed in Hugerth et al. (2014), Piredda et al. (2017), and Clarke et al. (2021), which include difficulty in amplifying some taxonomic groups such as Amoebozoa and Foraminifera, and the current length limit of Illumina sequencing technology. However, each primer set will have some bias, for example, based on an *in silico* test using the Silva dataset, the V4 primers modified from Piredda et al. (2017) tend to be biased against Haptophyta, Excavata, Discoba, Cercozoa, and Retaria. We decided to use this primer set as the V4 region is more taxonomically informative than other hypervariable regions (Hugerth et al., 2014), and we used the original primer set described by Stoeck et al. (2010) in order to be able to compare our data to published works (Massana et al., 2015; Swalethorp et al., 2019; Giner et al., 2020). To reduce the bias due to amplification, each PCR was carried out in triplicate and pooled before being sent to the sequencing center (Lahr and Katz, 2009).

Bioinformatics

To analyze the amplicon data, two datasets were considered: the paired-end read (P-E) and the forward read (FWD) datasets. The first is more sensible for assigning taxonomy as DNA fragments are longer but is more subject to issues related to the pair-end process (reverse reads of poor quality, an overlapping region that is too short, variable fragment size). The forward read dataset alone could possibly access a more "complete" community. The datasets were analyzed as previously described (Sisson et al., 2018; Grattepanche et al., 2019). In summary, paired-end reads were merged using BBMerge (Bushnell et al., 2017), and then both datasets were dereplicated using Vsearch (Rognes et al., 2016). Reads with unknown characters (N) were discarded, and OTUs were picked using SWARM2 and a distance of 1 (Mahe et al., 2015). We compared the diversity assessment using our current method, which involved SWARM to a pipeline using DADA2 (Callahan et al., 2016) in a previous paper (Grattepanche and Katz, 2020). In summary, both approaches were similar in the diversity assessment. However, we observed that some reads were discarded by DADA2 and considered as noise, while many others were kept (overestimation of diversity). Another big difference is that DADA2 analyzes each sample independently, while SWARM analyzes all the samples at once, which allows consideration as outliers if they appear in multiple samples. We decided to use SWARM to better control the OTU library, which includes correction of PCR and sequencing errors. Chimeras were identified using Uchime-*de novo* (Edgar et al., 2011) implemented in Vsearch and removed; singletons (OTU with only 1 read) and contaminants were discarded using local alignment water implemented in EMBOSS (Rice et al., 2000) and a cutoff similarity of 50%. The resulting sequence file was aligned against a guided alignment of PR2 data (Guillou et al., 2012). Phylogenic trees were built to identify non-eukaryotic OTUs for removal using RAxML-EPA (Stamatakis, 2014; Barbera et al., 2019). These phylogenies and a similarity approach (assignment by similarity using usearch_global implemented in Vsearch) were used to assign the taxonomy to each OTU, including at least 3 taxonomic ranks (e.g., SAR, Stramenopila, Ochrophyta or Opisthokonta, Choanoflagellata, Acanthoecida). Alignments are visually inspected in case of disagreement between the two methods of taxonomic assignment.

Statistics

Principal component analysis on the environmental data was performed to identify distribution patterns (by a depth layer, size, geographical location, related to nutrients, etc.), and the data interpolating empirical orthogonal function were used to extrapolate missing data (Beckers and Rixen, 2003).

To compare the community composition across our samples from different size fractions, stations, and depth layers, each sample was rarefied at 25,000 reads for the paired-end read (P-E) dataset. The same analyses were performed for the forward read (FWD) dataset, but without rarefaction to avoid some bias (e.g., introduction of artificial variation) and using proportions instead of number of reads (McMurdie and Holmes, 2014).

Non-metric multidimensional scaling (NMDS) with the Fast Unifrac dissimilarity index (Hamady et al., 2009) was used to assess the similarity between samples with the phyloseq and phyloseqCompanion packages (McMurdie and Holmes, 2013; Stagaman, 2019) implemented in R (R Core Team, 2021). To confirm the community group observed, ANOVA was performed using adonis2 implemented in the vegan package (Oksanen et al., 2020) from R, in which the data were randomly permuted 999 times, and the best model selected based on lowest Akaike information criterion corrected. The function envfit implemented in the vegan package was used to relate the axis of our ordination to environmental factors.

RESULTS

Environmental Pattern

The stations sampled varied in depth, ranging from 135 to 1,400 m, with the shallower depths near shore across the latitudinal range. The salinity, temperature, and oxygen ranged from 33.17 to 34.20 PSU, 1.8–0.9°C, and 5.9–7.9 ml L^{-1}, respectively. The chlorophyll a concentration ranged from 0.1 to 3.25 mg m^{-3} (**Table 1**). The depth of the mixed layer (ZML) and the depth of the deep chlorophyll maximum (ZCM) showed a negative relationship with the latitude and longitude (**Supplementary Figure 1A**), indicating shallower mixed layer and deep chlorophyll maximum depths in the northern stations, compared to the southern (**Table 1**). Overall, temperatures (air and water), ice coverage (% of floating ice observed at the sea surface), conductivity, and nutrients decreased significantly going southward (**Table 1** and **Supplementary Figure 1A**).

To have a better understanding of how the environmental parameters were distributed across "habitats," principal component analysis was performed using salinity, conductivity, water, and air temperature, dissolved oxygen, DO saturation, fluorescence, beam transmission, maximal depth, sampling depth, ice coverage, PAR and surface PAR, depths of the deep chlorophyll maximum of the euphotic zone and of the mixed layer (**Figure 1B**). The first two axes of the PCA explain more than 47% of the variability in our dataset. Overall, no clear distinction between the three depth layers sampled was observed: surface (sampled with a bucket), sub-surface (1 m, sampled with the CTD-rosette), and DCM samples, because the different depth layers for the same station tend to cluster close to each other (**Figure 1B**). Five groups were identified from the analysis of environmental parameters that related to their geographical location: a southern group located in Marguerite Bay (MB hereafter), a northern group located in Gerlache Strait (GS hereafter), two middle groups situated between Grandidier Channel (GC) and Anvers Island, where the USAP Palmer station is located (PS hereafter) and, lastly, an offshore group (OFF hereafter).

The GS group is composed of samples with higher conductivity and temperature, and, in some cases, a higher PAR. This group of samples represented a shallower mixed layer.

PS and GC groups are composed of stations with a deeper photic zone, a higher beam transmission, a lower fluorescence, and more extensive ice coverage. Lower bacterial abundance and productivity were observed for these groups (**Table 1**). The PS stations also showed the highest NH_4^+ concentration (**Table 1**).

The OFF group is composed of stations with higher oxygen saturation that tend to have a deeper mixed layer and a deeper chlorophyll maximum depth, while the PAR is lower (**Table 1**).

The MB stations also had higher oxygen concentrations and a deeper mixed layer. The MB stations also presented the lowest concentration of nitrite/nitrate and high concentration of chlorophyll (**Table 1**).

Overall Community Composition

Richness, Alpha Diversity, and Reads Number

Overall, the eukaryotic community, assessed from 18S rRNA, was composed of 200,760 OTUs from almost 3.8 million reads in the dataset composed of OTUs with paired-end reads (P-E reads hereafter; **Supplementary Dataset 1**). Of these OTUs, nearly 64% were present in only one sample and accounted for less than 4% of the paired-end reads. Conversely, only 2 OTUs (i.e., 0.001% of the OTUs), which encompassed 10% of the paired-end reads (386,817 P-E reads), were observed in all the samples (location, depth, and size fractions). The second dataset, which is composed of only forward reads (FWD reads hereafter; **Supplementary Dataset 2**), was used to assess the bias related to length of the sequence and issues with paired-end assembling. This dataset is composed of 87,214 OTUs, for a total of almost 3.5 million FWD reads. Overall, this dataset showed the same trend with a large number of OTUs observed in only 1 sample (29,891 OTUs, i.e., 34% of the OTUs and 64,704 FWD reads, i.e., almost 2% of FWD reads), and 5 OTUs observed in all the samples, representing almost 15% of the FWD reads (525,160 FWD reads).

To look at the distribution within the samples, stations, depth layers, and size fractions, only OTUs with at least 100 reads are considered in our subsequent analyses (labeled as abundant OTUs hereafter; **Supplementary Dataset 3**), and the samples were rarefied at 25,000 reads, which represented 1,857 abundant and active OTUs for more than 2 million paired-end reads. Each sample was represented by an average of 574 abundant OTUs (from 333 to 943 OTUs). The surface samples had an average of 588 abundant OTUs (from 333 to 790; 38 samples), and the DCM samples had 558 OTUs (between 375 and 943; 39 samples). Only a few OTUs showed a clear relationship for a single depth layer (1 and 9 abundant OTUs representing 40 and 496 reads for surface and DCM layers, respectively). Even considering a cutoff (i.e., if 95% of the reads for the OTU are observed in one depth layer, then the OTUs are considered as specific to this depth layer only, the 5% representing potential bias in the filtration or in the molecular steps), this trend is persistent (4 and 24 abundant OTUs representing 298 and 8,896 reads for surface and DCM layers, respectively). This suggests that most taxa are not restricted to a sampling depth but are active across layers at a given station during our cruise.

Size Distribution

The diversity was then examined within each size fraction. The nano-size fractions tended to have higher richness (an average of 672 and 656 abundant OTUs for surface and DCM layers,

TABLE 1 | Mean (standard deviation) of environmental parameters observed during the austral spring 2019 in different regions of the WAP.

						DCM					Surface				
	Gerlache	**Palmer**	**Grandidier**	**Offshore**	**Marguerite**	**Gerlache**	**Palmer**	**Grandidier**	**Offshore**	**Marguerite**	**Gerlache**	**Palmer**	**Grandidier**	**Offshore**	**Marguerite**
ZML (m)	18.81 ± 4.93	13.12 ± 1.73	16.24 ± 2.17	30.58 ± 18.81	35.64 ± 5.75										
Ze (m)	39.94 ± 9.39	52.1 ± 5.52	63.16 ± 6.51	57.2 ± 14.84	43.56 ± 4.91										
ZCM (m)	16.5 ± 11.07	17.2 ± 15.32	7.72 ± 1.08	28.38 ± 11.82	23.51 ± 16.25										
Bottom (m)	437.67 ± 234.24	1,156 ± 343.05	175 ± 0	541.11 ± 100.46	427.25 ± 253.8										
Ice (%)	3.33 ± 5.16	92.5 ± 4.63	70 ± 0	42.22 ± 44.1	2.5 ± 4.63										
Air T (oC)	0.6 ± 0.91	−1.44 ± 0.11	−1.32 ± 0.16	−1.39 ± 0.17	−3.05 ± 3.12										
Surf_PAR	716.79 ± 529.61	352.15 ± 255.08	108.22 ± 25.33	451.46 ± 291.97	219.41 ± 124.77										
Depth (m)	11.88 ± 17.33	14.48 ± 17.59	10.5 ± 14.78	15.84 ± 20	18.93 ± 19.01	22.77 ± 19.88	32.01 ± 16.46	24.75 ± 14	33.91 ± 16.81	35.89 ± 8.72	0.99 ± 0	3.96 ± 6.1	0.99 ± 0	1.39 ± 0.54	1.98 ± 0.81
Watert (oC)	0.14 ± 0.57	−1.59 ± 0.16	−1.46 ± 0.11	−1.63 ± 0.22	−1.59 ± 0.12	0.03 ± 0.38	−1.51 ± 0.15	−1.42 ± 0.03	−1.58 ± 0.27	−1.57 ± 0.14	0.26 ± 0.79	−1.64 ± 0.16	−1.49 ± 0.14	−1.67 ± 0.2	−1.62 ± 0.11
Conductivity (mS cm^{-1})	28.43 ± 0.43	26.68 ± 0.32	26.88 ± 0.1	26.81 ± 0.24	26.63 ± 0.13	28.4 ± 0.29	26.86 ± 0.28	26.96 ± 0.12	26.93 ± 0.24	26.67 ± 0.15	28.47 ± 0.61	26.57 ± 0.32	26.83 ± 0.07	26.71 ± 0.2	26.58 ± 0.11
Salinity (PSU)	34.03 ± 0.16	33.6 ± 0.32	33.73 ± 0.12	33.83 ± 0.14	33.53 ± 0.04	34.1 ± 0.17	33.75 ± 0.29	33.79 ± 0.18	33.92 ± 0.06	33.54 ± 0.04	33.95 ± 0.15	33.51 ± 0.33	33.7 ± 0.07	33.75 ± 0.15	33.51 ± 0.04
PAR	252.79 ± 393.62	213.09 ± 322.5	34.2 ± 25.94	67.35 ± 62.8	30.97 ± 31.8	18.15 ± 14.21	17.84 ± 17.95	7.17 ± 4.37	7.67 ± 8.23	2.27 ± 2.69	487.42 ± 471.15	330.23 ± 368.93	52.21 ± 10.92	115.09 ± 37.77	59.66 ± 12.52
BeamTrans (%)	92.37 ± 5.59	97.96 ± 1.44	98.75 ± 0.26	98.27 ± 0.91	96.58 ± 0.86	93.02 ± 5.29	98.54 ± 1.1	98.83 ± 0.36	98.57 ± 0.76	96.67 ± 0.86	91.72 ± 6.99	97.61 ± 1.62	98.69 ± 0.24	98.04 ± 1.04	96.5 ± 0.98
NH_4^+ (μM)	1.26 ± 0.07	1.44 ± 0.06	1.29 ± 0.05	1.28 ± 0.07	1.29 ± 0.01	1.25 ± 0.04	1.4 ± 0.07	1.27 ± 0.06	1.25 ± 0.04	1.29 ± 0.01	1.27 ± 0.1	1.47 ± 0.01	1.32 ± 0.02	1.31 ± 0.09	1.29 ± 0.02
NO_2^-/NO_3^- (μM)	29.32 ± 1.67	29.75 ± 1.71	30.55 ± 0.3	29.1 ± 0.83	26.08 ± 0.73	29.85 ± 1.08	30.24 ± 1.64	30.6 ± 0.13	29.44 ± 0.85	26.49 ± 0.9	28.78 ± 2.22	29.26 ± 2.27	30.51 ± 0.5	28.77 ± 0.76	25.68 ± 0.15
PO_4^{3-} (μM)	3.12 ± 0.15	3.18 ± 0.15	3.13 ± 0.13	3.12 ± 0.18	2.93 ± 0.17	3.17 ± 0.11	3.19 ± 0.16	3.21 ± 0.06	3.24 ± 0.14	2.96 ± 0.09	3.06 ± 0.18	3.17 ± 0.19	3.05 ± 0.16	3 ± 0.11	2.9 ± 0.24
oxygen (mL L^{-1})	6.87 ± 0.65	7.07 ± 0.53	6.46 ± 0.06	7.31 ± 0.36	7.71 ± 0.18	6.63 ± 0.69	7.07 ± 0.28	6.4 ± 0.05	7.2 ± 0.43	7.63 ± 0.17	7.12 ± 0.62	7.07 ± 0.68	6.5 ± 0.02	7.4 ± 0.32	7.79 ± 0.17
Oxygen Saturation (mL L^{-1})	8.04 ± 0.11	8.44 ± 0.05	8.4 ± 0.02	8.43 ± 0.05	8.44 ± 0.03	8.05 ± 0.08	8.41 ± 0.04	8.39 ± 0.01	8.42 ± 0.06	8.44 ± 0.03	8.02 ± 0.16	8.45 ± 0.05	8.41 ± 0.03	8.45 ± 0.05	8.45 ± 0.03
Fluorescence (mg m^{-3})	1.65 ± 1.25	0.62 ± 0.45	0.33 ± 0.14	0.41 ± 0.24	1.68 ± 0.6	2.19 ± 1.51	0.6 ± 0.52	0.33 ± 0.21	0.47 ± 0.31	1.92 ± 0.63	1.11 ± 0.85	0.63 ± 0.46	0.34 ± 0.14	0.35 ± 0.18	1.43 ± 0.53
Chlorophyll a (mg m^{-3})	1.53 ± 1.02	0.73 ± 0.42	0.28 ± 0.13	0.35 ± 0.16	1.11 ± 0.23	1.29 ± 0.7	0.5 ± 0.39	0.22 ± 0.16	0.3 ± 0.12	1.05 ± 0.15	1.77 ± 1.39	0.89 ± 0.42	0.32 ± 0.11	0.38 ± 0.19	1.17 ± 0.31
Primary production (μgC L^{-1} d^{-1})	14.54 ± 0.54	4.8 ± 4.15	1.16 ± 0.69	2.07 ± 1.26	5.07 ± 1.31	2.1 ± 1.24	0.92 ± 0.8	2.14 ± 2	4.27 ± 1.1		6.6 ± 4.64	1.33 ± 0.74	2.01 ± 0.71	5.87 ± 1.05	
Bacteria (10^8 L^{-1})	1.97 ± 0.6	1.68 ± 0.45	1.03 ± 0.16	2.08 ± 0.67	1.52 ± 0.46	2.11 ± 0.74	1.59 ± 0.05	1.17 ± 0.08	1.85 ± 0.91	1.53 ± 0.46	1.84 ± 0.67	1.75 ± 0.62	0.94 ± 0.14	2.24 ± 0.52	1.5 ± 0.53
Bacterial production (μgC L^{-1} d^{-1})	6.97 ± 3.64	7.2 ± 4.99	1.92 ± 1.04	3.36 ± 2.52	7.42 ± 1.78	6.85 ± 4.35	6.26 ± 8	1.44 ± 1.17	2.03 ± 1.53	6.98 ± 2.44	7.08 ± 3.76	7.76 ± 3.25	2.24 ± 1.05	4.43 ± 2.78	7.86 ± 0.96
Richness	964 ± 564	1,043 ± 94	1,179 ± 543	1,132 ± 147	937 ± 86	1,031 ± 602	1,061 ± 60	1,131 ± 233	1,062 ± 185	970 ± 111	897 ± 653	1,032 ± 116	1,227 ± 710	1,187 ± 95	905 ± 47
Chao1 index	1,536 ± 904	1,616 ± 195	1,945 ± 902	1,762 ± 226	1,462 ± 126	1,621 ± 980	1,636 ± 21	1,818 ± 402	1,721 ± 340	1,506 ± 120	1,450 ± 1,036	1,605 ± 256	2,071 ± 1,196	1,795 ± 111	1,418 ± 132
Shannon index	3.25 ± 1.78	3.56 ± 0.21	3.51 ± 1.59	3.74 ± 0.37	3.12 ± 0.24	3.47 ± 2	3.58 ± 0.29	3.46 ± 0.45	3.48 ± 0.3	3.13 ± 0.35	3.04 ± 1.95	3.56 ± 0.18	3.56 ± 2.06	3.96 ± 0.29	3.11 ± 0.1
pico.Richness	964 ± 564	1,043 ± 94	1,179 ± 543	1,132 ± 147	937 ± 86	1,031 ± 602	1,061 ± 60	1,131 ± 233	1,062 ± 185	970 ± 111	897 ± 653	1,032 ± 116	1,227 ± 710	1,187 ± 95	905 ± 47
nano.Richness	966 ± 499	1,090 ± 261	1,133 ± 676	1,381 ± 496	1,327 ± 157	1,004 ± 580	1,150 ± 366	921 ± 789	1,320 ± 142	1,311 ± 208	928 ± 536	1,054 ± 218	1,344 ± 777	1,442 ± 680	1,343 ± 117
micro.Richness	697 ± 395	703 ± 26	643 ± 342	1,075 ± 378	980 ± 132	606 ± 378	707 ± 9	572 ± 170	1,088 ± 377	966 ± 184	788 ± 485	701 ± 34	715 ± 462	1,064 ± 423	995 ± 77

ZML = mixed layer depth, ZML_T estimated using temperature, ZML_TS using temperature and salinity, and ZML_TSP using temperature, salinity, and pressure. Ze = depth of the (eu)photic zone, ZCM = depth of chlorophyll maximum, bottom = maximum depth, time is Julian day,% ice is the estimated percentage of ice coverage, airT = air temperature, surfPAR = surface photo-active radiation, waterT = water temperature, beamTrans = beam transmission.

respectively), while the pico-size fractions tended to show lower richness (an average of 530 and 519 abundant OTUs for surface and DCM layers, respectively; **Supplementary Figure 2A**). At least 12% of the abundant OTUs were specific to a size fraction and represented less than 3% of the reads (i.e., 10.2, 0.3, and 1.6% of the abundant OTUs were specific to the micro-, nano-, and pico-size fractions, respectively). Considering the same cutoff as before (i.e., 95% of the reads), almost 40% of the abundant OTUs for a third of the reads showed a clear size fraction signature, with 28, 5, and 6% of the abundant OTUs representing 27, 2, and 5% of the reads that were classified as specific to the micro-, nano-, and pico-size fractions, respectively. This trend is also consistent when grouping OTUs in morphospecies (based on assignment to known taxa; **Supplementary Figure 2B**). This suggests that the taxa do not tend to vary in their size distribution, especially for the micro-size fraction. It is interesting to note that only 14 OTUs (for a total of 1,857 abundant OTUs), representing 6,089 reads (out of more than 2 million reads), were present in both the micro- and pico-size fractions, suggesting that our filtration methods and a molecular approach were appropriate, and/or that size disjunction within microbial eukaryotes is rare.

Species Composition

Overall, diatoms dominated the micro-size fractions, while dinoflagellates, ciliates, diatoms, and cryptophytes dominated the nano- and pico-size fractions assessed from 18S rRNA (**Figure 2A** and **Supplementary Figure 3A**). Other groups were also present but in lower proportions, and included Haptophyta, Chlorophyta, Opalozoa, Picozoa, Pseudofungi, Sagenista lineages, and the clade named Opisthokonta_X in the PR2 database (Guillou et al., 2012). Our OTUs showed similarity to 1,139 morphospecies reported in our database, with 20% of these taxa observed in at least 50% of the samples, and 14 taxa in all the samples (taxa can be represented by multiple OTUs). The SAR clade [Stramenopiles (representing 37% of the reads), Alveolata (31%) and Rhizaria (< 1%)] was the dominant group in our samples with 867 morphospecies (76% of the morphospecies) and 68% of the FWD reads. The diatoms had the most taxa identified with 296 taxa, followed by 276 dinoflagellate and 139 ciliate taxa. Within the dominant taxa, we observed *Corethron inerme* (Stramenopiles), *Heterocapsa rotundata* (Dinoflagellata), *Prorocentrum* sp. (Dinoflagellata), *Geminigera cryophila* (Cryptophyta), *Porosira pseudodenticulata* (Stramenopiles), *Pelagomona scalceolata* (Stramenopiles), *Strombidium caudispina* (Ciliophora), *Phaeocystis antarctica* (Haptophyta), and *Micromonas polaris* (Chlorophyta), each representing more than 1% of the total read number. Unsurprisingly, more than 20% of the reads were represented by uncharacterized OTUs (low similarity to known sequences in our database). No foraminifera were detected using our 18S rRNA primer set, while some were observed using a binocular microscope during the samplings.

Community Pattern

Geographical Distribution

Overall, the diversity is relatively constant across latitude, with a slight increase in the samples collected in Marguerite Bay (MB), especially for the micro- and the nanoplankton (**Supplementary Figure 2**). Alpha diversity assessed by richness (number of OTUs), Shannon or Chao1 indices, using OTUs or morphospecies showed the same trend: higher alpha diversity for the samples collected in Marguerite Bay. This higher diversity for the MB group is particularly marked when using Shannon index, indicating a more diverse community, with an even distribution of abundance (as estimated by the number of reads). The alpha diversity estimated using OTU number and Chao1 index was generally stable for the surface (bucket), sub-surface, and DCM layers and for the three size fractions (**Supplementary Figure 2A**). This suggests that the total number of OTUs (including the missing ones as estimated by the Chao1 diversity index) for each sample is very similar. While the numbers tend to be lower when considering the morphospecies, we observed the same trend, i.e., higher diversity in the MB group, especially for the microplankton (**Supplementary Figure 2B**). The picoplankton diversity was relatively stable whatever the station or depth layer and tended to slightly decrease with time [from our first station (A) to our last station (R)]. As previously mentioned, the cruise track doubled back on itself so that some of the later stations were geographically close to the earliest stations.

The non-metric multidimensional scaling (NMDS) with the Fast Unifrac dissimilarity index showed that the microbial eukaryotic community, assessed from 18S rRNA, was strongly impacted by the environmental parameters (**Figure 1C**). However, the biggest factor differentiating the protist assemblage was size fraction. In fact, using permutational multivariate ANOVA of distance matrices (adonis), the size significantly explains 22% of the variance of our communities (**Supplementary Table 1**). Then, the size, in conjunction with the groups observed with our environmental parameters, explains another 12% of the variance, while the groups alone are responsible for 10% of the variance within our communities (**Supplementary Table 1**). So, almost 45% of the variance of our community is explained by the size fraction and its location (i.e., community groups match the environmental groups).

The NMDS and envfit analyses were performed independently for each size fraction. The distribution of the picoplankton was related to the location (longitude and latitude), the depth of sampling, salinity, oxygen concentration, and, to the date of sample collection (**Figure 1C** and **Supplementary Table 1A**). The nanoplankton distribution was significantly associated with the location (longitude and latitude), the percentage of ice coverage and with the oxygen concentration (**Figure 1C** and **Supplementary Table 1A**). The distribution of the microplankton was related to the location (longitude and latitude), oxygen concentration, fluorescence (proxy for the phytoplankton biomass), and to the beam transmission (proxy for the number of particles in the water column; **Figure 1C** and **Supplementary Table 1A**).

Some lineages were significantly related—either positively or negatively—to environmental parameters (**Supplementary Table 1**). Some lineages showed a latitudinal gradient such as the Cryptophyceae (decrease in proportion southward) and spirotrich and other ciliates (increase southward; **Supplementary Figure 1B** and **Figure 2B**). These relationships can also

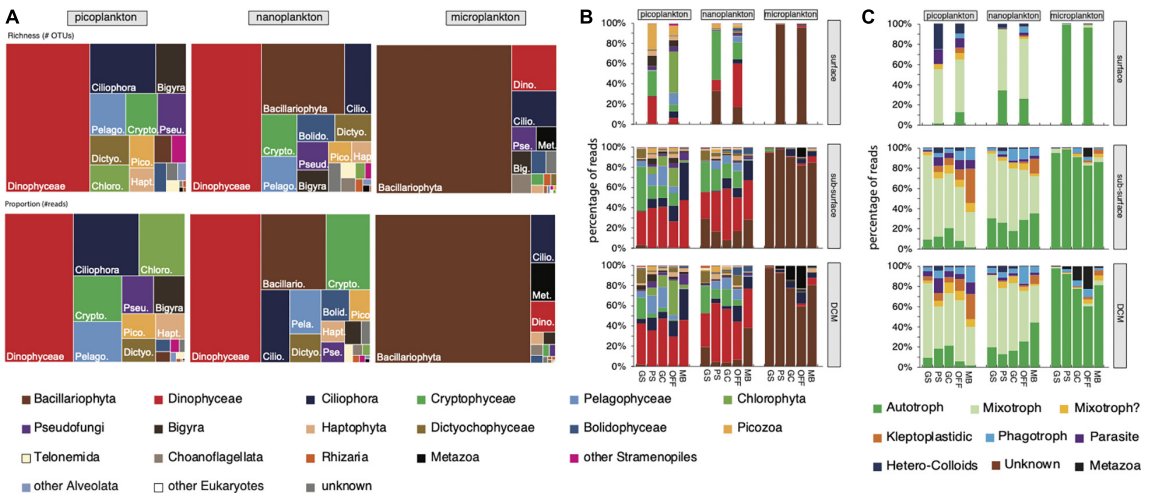

FIGURE 2 | Distribution of **(A)** lineages per size fraction, and **(B)** lineages and **(C)** trophic mode by size fraction, depth and group, showing the distinct composition of micro-, nano-, and picoplankton and the pattern related to the geographical location. Surface and sub-surface samples showed a different distribution, while subsurface and DCM samples shared a more comparable composition. **(B,C)** Bar graphs used the abundant OTUs, while **(A)** the treemap graph used all P-E OTUs.

be related to the temperature (positive relationship between cryptophyte and water temperature, and, inversely, negative correlation between spirotrich ciliates and temperature) or ice coverage (negative correlation between spirotrich ciliates and ice coverage; **Supplementary Figure 1B**). Pelagophyceae showed a significant and positive relationship with ice coverage and nitrite/nitrate and tended to decrease in proportion southward (**Supplementary Figure 1B**).

Dominant Taxa

The community from Marguerite Bay (MB) shows the most distinctive assemblage compared to the other groups for the three size fractions. Overall, 28 abundant OTUs represented more than 57% of the reads (Dataset S3). These 28 abundant OTUs accounted for 25–84%, 41–69%, and 42–78% of the reads of the micro-, nano-, and pico-plankton, respectively. The microplanktonic OTUs related to *Pirsonia formosa* (Oomycetes), a parasitoid of diatoms, and to the diatom *Porosira pseudodenticulata* (**Supplementary Figure 3B**) that dominated the community in the MB group, while the other groups were dominated by OTUs related to the diatom *Corethron inerme*. A larger number of OTUs were related to Ciliophora, including the Oligotrich *Strombidium caudispina* and the tintinnid *Cymatocylis calcyformis* present in all size fractions but mostly in the nano- and pico-plankton (**Supplementary Figure 3B**). A large portion of the nano- and picoplankton was composed of dinoflagellates.

The spatial distribution of each OTU was considered to identify an OTU specific to a depth layer or to a group (i.e., at least 90% of its reads were observed in this depth layer or group). For this analysis, only abundant OTUs that occurred in at least 2 samples were considered, which reduced the number of OTUs from 1,857 to 1,856. Only a small fraction of the OTUs is specific to a depth layer. Only 1 OTU accounting for 395 reads was specific to the bucket samples, 2 and 35 OTUs were specific to the sub-surface and DCM samples, respectively (accounting for 186 and 15,580 reads, respectively). The most abundant DCM-specific OTUs are related to ciliates (e.g., OTUs related to *Leegardiella* and other Strombidiidae). We also observed 112 OTUs specific to a group, representing 56,417 reads (i.e., 5% of the OTUs for less than 3% of the reads). Half of these OTUs are the members of the Bacillariophyta (61 OTUs for 24,577 reads). Most of the group specific OTUs are from the MB area with 83 OTUs and 48,173 reads (75% of the area-specific OTUs and 85% of the area-specific reads), with 47 and 37% of the reads represented by Bacillariophyta and the parasite *Pirsonia* (**Supplementary Figure 4**).

Trophic Mode

The trophic mode of each abundant OTU was estimated based on the literature (Leles et al., 2017; Faure et al., 2019; see **Supplementary Dataset 3** for additional references) to better understand the relationship between the geographical distribution and the community pattern (**Figure 2C**). Overall, the microplankton was mostly composed of phytoplankton, especially diatoms; a big proportion of nano- and pico-plankton corresponds to mixoplankton, including mixotrophic dinoflagellates, such as *Heterocapsa rotundata*, *Prorocentrum* sp., and *Warnowia* sp., cryptophytes (*Geminigera cryophila*) and *Micromonas polaris*. The contribution of phagotrophic (heterotrophic dinoflagellates such as *Gyrodinium* cf. *spirale; Leegardiella* sp. and other unknown ciliates) and kleptopladistidic (mostly oligotrich ciliates) lineages tends to increase going southward. Parasites were also present but had only a limited contribution (less than 4% of the total read number; **Figure 2C**). While the depth layers showed slightly different lineage proportions—more cryptophytes in the sub-surface layer compared to the DCM layer, more Dinophyceae and Mamiellophyceae (mostly *Micromonas polaris*) in the DCM layer, the trophic mode distribution was mostly similar between

the sub-surface and the DCM depths. We noted the large contribution of picozoa (*Picomonas*), known as consumers of colloid particles, in the surface layer (collected with a bucket).

DISCUSSION

In the austral late spring and early summer, the microbial eukaryotic community along the western Antarctic peninsula was strongly influenced by environmental factors that presented a distribution related to the sampling location. Five groups were observed in all three size fractions — micro-, nano-, and pico-size fractions (**Figure 1C**). These groups were also examined against the environmental parameters, including temperature, salinity, PAR, oxygen, amount of particulates in the water column (beam transmission), and structure of the water column (depths of the mixed layer, the euphotic zone, and, to a lesser extent, to the deep chlorophyll maximum; **Figure 1B**). The most dissimilar community assessed using 18S rRNA, compared to the others, was observed in Marguerite Bay (MB), i.e., our southernmost sampling location. Conversely, the communities from the near shore stations in the Gerlache Strait (GS) and Grandidier Channel (GC) were phylogenetically most similar, especially for the pico- and nano-plankton and grouped together despite the differences in environmental parameters shown in the PCA (**Figures 1B,C**). The latitudinal gradient for the environmental factors and for the community composition corresponds also to a gradient in a trophic mode with an increase of heterotrophy (as we analyzed RNA, which combines both presence and activity), including both phagotrophy and mixotrophy, toward the south.

Spring in the Western Antarctic Peninsula

Overall, much of the data on eukaryotic microorganisms, especially phytoplankton, for the WAP come from January or later in the year—in particular from cruises associated with the Palmer Station Long-Term Ecological Research program (Ducklow et al., 2007). The late spring/early summer period of the year in this area still has a considerable amount of sea ice, which limits the ability to a sample. Consequently, most of the studies focusing on the microbial eukaryotes in the Southern Ocean, including phytoplankton, were carried out during the January-April (summer/autumn) period when more open water and light availability have already produced the annual phytoplankton bloom (Flaviani et al., 2018; Clarke et al., 2019; Christaki et al., 2021; Lin et al., 2021). However, phytoplankton dynamics and environmental factors affecting them were examined by Arrigo et al. (2017) in early spring during the beginning of the bloom period. Light, and, consequently, the extent of sea ice seemed to be more important than nutrients in controlling phytoplankton production in early spring (Arrigo et al., 2017). Higher abundances of planktonic organisms were reported during the fall compared to the spring when the lowest abundance of nanoflagellates and bacteria was recorded (Clarke and Leakey, 1996; Ducklow et al., 2007; Trefault et al., 2021). Nevertheless, most of our environmental parameters, including inorganic nutrients, salinity, fluorescence, were in the same range as previously reported (Clarke and Leakey, 1996; Ducklow et al., 2013; Schofield et al., 2018; Christaki et al., 2021), especially prior to the phytoplankton bloom (Petrou et al., 2016; Arrigo et al., 2017; Trefault et al., 2021).

The mixed layer was shallower in our northern regions compared to southern regions (Factor 2; **Table 1**) comparable to previous observation (Schofield et al., 2018). Overall, the mixed layer was deeper than the chlorophyl maximum depth across the cruise, explaining the relative similarity between the samples taken at the sub-surface and at the DCM layer regarding both environmental parameters and planktonic community (**Table 1** and **Figures 1B,C**). As noted above, reduced sea ice has been identified as a good predictor of net community production (Lin et al., 2021). The decrease in coverage and duration of sea ice observed prior to 2008 reversed temporarily and began increasing (Ducklow et al., 2013; Schofield et al., 2018). However, since 2015, the sea ice coverage has returned to its lower level of 2008, and the sea ice duration is continuing to decrease (see LTER data).[1] This is expected to impact the productivity of the WAP system and could also affect community composition. A similar relationship has been observed between ice and heterotrophic protists in the Beauford Sea (Canadian Arctic), resulting in increased ammonium (Riedel et al., 2007). While a higher concentration of ammonium compared to previous studies was observed in the Southern Ocean as well (Clarke and Leakey, 1996; Christaki et al., 2021), this trend was not related to the ice coverage (**Table 1**). DIN, particularly nitrate/nitrate concentration, showed a latitudinal gradient and was negatively correlated to fluorescence and chlorophyll, suggesting a switch from new production supported by nitrite/nitrate in the northern regions to a more regenerated production in MB. However, we acknowledge that interpretation from a limited dataset (one cruise) can be risky, even if the correlation analysis is informative as a starting point (**Supplementary Figure 1**).

Environment Differently Impacts the Diversity of the Pico-, Nano-, and Micro-Plankton

Overall, the diversity (richness and Chao1 index; **Supplementary Figure 2A**), assessed using 18S rRNA, was comparable to what was previously reported in other parts of the world ocean (de Vargas et al., 2015) and in the same region in other periods of the year (Lin et al., 2021). As noted previously, the spring corresponds to a low abundance of protists (Trefault et al., 2021), although, Arrigo et al. (2017) reported some areas of relatively high chlorophyll in early spring. Yet, even with the low abundance, each sample had an average of 1,000 OTUs (comparable to reports in other seasons; Lin et al., 2021), suggesting that most of these OTUs were active but in low abundance (a low signal in our community analysis based on RNA). This raises the question of the effect of environmental changes on this community.

Oxygen, salinity, temperature, and depth of the mixed layer are known factors playing a role in the eukaryotic

[1] http://pal.lternet.edu/data

richness (Raes et al., 2018), and, as mentioned before, sea ice and temperature are also good predictors of protist diversity in the WAP during the autumn (Lin et al., 2021), as they are, for this study, in late spring/early summer (**Table 1** and **Figure 1C**). Lower diversity, in particular for the picoplankton, was observed in areas with less ice coverage, while a deeper mixed layer seemed to enhance the diversity of nanoplankton (**Table 1**). The difference in diversity in the north region compared to the south region of WAP has already been reported and linked with the depth of the mixed layer, the sea surface temperature, and the amount of sea ice (Schofield et al., 2018; Lin et al., 2021; Trefault et al., 2021), which mostly matches our own observations. It has also been noted that changes in productivity are related to the depth of the mixed layer (Montes-Hugo et al., 2009), with a shallower ZML, resulting in enhanced carbon fixation by phytoplankton (Schofield et al., 2018). In fact, increased sea ice correlated with an increase of photosynthetic efficiency because more micronutrients from the continental shelf were available, resulting in higher photosynthetic rates (Schofield et al., 2018). Low diversity in the Southern Ocean has been related to the bloom in summer months when phytoplankton biomass peaks and dissolved micronutrients tend to decrease (Arrigo et al., 2008; Ibarbalz et al., 2019). Based on these data, it is not unreasonable to expect that higher productivity associated with reduced sea ice will tend to decrease the protist diversity.

Endemism in West Antarctic Peninsula

The late spring/early summer protistan community was dominated by the members of the SAR clade (Stramenopiles, Alveolates, and Rhizaria), with different compositions based on size fractions. Dominance of the eukaryotic SAR clade has been reported in almost all oceans (de Vargas et al., 2015; Pernice et al., 2015), including the Southern Ocean (Flaviani et al., 2018; Lin et al., 2021). Compared to a survey carried out in the world oceans (de Vargas et al., 2015), neither high proportion nor diversity of Foraminifera, Diplonemida or Collodaria was observed. Several possibilities exist that explain this observation. For example, it is strongly probable that Collodaria, which are mostly mesoplankton, were not captured in the Niskin bottles due to their large size (Biard et al., 2016). It is also possible that our primers did not amplify some lineages, such as Foraminifera, which has a limited diversity (Morard et al., 2018). Finally, these lineages may be rare, absent, not active, or seasonal in the Southern Ocean. Indeed, other surveys carried out in the Southern Ocean have not reported a large diversity or prevalence of Collodaria, Diplonemea, or Foraminifera (Sassenhagen et al., 2020; Lin et al., 2021).

The abundant and active taxa of late spring/early summer protistan community include *Corethron inerme* (also known as *Corethron criophilum var. inerme), Fragilariopsis kerguelensis, Porosira pseudodenticulata, Geminigera cryophila, and Phaeocystis antarctica*, which have been only described in Antarctica so far (Scott and Marchant, 2005). In addition to these phototrophic taxa, the ciliate *Cymatocylis calcyformis* has only been recently identified in the Southern Ocean (Kim et al., 2013). Other taxa have been described in similar environments such as *Micromonas polaris* in polar environments (Simon et al., 2017), or in different environments, such as the diatom parasites *Pirsonia formosa* and *P. guinardiae* in the North Sea (Kühn et al., 2004) and in WAP (Cleary and Durbin, 2016), the ciliate *Strombidium caudispina* in the South China Sea (Song et al., 2015), and the mixotrophic dinoflagellate *Heterocapsa rotundata* in the Northern hemisphere (Millette et al., 2015; Guiry and Guiry, 2018). Something to consider here too is that the taxonomic assignment of dinoflagellates using a short fragment of the SSU ribosomal DNA (or 18S rRNA) is difficult, given the lack of variability, resulting in multiple taxa matching the same OTU at the same level of similarity. For example, our taxonomic analysis by similarity concludes that most of the OTUs related to dinoflagellates were closely related to *Heterocapsa rotundata* KY980129 or *(1) Gyrodinium cf. spirale* KP790157*, or (2) Prorocentrum sp.* MN824022, without a clear cutoff. In the same way, we can also identify OTUs matching *Symbiodinium* by similarity but *Gyrodinium spirale, Gymnodinium* sp. or unidentified dinoflagellates by phylogeny (**Supplementary Figure 3B**).

Community and Size Fractions

The use of three size fractions allows us to look at community structure at a finer scale. Overall, each size fraction is impacted differently by environmental factors. For example, picoplankton distribution has a stronger association with salinity compared to nano- and micro-plankton, while oxygen showed a slightly stronger impact on micro- and nano-plankton (**Figure 1** and **Supplementary Figure 1**). The dominance of diatoms and dinoflagellates has been reported in the Ross Sea during the austral summer and in WAP during the fall (Wolf et al., 2013; Lin et al., 2021) and early spring (Arrigo et al., 2017). The diatoms were dominant but mostly within the microplankton (>20 μm), while dinoflagellates were abundant in the pico- and nano-size fractions (0.2–5 and 5–20 μm, respectively). As, in January of 2012–2016 (Lin et al., 2021), our dinoflagellate community was dominated by the genus *Gyrodinium*. However, the diatom community is mostly different as our microplanktonic community was dominated by the large diatom *Corethron inerme,* while the phytoplankton community was dominated by *Fragilariopsis, Chaetoceros*, and *Proboscia* in January–February 2014 (Lin et al., 2017), and by *Thalassiosira*, *Odontella*, *Porosira*, *Actinocyclus*, *Proboscia*, and *Chaetoceros* in January 2012–2016 (Lin et al., 2021), or *Eucampia* in the Amundsen Sea in 2010 (Wolf et al., 2013). In early spring, Arrigo et al. (2017) found *Phaeocystis antarctica* and diatoms to consistently exceed 90% of the phytoplankton biomass in pigment and microscopic analyses, with *P. antarctica* and diatoms positively and negatively correlated, respectively, with sea ice. Cryptophytes and chlorophytes were occasionally significant components in their study, but dinoflagellates never contributed more than a few percent to the phytoplankton community (Arrigo et al., 2017).

Large diatoms are known consumers of nitrate, especially during the early summer (Clarke and Leakey, 1996), and the concentration of DIN (both NH_4^+ and NO_3^-/NO_2^-) was relatively high during the study period, which was also marked by a high level of light. Some diatoms (e.g., *Corethron*) are adapted to higher UV intensity by downregulating protein

to protect their photosystem II, mitigating the impact of photosynthetic inhibition (Read et al., 2019). This can explain the inverse relationship between PAR and the concentration of dissolved oxygen or oxygen saturation observed due to a reduced photosynthesis rate (**Supplementary Table 1** and **Figure 1**). Dominance of large diatoms can be related to shallow mixed layer water masses in the north regions, while nanoflagellates are more abundant in a deeper mixed layer zone because of their photoadaptation (Sakshaug and Holm-Hansen, 1986; Villafañe et al., 1995). In our study, the mixed layer depths were deeper in the MB and OFF groups, where higher importance of picophytoplankton, such as *Micromonas* and *Pelagomonas*, and nanoplanktonic diatoms, such as *Chaetoceros* (**Figures 1**, **2**), was observed. In addition, *Pelagomonas* can frequently dominate nitrate assimilation in other environments (Dupont et al., 2015) as this taxon relies on nitrate as the primary source of N (Choi et al., 2020) and has been reported as an important player in oligotrophic environments.

Heterotrophy and Diversity

Heterotrophic protists, including dinoflagellates, have been related to higher concentrations of ammonium, mostly due to their role in regenerating NH_4^+ (Glibert, 1993, 1998) and the key role of NH_4^+ in the ice environments (Riedel et al., 2007). Heterotrophic protists, in particular ciliates, showed a positive relationship with the amount of ice in the Amundsen Sea (Wolf et al., 2013), while the opposite trend was observed here (**Supplementary Figure 1B**). Ciliates are considered to have an important role in the consumption of pico-nanoplankton during night migration in summer along the WAP (Alcamán-Arias et al., 2018). In our data, an inverse relation between ciliates and cryptophytes was observed, which can suggest a predator-prey relationship (**Figure 2B**). However, the presence/dominance of cryptophytes in low salinity and warm stratified water in WAP was previously observed and related to their preferential growth within the surface of melting water (Ferreira et al., 2020; Lin et al., 2021), which also may explain the inverse relationship observed between ice coverage and ciliates. However, the collinearity within our measured environmental parameters, mostly related to the latitudinal gradient, complicates the assessment of the impact of each environmental parameter on the community distribution (**Supplementary Table 2**). Nevertheless, permutational multivariate ANOVA using distance matrices (adonis2), and an Akaike information criterion corrected showed that the pico- and nano-plankton are mostly impacted by latitude (21%) and NO_2NO_3 (12%), while the microplankton is also shaped by the latitude (23%), the depth of the photic zone (11%), and the number of particles in the water (7%; beam transmission; **Supplementary Table 3**) played a role in the distribution of the microplanktonic community. However, additional data are needed to confirm this observation and disentangle the effect of the latitudinal gradient to the effect of each environmental parameter.

The overall diversity, based on 18S rRNA (**Supplementary Figure 2**), tends to increase toward the south, which also corresponded to an increase of heterotrophy, including both phagotrophy and mixotrophy. Overall, the ratio autotroph/heterotroph decreases with an increasing latitude toward the south. Most of this change is related to an increase in the kleptoplastidic ciliates, heterotroph dinoflagellates, and parasitic Stramenopiles, while mixotrophic cryptophytes decrease (**Figure 2**). Garzio and Steinberg (2013) showed an increase of microzooplankton (heterotrophic protists) abundance and biomass toward the south in WAP, with higher values observed in the MB area. The Marguerite Bay is a known biodiversity hotspot due to currents bringing warmer water and nutrients from the deep water (Martinson et al., 2008; Ducklow et al., 2012), resulting in high primary production (Clarke et al., 2008; Vernet et al., 2008) and high populations of krill and penguins (Ashjian et al., 2004; Friedlaender et al., 2011). The higher proportion of heterotrophs may have led to a more complex and diversified community and, therefore, to higher diversity.

CONCLUSION

The results of the current study show a strong latitudinal gradient in protistan diversity and activity that is in agreement with other studies, describing phytoplankton and microzooplankton, mostly later in the spring (Garzio and Steinberg, 2013; Arrigo et al., 2017; Lin et al., 2021). Overall, the Marguerite Bay area showed the most distinctive environmental parameters, the most distinct pico-, nano-, and micro-planktonic communities, and the highest number of specific OTUs, suggesting that the environment played an important role in shaping the community in the WAP. Although these differences in diversity and activity were relatively small, so were the environmental changes, suggesting that the climate change, either directly (temperature) or indirectly, could have a significant effect on the microbial eukaryotic community for which we gathered these initial data.

DATA AVAILABILITY STATEMENT

The datasets presented in this study can be found in online repositories. The names of the repository/repositories and accession number(s) can be found below: NCBI – PRJNA807326. **Supplementary Datasets 1–3** can be found here: doi: 10.6084/m9.figshare.19514110.v3.

AUTHOR CONTRIBUTIONS

J-DG, WJ, and RS participated in the cruise, and with RG conceived and designed the experiments. J-DG performed the RNA community experiments and analyzed the data. WJ performed the nutrients and production analyses. J-DG wrote the manuscript with contribution from all the authors. All authors read and approved the final manuscript.

FUNDING

This work was supported by the National Science Foundation (Grant Nos. ANT 1744767 to RS, ANT 1744663 to RG, and

ANT 1744638 to WJ). This research was based, in part, upon sequencing conducted using the Rhode Island Genomics and Sequencing Center, which was supported in part by the National Science Foundation (MRI Grant No. DBI-0215393 and EPSCoR Grant Nos. 0554548 and EPS-1004057), the US Department of Agriculture (Grant Nos. 2002-34438-12688 and 2003-34438-13111), and the University of Rhode Island. This research includes calculations carried out on Temple University HPC resources supported in part by the National Science Foundation through major research instrumentation (Grant No. 1625061) and by the US Army Research Laboratory under (Contract No. W911NF-16-2-0189).

ACKNOWLEDGMENTS

We gratefully acknowledge the captain and crew of Nathanial B. Palmer for logistical support. We thank Leila Harris and Chris Carnivale for assistance in collecting samples. Opinions and conclusions expressed in this manuscript are those of the authors and do not necessarily reflect the views of the National Science Foundation.

SUPPLEMENTARY MATERIAL

The Supplementary Material for this article can be found online at: https://www.frontiersin.org/articles/10.3389/fmicb.2022.844856/full#supplementary-material

Supplementary Dataset 1 | The OTU table using paired-end reads. T1-5 are the taxonomic ranks, acc the GenBank accession number of the corresponding reference, id% is the percentage of identity, occurrence represents the number of samples in which the OTUs were present, read number the total read number. The samples are labeled as following: station_depthlayer_size._20 for the microsize, _5 for the nanosize, and _0.2 for the picosize.

Supplementary Dataset 2 | The OTU table using forward reads. Accession is the GenBank accession number of the corresponding reference; Btaxo_rank1-6, Bgenus, and Bsp are the taxonomic ranks from PR2, occurrence represents the number of samples in which the OTUs was present, read number the total read number. The samples are labeled as the following: station_depthlayer_size. _20 for the microsize, _5 for the nanosize, and _0.2 for the picosize.

Supplementary Dataset 3 | The OTU table using paired-end reads with at least 10 reads and then rarefied. T1-5 are the taxonomic ranks, acc the GenBank accession number of the corresponding reference, id% is the percentage of identity, Trophic is the trophic mode for the OTUs based on the literature. Reference_Trophic is the reference if different from the main text, occurrence represents the number of the samples in which the OTUs were present, read number the total read number. The samples are labeled as the following: station_depthlayer_size; _20 for the microsize, _5 for the nanosize, and _0.2 for the picosize.

REFERENCES

Alcamán-Arias, M. E., Farías, L., Verdugo, J., Alarcón-Schumacher, T., and Díez, B. (2018). Microbial activity during a coastal phytoplankton bloom on the Western Antarctic Peninsula in late summer. *FEMS Microbiol. Lett.* 365:fny090.

Anderson, R., Charvet, S., and Hansen, P. J. (2018). Mixotrophy in chlorophytes and haptophytes—effect of irradiance, macronutrient, micronutrient and vitamin limitation. *Front. Microbiol.* 9:1704. doi: 10.3389/fmicb.2018.01704

Arrigo, K. R., van Dijken, G. L., Alderkamp, A., Erickson, Z. K., Lewis, K. M., Lowry, K. E., et al. (2017). Early spring phytoplankton dynamics in the Western Antarctic Peninsula. *J. Geophys. Res. Oceans* 122, 9350–9369. doi: 10.1002/2017jc013281

Arrigo, K. R., van Dijken, G. L., and Bushinsky, S. (2008). Primary production in the Southern Ocean, 1997–2006. *J. Geophys. Res. Oceans* 113:C08004.

Ashjian, C. J., Rosenwaks, G. A., Wiebe, P. H., Davis, C. S., Gallager, S. M., Copley, N. J., et al. (2004). Distribution of zooplankton on the continental shelf off Marguerite Bay, Antarctic Peninsula, during austral fall and winter, 2001. *Deep Sea Res. Part II Top. Stud. Oceanogr.* 51, 2073–2098. doi: 10.1016/j.dsr2.2004.07.025

Baldrian, P., Kolařík, M., Štursová, M., Kopecký, J., Valášková, V., Větrovský, T., et al. (2012). Active and total microbial communities in forest soil are largely different and highly stratified during decomposition. *ISME J.* 6, 248–258. doi: 10.1038/ismej.2011.95

Barbera, P., Kozlov, A. M., Czech, L., Morel, B., Darriba, D., Flouri, T., et al. (2019). EPA-ng: massively parallel evolutionary placement of genetic sequences. *Syst. Biol.* 68, 365–369. doi: 10.1093/sysbio/syy054

Beckers, J.-M., and Rixen, M. (2003). EOF calculations and data filling from incomplete oceanographic datasets. *J. Atmos. Ocean. Technol.* 20, 1839–1856. doi: 10.1175/1520-0426(2003)020<1839:ecadff>2.0.co;2

Biard, T., Stemmann, L., Picheral, M., Mayot, N., Vandromme, P., Hauss, H., et al. (2016). In situ imaging reveals the biomass of giant protists in the global ocean. *Nature* 532, 504–507. doi: 10.1038/nature17652

Brown, M. S., Bowman, J. S., Lin, Y., Feehan, C. J., Moreno, C. M., Cassar, N., et al. (2021). Low diversity of a key phytoplankton group along the West Antarctic Peninsula. *Limnol. Oceanogr.* 66, 2470–2480. doi: 10.1002/lno.11765

Brown, M. S., Munro, D. R., Feehan, C. J., Sweeney, C., Ducklow, H. W., and Schofield, O. M. (2019). Enhanced oceanic CO 2 uptake along the rapidly changing West Antarctic Peninsula. *Nat. Clim. Chang.* 9, 678–683. doi: 10.1038/s41558-019-0552-3

Bushnell, B., Rood, J., and Singer, E. (2017). BBMerge–Accurate paired shotgun read merging via overlap. *PLoS One* 12:e0185056. doi: 10.1371/journal.pone.0185056

Callahan, B. J., McMurdie, P. J., Rosen, M. J., Han, A. W., Johnson, A. J. A., and Holmes, S. P. (2016). DADA2: high-resolution sample inference from Illumina amplicon data. *Nat. Methods* 13:581. doi: 10.1038/nmeth.3869

Caron, D. A., and Hu, S. K. (2019). Are we overestimating Protistan diversity in nature? *Trends Microbiol.* 27, 197–205. doi: 10.1016/j.tim.2018.10.009

Cavanagh, R. D., Melbourne-Thomas, J., Grant, S. M., Barnes, D. K. A., Hughes, K. A., Halfter, S., et al. (2021). Future risk for southern ocean ecosystem services under climate change. *Front. Mar. Sci.* 7:615214. doi: 10.3389/fmars.2020.615214

Choi, C. J., Jimenez, V., Needham, D., Poirier, C., Bachy, C., Alexander, H., et al. (2020). Seasonal and geographical transitions in eukaryotic phytoplankton community structure in the Atlantic and Pacific Oceans. *Front. Microbiol.* 11:542372. doi: 10.3389/fmicb.2020.542372

Christaki, U., Gueneugues, A., Liu, Y., Blain, S., Catala, P., Colombet, J., et al. (2021). Seasonal microbial food web dynamics in contrasting Southern Ocean productivity regimes. *Limnol. Oceanogr.* 66, 108–122. doi: 10.1002/lno.11591

Clarke, A., and Leakey, R. J. G. (1996). The seasonal cycle of phytoplankton, macronutrients, and the microbial community in a nearshore Antarctic marine ecosystem. *Limnol. Oceanogr.* 41, 1281–1294. doi: 10.4319/lo.1996.41.6.1281

Clarke, A., Meredith, M. P., Wallace, M. I., Brandon, M. A., and Thomas, D. N. (2008). Seasonal and interannual variability in temperature, chlorophyll and macronutrients in northern Marguerite Bay, Antarctica. *Deep Sea Res. Part II Top. Stud. Oceanogr.* 55, 1988–2006. doi: 10.1016/j.dsr2.2008.04.035

Clarke, L. J., Bestley, S., Bissett, A., and Deagle, B. E. (2019). A globally distributed Syndiniales parasite dominates the Southern Ocean micro-eukaryote community near the sea-ice edge. *ISME J.* 13, 734–737. doi: 10.1038/s41396-018-0306-7

Clarke, L. J., Suter, L., Deagle, B. E., Polanowski, A. M., Terauds, A., Johnstone, G. J., et al. (2021). Environmental DNA metabarcoding for monitoring metazoan biodiversity in Antarctic nearshore ecosystems. *PeerJ* 9:e12458. doi: 10.7717/peerj.12458

Cleary, A. C., and Durbin, E. G. (2016). Unexpected prevalence of parasite 18S rDNA sequences in winter among Antarctic marine protists. *J. Plankton Res.* 38, 401–417. doi: 10.1093/plankt/fbw005

Clem, K., Barreira, S., Fogt, R., Colwell, S., Keller, L., Lazzara, M., et al. (2020). Atmospheric circulation and surface observations [in "State of the Climate in 2019"]. *Bull. Am. Meteorol. Soc.* 101, S293–S296.

Comiso, J. C., Gersten, R. A., Stock, L. V., Turner, J., Perez, G. J., and Cho, K. (2017). Positive trend in the Antarctic sea ice cover and associated changes in surface temperature. *J. Clim.* 30, 2251–2267. doi: 10.1175/jcli-d-16-0408.1

Cordier, T., Angeles, I. B., Henry, N., Lejzerowicz, F., Berney, C., Morard, R., et al. (2022). Patterns of eukaryotic diversity from the surface to the deep-ocean sediment. *Sci. Adv.* 8:eabj9309. doi: 10.1126/sciadv.abj9309

Cristescu, M. E. (2019). Can environmental RNA revolutionize biodiversity science? *Trends Ecol. Evol.* 34, 694–697. doi: 10.1016/j.tree.2019.05.003

de Vargas, C., Audic, S., Henry, N., Decelle, J., Mahe, F., Logares, R., et al. (2015). Ocean plankton. Eukaryotic plankton diversity in the sunlit ocean. *Science* 348:1261605. doi: 10.1126/science.1261605

Dolan, J. R., Yang, E. J., Kang, S.-H., and Rhee, T. S. (2016). Declines in both redundant and trace species characterize the latitudinal diversity gradient in Tintinnid ciliates. *ISME J.* 10, 2174–2183. doi: 10.1038/ismej.2016.19

Ducklow, H. W., Baker, K., Martinson, D. G., Quetin, L. B., Ross, R. M., Smith, R. C., et al. (2007). Marine pelagic ecosystems: the west Antarctic Peninsula. *Philos. Trans. R. Soc. B Biol. Sci.* 362, 67–94. doi: 10.1098/rstb.2006.1955

Ducklow, H. W., Fraser, W. R., Meredith, M. P., Stammerjohn, S. E., Doney, S. C., Martinson, D. G., et al. (2013). West Antarctic Peninsula: an ice-dependent coastal marine ecosystem in transition. *Oceanography* 26, 190–203. doi: 10.5670/oceanog.2013.62

Ducklow, H., Clarke, A., Dickhut, R., Doney, S. C., Geisz, H., Huang, K., et al. (2012). "The marine system of the Western Antarctic Peninsula," in *Antarctic Ecosystems: An Extreme Environment in a Changing World*, eds A. D. Rogers, N. M. Johnston, E. J. Murphy, and A. Clarke (Chichester: John Wiley & Sons, Ltd), 121–159.

Dupont, C. L., McCrow, J. P., Valas, R., Moustafa, A., Walworth, N., Goodenough, U., et al. (2015). Genomes and gene expression across light and productivity gradients in eastern subtropical Pacific microbial communities. *ISME J.* 9, 1076–1092. doi: 10.1038/ismej.2014.198

Edgar, R. C., Haas, B. J., Clemente, J. C., Quince, C., and Knight, R. (2011). UCHIME improves sensitivity and speed of chimera detection. *Bioinformatics* 27, 2194–2200. doi: 10.1093/Bioinformatics/Btr381

Faure, E., Not, F., Benoiston, A. S., Labadie, K., Bittner, L., and Ayata, S. D. (2019). Mixotrophic protists display contrasted biogeographies in the global ocean. *ISME J.* 13, 1072–1083. doi: 10.1038/s41396-018-0340-5

Ferreira, A., Costa, R. R., Dotto, T. S., Kerr, R., Tavano, V. M., Brito, A. C., et al. (2020). Changes in phytoplankton communities along the Northern Antarctic Peninsula: causes, impacts and research priorities. *Front. Mar. Sci.* 7:576254. doi: 10.3389/fmars.2020.576254

Flaviani, F., Schroeder, D. C., Lebret, K., Balestreri, C., Highfield, A. C., Schroeder, J. L., et al. (2018). Distinct oceanic microbiomes from viruses to protists located near the Antarctic circumpolar current. *Front. Microbiol.* 9:1474. doi: 10.3389/fmicb.2018.01474

Friedlaender, A. S., Johnston, D. W., Fraser, W. R., Burns, J., and Costa, D. P. (2011). Ecological niche modeling of sympatric krill predators around Marguerite Bay, Western Antarctic Peninsula. *Deep Sea Res. Part II Top. Stud. Oceanogr.* 58, 1729–1740. doi: 10.1016/j.dsr2.2010.11.018

Garzio, L. M., and Steinberg, D. K. (2013). Microzooplankton community composition along the Western Antarctic Peninsula. *Deep Sea Res. Part I Oceanogr. Res. Pap.* 77, 36–49. doi: 10.1016/j.dsr.2013.03.001

Giner, C. R., Pernice, M. C., Balagué, V., Duarte, C. M., Gasol, J. M., Logares, R., et al. (2020). Marked changes in diversity and relative activity of picoeukaryotes with depth in the world ocean. *ISME J.* 14, 437–449. doi: 10.1038/s41396-019-0506-9

Glibert, P. M. (1993). The interdependence of uptake and release of NH4+ and organic nitrogen. *Mar. Microb. Food Webs* 7, 53–67.

Glibert, P. M. (1998). "Interactions of top-down and bottom-up control in planktonic nitrogen cycling," in *Eutrophication in Planktonic Ecosystems: Food Web Dynamics and Elemental Cycling*, eds T. Tamminen and H. Kuosa (Dordrecht: Springer), 1–12. doi: 10.1007/s00248-016-0899-1

Gonzalez, J. M., Sherr, B. F., and Sherr, E. (1993). Digestive enzyme activity as a quantitative measure of protistan grazing: the acid lysozyme assay for bacterivory. *Mar. Ecol. Prog. Ser.* 100, 197–206. doi: 10.3354/meps100197

Grattepanche, J.-D., and Katz, L. A. (2020). Top-down and bottom-up controls on microeukaryotic diversity (ie, amplicon analyses of SAR lineages) and function (ie, metatranscriptome analyses) assessed in microcosm experiments. *Front. Mar. Sci.* 6:818. doi: 10.3389/fmars.2019.00818

Grattepanche, J.-D., Juarez, D. L., Wood, C. C., McManus, G. B., and Katz, L. A. (2019). Incubation and grazing effects on Spirotrich ciliate diversity inferred from molecular analyses of microcosm experiments. *PLoS One* 14:e0215872. doi: 10.1371/journal.pone.0215872

Grattepanche, J.-D., Walker, L. M., Ott, B. M., Paim Pinto, D. L., Delwiche, C. F., Lane, C. E., et al. (2018). Microbial diversity in the eukaryotic SAR clade: illuminating the darkness between morphology and molecular data. *BioEssays* 40:e1700198. doi: 10.1002/bies.201700198

Guillou, L., Bachar, D., Audic, S., Bass, D., Berney, C., Bittner, L., et al. (2012). The Protist Ribosomal Reference database (PR2): a catalog of unicellular eukaryote small sub-unit rRNA sequences with curated taxonomy. *Nucleic Acids Res.* 41, D597–D604. doi: 10.1093/nar/gks1160

Guiry, M. D., and Guiry, G. M. (2018). *AlgaeBase*. Galway: World-Wide Electronic Publication, National University of Ireland.

Hamady, M., Lozupone, C., and Knight, R. (2009). Fast UniFrac: facilitating high-throughput phylogenetic analyses of microbial communities including analysis of pyrosequencing and PhyloChip data. *ISME J.* 4, 17–27. doi: 10.1038/ismej.2009.97

Hempel, I. (1985). "Variation in geographical distribution and abundance of larvae of Antarctic Krill, Euphausia superba, in the Southern Atlantic Ocean," in *Antarctic Nutrient Cycles and Food Webs*, eds W. R. Siegfried, P. R. Condy, and R. M. Laws (Berlin: Springer), 304–307. doi: 10.1007/978-3-642-82275-9_43

Holmes, R. M., Aminot, A., Kérouel, R., Hooker, B. A., and Peterson, B. J. (1999). A simple and precise method for measuring ammonium in marine and freshwater ecosystems. *Can. J. Fish. Aquat. Sci.* 56, 1801–1808. doi: 10.1139/f99-128

Hopkins, T. L. (1985). The zooplankton community of Croker passage, Antarctic Peninsula. *Polar Biol.* 4, 161–170. doi: 10.1007/bf00263879

Hugerth, L. W., Muller, E. E. L., Hu, Y. O. O., Lebrun, L. A. M., Roume, H., Lundin, D., et al. (2014). Systematic design of 18S rRNA gene primers for determining eukaryotic diversity in microbial consortia. *PLoS One* 9:e95567. doi: 10.1371/journal.pone.0095567

Ibarbalz, F. M., Henry, N., Brandão, M. C., Martini, S., Busseni, G., Byrne, H., et al. (2019). Global trends in marine plankton diversity across kingdoms of life. *Cell* 179, 1084–1097. doi: 10.1016/j.cell.2019.10.008

Irion, S., Jardillier, L., Sassenhagen, I., and Christaki, U. (2020). Marked spatiotemporal variations in small phytoplankton structure in contrasted waters of the Southern Ocean (Kerguelen area). *Limnol. Oceanogr.* 65, 2835–2852. doi: 10.1002/lno.11555

Keeling, P. J. (2019). Combining morphology, behaviour and genomics to understand the evolution and ecology of microbial eukaryotes. *Philos. Trans. R. Soc. B* 374:20190085. doi: 10.1098/rstb.2019.0085

Kim, S. Y., Choi, J. K., Dolan, J. R., Shin, H. C., Lee, S., and Yang, E. J. (2013). Morphological and ribosomal DNA-based characterization of six Antarctic ciliate morphospecies from the Amundsen Sea with phylogenetic analyses. *J. Eukaryot. Microbiol.* 60, 497–513. doi: 10.1111/jeu.12057

Kühn, S., Medlin, L., and Eller, G. (2004). Phylogenetic position of the parasitoid nanoflagellate Pirsonia inferred from nuclear-encoded small subunit ribosomal DNA and a description of *Pseudopirsonia* n. gen. and *Pseudopirsonia mucosa* (Drebes) comb. nov. *Protist* 155, 143–156. doi: 10.1078/143446104774199556

Lahr, D. J. G., and Katz, L. A. (2009). Reducing the impact of PCR-mediated recombination in molecular evolution and environmental studies using a new-generation high-fidelity DNA polymerase. *Biotechniques* 47, 857–863. doi: 10.2144/000113219

Lanzén, A., Jørgensen, S. L., Bengtsson, M. M., Jonassen, I., Øvreås, L., and Urich, T. (2011). Exploring the composition and diversity of microbial communities at the Jan Mayen hydrothermal vent field using RNA and DNA. *FEMS Microbiol. Ecol.* 77, 577–589. doi: 10.1111/j.1574-6941.2011.01138.x

Leles, S. G., Mitra, A., Flynn, K. J., Stoecker, D. K., Hansen, P. J., Calbet, A., et al. (2017). Oceanic protists with different forms of acquired phototrophy display contrasting biogeographies and abundance. *Proc. R. Soc. B Biol. Sci.* 284:20170664. doi: 10.1098/rspb.2017.0664

Leles, S. G., Polimene, L., Bruggeman, J., Blackford, J., Ciavatta, S., Mitra, A., et al. (2018). Modelling mixotrophic functional diversity and implications for ecosystem function. *J. Plankton Res.* 40, 627–642. doi: 10.1093/plankt/fby044

Lin, Y., Cassar, N., Marchetti, A., Moreno, C., Ducklow, H., and Li, Z. (2017). Specific eukaryotic plankton are good predictors of net community production in the Western Antarctic Peninsula. *Sci. Rep.* 7:14845. doi: 10.1038/s41598-017-14109-1

Lin, Y., Moreno, C., Marchetti, A., Ducklow, H., Schofield, O., Delage, E., et al. (2021). Decline in plankton diversity and carbon flux with reduced sea ice extent along the Western Antarctic Peninsula. *Nat. Commun.* 12:4948. doi: 10.1038/s41467-021-25235-w

Mahe, F., Rognes, T., Quince, C., de Vargas, C., and Dunthorn, M. (2015). Swarm v2: highly-scalable and high-resolution amplicon clustering. *PeerJ* 3:e1420. doi: 10.7717/peerj.1420

Martinson, D. G., Stammerjohn, S. E., Iannuzzi, R. A., Smith, R. C., and Vernet, M. (2008). Western Antarctic Peninsula physical oceanography and spatio–temporal variability. *Deep Sea Res. Part II Top. Stud. Oceanogr.* 55, 1964–1987. doi: 10.1016/j.dsr2.2008.04.038

Massana, R., Gobet, A., Audic, S., Bass, D., Bittner, L., Boutte, C., et al. (2015). Marine protist diversity in European coastal waters and sediments as revealed by high-throughput sequencing. *Environ. Microbiol* 17, 4035–4049. doi: 10.1111/1462-2920.12955

Matrai, P. A., Vernet, M., Hood, R., Jennings, A., Brody, E., and Saemundsdottir, S. (1995). Light-dependence of carbon and sulfur production by polar clones of the genus *Phaeocystis*. *Mar. Biol.* 124, 157–167. doi: 10.1007/bf00349157

McKie-Krisberg, Z. M., and Sanders, R. W. (2014). Phagotrophy by the picoeukaryotic green alga *Micromonas*: implications for arctic oceans. *ISME J.* 8, 1953–1961. doi: 10.1038/ismej.2014.16

McMurdie, P. J., and Holmes, S. (2013). phyloseq: an R package for reproducible interactive analysis and graphics of microbiome census data. *PLoS One* 8:e61217. doi: 10.1371/journal.pone.0061217

McMurdie, P. J., and Holmes, S. (2014). Waste not, want not: why rarefying microbiome data is inadmissible. *PLoS Comput. Biol.* 10:e1003531. doi: 10.1371/journal.pcbi.1003531

Millette, N. C., Stoecker, D. K., and Pierson, J. J. (2015). Top-down control by micro-and mesozooplankton on winter dinoflagellate blooms of *Heterocapsa rotundata*. *Aquat. Microb. Ecol.* 76, 15–25. doi: 10.3354/ame01763

Moline, M. A., Claustre, H., Frazer, T. K., Schofield, O., and Vernet, M. (2004). Alteration of the food web along the Antarctic Peninsula in response to a regional warming trend. *Glob. Chang. Biol.* 10, 1973–1980. doi: 10.1111/j.1365-2486.2004.00825.x

Montes-Hugo, M., Doney, S. C., Ducklow, H. W., Fraser, W., Martinson, D., Stammerjohn, S. E., et al. (2009). Recent changes in phytoplankton communities associated with rapid regional climate change along the western Antarctic Peninsula. *Science* 323, 1470–1473. doi: 10.1126/science.1164533

Morard, R., Garet-Delmas, M.-J., Mahé, F., Romac, S., Poulain, J., Kucera, M., et al. (2018). Surface ocean metabarcoding confirms limited diversity in planktonic foraminifera but reveals unknown hyper-abundant lineages. *Sci. Rep.* 8:2539. doi: 10.1038/s41598-018-20833-z

Murphy, E. J., Watkins, J. L., Trathan, P. N., Reid, K., Meredith, M. P., Thorpe, S. E., et al. (2007). Spatial and temporal operation of the Scotia Sea ecosystem: a review of large-scale links in a krill centred food web. *Philos. Trans. R. Soc. B Biol. Sci.* 362, 113–148. doi: 10.1098/rstb.2006.1957

Oksanen, J., Blanchet, F. G., Friendly, M., Kindt, R., Legendre, P., McGlinn, D., et al. (2020). *vegan: Community Ecology Package. R Package Version 2.5-6. 2019*.

Orsi, A. H., Whitworth, T. III, and Nowlin, W. D. Jr. (1995). On the meridional extent and fronts of the Antarctic Circumpolar Current. *Deep Sea Res. Part I Oceanogr. Res. Pap.* 42, 641–673. doi: 10.1038/s41467-021-24264-9

Parsons, T. R., Maita, Y., and Lalli, C. M. (1984). *A Manual of Chemical and Biological Methods for Seawater Analysis*. Oxford: Pergammon Press.

Pernice, M. C., Forn, I., Gomes, A., Lara, E., Alonso-Sáez, L., Arrieta, J. M., et al. (2015). Global abundance of planktonic heterotrophic protists in the deep ocean. *ISME J.* 9, 782–792. doi: 10.1038/ismej.2014.168

Petrou, K., Kranz, S. A., Trimborn, S., Hassler, C. S., Ameijeiras, S. B., Sackett, O., et al. (2016). Southern Ocean phytoplankton physiology in a changing climate. *J. Plant Physiol.* 203, 135–150. doi: 10.1016/j.jplph.2016.05.004

Piredda, R., Tomasino, M. P., D'erchia, A. M., Manzari, C., Pesole, G., Montresor, M., et al. (2017). Diversity and temporal patterns of planktonic protist assemblages at a Mediterranean Long Term Ecological Research site. *FEMS Microbiol. Ecol.* 93:fiw200. doi: 10.1093/femsec/fiw200

R Core Team (2021). *R: A Language and Environment for Statistical Computing.(Version 4.1. 0)[Computer software]*. Vienna: R Foundation for Statistical Computing.

Rachik, S., Christaki, U., Li, L. L., Genitsaris, S., Breton, E., and Monchy, S. (2018). Diversity and potential activity patterns of planktonic eukaryotic microbes in a mesoeutrophic coastal area (eastern English Channel). *PLoS One* 13:e0196987. doi: 10.1371/journal.pone.0196987

Raes, E. J., Bodrossy, L., Van De Kamp, J., Bissett, A., Ostrowski, M., Brown, M. V., et al. (2018). Oceanographic boundaries constrain microbial diversity gradients in the South Pacific Ocean. *Proc. Natl. Acad. Sci. U.S.A.* 115, E8266–E8275. doi: 10.1073/pnas.1719335115

Read, R. W., Vuono, D. C., Neveux, I., Staub, C., and Grzymski, J. J. (2019). Coordinated downregulation of the photosynthetic apparatus as a protective mechanism against UV exposure in the diatom *Corethron hystrix*. *Appl. Microbiol. Biotechnol.* 103, 1837–1850. doi: 10.1007/s00253-018-9544-x

Rice, P., Longden, I., and Bleasby, A. (2000). EMBOSS: the European molecular biology open software suite. *Trends Genet.* 16, 276–277. doi: 10.1016/S0168-9525(00)02024-2

Riedel, A., Michel, C., Gosselin, M., and LeBlanc, B. (2007). Enrichment of nutrients, exopolymeric substances and microorganisms in newly formed sea ice on the Mackenzie shelf. *Mar. Ecol. Prog. Ser.* 342, 55–67. doi: 10.3354/meps342055

Rognes, T., Flouri, T., Nichols, B., Quince, C., and Mahé, F. (2016). VSEARCH: a versatile open source tool for metagenomics. *PeerJ* 4:e2584. doi: 10.7717/peerj.2584

Saba, G. K., Fraser, W. R., Saba, V. S., Iannuzzi, R. A., Coleman, K. E., Doney, S. C., et al. (2014). Winter and spring controls on the summer food web of the coastal West Antarctic Peninsula. *Nat. Commun.* 5:4318. doi: 10.1038/ncomms5318

Sakshaug, E., and Holm-Hansen, O. (1986). Photoadaptation in Antarctic phytopfankton: variations in growth rate, chemical composition and P versus I curves. *J. Plankton Res.* 8, 459–473. doi: 10.1093/plankt/8.3.459

Sassenhagen, I., Irion, S., Jardillier, L., Moreira, D., and Christaki, U. (2020). Protist interactions and community structure during early autumn in the Kerguelen region (Southern Ocean). *Protist* 171:125709. doi: 10.1016/j.protis.2019.125709

Schnetger, B., and Lehners, C. (2014). Determination of nitrate plus nitrite in small volume marine water samples using vanadium (III) chloride as a reduction agent. *Mar. Chem.* 160, 91–98. doi: 10.1016/j.marchem.2014.01.010

Schofield, O., Brown, M., Kohut, J., Nardelli, S., Saba, G., Waite, N., et al. (2018). Changes in the upper ocean mixed layer and phytoplankton productivity along the West Antarctic Peninsula. *Philos. Trans. R. Soc. A Math. Phys. Eng. Sci.* 376:20170173. doi: 10.1098/rsta.2017.0173

Schofield, O., Ducklow, H. W., Martinson, D. G., Meredith, M. P., Moline, M. A., and Fraser, W. R. (2010). How do polar marine ecosystems respond to rapid climate change? *Science* 328, 1520–1523. doi: 10.1126/science.1185779

Schofield, O., Saba, G., Coleman, K., Carvalho, F., Couto, N., Ducklow, H., et al. (2017). Decadal variability in coastal phytoplankton community composition in a changing West Antarctic Peninsula. *Deep Sea Res. Part I Oceanogr. Res. Pap.* 124, 42–54. doi: 10.1016/j.dsr.2017.04.014

Scott, F. J., and Marchant, H. J. (2005). *Antarctic Marine Protists*. Canberra, ACT: Australian Biological Resources Study.

Simon, N., Foulon, E., Grulois, D., Six, C., Desdevises, Y., Latimier, M., et al. (2017). Revision of the genus *Micromonas* Manton et parke (Chlorophyta, Mamiellophyceae), of the type species M. *Pusilla* (Butcher) Manton & Parke and of the Species M. *commoda* van Baren, Bachy and worden and description of two new species based on the genetic and phenotypic characterization of cultured isolates. *Protist* 168, 612–635. doi: 10.1016/j.protis.2017.09.002

Sisson, C., Gulla-Devaney, B., Katz, L. A., and Grattepanche, J.-D. (2018). Seed bank and seasonal patterns of the eukaryotic SAR (Stramenopila, Alveolata and Rhizaria) clade in a New England vernal pool. *J. Plankton Res.* 40, 376–390. doi: 10.1093/plankt/fby020

Smith, D. C., and Azam, F. (1992). A simple, economical method for measuring bacterial protein synthesis rates in seawater using 3H-leucine. *Mar. Microb. Food Webs* 6, 107–114.

Sogin, M. L., Morrison, H. G., Huber, J. A., Mark Welch, D., Huse, S. M., Neal, P. R., et al. (2006). Microbial diversity in the deep sea and the underexplored "rare biosphere". *Proc. Natl. Acad. Sci. U.S.A.* 103, 12115–12120. doi: 10.1073/Pnas.0605127103

Song, W., Zhao, X., Liu, W., Hu, X., Al-Farraj, S. A., Al-Rasheid, K. A. S., et al. (2015). Biodiversity of oligotrich ciliates in the South China Sea: description of three new *Strombidium* species (Protozoa, Ciliophora, Oligotrichia) with phylogenetic analyses. *Syst. Biodivers.* 13, 608–623. doi: 10.1080/14772000.2015.1081992

Stagaman, K. (2019). *phyloseqCompanion Package Version 0.3: Provides Additional Functions to Work with phyloseq Objects. GitHub*. Available online at: https://github.com/kstagaman/phyloseqCompanion (accessed December 9, 2021).

Stamatakis, A. (2014). RAxML version 8: a tool for phylogenetic analysis and post-analysis of large phylogenies. *Bioinformatics* 30, 1312–1313. doi: 10.1093/Bioinformatics/Btu033

Stammerjohn, S., Massom, R., Rind, D., and Martinson, D. (2012). Regions of rapid sea ice change: an inter-hemispheric seasonal comparison. *Geophys. Res. Lett.* 39:L06501.

Stoeck, T., Bass, D., Nebel, M., Christen, R., Jones, M. D. M., Breiner, H. W., et al. (2010). Multiple marker parallel tag environmental DNA sequencing reveals a highly complex eukaryotic community in marine anoxic water. *Mol. Ecol.* 19, 21–31. doi: 10.1111/j.1365-294X.2009.04480.x

Stoecker, D. K., Hansen, P. J., Caron, D. A., and Mitra, A. (2016). Mixotrophy in the marine Plankton. *Ann. Rev. Mar. Sci.* 9, 311–335. doi: 10.1146/annurev-marine-010816-060617

Swalethorp, R., Dinasquet, J., Logares, R., Bertilsson, S., Kjellerup, S., Krabberød, A. K., et al. (2019). Microzooplankton distribution in the Amundsen Sea Polynya (Antarctica) during an extensive *Phaeocystis antarctica* bloom. *Prog. Oceanogr.* 170, 1–10. doi: 10.1016/j.pocean.2018.10.008

Trefault, N., De la Iglesia, R., Moreno-Pino, M., Dos Santos, A. L., Ribeiro, C. G., Parada-Pozo, G., et al. (2021). Annual phytoplankton dynamics in coastal waters from Fildes Bay, Western Antarctic Peninsula. *Sci. Rep.* 11:1368. doi: 10.1038/s41598-020-80568-8

Tréguer, P., and Jacques, G. (1992). "Review Dynamics of nutrients and phytoplankton, and fluxes of carbon, nitrogen and silicon in the Antarctic Ocean," in *Weddell Sea Ecology*, ed. G. Hempel (Berlin: Springer), 149–162. doi: 10.1007/978-3-642-77595-6_17

Turner, J., Lu, H., White, I., King, J. C., Phillips, T., Hosking, J. S., et al. (2016). Absence of 21st century warming on Antarctic Peninsula consistent with natural variability. *Nature* 535, 411–415. doi: 10.1038/nature18645

Vaughan, D. G., Marshall, G. J., Connolley, W. M., Parkinson, C., Mulvaney, R., Hodgson, D. A., et al. (2003). Recent rapid regional climate warming on the Antarctic Peninsula. *Clim. Change* 60, 243–274.

Vernet, M., Martinson, D., Iannuzzi, R., Stammerjohn, S., Kozlowski, W., Sines, K., et al. (2008). Primary production within the sea-ice zone west of the Antarctic Peninsula: I—Sea ice, summer mixed layer, and irradiance. *Deep Sea Res. Part II Top. Stud. Oceanogr.* 55, 2068–2085. doi: 10.1016/j.dsr2.2008.05.021

Villafañe, V. E., Helbling, E. W., Holm-Hansen, O., and Chalker, B. E. (1995). Acclimatization of Antarctic natural phytoplankton assemblages when exposed to solar ultraviolet radiation. *J. Plankton Res.* 17, 2295–2306. doi: 10.1093/plankt/17.12.2295

Ward, B. A. (2019). Mixotroph ecology: more than the sum of its parts. *Proc. Natl. Acad. Sci. U.S.A.* 116, 5846–5848. doi: 10.1073/pnas.1902106116

Whitehouse, M. J., Meredith, M. P., Rothery, P., Atkinson, A., Ward, P., and Korb, R. E. (2008). Rapid warming of the ocean around South Georgia, Southern Ocean, during the 20th century: forcings, characteristics and implications for lower trophic levels. *Deep Sea Res. Part I Oceanogr. Res. Pap.* 55, 1218–1228. doi: 10.1016/j.dsr.2008.06.002

Wolf, C., Frickenhaus, S., Kilias, E. S., Peeken, I., and Metfies, K. (2013). Regional variability in eukaryotic protist communities in the Amundsen Sea. *Antarct. Sci.* 25, 741–751. doi: 10.1017/s0954102013000229

Conflict of Interest: The authors declare that the research was conducted in the absence of any commercial or financial relationships that could be construed as a potential conflict of interest.

Publisher's Note: All claims expressed in this article are solely those of the authors and do not necessarily represent those of their affiliated organizations, or those of the publisher, the editors and the reviewers. Any product that may be evaluated in this article, or claim that may be made by its manufacturer, is not guaranteed or endorsed by the publisher.

frontiers | Frontiers in Microbiology

ORIGINAL RESEARCH
published: 17 May 2022
doi: 10.3389/fmicb.2022.867340

Characterizing the Piezosphere: The Effects of Decompression on Microbial Growth Dynamics

Anaïs Cario[1]†‡, Gina C. Oliver[1†‡] and Karyn L. Rogers[1,2]**

[1]Department of Earth and Environmental Sciences, Rensselaer Polytechnic Institute, Troy, NY, United States, [2]Rensselaer Astrobiology Research and Education Center, Rensselaer Polytechnic Institute, Troy, NY, United States

OPEN ACCESS

Edited by:
Andreas Teske,
University of North Carolina at Chapel Hill, United States

Reviewed by:
Philippe M. Oger,
UMR5240 Microbiologie, Adaptation et Pathogenie (MAP), France
Aude Picard,
University of Nevada, Las Vegas, United States

***Correspondence:**
Anaïs Cario
anais.cario@cnrs.fr
Karyn L. Rogers
rogerk5@rpi.edu

†Present addresses:
Anaïs Cario,
CNRS, Univ. Bordeaux, Bordeaux INP, ICMCB, Pessac, France
Gina C. Oliver,
Department of Earth and Spatial Sciences San Bernardino Valley College, San Bernardino, CA, United States

‡These authors have contributed equally to this work

Specialty section:
This article was submitted to Extreme Microbiology, a section of the journal Frontiers in Microbiology

Received: 01 February 2022
Accepted: 20 April 2022
Published: 17 May 2022

Citation:
Cario A, Oliver GC and Rogers KL (2022) Characterizing the Piezosphere: The Effects of Decompression on Microbial Growth Dynamics. Front. Microbiol. 13:867340. doi: 10.3389/fmicb.2022.867340

The extent to which the full diversity of the subsurface microbiome can be captured *via* cultivation is likely hindered by the inevitable loss of cellular viability from decompression during sampling, enrichment, and isolation. Furthermore, the pressure tolerance of previously isolated strains that span surface and subsurface ecosystems can shed light into microbial activity and pressure adaptation in these transition zones. However, assessments of the effects of elevated pressure on the physiology of piezotolerant and piezosensitive species may be biased by high-pressure enrichment techniques. Here, we compared two high-pressure cultivation techniques—one that requires decompression of the whole cultures during sampling and one that employs the previously described isobaric PUSH devices—to explore the effects of repeated decompression during incubations performed to characterize isolates from deep environments. Two model sulfate-reducing prokaryotes were used to test the effects of decompression/repressurization cycles on growth rates, cell yields, and pressure tolerance. The mesophilic bacterium *Desulfovibrio salexigens* was cultivated from 0.1 to 50 MPa, and the hyperthermophilic archaeon *Archaeoglobus fulgidus* was tested from 0.1 to 98 MPa. For both cultivation methods, *D. salexigens* showed exponential growth up to 20 MPa, but faster growth rates were observed for isobaric cultivation. Furthermore, at 30 MPa minor growth was observed in *D. salexigens* cultures only for isobaric conditions. Isobaric conditions also extended exponential growth of *A. fulgidus* to 60 MPa, compared to 50 MPa when cultures were decompressed during subsampling. For both strains, growth rates and cell yields decreased with increasing pressures, and the most pronounced effects of decompression were observed at the higher end of the pressure ranges. These results highlight that repeated decompression can have a significant negative impact on cell viability, suggesting that decompression tolerance may depend on habitat depth. Furthermore, sampling, enrichment, and cultivation in isobaric devices is critical not only to explore the portion of the deep biosphere that is sensitive to decompression, but also to better characterize the pressure limits and growth characteristics of piezotolerant and piezosensitive species that span surface and subsurface ecosystems.

Keywords: *Desulfovibrio salexigens*, *Archaeoglobus fulgidus*, high-pressure microbiology, microbial physiology, deep marine biosphere

INTRODUCTION

Most of the bacterial and archaeal biomass on Earth is in deep-sea and subsurface environments at elevated pressures (Whitman et al., 1998; Kallmeyer et al., 2012; Parkes et al., 2014; Bar-On et al., 2018). These microorganisms have been shown to be well-adapted to the elevated pressures of their natural habitats (e.g., Somero, 1992; Allen and Bartlett, 2002; Simonato et al., 2006; Jebbar et al., 2015; Peoples and Bartlett 2017). Despite this, pressure seems to be one of the least explored parameters for microbial growth, as relatively few microorganisms from these deep environments have been isolated and/or grown under *in situ* pressures. To date, fewer than 100 species have been reported to be piezotolerant or piezophilic (Picard and Daniel, 2013; Jebbar et al., 2015; Cario et al., 2019; Oliver et al., 2020; Alain et al., 2021; Courtine et al., 2021; Li et al., 2021; Yu et al., 2021; Zhang et al., 2022), and few obligate piezophiles have been identified (Bartlett, 2002; Zeng et al., 2009). Therefore, our knowledge of active microbial species, their physiological and metabolic potential, and community diversity in these deep environments is limited.

Exploration of high-pressure life is limited by the difficulty in both sampling from high-pressure environments and replicating those pressure conditions in the laboratory during cultivation, isolation, and characterization. For obligate piezophiles, high-pressure sampling and cultivation is the only route to isolate novel species (Yayanos and Dietz, 1983; Jannasch and Wirsen, 1984). However, facultative piezophiles and piezotolerant microorganisms can often withstand lower sampling and transfer pressures (Jannasch and Wirsen, 1984). In these cases, the total change in pressure, duration of decompression, and number of subsequent decompression/repressurization cycles can impact the successful isolation of piezophiles (Yayanos, 2001; Park and Clark, 2002; Peoples and Bartlett, 2017). The pressure condition of cultivation experiments may also impose a selection bias on enrichment and isolation experiments that favor species more tolerant to decompression or lower growth pressures (Jannasch et al., 1992; Yayanos, 1995; Grossart and Gust, 2009). Furthermore, Park and Clark (2002) showed that rates of decompression could also impact microbial survival during decompression. For example, accelerated rates of decompression (26 MPa/s) caused the piezophile, *Methanococcus jannaschii* cells to rupture while slower rates of decompression (5.2 MPa/min) over the same pressure range increased viable cell yields (Park and Clark, 2002). Additionally, many piezophiles recovered from the intestinal systems of deep-sea macro fauna (Yayanos et al., 1979; Deming et al., 1981; Jannasch and Wirsen, 1984), show a greater tolerance to sample decompression, but the loss of species from decompression has yet to be quantified and any correlation with habitat depth has yet to be explored (Yayanos, 1978).

Deep biosphere species are often exposed to decompression during sample recovery, as well as during transfer, enrichment, and isolation. Therefore, significant effort has gone into developing pressure-retaining vessels to sample from the deep ocean habitats and carry out enrichment and isolation experiments without decompression (Tabor and Colwell, 1976; Jannasch and Wirsen, 1977; Yayanos, 1977; Cahet et al., 1990; Bianchi et al., 1999; Tamburini et al., 2003; Kato et al., 2008; McNichol et al., 2016; Cario et al., 2019). Such variable volume, floating piston devices can maintain elevated pressure during subsampling, inoculation, and/or transfer (Bianchi et al., 1999; Tamburini et al., 2003; Garel et al., 2019). Recent application of these new technologies has confirmed that higher rates of microbial activity and cell growth are achieved in incubation studies of bathypelagic samples maintained at *in situ* pressures without decompression, compared to parallel, decompressed, ambient pressure experiments (Tamburini, 2006; Tamburini et al., 2013; Garel et al., 2019, 2021). These high-pressure incubation experiments emphasize the need to study deep-sea microbes under *in situ* pressure conditions in order to accurately quantify deep-sea prokaryotic activity.

For enrichments and isolation, common methods involve growth in syringes, plastic bulbs, or heat-sealed plastic bags, in static pressure vessels (reviewed in Yayanos, 2001). However, subsampling to monitor cell growth over time requires decompression of the entire system followed by repressurization for continued cultivation. Inoculating such devices for high-pressure enrichment experiments also usually requires ambient pressure conditions. Other alternatives to study microorganisms under *in situ* pressure conditions include (i) the implementation of optic windows in the high-pressure vessels to monitor growth and motility (Maldonado et al., 2016; Garel et al., 2019); (ii) using high-pressure capillaries or other high-pressure cells coupled with microscopy to study molecular behaviors under extreme conditions with specific high-pressure cell using fluorescence microscopy (Raber et al., 2006; Usui et al., 2012; Patra et al., 2017; Bourges et al., 2020); and (iii) application of spectroscopy techniques to characterize microbial metabolism under high-pressure conditions (Kato and Fujisawa, 1998; Picard et al., 2007, 2015; Peters et al., 2014; Martinez et al., 2016; Osman et al., 2021). These alternatives are promising but require both specific and costly equipment and expertise to perform high-pressure *in situ* monitoring, and are not-yet widespread.

Here, we compare microbial growth in traditional static pressure vessels with cultivation in variable volume, floating piston isobaric high-pressure vessels to explore how decompression affects microbial growth patterns and the range of growth pressures at HHP for two model subsurface sulfate-reducing prokaryotes. Building upon previous designs (Bianchi et al., 1999; Tamburini et al., 2003), we recently collaborated with TOP Industrie© (Vaux Le Peńil, France) to develop a high-pressure, high temperature (HT; 100 MPa, 121°C), floating piston device with a 50 ml PEEK-lined reservoir (Cario et al., 2019). These pressurized underwater sample handler (PUSH) vessels were designed to sample from deep-sea environments and enable subsequent high-pressure enrichment and isolation without decompression (Oliver et al., 2021). These PUSH vessels were used to grow two sulfate-reducing prokaryotes, in high hydrostatic pressure (HHP) batch cultivation experiments that compared growth rates between cultures that experienced several cycles of decompression/repressurization, and those that were maintained at constant pressures throughout the experiment. High-pressure growth of *Desulfovibrio salexigens*, a mesophilic

bacterium previously reported to be piezosensitive (Bale et al., 1997) was tested up to 50 MPa at 30°C (optimum temperature at 0.1 MPa). We have previously reported piezotolerant growth of *Archaeoglobus fulgidus* (Oliver et al., 2020), a hyperthermophilic archaeon, under high-pressure conditions with cycles of decompression/repressurization, and here explore growth at constant incubation pressures from 0.1 to 98 MPa at 83°C (optimum temperature at 0.1 MPa).

MATERIALS AND METHODS

High Temperature, High Hydrostatic Pressure Equipment

Pressurized Underwater Sample Handler Vessel Batch Culture System

The PUSH vessels, similar to those vessels described in Bianchi et al. (1999) and Garel et al. (2019), and purchased through TOP Industrie©, were used for HT and HHP microbial batch cultivation without whole sample decompression and repressurization cycles during subsampling periods (Oliver et al., 2020). The PUSH vessels have a maximum pressure and temperature range of 0.1–100 MPa and 25°C–160°C, respectively, (as detailed in Oliver et al., 2021). For HT conditions, the temperature was controlled by a heating jacket and thermocouple system constructed for each PUSH vessel. The heating jackets, thermocouples, and temperature controllers were purchased from OMEGA™. Each vessel had an insulation wrap over the heating jacket and thermocouple. This heating system can be moved into an anaerobic chamber and plugged into a DC to AC converter powered by a 12-volt battery to maintain HT conditions during anaerobic preparations so that stable pressures could be reached upon pressurization (**Supplementary Figures S1B,C**). A decompression line was constructed to mitigate rapid pressure changes during subsampling that might induce cell shearing or death (Park and Clark, 2002; Foustoukos and Pérez-Rodríguez, 2015). The line included a micrometering valve to slowly subsample while operating the HHP screw pump to maintain vessel pressures (**Supplementary Figure S1E**).

Syringes in Static Pressure Vessels for HT-HHP Batch Cultures

Similar to several previous high-pressure growth experiments (e.g., Marteinsson et al., 1997; Takai et al., 2008; Oliver et al., 2020) syringes were used as reaction vessels in heated static pressure vessels, which were decompressed and repressurized at each sampling point. *Desulfovibrio salexigens* was grown in plastic syringes, and *A. fulgidus* was grown in glass syringes (Hamilton© 10 ml, 1,000 series luer lock gastight glass syringes) to maintain anoxia in the *A. fulgidus* growth medium, as previously described (Oliver et al., 2020; glass syringes were required at the higher incubation temperature for this strain to limit oxygen diffusion into the anoxic growth medium during incubation). To prevent syringe leakage at HT-HHP, custom-made butyl rubber stoppers served as an extra seal between the growth medium and the syringe piston. For incubation in both plastic and glass syringes with Luer lock fittings, the needle hub was embedded in butyl rubber stoppers before being transferred into the pressure vessels. Four High Pressure Equipment Co.© (HiP©), OC-1 O-Ring static pressure vessels were equipped with individual pressure gauges, and heating systems were similar to those described above for the PUSH vessels. Each 125 ml vessel held one 10 ml glass syringe. The temperature range of this system is 25°C–121°C and accommodates pressures from 0.1 to 100 MPa (based on the maximum working pressure capacities of the HiP© vessels and the temperature range of the BUNA O-Rings).

Microbial Strains and Growth Medium

Selection of Target Strains for HT-HHP Growth

The choice of *D. salexigens* and *A. fulgidus* allowed for a comparison between two strains with similar metabolic strategies (heterotrophic sulfate reduction) over a range of temperatures (*D. salexigens* is a mesophile, while *A. fulgidus* is a thermophile) for two genera that are ubiquitous in subsurface environments and also represent both prokaryote. Each of these strains have had previous indications of growth at elevated pressure, belong to genera with other piezotolerant/piezophilic species, and also have been identified in high-pressure ecosystems. For example, a previous study, based on sulfide production measurements, showed that *D. salexigens* was active up to 5 MPa (Bale et al., 1997), and three other *Desulfovibrio* species have been isolated from subsurface environments (*D. profundus*, *D. hydrothermalis*, and *D. piezophiles*; Bale et al., 1997; Alazard et al., 2003; Khelaifia et al., 2011). While *A. fulgidus* type strain VC-16 was isolated from a shallow marine vent (Stetter et al., 1987, 1988), this strain has been identified in a number of deep-sea and deep subsurface environments (1–4 km and ~10–40 MPa; Stetter et al., 1987; Beeder et al., 1994; L'Haridon et al., 1995; Nakagawa et al., 2005; Fardeau et al., 2009). Additional species within the genus *Archaeoglobus* have been isolated from deep-sea environments (e.g., *Archaeoglobus veneficus* was isolated from the Mid Atlantic Ridge at 3.5 km depth, Huber et al., 1997), and archaeal sequences belonging to *Archaeoglobaceae* have been identified at the Mid-Cayman Rise, the deepest known hydrothermal system that reaches 4.96 km depths (~50 MPa; Reveillaud et al., 2016). Further, we have previously reported high-pressure growth of *A. fulgidus* (Oliver et al., 2020), showing that this strain is tolerant up to ~30–40 MPa (with decompression), which is consistent with the depths and pressures of deep-sea and deep subsurface environments where it has been identified.

Growth Conditions for *Desulfovibrio salexigens* and *Archaeoglobus fulgidus*

Desulfovibrio salexigens (DSM 2638), a marine sulfate-reducing bacterium (Postgate and Campbell, 1966) was obtained from the Deutsche Sammlung von Mikroorganismen und Zellkulturen (Germany) and grown anaerobically in DSMZ medium 163 (Solution A: NaCl 25 $g L^{-1}$, K_2HPO_4 0.5 $g L^{-1}$, NH_4Cl 1.0 $g L^{-1}$, Na_2SO_4 1.0 $g L^{-1}$, $CaCl_2.2H_2O$ 2.0 $g L^{-1}$, $MgSO_4.7H_2O$ 2.0 $g L^{-1}$,

Na-DL-lactate 2.0 g L^{-1}, Yeast Extract 1.0 g L^{-1}, resazurin solution (0.1% w/v) 0.5 ml L^{-1}, distilled water 980 ml; Solution B: $FeSO_4.7H_2O$ 0.5 g/10 ml and Solution C: Na-thioglycolate 0.1 g/10 ml, ascorbic acid 0.1 g/10 ml), similar to Postgate and Campbell (1966), with the exception that the media was enriched in calcium (1.5 times) and reduced in iron (1:100). Solutions B and C were added to solution A under N_2 and the pH was adjusted to 7.8 with NaOH.

Archaeoglobus fulgidus strain VC-16 (DSM 4304) was obtained from the Deutsche Sammlung von Mikroorganismen und Zellkulturen GmbH (DSMZ, Braunschweig, Germany). *Archaeoglobus fulgidus* VC-16 is an anaerobic, hyperthermophilic sulfate-reducing archaeon. Here, *A. fulgidus* was grown chemolithoheterotrophically in a lactate–sulfate-rich medium. The composition of the culture medium followed Hartzell and Reed (2006) and sterile anaerobic conditions were maintained following Balch et al. (1979). The medium was reduced prior to inoculation by adding $Na_2S.9H_2O$ to a final concentration of 0.1% prior to inoculation (Cario et al., 2016).

Desulfovibrio salexigens cultivations with or without decompression (static pressure vessels, and PUSH vessels, respectively) were tested at 0.1, 10, 20, 30, 40, and 50 MPa. Subsamples were taken at ~12 h intervals for 72 h to obtain a robust growth curve. For the higher pressures (30–50 MPa), a cell count after 150 h of growth was performed to enumerate cell density (death or survival) according to the pressure cultivation technique. Cell recovery experiments were performed for this strain in order to evaluate the impact of elevated pressure on cell growth recovery. The protocol and the obtained results are detailed in **Table 1**. *Archaeoglobus fulgidus* VC-16 was cultivated from 0.1 to 98 MPa in ~10 MPa increments at 83°C in PUSH vessels and in static pressure vessels. Six to eight subsamples were taken at regular time intervals for standard growth curves. *Archaeoglobus fulgidus* cells grown in the glass syringes were decompressed and repressurized a maximum of nine times throughout each batch culture experiment.

HT-HHP Culture Experiments

Pre-cultures and Inoculation

For triplicate HT-HHP culture experiments with and without sample decompression, the sterile media and pre-cultures were prepared for four PUSH vessels and four syringes incubated in static pressure vessels, corresponding to three inoculated culture replicates and one uninoculated experiment to serve as a negative control. Each strain was first grown from a frozen stock (−80°C) and transferred into sterile anaerobic growth medium. Exponential growth of this culture was used as inoculum for three independent pre-cultures. After reaching logarithmic-phase growth, each of these pre-cultures was used to inoculate fresh sterile growth medium in three serum bottles. Immediately following inoculation, 8–10 ml from each inoculated serum bottle were transferred into sterile syringes and the remaining 45–47 ml were transferred into each PUSH vessel. The *D. salexigens* culture started at 1.10^6 cells/ml and incubations were carried out in static pressure vessels and PUSH vessels at 30°C. Inoculation and transfer of *A. fulgidus* cultures were carried out in the anaerobic chamber in pre-heated PUSH vessels. Starting cell concentrations for *A. fulgidus* experiments were ~6.7×10^6 cells/ml, and incubations were carried out at 83°C.

TABLE 1 | The percentage of *D. salexigens* cell recovery after 36 h of growth at different elevated pressures, with or without decompression steps, and transfer at ambient pressure.

Cultivating pressures	Dilutions	Percentage of growth recovery after transfer at ambient pressure							
		After 24 h of growth				After 48 h of growth			
		Decompressed		No decompressed		Decompressed		No decompressed	
		%	SD	%	SD	%	SD	%	SD
10 MPa	1	50.7	1.7	90	2.2	76.7	12.5	99	0.5
	10	81.8	5.1	82	1.7	84.8	8.3	97	1.2
	100	52.5	17.2	81	3.6	95.5	3.9	99	0.8
20 MPa	1	20.2	2.2	76	2.8	69.1	14.8	98	1.1
	10	12.6	3.5	68	1.7	78.3	18.8	99	0.2
	100	10.2	3.7	71	5.2	64.2	15.1	99	0.8
30 MPa	1	NG		50	4.3	NG		89	2.5
	10			48	2.6			91	3.1
	100			55	3.8			85	5.8
40 MPa	1	NG		37	6.2	NG		80	5.2
	10			39	2.5			78	3.9
	100			31	4.8			81	8.7
50 MPa	1	NG		25	5.7	NG		78	10.2
	10			22	7.2			72	8.9
	100			17	12.3			70	15.2

The cell counts were measured after 24 and 48 h of growth at ambient pressure after the transfer from high-pressure to ambient pressure. For each pressure condition (P), one non-pressurized culture (ambient pressure) was used as a control (U). The average ratio of the growth recovery (U/P) was calculated for each dilution series and was performed at least in triplicate. SD, standard deviation and NG, no growth was observed. Significant differences were determined by Student's t-test (value of $p < 0.01$).

PUSH Vessel Preparation, Pressurization, and Subsampling

For each batch culture HT-HHP experiment, four PUSH vessels were sterilized, assembled, and pre-heated before inoculation and transfer (**Supplementary Information 1**, **Supplementary Figure S1**). After pre-assembly, each PUSH was individually wrapped in an insulated temperature-controlled system with thermocouple and heating jacket to 30°C and 83°C, for *D. salexigens* and *A. fulgidus*, respectively (**Supplementary Information 1**, **Supplementary Figure S1B**). Once pre-heated, all four vessels were transferred with their respective temperature-control systems into an anaerobic chamber (Bactron Shellab), and each temperature-control system was plugged into the DC to AC power converter allowing for continual vessel heating throughout the anaerobic inoculation process. In the anaerobic chamber, the PEEK reservoirs of each of the four PUSH vessels were filled with ~45–47 ml of pre-inoculated growth medium (triplicate) or sterile growth medium (**Supplementary Information 1**, **Supplementary Figure S1C**). The PEEK reservoir screw cap and lid was then closed completely and the valves were closed while in the anaerobic chamber. The vessels were then transported out of the anaerobic chamber for pressurization.

Each PUSH vessel was individually pressurized to the target pressure with a hydraulic screw pump with an in-line pressure gauge connected to the PEEK piston valve (**Supplementary Information 1**, **Supplementary Figure S1D**). Once pressurized, an initial 0.5 ml subsample was taken and fixed in 2.5% glutaraldehyde from each PUSH vessel using the decompression line (see below). Initial sampling and pressurization of the all of the PUSH vessels and syringes were done within 1 h of inoculation in the anaerobic chamber. To assure pressure stability, potential pressure loss from vessel leakage was closely monitored for the first 3 h after inoculation. Up to nine subsamples were obtained from each PUSH vessel for every HT-HHP batch culture growth experiment. For subsampling, the average decompression rate was of 15–25 MPa/min (**Supplementary Information 1**, **Supplementary Figure S1E**). The first 3 ml of medium sampled were discarded as waste from flushing the decompression line before taking a 0.5 ml aliquot sample for enumeration. A maximum of 10% pressure loss occurred during subsampling, but in all cases the pressure was rapidly re-established. The decompression line was cleaned with 70% ethanol and ultrapure water (18.2 MΩ) before and after subsampling each PUSH vessel.

Syringe Preparation, Pressurization, and Subsampling

For both strains, *D. salexigens* and *A. fulgidus*, four 10 ml syringes were used for HT-HHP batch cultivation with sample decompression. Ten milliliter sterile plastic syringes were used for *D. salexigens* and 10 ml glass syringes were used for *A. fulgidus*. Both plastic and glass syringes were flushed with N_2 and the syringe needles were then embedded into butyl stoppers (**Supplementary Figure S2B**). The assembled syringes were then inoculated in the anaerobic chamber by transferring 8–10 ml of inoculated medium into each of the three 10 ml glass/or plastic syringes. For a negative control, 8–10 ml of sterile medium was transferred in the fourth 10 ml glass/or plastic syringe (**Supplementary Information 2** and **Supplementary Figure S2C**). The syringes were removed from the anaerobic chamber and an initial 0.5 ml subsample was fixed in 2.5% glutaraldehyde for enumeration. Finally, each syringe was placed in one of the four pre-heated HiP© vessels, filled with water, and pressurized by connecting each vessel to a HHP screw pump to obtain the target growth pressure (**Supplementary Information 2**, **Supplementary Figure S2D**). For syringe subsampling, each vessel was decompressed at an average rate of 19 MPa/min and a 0.5 ml aliquot sample was taken and fixed in 2.5% glutaraldehyde from each syringe. After subsampling, the syringes were returned to the vessels and again pressurized to the target growth pressure.

Light Microscopy and Cell Enumeration

Cell enumeration was estimated by direct counts from fixed cells [2.5% (v/v) glutaraldehyde] in a Thoma-chamber (depth: 0.02 mm; Brand, Wertheim, Germany) using a light microscope (model XM: Olympus) under 80x magnification (e.g., Huber et al., 1989; Hei and Clark, 1994; Blöchl et al., 1997; Cario et al., 2016). Specific growth rates (μ^{-hr}) were calculated from linear regressions of the exponential portion of the growth curves from triplicate experiments using the LINEST function in Excel. Error bars indicate the standard error from linear regressions of triplicate experiments. Cell densities quantified at ~36 h for *A. fulgidus* and 48 h for *D. salexigens* were used to evaluate the effects of different cultivation conditions on overall cell yields. As some pressure conditions led to cell death, maximum cell densities could not be used for comparison. Error bars indicate SD from triplicate experiments. Significant differences were determined by Student's *t*-test (value of $p < 0.01$).

RESULTS

Desulfovibrio salexigens Growth at Elevated Pressure

Elevated pressure experiments were performed from ambient (0.1 MPa) up to 50 MPa for *D. salexigens* using both static pressure vessels (i.e., with cyclic decompression) and variable volume PUSH vessels (i.e., isobaric) for experiments that lasted 76–150 h. Growth curves, growth rates, and cell density data are summarized in **Figure 1**, **Supplementary Table S1**. At some elevated pressures, cell numbers decreased with time (e.g., cell death). To account for both cell growth and cell death at different conditions, cell densities are compared at 48 h over the entire pressure range of the experiments (**Figure 1D**).

Exponential growth of *D. salexigens* was observed up to 20 MPa both in the static and PUSH vessels (**Figures 1A,B**). The highest growth rates were observed at ambient pressure (0.1 MPa) and 30°C, and were nearly identical for cultivation in serum bottles and the PUSH vessels ($0.19 \pm 0.005\,h^{-1}$ and $0.19 \pm 0.004\,h^{-1}$, respectively). The same growth rate was confirmed with *D. salexigens* incubation, performed in syringes, at ambient pressure and 30°C (data not shown). Overall growth rates

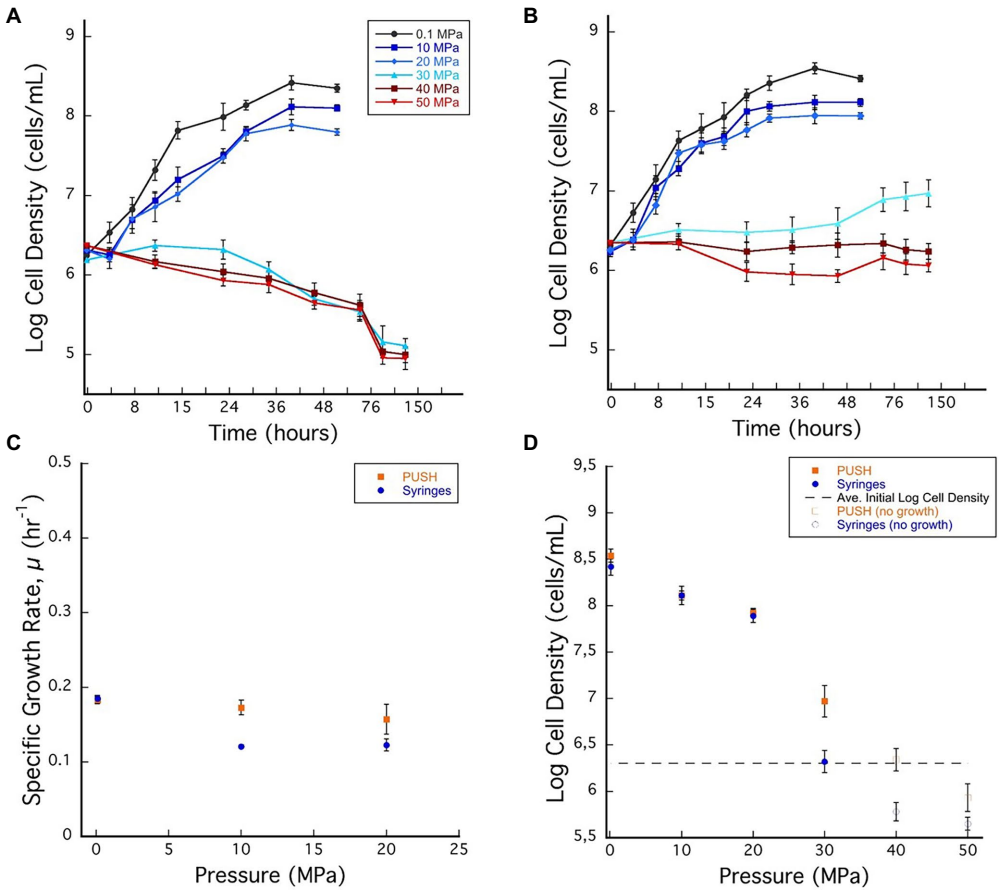

FIGURE 1 | (A) *Desulfovibrio salexigens* growth curves in plastic syringes with multiple sample decompression and **(B)** *D. salexigens* growth curves in the pressurized underwater sample handler (PUSH) vessels without multiple sample decompression from 0.1 to 50 MPa. **(C)** *Desulfovibrio salexigens* specific growth rates in the PUSH vessels (orange squares) and in syringes (blue circles). **(D)** *Desulfovibrio salexigens* maximum log cell densities in the PUSH vessels (orange squares) and in syringes (blue circles), open orange squares and blue circle indicate maximum cell densities in samples with no observed growth or observed cell densities lower than the average initial cell densities (dashed lines in **D**). Error bars are the SDs from the average of triplicate experiments. Significant differences were determined by Student's *t*-test (value of $p < 0.01$).

decreased with pressure, but declining growth rates were less pronounced for isobaric enrichments (**Figure 1C**; **Supplementary Table S1**). For example, at 10 MPa the growth rate for isobaric cultivation was $0.17 \pm 0.2\,h^{-1}$, ~10.5% lower than optimal conditions, while cultivation with decompression had a ~36.8% drop in growth rate to $0.12 \pm 0.1\,h^{-1}$. Furthermore, the upper pressure limit for growth was higher in isobaric experiments, with slow growth observed at 30 MPa in PUSH vessels ($0.02\,h^{-1}$), compared to distinct cell death in decompressed experiments (**Figures 1A–C**).

While differences in growth rates were notable between the two cultivation techniques at moderate pressures (0.1–20 MPa), there were negligible effects on cell yields in this pressure range (**Figure 1D**; **Supplementary Table S1**). However, at supra-optimal pressures (≥30 MPa for *D. salexigens*), differences in cell densities (quantified at 48 h) were more significant. For cultivation experiments that included cyclic decompression, cell numbers decreased markedly with time at 30, 40, and 50 MPa, indicating cell death. Conversely, isobaric cultivation at these pressures led to only minor changes in cell density with time. For example, at 40 MPa, cell density decreased from an initial value of $10^{6.30}$–$10^{5.78}$ after 48 h, while the isobaric culture had a cell density of $10^{6.34}$ after 48 h and no decompression (**Figure 1D**). When considering changes in cell yields, decompression had a more significant impact at supra-optimal pressures, inducing cell death, as opposed to isobaric conditions, which only limited growth.

To further explore the impact of decompression on *D. salexigens* cell viability, cells were incubated at various elevated pressures (10–50 MPa) for 36 h, with or without decompression. They were then transferred to ambient pressure, incubated in fresh growth medium at several dilutions (1:1, 1:10, and 1:100, v/v), and cell recovery was estimated after 24 and 48 h of growth. Because the syringe cultivation technique requires decompression of the high-pressure vessels for subsampling, each vessel was subjected to six decompression/repressurization cycles with a minimum of 4 h between cycles. For both static pressure vessels and PUSH vessels, cells from

the 10 and 20 MPa growth conditions were able to recover the optimal pressure cell density (see **Table 1**). However, when the cells were incubated at higher pressure (≥30 MPa) with cyclic decompression the cells were not able to recover and did not grow after 24 or 48 h of transfer at ambient pressure (nor after 1 week of incubation, data not shown). In comparison, cells exposed to 30–50 MPa in the PUSH without decompression remained viable, though were slower to recover as pressures increased. After transfer to and growth at ambient pressure (0.1 MPa) for 48 h, cell densities were only slightly lower (90% for 30 MPa and 70% for 50 MPa) than those observed for cells never exposed to elevated pressure (**Table 1**).

Archaeoglobus fulgidus Growth at Elevated Pressure

Archaeoglobus fulgidus VC-16 (type strain) was grown in batch cultivation experiments at 83°C over a range of pressures (0.1–98 MPa, at ~10 MPa increments) in PUSH vessels (isobaric) and in static pressure vessels (cyclic decompression) and cell densities were monitored up to 115 h. Growth curves, growth rates, and cell density data are summarized in **Figure 2**; **Supplementary Table S1**. To assess the impact of decompression on cell yields even in the cases of cell death, cell densities at 36 h are reported over the entire pressure range (**Figure 2D**). This time aligns with the generally faster growth of this strain, captures the exponential phase at lower pressures, and accurately represents cell death at elevated pressures.

Based on the growth curves shown in **Figures 2A,B**, *A. fulgidus* growth rates were calculated for pressures between 0.1 and 60 MPa (**Figure 2C**). Overall, *A. fulgidus* growth characteristics showed trends with pressure similar to those observed for *D. salexigens*. Exponential growth was observed in the PUSH vessels at 60 MPa until ~29 h, after which cell numbers decreased. In static pressure vessels at this pressure, only minor increases in cell density ($1.34 \pm 0.11 \times 10^7$ cells/ml) relative to initial values ($6.03 \times 10^6 \pm 1.02$ cells/ml) were observed, but were not consistent with a true exponential growth phase (**Figure 2A**). Growth was generally faster with higher maximum cell densities (with the exception at 10 MPa) in PUSH vessels compared to static pressure vessels, especially at the higher end of the pressure range (**Figures 2C,D**). The fastest growth rate in the PUSH vessels was measured at 0.1 MPa ($0.326 \pm 0.017\ \mu^{-hr}$), though growth rates were only slightly slower from 10 to 30 MPa (0.258 ± 0.026–$0.302 \pm 0.011\ \mu^{-hr}$). The largest difference in growth rates between the two cultivation methods was observed at 30 and 40 MPa (15.3% and 44%, respectively). Overall, growth rates indicate that *A. fulgidus* VC-16 is piezosensitive with a maximum exponential growth pressure of 60 MPa in isobaric conditions and 50 MPa for cultivation that included cyclic decompression.

Similar to the mesophilic strain, *D. salexigens*, the two cultivation techniques had a more significant impact on *A. fulgidus* cell density in the supra-optimal pressure range (≥50 MPa), while density was largely unaffected at the lower pressures. For example, from 0.1 to 40 MPa the largest difference in density at ~36 h was at 30 MPa ($10^{8.66}$, isobaric vs. $10^{8.56}$, decompressed). Comparing isobaric growth to cultivation with cyclic decompression shows that the largest disparities in cell density (measured at ~36 h) were observed at 60 MPa when growth was observed and at 90 MPa when only cell death was recorded. Again, these data suggest that cycles of decompressions can accelerate loss of cell viability. Loss of cell viability was also tested *via* high-pressure incubation experiments in which *A. fulgidus* cells were incubated at 80 MPa for 115 h and subsequently transferred (10% v/v) to fresh growth medium and incubated at 0.1 MPa and 83°C. Ambient pressure cultures were monitored visually and no growth was observed after a week of incubation.

Pressure-Induced Effects on Cell Mobility and Morphology

We also observed significant effects of elevated pressure on the mobility and the morphology of *D. salexigens* cells using a light microscope (**Supplementary Figure S3**). Under optimal pressure conditions (i.e., ambient pressure, 0.1 MPa), the cells were highly motile and formed 3–4 μm vibrios and up to 20 μm cell long when reaching the late exponential and stationary phases (**Supplementary Figure S3**). Under high-pressure cultivation conditions (10 and 20 MPa) and subsequent sampling, the cells were barely motile and formed short vibrios (2–3 μm). After longer incubation times they also formed filamentous cells (**Supplementary Figure S1**). At higher cultivation pressures without decompression steps (30–50 MPa) and subsequent sampling, the cells were also immotile. When they were transferred for growth at ambient pressure, the cell division appeared altered with formation of cells arranged in chains (**Supplementary Figure S4**). Irregular and elongated cell morphologies were previously observed in *A. fulgidus* at elevated pressures (Oliver et al., 2020). This morphological feature has been reported in several studies, where elevated pressure inhibited the cell division protein FtsZ (e.g., Ishii et al., 2004; Abe et al., 2013). Morphological changes are a common stress response (e.g., Zobell and Oppenheimer, 1950; Donaldson et al., 1989) and might be a global stress response to high-pressure (e.g., Bidle and Bartlett, 1999; Aertsen et al., 2004).

Additionally, for elevated pressure conditions (10–50 MPa) we noticed the presence of cyst-like cells (**Supplementary Figure S3**), a constitutive dormancy behavior characteristic of some non-spore forming bacteria (Suzina et al., 2004). As pressure increased from 10 to 50 MPa, we observed an increasing abundance (approximately 2-fold) of such pleiomorphic cells (**Supplementary Figure S5**). However, after transferring these cultures to ambient pressure, we observed the release of cells resembling the development of vegetative cells, suggesting that these structures could be cysts (**Supplementary Figure S4**). The formation of various types of structures, such as endospores, exospores, or cysts, is previously recognized survival strategy of many bacteria under unfavorable conditions induce (Sudo and Dworkin, 1973). The pressures at which we observed changes morphologies and structures are consistent with the growth data that indicated the onset global stress, as indicated by slower growth rates and decreasing cell numbers. Interestingly, among the dissimilatory

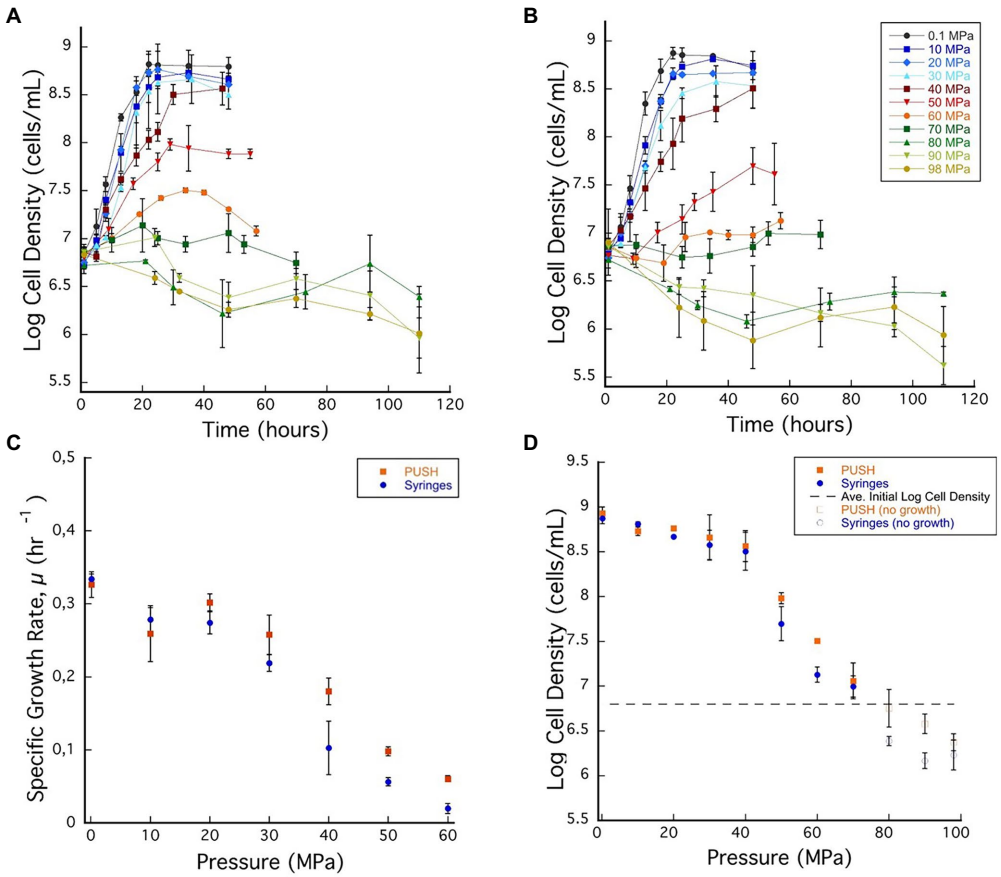

FIGURE 2 | (A) *Archaeoglobus fulgidus* growth curves in glass syringes with multiple sample decompression and **(B)** *A. fulgidus* growth curves in the PUSH vessels without multiple sample decompression from 0.1 to 98 MPa. **(C)** *Archaeoglobus fulgidus* specific growth rates in the PUSH vessels (orange squares) and in syringes (blue circles). **(D)** *Archaeoglobus fulgidus* maximum log cell densities in the PUSH vessels (orange squares) and in syringes (blue circles), open orange squares and blue circle indicate maximum cell densities in samples with no observed growth or observed cell densities lower than the average initial cell densities (dashed lines in **D**). Error bars are the SDs from the average of triplicate experiments. Significant differences were determined by Student's *t*-test (value of $p < 0.01$).

sulfate-reducing bacteria, the genus *Desulfovibrio* was characterized as non-sporulating compared to the closely related genus *Desulfotomaculum* (Postgate and Campbell, 1966). Such behavior might help this species to cope with extreme growth conditions, such as elevated pressure conditions, and might be an important contribution for microbial dissemination in various environments. These specific structures deserve more investigations to determine the developmental steps and the ultrastructural properties of this species when growing under unfavorable growth conditions.

DISCUSSION

A majority of the Earth's biosphere thrives in high-pressure, subsurface environments (Fang et al., 2010; Oger and Jebbar, 2010; Picard and Daniel, 2013), and like many natural ecosystems, studies of subsurface diversity reveal a vast number of uncultured species, often only identified through the presence of their genetic material. The difference between the diversity observed in molecular studies and the strains cultivated from natural systems is likely due to the loss of cell viability during sampling, or the enrichment and isolation protocols. The importance of using growth media compositions to target unique metabolic strategies and thus increase the diversity of cultured species has been discussed elsewhere (e.g., Alain and Querellou, 2009; Overmann et al., 2017). Furthermore, the idea of reducing sample exposure to conditions that cause cell death is regularly used, as is the case for obligate anaerobes, specifically methanogens. More recently, similar reasoning has been applied to the high-pressure biosphere; with novel technologies being deployed to capture and characterize microbes at elevated pressure (e.g., Garel et al., 2019; Peoples et al., 2019). Nonetheless, widespread application of high-pressure techniques throughout sampling, transfer, enrichment, and isolation is limited by challenges associated with cost, technology development, and technical expertise that are amplified when considering high-pressure sampling and cultivation (Cario et al., 2019). Furthermore, even when enrichments or isolates are cultivated at elevated pressures in laboratory settings, traditional methods that use static pressure vessels require decompression during subsampling (e.g., Takai et al., 2008), and the effects of decompression on experimental results for laboratory

cultivation experiments has not been thoroughly or systematically investigated.

To explore the potential effects of decompression on microbial growth dynamics, we used two model sulfate reducers, *D. salexigens* and *A. fulgidus* to compare growth rates, cell yields, and maximum growth pressures between cultivation experiments that included several cycles of decompression and repressurization during subsampling, and those that maintained cultures at constant pressure throughout. Both strains showed significant exponential growth at elevated pressure for both types of cultivation conditions, although both had maximum growth rates at ambient pressure, classifying them as piezosensitive strains. We note that in previous studies we observed piezophilic behavior with maximum growth rates at 20 MPa (Oliver et al., 2020), and found that the growth rate measured at 0.1 MPa was particularly sensitive to the presence of a gas phase. Additionally, the maximum pressure for exponential growth for both strains was extended under isobaric conditions, confirming that cultivation techniques can impact experimentally determined growth characteristics of isolated strains.

In general, the impacts of the two cultivation techniques (isobaric vs. cyclic decompression) followed similar patterns for both *D. salexigens* and *A. fulgidus*, even though the specific pressure ranges, growth rates, and cell yields were strain-specific. Comparing cultivation techniques across both species, growth dynamics can be delineated into three different pressure regimes. The low-pressure regime (LP) has robust exponential growth with only marginal decreases in growth rates as pressures increase and little variation in maximum cell density. The high-pressure regime (HP) includes the range that exceeds the maximum pressure for exponential growth and is often characterized by cell death. The transitional pressure regime (TP) lies in between, is characterized by markedly lower growth rates and cell yields than those observed in the LP, and sometimes exponential growth is hard to discern. Within the TP the impacts of several cycles of decompression and repressurization are most noticeable for both growth rates and maximum cell yields.

The LP regime of *D. salexigens* is 0.1–20 and 0.1–40 MPa for *A. fulgidus*. For both strains, exponential growth rates decreased with increasing pressure, but maximum cell densities were similar at the end of the exponential growth phase. In this low-pressure regime, the effects of cyclic decompression are pronounced for growth rates, which are lower for cyclic decompression cultivation compares to isobaric experiments. However, little to no discernible impact was observed for cell densities. Growth rates and cell densities are more variable in the TP and HP regimes. For *D. salexigens* the transition pressure range is 30–40 MPa. While exponential growth is not discernible at 30 MPa for either condition, there are measurable increases in cell density late in the isobaric cultivation, while only cell death is observed with cyclic decompression cultivation (**Figure 1A**). It is also in the TP range that the largest difference in cell density is observed (**Figure 1D**). A similar pattern is observed for *A. fulgidus* for which the transition pressure range is 40–70 MPa. Exponential growth is observed in isobaric cultures up to 60 MPa, while the limit for cell division in cyclic decompression cultivation is 50 MPa. Overall, significantly slower growth rates (**Figure 2C**) were observed in *A. fulgidus* subjected to decompression from 40 to 60 MPa. Furthermore, the impact of decompression on cell density was also most apparent at 50 and 60 MPa (**Figure 2D**). Finally, while the HP regime is generally characterized by cell death (decreasing cell density with time) there are still noticeable differences between the two cultivation techniques. For *D. salexigens* no growth was obvious at 40 or 50 MPa, however cells subjected to cyclic decompression exhibited clearly higher rates of cell death (**Figure 1A**). Additionally for *A. fulgidus*, decreases in cell density with time were slower for isobaric cultivation.

The processes that might cause the largest differences in both growth rate and cell yield in the TP and HP are not immediately apparent. However, the robust exponential growth in the LP indicates that cells in this lower pressure range are not significantly impacted by these conditions. As both *D. salexigens* and *A. fulgidus* are piezosensitive strains that were isolated and optimized at ambient pressure conditions (0.1 MPa), it follows that decompression from moderate pressures to ambient pressure (their optimum pressure for growth) has little impact on growth rates and cell yields. However, for piezotolerant and piezophilic organisms, decompression would repeatedly expose cells to sub-optimal pressure conditions. In these cases, we hypothesize that cyclic decompression would have a more significant negative impact on growth. Additionally, if extended exposure to elevated pressure were inducing adaptation, even in a subpopulation of the culture, these cells would be selected against during decompression. Further characterization of these and other piezotolerant and piezophilic strains are critical next steps to better understand the effects of cyclic decompression on laboratory characterization of isolated species. Overall, we expect that the difference between isobaric cultivation and cultivation with cyclic decompression will be more pronounced in piezotolerant and piezophilic strains.

CONCLUDING REMARKS

For two deep biosphere species investigated here, *A. fulgidus* and *D. salexigens*, growth was negatively impacted by sample decompression, and these detriments to growth were more significant at pressures further from optimum pressures. These results highlight the need to maintain constant pressure without decompression during cultivation of high-pressure strains. Such an approach is likely to increase the pressure ranges of piezotolerant species, potentially reclassify other strains as piezophilic, and ultimately expand our knowledge of the diversity of known piezophiles, putting into perspective the habitat constraints for many strains whose pressure ranges have been underestimated. Even the piezophilic and piezotolerant organisms that are in culture have likely been isolated after decompression, inevitably selecting against strains more sensitive to decompression. For high-pressure samples that are decompressed and subsequently enriched at elevated *in situ* pressures, those strains that are somewhat tolerant to decompression, like *A. fulgidus*, would outcompete more sensitive strains, and results

of any subsequent analyses would not necessarily be representative of the active *in situ* microbial communities.

Furthermore, maintaining *in situ* pressures becomes even more critical when retrieving samples from deep ecosystems, for example, 5–6 km—habitats more likely to host obligate piezophiles—for which decompression would subject native communities to pressure changes of over 50 MPa. Thus far, most of the obligate piezophiles identified have been psychrophilic bacteria sampled from depths greater that 6 km (i.e., ~60 MPa pressures; for example, Yayanos et al., 1981; Deming et al., 1988; Kato et al., 1998; Nogi et al., 2004) and only one obligate piezophilic hyperthermophilic archaeon, *Pyrococcus yayanosii*, has been identified from a hydrothermal vent at 4.1 km depth (Birrien et al., 2011). Given the extent of the subsurface biosphere, it is unlikely that these few obligate piezophiles represent the full diversity of Earth's largest microbiome. Variable volume, high-pressure devices like the PUSH and others (reviewed in Cario et al., 2019), can be used not only to retrieve samples from up to ~9–10 km water depth, but all can be connected in series (as shown here and in Garel et al., 2019), so that sample transfer and enrichment can also be carried out without decompression. Such an approach will be more selective for piezophiles and obligate piezophiles, and greatly expand our understanding of the activity and physiology of the deep biosphere microbiome.

DATA AVAILABILITY STATEMENT

The original contributions presented in the study are included in the article/**Supplementary Material**; further inquiries can be directed to the corresponding authors.

AUTHOR CONTRIBUTIONS

GO, AC, and KR designed this research project and analyzed data. GO and AC performed the experiments and collected data and wrote the original draft. KR edited and wrote sections of the manuscript. All authors contributed to revisions of the manuscript, tables, and figures and approved the submitted version.

FUNDING

Funding for this work was provided by the NASA Exobiology and PSTAR Programs (NNX13AP2G9 and 80NSSC17K0252 to KR), the Deep Carbon Observatory (Subawards: 10371-07, 10561-01, and 10311-11 to KR), an NSF Graduate Fellowship (FAIN 1247271 and 1744655 to GO), and a GSA Research grant to GO. Additional support was provided by startup funds from Rensselaer Polytechnic Institute to KR.

ACKNOWLEDGMENTS

We thank Bruce Watson for generously gifting us four pressure vessels that allowed us to perform these growth experiments.

SUPPLEMENTARY MATERIAL

The Supplementary Material for this article can be found online at: https://www.frontiersin.org/articles/10.3389/fmicb.2022.867340/full#supplementary-material

REFERENCES

Abe, A., Furukawa, S., Migita, Y., Tanaka, M., Ogihara, H., and Morinaga, Y. (2013). Sublethal high hydrostatic pressure treatment reveals the importance of genes coding cytoskeletal protein in *Escherichia coli* morphogenesis. *Curr. Microbiol.* 67, 515–521. doi: 10.1007/s00284-013-0392-8

Aertsen, A., Van Houdt, R., Vanoirbeek, K., and Michiels, C. W. (2004). An SOS response induced by high pressure in *Escherichia coli*. *J. Bacteriol.* 186, 6133–6141. doi: 10.1128/JB.186.18.6133-6141.2004

Alain, K., and Querellou, J. (2009). Cultivating the uncultured: limits, advances and future challenges. *Extremophiles* 13, 583–594. doi: 10.1007/s00792-009-0261-3

Alain, K., Vince, E., Courtine, D., Maignien, L., Zeng, X., Shao, Z., et al. (2021). *Thermococcus henrietii* sp. nov., a novel extreme thermophilic and piezophilic sulfur-reducing archaeon isolated from a deep-sea hydrothermal chimney. *Int. J. Syst. Evol. Microbiol.* 71:004895. doi: 10.1099/ijsem.0.004895

Alazard, D., Dukan, S., Urios, A., Verhé, F., Bouabida, N., Morel, F., et al. (2003). *Desulfovibrio hydrothermalis sp. nov*., a novel sulfate-reducing bacterium isolated from hydrothermal vents. *Int. J. Syst. Evol. Microbiol.* 53, 173–178. doi: 10.1099/ijs.0.02323-0

Allen, E. E., and Bartlett, D. H. (2002). Piezophiles: microbial adaptation to the deep-sea environment. *Extremophiles* III, 231–255.

Balch, W. E., Fox, G. E., Magrum, L. J., Woese, C. R., and Wolfe, R. S. (1979). Methanogens: reevaluation of a unique biological group. *Microbiol. Rev.* 43, 260–296. doi: 10.1016/j.watres.2010.10.010

Bale, S. J., Goodman, K., Rochelle, P. A., Marchesi, J. R., Fry, J. C., Weightman, A. J., et al. (1997). *Desulfovibrio profundus* sp. nov., a novel barophilic sulfate-reducing bacterium from deep sediment layers in the Japan Sea. *Int. J. Syst. Evol. Microbiol.* 47, 515–521.

Bar-On, Y. M., Phillips, R., and Milo, R. (2018). The biomass distribution on Earth. *Proc. Natl. Acad. Sci.* 115, 6506–6511. doi: 10.1073/pnas.1711842115

Bartlett, D. H. (2002). Pressure effects on in vivo microbial processes. *Biochim. Biophys. Acta Protein Struct. Mol. Enzymol.* 1595, 367–381. doi: 10.1016/S0167-4838(01)00357-0

Beeder, J., Nilsen, R. K., Rosnes, J. T., Torsvik, T., and Lien, T. (1994). *Archaeoglobus fulgidus* isolated from hot North Sea oil field waters. *Appl. Environ. Microbiol.* 60, 1227–1231. doi: 10.1128/aem.60.4.1227-1231.1994

Bianchi, A., Garcin, J., and Tholosan, O. (1999). A high-pressure serial sampler to measure microbial activity in the deep sea. *Deep-Sea Res. I: Oceanogr. Res. Pap.* 46, 2129–2142. doi: 10.1016/S0967-0637(99)00039-4

Bidle, K. A., and Bartlett, D. H. (1999). RecD function is required for high-pressure growth of a deep-sea bacterium. *J. Bacteriol.* 181, 2330–2337. doi: 10.1128/JB.181.8.2330-2337.1999

Birrien, J. L., Zeng, X., Jebbar, M., Cambon-Bonavita, M. A., Quérellou, J., Oger, P., et al. (2011). *Pyrococcus yayanosii* sp. nov., an obligate piezophilic hyperthermophilic archaeon isolated from a deep-sea hydrothermal vent. *Int. J. Syst. Evol. Microbiol.* 61, 2827–2881. doi: 10.1099/ijs.0.024653-0

Blöchl, E., Rachel, R., Burggraf, S., Hafenbradl, D., Jannasch, H. W., and Stetter, K. O. (1997). *Pyrolobus fumarii*, gen. and sp. nov., represents a novel group of archaea, extending the upper temperature limit for life to 113 degrees C. *Extremophiles* 1, 14–21. doi: 10.1007/s007920050010

Bourges, A. C., Lazarev, A., Declerck, N., Rogers, K. L., and Royer, C. A. (2020). Quantitative high-resolution imaging of live microbial cells at high hydrostatic pressure. *Biophys. J.* 118, 2670–2679. doi: 10.1016/j.bpj.2020.04.017

Cahet, G., Daumas, R., and Sibuet, M. (1990). In situ experimentation at the water/sediment interface in the deep sea: 2. Biotransformation of dissolved organic substrates by microbial communities at 2000m depth in the Bay of Biscay. *Prog. Oceanogr.* 24, 169–178. doi: 10.1016/0079-6611(90)90028-Z

Cario, A., Jebbar, M., Thiel, A., Kervarec, N., and Oger, P. M. (2016). Molecular chaperone accumulation as a function of stress evidences adaptation to high hydrostatic pressure in the piezophilic archaeon *Thermococcus barophilus*. *Sci. Rep.* 6:29483. doi: 10.1038/srep29483

Cario, A., Oliver, G. C., and Rogers, K. L. (2019). Exploring the deep marine biosphere: challenges, innovations, and opportunities. *Front. Earth Sci.* 7:225. doi: 10.3389/feart.2019.00225

Courtine, D., Vince, E., Maignien, L., Philippon, X., Gayet, N., Shao, Z., et al. (2021). *Thermococcus camini* sp. nov., a hyperthermophilic and piezophilic archaeon isolated from a deep-sea hydrothermal vent at the Mid-Atlantic Ridge. *Int. J. Syst. Evol. Microbiol.* 71:7. doi: 10.1099/ijsem.0.004853

Deming, J. W., Somers, L. K., Straube, W. L., Swartz, D. G., and Macdonell, M. T. (1988). Isolation of an obligately barophilic bacterium and description of a new genus, *Colwellia* gen. nov. *Syst. Appl. Microbiol.* 10, 152–160. doi: 10.1016/S0723-2020(88)80030-4

Deming, J. W., Tabor, P. S., and Colwell, R. R. (1981). Barophilic growth of bacteria from intestinal tracts of deep-sea invertebrates. *Microb. Ecol.* 7, 85–94. doi: 10.1007/BF02010480

Donaldson, E. C., Knapp, R. M., Yen, T. F., and Chilingarian, G. V. (1989). "The subsurface environment," *Developments in Petroleum Science Vol. 22*. Elsevier. doi: 10.1016/S0376-7361(09)70090-1

Fang, J., Zhang, L., and Bazylinski, D. A. (2010). Deep-sea piezosphere and piezophiles: geomicrobiology and biogeochemistry. *Trends Microbiol.* 18, 413–422. doi: 10.1016/j.tim.2010.06.006

Fardeau, M.-L., Goulhen, F., Bruschi, M., Khelifi, N., Cayol, J.-L., Ignatiadis, I., et al. (2009). Thermophilic isolates from deep geothermal water of the Paris Basin. *Geomicrobiol J.* 26, 119–130. doi: 10.1080/01490450802674970

Foustoukos, D. I., and Pérez-Rodríguez, I. (2015). A continuous culture system for assessing microbial activities in the piezosphere. *Appl. Environ. Microbiol.* 81, 6850–6856. doi: 10.1128/AEM.01215-15

Garel, M., Bonin, P., Martini, S., Guasco, S., Roumagnac, M., Bhairy, N., et al. (2019). Pressure-retaining sampler and high-pressure systems to study deep-sea microbes under in situ conditions. *Front. Microbiol.* 10:453. doi: 10.3389/fmicb.2019.00453

Garel, M., Panagiotopoulos, C., Boutrif, M., Repeta, D., Sempere, R., Santinelli, C., et al. (2021). Contrasting degradation rates of natural dissolved organic carbon by deep-sea prokaryotes under stratified water masses and deep-water convection conditions in the NW Mediterranean Sea. *Mar. Chem.* 231:103932. doi: 10.1016/j.marchem.2021.103932

Grossart, H. P., and Gust, G. (2009). Hydrostatic pressure affects physiology and community structure of marine bacteria during settling to 4000 m: an experimental approach. *Marine Ecology Progress Series* 390, 97–104. doi: 10.3354/meps08201

Hartzell, P., and Reed, D. W. (2006). "The genus archaeoglobus," in *The Prokaryotes*, (eds.) M. Dworkin, S. Falkow, E. Rosenberg, K.-H. Schleifer and E. Stackebrandt (New York, NY: Springer) 82–100.

Hei, D. J., and Clark, D. S. (1994). Pressure stabilization of proteins from extreme thermophiles. *Appl. Environ. Microbiol.* 60, 932–939. doi: 10.1128/aem.60.3.932-939.1994

Huber, H., Jannasch, H., Rachel, R., Fuchs, T., and Stetter, K. O. (1997). Archaeoglobus veneficus sp. nov., a novel facultative chemolithoautotrophic hyperthermophilic sulfite reducer, isolated from abyssal black smokers.. *Syst. Appl. Microbiol.* 20, 374–380.

Huber, R., Woese, C. R., Langworthy, T. A., Fricke, H., and Stetter, K. O. (1989). *Thermosipho africanus* gen. Nov., represents a new genus of thermophilic eubacteria within the "Thermotogales". *Syst. Appl. Microbiol.* 12, 32–37. doi: 10.1016/S0723-2020(89)80037-2

Ishii, A., Sato, T., Wachi, M., Nagai, K., and Kato, C. (2004). Effects of high hydrostatic pressure on bacterial cytoskeleton FtsZ polymers in vivo and in vitro. *Microbiology* 150, 1965–1972. doi: 10.1099/mic.0.26962-0

Jannasch, H. W., and Wirsen, C. O. (1977). Retrieval of concentrated and undecompressed microbial populations from the deep sea. *Appl. Environ. Microbiol.* 33, 642–646. doi: 10.1128/aem.33.3.642-646.1977

Jannasch, H. W., and Wirsen, C. O. (1984). Variability of pressure adaptation in deep-sea bacteria. *Arch. Microbiol.* 139, 281–288. doi: 10.1007/BF00408367

Jannasch, H. W., Wirsen, C. O., Molyneaux, S. J., and Langworthy, T. A. (1992). Comparative physiological studies on hyperthermophilic archaea isolated from deep-sea hot vents with emphasis on *Pyrococcus* strain GB-D. *Appl. Environ. Microbiol.* 58, 3472–3481. doi: 10.1128/aem.58.11.3472-3481.1992

Jebbar, M., Franzetti, B., Girard, E., and Oger, P. (2015). Microbial diversity and adaptation to high hydrostatic pressure in deep-sea hydrothermal vents prokaryotes. *Extremophiles* 19, 721–740. doi: 10.1007/s00792-015-0760-3

Kallmeyer, J., Pockalny, R., Adhikari, R. R., Smith, D. C., and D'Hondt, S. (2012). Global distribution of microbial abundance and biomass in subseafloor sediment. *Proc. Natl. Acad. Sci.* 109, 16213–16216. doi: 10.1073/pnas.1203849109

Kato, M., and Fujisawa, T. (1998). High-pressure solution X-ray scattering of protein using a hydrostatic cell with diamond windows. *J. Synchrotron Radiat.* 5, 1282–1286. doi: 10.1107/S0909049598000788

Kato, C., Li, L., Nakamura, Y., Nogi, Y., Tamaoka, J., and Horikoshi, K. (1998). Properties of hyper-barophilic bacteria isolated from the Mariana trench at a depth of 11,000m. *Rev. High Press. Sci. Technol.* (eds.) C. Michiels, D. H. Bartlett, and A. Aertsen (Washington, DC: © 2008 ASM Press). 7, 1274–1276. doi: 10.4131/jshpreview.7.1274

Kato, C., Nogi, Y., and Arakawa, S. (2008). "Isolation, cultivation, and diversity of deep-sea piezophiles" in *High-Pressure Microbiology*, 203–217.

Khelaifia, S., Fardeau, M. L., Pradel, N., Aussignargues, C., Garel, M., Tamburini, C., et al. (2011). *Desulfovibrio piezophilus* sp. nov., a piezophilic, sulfate-reducing bacterium isolated from wood falls in the Mediterranean Sea. *Int. J. Syst. Evol. Microbiol.* 61, 2706–2711. doi: 10.1099/ijs.0.028670-0

L'Haridon, S., Reysenbacht, A. L., Glenat, P., Prieur, D., and Jeanthon, C. (1995). Hot subterranean biosphere in a continental oil reservoir. *Nature* 377, 223–224. doi: 10.1038/377223a0

Li, X. G., Tang, H. Z., Zhang, W. J., Qi, X. Q., Qu, Z. G., Xu, J., et al. (2021). *Thermococcus aciditolerans* sp. nov., a piezotolerant, hyperthermophilic archaeon isolated from a deep-sea hydrothermal vent chimney in the southwest Indian ridge. *Int. J. Syst. Evol. Microbiol.* 71:004934. doi: 10.1099/ijsem.0.004934

Maldonado, J. A., Schaffner, D. W., Cuitiño, A. M., and Karwe, M. V. (2016). In situ studies of microbial inactivation during high pressure processing. *High Pressure Res.* 36, 79–89. doi: 10.1080/08957959.2015.1111887

Marteinsson, V. T., Moulin, P., Birrien, J., Gambacorta, A., Vernet, M., and Prieur, D. (1997). Physiological responses to stress conditions and barophilic behavior of the hyperthermophilic vent archaeon *Pyrococcus abyssi*. *Appl. Environ. Microbiol.* 63, 1230–1236. doi: 10.1128/aem.63.4.1230-1236.1997

Martinez, N., Michoud, G., Cario, A., Ollivier, J., Franzetti, B., Jebbar, M., et al. (2016). High protein flexibility and reduced hydration water dynamics are key pressure adaptive strategies in prokaryotes. *Sci. Rep.* 6, 1–11. doi: 10.1038/srep32816

McNichol, J., Sylva, S. P., Thomas, F., Taylor, C. D., Sievert, S. M., and Seewald, J. S. (2016). Assessing microbial processes in deep-sea hydrothermal systems by incubation at in situ temperature and pressure. *Deep Sea Res. Part I Oceanogr. Res. Pap.* 115, 221–232. doi: 10.1016/j.dsr.2016.06.011

Nakagawa, S., Takai, K., Inagaki, F., Chiba, H., Ishibashi, J. I., Kataoka, S., et al. (2005). Variability in microbial community and venting chemistry in a sediment-hosted backarc hydrothermal system: impacts of subseafloor phase-separation. *FEMS Microbiol. Ecol.* 54, 141–155. doi: 10.1016/j.femsec.2005.03.007

Nogi, Y., Hosoya, S., Kato, C., and Horikoshi, K.. (2004). Colwellia piezophila sp. nov., a novel piezophilic species from deep-sea sediments of the Japan Trench. *Int. J. Syst. Evol. Microbiol.* 54, 1627–1631. doi: 10.1099/ijs.0.03049-0

Oger, P. M., and Jebbar, M. (2010). The many ways of coping with pressure. *Res. Microbiol.* 161, 799–809. doi: 10.1016/j.resmic.2010.09.017

Oliver, G. C., Cario, A., and Rogers, K. L. (2020). Rate and extent of growth of a model extremophile, *Archaeoglobus fulgidus*, under high hydrostatic pressures. *Front. Microbiol.* 11:1023. doi: 10.3389/fmicb.2020.01023

Oliver, G. C., Cario, A., and Rogers, K. L. (2021). High temperature and high hydrostatic pressure cultivation, transfer, and filtration systems for investigating deep marine microorganisms. [Preprints]. doi: 10.20944/preprints202104.0453.v1.

Osman, J. R., Cardon, H., Montagnac, G., Picard, A., and Daniel, I. (2021). Pressure effects on sulfur-oxidizing activity of *Thiobacillus thioparus*. *Environ. Microbiol. Rep.* 13, 169–175. doi: 10.1111/1758-2229.12922

Overmann, J., Abt, B., and Sikorski, J. (2017). Present and future of culturing bacteria. *Annu. Rev. Microbiol.* 71, 711–730. doi: 10.1146/annurev-micro-090816-093449

Park, C. B., and Clark, D. S. (2002). Rupture of the cell envelope by decompression of the deep-sea methanogen *Methanococcus jannaschii*. *Appl. Environ. Microbiol.* 68, 1458–1463. doi: 10.1128/AEM.68.3.1458-1463.2002

Parkes, R. J., Cragg, B., Roussel, E., Webster, G., Weightman, A., and Sass, H. (2014). A review of prokaryotic populations and processes in sub-seafloor sediments, including biosphere: geosphere interactions. *Mar. Geol.* 352, 409–425. doi: 10.1016/j.margeo.2014.02.009

Patra, S., Anders, C., Erwin, N., and Winter, R. (2017). Osmolyte effects on the conformational dynamics of a DNA hairpin at ambient and extreme environmental conditions. *Angew. Chem.* 129, 5127–5131. doi: 10.1002/ange.201701420

Peoples, L. M., and Bartlett, Douglas H. (2017). "Ecogenomics of Deep-Ocean Microbial Bathytypes," in *Microbial Ecology of Extreme Environments*. 7–50. doi: 10.1007/978-3-319-51686-8

Peoples, L. M., Norenberg, M., Price, D., McGoldrick, M., Novotny, M., Bochdansky, A., et al. (2019). A full-ocean-depth rated modular lander and pressure-retaining sampler capable of collecting hadal-endemic microbes under in situ conditions. *Deep-Sea Res. I Oceanogr. Res. Pap.* 143, 50–57. doi: 10.1016/j.dsr.2018.11.010

Peters, J., Martinez, N., Michoud, G., Cario, A., Franzetti, B., Oger, P., et al. (2014). Deep sea microbes probed by incoherent neutron scattering under high hydrostatic pressure. *Z. Phys. Chem.* 228, 1121–1133. doi: 10.1515/zpch-2014-0547

Picard, A., and Daniel, I. (2013). Pressure as an environmental parameter for microbial life: a review. *Biophys. Chem.* 183, 30–41. doi: 10.1016/j.bpc.2013.06.019

Picard, A., Daniel, I., Montagnac, G., and Oger, P. (2007). In situ monitoring by quantitative Raman spectroscopy of alcoholic fermentation by *Saccharomyces cerevisiae* under high pressure. *Extremophiles* 11, 445–452. doi: 10.1007/s00792-006-0054-x

Picard, A., Testemale, D., Wagenknecht, L., Hazael, R., and Daniel, I. (2015). Iron reduction by the deep-sea bacterium *Shewanella profunda* LT13a under subsurface pressure and temperature conditions. *Front. Microbiol.* 5:796. doi: 10.3389/fmicb.2014.00796

Postgate, J. R., and Campbell, L. L. (1966). Classification of *Desulfovibrio* species, the nonsporulating sulfate-reducing bacteria. *Bacteriol. Rev.* 30, 732–738. doi: 10.1128/br.30.4.732-738.1966

Raber, E. C., Dudley, J. A., Salerno, M., and Urayama, P. (2006). Capillary-based, high-pressure chamber for fluorescence microscopy imaging. *Rev. Sci. Instrum.* 77:096106. doi: 10.1063/1.2349303

Reveillaud, J., Reddington, E., McDermott, J., Algar, C., Meyer, J. L., Sylva, S., et al. (2016). Subseafloor microbial communities in hydrogen-rich vent fluids from hydrothermal systems along the mid-Cayman rise. *Environ. Microbiol.* 18, 1970–1987. doi: 10.1111/1462-2920.13173

Simonato, F., Campanaro, S., Lauro, F. M., Vezzi, A., D'Angelo, M., Vitulo, N., et al. (2006). Piezophilic adaptation: a genomic point of view. *J. Biotechnol.* 126, 11–25. doi: 10.1016/j.jbiotec.2006.03.038

Somero, G. N. (1992). Adaptations to high hydrostatic pressure. *Annu. Rev. Physiol.* 54, 557–577. doi: 10.1146/annurev.ph.54.030192.003013

Stetter, K. O. (1988). *Archaeoglobus fulgidus* gen. nov., sp. nov.: a new taxon of extremely thermophilic archaebacteria. *Syst. Appl. Microbiol.* 10, 172–173. doi: 10.1016/S0723-2020(88)80032-8

Stetter, K. O., Lauerer, G., Thomm, M., and Neuner, A. (1987). Isolation of extremely thermophilic sulfate reducers: evidence for a novel branch of archaebacteria. *Science* 236, 822–824. doi: 10.1126/science.236.4803.822

Sudo, S. Z., and Dworkin, M. (1973). Comparative biology of prokaryotic resting cells. *Adv. Microb. Physiol.* 9, 153–224. doi: 10.1016/S0065-2911(08)60378-1

Suzina, N. E., Mulyukin, A. L., Kozlova, A. N., Shorokhova, A. P., Dmitriev, V. V., Barinova, E. S., et al. (2004). Ultrastructure of resting cells of some non-spore-forming bacteria. *Microbiology* 73, 435–447. doi: 10.1023/B:MICI.0000036990.94039.af

Tabor, P., and Colwell, R. (1976). Initial investigations with a deep ocean in situ sampler. in *IEEE OCEANS'76 September 1976*, 324–327.

Takai, K., Nakamura, K., Toki, T., Tsunogai, U., Miyazaki, M., Miyazaki, J., et al. (2008). Cell proliferation at 122 C and isotopically heavy CH4 production by a hyperthermophilic methanogen under high-pressure cultivation. *Proc. Natl. Acad. Sci.* 105, 10949–10954. doi: 10.1073/pnas.0712334105

Tamburini, C. (2006). "Life under pressure. Deep-sea microbial ecology" in *Life As We Know It. Series: Cellular Origin and Life in Extreme Habitats and Astrobiology* ed. J. Seckbach (Berlin: Springer), 1–17.

Tamburini, C., Boutrif, M., Garel, M., Colwell, R. R., and Deming, J. W. (2013). Prokaryotic responses to hydrostatic pressure in the ocean–a review. *Environ. Microbiol.* 15, 1262–1274. doi: 10.1111/1462-2920.12084

Tamburini, C., Garcin, J., and Bianchi, A. (2003). Role of deep-sea bacteria in organic matter mineralization and adaptation to hydrostatic pressure conditions in the NW Mediterranean Sea. *Aquat. Microb. Ecol.* 32, 209–218. doi: 10.3354/ame032209

Usui, K., Hiraki, T., Kawamoto, J., Kurihara, T., Nogi, Y., Kato, C., et al. (2012). Eicosapentaenoic acid plays a role in stabilizing dynamic membrane structure in the deep-sea piezophile *Shewanella violacea*: a study employing high-pressure time-resolved fluorescence anisotropy measurement. *Biochim. Biophys. Acta Biomembr.* 1818, 574–583. doi: 10.1016/j.bbamem.2011.10.010

Whitman, W. B., Coleman, D. C., and Wiebe, W. J. (1998). Prokaryotes: the unseen majority. *Proc. Natl. Acad. Sci.* 95, 6578–6583. doi: 10.1073/pnas.95.12.6578

Yayanos, A. A. (1977). Simply actuated closure for a pressure vessel: design for use to trap deep-sea animals. *Rev. Sci. Instrum.* 48, 786–789. doi: 10.1063/1.1135150

Yayanos, A. A. (1978). Recovery and maintenance of live amphipods at a pressure of 580 bars from an ocean depth of 5700 meters. *Science* 200, 1056–1059. doi: 10.1126/science.200.4345.1056

Yayanos, A. A. (1995). "Microbiology to 10,500 Meters in the Deep Sea," *Annual Review of Microbiology* 49, 777–805. doi: 10.1146/annurev.micro.49.1.777

Yayanos, A. A. (2001). 30 deep-sea piezophilic bacteria. *Methods Microbiol.* 30, 615–637. doi: 10.1016/S0580-9517(01)30065-X

Yayanos, A. A., and Dietz, A. S. (1983). Death of a Hadal deep-sea bacterium after decompression. *Science* 220, 497–498. doi: 10.1126/science.220.4596.497

Yayanos, A. A., Dietz, A. S., and Van Boxtel, R. (1979). Isolation of a deep-sea barophilic bacterium and some of its growth characteristics. *Science* 205, 808–810. doi: 10.1126/science.205.4408.808

Yayanos, A. A., Dietz, A. S., and Van Boxtel, R. (1981). Obligately barophilic bacterium from the Mariana trench. *Proc. Natl. Acad. Sci.* 78, 5212–5215. doi: 10.1073/pnas.78.8.5212

Yu, L., Jian, H., Gai, Y., Yi, Z., Feng, Y., Qiu, X., et al. (2021). Characterization of two novel psychrophilic and piezotolerant strains, *Shewanella psychropiezotolerans* sp. nov. and *Shewanella eurypsychrophilus* sp. nov, adapted to an extreme deep-sea environment. *Syst. Appl. Microbiol.* 44:126266. doi: 10.1016/j.syapm.2021.126266

Zeng, X., Birrien, J.-L., Fouquet, Y., Cherkashov, G., Jebbar, M., Querellou, J., et al. (2009). *Pyrococcus CH1*, an obligate piezophilic hyperthermophile: extending the upper pressure-temperature limits for life. *ISME J.* 3, 873–876. doi: 10.1038/ismej.2009.21

Zhang, H., Fang, J., Zhang, H., and Cao, J. (2022). Complete genome sequence of a psychrotolerant and piezotolerant bacterium *Parasedimentitalea marina* W43T, isolated from deep-sea water of the New Britain trench. *Mar. Genomics* 61:100915. doi: 10.1016/j.margen.2021.100915

Zobell, C. E., and Oppenheimer, C. H. (1950). Some effects of hydrostatic pressure on the Multiplication and morphology of marine bacteria. *Journal of Bacteriology* 60, 771–781.

Conflict of Interest: The authors declare that the research was conducted in the absence of any commercial or financial relationships that could be construed as a potential conflict of interest.

frontiers | Frontiers in Microbiology

ORIGINAL RESEARCH
published: 23 May 2022
doi: 10.3389/fmicb.2022.866681

High-Pressure Microfluidics for Ultra-Fast Microbial Phenotyping

Anaïs Cario[1], Marina Larzillière[1,2], Olivier Nguyen[1], Karine Alain[2] and Samuel Marre[1]**

[1]Univ. Bordeaux, CNRS, Bordeaux INP, ICMCB, UMR 5026, Pessac, France, [2]CNRS, Univ. Brest, Ifremer, IRP 1211 MicrobSea, Unité de Biologie et Ecologie des Ecosystèmes Marins Profonds BEEP, IUEM, Plouzané, France

Here, we present a novel methodology based on high-pressure microfluidics to rapidly perform temperature-based phenotyping of microbial strains from deep-sea environments. The main advantage concerns the multiple on-chip temperature conditions that can be achieved in a single experiment at pressures representative of the deep-sea, overcoming the conventional limitations of large-scale batch metal reactors to conduct fast screening investigations. We monitored the growth of the model strain *Thermococcus barophilus* over 40 temperature and pressure conditions, without any decompression, in only 1 week, whereas it takes weeks or months with conventional approaches. The results are later compared with data from the literature. An additional example is also shown for a hydrogenotrophic methanogen strain (*Methanothermococcus thermolithotrophicus*), demonstrating the robustness of the methodology. These microfluidic tools can be used in laboratories to accelerate characterizations of new isolated species, changing the widely accepted paradigm that high-pressure microbiology experiments are time-consuming.

Keywords: high-pressure microfluidics, deep-sea microorganisms, real time investigations, phenotyping, fast screening

OPEN ACCESS

Edited by:
Andreas Teske, University of North Carolina at Chapel Hill, United States

Reviewed by:
Philippe M. Oger, UMR5240 Microbiologie, Adaptation et Pathogenie (MAP), France
Krishnendu Chakrabarty, Government College of Engineering and Ceramic Technology, India

****Correspondence:***
Anaïs Cario
anais.cario@cnrs.fr
Samuel Marre
samuel.marre@cnrs.fr

Specialty section:
This article was submitted to Extreme Microbiology, a section of the journal Frontiers in Microbiology

Received: *31 January 2022*
Accepted: *27 April 2022*
Published: *23 May 2022*

Citation:
Cario A, Larzillière M, Nguyen O, Alain K and Marre S (2022) High-Pressure Microfluidics for Ultra-Fast Microbial Phenotyping. Front. Microbiol. 13:866681. doi: 10.3389/fmicb.2022.866681

INTRODUCTION

The study of the deep biosphere is particularly concerned with the discovery and investigation of the deep microbial life inhabiting this remote environment. The case of marine environment is particularly interesting since if we consider that the deep biosphere begins in the ocean at depths greater than 1,000 m (Jannasch and Taylor, 1984) the deep-sea represents 65% of the Earth's surface and 95% of its habitable space. The deep biosphere is estimated to account for more than ~15% of the total biomass on Earth (Whitman et al., 1998; Bar-On et al., 2018), and is known to be a major contributor to biogeochemical cycles (D'Hondt et al., 2004; Kallmeyer et al., 2012). In recent years, the deep ocean has been the focus of much attention because it hosts various ecosystems, contains biological resources—especially microbial—and mineral resources, and plays key functions for our planet (e.g., carbon storage, climate regulation, microbial degradation, receptacle of pollutants, etc.). However, despite its importance, the deep-sea remains sparsely documented, as does the deep microbial biosphere (Ramirez-Llodra et al., 2010). Knowledge of the deep biosphere is notably hampered by the difficulties inherent to its access, the technical difficulties to sample it, and the investigations at laboratory scale under realistic pressure conditions (up to 100 MPa), which require adapted equipment (Cario et al., 2019; Garel et al., 2019). Therefore, phenotyping (i.e., determining the detectable physical and biochemical characteristics of an organism or microbial strain) of microbial strains from

deep-sea environments is time-consuming, given the large number of long and distinct experiments that must be performed—and repeated—in order to characterize a new strain, a mutant or simply to perform basic growth studies.

Since microorganisms in the deep biosphere experience diverse and severe conditions (Jørgensen and Boetius, 2007; Orcutt et al., 2013), characterization of microbial species at the laboratory scale requires specific high-pressure equipment and robust methodologies. Various culture-based and culture-independent approaches have attempted to describe both the microbial diversity and the array of metabolic capabilities present in these singular ecosystems, but with more effort devoted to omics-based studies in recent years at the expense of time-consuming culture-based approaches (Connon and Giovannoni, 2002; DeSantis et al., 2007; Rinke et al., 2013; Chen et al., 2021). The cutting-edge approaches for isolation and cultivation of prokaryotes such as microencapsulation, single-cell and droplet-based cultivation, and cell sorting based cultivation (e.g., reverse genomics; Zengler et al., 2005; Nichols et al., 2010; Boitard et al., 2015; Jiang et al., 2016; Berdy et al., 2017; Terekhov et al., 2018; Hu et al., 2020; Lewis et al., 2021) are very promising but cannot be applied to all microbial taxa as they do not mimic all environmental conditions, and in particular high temperature and pressure. Despite these significant achievements, the vast majority of the genera and phyla of bacteria and archaea on Earth, including those from the deep biosphere, do not have cultured representatives (Whitman et al., 1998; Lloyd et al., 2018). The low cultivation scores can be explained in part by the fact that many cultures are grown at atmospheric pressure, whereas in their *in situ* habitat, microorganisms are subjected to high hydrostatic pressures. Together with temperature and chemistry, pressure is one of the parameters driving the distribution and the microbial activities in the biosphere (Fry et al., 2008; Reith, 2011; Picard and Daniel, 2013; Jebbar et al., 2015) and is of great importance to isolate new strains and to study their physiology. Having a larger number of deep biosphere isolates grown under different catabolic conditions and characterized in terms of temperature range and growth pressure would shed light on their putative function in their natural habitat and in the geochemical cycles of their ecosystem.

To reproduce the extreme conditions of pressure, temperature and geochemistry at the laboratory scale, the conventional equipment is large reactors (from a few tens of milliliters to a few liters) made of stainless steel or other metals (e.g., Inconel, Hastelloy, titanium alloys, etc.), which have demonstrated excellent thermo-mechanical properties along with acceptable chemical compatibility and bio compatible properties (Kato et al., 1996; Deusner et al., 2010; Czernichowski-Lauriol et al., 2017; Garel et al., 2019). Such reactors are used to achieve desired culture conditions representative of the deep biosphere environment to mimic the conditions encountered by deep environment microbes, while beneficiating from a laboratory-scale environment (Yayanos, 1986; Jannasch et al., 1996; Nauhaus et al., 2002; Kato, 2011). Although several new and/or updated sampling equipment and bioreactors have been developed allowing pressure and temperature conditions to be maintained (Garel et al., 2019; Peoples et al., 2019), there is still a lack of research equipment that allows for both (i) pressure-retention during analysis, (ii) ability to implement *in situ* characterization techniques—such as simple visualization, and (iii) fast screening capabilities. Several recent developments have overcome some of these limitations by allowing equi-pressure transfer of samples from reactor to reactor (Garel et al., 2019; Oliver et al., 2021) or by inserting sapphire windows within metal reactors, allowing performing microscopic or spectroscopy investigations (Bao et al., 2010; Maldonado et al., 2016). Such developments have somehow reduced the need for depressurization during analysis but remain scattered. Besides, some limitations remain: large-scale reactors can generate undesirable gradients—temperature, chemical composition—which could induce a bias in the analysis. In addition, these experimental set-ups do not allow for rapid screening experimentation, generally requiring weeks or even months to fully characterize a strain, which significantly slows the speed at which phenotyping can be performed. Therefore, the field of high-pressure microbiology needs to focus on new approaches and instruments to overcome the classical limitations of culturing and studying deep biosphere microorganisms, which are critical for advancing environmental microbiological research. An interesting option to address this gap involves the use of microfluidic reactors.

Over the past 20 years, microfluidics has greatly contributed to the progress of (micro)biology research, including the integration of analytical techniques (Demello, 2006) with cell handling (El-Ali et al., 2006), biochemical assays, which have been dedicated to various research areas such as medical investigations (Sackmann et al., 2014), environmental microbiology (Dusny and Schmid, 2015; Kaminski et al., 2016), etc. These tools offer several advantages over conventional large-scale devices. Indeed, microreactors offer a solution for temperature and feed flow control, reproducibility, *in situ* monitoring (Demello, 2006), rapid parameter screening (Jensen et al., 2000), fast mass and heat transfer (Gervais and Jensen, 2006), and low sample consumption. The combination of size reduction, single-phase and/or multi-phase *in situ* flows and improved reliability, can be recorded in a fast screening methodology development policy. Indeed, microfluidics generates a large amount of data and is already used as a high-throughput cultivation platform for conventional microbiology (i.e., non-extremophilic microorganisms) where hundreds to thousands of microbial colonies at a single-cell level can be studied by automated time-lapse microscopy, leading to a better understanding of microbial behavior and physiology (Moffitt et al., 2012; Grünberger et al., 2015). Conventional microfluidics uses PDMS (polydimethylsiloxane) materials, a polymer that is not compatible with extreme cultivation conditions (e.g., anoxic, high salinity, and high-pressure conditions). Nevertheless, microreactors have been already used to study environmental soil microbiology (Pucetaite et al., 2021) but also marine microbiology, under normal conditions (i.e., non-extremophilic) using droplet-based microfluidics (Girault et al., 2019). Meanwhile, technological developments have been made to use microfluidics for geochemical and microbiological investigations in deep-sea waters, considering microreactors as

in situ (bio)chemical sensors/detectors (Wang et al., 2009; Beaton et al., 2022). In that case, the microreactor undergoes isostatic pressure both externally and internally, therefore not requiring mechanically resistant materials for its fabrication. Besides, microflows have also permitted to develop flow cytometry (Adan et al., 2017) at single cell level for the sorting and further identification of strains in complex environmental samples using either shape and/or fluorescence (fluorescent labeling molecules) detection, although no demonstration has been reported so far for high-pressure conditions. In order to extend the range of microfluidics to high-pressure microbiology investigations as well as deep environmental microbiology at laboratory scale, two strategies have been considered. First, researchers have used transparent capillary tubings (e.g., glass, silica, and sapphire), either with circular or square crossed section, for studying deep environment microorganisms using visible or fluorescence imaging (Beney et al., 1997; Raber et al., 2006; Bourges et al., 2020). Such capillaries offer affordable and easy strategies to access microbial characterization under high pressure, up to 100 MPa. Secondly, the use of diamond anvil cell or specific high-pressure cells, combined to spectroscopy techniques are also used for *in situ* monitoring and characterization studies under high-pressure conditions (Kato and Fujisawa, 1998; Molina-Gutierrez et al., 2002; Oger et al., 2006; Picard et al., 2007; Peters et al., 2014) but are not yet widespread because of specific and costly equipment.

Despite their ease of implementation, capillaries suffer from difficulties in accessing elaborate fluidic designs and controlling temperature. Therefore, it is difficult to envision their use for high throughput screening studies, in particular, for microbial phenotyping.

To address these limitations, on chip high-pressure microreactors have been recently developed (Marre et al., 2010) and utilized for instance for thermodynamics investigations (Xu et al., 2017; Gavoille et al., 2019) or deep underground fluids flow and geochemistry studies (Morais et al., 2016, 2020). High-pressure microreactors can be made out of silicon and Pyrex (semi-transparent), glass–glass (Murphy et al., 2007; Tiggelaar et al., 2007), or even sapphire (i.e., fully transparent; Marre et al., 2021). Such tools benefit from all the advantages of microfluidics, while being compatible with the representative pressure and temperature conditions inherent to deep environment. With the same ability than their room pressure counter-parts, high-pressure on-chip microreactors provide the ability to screen multiple conditions in a single experiment, paving the way for the study of the deep biosphere in the laboratory using new rapid screening methodologies.

In this article, we demonstrate for the first time the use of a novel transparent, high-pressure, biocompatible microfluidic platform for ultra-fast screening of temperature-dependent growth conditions of microorganisms from deep environments. The concept is demonstrated using two marine species with different metabolic strategies: *Thermococcus barophilus* MP^T (Marteinsson et al., 1999), a model piezo-hyperthermophilic and heterotrophic strain isolated from a deep-sea hydrothermal vent and *Methanothermococcus thermolithotrophicus*, a thermophilic and a model hydrogenotrophic methanogen strain isolated from a seafloor geothermal spring (Huber et al., 1982). After introducing the overall methodology, design and fabrication of the microreactor, we present the investigation protocol and the obtained results, which are compared to the literature data.

MATERIALS AND METHODS

Model Strains and Growth Media

We detailed hereafter the two considered strains along with the associated growth media, which were used in this study.

Thermococcus barophilus

Thermococcus barophilus strain MP^T (DSM 11836) was obtained from the DSMZ collection (Deutsche Sammlung von Mikroorganismen und Zellkulturen, Braunschweig, Germany). It is a piezo-hyperthermophilic strain, which was isolated from a deep-sea hydrothermal vent (Snake Pit) on the Mid-Atlantic Ridge (depth, 3,550 m; Marteinsson et al., 1999). It grows from ambient pressure to 80 MPa and exhibits an optimal temperature for growth of 85°C over a wide pressure range (0.3–40 MPa; Marteinsson et al., 1999; Zeng et al., 2009). In this study, the *T. barophilus* cultures were carried out in a *Thermococcales* Rich Medium (TRM, pH 6.8; Zeng et al., 2009), under anoxic conditions. After autoclaving at 121°C during 30 min, the medium was aliquoted into several sterile Hungate tubes (10 ml), sealed with butyl rubber septa, reduced by adding 0.5% reductant (v/v, polysulfides stock solution of 0.05 M; Ikeda et al., 1972), and placed under an inert atmosphere (Ar, 30 kPa). The reductant was also used as a soluble source of sulfur for *T. barophilus* cells.

Methanothermococcus thermolithotrophicus

Methanothermococcus thermolithotrophicus strain $SN\text{-}1^T$ (DSM 2095) was obtained from the DSMZ collection (Deutsche Sammlung von Mikroorganismen und Zellkulturen, Braunschweig, Germany). It is a thermophilic and hydrogenotrophic methanogen archaeon isolated from a geothermally heated seafloor in Italy (Huber et al., 1982). This strain is able to grow on a wide temperature range, from 30°C to 70°C (Huber et al., 1982) with an optimum temperature at 65°C, and displays a piezophilic behavior when growing under elevated pressure conditions (i.e., 50 MPa; Bernhardt et al., 1988). In this study, *M. thermolithotrophicus* was cultivated in the AGW (Artificial Ground Water) medium (Dupraz et al., 2013) supplemented with 120 mM HEPES. The anoxic cultures were performed optimally at 65°C in serum flasks and with a 0.2 MPa gas mixture (mol/mol) of 80% H_2 and 20% CO_2, with a final cell density in stationary phase reaching 2×10^8 cells.ml^{-1}. When growing at elevated pressure conditions, the H_2/CO_2 partial pressure was established either at 2 or 3 MPa and supplemented with inert gas (Nitrogen) to reach the desired total pressure in the set up (i.e., 5 and 10 MPa, respectively). Only the initial (T_0) and end-points (T = 18 h of growth) were considered to evaluate the growth of this strain into the high-pressure microfluidic temperature gradient setup.

In all cases, the pre-cultures in mid-exponential phase of growth were used to inoculate Hungate tube and then transferred to the high-pressure microfluidic reactors with an initial cell concentration of ~5.10^6 cells.ml^{-1}. In the case of *T. barophilus*, for which a full phenotyping study was performed, cell concentrations in control culture tubes at 85°C (Hungate tube for ambient pressure condition and high-pressure vessels for high-pressure conditions) were assessed by direct cell counting onto a Thoma chamber (Preciss, France; surface area: 0.0025 mm^2, depth: 0.1 mm) using a DM2000 LED phase contrast optical microscope (Leica Microsystems CMS GmbH, Germany).

Microreactor Design and Set-up

The overall strategy for performing multi-temperature culture of microorganisms under pressure on a chip is to take advantage of microfluidic pools, which will serve as micro-wells, each exposed to a particular temperature condition. Microbial growth can then be monitored directly *in situ* for each pool by microscopic counting. We detail hereafter the microreactor design and dimensioning strategy employed to achieve this goal.

The microreactors were fabricated using the well-known silicon/Pyrex technology (Marre et al., 2010). This microfabrication technology is chosen for: (i) the optical access through the Pyrex side, allowing *in situ* characterization by optical microscopy, (ii) the excellent thermomechanical properties of silicon and Pyrex, allowing to work in a wide range of pressure and temperature conditions, and (iii) the biochemical inertness of both materials ensuring a good biocompatibility. The microreactors were fabricated using standard photolithography, wet etching and anodic bonding process, as previously described in the literature (Marre et al., 2010). The microreactor (**Figure 1A**) consists of one inlet and one outlet, used to inject the inoculated growth medium. It displays a U-shaped central microchannel (width: $w = 200\,\mu m$, depth: $d = 30\,\mu m$ and length: $L = 95\,mm$), which is used to deliver the fluid to 10 pairs of regularly spaced quasi-circular culture micropools on each branch, in which the microorganisms grow (diameter: $D = 300\,\mu m$, depth: $d = 30\,\mu m$, $V = 1.5\,nl$ or 1.9 nl, depending on the experiments). Each pool are placed on either side of the main channel and connected by a restriction channel (50 µm wide).

The main interest of this design stands in the possibility not only to work in a single phase mode were the inoculum occupied both the micro-chambers and the main channel but also to work in diphasic mode aiming at using a fluid non miscible with the inoculum for both "sealing" and feeding the micro-chambers with molecules through phase transfer (**Figure 1B**). In these cases, both liquids and gases may be considered. The microreactor surface being hydrophilic, the wetting phase is the inoculum. Hence, the wettability properties favor the inoculum to stay inside the micro-chamber (**Figure 1B**). However, the restriction channels are used to prevent any invasion of the micro-chambers with the second phase due to fluid flows during the microreactor filling procedure.

The microreactor is in contact with a temperature gradient generating device ensuring a linear temperature gradient between a T_{min} (either 60.1°C or 72.5°C for *M. thermolithotrophicus* and *T. barophilus*, respectively) and a T_{max} (either 70°C or 95°C for *M. thermolithotrophicus* and *T. barophilus*, respectively) along the microchip (**Figure 2**; **Supplementary Information 1**). Thus, 10 different temperatures could be examined simultaneously in a single experiment, while four different microchambers were subjected to the same temperature, providing a fourfold measurement to estimate the variability of results (**Supplementary Figure S1**). For *T. barophilus*, experiments were performed at three different pressures, 0.1, 5, and 10 MPa, in microreactors with 1.5 nl chambers. In parallel, experiments at 0.1 MPa (control) and 15 MPa were performed in microreactors with 1.9 nl chambers to demonstrate the robustness of the approach, independent of the microreactor itself. The microreactor with the 1.9 nl chambers was used for *M. thermolithotrophicus* experiments.

In a typical experimental set-up (**Figure 2**), the high-pressure temperature-gradient microreactor is connected to external fluid management equipment using a compression part, as described previously (Marre et al., 2010), made of polyetheretherketone (PEEK) for its biocompatibility characteristics and thermomechanical stability. The microreactor is placed on the temperature gradient system, which consists of an insulating block made of PEEK (for its thermal insulation properties) inside which two copper cylinders are inserted. A heating cartridge is inserted in the first cylinder, to generate a stable hot temperature zone using a Eurotherm temperature controller. The second cylinder is cooled to a targeted low temperature using a water flow provided by a circulating cryostat bath. To ensure a perfectly linear thermal gradient, an aluminum plate is placed in contact between the two copper cylinders, right below the microreactor (**Figure 2**; **Supplementary Figure S1**). A thermal paste is deposited between the aluminum and the microreactor to ensure excellent heat transfer. The whole assembly (i.e., microreactor + compression part + temperature gradient device) is placed under a confocal LASER scanning microscope. The compression part is connected to transparent tubes containing the fluids and equipped with movable pistons, in order to push the fluids into the microreactor.

Experimental Protocol

We have used two distinct protocols depending on both the considered strain and their growth strategy. Each protocol corresponds to a specific method depending on whether we considered a single fluid, a diphasic liquid–liquid or a gas–liquid approach. In a typical high-pressure microfluidic experiment, the inoculation was performed in sterile and anoxic ways with either *T. barophilus* or *M. thermolithotrophicus*.

First, a Hungate tube containing 10 ml of either TRM medium supplemented with polysulfides for *T. barophilus* or AGW medium for *M. thermolithotrophicus* (see the growth medium above) was inoculated from a mid-exponential phase pre-culture to reach a final cell concentration of 5×10^6 cells.ml^{-1}. This cell concentration was chosen to ensure filling all the micropools in the microfluidic setup with 5–10 cells. Indeed, preliminary tests have shown that by considering a lower cell concentration, some micropools were empty. After inoculation, the Hungate tube was homogenized and 2.0 ml were transferred in a 5 ml high-pressure transparent tube equipped with a movable piston (Tubing 1, **Figure 2**), which had been first degassed (five cycles

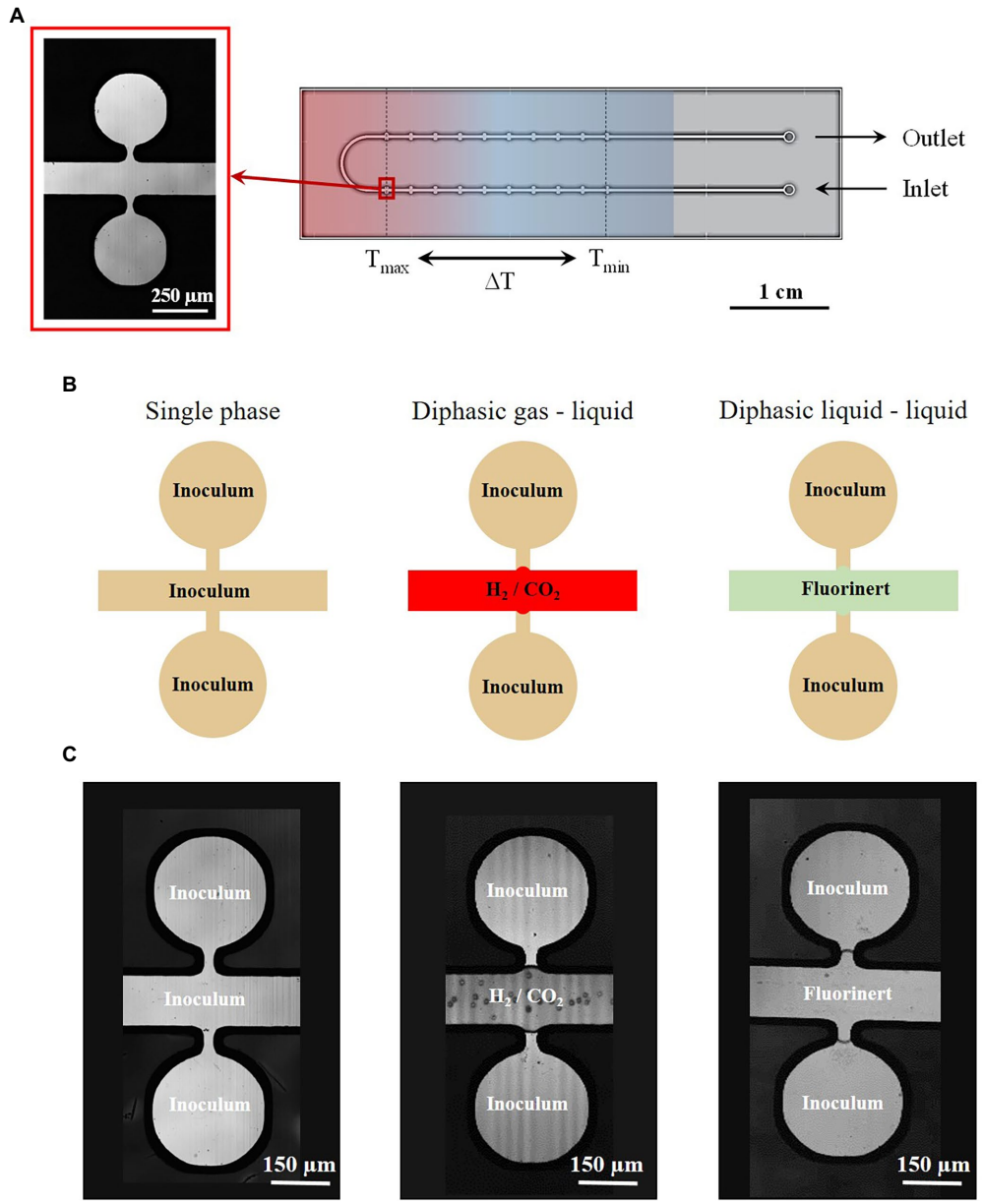

FIGURE 1 | (A) Design of the temperature-gradient microreactor developed and used in this study with a microscope picture of the micropools used for both *Thermococcus barophilus* and *Methanothermococcus thermolithotrophicus* cultivation. **(B)** Different feeding strategies implemented into the microfluidic setup using growth medium phases and several interfaces. **(C)** Pictures of the concerning cultivation interfaces into the microreactor.

of N_2–30 kPa/vacuum) to maintain anoxic conditions. This latter was then closed and connected *via* PEEK caps and connectors to a Teledyne ISCO high-pressure piston pump, previously filled with DI water as a pressurization fluid through a 3-way valve (V_1, **Figure 2**). The pressure was applied by pushing with DI water on the mobile piston. The microreactor was first vacuumed to remove the air phase inside the device and later flushed with inert gas (N_2) by opening valves V_3 and V_4 (**Figure 2**). This cycle was reproduced three times and the microreactor was finally left under vacuum to ensure getting rid of any gas bubbles in the micro-chambers during the filling procedure. Then, the microreactor was filled by delivering the inoculated growth medium at a flowrate of 50 µl.min^{-1} by opening V_2 and V_4 (**Figure 2**). The pressure inside the full set-up was maintained thanks to a membrane back pressure regulator (Equilibar) placed downstream the microreactor, enabling precise control of the pressure down to ultra-low flowrates (**Figure 2**).

When considering single-phase growth strategy (i.e., with *T. barophilus*), the pressure was slowly increased using the ISCO syringe pump (30 MPa.h^{-1}) to the desired conditions. The pump was then set into a pressure constant mode at the

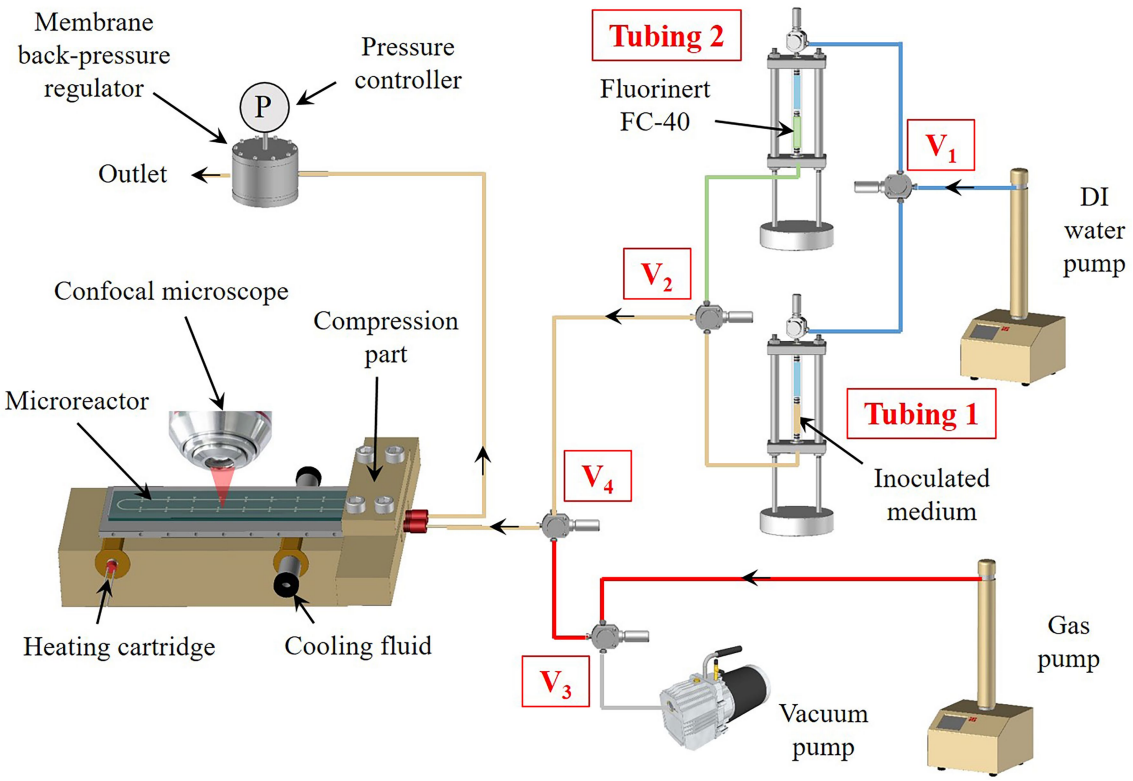

FIGURE 2 | Set-up of the high-pressure microfluidics platform for phenotyping microorganisms at temperature (see the description in the text).

working pressure. The remaining 8.0 ml of the inoculated medium was divided to serve as both a high-pressure positive control (4.0 ml corresponding to the high-pressure experimental pressure conditions) and a room pressure control (4.0 ml), at 85°C. In parallel, a 10-ml negative control (growth medium without inoculum) was performed to ensure there would be no contamination issues during the experiment.

When considering a diphasic gas–liquid growth strategy (i.e., with *M. thermolithotrophicus*), once the microreactor has been filled with the liquid inoculum, the pressure was set to the desired operating pressure and valve V_2 was closed. Then, the gas phase (H_2/CO_2 mixture, 80/20 mol/mol, supplemented with N_2 to reach the desired total pressure) was first pressurized inside the high-pressure syringe pump (Gas pump, **Figure 2**) up to the working pressure. Valve V_3 was opened in order to inject the gas phase inside the microreactor at a slow flowrate ($1\,\mu l.min^{-1}$) to avoid any undesirable invasion of the microchambers by the gas phase, resulting in gas–liquid interfaces between the microchambers and the main microchannel (**Figures 1B,C**).

Potentially, in the case of a diphasic liquid/liquid growth strategy (not utilized in this study), the same procedure can be applied: first, a pressurization of the microreactor with the inoculum, followed by the injection of an immiscible liquid (e.g. Fluorinert FC40), through the switch of the three-way valves V_1 and V_2 to inject the Fluorinert from Tubing 2 (**Figure 2**) to the microreactor. Similarly, as for gases, a low flowrate is applied ($1\,\mu l.min^{-1}$) to avoid any invasion of the microchambers by the inert fluid (**Figures 1B,C**).

Image Analysis: Pool Area Measurement and Cell Counting

The initial cell concentration (about $4–5 \times 10^6$ cells.ml^{-1} depending on the micropool volume) was experimentally confirmed by counting the cells in each micropool. As a starting point, the number of cells per pool was typically 8 ± 3 cells. Then, the growth rate in each micropool was determined as follows (**Figure 3A**). First, the volume of each pool was accurately determined using 3D confocal imaging followed by image analysis (ImageJ©), as detailed in **Supplementary Information 3**. Cell counting overtime (**Figure 3B**) was then performed based on image captures made with a confocal microscope (Leica Microsystems, SP8), at 40× objective (in reflection mode) using the Leica LasX© software. OpenCFU software (Geissmann, 2013) was used for semi-automatic counting and for more accurate cell counting. Since both *T. barophilus* and *M. thermolithotrophicus* cells are tiny cocci (0.8–2.0 µm diameter; Huber et al., 1982; Marteinsson et al., 1999), the processing parameters of OpenCFU were adjusted to detect both species in the micro-chambers (see **Supplementary Information 3** for details concerning the choosen OpenCFU parameters). Data were then combined to plot the growth curve for each micropool (**Figure 3C**), which all exhibit the classical shape of microbial

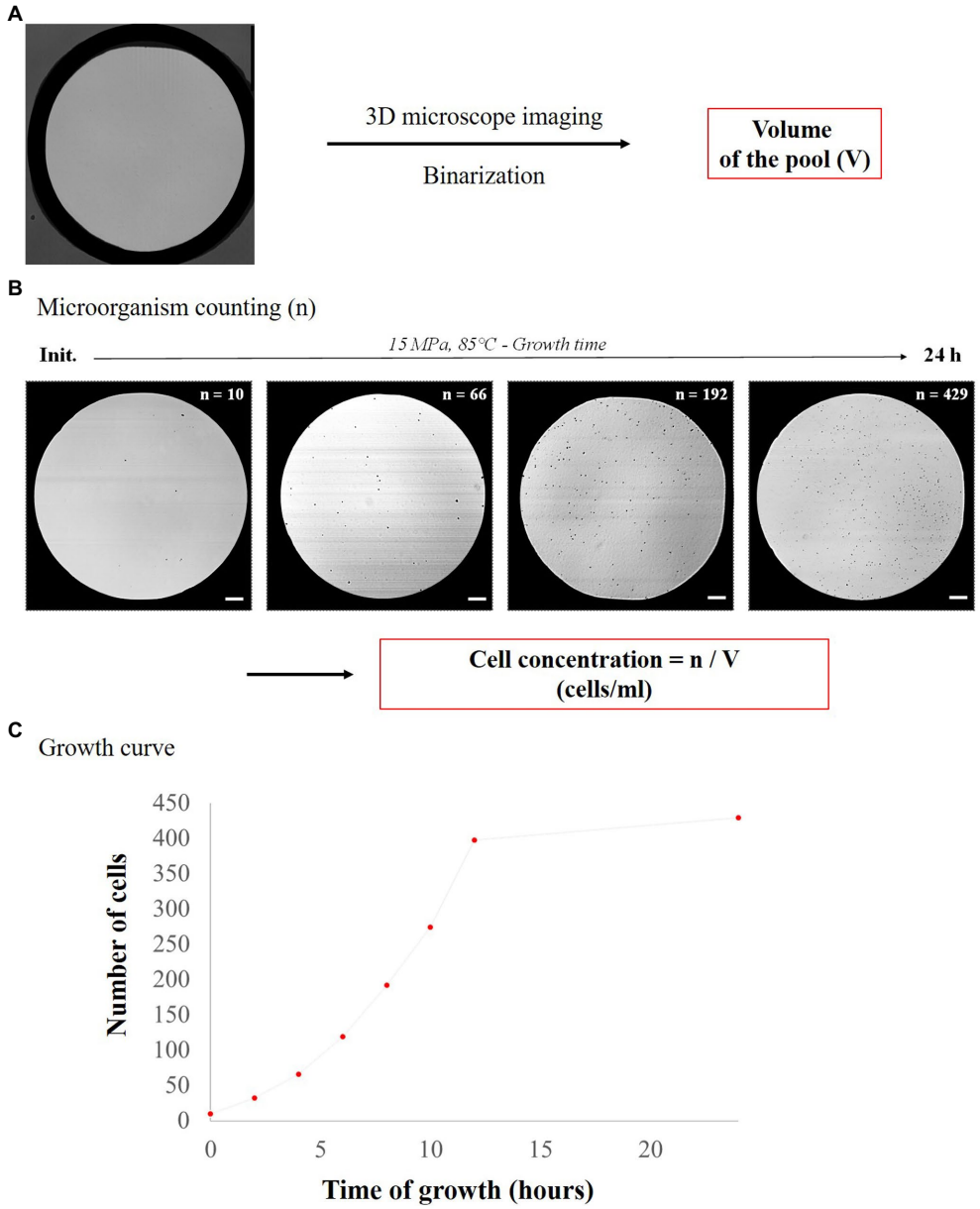

FIGURE 3 | Schematic flowsheet for determination of cell concentration in each pool. **(A)** Determination of micropool volumes using 3D confocal microscopy and ImageJ analysis and **(B)** examples of pictures of *Thermococcus barophilus* growth over time with the corresponding cell number (*n*) at 15 MPa and 85°C (scale bar = 25 µm), allowing determination of cell concentration (cells.ml^{-1}). **(C)** Growth curve with cell number versus time (15 MPa, 85°C).

growth curve (**Supplementary Figure S2**; i.e., lag phase, exponential phase and stationary phase—the death phase was not detected in here due to the "short" incubation time of 24 h max considered in our experiments). Finally, an extrapolation of the number of cells in the micropools was performed to obtain a normalized cell concentration (cells.ml^{-1}) over time (**Supplementary Figure S2**). This extrapolation was done using the following formula:

$C = n/V$.

with C corresponding to the cell concentration (cells.ml^{-1}), V to the volume of the micropool and n to the number of cells per pool. After conversion of cell concentrations to logarithmic values, growth rates were calculated from the logarithmic growth phase slopes of quadruplicate micropool culture experiments using the LINEST function in Excel. Error bars indicate the standard error from linear regressions of quadruplicate experiments (four micropools for one temperature data point) using the microfluidic temperature gradient chip (**Figure 4**). Maximum cell densities were measured from the stationary phase for all pressure conditions and error bars indicate standard deviation of quadruplicate experiments (**Figure 4** for *T. barophilus* and **Figure 5** for *M. thermolithotrophicus*). For *T. barophilus*, an

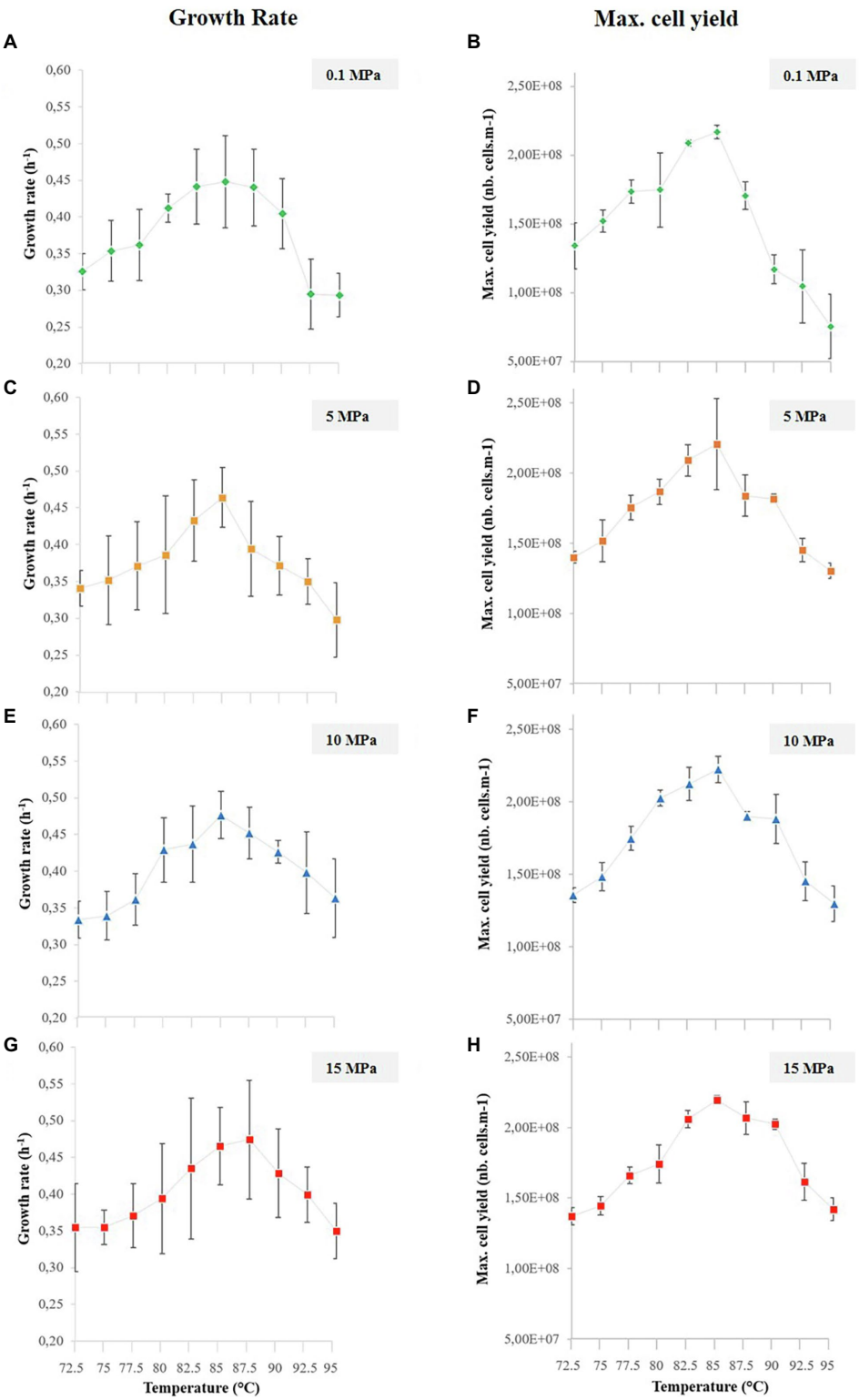

FIGURE 4 | *Thermococcus barophilus* growth rates (left column) and maximal cell yields (right column) over 10 temperature conditions (i.e., 72.5°C–95°C) for several pressure conditions, while growing in the temperature gradient on-a-chip: **(A)** *T. barophilus* growth rates at 0.1 MPa. **(B)** *T. barophilus* maximum cell densities at 0.1 MPa. **(C)** *T. barophilus* growth rates at 5 MPa. **(D)** *T. barophilus* maximum cell densities at 5 MPa. **(E)** *T. barophilus* growth rates at 10 MPa. **(F)** *T. barophilus* maximum cell densities at 10 MPa. **(G)** *T. barophilus* growth rates at 15 MPa. **(H)** *T. barophilus* maximum cell densities at 15 MPa. Error bars represent the SD from the four replicates on a single experiment using the gradient on chip microfluidic setup.

overnight positive control (batch culture in 10 ml flask for atmospheric pressure and 5 ml for high-pressure millifluidic vessel under high-pressure conditions) at 85°C with the same cell inoculum as in the microfluidic experiment was always performed to ensure cell viability. Since the conventional high-pressure experiment requires decompression, only an endpoint measurement (after 12 h of growth) was considered for cell counting and compared to microfluidic growth at the same time-period, to avoid any growth bias due to decompression.

RESULTS

Thermococcus barophilus Phenotyping

Images taken overtime showed an increasing number of cells in the micropools (up to 24 h of growth), regardless of the pressure or temperature considered. This allowed us to estimate the evolutionary growth of *T. barophilus* (**Figures 3B,C, 4**) as a function of temperature for different pressures. Each experiment is performed at a single pressure (0.1, 5, 10, and 15 MPa, respectively), but gathers 10 different temperature conditions (72.5°C–95°C) in quadruplicate (i.e., 40 micro-batch experiments in a single run). Based on these images, cell numbers were correlated to the corresponding cell concentrations in cells. ml^{-1}, allowing the phenotype of *T. barophilus* to be screened under 40 different P/T conditions and obtaining 40 growth curves in only 1 week of experiments (**Supplementary Figure S2**).

To compare the combined effects of high pressure (without decompression) and temperature on *T. barophilus* growth already reviewed in the literature, we plotted the growth rates and maximum cell yields (**Figure 4**) obtained in each pressure experiments on the temperature gradient on-a-chip. Average growth rates and maximal cell yields correspond to replicate of four microbial growths in a single experiment. The average growth rates ranged from 0.29 ± 0.03 to 0.45 ± 0.06, 0.30 ± 0.05 to 0.46 ± 0.04, 0.33 ± 0.02 to 0.48 ± 0.03 h, and 0.35 ± 0.04 to $0.47 \pm 0.05\,h^{-1}$ for 0.1, 5, 10, and 15 MPa pressure conditions, respectively (**Figures 4A,C,E,G** left column). The temperature-dependent pattern was similar for all four pressure conditions: growth rates were the highest for a temperature close to the known optimal temperature for *T. barophilus* (i.e., 85°C; Marteinsson et al., 1999), and decreased when moving away from the optimum, which is in accordance with previously published data. It is interesting to note that, due to the large amount of data available, the growth rate curves could be plotted with slightly better accuracy (2.5°C shift between each condition) than that obtained with the classical approach. It can also be observed that the temperature evolution of the growth rates shifted slightly to higher temperature values when growth was performed at higher pressure conditions (5, 10, and 15 MPa), however, the optimal growth temperature was not affected by the pressure variations in the explored range.

This shift was also observed with the maximum cell yields which ranged from $7.54 \pm 2.33 \times 10^7$ to $2.17 \pm 0.05 \times 10^8$, $1.30 \pm 0.05 \times 10^8$ to $2.17 \pm 0.32 \times 10^8$, $1.30 \pm 0.12 \times 10^8$ to $2.22 \pm 0.09 \times 10^8$, and $1.37 \pm 0.06 \times 10^8$ to $2.19 \pm 0.30 \times 10^8$ cells. ml^{-1} for 0.1, 5, 10, and 15 MPa pressure conditions, respectively (**Figures 4B,D,F,H** right column). For comparison, parallel experiments in millifluidic high-pressure vessels were performed for each pressure at 85°C, as positive controls. *T. barophilus* growth was checked after one night of growth and reached the plateau of 2.10^8 cells.ml^{-1} for each high-pressure experiment (data not shown), thus in good agreement with the results of the microfluidic approach.

Experiments With *Methanothermococcus thermolithotrophicus*

The high-pressure microfluidic temperature gradient setup was also implemented with the cultivation of a methanogen strain in order to show the cultivation versatility of this setup. As the model strain is a thermophilic and hydrogenotrophic methanogen, it requires the supply of a gas phase (H_2/CO_2) to grow. The temperature range was chosen as a function of the literature (i.e., 60°C–70°C, Bernhardt et al., 1988) for two pressure conditions, 5 and 10 MPa (i.e., total pressure) with a partial gas pressure (H_2/CO_2, 80/20% mol/mol) of 2 MPa and 3 MPa, respectively. As this strain was previously described to better grow under elevated pressure conditions (Bernhardt et al., 1988), these partial pressures were chosen in order to screen rapidly the effects of dissolved gases (H_2 and CO_2) at 10 different temperatures on *M. thermolithotrophicus* growth (i.e., cell yield in stationary phase). To do so, a quadruplicate counting was performed for these 10 temperature conditions, both at the initial time point and after 18 h of growth, for both pressure conditions considered in this study (5 and 10 MPa; **Figure 5**; **Supplementary Figure S3A**).

Interestingly, the cell yields at 5 MPa ($P_i = 2$ MPa) reach the optimal cell density observed at atmospheric pressure conditions (about 2×10^8 cells.ml^{-1}) for both the optimum growth temperature and the above ones (i.e., 65°C–70°C; **Supplementary Figure S3A**). However, for growth temperatures below the optimum (i.e., 60.1°C–63.4°C), the cell yields reach a lower cell density, approximatively two-fold less (about 1.25×10^8 cells.ml^{-1}) with an intermediate temperature at 64.5°C (about 1.5×10^8 cells. ml^{-1}; **Supplementary Figure S3A**). When considering the initial cell density into the micropools, *M. thermolithotrophicus* cells seem to grow better at temperatures between 66.7°C and 68.9°C (**Figure 5**). The same growth temperature pattern is observed when *M. thermolithotrophicus* is cultivated at 10 MPa (Pi = 3 MPa). Indeed, the strain displays a higher cell yield when growing at temperatures between 65.6°C and 68.9°C. However, the highest cell density is 2-fold lower than the optimum cell density known for this strain (**Figure 5**; **Supplementary Figure S3A**).

DISCUSSION

In this study, we provide proof-of-concept for the operation of a novel high-pressure microfluidic culture approach and demonstrate that it can rapidly screen the effects of temperature on the growth of the piezo-hyperthermophilic model of deep hydrothermal origin *T. barophilus* strain MP^T (Marteinsson et al., 1999) along with a marine thermophile strain *Methanothermoccus thermolithotrophicus*. *Thermococcus barophilus* uses molecular

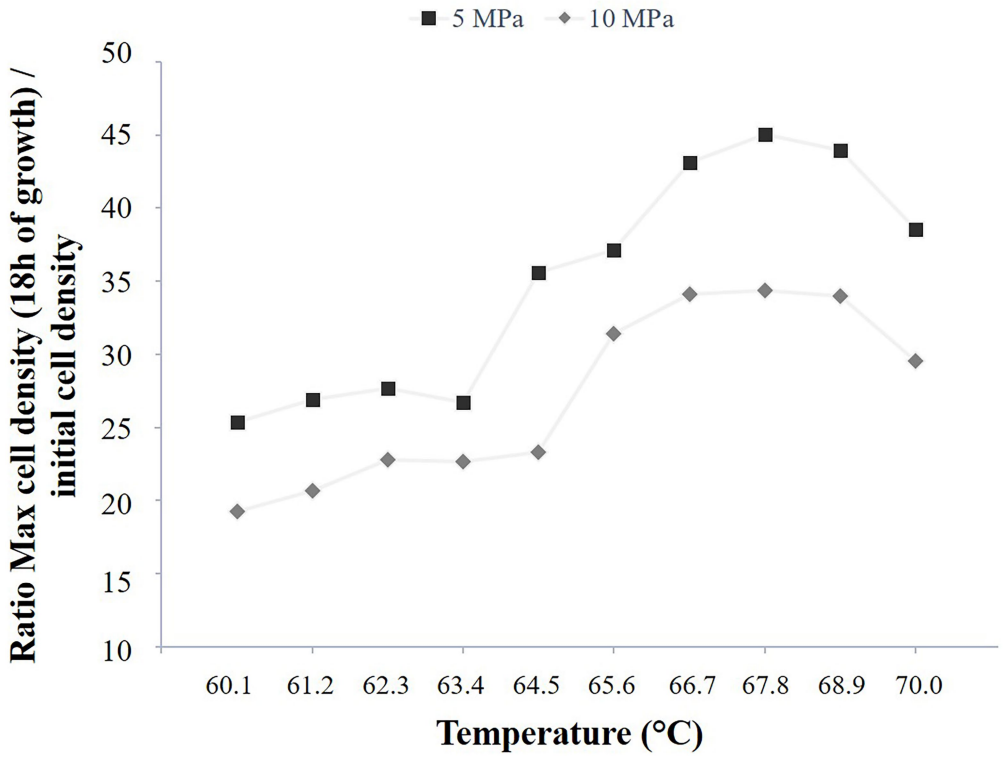

FIGURE 5 | *Methanothermococcus thermolithotrophicus* growth comparison in a temperature gradient-on-a-chip between two-pressure conditions, 5 and 10 MPa total pressure (2 and 3 MPa of partial pressure of H_2/CO_2, respectively). Ratio of the mean cell density after 18 h of growth to the corresponding mean initial cell density, for two temperature gradient microfluidic experiments (temperature: 60.1°C–70°C).

and structural adaptation to thrive in its harsh environment, being able to cope with high pressure and fluctuating salinity and temperature conditions (Vannier et al., 2015; Cario et al., 2015a,b, 2016). This piezophilic model is easy to manipulate (Thiel et al., 2014) and is a versatile microorganism with unique metabolic attributes for adaptation to deep-sea vent conditions (Le Guellec et al., 2021). In addition, this archaeal species exhibits several other deep-sea vent clones with other metabolic properties (Kozhevnikova et al., 2016; Oger et al., 2016) expanding the catabolic capabilities of this species. Therefore, this strain was a prime model for this study. Meanwhile, *M. thermolithotrophicus* is a model methanogenic strain, already cultivated and studied under elevated pressure conditions (Bernhardt et al., 1988; Jaenicke et al., 1988; Miller et al., 1988).

Microorganisms in the deep biosphere flourish under extreme environmental conditions and only a small fraction of them have been isolated to date. Working on isolates remains a technical challenge but the best opportunity to understand the microbial mechanisms enabling life at depth and the limits of life on Earth. Studying growth behaviors under such extreme conditions provides insight into the molecular and cellular processes developed by piezophilic strains for microbial adaptation to high pressure. Recreating the *in situ* pressure conditions require specific culture approaches and is extremely time-consuming for strain phenotyping. Classical microbiology approaches have overcome some of these time issues by using spectrophotometry and other automated counting methods (e.g. cell sorting and FACS) to estimate microbial growth and phenotype (Zuleta et al., 2014; García-Timermans et al., 2020). However, characterizing cells within a culture without disturbing conditions (i.e., microorganisms live imaging; Bourges et al., 2020) while mimicking *in situ* pressures (from the deep biosphere) remains a challenge whenever high-pressure vessels are not equipped with a sapphire or optic window for cell characterization.

In this study, the high-pressure microfluidic screening approach yielded 40 growth curves at different pressure and temperature conditions in a record time.

For *T. barophilus*, the final growth rates are comparable with the literature at ambient pressure and temperatures between 75°C and 90°C (Marteinsson et al., 1999) and at 85°C and for pressure conditions below 20 MPa (i.e., 0.35–0.45 h^{-1}; Vannier et al., 2015). Marteinsson and colleagues reported that *T. barophilus* was an obligate piezophile for temperature above 95°C. Our study confirmed that *T. barophilus* shifts its tolerance to higher temperatures when growing under higher-pressure conditions (**Figures 4**, **6**), and showed that it is still able to grow at atmospheric pressure and 95°C (well-defined environment with a precise temperature measurement, **Figure 1**; **Supplementary Information 1**). At atmospheric pressure, growth slowed as did cell density, which was the lowest at this extreme temperature. It is well-known in the literature that elevated pressures significantly increase the metabolism

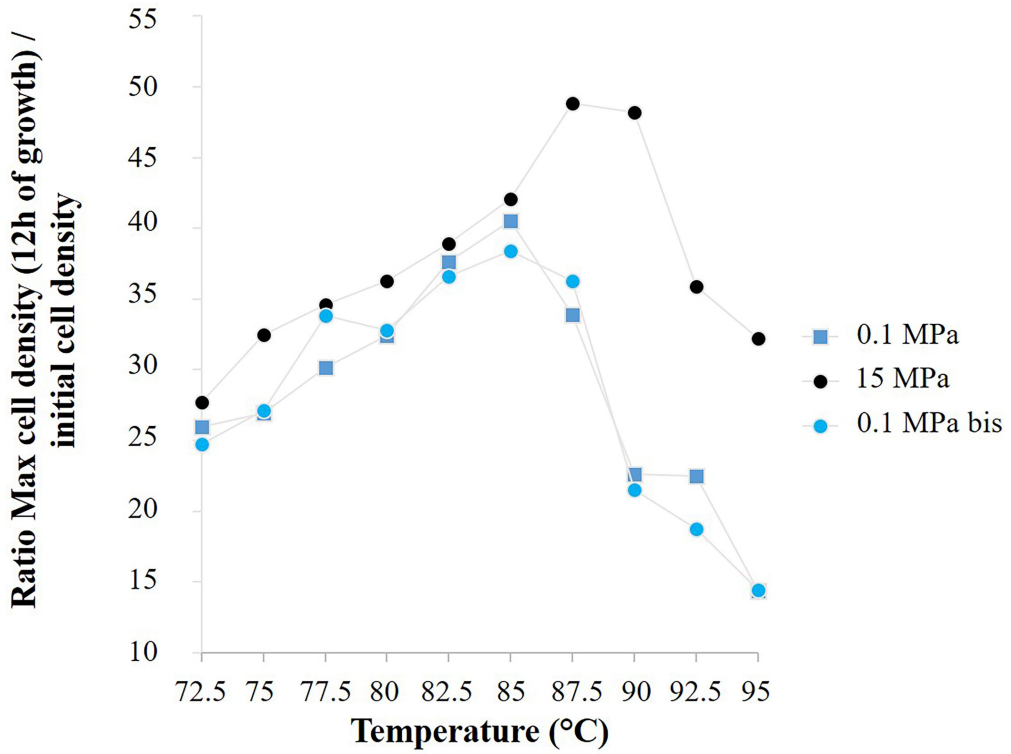

FIGURE 6 | Ratio of the mean cell density of *Thermococcus barophilus* after 12 h of growth to the corresponding mean initial cell density, for three temperature gradient microfluidic experiments (72.5°C–95°C): atmospheric pressure (0.1 MPa) in a microchip of 1.5 nl pool volume, both 15 MPa and atmospheric pressure (0.1 MPa bis) in a microchip of 1.9 nl pool volume.

of deep-sea strains while growing at elevated temperatures (Miller et al., 1988; Takai et al., 2008). In addition, the high-pressure shifts the upper temperature range of hyperthermophilic strains (Miller et al., 1988; Pledger et al., 1994; Canganella et al., 1997; Marteinsson et al., 1999), which was also observed in this study (**Figure 6**). The culture approach is important for studying the upper temperature limit of life in hyperthermophilic microorganisms, and even more so when they are piezophilic, as high-pressure is an essential metabolic driving force for these strains isolated from the deep-sea (Takai et al., 2008; Oliver et al., 2020). In this study, combining several conditions of high temperature and pressure (without decompression) in a single experiment provided a rapid mean for characterizing the temperature range of a model strain of deep hydrothermal origin. Furthermore, this work demonstrates that high-pressure microfluidics is a robust and reproducible technique to examine microbial growth at different pressure conditions. Indeed, *T. barophilus* displayed the same temperature profile when growing in different micropools volume (1.5 and 1.9 nl; **Figure 6**).

Concerning *M. thermolithotrophicus*, this microfluidic setup allowed us to cultivate the methanogen strain under elevated pressure conditions (i.e., 5 and 10 MPa) with two different partial pressure conditions of H_2/CO_2 (i.e., 2 and 3 MPa, respectively). *M. thermolithotrophicus* cells were easily detected in the micropools using reflective mode (Visible), and can also be monitored thanks to their putative autofluorescence (**Supplementary Figure S3**). The growth of this strain is known to be enhanced under elevated pressure conditions (i.e., 50 MPa, see Bernhardt et al., 1988). Thus, we screened the effects of partial gas pressure (H_2/CO_2) on the cell yields, at two pressure conditions and over 10 temperature conditions. Interestingly, this strain seems to have a better growth under lower partial pressure of H_2/CO_2 over the range of temperature conditions tested (60°C–70°C). This study needs further investigations (e.g., gas solubility calculations according to the thermodynamic parameters) as well as to be confirmed with growth rate experiments in order to evaluate the toxicity of H_2 and/or CO_2 at higher partial pressures for this strain (Dupraz et al., 2013).

Beyond this first demonstration, this setup is adaptable and evolutive and will allow in the short term to cover a wider range of temperature and pressure conditions (0°C–150°C at up to 70 MPa with the new sapphire reactor technology; Marre et al., 2021) to better appreciate the growth (limits and tolerance) of a strain under extreme culture conditions. An interesting outcome is the implementation of various cultivation strategies in order to capture a wide variety of microorganisms with different metabolic requirements: (i) anaerobes and heterotrophs using a single-phase medium; (ii) autotrophs using a diphasic gas–liquid interface; and (iii) aerobes using a diphasic liquid–liquid interface where the immiscible oil serves as an oxygen supplier (Tanet et al., 2019;

Figure 1). This microfluidic setup could provide new opportunities to screen known piezophiles and see how high pressure without decompression could extend the upper temperature range, e.g., for *T. barophilus* and other strict piezophiles such as *Pyrococcus yayanosii* CH1 (Zeng et al., 2009). In addition, high-pressure microfluidics could also be used as a fast-screening tool to characterize new isolates from the deep biosphere and to study the effect of pressure on growth in the vast majority of previously isolated strains in which this parameter has never been studied. Indeed, as an example, of the 129 bacterial species and 55 archaeal species that have been isolated from deep-sea hydrothermal vents to date and are recognized by the International Committee on Systematics of Prokaryotes (ICSP), only 23 have been examined for the effect of hydrostatic pressure on growth (Jebbar et al., 2015; Zeng et al., 2021).

Compared to conventionally studied batch microbial growth (i.e., large volume cultures at the ml or liter scale), microfluidics handles small volumes for batch culture (i.e., pl to µl) and such a volume variation could lead to a substantial change in microbial behavior when considering different situations such as surface area to volume ratio and nutritional aspect. The low cultivability scores in the laboratory of strains from natural environments have multiple explanations largely reviewed in the literature (e.g., Alain and Querellou, 2009; Lewis et al., 2021). Growth defects may be due to intrinsic environmental differences related, among others, to both accessible nutrients and the confined space available for growth. This variation in volume, known as the "bottle effect" is mainly reported in the literature for natural communities in aquatic environments (Hammes et al., 2010). Depending on the strain and its site of isolation, the effect of containment may be species-dependent and the size of the compartmentalization may trigger or constrain a microbial strain-specific phenotype. The model strain studied here, i.e. *T. barophilus*, comes from a deep hydrothermal vent, which is an environment with significant local chemical and physical gradients at the millimeter to the centimeter scale, changing in time and space, and containing a multitude of microniches for the growth of microorganisms (Dick, 2019). Microfluidics enables the handling of local gradients on a very small scale. It therefore appears to be a relevant cultivation approach to understand cell behavior (i.e., the microbial response to the local environment) or even cell interaction on a small scale. Such a confined environment for microbial cultivation does not account for larger scale processes (e.g., microbial dispersion and colonization) and depending on the type of study, multi-scale controls are needed to avoid biases induced by confined cultures. Here, *T. barophilus* and *M. thermolithotrophicus* cells were able to grow in a confined environment (mono- or diphasic) over several cell generations (about 2 log) in a similar fashion to dynamic growth in a "large" batch liquid culture (i.e., ml cultures in a closed vial). Thus, high-pressure microfluidics is a complementary approach to study microbial behavior under *in situ* pressure conditions.

Despite the reproducibility of this cultivation approach, such a confined environment presents a local nutrient gradient and motile microorganisms could use of their swimming abilities to seek out favorable available resources and/or conditions (Stocker and Seymour, 2012). *Thermococcus barophilus* is a motile microorganism but low-pressure conditions abolish its swimming capabilities (Vannier et al., 2015). Therefore, this approach on-a-chip is suitable at pressure conditions below 20 MPa, as *T. barophilus* cells are non-motile at these low pressure conditions and will not migrate from one pool to another. Concerning the application of this methodology to motile microorganisms, future developments will consider the use of non-miscible inert fluid (such as Fluorinert©) injected in the main microchannel to "seal" the micropools during the experiment, therefore preventing cell migration (see **Figure 1** and the concerning protocol in the method section). Nevertheless, one can also think of taking advantage of connections between pore-like structures (e.g., porous media) on-a-chip with temperature and/or chemical gradients to get insights into cell motility towards better living conditions, which can be investigating in real time and under pressure with such approach. In summary, microspatial structures matter for phenotyping studies, thus it is important to design the appropriate microreactor in order to take into account variable parameters (e.g., cell migration, nutrient availability, diffusion coefficient) to ensure both the reproducibility and the closest representativeness of microbial habitats.

CONCLUSION AND PERSPECTIVES

This study highlighted the potentialities of high-pressure microfluidics for microbial strain phenotyping and validated high-pressure microfluidics as a valuable complementary tool for temperature range screening of extremophilic microorganisms, under pressure. It demonstrated that microfluidics can be used in order to accelerate microbial phenotyping of microorganisms (here piezo-hyper/thermophilic models) and provided a proof-of-concept for the operation, efficiency and reliability of microfluidics to screen several parameters at a time (e.g., temperature, pressure, and also nutrients gradient) and get the overall and combined phenotype of a single strain in a record time. This set up also demonstrated its versatility with the ability to target various metabolic requirements, reflecting the wide variety of the microbial metabolisms in the deep biosphere.

In this study, one pressure condition experiment (in quadruplicate) took only a few days (pre-culture plus cultivation test) to perform 10 temperature conditions whereas the conventional high-pressure microbiology approach would have taken weeks or months to get these data. High-pressure microfluidic technology can acquire large amounts of data in a short time, resulting in a huge amount of data to process (i.e., image capture, image analysis, and data processing). Our future goal is to implement automation of cell image capture and cell counting using artificial intelligence (machine learning in particular). Indeed, machine learning could help speed up counting but also increase accuracy and reduce errors (Qu et al., 2019). Such a methodology coupled to high-pressure microfluidics, would promote in-depth investigations (e.g., morphologies, catabolisms, and effects of chemicals) of various

microorganisms from the deep-biosphere and greatly increase our knowledge of this remote biosphere.

Microfluidics provides an excellent opportunity to better document microbial phenotypes in a short time. This technology is widely applicable to other extremophiles (e.g., halophiles, psychrophiles) and could be adapted to diverse and more challenging culture conditions in order to explore the vast extremophilic microbial realm on Earth. The development of resilient microfabrication materials for extreme microfluidics (e.g., sapphire microreactors – (Marre et al., 2021)) is worth considering and could afford unique features to capture the large as-yet uncultured microbial fraction.

DATA AVAILABILITY STATEMENT

The original contributions presented in the study are included in the article/**Supplementary Material**, and further inquiries can be directed to the corresponding authors.

AUTHOR CONTRIBUTIONS

AC and SM designed this research project, made the microreactor design, analyzed data, and wrote the original draft. AC, SM, and ON developed the set-up. ON developed the temperature gradient device. AC and ML performed the experiments and collected data. AC, ON, and KA edited and wrote sections of the manuscript. All authors contributed to revisions of the manuscript, tables, and figures and approved the submitted version.

FUNDING

Funding for this work was provided by the European Research Council (ERC) under the European Union's Horizon 2020 research and innovation program (grant agreement no. 725100, project Big Mac).

ACKNOWLEDGMENTS

The authors are grateful to Fabien Palencia for the 3D printing of a specific microscopic frame enabling to fit the temperature gradient setup under the microscope and take pictures in the micropools over time.

SUPPLEMENTARY MATERIAL

The Supplementary Material for this article can be found online at: https://www.frontiersin.org/articles/10.3389/fmicb.2022.866681/full#supplementary-material

REFERENCES

Adan, A., Alizada, G., Kiraz, Y., Baran, Y., and Nalbant, A. (2017). Flow cytometry: basic principles and applications. *Crit. Rev. Biotechnol.* 37, 163–176. doi: 10.3109/07388551.2015.1128876

Alain, K., and Querellou, J. (2009). Cultivating the uncultured: limits, advances and future challenges. *Extremophiles* 13, 583–594. doi: 10.1007/s00792-009-0261-3

Bao, C., Gai, Y., Lou, K., Jiang, C., and Ye, S. (2010). High-hydrostatic-pressure optical chamber system for cultivation and microscopic observation of deep-sea organisms. *Aquat. Biol.* 11, 157–162. doi: 10.3354/ab00303

Bar-On, Y. M., Phillips, R., and Milo, R. (2018). The biomass distribution on earth. *Proc. Natl. Acad. Sci. U. S. A.* 115, 6506–6511. doi: 10.1073/pnas.1711842115

Beaton, A. D., Schaap, A. M., Pascal, R., Hanz, R., Martincic, U., Cardwell, C. L., et al. (2022). Lab-on-chip for *in situ* analysis of nutrients in the deep sea. *ACS sensors* 7, 89–98. doi: 10.1021/acssensors.1c01685

Beney, L., Perrier-Cornet, J. M., Hayert, M., and Gervais, P. (1997). Shape modification of phospholipid vesicles induced by high pressure: influence of bilayer compressibility. *Biophys. J.* 72, 1258–1263. doi: 10.1016/S0006-3495(97)78772-1

Berdy, B., Spoering, A. L., Ling, L. L., and Epstein, S. S. (2017). *In situ* cultivation of previously uncultivable microorganisms using the ichip. *Nat. Protoc.* 12, 2232–2242. doi: 10.1038/nprot.2017.074

Bernhardt, G., Distèche, A., Jaenicke, R., Koch, B., Lüdemann, H. D., and Stetter, K. O. (1988). Effect of carbon dioxide and hydrostatic pressure on the pH of culture media and the growth of methanogens at elevated temperature. *App. Microbiol. Biotechnol.* 28, 176–181.

Boitard, L., Cottinet, D., Bremond, N., Baudry, J., and Bibette, J. (2015). Growing microbes in millifluidic droplets. *Eng. Life Sci.* 15, 318–326. doi: 10.1002/elsc.201400089

Bourges, A. C., Lazarev, A., Declerck, N., Rogers, K. L., and Royer, C. A. (2020). Quantitative high-resolution imaging of live microbial cells at high hydrostatic pressure. *Biophys. J.* 118, 2670–2679. doi: 10.1016/j.bpj.2020.04.017

Canganella, F., Gonzalez, J. M., Yanagibayashi, M., Kato, C., and Horikoshi, K. (1997). Pressure and temperature effects on growth and viability of the hyperthermophilic archaeon *Thermococcus peptonophilus*. *Arch. Microbiol.* 168, 1–7. doi: 10.1007/s002030050462

Cario, A., Grossi, V., Schaeffer, P., and Oger, P. M. (2015a). Membrane homeoviscous adaptation in the piezo-hyperthermophilic archaeon *Thermococcus barophilus*. *Front. Microbiol.* 6:1152. doi: 10.3389/fmicb.2015.01152

Cario, A., Jebbar, M., Thiel, A., Kervarec, N., and Oger, P. M. (2016). Molecular chaperone accumulation as a function of stress evidences adaptation to high hydrostatic pressure in the piezophilic archaeon *Thermococcus barophilus*. *Sci. Rep.* 6, 1–8. doi: 10.1038/srep29483

Cario, A., Lormières, F., Xiang, X., and Oger, P. (2015b). High hydrostatic pressure increases amino acid requirements in the piezo-hyperthermophilic archaeon *Thermococcus barophilus*. *Res. Microbiol.* 166, 710–716. doi: 10.1016/j.resmic.2015.07.004

Cario, A., Oliver, G. C., and Rogers, K. L. (2019). Exploring the deep marine biosphere: challenges, innovations, and opportunities. *Front. Earth Sci.* 7:225. doi: 10.3389/feart.2019.00225

Chen, P, Zhou, H, Huang, Y, Xie, Z, Zhang, M, Wei, Y, et al. (2021). Revealing the full biosphere structure and versatile metabolic functions in the deepest ocean sediment of the challenger deep. bioRxiv [Preprint].

Connon, S. A., and Giovannoni, S. J. (2002). High-throughput methods for culturing microorganisms in very-low-nutrient media yield diverse new marine isolates. *Appl. Environ. Microbiol.* 68, 3878–3885. doi: 10.1128/AEM.68.8.3878-3885.2002

Czernichowski-Lauriol, I., Czop, V., Dupraz, S., Farret, R., Gombert, P., Husson, G., et al. (2017). "CO_2 capture, transport and storage research facilities from the French node of ECCSEL available for access by the European scientific community." in *9th "Trondheim Conference on CO_2 Capture, Transport and Storage" (TCCS-9)*. June 2017 (Trondheim, Norway).

Demello, A. J. (2006). Control and detection of chemical reactions in microfluidic systems. *Nature* 442, 394–402. doi: 10.1038/nature05062

DeSantis, T. Z., Brodie, E. L., Moberg, J. P., Zubieta, I. X., Piceno, Y. M., and Andersen, G. L. (2007). High-density universal 16S rRNA microarray analysis

reveals broader diversity than typical clone library when sampling the environment. *Microb. Ecol.* 53, 371–383. doi: 10.1007/s00248-006-9134-9

Deusner, C., Meyer, V., and Ferdelman, T. G. (2010). High-pressure systems for gas-phase free continuous incubation of enriched marine microbial communities performing anaerobic oxidation of methane. *Biotechnol. Bioeng.* 105, 524–533. doi: 10.1002/bit.22553

D'Hondt, S., Jørgensen, B. B., Miller, D. J., Batzke, A., Blake, R., Cragg, B. A., et al. (2004). Distributions of microbial activities in deep subseafloor sediments. *Science* 306, 2216–2221. doi: 10.1126/science.1101155

Dick, G. J. (2019). The microbiomes of deep-sea hydrothermal vents: distributed globally, shaped locally. *Nat. Rev. Microbiol.* 17, 271–283. doi: 10.1038/s41579-019-0160-2

Dupraz, S., Fabbri, A., Joulian, C., Dictor, M. C., Battaglia-Brunet, F., Menez, B., et al. (2013). Impact of CO_2 concentration on autotrophic metabolisms and carbon fate in saline aquifers–A case study. *Geochim. Cosmochim. Acta* 119, 61–76. doi: 10.1016/j.gca.2013.05.027

Dusny, C., and Schmid, A. (2015). Microfluidic single-cell analysis links boundary environments and individual microbial phenotypes. *Environ. Microbiol.* 17, 1839–1856. doi: 10.1111/1462-2920.12667

El-Ali, J., Sorger, P. K., and Jensen, K. F. (2006). Cells on chips. *Nature* 442, 403–411. doi: 10.1038/nature05063

Fry, J. C., Parkes, R. J., Cragg, B. A., Weightman, A. J., and Webster, G. (2008). Prokaryotic biodiversity and activity in the deep subseafloor biosphere. *FEMS Microbiol. Ecol.* 66, 181–196. doi: 10.1111/j.1574-6941.2008.00566.x

García-Timermans, C., Rubbens, P., Heyse, J., Kerckhof, F. M., Props, R., Skirtach, A. G., et al. (2020). Discriminating bacterial phenotypes at the population and single-cell level: a comparison of flow cytometry and Raman spectroscopy fingerprinting. *Cytometry A* 97, 713–726. doi: 10.1002/cyto.a.23952

Garel, M., Bonin, P., Martini, S., Guasco, S., Roumagnac, M., Bhairy, N., et al. (2019). Pressure-retaining sampler and high-pressure systems to study deep-sea microbes under *in situ* conditions. *Front. Microbiol.* 10:453. doi: 10.3389/fmicb.2019.00453

Gavoille, T., Pannacci, N., Bergeot, G., Marliere, C., and Marre, S. (2019). Microfluidic approaches for accessing thermophysical properties of fluid systems. *React. Chem. Eng.* 4, 1721–1739. doi: 10.1039/C9RE00130A

Geissmann, Q. (2013). OpenCFU, a new free and open-source software to count cell colonies and other circular objects. *PLoS One* 8:e54072. doi: 10.1371/journal.pone.0054072

Gervais, T., and Jensen, K. F. (2006). Mass transport and surface reactions in microfluidic systems. *Chem. Eng. Sci.* 61, 1102–1121. doi: 10.1016/j.ces.2005.06.024

Girault, M., Beneyton, T., Del Amo, Y., and Baret, J.-C. (2019). Microfluidic technology for plankton research. *Curr. Opin. Biotechnol.* 55, 134–150. doi: 10.1016/j.copbio.2018.09.010

Grünberger, A., Probst, C., Helfrich, S., Nanda, A., Stute, B., Wiechert, W., et al. (2015). Spatiotemporal microbial single-cell analysis using a high-throughput microfluidics cultivation platform. *Cytometry A* 87, 1101–1115. doi: 10.1002/cyto.a.22779

Hammes, F., Vital, M., and Egli, T. (2010). Critical evaluation of the volumetric "bottle effect" on microbial batch growth. *Appl. Environ. Microbiol.* 76, 1278–1281. doi: 10.1128/AEM.01914-09

Hu, B., Xu, B., Yun, J., Wang, J., Xie, B., Li, C., et al. (2020). High-throughput single-cell cultivation reveals the underexplored rare biosphere in deep-sea sediments along the Southwest Indian Ridge. *Lab Chip* 20, 363–372. doi: 10.1039/C9LC00761J

Huber, H., Thomm, M., König, H., Thies, G., and Stetter, K. O. (1982). *Methanococcus thermolithotrophicus*, a novel thermophilic lithotrophic methanogen. *Arch. Microbiol.* 132, 47–50. doi: 10.1007/BF00690816

Ikeda, S., Satake, H., Hisano, T., and Terazawa, T. (1972). Potentiometric argentimetric method for the successive titration of sulphide and dissolved sulphur in polysulphide solutions. *Talanta* 19, 1650–1654. doi: 10.1016/0039-9140(72)80240-6

Jaenicke, R., Bernhardt, G., Lüdemann, H. D., and Stetter, K. O. (1988). Pressure-induced alterations in the protein pattern of the thermophilic archaebacterium *Methanococcus thermolithotrophicus*. *Appl. Environ. Microbiol.* 54, 2375–2380. doi: 10.1128/aem.54.10.2375-2380.1988

Jannasch, H. W., and Taylor, C. D. (1984). Deep-sea microbiology. *Annu. Rev. Microbiol.* 38:487. doi: 10.1146/annurev.mi.38.100184.002415

Jannasch, H. W., Wirsen, C. O., and Doherty, K. W. (1996). A pressurized chemostat for the study of marine barophilic and oligotrophic bacteria. *Appl. Environ. Microbiol.* 62, 1593–1596. doi: 10.1128/aem.62.5.1593-1596.1996

Jebbar, M., Franzetti, B., Girard, E., and Oger, P. (2015). Microbial diversity and adaptation to high hydrostatic pressure in deep-sea hydrothermal vents prokaryotes. *Extremophiles* 19, 721–740. doi: 10.1007/s00792-015-0760-3

Jensen, K. F., Ajmera, S. K., Firebaugh, S. L., Floyd, T. M., Franz, A. J., Losey, M. W., et al. (2000). *Microfabricated Chemical Systems for Product Screening and Synthesis. Automated Synthetic Methods for Speciality Chemicals*. ed. W. Hoyle (London: Royal Society of Chemistry), 14–24.

Jiang, C.-Y., Dong, L., Zhao, J.-K., Hu, X., Shen, C., Qiao, Y., et al. (2016). High-throughput single-cell cultivation on microfluidic streak plates. *Appl. Environ. Microbiol.* 82, 2210–2218. doi: 10.1128/AEM.03588-15

Jørgensen, B. B., and Boetius, A. (2007). Feast and famine—microbial life in the deep-sea bed. *Nat. Rev. Microbiol.* 5, 770–781. doi: 10.1038/nrmicro1745

Kallmeyer, J., Pockalny, R., Adhikari, R. R., Smith, D. C., and D'Hondt, S. (2012). Global distribution of microbial abundance and biomass in subseafloor sediment. *Proc. Natl. Acad. Sci.* 109, 16213–16216. doi: 10.1073/pnas.1203849109

Kaminski, T. S., Scheler, O., and Garstecki, P. (2016). Droplet microfluidics for microbiology: techniques, applications and challenges. *Lab Chip* 16, 2168–2187. doi: 10.1039/C6LC00367B

Kato, C. (2011). *Cultivation Methods for Piezophiles. Extremophiles Handbook* Tokyo: Springer, 719–726.

Kato, M., and Fujisawa, T. (1998). High-pressure solution X-ray scattering of protein using a hydrostatic cell with diamond windows. *J. Synchrotron Radiat.* 5, 1282–1286. doi: 10.1107/S0909049598000788

Kato, C., Inoue, A., and Horikoshi, K. (1996). Isolating and characterizing deep-sea marine microorganisms. *Trends Biotechnol.* 14, 6–12. doi: 10.1016/0167-7799(96)80907-3

Kozhevnikova, D., Taranov, E., Lebedinsky, A., Bonch-Osmolovskaya, E., and Sokolova, T. (2016). Hydrogenogenic and sulfidogenic growth of *Thermococcus* archaea on carbon monoxide and formate. *Microbiology* 85, 400–410. doi: 10.1134/S0026261716040135

Le Guellec, S., Leroy, E., Courtine, D., Godfroy, A., and Roussel, E. G. (2021). H_2-dependent formate production by hyperthermophilic Thermococcales: an alternative to sulfur reduction for reducing-equivalents disposal. *ISME J.* 15, 3423–3436. doi: 10.1038/s41396-021-01020-x

Lewis, W. H., Tahon, G., Geesink, P., Sousa, D. Z., and Ettema, T. J. (2021). Innovations to culturing the uncultured microbial majority. *Nat. Rev. Microbiol.* 19, 225–240. doi: 10.1038/s41579-020-00458-8

Lloyd, K. G., Steen, A. D., Ladau, J., Yin, J., and Crosby, L. (2018). Phylogenetically novel uncultured microbial cells dominate earth microbiomes. *mSystems* 3, e00055–e00018. doi: 10.1128/mSystems.00055-18

Maldonado, J. A., Schaffner, D. W., Cuitiño, A. M., and Karwe, M. V. (2016). *In situ* studies of microbial inactivation during high pressure processing. *High Pressure Res.* 36, 79–89. doi: 10.1080/08957959.2015.1111887

Marre, S., Adamo, A., Basak, S., Aymonier, C., and Jensen, K. F. (2010). Design and packaging of microreactors for high pressure and high temperature applications. *Ind. Eng. Chem. Res.* 49, 11310–11320. doi: 10.1021/ie101346u

Marre, S., Lecoutre, C., Garrabos, Y., Fauveau, C., Cario, A., and Nguyen, O. (2021). Sapphire microreactors. International Patent No WO 2021/2051 15 A1. WIPO, PCT

Marteinsson, V. T., Birrien, J. L., Reysenbach, A. L., Vernet, M., Marie, D., Gambacorta, A., et al. (1999). *Thermococcus barophilus* sp. nov., a new barophilic and hyperthermophilic archaeon isolated under high hydrostatic pressure from a deep-sea hydrothermal vent. *Int. J. Syst. Bacteriol.* 49, 351–359.

Miller, J. F., Shah, N. N., Nelson, C. M., Ludlow, J. M., and Clark, D. S. (1988). Pressure and temperature effects on growth and methane production of the extreme thermophile *Methanococcus jannaschii*. *Appl. Environ. Microbiol.* 54, 3039–3042. doi: 10.1128/aem.54.12.3039-3042.1988

Moffitt, J. R., Lee, J. B., and Cluzel, P. (2012). The single-cell chemostat: an agarose-based, microfluidic device for high-throughput, single-cell studies of bacteria and bacterial communities. *Lab Chip* 12, 1487–1494. doi: 10.1039/c2lc00009a

Molina-Gutierrez, A., Stippl, V., Delgado, A., Gänzle, M. G., and Vogel, R. F. (2002). *In situ* determination of the intracellular pH of *Lactococcus lactis* and *Lactobacillus plantarum* during pressure treatment. *Appl. Environ. Microbiol.* 68, 4399–4406. doi: 10.1128/AEM.68.9.4399-4406.2002

Morais, S., Cario, A., Liu, N., Bernard, D., Lecoutre, C., Garrabos, Y., et al. (2020). Studying key processes related to CO 2 underground storage at the pore scale using high pressure micromodels. *React. Chem. Eng.* 5, 1156–1185. doi: 10.1039/D0RE00023J

Morais, S., Liu, N., Diouf, A., Bernard, D., Lecoutre, C., Garrabos, Y., et al. (2016). Monitoring CO 2 invasion processes at the pore scale using geological labs on chip. *Lab Chip* 16, 3493–3502. doi: 10.1039/C6LC00830E

Murphy, E. R., Inoue, T., Sahoo, H. R., Zaborenko, N., and Jensen, K. F. (2007). Solder-based chip-to-tube and chip-to-chip packaging for microfluidic devices. *Lab Chip* 7, 1309–1314. doi: 10.1039/b704804a

Nauhaus, K., Boetius, A., Krüger, M., and Widdel, F. (2002). *In vitro* demonstration of anaerobic oxidation of methane coupled to sulphate reduction in sediment from a marine gas hydrate area. *Environ. Microbiol.* 4, 296–305. doi: 10.1046/j.1462-2920.2002.00299.x

Nichols, D., Cahoon, N., Trakhtenberg, E., Pham, L., Mehta, A., Belanger, A., et al. (2010). Use of ichip for high-throughput in situ cultivation of "uncultivable" microbial species. *Appl. Environ. Microbiol.* 76, 2445–2450. doi: 10.1128/AEM.01754-09

Oger, P. M., Daniel, I., and Picard, A. (2006). Development of a low-pressure diamond anvil cell and analytical tools to monitor microbial activities *in situ* under controlled P and T. *Biochim Biophys Acta* 1764, 434–442. doi: 10.1016/j.bbapap.2005.11.009

Oger, P., Sokolova, T. G., Kozhevnikova, D. A., Taranov, E. A., Vannier, P., Lee, H. S., et al. (2016). Complete genome sequence of the hyperthermophilic and piezophilic archaeon *Thermococcus barophilus* Ch5, capable of growth at the expense of hydrogenogenesis from carbon monoxide and formate. *Genome Announc.* 4, e01534–e01515. doi: 10.1128/genomeA.01534-15

Oliver, G. C., Cario, A., and Rogers, K. L. (2020). Rate and extent of growth of a model extremophile, *Archaeoglobus fulgidus*, under high hydrostatic pressures. *Front. Microbiol.* 11:1023. doi: 10.3389/fmicb.2020.01023

Oliver, G. C., Cario, A., and Rogers, K. L. (2021). High temperature and high hydrostatic pressure cultivation, transfer, and filtration Systems for Investigating Deep Marine Microorganisms. Preprints 2021, 2021040453. doi: 10.20944/preprints202104.0453.v1.

Orcutt, B. N., LaRowe, D. E., Biddle, J. F., Colwell, F. S., Glazer, B. T., Reese, B. K., et al. (2013). Microbial activity in the marine deep biosphere: progress and prospects. *Front. Microbiol.* 4:189. doi: 10.3389/fmicb.2013.00189

Peoples, L. M., Norenberg, M., Price, D., McGoldrick, M., Novotny, M., Bochdansky, A., et al. (2019). A full-ocean-depth rated modular lander and pressure-retaining sampler capable of collecting hadal-endemic microbes under in situ conditions. *Deep-Sea Res. I Oceanogr. Res. Pap.* 143, 50–57. doi: 10.1016/j.dsr.2018.11.010

Peters, J., Martinez, N., Michoud, G., Cario, A., Franzetti, B., Oger, P., et al. (2014). Deep sea microbes probed by incoherent neutron scattering under high hydrostatic pressure. *Z. Phys. Chem.* 228, 1121–1133. doi: 10.1515/zpch-2014-0547

Picard, A., and Daniel, I. (2013). Pressure as an environmental parameter for microbial life—a review. *Biophys. Chem.* 183, 30–41. doi: 10.1016/j.bpc.2013.06.019

Picard, A., Daniel, I., Montagnac, G., and Oger, P. (2007). *In situ* monitoring by quantitative Raman spectroscopy of alcoholic fermentation by *Saccharomyces cerevisiae* under high pressure. *Extremophiles* 11, 445–452. doi: 10.1007/s00792-006-0054-x

Pledger, R. J., Crump, B. C., and Baross, J. A. (1994). A barophilic response by two hyperthermophilic, hydrothermal vent *Archaea*: an upward shift in the optimal temperature and acceleration of growth rate at supra-optimal temperatures by elevated pressure. *FEMS Microbiol. Ecol.* 14, 233–241. doi: 10.1111/j.1574-6941.1994.tb00109.x

Pucetaite, M., Ohlsson, P., Persson, P., and Hammer, E. (2021). Shining new light into soil systems: spectroscopy in microfluidic soil chips reveals microbial biogeochemistry. *Soil Biol. Biochem.* 153:108078. doi: 10.1016/j.soilbio.2020.108078

Qu, K., Guo, F., Liu, X., Lin, Y., and Zou, Q. (2019). Application of machine learning in microbiology. *Front. Microbiol.* 10:827. doi: 10.3389/fmicb.2019.00827

Raber, E. C., Dudley, J. A., Salerno, M., and Urayama, P. (2006). Capillary-based, high-pressure chamber for fluorescence microscopy imaging. *Rev. Sci. Instrum.* 77:096106. doi: 10.1063/1.2349303

Ramirez-Llodra, E, Brandt, A, Danovaro, R, De Mol, B, Escobar, E, German, CR, et al. (2010). Deep, diverse and definitely different: unique attributes of the world's largest ecosystem. *Biogeosciences* 7, 2851–2899. doi: 10.5194/bg-7-2851-2010

Reith, F. (2011). Life in the deep subsurface. *Geology* 39, 287–288. doi: 10.1130/focus032011.1

Rinke, C., Schwientek, P., Sczyrba, A., Ivanova, N. N., Anderson, I. J., Cheng, J.-F., et al. (2013). Insights into the phylogeny and coding potential of microbial dark matter. *Nature* 499, 431–437. doi: 10.1038/nature12352

Sackmann, E. K., Fulton, A. L., and Beebe, D. J. (2014). The present and future role of microfluidics in biomedical research. *Nature* 507, 181–189. doi: 10.1038/nature13118

Stocker, R., and Seymour, J. R. (2012). Ecology and physics of bacterial chemotaxis in the ocean. *Microbiol. Mol. Biol. Rev.* 76, 792–812. doi: 10.1128/MMBR.00029-12

Takai, K., Nakamura, K., Toki, T., Tsunogai, U., Miyazaki, M., Miyazaki, J., et al. (2008). Cell proliferation at 122°C and isotopically heavy CH_4 production by a hyperthermophilic methanogen under high-pressure cultivation. *Proc. Natl. Acad. Sci.* 105, 10949–10954. doi: 10.1073/pnas.0712334105

Tanet, L., Tamburini, C., Baumas, C., Garel, M., Simon, G., and Casalot, L. (2019). Bacterial bioluminescence: light emission in *Photobacterium phosphoreum* is not under quorum-sensing control. *Front. Microbiol.* 10:365. doi: 10.3389/fmicb.2019.00365

Terekhov, S. S., Smirnov, I. V., Malakhova, M. V., Samoilov, A. E., Manolov, A. I., Nazarov, A. S., et al. (2018). Ultrahigh-throughput functional profiling of microbiota communities. *Proc. Natl. Acad. Sci.* 115, 9551–9556. doi: 10.1073/pnas.1811250115

Thiel, A., Michoud, G., Moalic, Y., Flament, D., and Jebbar, M. (2014). Genetic manipulations of the hyperthermophilic piezophilic archaeon *Thermococcus barophilus*. *Appl. Environ. Microbiol.* 80, 2299–2306. doi: 10.1128/AEM.00084-14

Tiggelaar, R. M., Benito-López, F., Hermes, D. C., Rathgen, H., Egberink, R. J., Mugele, F. G., et al. (2007). Fabrication, mechanical testing and application of high-pressure glass microreactor chips. *Chem. Eng. J.* 131, 163–170. doi: 10.1016/j.cej.2006.12.036

Vannier, P., Michoud, G., Oger, P., þór Marteinsson, V., and Jebbar, M. (2015). Genome expression of *Thermococcus barophilus* and *Thermococcus kodakarensis* in response to different hydrostatic pressure conditions. *Res. Microbiol.* 166, 717–725. doi: 10.1016/j.resmic.2015.07.006

Wang, F., Zhou, H., Meng, J., Peng, X., Jiang, L., Sun, P., et al. (2009). GeoChip-based analysis of metabolic diversity of microbial communities at the Juan de Fuca Ridge hydrothermal vent. *Proc. Natl. Acad. Sci.* 106, 4840–4845. doi: 10.1073/pnas.0810418106

Whitman, W. B., Coleman, D. C., and Wiebe, W. J. (1998). Prokaryotes: The unseen majority. *Proc. Natl. Acad. Sci.* 95, 6578–6583. doi: 10.1073/pnas.95.12.6578

Xu, Y., Riordon, J., Cheng, X., Bao, B., and Sinton, D. (2017). The full pressure–temperature phase envelope of a mixture in 1000 microfluidic chambers. *Angew. Chem.* 129, 14150–14155. doi: 10.1002/ange.201708238

Yayanos, A. A. (1986). Evolutional and ecological implications of the properties of deep-sea barophilic bacteria. *Proc. Natl. Acad. Sci.* 83, 9542–9546. doi: 10.1073/pnas.83.24.9542

Zeng, X., Alain, K., and Shao, Z. (2021). Microorganisms from deep-sea hydrothermal vents. *Marine Life Sci. Technol.* 3, 204–230.

Zeng, S., Birrien, J., Fouquet, Y., Cherkashov, G., Jebbar, M., Querellou, J., et al. (2009). *Pyrococcus* CH1, an obligate piezophilic hyperthermophile: extending the upper pressure-temperature limits for life. *ISME J.* 3, 873–876. doi: 10.1038/ismej.2009.21

Zengler, K., Walcher, M., Clark, G., Haller, I., Toledo, G., Holland, T., et al. (2005). High-throughput cultivation of microorganisms using microcapsules. *Methods Enzymol.* 397, 124–130. doi: 10.1016/S0076-6879(05)97007-9

Zuleta, I. A., Aranda-Díaz, A., Li, H., and El-Samad, H. (2014). Dynamic characterization of growth and gene expression using high-throughput automated flow cytometry. *Nat. Methods* 11, 443–448. doi: 10.1038/nmeth.2879

Conflict of Interest: The authors declare that the research was conducted in the absence of any commercial or financial relationships that could be construed as a potential conflict of interest.

frontiers | Frontiers in Microbiology

ORIGINAL RESEARCH
published: 25 May 2022
doi: 10.3389/fmicb.2022.861795

Metagenomics Reveals Dominant Unusual Sulfur Oxidizers Inhabiting Active Hydrothermal Chimneys From the Southwest Indian Ridge

Yong Wang[1†], Hong-Yu Bi[2†], Hua-Guan Chen[2,3], Peng-Fei Zheng[2], Ying-Li Zhou[2,3] and Jiang-Tao Li[4]*

[1] Institute for Marine Engineering, Shenzhen International Graduate School, Tsinghua University, Shenzhen, China, [2] Institute of Deep Sea Science and Engineering, Chinese Academy of Sciences, Sanya, China, [3] College of Marine Sciences, University of Chinese Academy of Sciences, Beijing, China, [4] State Key Laboratory of Marine Geology, Tongji University, Shanghai, China

OPEN ACCESS

Edited by:
Philippe M. Oger,
UMR 5240 Microbiologie, Adaptation et Pathogenie (MAP), France

Reviewed by:
Mirjam Perner,
GEOMAR Helmholtz Center for Ocean Research Kiel, Helmholtz Association of German Research Centres (HZ), Germany
Anaïs Cario,
UMR 5026 Institut de Chimie de la Matière Condensée de Bordeaux (ICMCB), France

***Correspondence:**
Yong Wang
wangyong@sz.tsinghua.edu.cn

[†] These authors have contributed equally to this work

Specialty section:
This article was submitted to Extreme Microbiology, a section of the journal Frontiers in Microbiology

Received: 25 January 2022
Accepted: 12 April 2022
Published: 25 May 2022

Citation:
Wang Y, Bi H-Y, Chen H-G, Zheng P-F, Zhou Y-L and Li J-T (2022) Metagenomics Reveals Dominant Unusual Sulfur Oxidizers Inhabiting Active Hydrothermal Chimneys From the Southwest Indian Ridge. Front. Microbiol. 13:861795. doi: 10.3389/fmicb.2022.861795

The deep-sea hydrothermal vents (DSHVs) in the Southwest Indian Ridge (SWIR) are formed by specific geological settings. However, the community structure and ecological function of the microbial inhabitants on the sulfide chimneys of active hydrothermal vents remain largely unknown. In this study, our analyses of 16S rRNA gene amplicons and 16S rRNA metagenomic reads showed the dominance of sulfur-oxidizing Ectothiorhodospiraceae, *Thiomicrorhabdus*, *Sulfurimonas,* and *Sulfurovum* on the wall of two active hydrothermal chimneys. Compared with the inactive hydrothermal sediments of SWIR, the active hydrothermal chimneys lacked sulfur-reducing bacteria. The metabolic potentials of the retrieved 82 metagenome-assembled genomes (MAGs) suggest that sulfur oxidation might be conducted by Thiohalomonadales (classified as Ectothiorhodospiraceae based on 16S rRNA gene amplicons), Sulfurovaceae, Hyphomicrobiaceae, Thiotrichaceae, Thiomicrospiraceae, and Rhodobacteraceae. For CO_2 fixation, the Calvin-Benson-Bassham and reductive TCA pathways were employed by these bacteria. In Thiohalomonadales MAGs, we revealed putative phytochrome, carotenoid precursor, and squalene synthesis pathways, indicating a possible capacity of Thiohalomonadales in adaptation to dynamics redox conditions and the utilization of red light from the hot hydrothermal chimneys for photolithotrophic growth. This study, therefore, reveals unique microbiomes and their genomic features in the active hydrothermal chimneys of SWIR, which casts light on ecosystem establishment and development in hydrothermal fields and the deep biosphere.

Keywords: deep-sea hydrothermal vents, SWIR, thiohalomonadales, metagenomics, red light photosynthesis

INTRODUCTION

Deep-sea hydrothermal vents (DSHVs) are located in tectonically active areas where plate boundaries move at different speeds along mid-ocean ridges. DSHV is an important conduit for the exchange of energy and materials between the Earth's interior and the ocean. Since the first report in 1977, DSHVs as a deep-sea extreme environment have attracted great concerns about the microbial extremophilic inhabitants with respect to early life form, chemoautotrophy, and adaptation (Corliss et al., 1979; Francheteau et al., 1979; Jannasch and Mottl, 1985;

Kelley et al., 2005; Dick, 2019). The mixture of cold, oxic deep-sea water, and highly reducing fluids with high concentrations of hydrogen, sulfide, and methane was ideal for chemoautotrophs and C1 oxidizers (Dick et al., 2013). The complex dynamic habitats have steep thermal and chemical gradients, and different microbial populations are simultaneously involved in many important biogeochemical processes, such as the nitrogen, sulfur, and carbon cycles that also occur in symbionts of megafauna around DSHV (Jannasch and Mottl, 1985; Connelly et al., 2012). Strong dynamics of geochemistry and temperature provide a wide range of habitats for deep-sea microorganisms, and therefore, niche specificity of microbes has been demonstrated in different environmental settings by previous studies (Dick, 2019 and references therein).

Sulfide samples from inactive and active hydrothermal vents are distinct in microbial community structure and ecological function in the Indian Ocean (Zhang et al., 2016; Han et al., 2018; Adam et al., 2020; Hou et al., 2020). Sulfur oxidizing bacteria (SOB) dominate various hydrothermal sediments and flumes and are classified to be aerobes (e.g., SUP05 and *Beggiatoa* from Gammaproteobacteria), microaerobes (e.g., *Sulfurimonas* and *Sulfurovum* from Epsilonbacteraeota), and anaerobes (e.g., *Caminibacter* and *Nautila* from Epsilonbacteraeota) (López-García et al., 2003; Dick, 2019; Meier et al., 2019; Hou et al., 2020) with preference to different electron donors. For the microaerobic SOB, the *cbb3*-type cytochrome c oxidase was involved in adaptation to low oxygen concentrations for respiration (Hou et al., 2020; Dong et al., 2021); however, the mechanism for reducing the damage by high oxygen flux is largely unknown. Considering the highly variable microenvironments adjacent to an active hydrothermal vent, there are perhaps much more SOB species that have evolved to adapt to the varying temperature and redox conditions. A photoautotrophic bacterium has been isolated from a hydrothermal chimney (Beatty et al., 2005). Evidence shows that this bacterial isolate from the *Prosthecochloris* genus can absorb weak ultra-red light as energy to fix CO_2 and oxidize H_2S. The abundance and distribution of such photoautotrophic SOB in the dark ocean are still unclear up to date.

Since the first report in the Southwest Indian Ridge (SWIR) more than a decade ago (German et al., 1998), multiple hydrothermal fields have been discovered in the Indian Ocean (Van Dover et al., 2001). Low-temperature hydrothermal activity because of the effect of an ultra-slow spreading speed of tectonic plates was reported in the SWIR (Tao et al., 2012). The discovery of hydrothermal fields in such an ultra-slow spreading ridge provides an unprecedented opportunity to understand microbially mediated biogeochemistry. A serpentinite-hosted hydrothermal site and distinct microbial community resembling those of the Lost City hydrothermal field in the Atlantic Ocean were reported in a magma-poor area of the eastern SWIR (Lecoeuvre et al., 2021). The relatively low temperature and serpentinization of SWIR hydrothermal fields (Zhou and Dick, 2013) had probably shaped the microbial inhabitants in the hydrothermal fields. However, microbial genomics studies on the SWIR hydrothermal areas are still limited. *Thiomicrorhabdus* has been reported as a dominant SOB in SWIR (Cao et al., 2014), and was also isolated from the other hydrothermal vents (Brazelton and Baross, 2010; Scott et al., 2019). A recent study revealed a large number of Gammaproteobacteria with sulfur oxidation potentials using nitrate and oxygen as electron acceptors in the SWIR inactive hydrothermal sediments (Dong et al., 2021). We employed metagenomics to compare the microbiomes in the active hydrothermal vents with those from inactive ones to reveal microbial community structure and ecological function driven by active "black-smoker" hydrothermal seepage in SWIR. We hereby report a unique microbiome exclusively composed of Thiohalomonadales-dominated SOB, which has not been reported in DSHVs and presumably plays a critical role in the initiation of the deep-sea hydrothermal ecosystem in SWIR.

MATERIALS AND METHODS

Sample Collection and Mineral Analysis

During the *R/V* DY35 cruise, the manned submersible "Jiaolong" collected sulfide samples from hydrothermal chimneys by dives no. 96 (49.65°E, 37.78°S; depth: 2,768) and no. 100 (49.65°E, 37.78°S; depth: 2,755 m) in SWIR (**Figure 1**, **Supplementary Table 1**, and **Supplementary Figure 1**). A sulfide chimney sample was obtained from an inactive hydrothermal vent (49.63°E, 37.77°S; depth: 2,789 m) by dive no. 95 at a depth of 2,789 m. The samples were stored in sterile bags and maintained at –80°C until use. The temperature and pH of the hydrothermal fluid were measured *in situ* with a Miniature Autonomous Plume Recorder (MAPR) (Baker and Milburn, 1997).

An X-ray diffraction (XRD) analysis was carried out to determine the major minerals of the sulfide chimneys using an Empyrean X-ray diffractometer (PANalytical, Malvern, United Kingdom). The detection parameters were Cu Kα radiation at 45 kV and 40 mA; Goniometer PW3050/60 (Theta/Theta); scanning from 3° to 85° with 0.03 step size (°2Th). The mineral components were converted to wt%.

High-Throughput Sequencing and Analyses of 16S rRNA Gene Amplicons

Genomic DNA of sulfide samples was extracted from a 2 g sample using the MO BIO Powersoil DNA isolation kit (Qiagen, Carlsbad, CA, United States). The quality and quantity of the DNA extractions were checked by the Qubit 2.0 fluorometer (Invitrogen, Carlsbad, CA, United States). Then, 16S rRNA gene fragments from V3–V4 regions were amplified with a set of universal primers 341F (5′-CCTAYGGGRBGCASCAG-3′) and 802R (5′-TACNVGGGTATCTAATCC-3′) (Wang and Qian, 2009) using 1 ng DNA as a template. PCR conditions of the amplification were performed as follows: initial denaturation at 98°C for 10 s; 28 cycles of denaturation at 98°C for 10 s, annealing at 50°C for 15 s, and extension at 72°C for 30 s; and a final extension at 72°C for 5 min. A PCR replicate was performed. The mixed barcoded 16S rRNA gene amplicons and 100 ng genomic DNA were used for Illumina library preparation using the TruSeq Nano DNA LT kit (Illumina, San Diego, CA, United States), separately, and were sequenced on an Illumina Miseq sequencer

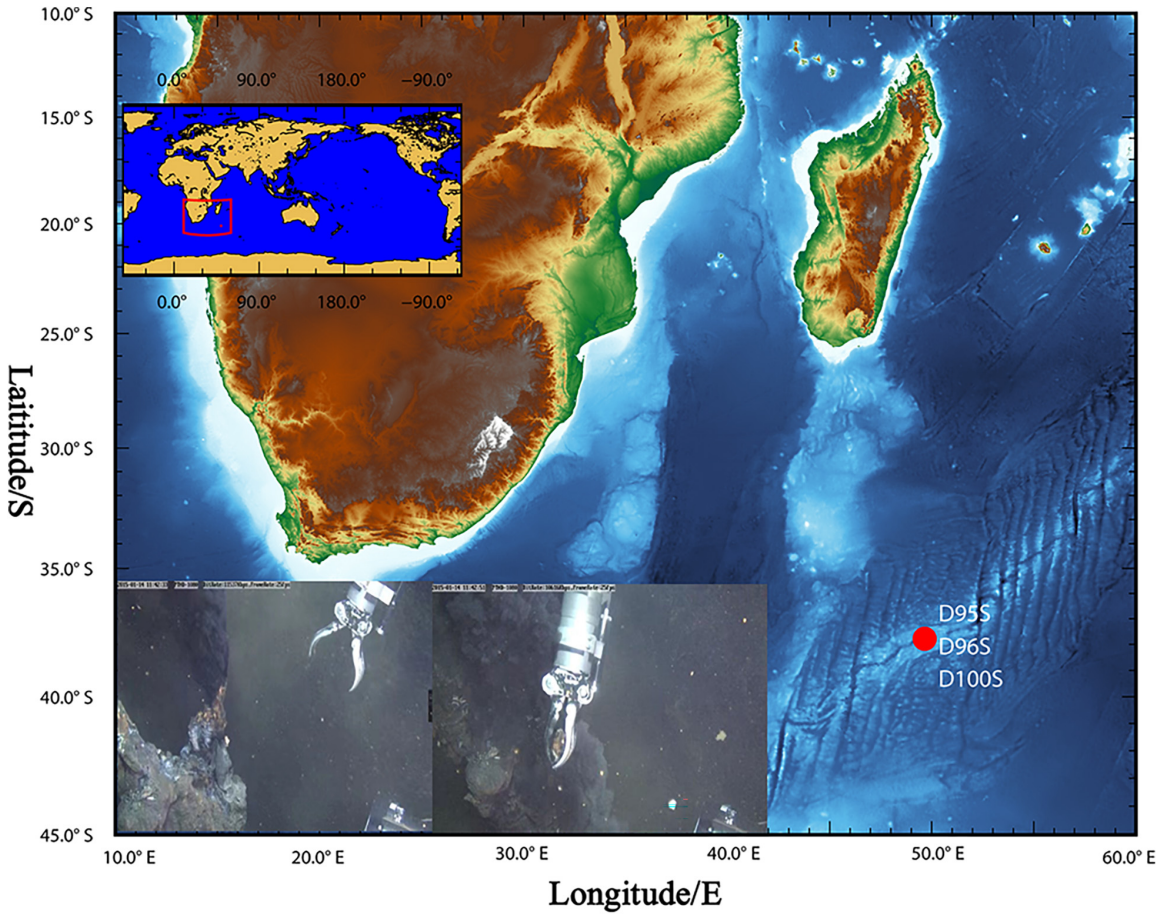

FIGURE 1 | Sampling site at "Longqi" hydrothermal field. During *R/V* DY35, two chimney rocks (D96S and D100S) were obtained by the "Jiaolong" submersible from active sulfide chimney bodies (inset figures) at "Longqi" hydrothermal field in the Southwest Indian Ocean. A sulfide sample (D95A) was also collected from a nearby inactive chimney by the submersible. The details of the samples are listed in **Supplementary Table 1**.

to obtain 2 × 300 bp paired-end sequencing reads (Illumina, San Diego, CA, United States).

The sequencing reads of 16S rRNA gene amplicons were checked by FASTQC (v0.11.8)[1] and merged by the QIIME 1 workflow (Kuczynski et al., 2011). The adaptors and low-quality reads were trimmed by the NGS QC Toolkit (v2.3.3) (Patel and Jain, 2012). Operational taxonomic units (OTUs) at 97% similarity were selected between the qualified reads by the QIIME 1 workflow (Kuczynski et al., 2011). Taxonomic classification of the OTUs was performed with vsearch against the SILVA database v138 (Quast et al., 2013). A principal component analysis (PCoA) was performed to estimate the similarity between the microbial communities at the family level using vegan in the R package (Dixon, 2003).

Metagenomics Analyses of Microbial Community and Metabolic Potentials

Raw reads of metagenomes were qualified by removing adapters and then filtered by using fastp (version 0.20.0) (Chen et al., 2018) with parameters (-w 16 -q 20 -u 20 -g -c -W 5 -3 -l 50). Low-quality reads (assigned by a quality score < 20 for >20% of the read length), and those shorter than 50 bp and unpaired were removed. Metagenomics reads that were mapped onto sequences in an in-house contaminant database (such as, sequences of human, mouse, and common laboratory contaminant bacterial genomes downloaded from the National Center for Biotechnology Information [NCBI]) (Huang et al., 2019) by Bowtie2 (version.2.4.1) (Langmead and Salzberg, 2012) were discarded.

Furthermore, 16S miTags were extracted from qualified metagenomic reads using rna_hmm3.py (Huang et al., 2019), which employs HMMER (version 3.1b2) to predict ribosomal RNA gene fragments from both forward and reverse metagenomic reads. An in-house python script was used to extract 16S miTags. The 16S miTags were imported into Qiime1 with a setting of –type "SampleData[Sequences]" and dereplicated redundancy to yield representative 16S miTag sequences. The classify-consensus-vsearch command in QIIME v1.9.1 (Kuczynski et al., 2011) was used to classify the representative 16S miTags using the SILVA

[1]http://www.bioinformatics.babraham.ac.uk/projects/fastqc/

SSU database v138 as a reference (Quast et al., 2013), as mentioned above.

The qualified reads were assembled using SPAdes (v3.13) (Nurk et al., 2013) with a kmer set of 21, 33, 55, 77, 99, and 127 under the "—careful" mode (metagenome mode). Genome binning from assembled contigs > 2 kbp was performed by running three tools MaxBin (Wu et al., 2016), MetaBAT (Kang et al., 2019), and CONCOCT (Alneberg et al., 2014) using their default settings. Raw genome bins resulting from the three approaches were combined, followed by a selection of the best genome for each genome set using the bin_refinement module in metaWRAP (v1.2) (Uritskiy et al., 2018). During the bin refinement, we applied CheckM_lineage (v1.0.12) (Parks et al., 2015) to evaluate completeness and contamination for each bin. The draft genomes with >50% completeness and <10% contamination were retained for further analysis. Metagenome-assembled genomes (MAGs) were treated with dRep software (Olm et al., 2017) to dereplicate the MAGs by an average nucleotide identity (ANI) threshold of 95% (dereplicate -p 40 -comp 50 -con 10 -pa 0.95 -sa 0.95 -l 10000 -nc 0.30). The taxonomic position of the genomes was identified using genome taxonomy database (GTDB)-tk v0.2.2 (Chaumeil et al., 2020), as well as the calculation of relative evolutionary distance (RED). Coding regions (CDS) for individual MAGs were predicted using Prodigal (version v2.6.3) (Hyatt et al., 2010) with option "-p meta." Annotation of CDSs was performed using KofamScan (version 1.1.0) (Aramaki et al., 2019) and using Blastp (E value = 1e-5) against the Clusters of Orthologous Gene (COG) and NCBI_nr databases. The results were visualized using the heatmap package of the R platform.

Phylogenetic Tree Construction

For phylogenomic analysis of Thiohalomonadales genomes, 43 conserved proteins were obtained by the CheckM program with default settings (Katoh et al., 2009) and were used for alignment with Mafft (v7.453, setting: –maxiterate 1000-localpair) (Katoh and Standley, 2013), followed by a further optimization with trimAl (v1.4) (Capella-Gutiérrez et al., 2009). A maximum likelihood (ML) tree was reconstructed using IQ-TREE (v1.6.10) (Nguyen et al., 2015) with the "LG + F + R6" model (Price et al., 2009). Bootstrap values were calculated based on 1,000 replicates.

RESULTS

Mineral Composition of the Southwest Indian Ridge Hydrothermal Chimneys

The "Longqi" hydrothermal area is located in the Southwest Indian Ridge. Two sulfide samples, D96S and D100S, were collected from the outer wall of active hydrothermal chimneys on 14 January and 4 February 2015 by the "Jiaolong" submersible (**Figure 1** and **Supplementary Table 1**) in dives nos. 96 and 100, respectively. The chimney rocks were about 10 cm away from the vents. Strong seepage from the hydrothermal vent could be observed. The temperature of the hydrothermal fluid was recorded to be 362 and 365°C for the vents near D96S and D100S, respectively, while the bottom seawater was ∼2.2°C. The pH of the fluid from the two vents was between 3.47 and 3.58. The surface of the D96S sample is gray and has been partially oxidized to grayish brown, while it was light yellow inward with metallic luster (**Supplementary Figure 1**). There was no megafauna attached to these chimneys. An XRD analysis revealed that D95S and D100S were exclusively composed of sphalerite (ZnS) with a small amount of pyrite (FeS_2) (<1%) (**Supplementary Figure 2**). Oxidized minerals were not present in the XRD results, which is in contrast to the dominance of copper-containing chalcopyrite ($CuFeS_2$) and kusachiite ($CuBi_2O_4$) in inactive hydrothermal sediments of SWIR (Cao et al., 2014).

Analysis of Prokaryotic Community Structure

Prokaryotic communities in our chimney samples were examined by sequencing and analysis of 16S rRNA gene amplicons and 16S rRNA gene tags in metagenomic reads (16S miTags), and were then compared with those of the sulfide samples from other SWIR sites (**Supplementary Table 1**; Dong et al., 2021). There are a total of 30,189 qualified 16S rRNA gene amplicons for the characterization of microbial communities. They were then clustered with 97% similarity into 6,994 OTUs (**Supplementary Table 2**). Proteobacteria dominated all the SWIR sulfide samples of this study (**Figure 2A**), except for D95S, in which Bacteroidetes (20%) were the most prevalent phylum. Epsilonbacteraeota was particularly enriched in the chimney samples, and Archaea was not present in these communities. At the family level, *Ectothiorhodospiraceae* (average 11.9%) and *Thiovulaceae* (average 6.8%) were the most abundant families in both the 16S rRNA gene amplicon- and miTag-based communities of the D96S sample. *Ectothiorhodospiraceae* is significantly more abundant in the active chimney samples (D96S and D100S) than in other SWIR hydrothermal sediments using the *U*-test ($p < 10^{-10}$). In contrast, D100S contains a high proportion (7.7–19.1%) of *Sulfurovaceae*, which outcompetes *Ectothiorhodospiraceae* (∼6.2%) and *Thiovulaceae* (∼3.2%) as the dominant SOB (**Figure 2B**). Sulfur reducing bacteria (SRB) represented by *Desulfobulbaceae* and *Thermodesulfovibrionaceae* are abundantly present only in D95S and the reference SWIR sulfide samples. *Thermodesulfovibrionaceae* (Nitrospirae) occupied 6.3% of the community in D95S. The distinct distribution of *Ectothiorhodospiraceae* and *Desulfobulbaceae* between active chimney samples (D96S and D100S) and other hydrothermal samples from the SWIR was further illustrated by a chord diagram (**Figure 3**). The plotting further revealed special enrichment of Thiotrichaceae as the major SOB in inactive hydrothermal sediments, particularly in the S12T1 sample. A PCoA plot separated the microbial communities of D96S and D100S from the references and D95S. For D96S and D100S, the community structures revealed by the 16S rRNA gene amplicon and miTags were consistent with respect to the PCoA clustering (**Figure 4**).

Metagenomics Analysis of Dominant Species Inhabiting Active Hydrothermal Chimney

To understand the ecological role of microbial inhabitants in the active hydrothermal vents, we obtained 12.1 Gb raw

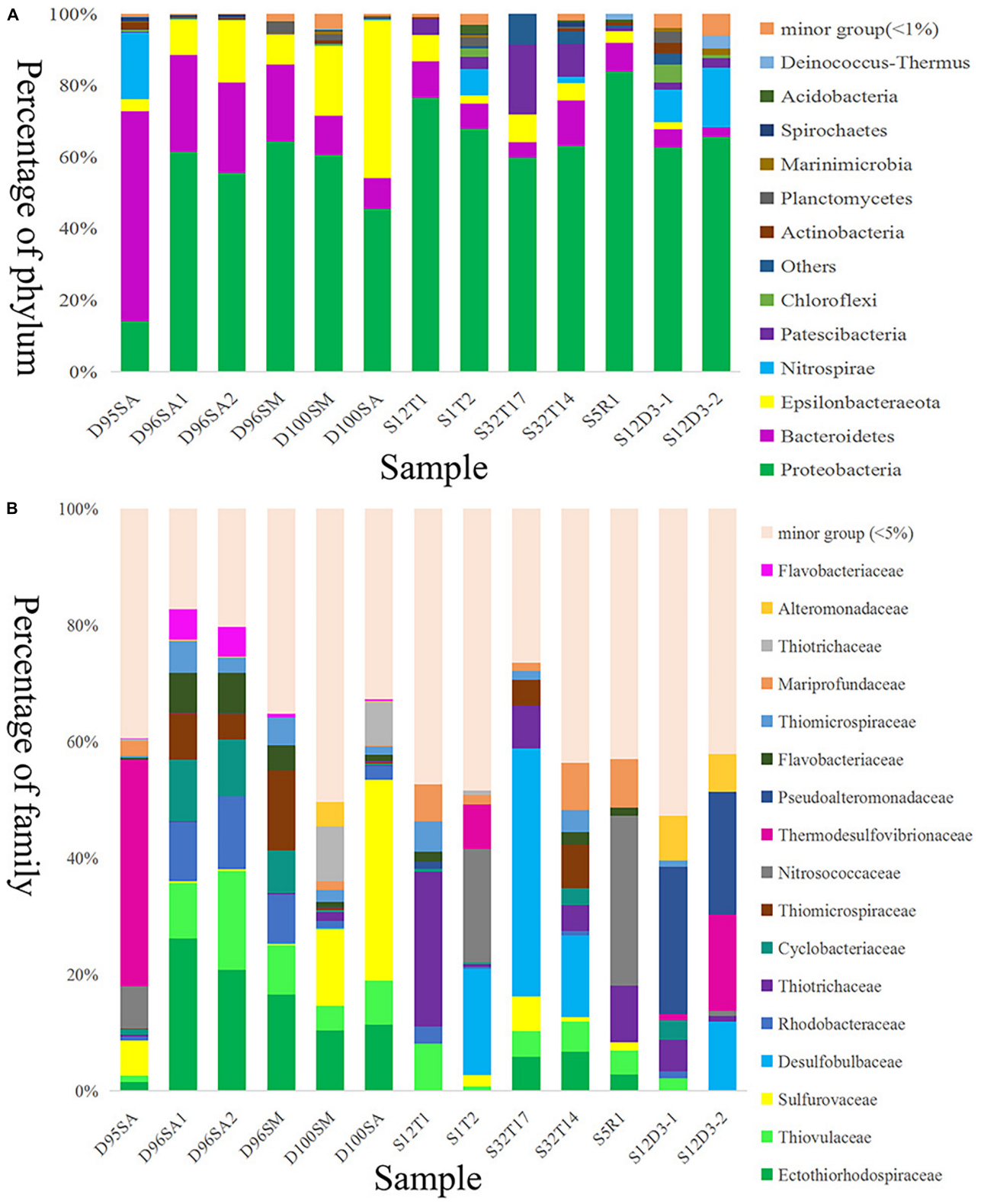

FIGURE 2 | Microbial community structures of hydrothermal samples. Taxonomic classification of operational taxonomic units (OTUs) at 97% similarity was performed by comparing with reference sequences of SILVA database v138. The microbial community structures were shown at phylum **(A)** and family **(B)** levels. D100SA, D96SA1, D96SA2, and D95SA refer to 16S rRNA gene amplicons; D100SM and D96SM are 16S miTags. The other samples are referred to **Supplementary Table 2**.

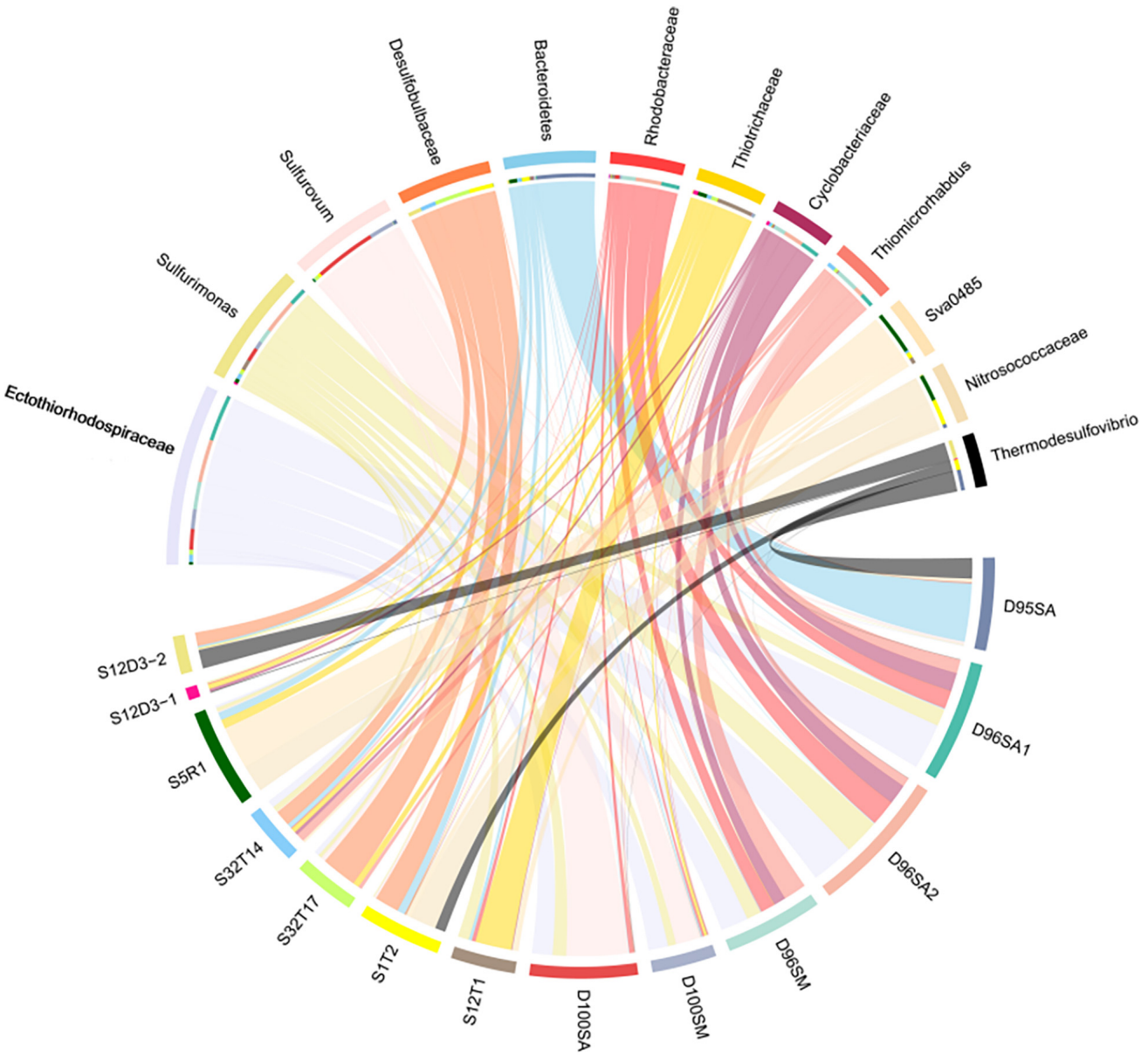

FIGURE 3 | The chord diagram chart showing the distribution of dominant genera. The analysis was performed using the microbial communities at the genus level. D100SA, D96SA1, D96SA2, and D95SA refer to 16S rRNA gene amplicons; D100SM and D96SM are 16S miTags obtained from the metagenomes. The other samples are referred in **Supplementary Table 2**.

Illumina Miseq paired-end sequencing data (2 × 300 bp) and retained 8.3 Gb clean data for subsequent metagenomics work of D96S and D100S (**Supplementary Table 3**). After assembly and genome binning, a total of 82 MAGs were retrieved from D96S and D100S metagenomic assemblies (**Supplementary Table 4**), among which 57 MAGs were of good quality (completeness > 80% and contamination < 5%). Taxonomic classification of the MAGs against GTDB indicates that they were affiliated with 12 prokaryotic phyla mainly composed of Proteobacteria ($n = 39$), Bacteroidota ($n = 20$), Campylobacterota ($n = 7$), and Desulfobacterota ($n = 5$; **Supplementary Table 4**). The abundant *Ectothiorhodospiraceae* in D96S and D100S identified by 16S rRNA gene amplicon sequencing were not present in the taxa of the MAGs. By searching the 16S rRNA gene amplicons of *Ectothiorhodospiraceae* against those extracted from the MAGs (>97% similarity), we reassigned *Ectothiorhodospiraceae* to the orders Thiohalomonadales SZUA-152 ($n = 8$) and SZUA-140 ($n = 1$) of Gammaproteobacteria in GTDB taxonomy. In a phylogenomics tree, these MAGs were clustered with the genomes obtained from hypersaline soda lake sediment, ground water, and other deep-sea hydrothermal vents, such as Mid-Atlantic Ridge, East Pacific Rise, and Lau Basin

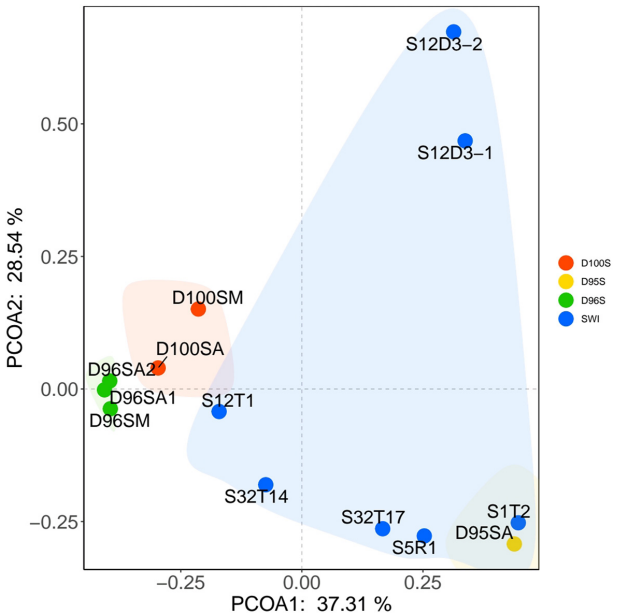

FIGURE 4 | The principal component analysis (PCoA) analysis of microbial communities. The PCoA analysis was performed using the microbial communities at family level. The community structures were based on the classification of 16S miTags (D100SM, D96SM, and the other SWIR reference samples) and 16S rRNA gene amplicons (D96SA1, D96SA2, D100SA, and D95SA) (**Supplementary Table 2**).

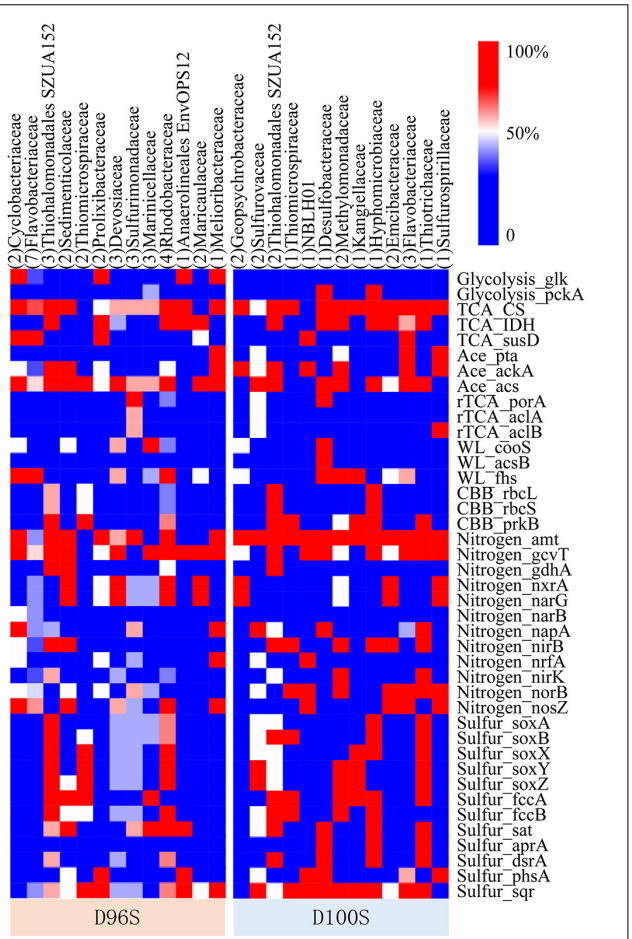

FIGURE 5 | Frequency of functional genes identified in metagenome-assembled genomes (MAGs) belonging to different families. The functional genes of 57 good-quality MAGs were identified by searching against Kyoto Encyclopedia of Genes and Genomes (KEGG) database. The number of MAGs in each genome taxonomy database (GTDB) family was included in the round brackets. The functions of the genes are shown in **Supplementary Table 5**. The full annotation of KEGG functions is shown in **Supplementary Table 6**.

of Tonga (**Figure 5**). Three phylogenetic groups were formed with most of our MAGs in Thiohalomonadales SZUA-152, a new order in GTDB.

On the basis of Kyoto Encyclopedia of Genes and Genomes (KEGG) gene annotation of the 57 good-quality MAGs, the functional genes for carbon, nitrogen, and sulfur metabolisms mediated by the major families of the chimney inhabitants were examined to predict their ecological functions. Hydrothermal vents discharge large amounts of hydrogen, methane, and hydrogen sulfide to deep waters (Jannasch and Mottl, 1985; Kawagucci et al., 2010; Dick, 2019). Thiosulfate oxidizing genes *soxABXYZ*, and sulfide oxidizing genes *dsrAB*, *fccAB,* and *sqr* were found in ≥50% of the MAGs for Thiohalomonadales (Gammaproteobacteria), *Thiomicrospiraceae* (Gammaproteobacteria), and *Rhodobacteraceae* (Alphaproteobacteria) MAGs from D96S; and in Thiohalomonadales, *Sulfurovaceae* (Campylobacterota), *Hyphomicrobiaceae* (Alphaproteobacteria), and *Thiotrichaceae* (Gammaproteobacteria) MAGs from D100S (**Figure 6**). In the periplasmic space, FccAB catalyzes oxidation of sulfide to elemental sulfur with electrons being transferred to cytochrome c; the SQR enzyme oxidizes sulfide to polysulfide (Schutz et al., 1999). The DsrAB encoded by the SOB carry out sulfide oxidation to sulfite (Anantharaman et al., 2014; Dong et al., 2021). This indicates the capacity of sulfide oxidation to S^0, polysulfide or sulfate by these SOB bacteria inhabiting our active chimney samples under different fluxes of electron acceptors. The *Rhodobacteraceae* MAGs also harbor nitrate reduction genes *narG*, suggesting the coupling of nitrate reduction and sulfide oxidation. *Sulfurimonadaceae* and *Sulfurovaceae* encoded the reverse tricarboxylic acid (rTCA) pathway for autotrophic CO_2 fixation. The other SOB, with the exception of *Thiotrichaceae,* may rely on the Calvin–Benson–Bassham (CBB) pathway for autotrophs, as ribulose-1,5-bisphosphate carboxylase (RuBisCO) genes *rbcLS* were found in their MAGs. Wood-Ljungdahl pathway as an alternative autotrophic process was only encoded by *Desulfobacteraceae* MAGs. Acetate metabolism is highly required by the bacterial inhabitant, as evidenced by the prevalence of acetate assimilatory genes *pta*, *acs,* and *ackA* in these MAGs. Genomics data also indicate that Gammaproteobacteria might use hydrogen released from the vents as alternative energy sources for carbon fixation and metabolic activities as indicated by the detection of [NiFe]-hydrogenase genes.

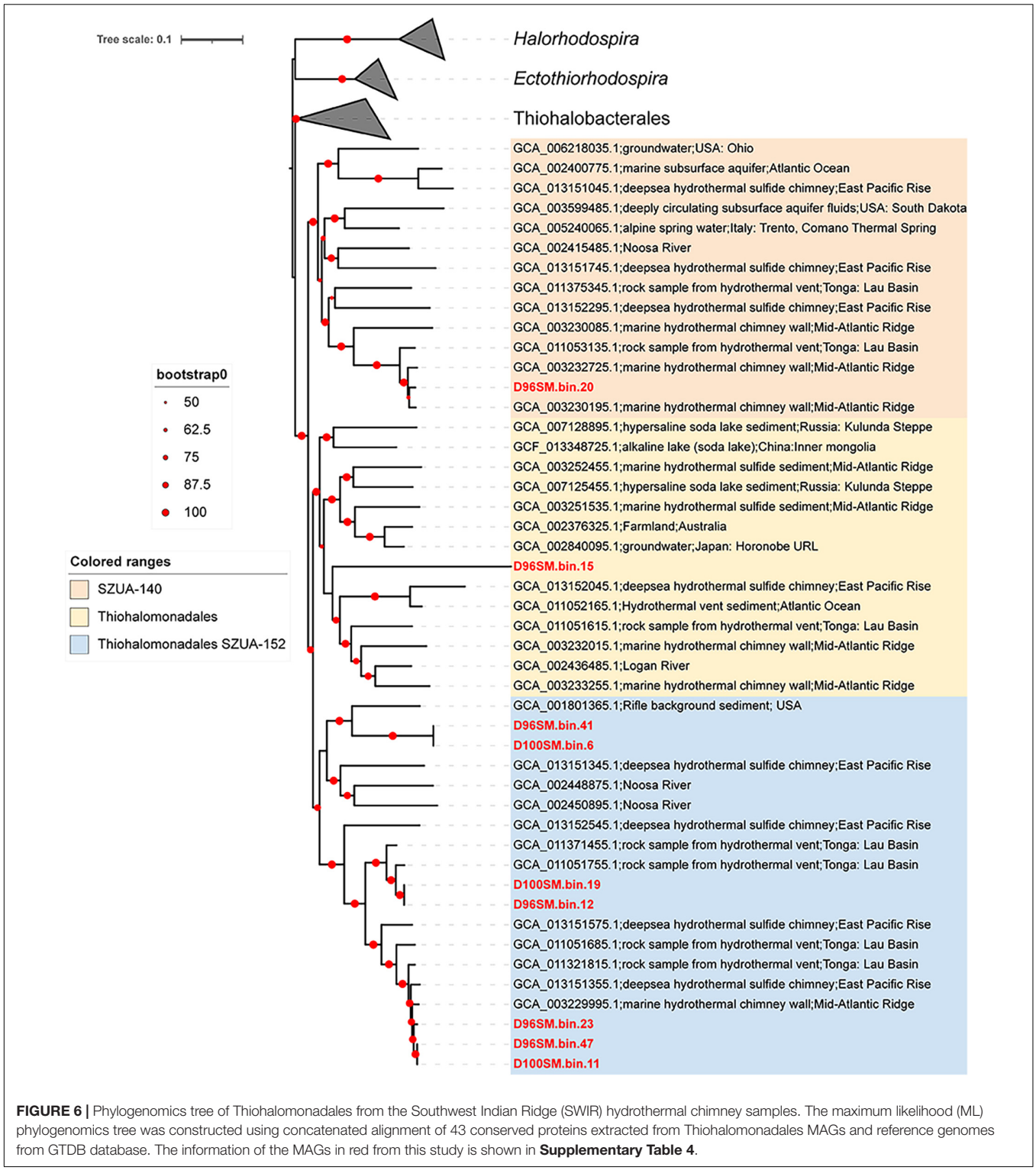

FIGURE 6 | Phylogenomics tree of Thiohalomonadales from the Southwest Indian Ridge (SWIR) hydrothermal chimney samples. The maximum likelihood (ML) phylogenomics tree was constructed using concatenated alignment of 43 conserved proteins extracted from Thiohalomonadales MAGs and reference genomes from GTDB database. The information of the MAGs in red from this study is shown in **Supplementary Table 4**.

Metabolism Potentials of Thiohalomonadales

We next examined the metabolic potentials and adaptive strategy of the dominant SOB, Thiohalomonadales, from our active hydrothermal vents using the annotation result of their five high-quality MAGs. The Thiohalomonadales MAGs harbor a complete set of sulfur-oxidizing genes, such as *soxABXYZ*, *fccABV*, *sqr*, *rdsrAB*, and *TST*, that may yield S^0, polysulfide, or sulfate (**Figure 7**). Nitrate assimilatory reduction may occur in the Thiohalomonadales as the MAGs contain *napAB* periplasmic

nitrate reduction genes and nitrite reduction genes (*nirBD*) that are involved in ammonia production. Thiohalomonadales might also rely on the CBB pathway for CO_2 fixation. Thiohalomonadales MAGs contain *cbb3* genes coding for phosphorylation respiration complex IV to overcome low oxygen conditions. Considering the high hydrogen content of the hydrothermal fluids, the microbes on the chimney are expected to be able to utilize hydrogen as an energy source. [NiFe] hydrogenase genes were present in the MAGs, along with *hup* genes responsible for the uptake and/or export of hydrogen. The Rnf complex as a cross-membrane proton pumping machine for the balance of cytoplasmic pH was encoded by the MAGs (Buckel and Thauer, 2013).

We identified all the related genes encoding the enzymes that participate in terpenoid backbone biosynthesis. Using geranylgeranyl diphosphate, Thiohalomonadales might generate phytoene, since the *crtB* gene encoding 15-cis-phytoene synthase was identified in the MAGs. The CrtB protein of Thiohalomonadales is most similar (82%) to a homolog of Thiotrichaceae from a subseafloor aquifer. Phytoene is a precursor of zeta-carotene and can be catalyzed by phytoene desaturase CtrI for carotene production (Lang et al., 1994). However, *ctrI* gene is missing from the MAGs, and the capacity of carotene biosynthesis by these SOB is thus questioned. The *crtB* gene was also present in the MAGs from RBG-16-57-12, Mariprofundaceae, Thiohalomonadales SZUA-140, and Melioribacteraceae. Most of these *crtB*-bearing MAGs also contain a farnesyl-diphosphate farnesyltransferase coding gene (*FDFT1*) that functions in squalene synthesis using farnesyl diphosphate.

In the Thiohalomonadales MAGs, a cph2 type bacteriophytochrome coding gene was identified to be 45% similar to a homolog from *Pseudomonas aeruginosa*. However, the putative bacteriophytochrome is featured with GGDEF and EAL domains but lacks GAF and PHY domains, indicating a discovery of a novel or malfunctional bacteriophytochrome (Gourinchas et al., 2019). The co-factor of bacteriophytochrome is biliverdin with a tetrapyrrolic structure. Heme synthesis pathway and biliverdin-producing heme oxygenase have been identified in the MAGs, which are vital for the potential function of bacteriophytochrome under red and far-red lights for Thiohalomonadales species (Vuillet et al., 2007; Gourinchas et al., 2019).

DISCUSSION

Discovery of Novel Microbiomes in Active Hydrothermal Chimneys

In this study, the "Jiaolong" manned submersible with robotic precision was employed to locate the vent structure of sulfide chimneys in the active SWIR hydrothermal areas. Using these chimney samples, we report the genomes of dominant microbial species and the prevalence of distinct SOB affiliated with Campylobacterota, Gammaproteobacteria, and Alphaproteobacteria inhabiting the sulfide chimney, all of which have been reported in deep-sea cold seeps recently (Li et al., 2021). The microbial community in the active SWIR hydrothermal vents was remarkably different from those from the SWIR inactive hydrothermal sulfide sediments (Cao et al., 2014; Dong et al., 2021) and others DSHVs (Dick, 2019; Hou et al., 2020; Zeng et al., 2021). Culturable Thiohalomonadales SOB, such as *Thiohalomonas denitrificans* had been isolated from the hydrothermal vents of the Suiyo Seamount in the Pacific Ocean (Mori et al., 2015). In addition, this study demonstrates their distribution in the DSHVs located in the Mid-Atlantic Ridge, East Pacific Rise, and Lau Basin. Given the finding of their relatives in other worldwide sites, the dominance of this order in DSHVs was, however, not reported previously (Flores et al., 2011; Urich et al., 2014; Meier et al., 2017). Dominant SOB differed even between D96S and D100S, owing to different combinations of Thiohalomonadales, *Thiomicrorhabdus*, *Sulfurovum,* and *Sulfurimonas*. This suggests a high diversity of SOB among active hydrothermal vents. Our genomics data predict other potential SOB, such as Hyphomicrobiaceae, Thiotrichaceae (represented by Beggiatoa), and Rhodobacteraceae in our samples, which have been rarely reported in other DSHVs. Considering the highly variable microenvironments adjacent to DSHVs, the composition of SOB inhabitants is predicted to be slightly diversified as reported for D96S and D100S by this study. In the late stages of hydrothermal vents, weak seepage of reducing fluids allows soaking of sulfide with oxic bottom water, which will gradually result in sulfide mineral oxidation and subsequent microbially mediated reduction processes (Li et al., 2017). The microbiomes of D96S and D100S were solely constituted by SOB, which is an indicator of the initial stage of a hydrothermal ecosystem. This has not been noticed in the SWIR and even global DSHVs.

The strong hydrothermal venting probably creates a reducing environment that covers the chimney, prohibiting oxidation of the chimney sulfide in this study. The mineral components in our samples indicate an early stage of the chimney formation at D100S, as there were not any oxidized mineral components. As a result, we could not detect SRB in D100S, while in contrast, prevalent *Thermodesulfovibrionaceaea* (SRB) was present in D95S. Although the sulfate concentration and nutrients of the samples were not analyzed due to their contact with sea water, we speculate that sulfate from sea water and produced by SOB might probably fuel the SRB in D95S. It seems that *Sulfurovaceae*, Thiohalomonadales, and *Thiovulaceae* were distributed differently in the hydrothermal chimneys possibly due to selection of different SOB families by local environmental variants. For example, *Sulfurovum* is more tolerant to oxygen (Meier et al., 2017) and might prefer a more oxic chimney with lower impact of hydrothermal fluid. In this study, Thiohalomonadales probably employed *cbb3* to cope with low oxygen; however, hypoxic exposure may also impair anaerobic and microaerobic microbial inhabitants (Lu and Imlay, 2021). We found that squalene as a bacterial hopanoid was likely synthesized by Thiohalomonadales, which is probably an efficient mechanism to scavenge single oxygen that may damage cell lipid by peroxidation (Kohno et al., 1995). The microbes in D96S and D100S have probably evolved to contain distinct gene profiles for adaptation to environmental changes due to the dynamics of gas and metal fluxes near active hydrothermal vents.

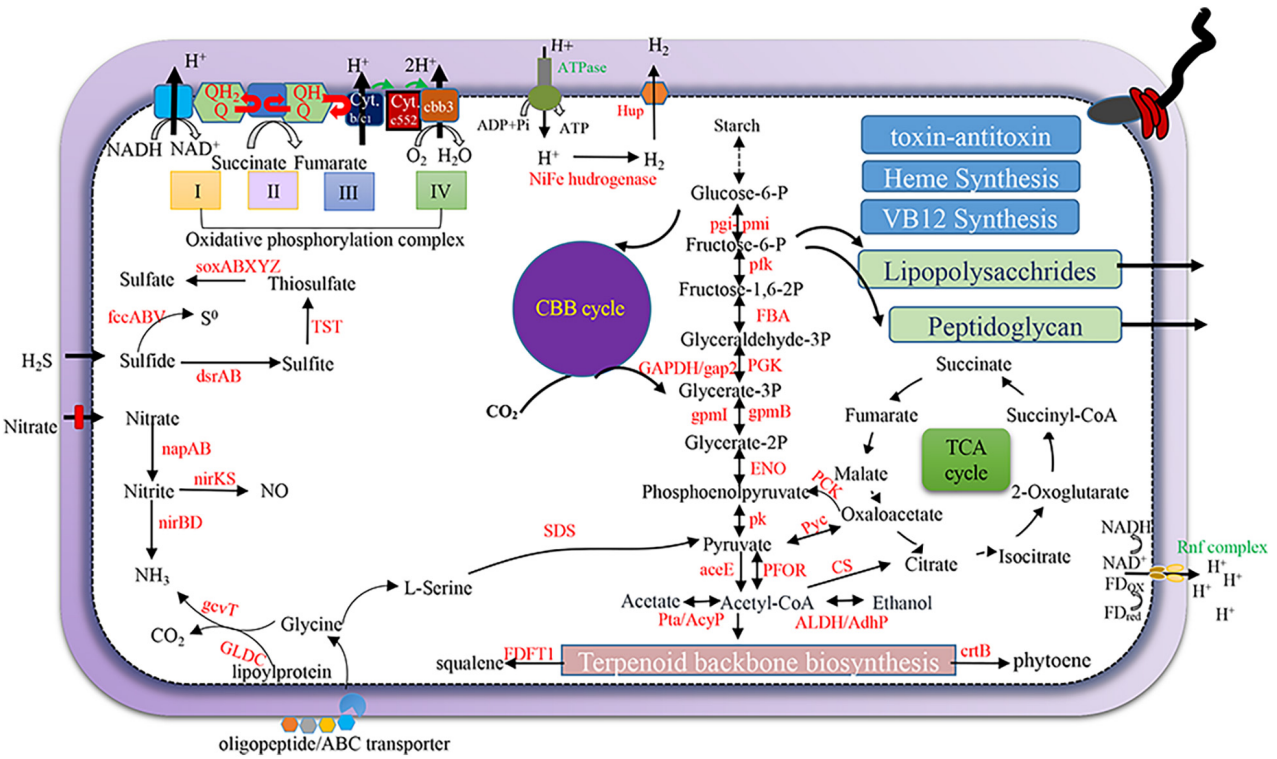

FIGURE 7 | Schematic metabolism of Thiohalomonadales (sulfur oxidizing bacteria) SOB. The metabolic pathways were predicted and depicted based on gene annotation of high-quality MAGs of Thiohalomonadales against KEGG and National Center for Biotechnology Information (NCBI)_nr databases.

Photolithoautotrophic Potential of Sulfur-Oxidizing Thiohalomonadales

Ectothiorhodospiraceae was previously a family of Chromatiales, but was recently reclassified into a new family of Thiohalomonadales. Members of the *Ectothiorhodospiraceae* are versatile in metabolisms, including photolithotrophic, photoheterotrophic, chemoheterotrophic, chemolithotrophic, and methylotrophic bacteria using various electron acceptors, such as nitrite, sulfur compounds, and arsenite (Hallberg et al., 2011; Slobodkina et al., 2016). So far, all isolates from hydrothermal fields belonging to this family are sulfur-oxidizing bacteria (Imhoff, 2006; Mori et al., 2015; Slobodkina et al., 2016). In this study, we discovered three phylogenetic groups in Thiohalomonadales belonging to SZUA152, SZUA140, and an unclassified clade. *Ectothiorhodospiraceae* members are able to capture red/far-red light for anaerobic photosynthesis, by which sulfide is oxidized to elemental sulfur and deposited in periplasm for further oxidation to sulfate (Imhoff, 2006). Bacteriophytochromes are photosensitive proteins employed by bacteria to capture red/far-red light to mediate growth (Vuillet et al., 2007; Gourinchas et al., 2019). At hydrothermal vents with a temperature of ∼350°C, most of the ambient light was detected to fall into near-infrared spectra between 750 and 1,050 nm (Dover et al., 1994). A recent report showed the promoted growth of a bacterial cultivation isolated from the Western Pacific DSHV under stimulation of infrared light at 940 nm (Liu et al., 2021). This is highly supported by a recent report that showed the presence of proteorhodopsin synthesis genes and photoautotrophic microbial groups in some metagenomes of active hydrothermal vents of SWIR (Chen et al., 2022). If the bacteriophytochromes and cofactor biliverdin are functional in Thiohalomonadales, they can probably sense red/near-infrared light from the hydrothermal vents to activate photosynthesis of Thiohalomonadales. In photosynthetic and non-photosynthetic organisms, carotenoids are synthesized to prevent the photooxidative damage (Glaeser and Klug, 2005). In the present study, although the gene coding for the enzyme catabolizing the final step of zeta-carotenoid was not found, there are still perhaps unknown genes responsible for carotenoid synthesis in the genomes. Aside from serving as light sensors, some bacteriophytochromes can be redox sensors to monitor the environmental changes, particularly in the environment approximate to hydrothermal vents where hot reductive fluid meets cold oxic sea water. Whether Thiohalomonadales can synthesize the *bona fide* bacteriophytochromes for photoautotrophy warrants future experimental efforts using cultivated strains of this order from DSHVs.

Overall, we identified an unusual, uncultivated sulfur-oxidizing bacterial group that is particularly prevalent in active hydrothermal chimneys. Their potential capacity of sulfur oxidization and photoautotrophic lifestyle casts lights on the possible relationship with ancient lineages inhabiting the early earth with similar hydrothermal environments billions of years

ago (Lunine, 2006). The finding of this SOB group can probably provide insights into the future evolutionary study of ancient microbial lineages under the climate change in the long history of the Earth.

DATA AVAILABILITY STATEMENT

The datasets presented in this study can be found in online repositories. The names of the repository/repositories and accession number(s) can be found in the article/ **Supplementary Material**.

AUTHOR CONTRIBUTIONS

H-YB and YW conceived the study and wrote the manuscript. H-GC, P-FZ, and Y-LZ performed the experiments. YW, H-YB, P-FZ, and Y-LZ analyzed the data and summarized the results. J-TL critically revised the manuscript. All authors contributed to the article and approved the submitted version.

FUNDING

This study was supported by the Major Scientific and Technological Projects of Hainan Province (ZDKJ2021028).

ACKNOWLEDGMENTS

We thank the cruise members of *D/V* DY35 and "Jiaolong" submersible pilots for their efforts in sampling. We appreciate the Supercomputing Center of University of Sanya for providing the computation assistance.

SUPPLEMENTARY MATERIAL

The Supplementary Material for this article can be found online at: https://www.frontiersin.org/articles/10.3389/fmicb.2022.861795/full#supplementary-material

REFERENCES

Adam, N., Kriete, C., Garbe-Schönberg, D., Gonnella, G., Krause, S., Schippers, A., et al. (2020). Microbial community compositions and geochemistry of sediments with increasing distance to the hydrothermal vent outlet in the Kairei field. *Geomicrobiol. J.* 37, 242–254. doi: 10.1080/01490451.2019.1694107

Alneberg, J., Bjarnason, B. S., De Bruijn, I., Schirmer, M., Quick, J., Ijaz, U. Z., et al. (2014). Binning metagenomic contigs by coverage and composition. *Nat. Methods* 11, 1144–1146.

Anantharaman, K., Duhaime, M. B., Breier, J. A., Wendt, K. A., Toner, B. M., and Dick, G. J. (2014). Sulfur oxidation genes in diverse deep-sea viruses. *Science* 344, 757–760. doi: 10.1126/science.1252229

Aramaki, T., Blanc-Mathieu, R., Endo, H., Ohkubo, K., Kanehisa, M., Goto, S., et al. (2019). KofamKOALA: KEGG ortholog assignment based on profile HMM and adaptive score threshold. *Bioinformatics* 36, 2251–2252. doi: 10.1093/bioinformatics/btz859

Baker, E. T., and Milburn, H. B. (1997). MAPR: a new instrument for hydrothermal plume mapping. *RIDGE Events* 8, 23–25.

Beatty, J. T., Overmann, J., Lince, M. T., Manske, A. K., Lang, A. S., Blankenship, R. E., et al. (2005). An obligately photosynthetic bacterial anaerobe from a deep-sea hydrothermal vent. *Proc. Natl. Acad. Sci. U.S.A.* 102, 9306–9310. doi: 10.1073/pnas.0503674102

Brazelton, W. J., and Baross, J. A. (2010). Metagenomic comparison of two Thiomicrospira lineages inhabiting contrasting deep-aea hydrothermal environments. *PLoS One* 5:e13530. doi: 10.1371/journal.pone.0013530

Buckel, W., and Thauer, R. K. (2013). Energy conservation via electron bifurcating ferredoxin reduction and proton/Na(+) translocating ferredoxin oxidation. *Biochim. Biophys. Acta* 1827, 94–113. doi: 10.1016/j.bbabio.2012.07.002

Cao, H., Wang, Y., Lee, O. O., Zeng, X., Shao, Z., and Qian, P. Y. (2014). Microbial sulfur cycle in two hydrothermal chimneys on the Southwest Indian Ridge. *mBio* 5, e980–e913. doi: 10.1128/mBio.00980-13

Capella-Gutiérrez, S., Silla-Martínez, J. M., and Gabaldón, T. (2009). trimAl: a tool for automated alignment trimming in large-scale phylogenetic analyses. *Bioinformatics* 25, 1972–1973. doi: 10.1093/bioinformatics/btp348

Chaumeil, P.-A., Mussig, A. J., Hugenholtz, P., and Parks, D. H. (2020). GTDB-Tk: a toolkit to classify genomes with the Genome Taxonomy Database. *Bioinformatics* , [Epub ahead of print]. doi: 10.1093/bioinformatics/btz848

Chen, H., Li, D. H., Jiang, A. J., Li, X. G., Wu, S. J., Chen, J. W., et al. (2022). Metagenomic analysis reveals wide distribution of phototrophic bacteria in hydrothermal vents on the ultraslow-spreading Southwest Indian Ridge. *Mar. Life Sci. Technol.* doi: 10.1007/s42995-021-00121-y

Chen, S., Zhou, Y., Chen, Y., and Gu, J. (2018). fastp: an ultra-fast all-in-one FASTQ preprocessor. *Bioinformatics* 34, i884–i890. doi: 10.1093/bioinformatics/bty560

Connelly, D. P., Copley, J. T., Murton, B. J., Stansfield, K., Tyler, P. A., German, C. R., et al. (2012). Hydrothermal vent fields and chemosynthetic biota on the world's deepest seafloor spreading centre. *Nat Commun* 3:620. doi: 10.1038/ncomms1636

Corliss, J. B., Dymond, J., Gordon, L. I., Edmond, J. M., Von Herzen, R. P., Ballard, R. D., et al. (1979). Submarine thermal sprirngs on the galapagos rift. *Science* 203, 1073–1083. doi: 10.1126/science.203.4385.1073

Dick, G. J. (2019). The microbiomes of deep-sea hydrothermal vents: distributed globally, shaped locally. *Nat. Rev. Microbiol.* 17, 271–283. doi: 10.1038/s41579-019-0160-2

Dick, G. J., Anantharaman, K., Baker, B. J., Li, M., Reed, D. C., and Sheik, C. S. (2013). The microbiology of deep-sea hydrothermal vent plumes: ecological and biogeographic linkages to seafloor and water column habitats. *Front. Microbiol.* 4:124. doi: 10.3389/fmicb.2013.00124

Dixon, P. (2003). VEGAN, a package of R functions for community ecology. *J. Veget. Sci.* 14, 927–930. doi: 10.1111/j.1654-1103.2003.tb02228.x

Dong, X., Zhang, C., Li, W., Weng, S., Song, W., Li, J., et al. (2021). Functional diversity of microbial communities in inactive seafloor sulfide deposits. *FEMS Microbiol. Ecol.* 97:fiab108. doi: 10.1093/femsec/fiab108

Dover, C. L. V., Reynolds, G. T., Chave, A. D., and Tyson, J. A. (1994). Light at deep-sea hydrothermal vents. *Geophys. Res. Lett.* 23, 2049–2052.

Flores, G. E., Campbell, J. H., Kirshtein, J. D., Meneghin, J., Podar, M., Steinberg, J. I., et al. (2011). Microbial community structure of hydrothermal deposits from geochemically different vent fields along the Mid-Atlantic Ridge. *Environ. Microbiol.* 13, 2158–2171. doi: 10.1111/j.1462-2920.2011.02463.x

Francheteau, J., Needham, H. D., Choukroune, P., Juteau, T., Séguret, M., Ballard, R. D., et al. (1979). Massive deep-sea sulphide ore deposits discovered on the East Pacific Rise. *Nature* 277, 523–528.

German, C. R., Baker, E. T., Mevel, C., Tamaki, K., and Team, F. S. (1998). Hydrothermal activity along the southwest Indian ridge. *Nature* 395, 490–493. doi: 10.1038/26730

Glaeser, J., and Klug, G. (2005). Photo-oxidative stress in Rhodobacter sphaeroides: protective role of carotenoids and expression of selected genes. *Microbiology* 151, 1927–1938. doi: 10.1099/mic.0.27789-0

Gourinchas, G., Etzl, S., and Winkler, A. (2019). Bacteriophytochromes – from informative model systems of phytochrome function to powerful tools in cell biology. *Curr. Opin. Struct. Biol.* 57, 72–83. doi: 10.1016/j.sbi.2019.02.005

Hallberg, K. B., Hedrich, S., and Johnson, D. B. (2011). Acidiferrobacter thiooxydans, gen. nov. sp. nov.; an acidophilic, thermo-tolerant, facultatively anaerobic iron- and sulfur-oxidizer of the family Ectothiorhodospiraceae. *Extremophiles* 15, 271–279. doi: 10.1007/s00792-011-0359-2

Han, Y., Gonnella, G., Adam, N., Schippers, A., Burkhardt, L., Kurtz, S., et al. (2018). Hydrothermal chimneys host habitat-specific microbial communities: analogues for studying the possible impact of mining seafloor massive sulfide deposits. *Sci. Rep.* 8:10386. doi: 10.1038/s41598-018-28613-5

Hou, J., Sievert, S. M., Wang, Y., Seewald, J. S., Natarajan, V. P., Wang, F., et al. (2020). Microbial succession during the transition from active to inactive stages of deep-sea hydrothermal vent sulfide chimneys. *Microbiome* 8:102. doi: 10.1186/s40168-020-00851-8

Huang, J. M., Baker, B. J., Li, J. T., and Wang, Y. (2019). New microbial lineages capable of carbon fixation and nutrient cycling in deep-sea sediments of the northern South China Sea. *Appl. Environ. Microbiol.* 85, e523–e519. doi: 10.1128/AEM.00523-19

Hyatt, D., Chen, G.-L., Locascio, P. F., Land, M. L., Larimer, F. W., and Hauser, L. J. (2010). Prodigal: prokaryotic gene recognition and translation initiation site identification. *BMC Bioinform.* 11:119. doi: 10.1186/1471-2105-11-119

Imhoff, J. F. (2006). "The Family Ectothiorhodospiraceae," in *The Prokaryotes: A Handbook on the Biology of Bacteria Volume 6: Proteobacteria: Gamma Subclass*, eds M. Dworkin, S. Falkow, E. Rosenberg, K.-H. Schleifer, and E. Stackebrandt (New York: Springer New York), 874–886. doi: 10.1007/0-387-30746-x_32

Jannasch, H. W., and Mottl, M. J. (1985). Geomicrobiology of deep-sea hydrothermal vents. *Science* 229, 717–725. doi: 10.1126/science.229.4715.717

Kang, D. D., Li, F., Kirton, E., Thomas, A., Egan, R., An, H., et al. (2019). MetaBAT 2: an adaptive binning algorithm for robust and efficient genome reconstruction from metagenome assemblies. *PeerJ* 7:e7359.

Katoh, K., Asimenos, G., and Toh, H. (2009). "Multiple alignment of DNA sequences with MAFFT," in *Bioinformatics for DNA Sequence Analysis*, Ed. P. David. (Berlin: Springer), 39–64. doi: 10.1007/978-1-59745-251-9_3

Katoh, K., and Standley, D. M. (2013). MAFFT multiple sequence alignment software version 7: improvements in performance and usability. *Mol. Biol. Evol.* 30, 772–780. doi: 10.1093/molbev/mst010

Kawagucci, S., Toki, T., Ishibashi, J., Takai, K., Ito, M., Oomori, T., et al. (2010). Isotopic variation of molecular hydrogen in 20 degrees-375 degrees C hydrothermal fluids as detected by a new analytical method. *J. Geophys. Res.* 115:G03021.

Kelley, D. S., Karson, J. A., Fruh-Green, G. L., Yoerger, D. R., Shank, T. M., Butterfield, D. A., et al. (2005). A serpentinite-hosted ecosystem: the Lost City hydrothermal field. *Science* 307, 1428–1434. doi: 10.1126/science.1102556

Kohno, Y., Egawa, Y., Itoh, S., Nagaoka, S.-I., Takahashi, M., and Mukai, K. (1995). Kinetic study of quenching reaction of singlet oxygen and scavenging reaction of free radical by squalene in n-butanol. *Biochim. Biophys. Acta* 1256, 52–56. doi: 10.1016/0005-2760(95)00005-w

Kuczynski, J., Stombaugh, J., Walters, W. A., Gonzalez, A., Caporaso, J. G., and Knight, R. (2011). Using QIIME to analyze 16S rRNA gene sequences from microbial communities. *Curr. Protoc. Bioinform.* Chapter 10:10.7.

Lang, H. P., Cogdell, R. J., Gardiner, A. T., and Hunter, C. N. (1994). Early steps in carotenoid biosynthesis: sequences and transcriptional analysis of the crtI and crtB genes of Rhodobacter sphaeroides and overexpression and reactivation of crtI in *Escherichia coli* and R. sphaeroides. *J. Bacteriol.* 176, 3859–3869. doi: 10.1128/jb.176.13.3859-3869.1994

Langmead, B., and Salzberg, S. (2012). Fast gapped-read alignment with Bowtie 2. *Nat. Methods* 9, 357–359.

Lecoeuvre, A., Menez, B., Cannat, M., Chavagnac, V., and Gerard, E. (2021). Microbial ecology of the newly discovered serpentinite-hosted Old City hydrothermal field (southwest Indian ridge). *ISME J.* 15, 818–832.

Li, J., Cui, J., Yang, Q., Cui, G., Wei, B., Wu, Z., et al. (2017). Oxidative weathering and microbial diversity of an inactive seafloor hydrothermal sulfide chimney. *Front. Microbiol.* 8:1378. doi: 10.3389/fmicb.2017.01378

Li, W. L., Dong, X., Lu, R., Zhou, Y. L., Zheng, P. F., Feng, D., et al. (2021). Microbial ecology of sulfur cycling near the sulfate-methane transition of deep-sea cold seep sediments. *Environ. Microbiol.* 23, 6844–6858. doi: 10.1111/1462-2920.15796

Liu, G., Shan, Y., Zheng, R., Liu, R., and Sun, C. (2021). Growth promotion of a deep-sea bacterium by sensing infrared light through a bacteriophytochrome photoreceptor. *Environ. Microbiol.* 23, 4466–4477. doi: 10.1111/1462-2920.15639

López-García, P., Duperron, S., Philippot, P., Foriel, J., Susini, J., and Moreira, D. (2003). Bacterial diversity in hydrothermal sediment and epsilon*proteobacteria*l dominance in experimental microcolonizers at the Mid-Atlantic Ridge. *Environ. Microbiol.* 5, 961–976. doi: 10.1046/j.1462-2920.2003.00495.x

Lu, Z., and Imlay, J. A. (2021). When anaerobes encounter oxygen: mechanisms of oxygen toxicity, tolerance and defence. *Nat. Rev. Microbiol.* 19, 774–785. doi: 10.1038/s41579-021-00583-y

Lunine, J. I. (2006). Physical conditions on the early Earth. *Philos. Trans. R. Soc. Lond. B Biol. Sci.* 361, 1721–1731. doi: 10.1098/rstb.2006.1900

Meier, D. V., Pjevac, P., Bach, W., Hourdez, S., Girguis, P. R., Vidoudez, C., et al. (2017). Niche partitioning of diverse sulfur-oxidizing bacteria at hydrothermal vents. *ISME J.* 11, 1545–1558. doi: 10.1038/ismej.2017.37

Meier, D. V., Pjevac, P., Bach, W., Markert, S., Schweder, T., Jamieson, J., et al. (2019). Microbial metal-sulfide oxidation in inactive hydrothermal vent chimneys suggested by metagenomic and metaproteomic analyses. *Environ. Microbiol.* 21, 682–701. doi: 10.1111/1462-2920.14514

Mori, K., Suzuki, K. I., Yamaguchi, K., Urabe, T., and Hanada, S. (2015). Thiogranum longum gen. nov., sp. nov., an obligately chemolithoautotrophic, sulfur-oxidizing bacterium of the family Ectothiorhodospiraceae isolated from a deep-sea hydrothermal field, and an emended description of the genus Thiohalomonas. *Int. J. Syst. Evol. Microbiol.* 65, 235–241. doi: 10.1099/ijs.0.070599-0

Nguyen, L.-T., Schmidt, H., Haeseler, A. V., and Minh, B. (2015). IQ-TREE: A Fast and Effective Stochastic Algorithm for Estimating Maximum-Likelihood Phylogenies. *Mol. Biol. Evol.* 32, 268–274. doi: 10.1093/molbev/msu300

Nurk, S., Bankevich, A., Antipov, D., Gurevich, A. A., Korobeynikov, A., Lapidus, A., et al. (2013). Assembling single-cell genomes and mini-metagenomes from chimeric MDA products. *J. Comput. Biol.* 20, 714–737.

Olm, M. R., Brown, C. T., Brooks, B., and Banfield, J. F. (2017). dRep: a tool for fast and accurate genomic comparisons that enables improved genome recovery from metagenomes through de-replication. *ISME J.* 11, 2864–2868.

Parks, D. H., Imelfort, M., Skennerton, C. T., Hugenholtz, P., and Tyson, G. W. (2015). CheckM: assessing the quality of microbial genomes recovered from isolates, single cells, and metagenomes. *Genom. Res.* 25, 1043–1055. doi: 10.1101/gr.186072.114

Patel, R. K., and Jain, M. (2012). NGS QC toolkit: A toolkit for quality control of next generation sequencing data. *PLoS One* 7:e30619. doi: 10.1371/journal.pone.0030619

Price, M. N., Dehal, P. S., and Arkin, A. P. (2009). FastTree: computing large minimum evolution trees with profiles instead of a distance matrix. *Mol. Biol. Evol.* 26, 1641–1650. doi: 10.1093/molbev/msp077

Quast, C., Pruesse, E., Yilmaz, P., Gerken, J., Schweer, T., Yarza, P., et al. (2013). The SILVA ribosomal RNA gene database project: improved data processing and web-based tools. *Nucleic Acids Res.* 41, D590–D596. doi: 10.1093/nar/gks1219

Schutz, M., Maldener, I., Griesbeck, C., and Hauska, G. (1999). Sulfide-quinone reductase from Rhodobacter capsulatus: requirement for growth, periplasmic localization, and extension of gene sequence analysis. *J. Bacteriol.* 181, 6516–6523. doi: 10.1128/JB.181.20.6516-6523.1999

Scott, K. M., Leonard, J. M., Boden, R., Chaput, D., Dennison, C., Haller, E., et al. (2019). Diversity in CO(2)-concentrating mechanisms among chemolithoautotrophs from the genera Hydrogenovibrio, Thiomicrorhabdus, and Thiomicrospira, ubiquitous in sulfidic habitats worldwide. *Appl. Environ. Microbiol.* 85, e2096–e2018. doi: 10.1128/AEM.02096-18

Slobodkina, G. B., Baslerov, R. V., Novikov, A. A., Viryasov, M. B., Bonch-Osmolovskaya, E. A., and Slobodkin, A. I. (2016). Inmirania thermothiophila gen. nov., sp. nov., a thermophilic, facultatively autotrophic, sulfur-oxidizing gammaproteobacterium isolated from a shallow-sea hydrothermal vent. *Int. J. Syst. Evol. Microbiol.* 66, 701–706. doi: 10.1099/ijsem.0.000773

Tao, C. H., Lin, J., Guo, S. Q., Chen, Y. J., Wu, G. H., Han, X. Q., et al. (2012). First active hydrothermal vents on an ultraslow-spreading center: southwest Indian Ridge. *Geology* 40, 47–50. doi: 10.1130/g32389.1

Urich, T., Lanzen, A., Stokke, R., Pedersen, R. B., Bayer, C., Thorseth, I. H., et al. (2014). Microbial community structure and functioning in marine sediments associated with diffuse hydrothermal venting assessed by integrated meta-omics. *Environ. Microbiol.* 16, 2699–2710. doi: 10.1111/1462-2920.12283

Uritskiy, G. V., Diruggiero, J., and Taylor, J. (2018). MetaWRAP—a flexible pipeline for genome-resolved metagenomic data analysis. *Microbiome* 6:158. doi: 10.1186/s40168-018-0541-1

Van Dover, C. L., Humphris, S. E., Fornari, D., Cavanaugh, C. M., Collier, R., Goffredi, S. K., et al. (2001). Biogeography and ecological setting of Indian Ocean hydrothermal vents. *Science* 294, 818–823. doi: 10.1126/science.1064574

Vuillet, L., Kojadinovic, M., Zappa, S., Jaubert, M., Adriano, J. M., Fardoux, J., et al. (2007). Evolution of a bacteriophytochrome from light to redox sensor. *EMBO J.* 26, 3322–3331. doi: 10.1038/sj.emboj.7601770

Wang, Y., and Qian, P.-Y. (2009). Conservative fragments in bacterial 16S rRNA genes and primer design for 16S ribosomal DNA amplicons in metagenomic studies. *PLoS One* 4:e7401. doi: 10.1371/journal.pone.0007401

Wu, Y. W., Simmons, B. A., and Singer, S. W. (2016). MaxBin 2.0: an automated binning algorithm to recover genomes from multiple metagenomic datasets. *Bioinformatics* 32, 605–607.

Zeng, X., Alain, K., and Shao, Z. (2021). Microorganisms from deep-sea hydrothermal vents. *Mar. Life Sci. Technol.* 3, 204–230.

Zhang, L., Kang, M., Xu, J., Xu, J., Shuai, Y., Zhou, X., et al. (2016). Bacterial and archaeal communities in the deep-sea sediments of inactive hydrothermal vents in the Southwest India Ridge. *Sci. Rep.* 6:25982. doi: 10.1038/srep25982

Zhou, H. Y., and Dick, H. J. B. (2013). Thin crust as evidence for depleted mantle supporting the Marion Rise. *Nature* 494, 195–200. doi: 10.1038/nature11842

Conflict of Interest: The authors declare that the research was conducted in the absence of any commercial or financial relationships that could be construed as a potential conflict of interest.

Publisher's Note: All claims expressed in this article are solely those of the authors and do not necessarily represent those of their affiliated organizations, or those of the publisher, the editors and the reviewers. Any product that may be evaluated in this article, or claim that may be made by its manufacturer, is not guaranteed or endorsed by the publisher.

frontiers | Frontiers in Microbiology

REVIEW
published: 02 June 2022
doi: 10.3389/fmicb.2022.891528

Advances in Defining Ecosystem Functions of the Terrestrial Subsurface Biosphere

*D'Arcy R. Meyer-Dombard**† and Judy Malas*†

Earth and Environmental Sciences, University of Illinois at Chicago, Chicago, IL, United States

The subsurface is one of the last remaining 'uncharted territories' of Earth and is now accepted as a biosphere in its own right, at least as critical to Earth systems as the surface biosphere. The terrestrial deep biosphere is connected through a thin veneer of Earth's crust to the surface biosphere, and many subsurface biosphere ecosystems are impacted by surface topography, climate, and near surface groundwater movement and represent a transition zone (at least ephemerally). Delving below this transition zone, we can examine how microbial metabolic functions define a deep terrestrial subsurface. This review provides a survey of the most recent advances in discovering the functional and genomic diversity of the terrestrial subsurface biosphere, how microbes interact with minerals and obtain energy and carbon in the subsurface, and considers adaptations to the presented environmental extremes. We highlight the deepest subsurface studies in deep mines, deep laboratories, and boreholes in crystalline and altered host rock lithologies, with a focus on advances in understanding ecosystem functions in a holistic manner.

Keywords: subsurface, continental, dark biosphere, extremophiles, catabolism and anabolism

OPEN ACCESS

Edited by:
Andreas Teske, University of North Carolina at Chapel Hill, United States

Reviewed by:
John R. Spear, Colorado School of Mines, United States
Shawn E. McGlynn, Earth-Life Science Institute, Tokyo Institute of Technology, Japan

****Correspondence:***
D'Arcy R. Meyer-Dombard
drmd@uic.edu

† These authors have contributed equally to this work

Specialty section:
This article was submitted to Extreme Microbiology, a section of the journal Frontiers in Microbiology

Received: *07 March 2022*
Accepted: *03 May 2022*
Published: *02 June 2022*

Citation:
Meyer-Dombard DR and Malas J (2022) Advances in Defining Ecosystem Functions of the Terrestrial Subsurface Biosphere. Front. Microbiol. 13:891528. doi: 10.3389/fmicb.2022.891528

INTRODUCTION

Defining the Terrestrial Subsurface

Defining what is meant by the label "deep biosphere" is not straightforward, as researchers have their own, personal interpretations and there is not a universal community consensus. It's equally interesting to consider how to define the "surface biosphere." Is the surface biosphere just the outermost skin of the planet? Does it extend through the entire soil profile or just the first meter (both of which are arbitrary and variable criteria)? Does it extend to the stratosphere? Microorganisms have been identified up to altitudes of 41–77 km in the stratosphere and mesosphere (Wainwright et al., 2004; Griffin, 2008; Pearce et al., 2009; DeLeon-Rodriguez et al., 2013), and are known to influence climate through cloud formation and triggering precipitation events as well as catalyzing atmospheric chemistry (Vaïtilingom et al., 2013; Fröhlich-Nowoisky et al., 2016). No study of the terrestrial deep biosphere has yet reached comparable depths into the subsurface. For comparison, the Chinese Continental Scientific Drilling project (CCSD) recovered continuous cores from depths up to 5,110 m (Zhang et al., 2005; Dai et al., 2021). The lowest reaches of the deep biosphere are currently unknown, but are likely to be governed by physical environmental stressors such as temperature and pressure, as well as the availability and activity of liquid water (Schulze-Makuch et al., 2017; Merino et al., 2019). For example, Dai et al. (2021) found

that no microorganisms were detectable in the CCSD cores below 4,850 m depth, estimated to be 137°C. Our ability to investigate fully the depth of the subsurface biosphere is currently hampered by our ability to reach those depths, while providing sufficiently clean samples (see discussions in; Moser et al., 2003; Davidson et al., 2011; Zhong et al., 2018).

Other recent work has reviewed diversity and function in the deep biosphere, from marine, terrestrial, extremophile, and planetary perspectives (e.g., Parkes et al., 2014; Kieft, 2016; Morono and Inagaki, 2016; Colman et al., 2017; Schulze-Makuch et al., 2017; Magnabosco et al., 2018; Merino et al., 2019), each with a different focus. We will consider only the terrestrial deep biosphere, and define this as including bedrock below the soil horizon, at whatever depth that might occur locally. Further, we will synergize recent advances in understanding the metabolic and ecological function of the terrestrial subsurface, highlighting ecosystems where the recent literature showcases efforts to understand the roles of taxa and of microbial communities in the subsurface biosphere.

Surface Influences on the Terrestrial Subsurface

A necessary topic of discussion, inevitably, is whether the terrestrial subsurface is truly divorced from influence from the surface biosphere. The terrestrial subsurface is hosted within a porous and permeable crust, through which groundwater moves, bringing with it nutrients, carbon, and biomass from the surface biosphere. It is possible that we are not yet technologically capable of reaching depths in the terrestrial subsurface that are truly independent of surface influence - modern or ancient. Many of the biomes commonly considered in the community as "terrestrial subsurface" - by nature of geology and physics - are significantly influenced by surface input. For example, cave biomes have a direct open conduit to the surface if a natural entrance exists, which have the potential to influence metabolic processes within the caves (e.g., Barton and Northup, 2007; Spear et al., 2007; De Waele et al., 2016; D'Angeli et al., 2019; Engel, 2019; Jones and Northup, 2021; Selensky et al., 2021 and references therein). Even without a natural entrance, caves are typically formed in shallow groundwater (Lauritzen, 2018). Another example can be found in the huge body of literature on ecosystems in and under glacial ice (inter- and subglacial ice, respectively), much of which involves discussions of contamination from drilling and sampling protocols, or whether the organisms found represent a paleo-surface signal (e.g., Miteva et al., 2014). The provenance of microorganisms found in interglacial ice is questioned as being endemic vs. sourced from past supraglacial communities or from surrounding biomes (e.g., Zhong et al., 2021). In fact, fluctuations in microbial abundance in interglacial ice has been shown to be correlated with dust load in annual snow (Margesin and Miteva, 2011, and refs. within). While convincing evidence has been presented showing that microorganisms trapped in interglacial ice can actively metabolize (Tung et al., 2005, 2006; Price, 2007; Rhodes et al., 2013; Miteva et al., 2016), these organisms may be recording a history of past climate conditions (Margesin and Miteva, 2011), rather than an endemic modern subsurface biosphere signal.

Another specific biome that is often hailed as a "window" or "portal" to the subsurface is surface springs that have characteristically long residence time or water-rock reaction progress (e.g., hydrothermal or serpentinizing springs). However, the "window" may be opaque and coated with a layer of surface biome. Magnabosco et al. (2014) examined the microbiology of both deep subsurface fracture fluids and related surface springs, and showed that the spring communities were distinct from their fracture fluid counterparts, bringing into question whether springs serve as a reflection of subsurface processes. Further, it has been demonstrated that local climate and topography can directly influence the nutrients and carbon that are present in surface springs. Schubotz et al. (2013) illustrated that the intact polar lipids from biofilms examined from the chemosynthetic zone of two hot springs of different topographic aspect (one seated at the bottom of a wooded slope and the other seated at the top of a mound of hydrothermal deposits) recorded distinct histories of carbon sources and usage. Isotopic analysis of the biomass, DIC, and DOC revealed that the Archaea and Bacteria of the topographically isolated spring recorded a ^{13}C enriched signature similar to the ^{13}C-DIC (indicating autotrophic growth), while the organisms in the topographically low spring recorded a signature of mixed carbon fixation and heterotrophic metabolisms supported by surface organic carbon. Climate/seasonality can also be a factor in exogenous vs. endogenous carbon use in surface springs as was demonstrated for a system of serpentinizing surface springs in the Philippines (Meyer-Dombard et al., 2019).

Figure 1 further demonstrates the impact of both topography and climate. The data in **Figure 1** come from a hydrothermal spring known as "Bison Pool" in Yellowstone National Park, which was serendipitously sampled immediately after a major precipitation event and 8 days following the event. "Bison Pool" is a wide, clear spring, seated nearly level with a surrounding meadow, where one can easily visualize that a window to the subsurface is being presented. **Figure 1** shows historic values for ^{13}C-biomass (relative to both ^{13}C-DIC and ^{13}C-DOC, black and gray points, respectively), moving from the source pool brimming with fluids recently in the subsurface to the surface-derived photosynthetic mat downstream. Historic data (encompassed in shaded boxes) show that biomass closest to the high temperature spring source typically incorporates DIC through non-photosynthetic carbon fixation, then trends toward more heterotrophic metabolisms near the 65–70°C section of the outflow channel, and finally returns to carbon fixation through photosynthesis at the end of the outflow (also demonstrated in Swingley et al., 2012). Following the precipitation event, we observed that overland flow was washing the soil and animal excrement from the ground into the pool source, turning the normally clear fluid a turbid brown. The biofilms in the hottest parts of the outflow channel immediately after the rain event (red and pink points) are depleted by as much as ∼5–15‰ relative to both DIC and DOC, indicating an incorporation of more surface derived organic carbon than is typical (compared to "historic"

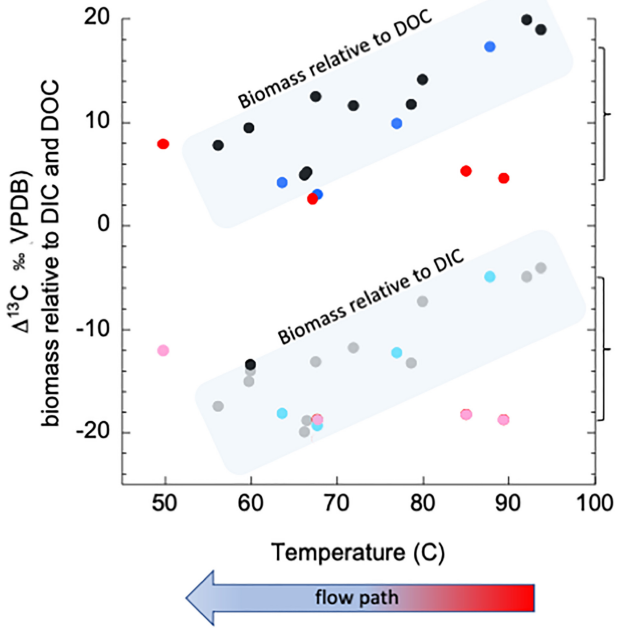

FIGURE 1 | Isotopic composition of carbon in biomass in sediments at "Bison Pool," Yellowstone National Park, relative to that of dissolved inorganic and organic carbon. Figure shows samples with flow down the outflow channel, with the hottest samples near the source at the right end of the *X*-axis. "Historic," multi year values are in black and gray points, within blue fields. Values immediately following the precipitation event are in red and pink. Values representing recovery after 8 days are in shades of blue. Methods can be found in **Supplementary Material**.

data, note brackets at right). Eight days following the event (light and dark blue points), the biomass had returned to "normal" values, indicating a return to incorporation of DIC in the hottest portions of the pool - the areas that are typically thought of as being "windows" to the subsurface.

This vignette reminds us that the subsurface biosphere, by definition, intersects the surface biosphere. Springs, caves, glaciers, and even aquifers are subsurface biomes that have at least intermittent connection to the surface biosphere. For example, near surface aquifers (e.g., Boyd et al., 2007; Anantharman et al., 2016) and boreholes into sedimentary units (e.g., Katsuyama et al., 2013; Dong et al., 2014; Frank et al., 2016; Hu et al., 2016; Thieringer et al., 2021) may have frequent contact with water, nutrients, and carbon that originated in the surface biome due to high permeability and porosity of host rock.

The degree of connection between the surface and subsurface at any given study area is often a subject of discussion or even concern, if the purpose of the study is to identify a true subsurface signal. While we posit that the connection between the subsurface and surface biospheres is equally as interesting as identifying a subsurface biosphere that is independent of all surface influence, to narrow the scope of this review we will focus on investigations of boreholes, deep mines, and subsurface laboratories, which we feel are the best, current examples of locations with minimized surface influence.

The Environment of the Deep Terrestrial Subsurface

Environmental conditions, modulators, and nutrient flow in the subsurface are necessarily directed by the type of bedrock that hosts the specific subsurface ecosystem. For example, porosity and permeability of the host rock will partly determine the access the system has to water, nutrients, and carbon sources that moving water may bring with it. Further, these properties may allow direct connection of the surface and subsurface biospheres (e.g., aquifers contaminated by surface sources). In general, environmental conditions that are likely ubiquitous in the terrestrial subsurface biosphere include anaerobicity or very low oxygen concentrations, high pressure, and nutrient limitation. Some locations may also host fluids of higher temperature and salinity than similar surface environments. Several studies have remarked on the probability that most deep subsurface microorganisms are likely surface-attached, or have demonstrated that biofilms form *in situ* on fracture surfaces, and one estimate suggests that biofilms make up 20–80% of the total subsurface biomass (Jägevall et al., 2011; Magnabosco et al., 2018; Flemming and Wuertz, 2019). These observations have direct implications for estimates of subsurface biomass and functioning of ecosystems in the host rock (e.g., Colman et al., 2016).

Regardless of aspect, the host rock water interaction is a key component of defining all terrestrial subsurface ecosystems. Except in cases where organic compounds from the surface biosphere are delivered to the deeper subsurface biosphere, energy and nutrients for life in the subsurface are defined by the interaction between the host rock and water. This interaction is also influenced by surface variables such as local climate and topography, which influence groundwater recharge and flow. Metabolisms that might take place in the subsurface are then guided by these environmental variables and the host rock mineralogy. Further, there is evidence that some water rock interactions may limit the ability for a subsurface community to survive. For example, groundwater interaction with evaporite sequences in the Boulby Mine subsurface were shown to produce brines, some of which resisted cultivation and DNA extraction efforts (Payler et al., 2019). This example illuminates and emphasizes the dependence of the terrestrial subsurface biosphere on the minerals present and groundwater origin and flow path. The systems examined here are hosted in a variety of parent rock and geologic settings, including from volcanic, metamorphic, and ultramafic assemblages, which have implications for resulting geochemistry, energy availability, and functional/taxonomic diversity in the subsurface ecosystem (Boyd et al., 2007; Magnabosco et al., 2018; Leong and Shock, 2020).

EXPLORING THE TERRESTRIAL DEEP BIOSPHERE

Arguably, the most direct access to the deep subsurface with minimal surface influence is in places where we have

physically entered the ecosystem *via* mining. The deep subsurface community has been making best use of economic mines for decades now, providing literature that explores the microbial ecosystems in solid rock and pore fluids. Some studies further drill directly into the walls of previously cut mine shafts and tunnels, to obtain more pristine materials. Several underground laboratories and observatories have been established, and modern DNA sequencing technologies are providing fresh perspectives. The deep subsurface has also been frequently accessed *via* drilling of boreholes directly into substrata. The advantage of removing material by drilling (whether from the surface or from within a mine), is that experimental and analytical apparatus can be inserted. Several studies mentioned in the following paragraphs utilize this technique, delivering short and long term incubation experiments and continuous fluid collection.

It must also be recognized that even these best examples of accessing the deeper terrestrial biosphere are not completely without interaction from surface environments. The act of mining by nature exposes the subsurface to the surface atmosphere and surface fluids. Drilling places materials downhole that aren't indigenous and may not be fully sterile. By necessity, a major focus of working in deep biosphere settings involves understanding, managing, and mitigating contamination. Creative solutions have been developed, particularly to address situations where cell numbers can be vanishingly small (e.g., Zhong et al., 2018, 2021), that have driven innovation in technology and technique (comprehensive descriptions in Hodgson et al., 2016; Kieft, 2016; Morono and Inagaki, 2016). For example, hot water drilling techniques were developed to clean access sediment cores beneath subglacial lake Whillans (Christner et al., 2014; Hodgson et al., 2016) and other technological advances are needed for fast moving ice shelves, or for work in remote locations (Hodgson et al., 2016). The studies highlighted below have shown reasonable attempts at ensuring a lack of surface signal, or defining where potential surface signal is found.

Deep Mines and Laboratories

We start our discussion of metabolism and ecological function in the terrestrial deep subsurface by reviewing recent work that has emerged from the world's deep mines and laboratories. The terrestrial subsurface community has long recognized that such direct access is invaluable for microbiological investigations. Leading the way in underground microbiological research are permanently established laboratory sites such as the Kidd Creek Mine Observatory, Äspö Hard Rock Laboratory, Olkiluoto Spent Nuclear Fuel tunnel (ONKALO), Mizunami Underground Research Laboratory, Mont Terri Rock Laboratory, the Boulby Underground Laboratory, and the Sanford Underground Research Laboratory (Stroes-Gascoyne et al., 2007; Fukuda et al., 2010; Pedersen, 2012, 2013; Osburn et al., 2014; Cockell et al., 2019; Lollar et al., 2019). Adding to this wealth of data are studies from retired and working mine locations, which provide additional opportunities for examining the limits of life in the subsurface (e.g., Chivian et al., 2008; Bagnoud et al., 2016; Payler et al., 2019).

Fennoscandian Shield Deep Laboratories: Aspö and Pyhäsalmi

One well studied site is the Äspö Hard Rock Laboratory (HRL) in Sweden, which has been established as a deep laboratory for decades (Kotelnikova and Pedersen, 1998). Äspö HRL is a coastal site, situated in the porphyritic granite-granodiorite of the Fennoscandian Shield, and intrusion ages (U-Pb) suggest ages between 1,760 and 1840 Ma (Johansson, 1988). Groundwater in the Äspö HRL is a mix of meteoric and seawater origins, depending on the depth of the boreholes (Kotelnikova and Pedersen, 1998). Fracture fluids are neutral pH, are reduced and depleted in dissolved oxygen and nitrate, but carry measurable amounts of DOC and bicarbonate, as well as sulfate (Kotelnikova and Pedersen, 1998; Wu et al., 2016).

Interest in a "hydrogen driven" subsurface biosphere and the determination that biogenic methane is produced in boreholes in the Fennoscandian Shield (Sherwood Lollar et al., 1993; Kotelnikova and Pedersen, 1998) encouraged an early focus on methanogenic and acetogenic organisms at the Äspö HRL (e.g., Pedersen, 1993; Stevens and McKinley, 1995). It was predicted that groundwaters in Äspö HRL provide an anaerobic and oligotrophic environment that could support nitrate, ferric iron, sulfate, and manganese reducing organisms (Hallbeck and Pedersen, 2012; Pedersen, 2013; Ionescu et al., 2015). Early work at Äspö HRL sites was focused on culture dependent methods. This included the use of a system that recirculates fracture fluids through refrigerated flow cell "cabinets" and then back through the fracture, while maintaining the 3.15 MPa *in situ* fluid pressure within a microbiology dedicated laboratory ("MICROBE," at 447 m depth) (Hallbeck and Pedersen, 2008). The flow cells allow experimentation with fracture water as well as on surfaces such as glass slides or mineral coupons.

Microorganisms capable of nitrate, sulfate, iron, and manganese reduction, methanogenesis, and acetogenesis were found in groundwater at the MICROBE site in densities $\sim 8 \times 10^7$ cells/ml (Hallbeck and Pedersen, 2008), and ^{14}C and ^{3}H labeled substrates were incorporated into biomass, demonstrating autotrophic and heterotrophic metabolic capabilities in a related location (Pedersen and Ekendahl, 1992; Ekendahl and Pedersen, 1994). Novel methanogens and sulfate reducing bacteria have been described from the Äspö HRL (Kotelnikova et al., 1998; Kotelnikova and Pedersen, 1998; Motamedi and Pedersen, 1998), and it has been suggested that this site is largely supported by hydrogen, a strong electron donor (Pedersen, 2012). The flow cell cabinets were used to experiment with *in situ* batch cultures, with hydrogen or acetate additives, to demonstrate that hydrogen can support a slow but sustainable level of microbial activity in Äspö HRL groundwaters (Pedersen, 2012).

Wu et al. (2016) further queried the planktonic communities in groundwaters of the Äspö HRL to determine the genetic potential for metabolic schema. This work examined three fluids of different age and origin. The resulting metagenomic analysis revealed that the fracture water of modern, marine origin likely represents a more surface impacted fluid. Populations in the modern, marine fracture fluids were shown to be able to primarily

ferment organic carbon, and potentially couple sulfide oxidation to nitrate reduction and fix carbon with the reductive pentose phosphate cycle (no other C-fixation pathways were represented). Geochemical data supports these conclusions; fracture water is depleted in nitrate but features measurable ammonium, as well as low sulfide but abundant sulfate. The metagenome from the older, saline fracture waters suggested, again, a large dependence on organic carbon, as well as nitrate and sulfur reduction, denitrification, and carbon and nitrogen fixation. Further, despite the previous demonstrations that a wide range of hydrogen supported, reducing metabolic pathways could be stimulated through enrichment, no genetic signal was found to suggest that these are dominant metabolic functions in the Äspö HRL groundwaters.

A second mine site in the Fennoscandian Shield offers an opportunity to explore different fracture water host rock relationships than the Äspö HRL mine site. In contrast to Äspö, the Pyhäsalmi mine in Finland is seated in Paleoproterozoic volcanogenic massive sulfides, where the lower mine stratigraphy is composed of felsic, tuffaceous volcanites and the upper mine is seated in mafic lavas, breccias, and pyroclastics (Miettinen et al., 2015). Bomberg et al. (2019) explored fracture waters in the upper mine, between 240–600 m depth using enrichments (focusing on iron based metabolisms) coupled with taxonomic diversity analysis, following up on a previous study by Kay et al. (2014). At these depths, the freshly exposed surfaces allow oxidation of the host rock, weathering the minerals and impacting the fracture fluids. Fracture fluids were at pH 1.4–2.3, reminiscent of acid mine drainage systems. Concurrently, the fluids contained high concentrations of the analyzed metals (such as Fe, Mn, Cu, Zn, Al), and both sulfate and sulfide. This study site presents a good example of a deep subsurface site that has been highly impacted by the surface biosphere, and illustrates the plasticity of the resident microbial communities. Enrichments targeted aerobic ferrous iron oxidizers and ferric iron reducers, and results showed a high microbial diversity. Dominant members differed with depth, and *Acidithiobacillus* and *Leptospirillum* dominated at shallower depth while *Ferrovum* and *Metallibacter* were the dominating bacterial genera at 600 m. Species of the heterotrophic genera, *Acidiphilum,* were detected in all samples and enrichments.

Purkamo et al. (2020) investigated the same mine using metagenomics, but at 2.4 km where the fracture fluids were alkaline and reduced, more typical of a deep subsurface mine fluid with less surface influence. Here, 96% of the 16S rRNA marker genes sequenced at this site were gamma and alpha Proteobacteria, and archaeal sequences were essentially not retrieved - it was estimated that only ∼50% of the bacterial richness was captured from these low biomass fluids. Notably, marker genes for sulfate reduction and methanogenesis were not detected. However, the complete dissimilatory nitrate reduction pathway and reductive pentose phosphate pathways were identified (KEGG reconstructions). Carbon cycling was primarily heterotrophic, much like the Äspö sites described above, and functional predictions indicated that chemoheterotrophy was a key ecological function in this environment, with indication that heterotrophy could be coupled with sulfate or sulfur respiration.

Together, these investigations of the deep biosphere seated in the Fennoscandian shield bedrocks point to a low biomass ecosystem that is driven by chemoheterotrophy, nitrate reduction, and reduction of sulfur compounds. Carbon fixation may occur through the reductive pentose phosphate cycle. However, the evidence of a hydrogen-driven ecosystem, with emphasis on methanogenesis, acetogenesis, and sulfate reduction is lacking in the most recent metagenomic-driven studies (Wu et al., 2016; Purkamo et al., 2020), despite earlier successes with targeted enrichments. Future work may elucidate the role of these metabolic options in these sites as supportive, rather than dominant, as in Lau et al. (2016). Further, while each deep mine highlighted here hosts fluids that are clearly impacted by the surface biosphere, truer signals of the subsurface biosphere were apparent at depth at both Äspö HRL and Pyhäsalmi.

Sanford Underground Research Facility and Deep Mine Microbial Observatory

At a depth intermediate between the Fennoscandian Shield Äspö HRL and Pyhäsalmi mine locations, the Sanford Underground Research Facility (SURF) in the former Homestake Gold Mine (South Dakota, United States) is home to the Deep Mine Microbial Observatory (DeMMO). The mine is seated in Paleoproterozoic metasediments that are iron rich, and the complex geologic history documents oceanic volcanisms and subsequent marine infilling (Osburn et al., 2019). A summary of primary minerals present in each of the major units at SURF can be found in Casar et al. (2021a), **Table 1**. Numerous boreholes, manifolds, and pools were available within the mine for sampling prior to the establishment of the DeMMO and new boreholes were drilled (horizontally) at the 1.48 km depth for fresh rock analyses (e.g., Osburn et al., 2014; Momper et al., 2017a). Fresh holes in differing lithologies and fluid flow rates were produced in 2016, some of which were fitted with custom made expandable packers (Osburn et al., 2019). The SURF laboratory and DeMMO locations have produced several studies dedicated to understanding metabolism and microbe-mineral interaction in the deep terrestrial subsurface.

Given the complex geologic history of the host rock, it is no surprise that the fracture fluids are geochemically diverse at different DeMMO locations. The concentration of cations in six sites of different depths (and thus different host formations) varies considerably from site to site, even while anions are relatively consistent (high sulfate with low carbonate, or moderate sulfate and carbonate) (Osburn et al., 2019). Redox sensitive chemical species are highly variable, and provide a wide range of energetic options for metabolic pathways (Osburn et al., 2014). Fluid chemistry is extremely consistent over time, suggesting that microbial communities may enjoy environmental stability. Further, it has been demonstrated repeatedly that the fracture fluids in DeMMO are distinct chemically and microbiologically from controls and service waters used in the mine (Osburn et al., 2014, 2019; Casar et al., 2020).

Surveys of diversity at various sites (∼240 m–1.48 km) reveal that among the boreholes, biofilms, pools, and manifolds,

TABLE 1 | Reactions considered in estimations of Gibbs Free Energy of Reaction shown in **Figure 2**. Aqueous forms were used for O_2, CH_4, H_2, N_2.

	Reaction	Electron acceptor	e^-/rxn
1	$O_2 + 2H_2 \leftrightarrow 2H_2O$	O_2	4
2	$4Fe^{+2} + O_2 + 6H_2O \leftrightarrow 4FeOOH + 8H^+$	O_2	4
3	$2NO_3^- + 2H^+ + 5H_2 \leftrightarrow N_2 + 6H_2O$	NO_3^-	10
4	$8NO_3^- + 3H^+ + 5HS^- \leftrightarrow 5SO_4^{-2} + 4N_2 + 4H_2O$	NO_3^-	40
5	$NO_3^- + H^+ + CH_4 \leftrightarrow HCO_3^- + NH_4^+$	NO_3^-	8
6	$SO_4^{-2} + H^+ + 4H_2 \leftrightarrow HS^- + 4H_2O$	SO_4^{-2}	8
7	$SO_4^{-2} + CH_4 \leftrightarrow HCO_3^- + HS^- + H_2O$	SO_4^{-2}	8
8	$4SO_4^{-2} + 5H^+ + 3CH_4 \leftrightarrow 3HCO_3^- + 4S^0 + 7H_2O$	SO_4^{-2}	24
9	$acetate + SO_4^{-2} \leftrightarrow 2HCO_3^- + HS^-$	SO_4^{-2}	8
10	$S^0 + H_2 \leftrightarrow H^+ + HS^-$	S^0	2
11	$HCO_3^- + H^+ + 4H_2 \leftrightarrow CH_4 + 3H_2O$	HCO_3^-	8
12	$4H_2 + H^+ + 2HCO_3^- \leftrightarrow acetate + 4H_2O$	HCO_3^-	4
13	$8FeOOH + acetate + 15H^+ \leftrightarrow 8Fe^{+2} + 2HCO_3^- + 12H_2O$	FeOOH	8
14	$Fe_2O_3 + H_2 + 4H^+ \leftrightarrow 2Fe^{+2} + 3H_2O$	Fe_2O_3	2
15	$Fe_3O_4 + H_2 + 6H^+ \leftrightarrow 3Fe^{+2} + 4H_2O$	Fe_3O_4	2

Bacteria dominate the communities with Archaea representing at most 5% of the populations. Site fluids differ in dominant taxa. For example, at ∼250 m depth, where fluids are only moderately reducing and have high concentrations of ferrous iron (up to 2.3 mg/L), the communities are dominated by *Ca. Omnitrophica* and various unclassified taxa. In contrast, the 600 m depth fluid is reduced and very rich in both ferrous iron and sulfate (2.8 and 1,800 mg/L, respectively), and is dominated by Betaproteobacteria and *Nitrospirae*. Finally, at 1.5 km, the fluids contain high concentrations of sulfate and methane and primarily host Deltaproteobacteria and *Firmicutes* (Osburn et al., 2014). Fracture fluids appear to support a much higher diversity and richness of organisms than rock-hosted samples (Momper et al., 2017a; Casar et al., 2020, 2021a,b).

A series of investigations fueled by metagenome and experimental methodologies paired with extensive catabolic modeling efforts have elucidated the genetic and metabolic potential of communities in DeMMO sites. At the time of this writing, 22 high quality "MAGs" (metagenome assembled genomes) that are > 90% complete were recovered from fluids at the 1.48 km DeMMO site and other fluids in the SURF complex (Momper et al., 2017b). The reductive Acetyl Co-A pathway was dominant, with a few select MAGS hosting complete pathways for the 3-hydroxypropionate/4-hydroxybutyrate and reductive pentose phosphate cycles (Momper et al., 2017b). The dominance of the reductive Acetyl-CoA pathway has also been noted in several other deep terrestrial biosphere sites (e.g., Nyyssönen et al., 2014; Lau et al., 2016; Magnabosco et al., 2016; Rempfert et al., 2017). The genetic capacity for methanogenesis and sulfate/sulfite reduction were identified in one and thirteen (out of 74) MAGS, respectively. Marker genes for nitrate reduction (both cytoplasmic and periplasmic) were present in several MAGs. However, while all genes needed for denitrification were identified, none were all present together in one MAG. Likewise, evidence for the genetic capacity for CO, thiosulfate, sulfur or sulfide, or iron redox was not found in this particular study (but read on!). These suggested metabolic functions of Bacteria in the fracture fluids agree well with the calculated energy density for these metabolic strategies (Osburn et al., 2014).

Despite the apparent lack of genetic markers for iron-based metabolism in DeMMO fluids, taxonomy and catabolic modeling studies suggested that iron cycling should likely play a large role in ecosystem dynamics. Experiments demonstrated growth of biofilms on surfaces of minerals bearing Fe (as well as S, Ti, Mn), spatially targeting these metals (Casar et al., 2020, 2021a). Biofilms on native rock coupons were enriched in taxa putatively capable of pyrite oxidation with nitrate, a thermodynamically favorable catabolic option that releases ferrous iron and sulfate. In light of this, both new and previously published metagenomes were specifically annotated with an Fe-centric pipeline. Casar et al. (2021b) found that the genetic capacity for iron oxidation existed at all sites analyzed, however, the specific genes present varied from site to site, apparently in accordance with local fracture fluid geochemistry. For example, the shallower, less reducing fluids contained the highest abundances of Cyc2 cluster 1, characteristic of neutrophilic iron oxidizers such as *Gallionella* (identified in MAGs). In general, Cyc2 was identified from most sites, affiliated with different families of Bacteria, demonstrating a wide spread genetic potential for iron oxidation. In addition, genes encoding for iron reduction (*OmcS*, *OmcZ*, and DFE) were abundant at some sites, suggesting that biofilm forming taxa identified in the MAGs can carry out iron/metal reduction on the surface of DeMMO minerals. These lines of genetic and modeling evidence point to iron cycling as a key metabolic function in the subsurface at this site.

These studies reveal a metabolic landscape in the subsurface at SURF. Modeling predicted modes of catabolism that should be favorable in the fluids, namely that the oxidation of sulfur, sulfide, ferrous iron, ammonium, and the reduction of manganese oxides are strong potential *in situ* energy sources, and that the energy density is highest at most sites examined using S^0, HS^-, NH_4^+, Fe^{+2}, and Mn^{+2} as electron donors, but lower using CH_4, CO, and H_2. Generally, the oxidation of S^0, HS^-, NH_4^+, and Fe^{+2} yields large reservoirs of energy in all fracture fluids (per kg of H_2O), regardless of the electron acceptor (Osburn et al., 2014; Rowe et al., 2020; Casar et al., 2021b). Hydrogen oxidation, methanogenesis, sulfate reduction, and aqueous iron reduction were found to yield little to no energy when normalized as energy density (Osburn et al., 2014). Metabolism associated with mineral surfaces, specifically of S, Fe, Ti, and Mn minerals (Casar et al., 2021a) was predicted to drive biofilm growth on solid rock. The reduction of oxidized iron minerals, such as ferrihydrite, magnetite, goethite, hematite, and lepidocrocite, using HS^- and the oxidation of siderite and pyrite with NO_3^- were shown to be particularly energy dense catabolic options for mineral biofilms, while planktonic communities have options for oxidation of aqueous iron (with NO_3^-) and reduction of particulate ferrihydrite (with HS^-) (Casar et al., 2021b). Combined with experimental and metagenomic evidence, this

evidence of likely catabolic processes in the subsurface is particularly convincing.

South African Mines

The mines in the Witwatersrand represent deep access to Archaean rocks and some of the deepest studies of the terrestrial subsurface biosphere have emerged from this region. This basin is made up of several supergroups of different host rock lithologies; namely, the 2.5 Ga Transvall Supergroup (dolomites, banded iron formation and volcanics), the 2.7 Ga Ventersdorp Supergroup (basaltic), and the 2.9 Ga Witwatersrand Supergroup (quartzite and shale). Below these lies a 3.4–3.0 Ga metamorphic and igneous complex basement, including granite, amphibolite, and gneiss (Nicolaysen et al., 1981). Two types of fracture waters in this region have been identified, ranging in age between 1.5–23 Ma (Lippmann-Pipke et al., 2011). At 0.8–2 km depths, in the Beatrix, Masimong, Merriespruit and Joel mines, paleo-meteoric waters contain hydrocarbon gasses of primarily microbial origin and very little H_2 gas (Ward et al., 2004; Lippmann-Pipke et al., 2011). Fluids at 2.7–3.6 km in the Kloof, Driefontein, Mponeng, and TauTona mines are saline and host high levels of H_2 gas (Sherwood Lollar et al., 2007; Lippmann-Pipke et al., 2011). Ancient waters, formed > 2 Ga, enter the fracture fluid by intersecting with fluid inclusions (Lippmann-Pipke et al., 2011). The "self-sufficient," deep subsurface *Candidatus Desulforudis audaxviator* (Lin et al., 2006a; Chivian et al., 2008) was identified from fracture fluids at 2.8 km depth in the Mponeng mine, with some of the highest contributions of the > 2 Ga fluids among all the fluids investigated by Lippmann-Pipke et al. (2011). Arguably, these mines represent some of the best access to the deep and ancient subsurface. Indications of temporal changes in fracture fluid composition have implications for long term community variability (Magnabosco et al., 2018).

Our discussion will include studies from four of the aforementioned mines, beginning at the shallower depths. Some early indications that shallower fracture fluids (e.g., Beatrix mine) are more microbially diverse than fluids from more saline fluids deeper in the basin (Lin et al., 2006b) may not hold up to scrutiny using modern sequencing methodologies. For example, when Magnabosco et al. (2014) compared samples from six different deep mines in the region, including Beatrix, Driefontein, and TauTona gold mines in the Witwatersrand, they found no statistical difference in the richness or evenness of taxa in fracture fluids between the shallower Beatrix site and the deeper mine sites, and 220/874 total taxa observed in the pooled sample set were shared between all locations. Using high-throughput DNA sequencing to study taxonomic diversity in these deep mines increased the number of identified taxa from previous studies (from 243 taxa), possibly by further identifying rare taxa (Magnabosco et al., 2014).

The Beatrix mine is at the southwestern edge of the Witwatersrand Basin where both the Transvaal Supergroup and Pilanesberg dikes are absent and the sequence is overlain by sedimentary strata. As such, the mine's fracture fluids flow through quartzite or between the contact of the quartzites and the sedimentary units. Simkus et al. (2016) used carbon isotopic analysis to reveal that fracture fluid biomass incorporated carbon from both biogenic methane and DIC derived from methane oxidation. A recent study by Magnabosco et al. (2018) focused on the methane oxidizing community in these 1.3 km deep fracture fluids, over both long and short time scales. Over a 2.5 year period, the Eh, sulfate, nitrate, and hydrogen concentrations shifted considerably, as did the abundances of specific Archaea and Bacteria. In particular, the methane oxidizing community shifted from a ANME-1- to a *Ca. M. nitroreducens*- dominated community over several years (based on abundances of *mcrA*, *mmo*, and 16S rRNA genes). These shifts correlated to an increase of nitrate over the same time period, and experiments using $^{13}CH_4$ coupled to NO_3^- as an electron acceptor resulted in an increase of $^{13}CO_2$, suggesting fluctuations of the two populations with shifting electron acceptors (Magnabosco et al., 2018). Metagenomic analysis showed that methanogens and methanotrophs represented < 5% of the total population, signaling that organisms at this depth are utilizing carbon processed by a very small fraction of the community (Simkus et al., 2016).

Extensive literature exists for the deeper mines in the Witwatersrand Basin, which includes the Driefontein, Mponeng, Kloof, and TauTona mines. At intermediate depths, (2.6–2.8 km), solid surfaces, such as crushed rock substrate and fracture surfaces were demonstrated to host biofilms on both basalt and quartzite exposed to fracture fluids (Baker et al., 2003; Wanger et al., 2006). Established *Desulfotomaculum spp*. could be induced to reduce sulfate on most probable number (MPN) plates enriched with lactate or hydrogen (Baker et al., 2003). Lin et al. (2006a) described a community from a 2.8 km depth fracture fluid in the Ventersdorp basalt (Mponeng mine) that was 88% composed of *Desulfotomaculum spp*. (based on molecular cloning methods), and isotopes of sulfur indicated potential microbial sulfate reduction. Chivian et al. (2008) further supported these works by assembling the genome of *Ca. Desulforudis audaxviator*, also from a fracture fluid at 2.8 km in the Mponeng mine, where communities are overwhelmingly dominated by this taxon. This sporulating, sulfate-reducing, chemoautotrophic thermophile likely fixes its own carbon and possibly nitrogen (Chivian et al., 2008), and is a dominant member of many fluids sampled below 1.5 km in the Witwatersrand Basin (e.g., Moser et al., 2003, 2005; Gihring et al., 2006; Lin et al., 2006a). These approaches show that sulfate reduction is likely an important catabolic path in the ∼2.7 km fluids passing through basalt and quartzite hot rock.

Magnabosco et al. (2016) and Simkus et al. (2016) investigated possible avenues for carbon cycling at > 3 km depths. Using metagenomic, isotopic, and "energy flux" analysis, they determined a variety of potential sources of anabolism, and evaluated the likelihood of several catabolic pathways that could support cellular growth. In the deeper, 3 km TauTona mine borehole "TT107," protein encoding genes (PEGs) for six different carbon fixation pathways were found in the fracture fluids, and the reductive acetyl-CoA pathway was the best represented among the 289 total identified taxa, dominated by Firmicutes (57.4%) and Euryarchaeota (22.3%) (Magnabosco et al., 2016). A second borehole at 3.14 km

depth in the same mine was dominated by putative enzymes associated with the 3-hydroxypropionate/4-hydroxybutyrate cycle (Simkus et al., 2016). Further, the oxidation of alkanes is suspected to proceed by reversing the reductive acetyl-CoA pathway, and the abundance of related PEGs related may instead be used to oxidize alkanes (Magnabosco et al., 2016). The presence of methyl-coenzyme M reductase may signal methanogenesis among the Euryarchaea identified, but anaerobic oxidation of hydrocarbons (e.g., sulfate reduction coupled to propane or butane oxidation) yields more energy in these fluids than methanogenesis. It was also determined that the methane carries a depleted carbon isotopic signature consistent with a primarily abiotic origin at this site (Simkus et al., 2016). Carbon monoxide dehydrogenase was abundant in the community, along with the carboxydovore genus *Desulfotomaculum*, and CO oxidation coupled to H_2O reduction was the second most energy yielding reaction considered (as energy flux, in units of kJ $cell^{-1}$ s^{-1}). These efforts expanded considerably what is known about carbon cycling in the deep terrestrial subsurface of the Witwatersrand Basin.

Finally, genes coding for enzymes involved in nitrogen cycling have been investigated in four Witwatersrand Basin mines. In all, seven nitrogen cycling genes (*Nar*V, NPD, *Nif* HDKEN) were found to be common to all samples analyzed (Lau et al., 2014). A further examination of the Beatrix fracture fluid utilized a combination of "omics" approaches to demonstrate that oxidation of sulfur species coupled to nitrate reduction by spp. of *Thiobacilus* and *Sulfuricella* accounted for 27.8% of the active microbial community (Lau et al., 2016). In addition, the key enzymes for dissimilatory nitrate reduction to ammonia, ANAMMOX, and nitrogen fixation were found in low quantities (Lau et al., 2016). However, isotopic evidence supports the conclusion that canonical denitrification is the primary nitrogen cycling process in this environment, with nitrate originating from either radiolytic oxidation or paleometeoric recharge (Silver et al., 2012). In order for *Thiobacilus* and *Sulfuricella* to drive this part of the nitrogen cycle, they require sufficient sulfur species to serve as electron donors. Lau et al. (2016) propose that these are produced by ANME-2 and sulfate reducing bacteria, which represent a smaller proportion of both the community and activity in this environment. In all, they describe an ecosystem that supports an "inverted" biomass pyramid, where the codependent methanogens and ANME members are active at low levels, and the sulfate reducing bacteria and methanogens are supported by the syntrophy with ANME and sulfur oxidizing bacteria. Carbon is moved through this system by autotrophy, primarily the reductive pentose phosphate cycle and reductive acetyl-CoA cycles, using DIC recycled through the methane cycling community. Contrary to previous assumptions supported by approaches that targeted hydrogen-driven metabolisms, this work showed that the bulk of the anabolic and catabolic activity in this 1.34 km fracture fluid did not use hydrogen as an electron donor, but rather hydrogen dependent metabolisms exist in syntrophy with coupled sulfur/nitrogen cycling (Lau et al., 2016), and called attention to the importance of the overlooked subsurface nitrogen cycle.

Boreholes

Boreholes offer an indirect path to the subsurface and provide a means for emplacing instrumentation and long term experimentation *in situ*. Borehole depths are often comparable to deep mine investigations, frequently reaching 500–2,500 m. Dai et al. (2021) were able to retrieve continuous cores up to 5.1 km. As with other drilling operations interested in obtaining clean and uncontaminated samples for microbiological research, methodologies have been developed for terrestrial deep borehole drilling (e.g., Templeton et al., 2021). Here we consider some of the deepest examples of microbial surveys in boreholes in the continental crust, focusing on altered and metamorphosed bedrocks with lower permeability than sedimentary units, and thus less opportunity for migration of surface microorganisms (Mailloux et al., 2003; Lau et al., 2014). The examples below highlight boreholes into altered bedrocks, such as serpentinized ophiolites, schists, and gneisses, which offer fluid and gas chemistries that differ from the fracture fluids in the deep mine and laboratory examples above.

Boreholes in Serpentinized Bedrock

When ophiolites, interact with groundwater, the hydration of olivine and pyroxene within the rocks leads to the formation of a variety of serpentine phases such lizardite, chrysotile, among others (Moody, 1976, *and references therein;* Dilek and Furnes, 2011). These reactions lead to a production of H_2, CH_4, alkaline fluids, and a liberation of Ca^{2+} ions (e.g., Neal and Stanger, 1983; McCollom and Bach, 2009), providing the potential for the establishment of terrestrial chemoautotrophic microbiological communities that are largely divorced from inputs at the surface. Indeed, there are active microbial ecosystems in the deep subsurface fueled by serpentinization (reviewed previously in Schrenk et al., 2013). The origin of microorganisms within these subsurface communities is thought to be related to transportation to the subsurface during ophiolite obduction or introduction from groundwater along slow regional flow pathways (Sabuda et al., 2020; Putman et al., 2021). Microbial communities dependent on serpentinization are of particular interest to theories of the origin of life and potential life elsewhere in the solar system such as Mars or icy moons (e.g., Schulte et al., 2006; Martin et al., 2008; Cardace and Hoehler, 2009; Sojo et al., 2016; Preiner et al., 2018; Cartwright and Russell, 2019; Russell and Ponce, 2020; Taubner et al., 2020).

Well studied ophiolites include the Coast Range Ophiolite, United States, the Tablelands ophiolite, Canada, the Santa Elena ophiolite, Costa Rica, the Voltri Massif ophiolite, Italy, and the Samail ophiolite, Oman, among others. Until recently, much of the research on serpentinizing systems came from studies of alkaline rich springs, where serpentinization influenced groundwater intersects with the surface (Morrill et al., 2013; Crespo-Medina et al., 2014; Sánchez-Murillo et al., 2014; Cardace et al., 2015; Meyer-Dombard et al., 2015; Quéméneur et al., 2015; Woycheese et al., 2015; Brazelton et al., 2017; CanovasIII, Hoehler and Shock, 2017; Rowe et al., 2017; Suzuki et al., 2017, 2018). Here, we focus on the direct sampling of fluids from borehole wells (see section " Surface Influences on the Terrestrial Subsurface"). In the last decade, drilling projects such

as the Coast Range Ophiolite Microbial Observatory (CROMO) and the multi-borehole observatory (MBO) established by the Oman Drilling Project, have enabled more direct access to the groundwater fluids in contact with the subsurface (Cardace et al., 2013; Kelemen et al., 2013, Kelemen et al., 2020). Prior to the establishment of these observatories, direct access to groundwater of serpentinizing systems was rare (Tiago et al., 2004; Daae et al., 2013; Tiago and Veriìssimo, 2013).

Recent work utilizes next generation DNA sequencing for taxonomic and functional classification of borehole fluids in combination with other techniques such as microcosm or enrichment based experiments (Crespo-Medina et al., 2014; Meyer-Dombard et al., 2018; Fones et al., 2021; Glombitza et al., 2021), stable isotope analyses (Nothaft et al., 2021a,b), radioisotope labeling (Fones et al., 2021; Glombitza et al., 2021; Templeton et al., 2021), and ecological/hydrological modeling (Putman et al., 2021). Transcriptomic and single cell genomics studies have also shown mechanisms of adaptation of microbial life to serpentinizing environments (Fones et al., 2019, 2021; Merino et al., 2020; Kraus et al., 2021). The borehole observatories have enhanced the spatial and temporal resolution of microbial dynamics within serpentinizing systems and highlight the differences between borehole fluids influenced by the surface and deeper, highly reducing groundwater fluids.

Both host rock composition and hydrologic context influence microbial community composition in subsurface serpentinizing systems, and recent work at the MBO in Oman highlights this concept (Miller et al., 2016; Rempfert et al., 2017; Fones et al., 2019; Kraus et al., 2021; Nothaft et al., 2021a). The Samail Ophiolite is composed of mafic gabbros and ultramafic peridotites, mainly harzburgite, both presumed to be undergoing active serpentinization, which fuel distinct microbial communities (Neal and Stanger, 1983; Miller et al., 2016; Rempfert et al., 2017; Fones et al., 2019; Nothaft et al., 2021a). Rempfert et al. (2017) distinguished between four different fluid types at the Samail ophiolite MBO wells, influenced by host rock lithology and hydrologic flow regime (long v. short residence time): hyperalkaline peridotite (pH > 10), alkaline peridotite (pH 8–10), gabbro, and peridotite/gabbro contact wells. Taxonomic analysis showed microbial communities clustered in accordance with these four fluid types at the Samail Ophiolite (Rempfert et al., 2017). Geochemical data showed alkaline peridotite and gabbro hosted wells were likely to be more surface influenced, and harbored more nitrogen cycling microorganisms (Rempfert et al., 2017). Hyperalkaline peridotite wells, characterized by high dissolved H_2, methane, and calcium, had more sulfate reducing Bacteria and methane cycling Archaea relative to other fluid types (Rempfert et al., 2017). Sixteen metagenome assemblies from the Samail MBO also showed metabolic potential correlated with fluid types associated with host rock lithologies (Fones et al., 2019). Metagenomes from hyperalkaline peridotite wells were more enriched in anaerobic respiration genes, including anaerobic sulfite reductase unit A, *AsrA*, while genes associated with aerobes were more enriched in the alkaline peridotite wells (< 10 pH) (Fones et al., 2019). The influence of hydrologic regime on geochemical composition, and thus microbial communities, was shown at the Samail Ophiolite through the use of packers to isolate discrete borehole sections in the mantle section of the ophiolite (Nothaft et al., 2021a). Nothaft et al. (2021a) sampled two boreholes at multiple discrete depths, up to 132 m, and subjected fluids to geochemical, isotopic, and 16s RNA sequencing. Fluids isolated from shallower, more oxidized parts of the groundwater contained more heterotrophic organisms capable of aerobic respiration, denitrification, and fermentation, while highly reacted Ca^{2+} – OH^- groundwaters were dominated by sulfate reducing chemolithoheterotrophs (Nothaft et al., 2021a).

Microbial communities in fluids most influenced by serpentinization are dominated by Bacteria, with variable archaeal abundances (< 1% to ∼30%), and generally consist of low richness and planktonic cell abundances ($\leq 10^6$ cells mL^{-1}) (e.g., Rempfert et al., 2017; Twing et al., 2017; Fones et al., 2019, 2021; Kraus et al., 2021; Putman et al., 2021; Sabuda et al., 2021). Studies associated with rock solids in these environments are uncommon, but microscopy and 16S rRNA sequencing from cores obtained during drilling at CROMO and at MBO indicated variable cell abundances (10^3–10^7 cells per gram) and low taxonomic richness (Cardace et al., 2013; Kelemen et al., 2020; Templeton et al., 2021). Selective pressures that affect community structure in these environments include low dissolved inorganic carbon (DIC) concentrations, high pH, low dissolved oxygen (DO), and energy limitations (Rempfert et al., 2017; Twing et al., 2017; Fones et al., 2019, 2021; Nothaft et al., 2021a; Putman et al., 2021). While microbial populations in highly reducing, hyperalkaline groundwater are generally limited by the lack of more energy rich electron acceptors (oxidants such as O_2, NO_3^-, and Mn; e.g., Twing et al., 2017), this may not be the most important limitation on microbial metabolisms (Crespo-Medina et al., 2014; Rempfert et al., 2017; Glombitza et al., 2021). Enrichment experiments show low DIC may be most limiting, driving the selection for unique adaptations such as higher rates of substrate assimilation to dissimilation, and methanogen diversification (Crespo-Medina et al., 2014; Fones et al., 2019, 2021; Kraus et al., 2021). Finally, ecological modeling has shown dispersal limitation due to low permeability and slow fluid flow imposes strong selective pressure on microbial communities within ophiolite hosted aquifers at CROMO (Putman et al., 2021), leading to microbial community differentiation.

As highlighted above, the functional potential of serpentinizing communities depends on the availability of substrates such as H_2 and CH_4, which can be highly variable depending on the depth, host rock lithology, and the extent of surface influence (Daae et al., 2013; Rempfert et al., 2017; Nothaft et al., 2021a; Sabuda et al., 2021). Some ophiolite hosted aquifers may retain ancient seawater from their marine origins, which contributes to increased salinity and dissolved sulfate in some sites, potentially providing a resource that could be utilized by microbial communities (Schwarzenbach et al., 2012; Sabuda et al., 2020; Nothaft et al., 2021a; Putman et al., 2021). Active microbially mediated sulfur cycle processes are abundant in aquifers with higher sulfate concentrations (Schrenk et al., 2013; Sabuda et al., 2020; Glombitza et al., 2021). Metagenomic sequencing has detected genes coding for the complete dissimilatory sulfate reduction pathway such as

sulfate adenylytransferase (*sat*), adenosine-5′-phosphosulfate reductase (*aprAB*) and dissimilatory sulfite reductase (*dsrAB*) (Sabuda et al., 2020; Glombitza et al., 2021). Low levels of sulfate reduction comparable with those found in deep subseafloor sediments, $< 10^{-3}$ to 2.1 pmol $mL^{-1}day^{-1}$, were detectable up to pH 12.3 in laboratory incubations of serpentine fluids isolated from both CROMO and MBO wells (Glombitza et al., 2021). Incubations of 10 cm core samples at pH 9.5 from MBO yielded sulfate reduction rates of 2–1,000 fmol $cm^{-3}day^{-1}$ (Templeton et al., 2021). At the CRO, sulfate reduction coupled to methane oxidation was found to be most thermodynamically favorable in the deeper wells, as well as sulfide and thiosulfate oxidation (Sabuda et al., 2020). Sulfate reducing bacteria (SRB) *Thermodesulfovibrionaceae* and *Desulforudaceae* are commonly found at both Coast Range and Samail ophiolite fluids (Sabuda et al., 2020; Glombitza et al., 2021; Nothaft et al., 2021a; Templeton et al., 2021). Glombitza et al. (2021) found that SRB constituted 39.59% of taxa in the Samail and Coast Range Ophiolites by screening taxonomic ranks for possession of *dsrAB* genes. It has been suggested that ophiolites serve as a vector for transporting sulfur compounds and microorganisms capable of sulfur metabolism from the seafloor to the continents, highlighting sulfur biogeochemistry taking place within ophiolites as a link between terrestrial and marine systems (Sabuda et al., 2020).

Metagenomic and 16S rRNA gene sequencing evidence for hydrogen metabolisms, nitrogen cycling metabolisms, carbon monoxide oxidation, carbon fixation, acetogenesis, sulfate reduction, sulfide oxidation, and to a lesser extent, methane oxidation have been found in serpentinizing boreholes *in situ* (e.g., Twing et al., 2017; Fones et al., 2019; Merino et al., 2020; Kraus et al., 2021; Sabuda et al., 2021). Ferrous iron has been measured in borehole samples, indicating the potential for iron redox metabolisms (Miller et al., 2016; Rempfert et al., 2017). Several methods have shown that microbially mediated iron reduction and oxidation occur in enrichment microcosms and batch culture experiments using fluids from subsurface borehole and hyperalkaline springs (Meyer-Dombard et al., 2018). While iron reduction is thought to be unfavorable in hyperalkaline conditions, local drops in pH (< 9 pH) driven by fractures, low flow voids, or biofilm protection can potentially create favorable conditions. Borehole measurements show that pH in the Samail and Coast Range ophiolites can range between ∼ 7.4 to > 12 pH (Rempfert et al., 2017; Putman et al., 2021), potentially providing the context necessary for iron oxidation at the lower end of this range.

Methanogenesis is often cited as an energetically favorable potential metabolism in serpentinizing fluids, however, the observation of isotopically heavy methane in the "abiotic" synthesis range has garnered some debate on the origin of methane in these systems (Etiope et al., 2016; Miller et al., 2016, CanovasIII, Hoehler and Shock, 2017; Etiope, 2017). It is likely that a combination of abiotic and biogenic methane is present in serpentinizing systems, as genetic evidence for methanogens within borehole fluids has been reported (Miller et al., 2016; Fones et al., 2021; Kraus et al., 2021; Nothaft et al., 2021b). Methanogenesis under DIC limitation has been shown to result in relatively high $\delta^{13}C$-CH_4 values, potentially providing a mechanistic explanation for the observed isotopically heavy methane (Miller et al., 2018). Methanotrophy may provide another mechanism for $\delta^{13}C$ enrichment (Nothaft et al., 2021b). It has been suggested that biological methanogenesis becomes energetically competitive with sulfate reduction at a threshold level of accumulation of reduced compounds such as H_2 or formate in the range of $10–10^2$ μmol per L in the Samail ophiolite, which is a higher threshold than other environments potentially due to increased energy expenditure to cope with high pH (Nothaft et al., 2021a). Several studies have identified methanogens affiliated with *Methanobacterium,* an autotrophic and hydrogenotrophic genus (Rempfert et al., 2017; Kraus et al., 2021; Nothaft et al., 2021a). Genomic and transcriptomic evidence suggest that *Methanobacterium* can be active in hyperalkaline groundwater up to pH 11.3 (Kraus et al., 2021). Taxonomic evidence for aerobic and anaerobic methane oxidation is available to lesser extent than methanogenesis, however, both are predicted to be energetically favorable in these environments (Miller et al., 2016; CanovasIII, Hoehler and Shock, 2017; Twing et al., 2017; Nothaft et al., 2021b; Sabuda et al., 2021). Methane produced either biogenically or abiotically may not be consumed to a significant degree by methanotrophs, and methane emissions from sites of serpentinization should be considered in global atmospheric methane budgets (Sabuda et al., 2021).

Boreholes in the Fennoscandian Shield

Boreholes fluids at the Outokumpu site (Finland) in the Fennoscandian Shield have been used extensively as an *in situ* experimental canvas. Here, the lithology of the first 1.3 km is organic rich mica schists below which continues an ophiolite, ultramafic sequence (Nyyssönen et al., 2014), providing a comparison with the serpentinized fluids discussed above. Emphasis has been placed on down hole experimentation, as well as use of inflatable packer systems to retrieve authentic deep subsurface fluid samples. Early work identified sulfate reduction in fracture fluids (*via* identification and enumeration of the *dsrB* gene) at varying depths (Itävaara et al., 2011; Purkamo et al., 2013). However, the organic rich schists of the Outokumpu site provides opportunity for fermentation and anaerobic respiration, and initial predictions of functional diversity indicated that carbon fixation processes were underrepresented in the microbial communities (Purkamo et al., 2015a,b), although the genetic capacity for the reductive acetyl-CoA pathway is found in fluids from 600–2,300 m (Nyyssönen et al., 2014). Enrichments with acetate, sulfate, H_2, and CO_2 in laboratory microcosms clarified that acetate induced growth of bacterial heterotrophs, thiosulfate reduction was more important that sulfate reduction, and methanogens were not present (Purkamo et al., 2017). However, a recent metagenomic survey of fluids at 600, 1,500, and 2,300 m detected the genetic capacity for methanogenesis from multiple pathways; acetoclastic and methylotrophic methanogenesis pathways were found at all depths, while hydrogenotrophic pathways were only found in the deepest sample (Nyyssönen et al., 2014). Further work demonstrated

that acetate was incorporated into biomass by archaeal members of the community, supporting previous indications that acetate is likely key for metabolism in the deep biosphere at 2.2 km at Outokumpu (Nuppunen-Puputti et al., 2018).

A variety of other locations provide fracture fluids within metamorphic units in the Fennoscandian Shield. Shallow boreholes provide access to Precambrian gneisses (e.g., at Olkiluoto, Romuvarra), where emphasis on cultivation and identification of sulfate reducing bacteria, nitrate reducing bacteria, acetogens, and methanogens has been the focus of much previous research (Nyyssönen et al., 2012; Pedersen, 2013; Bomberg et al., 2015, 2016; Kutvonen et al., 2015; Miettinen et al., 2018). For example, in shallow fluids (up to 600 m), sulfate reduction and methanotrophy were induced when hydrogen and methane were introduced in flow cells using fluid from a borehole in the ONKALO tunnel (Olkiluoto, Finland; Pedersen, 2013), and active nitrate and ammonium based catabolism were also indicated (Kutvonen et al., 2015; Miettinen et al., 2018). In contrast to many other Fennoscandian Shield sites, at Romuvaara, groundwaters are not saline, and Purkamo et al. (2018) postulated that this was the reason for a different suite of microbial community compositions, despite similar host rock as Olkiluoto. Interestingly, Romuvaara groundwaters from ∼600 m depth demonstrated a similar suite of predicted functional diversity as that found in Olkiluoto. One study investigated metabolic functions at much greater depth; a deep borehole (4.5 km) into gneiss bedrock was obtained at the Otaniemi site in Finland. Here, the functional diversity of retrieved rock (as opposed to groundwater) was determined *via* qPCR of *drsB*, *narG*, and *mcrA* genes (Purkamo et al., 2020). This work was only able to retrieve copies of the *narG* gene from this deeper borehole site, potentially suggesting that nitrate reduction outcompetes sulfate reduction and methanogenesis at depths greater than 600 m in gneissic bedrock. Other potential metabolic processes were predicted from 16S rRNA data, and indicated that a variety of chemoheterotrophic and methylotrophic metabolic options could also be present at these depths.

It is tempting to compare the functional diversity of the schist-hosted vs. gneiss-hosted deep biosphere in the Fennoscandian Shield, at depths > 1 km. It could be said that the schist hosted deep biosphere appears to support a more acetate driven ecosystem, with indications that thiosulfate reduction is also important, and that nitrogen cycling may be more important in the gneiss hosted deep biosphere. However, caution should be taken in these broad conclusions as different specific metabolic functions were the target of the searches in each location. For example, while experimental approaches have shown that $^{15}NH_4^+$ and $^{15}NO_3^-$ is taken up into biomass at Olkiluoto (100 m; Kutvonen et al., 2015), similar experiments have not yet been applied to verify the activity of the nitrogen cycling genes at greater depths at this site (Purkamo et al., 2020). Metagenomic data suggests that nitrogen cycling may be important in the schist/serpentine hosted Outokumpu groundwaters, but data showing activity of these genes are not yet available. Future analyses that broadly compare functional capacity and show activity of the genes involved or uptake into biomass will enhance our understanding of metabolic regimes across host rock types and geochemical profiles.

SYNTHESIS *VIA* CATABOLIC MODELING

Many have predicted the energetic landscape that might be presented in the terrestrial subsurface (e.g., Stevens and McKinley, 1995; Amend and Teske, 2005; Osburn et al., 2014; Magnabosco et al., 2016; CanovasIII, Hoehler and Shock, 2017). Because the interplay between climate, topography, host rock, and groundwater defines the terrestrial subsurface environment, it has been suggested that, other environmental parameters being equal, the energetic landscape of the subsurface biosphere is dependent on the mineralogy of the host rock. Specifically, the host rock determines the mineralogy of the substrates that then serve as the backbone of the energetic "buffet" for chemosynthetic organisms (e.g., Swanner and Templeton, 2011; Casar et al., 2021a,b). Further, groundwaters connect diverse rock types, adding the history of the water rock interaction along the flow path with the local host rock, producing a distinctive fracture fluid chemistry (e.g., Sahl et al., 2008; Osburn et al., 2019).

This geochemical reality provides a stunning array of possibilities to supply the subsurface with energy and carbon. On the whole, the community has generally and historically made the assumptions that, (1) when methane or hydrogen gas are measurable in subsurface fluids, the biosphere is likely dominated by sulfate reduction and methanogenesis, and (2) presence of heterotrophic metabolisms indicates influence from the surface biosphere. These assumptions made a great deal of sense several decades ago, but have been consistently shown to be less relevant in many locations as more data are acquired, reduced sulfur species, ammonium, ferrous iron and other metals are shown to be important sources of electrons, and abiotic reactions resulting in synthesis of organic carbon are known to provide fuel for biomass synthesis (Amend and Teske, 2005; McCollom et al., 2010; Shock and Canovas, 2010; Osburn et al., 2014; Bomberg et al., 2019). Very recent considerations of the structure of the energetic landscape in deep continental biosphere settings have begun to paint a picture that methanogenesis may be limited at greater depths, or more prevalent where fresh groundwater mixes with deeper fluids (e.g., Osburn et al., 2014; Leong and Shock, 2020). Holistic and comprehensive analysis of functional diversity, capacity, and profiling of energy availability using updated databases and culture independent methods are suggesting that, where methanogens or the genetic capacity for methanogenesis are found in low levels in fracture fluids (and are not necessarily universally found, e.g., Lau et al., 2014), methanogenesis may not be the dominant metabolic process but rather may be providing a support for other organisms (Lau et al., 2016; Purkamo et al., 2016; Simkus et al., 2016). Additional ecological functions such as nitrogen cycling, methane oxidation, and iron cycling have emerged as metabolisms of interest in discussions of terrestrial deep subsurface sites (Swanner and Templeton, 2011; Lau et al., 2014, 2016; Magnabosco et al., 2016; Momper et al., 2017b; Purkamo et al., 2020; Casar et al., 2021b).

To better ascertain whether there is a universality to energy availability in terrestrial subsurface sites, we attempted to canvas the known literature for published values to compare sites. The representation of "energy" is not standardized, and available data are presented in a dazzling variety of metrics and normalizations. Data are often presented only in figures, preventing the conversion of published data to a consistent metric across sites. Further complicating the process is variable reporting of geochemical data. For example, aqueous chemistry is frequently presented without corresponding gas data, measurements of redox sensitive compounds (such as NH_4^+, HS^-), or fluid conductivity, which are essential for calculation of ΔG_r. We have used geochemical data where available to estimate energy availability and density for deep subsurface fracture waters across five different deep mine laboratory locations – Äspö, Beatrix, Pyhäsalmi, SURF/MeMMO, and TauTona. We chose fifteen reactions of interest to further our discussion of the energetic landscape for these systems, shown in **Table 1**. The results of our estimates are found in **Figure 2** and in **Supplementary Table 1**, where we present the data as both "energy density" and in the semi standard metric of ΔG_r, normalized per mole of electrons involved in each reaction. Convincing arguments have been made for these metrics and normalizations, which present the data as volumetric and molar distributions of energy, respectively (McCollom, 2000; Amend and Shock, 2001; LaRowe and Amend, 2014, 2019).

We include reactions that are commonly exergonic in terrestrial deep biosphere systems (e.g., reactions 1, 6, 11), and that include nitrate and oxidized iron minerals as an electron acceptor (processes currently of interest). We also chose reactions that specifically do not involve hydrogen as an electron donor to compare to reactions that do (e.g., reactions 3 vs. 4, 6 vs. 9). We represent sulfate reduction with both hydrogen and methane, but also acetate, and chose to reduce HCO_3^- to methane because that is the dominant species at the pH ranges of the systems in question. Further, in **Figure 2** we highlight the electron acceptors involved in each reaction, as fluids at all examined sites are reducing and these are the chemical species receiving the transferred electrons.

In general, on a molar basis, the most exergonic reactions across all sites are those using electron acceptors in the order $O_2 > NO_3^- > S^0 > SO_4^{-2} > HCO_3^- >$ Fe-minerals (**Figure 2**, right side). Under this lens, there is little variability in the energy available per reaction across the five locations, with most reactions varying < 10 kJ(mol e^-)$^{-1}$. Of interest are the reactions that play across the zero line, showing that the reaction is only (barely) exergonic at some sites. These are methanogenesis, acetogenesis, sulfate reduction with methane, and reduction of iron bearing minerals with H_2 (reactions 11, 12, 8, 14, and 15, respectively). These same reactions also provide the least energy on a volumetric basis, with Aspö fluids providing the most energy of the five sites (**Figure 2**, right side). The "top 5" exergonic reactions differ considerably when assessed as volumetric vs. molar normalizations. Normalized per a volumetric basis, the most exergonic reactions across all sites are 7, 1, 10, 9, and 2, which include sulfate reduction with methane or acetate (7, 9), sulfur reduction with H_2 (10), and ferrous iron oxidation (2). Normalized per a molar basis, only one of these reactions remains in the "top 5" - reaction 1 - joined by nitrate reduction with H_2, HS^-, and CH_4, and ferrihydrite reduction coupled with acetate (reactions 3–5, and 13, respectively). Note that there is considerable variability in the energy density for the "top 5" reactions among sites, with the DeMMO fracture fluids presenting far less energy density for the top 3 reactions than all the other sites (reaction 2 is actually the most energy dense for DeMMO fluids).

We can choose thresholds by which to compare the sites' energy density. On a site by site comparison, there are seven reactions for which the Aspö fluids yield > -2 (log J/kg H_2O) and only 4–5 reactions in this range for all the other sites. If we look at the lower energy density threshold of < -4 (log J/kg H_2O), there are ten reactions for which the DeMMO fluid yields this or less energy on a volumetric basis, and none of the Aspö reactions fall in this range. Ranking the sites in this way, the Aspö site had the greatest number of high energy density reactions, the DeMMO fluids had the least, and Beatrix, TauTona, and Pyhäsalmi were midrange, in descending order. Fracture fluids at Aspö are flowing through basaltic units, while Beatrix and TauTona are hosted in quartzites. Both Pyhäsalmi and DeMMO fluids experience more complex geologic settings and reaction pathways. One might conclude that there is a pattern here, from the most energy dense site to the least, with sites hosted in similar geologic settings arranged in a gradient, but more data would be needed to verify this. Pan-metagenomic analysis of global subsurface sites suggests that community variations are correlated to lithology, so the possibility exists that this trend would hold up to deeper scrutiny (Magnabosco et al., 2018).

Looking at specific reactions of interest, we can compare the reduction of nitrate and sulfate with and without hydrogen, toward considering whether the subsurface might be dependent on hydrogen as an electron donor. Reactions 3 and 4 (nitrate reduction with hydrogen and with sulfide, respectively) yield roughly the same energy density for nearly all sites, although DeMMO fluids are significantly more energy dense when sulfide is the electron donor. Reactions 6–9 all reduce sulfate; of these, reducing sulfate with hydrogen is one of the least energy dense options. Reduction of sulfate to sulfide with methane is the most energy dense of all the reactions, but reducing sulfate to elemental sulfur with methane yields considerably less energy density. Sulfate reduction with methane, acetate, and hydrogen are all more energy dense than methanogenesis, for each site. Stacking the four yellow bars in the left plot of **Figure 2** covers the entire range of energy density shown on the plot, when all samples are included. This indicates that sulfate reduction is highly site and reaction specific, which should be taken into consideration when discussing this as a metabolic option in the subsurface. Nitrate reduction is a metabolism that has been highlighted above in several deep subsurface mine publications, and notably, reactions 3–5 are among the most exergonic when considered on a molar basis and are also in the middle range of the scale when considered on a volumetric basis. Further, across all sites there is less range in the energy density available for nitrate reduction, indicating that it is less site and reaction specific. We believe that reactions utilizing nitrate as an electron acceptor warrant

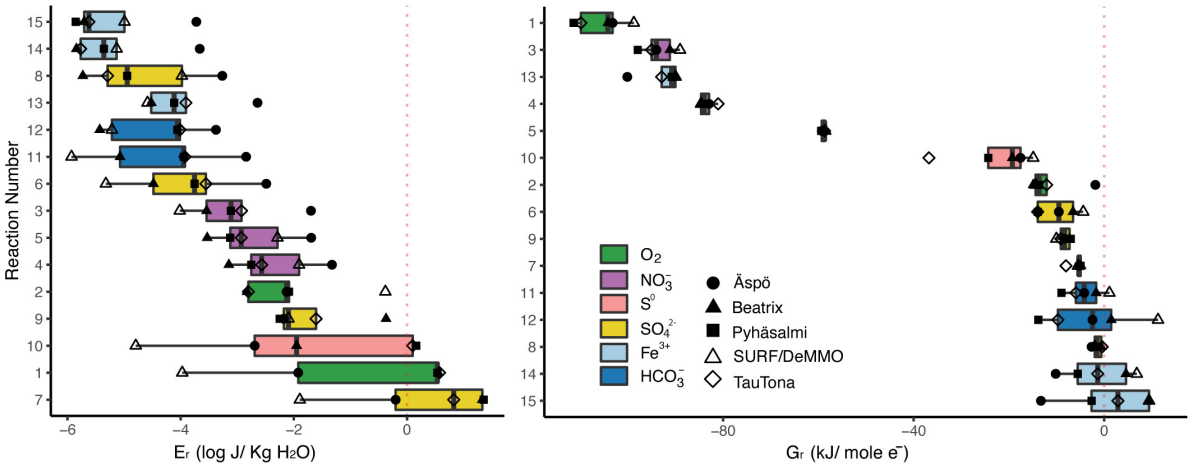

FIGURE 2 | Estimated energetic landscape of the fifteen reactions presented in **Table 1** for five selected deep fracture fluids, as accessed in subsurface laboratories. Calculated energy densities are presented at left, and ΔG_r estimates are at right (normalized as kJ/mol and the number of electrons involved in the reaction). Electron acceptors for each reaction are highlighted. Fracture fluid geochemistry data are from: Aspö - Hallbeck and Pedersen (2008), sample "KJ0052F01/2006-03-23/43.70-43.90 m;" Beatrix mine – Lin et al. (2006b), sample "BE325;" Pyhäsalmi – Miettinen et al. (2015), sample "R-2247;" SURF – Osburn et al. (2014), sample "'Manifold B;" TauTona – Magnabosco et al. (2016), sample "TT107." Methods for estimated values may be found in **Supplementary Material**.

closer inspection and consideration in metabolic profiling for subsurface fracture fluids, especially given recent discoveries concerning the genetic capacity for these processes (Swanner and Templeton, 2011; Lau et al., 2014, 2016; Magnabosco et al., 2016; Momper et al., 2017b; Purkamo et al., 2020). Whether methane oxidation (reaction 5, 7, and 8) is an energy dense option depended on what is being used as the electron acceptor, and those data overlap to cover the entire x-axis range in **Figure 2**. Again, this indicates that methane oxidation as an energy dense option depends highly on site chemistry and reaction specifics. Magnabosco et al. (2018) isotopically traced methane oxidation with nitrate in fracture fluids in the Beatrix mine, and our estimates indicate that, at least with reaction 5, there is a high energy density present for this process. Finally, we considered whether iron cycling is a favorable process in these fluids. This is site dependent. For the most part, reduction of iron bearing minerals is not a highly exergonic option, considering both volumetric and molar values of energy. However, reaction 13 yielded as much energy in the Aspö fluids as ferrous iron oxidation (reaction 2) on a volumetric basis and the reaction is highly exergonic on a molar basis. Ferrous iron oxidation with oxygen is one of the "top 5" reactions for all sites on a volumetric basis. Iron cycling may be a possible source of energy in subsurface fracture fluids, but generalizations can't be drawn across sites.

We recognize that the presence of energy availability does not confer the guarantee of the importance of a given process to an ecosystem, any more than identification of taxonomic or functional diversity might. While the choice of how metrics of energy availability and flux are normalized depends largely on the questions being asked in a given study, it is certain that more cross-site comparisons could be made if, at the very least, the ΔG_r value is reported along with the normalized data as a discipline standard. Further, some basic standards could be suggested for data collection that would enable others to assess the energy availability of a system, even if the study's authors are disinterested in that topic. For example, analysis of temperature, pH and conductivity, as well as redox pairs (nitrate and ammonia/ammonium, sulfate and sulfide, for example) and gas chemistry that includes dissolved oxygen, hydrogen, nitrogen, and methane, could serve as a general "basic set" of useful analyses (with acknowledgment that analytical capacity varies widely in the field). The most convincing investigations of ecosystem function combine modeling of energy options, functional diversity surveys, and experimental approaches. We look forward to the community putting the "nail in the coffin" by adding proteomic analysis to such suites of data, which will greatly enhance our ability to draw connections between geology, geochemistry, and community diversity to describe ecosystem functions and services in the deep terrestrial subsurface biosphere.

CONCLUSION

The mass of the terrestrial subsurface biosphere has been frequently estimated, with current values conservatively approaching 23–31 Pg of carbon C (PgC) (Magnabosco et al., 2018). There are many environmental factors that are very similar in most terrestrial subsurface sites, and several studies have considered taxonomic and functional diversity from a global perspective. Several taxa have been noted in many subsurface sites globally, regardless of geochemical provenance (Colman et al., 2017). Among these are members of the Firmicutes and Proteobacteria. Firmicutes are shown to dominate taxonomic diversity surveys in deeper subsurface sites in South Africa (Magnabosco et al., 2016), various serpentinite sites including surface springs (Brazelton et al., 2013; Suzuki et al., 2013;

Twing et al., 2017), and fracture fluids in boreholes and deep laboratories of the Fennoscandian Shield (Itävaara et al., 2011; Purkamo et al., 2016), while Proteobacteria dominate in shallower sites that mix with younger and less saline groundwaters (Itävaara et al., 2011; Magnabosco et al., 2016). The well-noted *Candidatus Desulforudis audaxviator*, a Firmicutes, has been found in subsurface fluids globally since first discovered in a South African gold mine (Baker et al., 2003; Cowen et al., 2003; Lin et al., 2006a,b; Aüllo et al., 2013; Tiago and Veriìssimo, 2013; Labonteì et al., 2015; Magnabosco et al., 2016; Jungbluth et al., 2017; Momper et al., 2017b). Notably, fluids across these sites are geochemically diverse, and the presence of the same taxonomic groups suggests both functional redundancy and functional generalists within the communities. Indeed, it was shown that distributions of functional genes are not correlated across sites, geochemistry, distance, or other physical/environmental parameters (Lau et al., 2014).

As we move forward in terrestrial subsurface research, it will be important to consider subjects such as functional redundancy and the ecosystems services that both generalist and specialist taxa provide. Narrowly targeting investigations to a few specific metabolic functions can help elucidate details, but holistic context should not be neglected. To facilitate such progress, we look forward to coordinated analyses that examine the energetic landscapes, taxonomic and functional diversity, and end point analyses such as proteomics and enzymatic assays.

AUTHOR CONTRIBUTIONS

Both authors listed have made a substantial, direct, and intellectual contribution to the work, and approved it for publication.

FUNDING

DM-D and JM was funded by NASA grant number 17-NAI8_2-0017.

ACKNOWLEDGMENTS

DM-D would like to thank A. J. Dombard and D. Cardace for helpful discussions. This is EDGElab contribution #9.

SUPPLEMENTARY MATERIAL

The Supplementary Material for this article can be found online at: https://www.frontiersin.org/articles/10.3389/fmicb.2022.891528/full#supplementary-material

REFERENCES

Amend, J. P., and Shock, E. L. (2001). Energetics of overall metabolic reactions of thermophilic and hyperthermophilic Archaea and Bacteria. *FEMS Microbiol. Rev.* 25, 175–243. doi: 10.1111/j.1574-6976.2001.tb00576.x

Amend, J. P., and Teske, A. (2005). Expanding frontiers in deep subsurface microbiology. *Paleogeography Paleoclimatol. Palaeoecol.* 219, 131–155. doi: 10.1016/b978-0-444-52019-7.50012-7

Anantharman, K., Brown, C. T., Hug, L. A., Sharon, I., Castelle, C. J., Probst, A. J., et al. (2016). Thousands of microbial genomes shed light on interconnected biogeochemical processes in an aquifer system. *Nat. Commun.* 7:13219.

Aüllo, T., Ranchou-Peyruse, A., Ollivier, B., and Magot, M. (2013). *Desulfotomaculum spp*. and related gram-positive sulfate-reducing bacteria in deep subsurface environments. *Front. Microbiol.* 4:362. doi: 10.3389/fmicb.2013.00362

Bagnoud, A., Chourey, K., Hettich, R. L., de Bruijn, I., Andersson, A. F., Leupin, O. X., et al. (2016). Reconstructing a hydrogen-driven microbial metabolic network in Opalinus Clay rock. *Nat. Commun.* 7:12770. doi: 10.1038/ncomms12770

Baker, B. J., Moser, D. P., MacGregor, B. J., Fishbain, S., Wagner, M., Fry, N. K., et al. (2003). Related assemblages of sulphate-reducing bacteria associated with ultradeep gold mines of South Africa and deep basalt aquifers of Washington State. *Environ. Microbiol.* 5, 267–277. doi: 10.1046/j.1462-2920.2003.00408.x

Barton, H. A., and Northup, D. E. (2007). Geomicrobiology in cave environments: past, current and future perspectives. *J. Cave Karst Stud.* 69, 163–178.

Bomberg, M., Lamminmäki, T., and Itävaara, M. (2016). Microbial communities and their predicted metabolic characteristics in deep fracture groundwaters of the crystalling bedrock at Olkiluoto, Finland. *Biogeosciences* 13, 6031–6047. doi: 10.5194/bg-13-6031-2016

Bomberg, M., Mäkinen, J., Salo, M., and Kinnunen, P. (2019). High diversity in iron cycling microbial communities in acidic, iron-rich water of the pyhäsalmi mine, Finland. *Geofluids* 2019:7401304. doi: 10.1155/2019/7401304

Bomberg, M., Nyyssönen, M., Pitkänen, P., Lehtinen, A., and Itävaara, M. (2015). Active microbial communities inhabit sulphate-methane interphase in deep bedrock fracture fluids in Olkiluoto, Finland. *BioMed Res. Int.* 2015:979530. doi: 10.1155/2015/979530

Boyd, E. S., Cummings, D. E., and Geesey, G. G. (2007). Mineralogy influences structure and diversity of bacterial communities associated with geological substrata in a pristine aquifer. *Microb. Ecol.* 54, 170–182. doi: 10.1007/s00248-006-9187-9

Brazelton, W. J., Morrill, P. L., Szponar, N., and Schrenk, M. O. (2013). Bacterial communities associated with subsurface geochemical processes in continental serpentinite springs. *Appl. Environ. Microbiol.* 79, 3906–3916. doi: 10.1128/AEM.00330-13

Brazelton, W. J., Thornton, C. N., Hyer, A., Twing, K. I., Longino, A. A., Lang, S. Q., et al. (2017). Metagenomic identification of active methanogens and methanotrophs in serpentinite springs of the Voltri Massif, Italy. *PeerJ* 5:e2945. doi: 10.7717/peerj.2945

Canovas, P. C. III, Hoehler, T., and Shock, E. L. (2017). Geochemical bioenergetics during low-temperature serpentinization: an example from the Samail ophiolite, Sultanate of Oman. *J. Geophys. Res. Biogeosci.* 122, 1821–1847. doi: 10.1002/2017JG003825

Cardace, D., and Hoehler, T. M. (2009). Serpentinizing fluids craft microbial habitat. *Northeastern Nat.* 16, 272–284. doi: 10.1656/045.016.0520

Cardace, D., Hoehler, T., McCollom, T., Schrenk, M., Carnevale, D., Kubo, M., et al. (2013). Establishment of the Coast Range ophiolite microbial observatory (CROMO): drilling objectives and preliminary outcomes. *Sci. Drilling* 16, 45–55. doi: 10.5194/sd-16-45-2013

Cardace, D., Meyer-Dombard, D. R., Woycheese, K. M., and Arcilla, C. A. (2015). Feasible metabolisms in high pH springs of the Philippines. *Front. Microbiol.* 6:10. doi: 10.3389/fmicb.2015.00010

Cartwright, J. H. E., and Russell, M. J. (2019). The origin of life: the submarine alkaline vent theory at 30. *Interface Focus* 9:20190104. doi: 10.1098/rsfs.2019.0104

Casar, C. P., Kruger, B. R., Flynn, T. M., and Osburn, M. R. (2020). Mineral-hosted biofilm communities in the continental deep subsurface, Deep Mine Microbial Observatory, SD, USA. *Geobiology* 18, 508–522. doi: 10.1111/gbi.12391

Casar, C. P., Kruger, B. R., and Osburn, M. R. (2021a). Rock-Hosted subsurface biofilms: mineral selectivity drives hotspots for intraterrestrial life. *Front. Microbiol.* 12:658988. doi: 10.3389/fmicb.2021.658988

Casar, C. P., Momper, L. M., Kruger, B. R., and Osburn, M. R. (2021b). Iron-Fueled life in the continental subsurface: deep mine microbial observatory, South Dakota, USA. *Appl. Environ. Microbiol.* 87:e00832-21. doi: 10.1128/AEM.00832-21

Chivian, D., Brodie, E. L., Alm, E. J., Culley, D. E., Dehal, P. S., DeSantis, T. Z., et al. (2008). Environmental genomics reveals a single-species ecosystem deep within Earth. *Science* 322, 275–278. doi: 10.1126/science.1155495

Christner, B. C., Priscu, J. C., Achberger, A. M., Barbante, C., Carter, S. P., Christianson, K., et al. (2014). A microbial ecosystem beneath the West Antarctic ice sheet. *Nature* 512, 310–313. doi: 10.1038/nature13667

Cockell, C. S., Holt, J., Campbell, J., Groseman, H., Josset, J.-L., Bontognali, T. R. R., et al. (2019). Subsurface scientific exploration of extraterrestrial environments (MINAR 5): analog science, technology and education in the Boulby Mine. UK. *Int. J. Astrobiol.* 18, 157–182. doi: 10.1017/s1473550418000186

Colman, D. R., Feyhl-Buska, J., Fecteau, K. M., Xu, H., Shock, E. L., and Boyd, E. S. (2016). Ecological differentiation in planktonic and sediment-associated chemotrophic microbial populations in Yellowstone hot springs. *FEMS Microbiol. Ecol.* 92:fiw137. doi: 10.1093/femsec/fiw137

Colman, D. R., Poudel, S., Stamps, B. W., Boyd, E. S., and Spear, J. R. (2017). The deep, hot biosphere: twenty-five years of retrospection. *Proc. Natl. Acad. Sci. U S A.* 113, 6895–6903. doi: 10.1073/pnas.1701266114

Cowen, J. P., Giovannoni, S. J., Kenig, F., Johnson, H. P., Butterfield, D., Rappeì, M. S., et al. (2003). Fluids from aging ocean crust that support microbial life. *Science* 299, 120–123. doi: 10.1126/science.1075653

Crespo-Medina, M., Twing, K. I., Kubo, M. D., Hoehler, T. M., Cardace, D., McCollom, T., et al. (2014). Insights into environmental controls on microbial communities in a continental serpentinite aquifer using a microcosm-based approach. *Front. Microbiol.* 5:604. doi: 10.3389/fmicb.2014.00604

Daae, F. L., Okland, I., Dahle, H., Jorgensen, S. L., Thorseth, I. H., and Pedersen, R. B. (2013). Microbial life associated with low-temperature alteration of ultramafic rocks in the Leka ophiolite complex. *Geobiology* 11, 318–339. doi: 10.1111/gbi.12035

Dai, X., Wang, Y., Luo, L., Pfiffner, S. M., Dong, Z., Xu, Z., et al. (2021). Detection of the deep biosphere in metamorphic rocks from the Chinese continental scientific drilling. *Geobiology* 19, 278–291. doi: 10.1111/gbi.12430

D'Angeli, I. M., Ghezzi, D., Leuko, S., Firrincieli, A., Parise, M., Fiorucci, A., et al. (2019). Geomicrobiology of a seawater-influenced active sulfuric acid cave. *PLoS One* 14:e0220706. doi: 10.1371/journal.pone.0220706

Davidson, M. M., Silver, B. J., Onstott, T. C., Moser, D. P., Gihring, T. M., Pratt, L. M., et al. (2011). Capture of planktonic microbial diversity in fractures by long-term monitoring of flowing boreholes, evander basin, South Africa. *Geomicrobiol. J.* 28, 275–300. doi: 10.1080/01490451.2010.499928

De Waele, J., Audra, P., Madonia, G., Vattano, M., Plan, L., D'Angeli, I. M., et al. (2016). Sulfuric acid speleogenesis (SAS) close to the water table: examples from southern France, Austria, and Sicily. *Geomorphology* 253, 452–467. doi: 10.1016/j.geomorph.2015.10.019

DeLeon-Rodriguez, N., Lathem, T. L., Rodriguez-R, L. M., Barazesh, J. M., Anderson, B. E., Beyersdorf, A. J., et al. (2013). Microbiome of the upper troposphere: species composition and prevalence, effects of tropical storms, and atmospheric implications. *Proc. Natl. Acad. Sci. U S A.* 110, 2575–2580. doi: 10.1073/pnas.1212089110

Dong, Y., Gupta Kumar, C., Chia, N., Kim, P.-J., Miller, P. A., Price, N. D., et al. (2014). Halomonas sulfidaeris-dominated microbial community inhabits a 1.8 km-deep subsurface Cambrian Sandstone reservoir. *Environ. Microbiol.* 16, 1695–1708. doi: 10.1111/1462-2920.12325

Dilek, Y., and Furnes, H. (2011). Ophiolite genesis and global tectonics: geochemical and tectonic fingerprinting of ancient oceanic lithosphere. *Geol. Soc. Am. Bullet.* 123, 387–411.

Ekendahl, S., and Pedersen, K. (1994). Carbon transformations by attached bacterial populations in granitic ground water from deep crystalline bed-rock of the Stripa research mine. *Microbiology* 140, 1565–1573. doi: 10.1099/13500872-140-7-1565

Engel, A. S. (2019). "Microbes," in *Encyclopedia of Caves*, eds W. B. White, D. C. Culver, and T. Pipan (Amsterdam: Elsevier).

Etiope, G. (2017). Abiotic methane in continental serpentinization sites: an overview. *Proc. Earth Plan. Sci.* 17, 9–12. doi: 10.1016/j.proeps.2016.12.006

Etiope, G., Vadillo, I., Whiticar, M. J., Marques, J. M., Carreira, P. M., Tiago, I., et al. (2016). Abiotic methane seepage in the Ronda peridotite massif, southern Spain. *Appl. Geochem.* 66, 101–113. doi: 10.1016/j.apgeochem.2015.12.001

Flemming, H.-C., and Wuertz, S. (2019). Bacteria and archaea on Earth and their abundance in biofilms. *Nat. Rev. Microbiol.* 17, 247–260. doi: 10.1038/s41579-019-0158-9

Fones, E. M., Colman, D. R., Kraus, E. A., Nothaft, D. B., Poudel, S., Rempfert, K. R., et al. (2019). Physiological adaptations to serpentinization in the Samail Ophiolite. Oman. *ISME J.* 13, 1750–1762. doi: 10.1038/s41396-019-0391-2

Fones, E. M., Colman, D. R., Kraus, E. A., Stepanauskas, R., Templeton, A. S., Spear, J. R., et al. (2021). Diversification of methanogens into hyperalkaline serpentinizing environments through adaptations to minimize oxidant limitation. *ISME J.* 15, 1121–1135. doi: 10.1038/s41396-020-00838-1

Frank, Y. A., Kadnikov, V. V., Gavrilov, S. N., Banks, D., Gerasimchuk, A. L., Podosokorskaya, O. A., et al. (2016). Stable and variable parts of microbial community in siberian deep subsurface thermal aquifer system revealed in a long-term monitoring study. *Front. Microbiol.* 7:2101. doi: 10.3389/fmicb.2016.02101

Fröhlich-Nowoisky, J., Kampf, C. J., Weber, B., Huffman, J. A., Pöhlker, C., Andreae, M. O., et al. (2016). Bioaerosols in the earth system: climate, health, and ecosystem interactions. *Atmospheric Res.* 182, 346–376. doi: 10.1016/j.atmosres.2016.07.018

Fukuda, A., Hagiwara, H., Ishimura, T., Kouduka, M., Ioka, S., Amano, Y., et al. (2010). Geomicrobiological properties of ultra-deep granitic groundwater from the Mizunami Underground Research Laboratory (MIU), Central Japan. *Microb. Ecol.* 60, 214–225. doi: 10.1007/s00248-010-9683-9

Gihring, T. M., Moser, D. P., Lin, L.-H., Davidson, M., Onstott, T. C., Morgan, L., et al. (2006). The distribution of microbial taxa in the subsurface water of the kalahari shield, South Africa. *Geomicrobiol. J.* 23, 415–430. doi: 10.1080/01490450600875696

Glombitza, C., Putman, L. I., Rempfert, K. R., Kubo, M. D., Schrenk, M. O., Templeton, A. S., et al. (2021). Active microbial sulfate reduction in fluids of serpentinizing peridotites of the continental subsurface. *Commun. Earth Environ.* 2:84. doi: 10.1038/s43247-021-00157-z

Griffin, D. W. (2008). Non-spore forming eubacteria isolated at an altitude for 20,000 m in Earth's atmosphere: extended incubation periods needed for culture-based assays. *Aerobiologia* 24, 19–25. doi: 10.1007/s10453-007-9078-7

Hallbeck, L., and Pedersen, K. (2008). Characterization of microbial processes in deep aquifers of the Fennoscandian Shield. *Appl. Geochem.* 23, 1796–1819. doi: 10.1016/j.apgeochem.2008.02.012

Hallbeck, L., and Pedersen, K. (2012). Culture-dependent comparison of microbial diversity in deep granitic groundwater from two sites considered for a Swedish final repository of spent nuclear fuel. *FEMS Microbiol. Ecol.* 81, 66–77. doi: 10.1111/j.1574-6941.2011.01281.x

Hodgson, D. A., Bentley, M. J., Smith, J. A., Klepacki, J., Makinson, K., Smith, A. M., et al. (2016). Technologies for retrieving sediment cores in Antarctic subglacial settings. *Philos. Trans. R. Soc. A* 374:20150056. doi: 10.1098/rsta.2015.0056

Hu, P., Tom, L., Singh, A., Thomas, B. C., Baker, B. J., Piceno, Y. M., et al. (2016). Genome-resolved metagenomic analysis reveals roles for candidate phyla and other microbial community members in biogeochemical transformations in oil reservoirs. *mBio* 7:e01669-15. doi: 10.1128/mBio.01669-15

Ionescu, D., Heim, C., Thiel, V., Ramette, A., Reitner, J., and de Beer, D. (2015). Diversity of iron oxidizing and reducing bacteria in bioreactors set in the Äspö Hard Rock Laboratory. *Geomicrobiology* 32, 207–220.

Itävaara, M., Nyyssönen, M., Kapanen, A., Mousiainen, A., Ahonen, L., and Kukkonen, I. (2011). Characterization of bacterial diversity to a depth of 1500m in the Outokumpu deep borehole, Fennoscandian Shield. *FEMS Microbiol. Ecol.* 77, 295–309. doi: 10.1111/j.1574-6941.2011.01111.x

Jägevall, S., Lisa Rabe, L., and Pedersen, K. (2011). Abundance and diversity of biofilms in natural and artificial aquifers of the äspö hard rock laboratory, Sweden. *Microbial Ecol.* 61, 410–422. doi: 10.1007/s00248-010-9761-z

Johansson, Å (1988). The age and geotectonic setting of the Småland-Värmland granite porphyry belt. *GFF* 110, 105–110. doi: 10.1080/11035898809452648

Jones, D. S., and Northup, D. E. (2021). Cave decorating with microbes: geomicrobiology of caves. *Elements* 17, 107–112. doi: 10.2138/gselements.17.2.107

Jungbluth, S. P., Glavina del Rio, T., Tringe, S. G., Stepanauskas, R., and Rappeì, M. S. (2017). Genomic comparisons of a bacterial lineage that inhabits both marine and terrestrial deep subsurface systems. *PeerJ* 5:e3134. doi: 10.7717/peerj.3134

Katsuyama, C., Nashimoto, H., Nagaosa, K., Ishibashi, T., Furuta, K., Kinoshita, T., et al. (2013). Occurrence and potential activity of denitrifiers and methanogens in groundwater at 140m depth in Pliocene diatomaceous mudstone of northern Japan. *FEMS Microbiol. Ecol.* 86, 532–543. doi: 10.1111/1574-6941.12179

Kay, C. M., Haanela, A., and Johnson, D. B. (2014). Microorganisms in subterranean acidic waters within Europe's deepest metal mine. *Res. Microbiol.* 165, 705–712. doi: 10.1016/j.resmic.2014.07.007

Kelemen, P. B., Matter, J. M., Teagle, D. A. H., Coggon, J. A., and The Oman Drilling Project Science Team. (2020). "Microbiology," in *Proceedings of the International Ocean Discovery Program*, (College Station, TX).

Kelemen, P., Rajhi, A. A., Godard, M., Ildefonse, B., Köpke, J., MacLeod, C., et al. (2013). Scientific drilling and related research in the samail ophiolite, sultanate of oman. *Sci. Drilling* 15, 64–71. doi: 10.5194/sd-15-64-2013

Kieft, T. L. (2016). "Microbiology of the deep continental biosphere," in *Their World: A Diversity of Microbial Environments, Advances in Environmental Microbiology*, ed. C. J. Hurst (Berlin: Springer), doi: 10.1007/978-3-319-28071-4_6

Kotelnikova, S., and Pedersen, K. (1998). Distribution and activity of methanogens and homoacetogens in deep granitic aquifers at Äspö Hard Rock Laboratory, Sweden. *FEMS Microbiol. Ecol.* 26, 121–134. doi: 10.1016/s0168-6496(98)00028-2

Kotelnikova, S., Macario, A. J. L., and Pedersen, K. (1998). Methanobacterium subterraneum, a new species of Archaea isolated from deep groundwater at the Äspö Hard Rock Laboratory, Sweden. *Int. J. Systematic Bacteriol.* 48, 357–367. doi: 10.1099/00207713-48-2-357

Kraus, E. A., Nothaft, D., Stamps, B. W., Remphert, K. R., Ellison, E. T., Matter, J. M., et al. (2021). Molecular evidence for an active microbial methane cycle in subsurface serpentinite-hosted groundwaters in the samail ophiolite, Oman. *Appl. Environ. Microbiol.* 87:e02068-20. doi: 10.1128/AEM.02068-2020

Kutvonen, H., Rajala, P., Carpén, L., and Bomberg, M. (2015). Nitrate and ammonia as nitrogen sources for deep subsurface microorganisms. *Front. Microbiol.* 6:1079. doi: 10.3389/fmicb.2015.01079

Labonteì, J. M., Field, E. K., Lau, M., Chivian, D., Van Heerden, E., Wommack, K. E., et al. (2015). Single cell genomics indicates horizontal gene transfer and viral infections in a deep subsurface Firmicutes population. *Front. Microbiol.* 6:349. doi: 10.3389/fmicb.2015.00349

LaRowe, D., and Amend, J. (2014). "Energetic constraints on life in marine deep sediments," in *Microbial Life of the Deep Biosphere*, eds J. Kallmeyer and D. Wagner (Berlin: Springer), 326. doi: 10.3389/fmicb.2014.00362

LaRowe, D., and Amend, J. (2019). "Energy limits for life in the subsurface," in *Deep Carbon*, eds B. N. Orcutt, I. Daniel, and R. Dasgupta (Cambridge: Cambridge University Press), 585–619. doi: 10.1017/9781108677950.019

Lau, M. C. Y., Kieft, T. L., Kuloyo, O., Linage-Alvarez, B., van Heerden, E., Lindsay, M. R., et al. (2016). Syntrophy in the oligotrophic deep subsurface. *Proc. Natl. Acad. Sci. U S A.* 113, E7927–E7936.

Lau, M. C., Cameron, C., Magnabosco, C., Brown, C. T., Schilkey, F., Grim, S., et al. (2014). Phylogeny and phylogeography of functional genes shared among seven terrestrial subsurface metagenomes reveal N-cycling and microbial evolutionary relationships. *Front. Microbiol.* 5:531. doi: 10.3389/fmicb.2014.00531

Lauritzen, S.-E. (2018). "Physiography of the Caves," in *Cave Ecology*, eds O. T. Moldovan, Ĺ Kovač, and S. Halse (Cham: Springer Nature Switzerland), 7–22. doi: 10.1007/978-3-319-98852-8_2

Leong, J. A. M., and Shock, E. L. (2020). Thermodynamic constraints on the geochemistry of low-temperature, continental, serpentinization-generated fluids. *Am. J. Sci.* 320, 185–235. doi: 10.2475/03.2020.01

Lin, L.-H., Wang, P.-L., Rumble, D., Lippmann-Pipke, J., Boice, E., Pratt, L. M., et al. (2006a). Long-term sustainability of a high-energy, low-diversity crustral biome. *Science* 314, 479–482. doi: 10.1126/science.1127376

Lin, L. H., Hall, J., Onstott, T. C., Gihring, T., Sherwood Lollar, B., Boice, E., et al. (2006b). Planktonic microbial communities associated with fracture-derived groundwater in a deep gold mine of South Africa. *Geomicrobiol. J.* 23, 475–497. doi: 10.1080/01490450600875829

Lippmann-Pipke, J., Sherwood Lollar, B., Niedermann, S., Stroncik, N. A., Naumann, R., van Heerden, E., et al. (2011). Neon identifies two billion year old fluid component in the Kaapvaal Craton. *Chem. Geol.* 283, 287–296. doi: 10.1016/j.chemgeo.2011.01.028

Lollar, G. S., Wart, O., Telling, J., Osburn, M. R., and Sherwood Lollar, B. (2019). 'Follow the water': hydrogeochemical constraints on microbial investigations 2.4km below surface at the Kidd Creek Deep Fluid and Deep Life Observatory. *Geomicrobiol. J.* 36, 859–872. doi: 10.1080/01490451.2019.1641770

Magnabosco, C., Lin, L.-H., Dong, H., Bomberg, M., Ghiorse, W., Stan-Lotter, H., et al. (2018). The biomass and biodiversity of the continental subsurface. *Nat. Geosci.* 11, 707–717. doi: 10.1038/s41561-018-0221-6

Magnabosco, C., Ryan, K., Lau, M. C. Y., Kuloyo, O., Sherwood Lollar, B., Kieft, T. L., et al. (2016). A metagenomic window into carbon metabolism at 3 km depth in Precambrian continental crust. *ISME J.* 10, 730–741. doi: 10.1038/ismej.2015.150

Magnabosco, C., Tekere, M., Lau, M. C. Y., Linage, B., Kuloyo, O., Erasmus, M., et al. (2014). Comparisons of the composition and biogeographic distribution of the bacterial communities occupying South African thermal springs with those inhabiting deep subsurface fracture water. *Front. Microbiol.* 5:679. doi: 10.3389/fmicb.2014.00679

Mailloux, B. J., Fuller, M. E., Onstott, T. C., Hall, J., Dong, H., DeFlaun, M. F., et al. (2003). The role of physical, chemical, and microbial heterogeneity on the field-scale transport and attachment of bacteria. *Water Resources Manag.* 39:hbox1142. doi: 10.1029/2002WR001591

Margesin, R., and Miteva, V. (2011). Diversity and ecology of psychrophilic microorganisms. *Res. Microbiol.* 162, 346–361. doi: 10.1016/j.resmic.2010.12.004

Martin, W., Baross, J., Kelley, D., and Russell, M. J. (2008). Hydrothermal vents and the origin of life. *Nat. Rev. Microbiol.* 6, 805–814. doi: 10.1038/nrmicro1991

McCollom, T. M. (2000). Geochemical constraints on primary productivity in submarine hydrothermal vent plumes. *Deep Sea Res. Part I: Oceanographic Res. Papers* 47, 85–101. doi: 10.1016/s0967-0637(99)00048-5

McCollom, T. M., and Bach, W. (2009). Thermodynamic constraints on hydrogen generation during serpentinization of ultramafic rocks. *Geochim. Cosmochimica Acta* 73, 856–875. doi: 10.1016/j.gca.2008.10.032

McCollom, T. M., Sherwood Lollar, B., Lacrampe-Couloume, G., and Seewald, J. S. (2010). The influence of carbon source on abiotic organic synthesis and carbon isotope fractionation under hydrothermal conditions. *Geochim. Cosmochimica Acta* 74, 2717–2740. doi: 10.1016/j.gca.2010.02.008

Merino, N., Aronson, H. S., Bojanova, D. P., Feyhl-Buska, J., Wong, M. L., Zhang, S., et al. (2019). Living at the extremes: extremophiles and the limits of life in a planetary context. *Front. Microbiol.* 10:780. doi: 10.3389/fmicb.2019.00780

Merino, N., Kawai, M., Boyd, E. S., Colman, D. R., McGlynn, S. E., Nealson, K. H., et al. (2020). Single-Cell genomics of novel actinobacteria with the wood–ljungdahl pathway discovered in a serpentinizing system. *Front. Microbiol.* 11:1031. doi: 10.3389/fmicb.2020.01031

Meyer-Dombard, D. R., Casar, C. P., Simon, A. G., Cardace, D., Schrenk, M. O., and Arcilla, C. A. (2018). Biofilm formation and potential for iron cycling in serpentinization-influenced groundwater of the Zambales and Coast Range ophiolites. *Extremophiles* 22, 407–431. doi: 10.1007/s00792-018-1005-z

Meyer-Dombard, D. R., Osburn, M. R., Cardace, D., and Arcilla, C. A. (2019). The effect of a tropical climate on available nutrient resources to springs in ophiolite-hosted, deep biosphere ecosystems in the Philippines. *Front. Microbiol.* 10:761. doi: 10.3389/fmicb.2019.00761

Meyer-Dombard, D. R., Woycheese, K. M., Yargı çoğlu, Cardace, D., Shock, E. L., Güleçal-Pektas, et al. (2015). High pH microbial ecosystems in a newly discovered, ephemeral, serpentinizing fluid seep at Yanastas (Chimera). *Front. Microbiol.* 5:723. doi: 10.3389/fmicb.2014.00723

Miettinen, H., Bomberg, M., and Vikman, M. (2018). Acetate activates deep subsurface fracture fluid microbial communities in Olkiluoto, Finland. *Geosciences* 8:399. doi: 10.3390/geosciences8110399

Miettinen, H., Kietäväinen, R., Sohlberg, E., Numminen, M., Ahonen, L., and Itävaara, M. (2015). Microbiome composition and geochemical characteristics of deep subsurface high-pressure environment, Pyhäsalmi mine Finland. *Front. Microbiol.* 6:1203. doi: 10.3389/fmicb.2015.01203

Miller, H. M., Chaudhry, N., Conrad, M. E., Bill, M., Kopf, S. H., and Templeton, A. S. (2018). Large carbon isotope variability during methanogenesis under

alkaline conditions. *Geochim. Cosmochimica Acta* 237, 18–31. doi: 10.1016/j.gca.2018.06.007

Miller, H. M., Matter, J. M., Kelemen, P., Ellison, E. T., Conrad, M. E., Fierer, N., et al. (2016). Modern water/rock reactions in Oman hyperalkaline peridotite aquifers and implications for microbial habitability. *Geochim. Cosmochimica Acta* 179, 217–241. doi: 10.1016/j.gca.2016.01.033

Miteva, V., Burlingame, C., Sowers, T., and Brenchley, J. (2014). Comparative evaluation of the indigenous microbial diversity vs. drilling fluid contaminants in the NEEM Greenland ice core. *FEMS Microbiol. Ecol.* 89, 238–256. doi: 10.1111/1574-6941.12286

Miteva, V., Sowers, T., Schüpbach, S., Fischer, H., and Brenchley, J. (2016). Geochemical and microbiological studies of nitrous oxide variations within the new NEEM Greenland ice core during the last glacial period. *Geomicrobiol. J.* 33, 647–660. doi: 10.1080/01490451.2015.1074321

Momper, L., Kiel Reese, B., Zinke, L., Wanger, G., Osburn, M. R., Moser, D., et al. (2017a). Major phylum-level differences between porefluid and host rock bacterial communities in the terrestrial deep subsurface. *Environ. Microbiol. Rep.* 9, 501–511. doi: 10.1111/1758-2229.12563

Momper, L., Jungbluth, S. P., Lee, M. D., and Amend, J. P. (2017b). Energy and carbon metabolisms in a deep terrestrial subsurface fluid microbial community. *ISME J.* 11, 2319–2333. doi: 10.1038/ismej.2017.94

Moody, J. B. (1976). Serpentinization: a review. *Lithos* 9, 125–138. doi: 10.1016/0024-4937(76)90030-x

Morono, Y., and Inagaki, F. (2016). Analysis of low-biomass microbial communities in the deep biosphere. *Adv. Appl. Microbiol.* 95, 149–178. doi: 10.1016/bs.aambs.2016.04.001

Morrill, P. L., Kuenen, J. G., Johnson, O. J., Suzuki, S., Rietze, A., Sessions, A. L., et al. (2013). Geochemistry and geobiology of a present-day serpentinization site in California: the Cedars. *Geochim. Cosmochimica Acta* 109, 222–240. doi: 10.1016/j.gca.2013.01.043

Moser, D. P., Gihring, T. M., Brockman, F. J., Fredrickson, J. K., Balkwill, D. L., Dollhopf, M. E., et al. (2005). *Desulfotomaculum* and *Methanobacterium spp*. Dominate a 4- to 5-Kilometer-Deep Fault. *Appl. Environ. Microbiol.* 71, 8773–8783. doi: 10.1128/AEM.71.12.8773-8783.2005

Moser, D. P., Onstott, T. C., Fredrickson, J. K., Brockman, F. J., Balkwill, D. L., Drake, G. R., et al. (2003). Temporal shifts in the geochemistry and microbial community structure of an ultradeep mine borehole following isolation. *Geomicrobiol. J.* 20, 517–548. doi: 10.1080/713851170

Motamedi, M., and Pedersen, K. (1998). Desulfovibrio aespoeensis sp. nov. a mesophilic sulfate-reducing bacterium from deep groundwater at Äspö Hard Rock Laboratory, Sweden. *Int. J. Systematic Bacteriol.* 48, 311–315. doi: 10.1099/00207713-48-1-311

Neal, C., and Stanger, G. (1983). Hydrogen generation from mantle source rocks in oman. *Earth Plan. Sci. Lett.* 66, 315–320. doi: 10.1016/0012-821x(83)90144-9

Nicolaysen, L. O., Hart, R. J., and Gale, N. H. (1981). The Vredefort radioelement profile extended to supracrustal strata at Carletonville, with implications for continental heat flow. *J. Geophys. Res.* 86, 10653–10661. doi: 10.1029/jb086ib11p10653

Nothaft, D. B., Templeton, A. S., Boyd, E. S., Matter, J. M., Stute, M., and Paukert Vankeuren, A. N. (2021a). Aqueous geochemical and microbial variation across discrete depth intervals in a peridotite aquifer assessed using a packer system in the samail ophiolite, oman. *J. Geophys. Res. Biogeosci.* 126:e2021JG006319. doi: 10.1029/2021jg006319

Nothaft, D. B., Templeton, A. S., Rhim, J. H., Wang, D. T., Labidi, J., Miller, H. M., et al. (2021b). Geochemical, biological, and clumped isotopologue evidence for substantial microbial methane production under carbon limitation in serpentinites of the samail ophiolite, oman. *J. Geophys. Res. Biogeosci.* 126:e2020JG006025. doi: 10.1029/2020jg006025

Nuppunen-Puputti, M., Purkamo, L., Kietäväinen, R., Nyyssönen, M., Itävaara, M., Ahonen, L., et al. (2018). Rare biosphere Archaea assimilate acetate in *Precambrian terrestrial* subsurface at 2.2 km depth. *Geosciences* 8:418. doi: 10.3390/geosciences8110418

Nyyssönen, M., Bomberg, M., Kapanen, A., Nousiainen, A., Pitkänen, P., and Itävaara, M. (2012). Methanogenic and sulphate-reducing microbial communities in deep groundwater of crystalline rock fractures in Olkiluoto, Finland. *Geomicrobiol. J.* 29, 863–878. doi: 10.1080/01490451.2011.635759

Nyyssönen, M., Hultman, J., Ahonen, L., Kukkonen, I., Paulin, L., Laine, P., et al. (2014). Taxonomically and functionally diverse microbial communities in deep crystalline rocks of the Fennoscandian shield. *ISME J.* 8, 126–138. doi: 10.1038/ismej.2013.125

Osburn, M. R., Kruger, B., Masterson, A. L., Casar, C. P., and Amend, J. P. (2019). Establishment of the deep mine microbial observatory (DeMMO), South Dakota, USA, a geochemically stable portal into the deep subsurface. *Front. Earth Sci.* 7:196. doi: 10.3389/feart.2019.00196

Osburn, M. R., LaRowe, D. E., Momper, L. M., and Amend, J. P. (2014). Chemolithotrophy in the continental deep subsurface: Sanford Underground Research Facility (SURF), USA. *Front. Microbiol.* 5:610. doi: 10.3389/fmicb.2014.00610

Parkes, R. J., Cragg, B., Roussel, E., Webster, G., Weightman, A., and Sass, H. (2014). A review of prokaryotic populations and processes in sub-seafloor sediments, including biosphere:geosphere interactions. *Mar. Geol.* 352, 409–425. doi: 10.1016/j.margeo.2014.02.009

Payler, S. J., Biddle, J. F., Sherwood Lollar, B., Fox-Powell, M. G., Edwards, T., Ngwenya, B. T., et al. (2019). An ionic limit to life in the deep subsurface. *Front. Microbiol.* 10:426. doi: 10.3389/fmicb.2019.00426

Pearce, D. A., Bridge, P. D., Hughes, K. A., Sattler, B., Psenner, R., and Russell, N. J. (2009). Microorganisms in the atmosphere over Antarctica. *FEMS Microbiol. Ecol.* 69, 143–157. doi: 10.1111/j.1574-6941.2009.00706.x

Pedersen, K. (1993). Bacterial processes in nuclear waste disposal. *Microbiol. Eur.* 1, 18–23.

Pedersen, K. (2012). Subterranean microbial populations metabolize hydrogen and acetate under *in situ* conditions in granitic groundwater at 450 m depth in the Äspö Hard Rock Laboratory, Sweden. *FEMS Microbiol. Ecol.* 81, 217–229. doi: 10.1111/j.1574-6941.2012.01370.x

Pedersen, K. (2013). Metabolic activity of subterranean microbial communities in deep granitic groundwater supplemented with methane and H2. *ISME J.* 7, 839–849. doi: 10.1038/ismej.2012.144

Pedersen, K., and Ekendahl, S. (1992). Incorporation of CO2 and introduced organic compounds by bacterial populations in groundwater from the deep crystalline bedrock of the Stripa mine. *J. General Microbiol.* 138, 369–376. doi: 10.1099/00221287-138-2-369

Preiner, M., Xavier, J. C., Sousa, F. L., Zimorski, V., Neubeck, A., Lang, S. Q., et al. (2018). Serpentinization: connecting geochemistry, ancient metabolism and industrial hydrogenation. *Life-Basel* 8:41. doi: 10.3390/life8040041

Price, P. B. (2007). Microbial life in glacial ice and implications for a cold origin of life. *FEMS Microbiol. Ecol.* 59, 217–231. doi: 10.1111/j.1574-6941.2006.00234.x

Purkamo, L., Bomberg, M., Nyyssönen, M., Kukkonen, I., Ahonen, L., and Itävaara, M. (2015a). Heterotrophic communities supplied by ancient organic carbon predominate in deep Fennoscandian bedrock fluids. *Microb. Ecol.* 69, 319–332. doi: 10.1007/s00248-014-0490-6

Purkamo, L., Bomberg, M., Kietäväinen, R., Salavirta, H., Nyyssönen, M., Nuppunen-Puputti, M., et al. (2015b). The keystone species of Precambrian deep bedrock biosphere belong to *Burkholderiales* and *Clostridiales*. *Biogeosci. Discussions* 12, 18103–18150.

Purkamo, L., Bomberg, M., Kietäväinen, R., Salavirta, H., Nyyssönen, M., Nuppunen-Puputti, M., et al. (2016). Microbial co-occurrence patterns in deep Precambrian bedrock fracture fluids. *Biogeosciences* 13, 3091–3108. doi: 10.5194/bg-13-3091-2016

Purkamo, L., Bomberg, M., Nyyssönen, M., Ahonen, L., Kukkonen, I., and Itävaara, M. (2017). Response of deep subsurface microbial community to different carbon sources and electron acceptors during ∼2 months incubation in microcosms. *Front. Microbiol.* 8:232. doi: 10.3389/fmicb.2017.00232

Purkamo, L., Bomberg, M., Nyyssönen, M., Kukkonen, I., Ahonen, L., Kietäväinen, R., et al. (2013). Dissecting the deep biosphere: retrieving authentic microbial communities from packer-isolated deep crystalline bedrock fracture zones. *FEMS Microbiol. Ecol.* 85, 324–337. doi: 10.1111/1574-6941.12126

Purkamo, L., Kietäväinen, R., Miettinen, H., Sohlberg, E., Kukkonen, I., Itavaara, M., et al. (2018). Diversity and functionality of archaeal, bacterial and fungal communities in deep Archaean bedrock groundwater. *FEMS Microbiol. Ecol.* 94:fiy116. doi: 10.1093/femsec/fiy116

Purkamo, L., Kietäväinen, R., Nuppunen-Puputti, M., Bomberg, M., and Cousins, C. (2020). Ultradeep microbial communities at 4.4 km within crystalline bedrock: implications for habitability in a planetary context. *Life* 10:2. doi: 10.3390/life10010002

Putman, L. I., Sabuda, M. C., Brazelton, W. J., Kubo, M. D., Hoehler, T. M., McCollom, T. M., et al. (2021). Microbial communities in a serpentinizing

aquifer are assembled through strong concurrent dispersal limitation and selection. *mSystems* 6:e0030021. doi: 10.1128/mSystems.00300-21

Quéméneur, M., Palvadeau, A., Postec, A., Monnin, C., Chavagnac, V., Ollivier, B., et al. (2015). Endolithic microbial communities in carbonate precipitates from serpentinite-hosted hyperalkaline springs of the *Voltri Massif* (Ligurian Alps, Northern Italy). *Environ. Sci. Pollution Res. Int.* 22, 13613–13624. doi: 10.1007/s11356-015-4113-7

Rempfert, K. R., Miller, H. M., Bompard, N., Nothaft, D., Matter, J. M., Kelemen, P., et al. (2017). Geological and geochemical controls on subsurface microbial life in the samail ophiolite, Oman. *Front. Microbiol.* 8:56. doi: 10.3389/fmicb.2017.00056

Rhodes, R. H., Faïn, X., Stowasser, C., Blunier, T., Chappelaz, J., McConnell, J. R., et al. (2013). Continuous methane measurements from a late Holocene Greenland ice core: atmospheric and in situ signals. *Earth Plan. Sci. Lett.* 368, 9–19. doi: 10.1016/j.epsl.2013.02.034

Rowe, A. R., Abuyen, K., Lam, B. R., Kruger, B., Casar, C. P., Osburn, M. R., et al. (2020). Electrochemical evidence for in situ microbial activity at the Deep Mine Microbial Observatory (DeMMO), South Dakota, USA. *Geobiology* 19, 173–188. doi: 10.1111/gbi.12420

Rowe, A. R., Yoshimura, M., LaRowe, D. E., Bird, L. J., Amend, J. P., Hashimoto, K., et al. (2017). In situ electrochemical enrichment and isolation of a magnetite-reducing bacterium from a high pH serpentinizing spring. *Environ. Microbiol.* 19, 2272–2285. doi: 10.1111/1462-2920.13723

Russell, M. J., and Ponce, A. (2020). Six 'Must-Have' minerals for life's emergence: olivine, pyrrhotite, bridgmanite, serpentine, fougerite and mackinawite. *Life-Basel* 10:291. doi: 10.3390/life10110291

Sabuda, M. C., Brazelton, W. J., Putman, L. I., McCollom, T. M., Hoehler, T. M., Kubo, M. D. Y., et al. (2020). A dynamic microbial sulfur cycle in a serpentinizing continental ophiolite. *Environ. Microbiol.* 22, 2329–2345. doi: 10.1111/1462-2920.15006

Sabuda, M. C., Putman, L. I., Hoehler, T. M., Kubo, M. D., Brazelton, W. J., Cardace, D., et al. (2021). Biogeochemical gradients in a serpentinization-influenced aquifer: implications for gas exchange between the subsurface and atmosphere. *J. Geophys. Res. Biogeosci.* 126:e2020JG006209. doi: 10.1029/2020jg006209

Sahl, J. W., Schmidt, R., Swanner, E. D., Mandernack, K. W., Templeton, A. S., Kieft, T. L., et al. (2008). Subsurface microbial diversity in deep granitic fracture water in Colorado. *Appl. Environ. Microbiol.* 74, 143–152. doi: 10.1128/AEM.01133-07

Sánchez-Murillo, R., Gazel, E., Schwarzenbach, E. M., Crespo-Medina, M., Schrenk, M. O., Boll, J., et al. (2014). Geochemical evidence for active tropical serpentinization in the Santa Elena Ophiolite, Costa Rica: an analog of a humid early Earth? *Geochem. Geophys. Geosystems* 15, 1783–1800. doi: 10.1002/2013gc005213

Schrenk, M. O., Brazelton, W. J., and Lang, S. Q. (2013). Serpentinization, Carbon, and deep life. *Rev. Mineral. Geochem.* 75, 575–606. doi: 10.2138/rmg.2013.75.18

Schubotz, F., Meyer-Dombard, D. R., Bradley, A. S., Fredricks, H. F., Hinrichs, K.-U., Shock, E. L., et al. (2013). Spatial and temporal variability of biomarkers and microbial diversity reveal metabolic and community flexibility in Streamer Biofilm Communities in the Lower Geyser Basin, Yellowstone National Park. *Geobiology* 11, 549–569. doi: 10.1111/gbi.12051

Schulte, M., Blake, D., Hoehler, T., and McCollom, T. (2006). Serpentinization and its implications for life on the early Earth and Mars. *Astrobiology* 6, 364–376. doi: 10.1089/ast.2006.6.364

Schulze-Makuch, D., Airo, A., and Schirmack, J. (2017). The adaptability of life on earth and the diversity of planetary habitats. *Front. Microbiol.* 8:2011. doi: 10.3389/fmicb.2017.02011

Schwarzenbach, E. M., Früh-Green, G. L., Bernasconi, S. M., Alt, J. C., Shanks Iii, W. C., Gaggero, L., et al. (2012). Sulfur geochemistry of peridotite-hosted hydrothermal systems: comparing the Ligurian ophiolites with oceanic serpentinites. *Geochim. Cosmochimica Acta* 91, 283–305. doi: 10.1016/j.gca.2012.05.021

Selensky, M. J., Masterson, A. L., Blank, J. G., Lee, S. C., and Osburn, M. R. (2021). Stable carbon isotope depletions in lipid biomarkers suggest subsurface carbon fixation in lava caves. *J. Geophys. Res. Biogeosci.* 126:e2021JG006430. doi: 10.1029/2021jg006430

Sherwood Lollar, B., Frape, S. K., Fritz, P., Macko, S. A., Welhan, J. A., Blomqvist, R., et al. (1993). Evidence for bacterially generated hydrocarbon gas in Canadian shield and Fennoscandian shield rocks. *Geochim. Cosmochimica Acta* 57, 5073–5085. doi: 10.1016/0016-7037(93)90609-z

Sherwood Lollar, B., Voglesonger, K., Lin, L. H., Lacrampe-Couloume, G., Telling, J., Abrajano, T. A., et al. (2007). Hydrogeologic controls on episodic H2 release from Precambrian fractured rocks: energy for deep subsurface life on Earth and Mars. *Astrobiology* 7, 971–986. doi: 10.1089/ast.2006.0096

Shock, E., and Canovas, P. (2010). THe potential for abiotic organic synthesis and biosynthesis at seafloor hydrothermal systems. *Geofluids* 10, 161–192. doi: 10.1002/9781444394900.ch12

Silver, B. J., Raymond, R., Sigman, D., Prokopeko, M., Lollar, B., Lacrampe-Couloume, G., et al. (2012). The origin of NO3− and N2 in deep subsurface fracture water of South Africa. *Chem. Geol.* 294-295, 51–62. doi: 10.1016/j.chemgeo.2011.11.017

Simkus, D. N., Slater, G. F., Lollar, B. S., Wilkie, K., Kieft, T. L., Magnabosco, C., et al. (2016). Variations in microbial car- bon sources and cycling in the deep continental subsurface. *Geochim. Cosmochimica Acta* 173, 264–283. doi: 10.1016/j.gca.2015.10.003

Sojo, V., Herschy, B., Whicher, A., Camprubi, E., and Lane, N. (2016). The origin of life in alkaline hydrothermal vents. *Astrobiology* 16, 181–197. doi: 10.1089/ast.2015.1406

Spear, J. R., Barton, H. A., Francis, C. A., Roberts, K. J., and Pace, N. R. (2007). Microbial community biofabrics in a geothermal mine adit. *Appl. Environ. Microbiol.* 73, 6172–6180. doi: 10.1128/AEM.00393-07

Stevens, T. O., and McKinley, J. P. (1995). Lithoautotrophic microbial ecosystems in deep basalt aquifers. *Science* 270, 450–454. doi: 10.1038/s41467-017-01288-8

Stroes-Gascoyne, S., Schippers, A., Schwyn, B., Poulain, S., Sergeant, C., Simonoff, M., et al. (2007). Microbial community analysis of Opalinus Clay drill core samples from the Mont Terri underground research laboratory, Switzerland. *Geomicrobiol. J.* 24, 1–17. doi: 10.1080/01490450601134275

Suzuki, S., Ishii, S., Hoshino, T., Rietze, A., Tenney, A., Morrill, P. L., et al. (2017). Unusual metabolic diversity of hyperalkaliphilic microbial communities associated with subterranean serpentinization at the Cedars. *ISME J.* 11, 2584–2598. doi: 10.1038/ismej.2017.111

Suzuki, S., Ishii, S., Wu, A., Cheung, A., Tenney, A., Wagner, G., et al. (2013). Microbial diversity in The Ceders, an ultrabasic, ultrareducing, and low salinity serpentinizing ecosystem. *Proc. Natl. Acad. Sci. U S A.* 110, 15336–15341. doi: 10.1073/pnas.1302426110

Suzuki, S., Nealson, K. H., and Ishii, S. (2018). Genomic and in-situ transcriptomic characterization of the candidate phylum NPL-UPL2 from highly alkaline highly reducing serpentinized groundwater. *Front. Microbiol.* 9:3141. doi: 10.3389/fmicb.2018.03141

Swanner, E. D., and Templeton, A. S. (2011). Potential for nitrogen fixation and nitrification in the granite-hosted subsurface at Henderson Mine, CO. *Front. Microbiol.* 2:254. doi: 10.3389/fmicb.2011.00254

Swingley, W. D., Meyer-Dombard, D. R., Shock, E. L., Alsop, E. B., Falenski, H. D., Havig, J. R., et al. (2012). Coordinating environmental genomics and geochemistry reveals metabolic transitions in a hot spring ecosystem. *PLoS One* 7:e38108. doi: 10.1371/journal.pone.0038108

Taubner, R. S., Olsson-Francis, K., Vance, S. D., Ramkissoon, N. K., Postberg, F., de Vera, J. P., et al. (2020). Experimental and simulation efforts in the astrobiological exploration of exooceans. *Space Sci. Rev.* 216:9. doi: 10.1007/s11214-020-0635-5

Templeton, A. S., Ellison, E. T., Glombitza, C., Morono, Y., Rempfert, K. R., Hoehler, T. M., et al. (2021). Accessing the subsurface biosphere within rocks undergoing active low-temperature serpentinization in the samail ophiolite (Oman Drilling Project). *J. Geophys. Res. Biogeosci.* 126:e2021JG006315. doi: 10.1029/2021jg006315

Thieringer, P. H., Honeyman, A. S., and Spear, J. R. (2021). Spatial and temporal constraints on the composition of microbial communities in subsurface boreholes of the Edgar Experimental Mine. *Microbiol. Spectrum.* 9:e00631-21. doi: 10.1128/Spectrum.00631-21

Tiago, I., and Veriissimo, A. (2013). Microbial and functional diversity of a subterrestrial high pH groundwater associated to serpentinization. *Environ. Microbiol.* 15, 1687–1706. doi: 10.1111/1462-2920.12034

Tiago, I., Chung, A. P., and Verissimo, A. (2004). Bacterial diversity in a nonsaline alkaline environment: heterotrophic aerobic populations.

Appl. Environ. Microbiol. 70, 7378–7387. doi: 10.1128/AEM.70.12.7378-7387.2004

Tung, H. C., Bramall, N. E., and Price, P. B. (2005). Microbial origin of excess methane in glacial ice and implications for life on Mars. *Proc. Natl. Acad. Sci. U S A.* 102, 18292–18296. doi: 10.1073/pnas.0507601102

Tung, H. C., Price, P. B., Bramall, N. E., and Vrdoljak, G. (2006). Microorganisms metabolizing on clay grains in 3-km-deep Greenland basal ice. *Astrobiology* 6, 69–86. doi: 10.1089/ast.2006.6.69

Twing, K. I., Brazelton, W. J., Kubo, M. D., Hyer, A. J., Cardace, D., Hoehler, T. M., et al. (2017). Serpentinization-Influenced groundwater harbors extremely low diversity microbial communities adapted to high pH. *Front. Microbiol.* 8:308. doi: 10.3389/fmicb.2017.00308

Vaïtilingom, M., Deguillaume, L., Vinatier, V., Sancelme, M., Amato, P., Chaumerliac, N., et al. (2013). Potential impact of microbial activity on the oxidant capacity and organic carbon budget in clouds. *Proc. Natl. Acad. Sci. U S A.* 110, 559–564. doi: 10.1073/pnas.1205743110

Wainwright, M., Wickramasinghe, N., Narlikar, J., and Rajaratnam, P. (2004). Microorganisms cultured from stratospheric air samples obtained at 41 km. *FEMS Microbiol. Lett.* 218, 161–165. doi: 10.1111/j.1574-6968.2003.tb11513.x

Wanger, G., Southam, G., and Onstott, T. C. (2006). Structural and chemical characterization of a natural fracture surface from 2.8 kilometers below land surface: biofilms in the deep subsurface. *Geomicrobiol. J.* 23, 443–452. doi: 10.1080/01490450600875746

Ward, J. A., Slater, G. F., Moser, D. P., Lin, L.-H., Lacrampe-Couloume, G., Bonin, A. S., et al. (2004). Microbial hydrocarbon gasses in the Witwatersrand Basin, South Africa: implications for the deep biosphere. *Geochim. Cosmochimica Acta* 68, 3239–3250. doi: 10.1016/j.gca.2004.02.020

Woycheese, K. M., Meyer-Dombard, D. R., Cardace, D., Argayosa, A. M., and Arcilla, C. A. (2015). Out of the dark: transitional subsurface-to-surface microbial diversity in a terrestrial serpentinizing seep (Manleluag, Pangasinan, the Philippines). *Front. Microbiol.* 6:44. doi: 10.3389/fmicb.2015.00044

Wu, X., Holmfeldt, K., Hubalek, V., Lundin, D., Åström, M., Bertilsson, S., et al. (2016). Microbial metagenomes from three aquifers in the Fennoscandian shield terrestrial deep biosphere reveal metabolic partitioning among populations. *ISME J.* 10, 1192–1203. doi: 10.1038/ismej.2015.185

Zhang, G., Dong, H., Xu, Z., Zhao, D., and Zhang, C. (2005). Microbial diversity in ultra-high-pressure rocks and fluids from the chinese continental scientific drilling project in China. *Appl. Environ. Microbiol.* 71, 3213–3227. doi: 10.1128/AEM.71.6.3213-3227.2005

Zhong, Z.-P., Solonenko, N. E., Gazituìa, M. C., Kenny, D. V., Mosley-Thompson, E., Rich, V. I., et al. (2018). Clean low-biomass procedures and their application to ancient ice core microorganisms. *Front. Microbiol.* 9:1094. doi: 10.3389/fmicb.2018.01094

Zhong, Z.-P., Tian, F., Roux, S., Gazitúa, M. C., Solonenko, N. E., Li, Y.-F., et al. (2021). Glacier ice archives nearly 15,000-year-old microbes and phages. *Microbiome* 9:160. doi: 10.1186/s40168-021-01106-w

Conflict of Interest: The authors declare that the research was conducted in the absence of any commercial or financial relationships that could be construed as a potential conflict of interest.

Publisher's Note: All claims expressed in this article are solely those of the authors and do not necessarily represent those of their affiliated organizations, or those of the publisher, the editors and the reviewers. Any product that may be evaluated in this article, or claim that may be made by its manufacturer, is not guaranteed or endorsed by the publisher.

frontiers | Frontiers in Microbiology

ORIGINAL RESEARCH
published: 06 July 2022
doi: 10.3389/fmicb.2022.881873

Multiple Adaptive Strategies of Himalayan *Iodobacter* sp. PCH194 to High-Altitude Stresses

Vijay Kumar[1†], *Prakriti Kashyap*[1†], *Subhash Kumar*[1,2], *Vikas Thakur*[1,2], *Sanjay Kumar*[1] *and Dharam Singh*[1,2*]

[1] *Biotechnology Division, CSIR-Institute of Himalayan Bioresource Technology, Palampur, India,* [2] *Academy of Scientific and Innovative Research (AcSIR), CSIR–Human Resource Development Centre (CSIR-HRDC), Ghaziabad, India*

Bacterial adaption to the multiple stressed environments of high-altitude niches in the Himalayas is intriguing and is of considerable interest to biotechnologists. Previously, we studied the culturable and unculturable metagenome microbial diversity from glacial and kettle lakes in the Western Himalayas. In this study, we explored the adaptive strategies of a unique Himalayan eurypsychrophile *Iodobacter* sp. PCH194, which can synthesize polyhydroxybutyrate (PHB) and violacein pigment. Whole-genome sequencing and analysis of *Iodobacter* sp. PCH194 (4.58 Mb chromosome and three plasmids) revealed genetic traits associated with adaptive strategies for cold/freeze, nutritional fluctuation, defense against UV, acidic pH, and the kettle lake's competitive environment. Differential proteome analysis suggested the adaptive role of chaperones, ribonucleases, secretion systems, and antifreeze proteins under cold stress. Antifreeze activity inhibiting the ice recrystallization at −9°C demonstrated the bacterium's survival at subzero temperature. The bacterium stores carbon in the form of PHB under stress conditions responding to nutritional fluctuations. However, violacein pigment protects the cells from UV radiation. Concisely, genomic, proteomic, and physiological studies revealed the multiple adaptive strategies of Himalayan *Iodobacter* to survive the high-altitude stresses.

Keywords: high-altitude Himalaya, bacterial adaptation, genomic traits, proteomic response, antifreeze proteins, polyhydroxybutyrate

OPEN ACCESS

Edited by:
Andreas Teske, University of North Carolina at Chapel Hill, United States

Reviewed by:
Grégoire Michoud, Swiss Federal Institute of Technology Lausanne, Switzerland
Salma Mukhtar, Connecticut Agricultural Experiment Station, United States

***Correspondence:**
Dharam Singh
dharamsingh@ihbt.res.in;
dharams14@gmail.com

[†] *These authors have contributed equally to this work*

Specialty section:
This article was submitted to Extreme Microbiology, a section of the journal Frontiers in Microbiology

Received: *23 February 2022*
Accepted: *01 June 2022*
Published: *06 July 2022*

Citation:
Kumar V, Kashyap P, Kumar S, Thakur V, Kumar S and Singh D (2022) Multiple Adaptive Strategies of Himalayan Iodobacter sp. PCH194 to High-Altitude Stresses. Front. Microbiol. 13:881873. doi: 10.3389/fmicb.2022.881873

INTRODUCTION

The Himalayas host a range of environmental niches such as permafrost, glacial streams, lakes, sediments, meadows, and deserts that contain distinct microbial communities (Stres et al., 2013; Kumar et al., 2018, 2019, 2022; Thakur et al., 2018; Dhakar and Pandey, 2020). High-altitude Himalayan environments are characterized by multiple stress factors such as high UV irradiation, oxidative stress, frequent freeze-thaw cycles, desiccation, oxygen limitation, nutritional fluctuation, and perennially cold temperatures (Singh and Singh, 2004; Stres et al., 2013). Microbes thriving in permanently cold environments have evolved many adaptive strategies at the molecular and physiological levels (Mykytczuk et al., 2013; De Maayer et al., 2014; Goordial et al., 2016; Kumar et al., 2020a). Thus, the microbes thriving in high-altitude Himalayan niches provide an interesting model system to study microbial adaptation strategies in response to the fluctuating environment.

Global warming has led to the rapid meltdown and receding of Himalayan glaciers (Bolch et al., 2012; Maurer et al., 2019), resulting in new environmental niches that provide opportunities

to study their microbial ecology (Hotaling et al., 2017). Glacial meltdown forms many enclosed depressions in a geographic area called kettle holes or kettle lakes (Corti et al., 2012). In fact, kettle lakes are exposed to frequent changes in physicochemical factors such as thermal, hydrodynamics, and nutrients (Reverey et al., 2018). Hence, such niches are a goldmine for studying biogeochemical cycles (Reverey et al., 2016, 2018), distinct microbial communities (Kumar et al., 2022), and commercially important bacteria (Kumar et al., 2021).

A recent glacial retreat has created a kettle lake at 4,200 m above sea level in the Sach Pass area of the Western Himalayas (Himachal Pradesh, India). The kettle lake is exposed to daily and seasonal fluctuations in thermal, hydrological, nutritional, and other physicochemical factors. The eurypsychrophilic bacterial strain *Iodobacter* sp. PCH194, which coproduces PHB and violacein pigment, was isolated from a sediment sample of this lake (Kumar et al., 2021). The genus *Iodobacter* is a minor member of microbial communities inhabiting rivers, streams, and low-temperature niches such as Arctic glacial lake sediment and the Antarctic Peninsula (Logan, 1989; Leblanc et al., 2009; Su et al., 2013; Atalah et al., 2020). *Iodobacter* and other violacein-producing bacteria are distinct in cold-water bodies and glacial environments. There are reports on violacein-producing bacteria from cold niches, studying the adaptive and ecological function of violacein pigment (Matz et al., 2004; Pantanella et al., 2007; Deines et al., 2009; Abboud and Arment, 2013; Mojib et al., 2013; Atalah et al., 2020). However, the unique features displayed by Himalayan *Iodobacter*, such as coproducing PHB and violacein and surviving in the freezing environment of high-altitude kettle lake, intrigue to explore its survival strategies.

This study investigated the adaptive strategies of Himalayan *Iodobacter* sp. PCH194 using genomic, proteomic, and physiological approaches. The bacterium possesses multiple genomic traits to cope with cold and freezing conditions, oxygen depletion, oxidative stress, starvation, acidic pH, and high UV irradiance in its high-altitude niche. Differential proteome and antifreeze activity analysis provides insight into a bacterial response to cold and freezing. In addition, physiological experiments demonstrated polyhydroxyalkanoate synthesis and violacein pigment-containing microbial mat formation as a key survival strategy. Our findings identify the multiple adaptive strategies of *Iodobacter* sp. PCH194 enable it to survive in the kettle lake environment of the high-altitude Himalaya.

MATERIALS AND METHODS

Phenotypic and Biochemical Characterization of *Iodobacter* sp. PCH194

Iodobacter sp. PCH194, isolated previously from high-altitude kettle lake sediment (Kumar et al., 2021), was used for the study. The pure culture was submitted in patent deposit to the Microbial Type Culture Collection (MTCC number 25171) at CSIR-IMTECH, Chandigarh, India. The colony morphology of the bacterium was observed after 72 h of agar plate incubation at 20°C on the Antarctic bacterial medium (AMB) (0.5% peptone, 0.2% yeast extract, and 2.0% agar). The carbohydrate and sugar utilization tests and catalase, oxidase, and nitrite reduction activity assays were performed using HiMedia kits (HiMedia, Mumbai, India).

Whole-Genome Sequencing and Genomic Insights of *Iodobacter* sp. PCH194

Genomic DNA isolation and library construction for *Iodobacter* sp. PCH194 were performed as described previously (Kumar et al., 2020a). The genomic library was evaluated using Qubit 2.0 (Invitrogen, Carlsbad, California, USA) and Bioanalyser (Agilent Technologies, Santa Clara, California, USA). Whole-genome sequencing (WGS) was carried out using the PacBio RSII system (PacBio, Menlo Park, California, USA), and genome assembly was performed using the RS Hierarchical Genome Assembly Process (HGAP) protocol version 3.0 (Chin et al., 2013). The complete genome sequence was submitted to the NCBI database with genome assembly accession number GCA_004194535.1, BioSample ID SAMN08324479, and BioProject ID PRJNA428922. Genome annotation was performed using Rapid Annotation and Subsystem Technology (RAST) (Aziz et al., 2008) and Prokaryotic Genome Annotation Pipeline (PGAP) version 3.1 (Tatusova et al., 2016). DNA-DNA hybridization (DDH) and average nucleotide identity (ANI) analyses were performed using online tools, *viz.,* Genome-to-Genome Distance Calculator (GGDC) (http://ggdc.dsmz.de/) (Meier-Kolthoff et al., 2013) and ANI calculator of Kostas lab (http://enve-omics.ce.gatech.edu/ani/) (Goris et al., 2007), respectively. Phylogenetic trees for the members of the genus *Iodobacter* were constructed based upon the available whole-genome sequences in the NCBI genome database. A phylogenetic tree was constructed using Type (Strain) Genome Server (TYGS) (https://tygs.dsmz.de/) by manually restricting the job to the input sequences (Meier-Kolthoff and Göker, 2019). Genes associated with adaptive traits such as carbon storage, respiration, chemotaxis, cold stress and oxidative stress response, acidic pH adaptation, defense against UV, and interspecies competition were mined by analyzing subsystem categories in RAST and NCBI PGAP files (Aziz et al., 2008; Tatusova et al., 2016).

Growth of *Iodobacter* sp. PCH194 at low Temperatures

Growth of *Iodobacter* sp. PCH194 was monitored in nutrient broth medium (g/l; meat extract 1.0, peptone 5.0, yeast extract 2.0, NaCl 5.0) at a temperature range of −5 to 37°C by observing the OD_{600} and OD_{460}. The specific growth rate (μ) of the bacterium was calculated in a static condition at temperatures of 0, 4, and 20°C and in a shaking condition at 20°C.

Proteomic Analysis of *Iodobacter* sp. PCH194 Growing at Different Temperatures

The bacterium culture was inoculated in nutrient broth and incubated at 20°C to prepare a seed culture of 1.0 OD_{460}. Seed culture (1.0%, v/v) was transferred to the same medium and incubated at temperatures of 20, 10, and 4°C. After 3 days of cold acclimation at 4°C (OD_{460} 0.567), the culture was transferred to 0°C and the growth was monitored. To further

evaluate the adaptive changes, a differential proteome study was performed.

Protein Extraction and In-Gel Digestion and MALDI-TOF-TOF Identification

Iodobacter sp. PCH194 was grown at 0, 4, and 20°C, and the culture was centrifuged at 9,600 *g* for 10 min to obtain the pellet. The bacterial pellet was resuspended in 10 mM Tris-HCl, pH 8.0, and total protein was extracted by sonicating the bacterial pellet. The protein was quantified using the Bradford assay with a standard curve of BSA at various concentrations. An equal amount of protein was loaded onto the 10% SDS PAGE to visualize differentially expressed proteins. The differentially expressed polypeptides from SDS-PAGE were excised, washed in deionized water, and destained in 100 mM NH_4HCO_3/50% acetonitrile for 15 min at room temperature (RT). Polypeptides were reduced with 10 mM dithiothreitol and alkylated with 55 mM iodoacetamide. The resulting alkylated polypeptides were dehydrated using acetonitrile followed by overnight digestion with a freshly prepared trypsin solution (25 mM NH_4HCO_3 with 5 ng/μl of trypsin, Sigma, USA) at 37°C. Trypsin was inactivated by incubating peptide samples in 0.1% formic acid (1.0 μl) for 40 min at 37°C. The digested peptides were extracted using extraction buffer (50% trifluoroacetic acid/50% acetonitrile) in an ultrasonic water bath at RT. Extracted peptides were mixed with MALDI matrix (0.5 μl) α-cyano-4-hydroxycinnamic acid (20 mg/ml) in 0.1% trifluoroacetic/30% (v/v) acetonitrile (1:2) and dried at RT followed by mass spectrometric analysis by MALDI-TOF/TOF-MS/MS using an UltrafleXtremeTM mass spectrometer (Bruker Daltonics Inc., Billerica, Massachusetts, USA). The instrument was set in positive ionization mode and was previously calibrated with a mass standard starter kit and standard tryptic BSA digest (Bruker). Proteins were identified using Mascot Software version 3.5 (https://matrixxscience.com) (Matrix Science, London, UK) at 1.2 Da MS/MS mass tolerance, in which SwissProt database was searched among Proteobacteria and one missed cleavage was allowed. Oxidation of methionine and carbamidomethylation of cysteine were considered variable and fixed modifications, respectively. Proteins identified from Mascot were functionally annotated by the UniProt database (https://www.uniprot.org).

Label-Free Quantification

Label-free relative quantification was performed according to the method described by Sharma et al. (2014) to identify and analyze the differentially expressed proteins at a low temperature. The total protein of *Iodobacter* sp. grown at different temperatures was quantified by the Bradford method. Total protein (200 μg) from each sample was lyophilized and resuspended in 100 μl of ammonium bicarbonate (100 mM). Protein suspension was reduced with 10 mM dithiothreitol and alkylated with iodoacetamide (55 mM), followed by trypsinization (Promega, Madison, Wisconsin, USA) for 12–16 h at 37°C. Trypsin was inactivated by incubating the sample with 0.1% formic acid (1 μl) for 40 min at 37°C. Digested peptides thus obtained were lyophilized and dissolved in 0.1% formic acid. The resuspended sample (10 μl) was loaded on an Advance Bio Peptide column (2.1, 100 mm, 2.7 μm) (Agilent Technologies, Santa Clara, California, USA) equilibrated with 0.1% (v/v) formic acid (Solvent A) for 3 min with a flow rate of 5 μl/min. For peptide separation, a linear gradient starting from 5 to 45% of solvent B (0.1%, v/v) formic acid (in acetonitrile) for 75 min was employed. Three replicates per sample were used for all data acquisition using 6550 UHPLC-Q-TOF-IMS (Agilent Technologies, Santa Clara, California, USA). The following parameters were set in the acquisition mode; MS minimum range (m/z): 50, MS maximum range (m/z): 1,700, and MS and MS/MS scan rate (spectra/sec): 3. The following parameters were fixed in precursor selection; maximum precursor selection per cycle: 3, threshold (absolute): 5,000, threshold (relative %): 0.010, and target (counts/spectrum): 25,000. The instrument was set in positive ionization mode. For protein identification by Spectrum Mill software (Agilent Technologies, Santa Clara, USA), the following search parameters were used; NCBI database (version 2010_09), having 16,365 protein sequences; fixed modification was carbamidomethylation; N-terminal acetylation, N and Q deamidation, and M oxidation, as variable modifications; missed cleavage: 1 and fragment error tolerance: 0.5 Da. Accession numbers retrieved from Spectrum Mill software were annotated using NCBI. The proteins identified using label-free quantification and MALDI-TOF/TOF-MS/MS were analyzed with BLAST2GO analysis and the UniProt database, and the matched protein GIs were functionally categorized.

Ice Recrystallization Inhibition Activity

The IRI activity of lysate was analyzed using a splat assay following Knight and Duman (1986), with slight modifications as mentioned by Kashyap et al. (2020). Total protein (1.0 mg/ml) in 30% sucrose was sandwiched in two coverslips and was flash-frozen at −20°C. It was allowed to recrystallize at −9°C for 40 min using a nanolitre osmometer (Otago Instruments, Dunedin, New Zealand). The growth of ice crystals was monitored under an upright Eclipse Ci Microscope (Nikon, Tokyo, Japan) at 10X resolution. BSA (2.0 mg/ml) was used as a negative control. Heat denaturation of crude lysate at 100°C for 10 min was performed to confirm that the activity was because of the protein content. The area of crystals was quantified using ImageJ software.

PHA Production Under Different Physiological Conditions

In the PHA production medium, PHA production by *Iodobacter* sp. PCH194 was assessed (g/l; K_2HPO_4 6.0, KH_2PO_4 3.0, NH_4Cl 0.5, NaCl 1.0, and 1.0 mM $MgSO_4$, 0.1 mM $CaCl_2$) under different environmental conditions, *viz.,* temperature, aeration, and pH. The bacterium was also tested to synthesize PHA at varying nutritional conditions of carbon to nitrogen ratio from 0.2 to 60 (where NH_4Cl concentration was kept constant at 0.05% and glucose concentration varied accordingly). Biomass and PHA production were quantified as described by us in earlier studies (Kumar et al., 2018, 2020a).

Morphology and Anatomy of *Iodobacter* sp. PCH194

The cell morphology of bacterial cells from the late log phase was examined using TEM analysis using JEOL JEM-1010 (JEOL, Akishima, Japan). The PHA granules formation by bacterial isolate was analyzed as per the methods described by Sandoval et al. (2007) with slight modification. The bacterial cells were grown to stationary phase in 2.0% glucose and harvested at 2,400 *g*, washed three times with phosphate buffer saline, and fixed by glutaraldehyde solution (2.0%, v/v) at 4°C. Samples were washed three times with PBS buffer and fixed with 1.0% osmium tetroxide for 60 min in the dark. The washing step was repeated, stained in blocks with uranyl acetate (30%), and embedded slowly in Embed 812 epoxy resin (Electron Microscopy Sciences, Hatfield, Pennsylvania, USA). Polymerization of blocks was carried out in an oven at 50°C for 72 h. Ultrathin sections of the samples were cut using an ultramicrotome, and further grids were prepared. Structural studies were performed with an FEI Technai G2200kV transmission electron microscope (FEI, Hillsboro, Oregon, USA).

Synthesis of Violacein Pigment by *Iodobacter* sp. PCH194 and Its UV Protective Role

Violacein was produced by *Iodobacter* sp. PCH194 growing in glucose and tryptone medium, and extracted as described by Kumar et al. (2021). For analyzing the protective role of violacein pigment against UV, the cells of *Iodobacter* sp. PCH194 were drawn at a different time interval at the initial log phase (when cells are non-pigmented), late log phase, and stationary phase (when cells produce pigments), washed in normal saline and diluted to 1.0 OD_{600}. Different dilutions were spread on a nutrient agar plate and treated with 302 nm UV radiation (UV B_{302}) from a distance of 1.4 feet by using UV torch (Analytik Jena, California, USA) for 1, 2, and 3 min. The dose of UV-B was 0.32 $Js^{-1}cm^{-2}$ (320 $mWcm^{-2}$) as measured by a UV light meter (Model UV340A, Lutron Electronic, Pennsylvania, USA). UV-untreated plates from each growth phase served as controls. Non-pigmented cells of *Iodobacter* sp. PCH194 were harvested after 16 h of growth, amended with methanol-extracted violacein pigment (100 μg/ml), and compared to non-pigmented cells without violacein in a UV exposure experiment as described. All plates were further incubated at 20°C for 2–3 days, and the number of colonies was counted and recorded as log cfu/ml. The significance of the experiment was determined by the *t*-test, and the level of significance was expressed as *P*-value at $^{*}\leq 0.05$, $^{**}\leq 0.01$, and $^{***}\leq 0.001$.

RESULTS

Sampling Site and Bacterium Description

The Bhoot ground lake at Sach Pass (Pangi Valley, Himachal Pradesh, India) is a shallow kettle lake formed due to the glacier retreat and remains frozen for almost half of the year (**Figure 1A**). The lake water temperature, pH, and UV radiation were 4°C, 4.5, and 50 $mWcm^{-2}$, respectively; measured at the site during the sampling (18 November 2016). Available N, P, K (kg/Ha), electrical conductivity (μS/cm), and pH of dried mud vary from 65.86 to 194.9, 11.68 to 25.76, 68.26 to 162.13, 88 to 95, and 4.1 to 4.26, respectively (**Supplementary Table 1**). The isolated bacterium *Iodobacter* sp. PCH194 forms violet-pigmented colonies (**Figure 1B**). The cells were found to be in straight round-ended rods, Gram-negative, facultative anaerobes, oxidase and catalase-positive, and glucose-fermenting. The bacterium can grow at −5 to 25°C, with optimum growth at 20°C (**Supplementary Table 2**).

General Description of the Genome and Phylogenomic Analysis

Whole-genome sequencing of *Iodobacter* sp. PCH194 has resulted in a single high-quality contig of a 4.44 Mb chromosome and three sizes of 76.7, 57.4, and 12.3 kb plasmids. The NCBI predicted 4,165 genes, 3,950 proteins, 31 rRNA, 76 tRNA, 04 ncRNAs, and 104 pseudogenes (**Table 1**). The phylogenomic analysis of *Iodobacter* sp. PCH194 with reference strains *I. fluviatilis* DSM 3764 and *I. fluviatilis* NCTC11159 showed a low value of ANI (80.81%) and DDH (25.90% and 26.40%). Similarly, other strains of *Iodobacter*, i.e., BJB302, H11R3, and HSC-16F04, also showed a low percentage in ANI and DDH analysis (**Supplementary Table 3**). The phylogenetic tree was constructed using the TYGS server based on the available whole-genome sequences in the NCBI database. *Iodobacter* sp. PCH194 showed a separate and distinct clade compared to the rest of the *Iodobacter* spp. (**Figure 1C**). The low ANI (79.99–80.81), DDH (25.70–26.40) score, and phylogenetic analysis of strain PCH194 clearly describe it as a putative novel species of the genus *Iodobacter*.

Genomic Insights for Adaptive Strategies of *Iodobacter* sp. PCH194

Genomic analysis of *Iodobacter* sp. PCH194 revealed multiple genes/proteins for stress adaptation (**Table 2**). The adaptive genomic traits are described in detail in the following subheads and are tabled in **Supplementary Data Set 1**.

Starvation and Storage of Carbon

The genome of *Iodobacter* sp. PCH194 showed the presence of key genes involved in nutritional starvation, viz., carbon sensing and downstream response mechanisms such as carbon starvation protein A (*cstA*), sigma factor (*rpoS*), stringent starvation proteins A and B (*sspAB*), bifunctional ppGpp synthetase, Clp proteases (*clpA,B,S,X,P*), and phosphate starvation-inducible protein (*psiF*). The genes for polyhydroxyalkanoate (PHA) synthesis, namely, polyhydroxyalkanoate synthase (*phaC*) and acetyl-3-hydroxybutyryl-CoA dehydrogenase (*phaB*), were found in two copies each, while acetyl-CoA-acyltransferase or thiolase (*phaA*) was found in a single copy. Additionally, one copy of PHA depolymerase (*phaZ*) and PHA regulatory

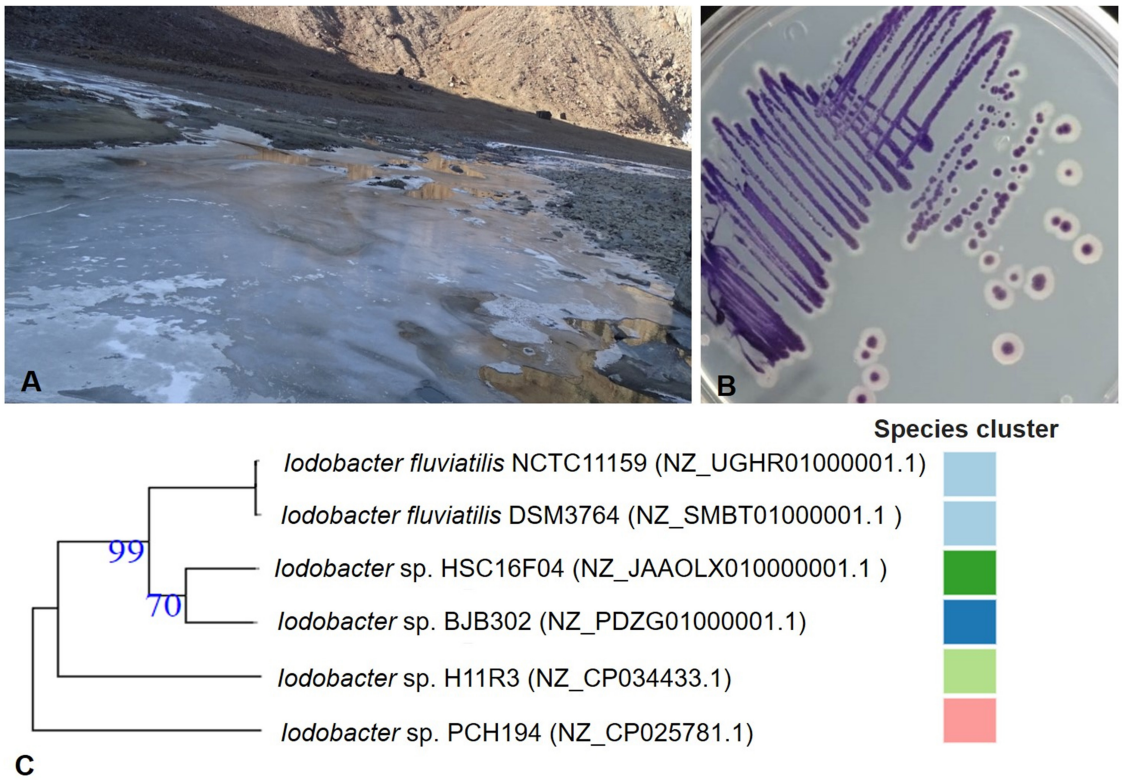

FIGURE 1 | Sampling site and Himalayan bacterium *Iodobacter* sp. PCH194. **(A)** A view of partially frozen kettle lake (Picture was taken on 18 November 2016) at an altitude of 4,160 masl and geographical coordinates of 33.006831°N, 76.248209°E at Sach Pass area in Chamba district of Himachal Pradesh, India, **(B)** isolated single colonies of *Iodobacter* sp. PCH194, and **(C)** a phylogenetic tree for genus *Iodobacter* based on the available whole-genome sequences. The number in parenthesis is the NCBI reference number for the respective genome assembly, and the color code represents the species cluster, where different colors represent the different species. The tree was constructed using an online TYGS server.

TABLE 1 | Genomic features of *Iodobacter* sp. PCH194.

Attributes	Value				
	Genome	**Chromosome**	**Plasmid 1**	**Plasmid 2**	**Plasmid 3**
RefSeq	–	NZ_CP025781.1	NZ_CP025783.1	NZ_CP025782.1	NZ_CP025784.1
Genome size (bases)	4,588,033	4,441,511	76,766	57,428	12,328
GC content (%)	47.50	47.50	50.36	40.90	51.21
Proteins	3,950	3,797	67	70	16
rRNAs	31	31	0	0	0
tRNAs	76	76	0	0	0
other RNAs	04	04	0	0	0
Genes	4,165	4,006	72	71	16
Pseudogenes	104	98	05	01	0

gene (*phaR*), two genes encoding for phasin family protein, and three copies of enoyl CoA (*fadB* or *phaJ*) were also present.

Respiration

The genomic insights revealed the presence of genes for various high-affinity terminal oxidases, *viz.*, cytochrome cbb_3 and cytochrome *bd*, and an operon of NADH-quinone oxidoreductase (*nuoABCEFGHIJKLMN*). The genome analysis also showed various genes encoding for fumarate/nitrate reduction transcriptional regulator Fnr (*fnr*), two-component system response regulator NarL (*narL*), and various reductases such as periplasmic nitrate reductase (*napABCF*), fumarate reductase (*frdABCD*), and arsenate reductase (*arsBCJ*).

TABLE 2 | Adaptive genomic traits of *Iodobacter* sp. PCH194. Adaptive strategies to stress conditions and related genes/proteins are tabulated along with their putative physiological and ecological functions.

Stress conditions	Adaptation strategies	Genes/proteins for adaptative strategies	Physiological functions
Low temperature	Cold stress response	*dnaJK, groES, groEL, hscAB, surA, hslO, clpB, betIAB* adhesins, AFP	Growth at low temperature, protection from freezing
Freezing	Antifreeze proteins		
Oxidative stress	Oxidative stress response	Superoxide dismutase, catalase, peroxidases, thioredoxin, peroxiredoxin	Prevention and detoxification from oxidative damage
Nutritional fluctuation and starvation	Chemotaxis and flagellar motility	*cheA,W,R,Y,D motABCD, flaABH, fliMNOPQRS, fliEFGI, flgBCDEFGHIJKL*	Sensing the nutrition and movement
	Starvation response proteins	ppGpp synthetase, *clpXP, psiF*	Starvation sensing, signaling and response
	Carbon storage	*phaC*, *phaB*, *phaA*, *phaR*, *phaZ*, *phaJ*, phasin protein	Carbon storage and energy reservoir
Low oxygen	Harvesting low oxygen and facultative anaerobic respiration	High affinity terminal oxidases (Cbb_3 and *bd*) *fnr, napABCF, frdABCD, arsBC J*	Respiration in low O_2 or anaerobic condition
UV irradiance	DNA repair, violacein production	*UvrABC,* photolyase *vioABCDE*	UV protection and tolerance
Predation and competitive stress	Biofilm and violacein pigment synthesis	*luxS, Q*, Enzymes of GT family, *vioABCDE*	Biofilm formation, antimicrobial and anti-predatory
Acidic pH	Efflux pump, Na^+/H^+ antiporters, amino acid dependent acid tolerance	*kdpFABC, nhaCR,* trkAD*, arcD*, ADI, OTC, CK, GAD	Removal, detoxification and consumption of H^+
Overall physio-chemical/environment stress	Toxin-antitoxin system, plasmids	Toxin-antitoxin system, genes for conjugation assembly proteins	Cell persistence, recombination, and adaptative role

Genomic Features for Cold, UV, Oxidative, and Osmotic Stress

NCBI annotation revealed genes for cold stress, i.e., cold-shock proteins, molecular chaperones, co-chaperone, chaperonin, fatty acid desaturase, and stress proteins. The genes encoding for the proteins involved in oxidative stress include superoxide dismutase, catalase, peroxiredoxin, thioredoxin, and various peroxidases, and the excinuclease repair system (*uvrABCD*) were also present in the genome. Additionally, genes encoding for choline ABC transporters and permease, betaine aldehyde dehydrogenase, and choline dehydrogenase involved in osmolyte glycine-betaine synthesis were present.

Violacein Biosynthesis and Biofilm Formation

A complete operon containing five genes, *vioABCDE* encoding enzymes involved in violacein pigment biosynthesis and quorum sensing regulatory genes (*luxS* and *luxQ*), was present in the genome. The bacterium possesses genes (*epsDEF GI*) for the biosynthesis of polysaccharides and export. Furthermore, the dbCAN meta server found genes encoding for 13 different glycosyltransferase (GT) family proteins in the genome.

Additional Adaptive Features

The genome of *Iodobacter* sp. PCH194 possesses key genes for chemotaxis (*cheA*, *D*, *W*, *R*, *Y*) and flagellar assembly (*motABCD*, *fliMNOPQRS*, *fliEFGI*, *flaABH*, *flgBCDEFGHIJKL*). The genome showed the presence of genes encoding for the cation-efflux pump, cation transporters and Na^+/H^+ (sodium:proton) antiporters, potassium channel protein, potassium transporter (Kup), and an operon *kdpFABC* encoding for the ATP-dependent potassium transporter system. The bacterium also possesses the genes encoding for the enzymes involved in amino acid-dependent acid tolerance, i.e., arginine-ornithine antiporter (ArcD), arginine deiminase (ADI), ornithine carbamoyltransferase (OTC) and carbamate kinase (CK), glutaminase, glutamate decarboxylase, lysine decarboxylase, and histidine decarboxylase. Apart from other mentioned strategies, the genome of *Iodobacter* sp. PCH194 possesses genes encoding for the toxin-antitoxin (TA) system on chromosomes and plasmid. Additionally, three plasmids possess various genes encoding for replication proteins, transposase, recombinase, replicase, mobilization protein, conjugal transfer protein TraA, and transcriptional regulators.

Proteomic Response of *Iodobacter* sp. PCH194 to Cold and Freezing Conditions

Growth Kinetics and General Proteome Response to Cold and Freeze

Iodobacter sp. PCH194 grew at a temperature ranging from −5 to 25°C, with optimum growth at 20°C. The growth rate (μ) of the bacterium calculated in NB medium (pH: 7.0) at

0, 4, and 20°C in static, and at 20°C with 150 rpm was 0.008, 0.038, 0.049, and 0.096 h^{-1}, respectively (**Figure 2A**). The bacterium under cold stress (at 4 and 0°C conditions) underwent proteome changes as visualized using SDS-PAGE (**Supplementary Figure 1**). A total of 19 differentially expressed polypeptides were observed and subjected to mass spectrometric identification using MALDI-TOF/TOF. After Mascot analysis, 68 upregulated and 17 downregulated protein targets were identified (**Supplementary Data Set 2**).

In contrast, the label-free proteomics data led to the quantitative identification of 558 proteins ($p < 0.05$), showing a ≥1.5-fold increase and ≤0.75 decrease in abundance upon cold/freeze stress (**Supplementary Data Set 3**). Based on the gel and gel-free approaches, 152 and 109 proteins were upregulated at 0 and 4°C, respectively, compared to 20°C (**Figure 2B).** Among all proteins that were upregulated at cold temperatures, 125 and 64 proteins were identified exclusively at 0 and 4°C, respectively. The bacterium also revealed downregulation of 252 and 263 proteins at 0 and 4°C, respectively (**Figure 2C**). These downregulated proteins include the majority of proteins expressed at 20°C. The gene ontology (GO) study of differently expressed proteins under cold (4°C) and freezing (0°C) conditions revealed upregulated and downregulated targets in the cellular component and biological process category (**Supplementary Figure 2**). Cellular components that were upregulated at 0°C as compared to 4°C included a higher number of membrane proteins and intrinsic components of membrane proteins. Other proteins belonging to these categories were found to be downregulated in both cold and freezing conditions. These results indicate an important role for membrane dynamics during freeze stress. The upregulated and downregulated protein targets were further functionally categorized using the UniProt database (**Figure 2D**, **Supplementary Data Set 4**). Upon cold stress, the bacterium showed differential regulation in cellular and metabolic processes such as nucleotide biosynthesis, transcription, translation, DNA recombination and repair, peptidoglycan, and fatty acid metabolism. Additionally, proteins involved in maintaining the structural and functional integrity of cells (cellular anatomical entity) and transmembrane transporters also exhibit different protein regulations during low temperatures. Since these categories show differential proteome responses, their functions in *Iodobacter* sp. PCH194 were further analyzed to reveal cold-adaptive strategies.

Differential Proteome Response for Important Functional Categories to Cold and Freeze

The proteome changes in *Iodobacter* sp. PCH194 in response to cold/freezing stress were functionally categorized (**Supplementary Table 4**). Cold and freeze stress cause misfolding of proteins. Therefore, chaperones and proteases play a crucial role during cold/freeze stress conditions. *Iodobacter* sp. PCH194 showed an abundance of molecular chaperones DnaJ and HscA at freezing temperatures. However, chaperone GroEL and co-chaperone GrpE exhibited a decreased abundance, while chaperone DnaK was slightly reduced during cold stress. Additionally, ATP-dependent Clp proteases were also found to be upregulated in both gel-based and gel-free studies during low-temperature stress. Cold/freeze stress-regulated not only chaperones and proteases but also RNA metabolism, mediated by cold shock proteins (CSPs) and ribonucleases (RNase). RNase E and RNase Z were found abundant at 0°C in *Iodobacter* sp. PCH194, whereas RNase II and RNase BN were not detected at low-temperature conditions.

Interestingly, the proteins of secretion system VI and IV families were found to be upregulated during cold/freeze stress. In addition, T4SS and T6SS, phage tail proteins closely resembling T6SS, were also upregulated at freezing temperature (0°C). Besides, the glycosyltransferase (family 1) protein that participated in biofilm formation was also upregulated during low temperatures. One of the strategies to survive under subzero temperatures is the production of antifreeze proteins such as adhesins. In *Iodobacter* sp. PCH194, adhesin was detected in all three temperatures, but its expression decreased during 4°C stress and then increased at 0°C. Furthermore, MafB adhesion was detected only at 0°C, indicating that it might also have a role as an antifreeze protein during freezing conditions.

Ice Recrystallization Inhibition Activity in *Iodobacter* sp. PCH194

Antifreeze activity in crude lysate proteins (1.0 mg/ml) of *Iodobacter* sp. PCH194 was validated by inhibition of ice recrystallization at −9°C, when *Iodobacter* sp. PCH194 lysate decreased the average area of ice crystals by a factor of 4 compared to BSA (1.0 mg/ml) as a negative control. Heat denaturation of the protein lysate resulted in the loss of the IRI activity and produced a 5-fold increase in the average area of ice crystals (**Figure 3**). The IRI activity in crude lysate indicated that antifreeze proteins are constitutively present in *Iodobacter* sp. PCH194.

Physiological Insights for Adaptive Strategies of *Iodobacter* sp. PCH194

Carbon Storage Under Different Physiological Conditions

Iodobacter sp. PCH194 showed the ability to synthesize PHB in different conditions of pH (4–10), temperature (4–25°C), varied carbon to nitrogen ratio, and in static as well as shaking conditions (**Figure 4**). The bacterium synthesizes 40–60% PHB to its dry cell mass in a wide range of carbon to nitrogen ratios of 0.2–60 (glucose and NH_4Cl as sole carbon and nitrogen sources). Though the growth is slow in the medium with a C/N ratio of 0.2, the bacterium can synthesize 40% of PHB to its dry cell mass. The TEM analysis of an ultrathin section of the stationary phase showed the formation of intercellular PHB granules.

Violacein Pigment Production and Formation of Biofilm

Physiological experiments showed that *Iodobacter* sp. PCH194 can grow and produce violacein pigment under static and shaking conditions in the NB medium. The cells adhered to the media's surface under static conditions and formed a violet-colored mat in 7–8 days of incubation at 4°C (**Figure 5A**). The bacterium also formed a violet-colored biofilm around cells under shaking

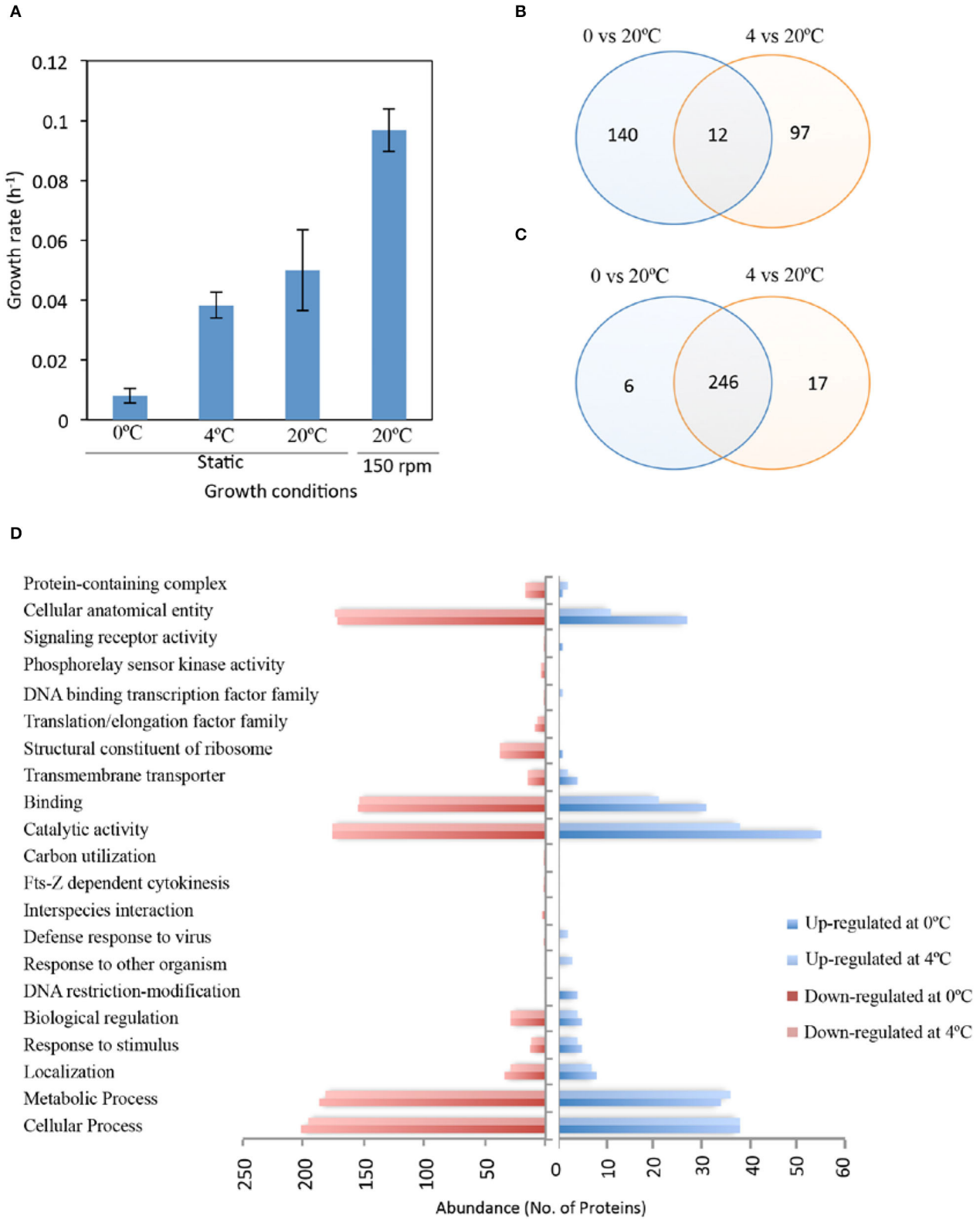

FIGURE 2 | Growth and proteomic response of *Iodobacter* sp. PCH194 in cold/freeze conditions. **(A)** Growth rate (OD_{460}) of *Iodobacter* sp. PCH194 at different temperatures in nutrient broth medium, **(B)** Venn diagram showing the total and shared number of upregulated, and **(C)** downregulated protein targets in response to cold (4°C) and freeze (0°C) compared to 20°C identified by gel-based and gel-free proteomics approaches, and **(D)** the abundance of upregulated and downregulated proteins with functional categorization by UniProt.

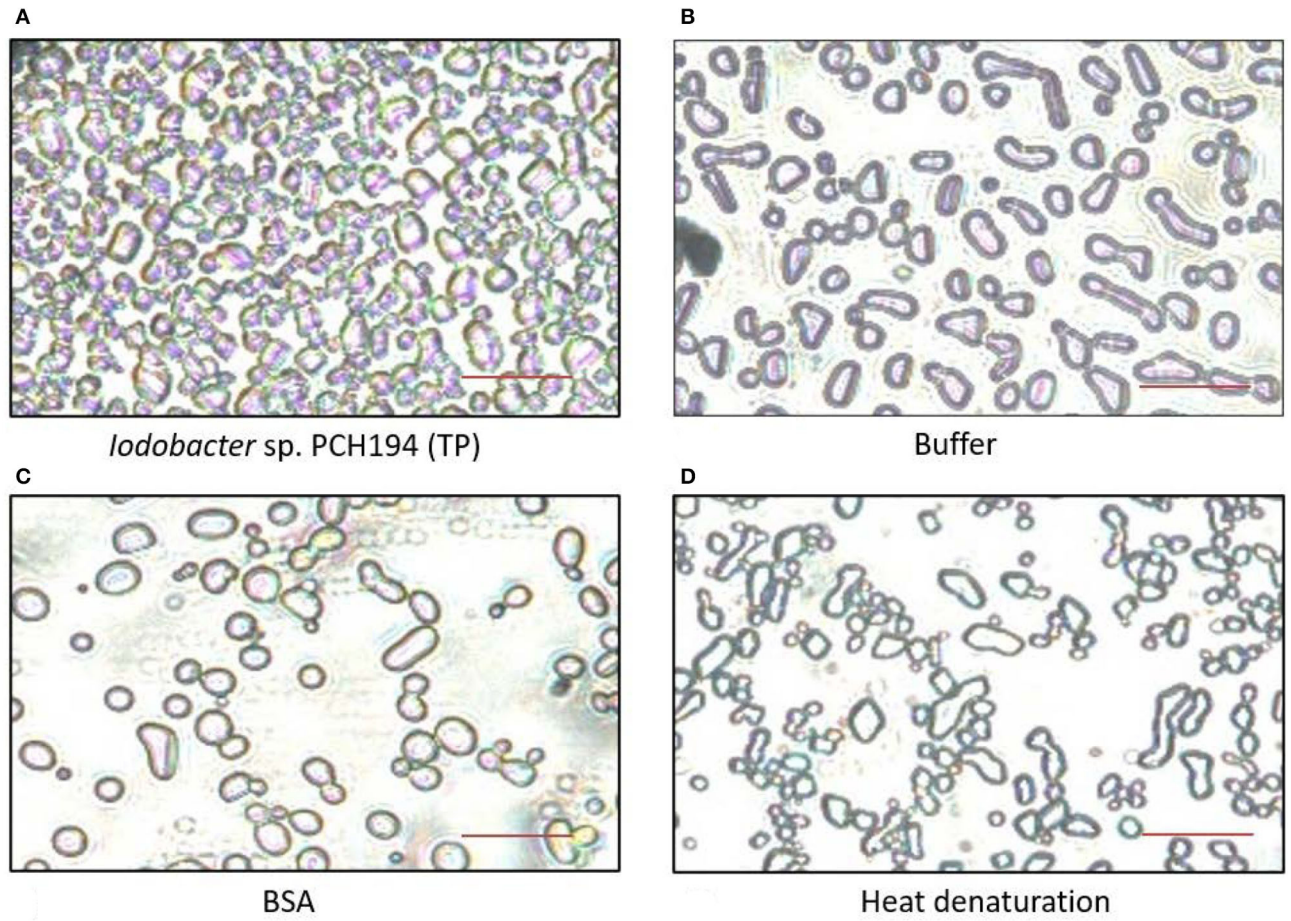

FIGURE 3 | Antifreeze activity exhibited by *Iodobacter* sp. PCH194. The ice recrystallization inhibition (IRI) was observed at −9°C after 40 min. **(A)** *Iodobacter* sp. PCH194 [total cell lysate protein (TP), 1.0 mg/ml] showed smaller ice crystals upon recrystallization in comparison to **(B)** buffer (20 mM Tris-HCl, pH 8.0), and **(C)** BSA (1.0 mg/ml) as a negative control, and **(D)** heat denaturation (at 100°C for 10 min) of *Iodobacter* sp. PCH194 (TP) resulted in the loss of activity. Scale bar = 200 μm.

conditions as well. The TEM analysis of stationary phase bacteria grown in NB at 20°C and 150 rpm showed intercellular PHB granules and a clear sheath-like structure around the cells (**Figures 5B,C**).

UV Protective Role of Violacein Pigment

The colonies of *Iodobacter* sp. PCH194 are violet pigmented, and they also produce violet pigment in a liquid medium. During undisturbed growth at 4°C, the bacterium produces a violet-colored mat at the medium's surface (**Figure 5A**). Violacein is likely to protect bacterial cells against UV irradiation at high altitudes. Therefore, to validate the role of violacein pigment against UV stress, the non-pigmented and pigmented cells of *Iodobacter* sp. PCH194 were subjected to a UVB irradiance of 320 $mWcm^{-2}$. The effect of UV irradiance on the bacterial cells from different growth stages showed that the pigmented cells have higher tolerance and survival under UV. Pigmented cells from the late log phase showed 21% higher survival at 1 and 2 min and 10% higher survival at 3 min of UV exposure. Similarly, pigmented cells from the stationary phase showed 13%, 7%, and 6% higher survival than the non-pigmented cells in 1, 2, and 3 min of UV exposure (**Figure 5D**). The violacein pigment treated (100 μg/ml) non-pigmented cells of *Iodobacter* sp. PCH194 showed better UV tolerance than untreated cells (**Figure 5E**).

DISCUSSION

This study unveiled multiple adaptive strategies of a unique Himalayan bacterium, *Iodobacter* sp. PCH194, ensuring its survival in high-altitude stresses (**Figure 6**). It also provides a complete genome sequence of Himalayan *Iodobacter* and highlights the adaptive traits in its genome. Furthermore, differential proteome response to cold and physiological experiments of antifreeze activity, PHB, and violacein synthesis supports its survival in the stress environment of high-altitude Himalayas. Additionally, the phylogenomic analysis suggested that *Iodobacter* sp. PCH194 is a putative novel bacterium in the genus *Iodobacter* with biotechnological importance. Herein, we

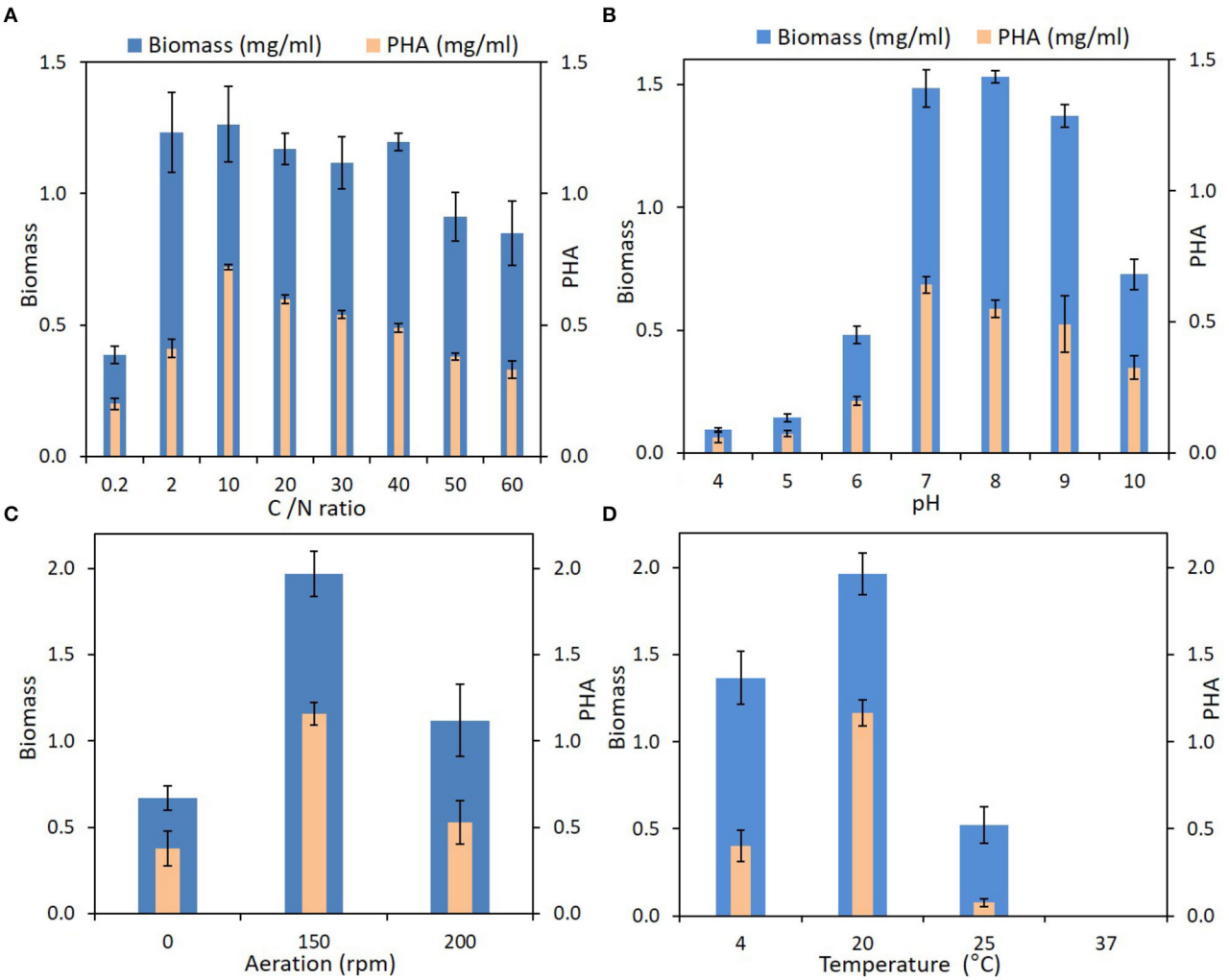

FIGURE 4 | PHA production by *Iodobacter* sp. PCH194 at different physicochemical and environmental conditions. **(A)** Carbon to nitrogen (g/g) ratio, **(B)** pH, **(C)** aeration, and **(D)** temperature.

discuss multiple adaptive strategies of *Iodobacter* sp. PCH194, supported by its genomic, proteomic, and physiological data.

Cold stress is one of the major environmental stresses in the high-altitude Himalayan lakes. *Iodobacter* sp. PCH194 showed adaptation to changes in temperature and can grow from subzero to 25°C. Wide temperature adaptability was supported by many genes encoding for cold/freeze and other stress adaptation functions. Previous studies also reported a high copy number of genes for general stress, cold shock, osmotic, and oxidative stress in bacteria from the Antarctic and Arctic cryo-environments (Mykytczuk et al., 2013; Goordial et al., 2016). In response to the cold, *Iodobacter* sp. PCH194 revealed a differential proteome expression. During cold stress, bacteria reduce cell growth, and there is a downshift in the efficiency of transcription and translational machinery with an increase in the Csps proteins (Polissi et al., 2003). The proteins that show the most significant changes upon cold stress have been known to be involved in nucleotide biosynthesis, translation processes, DNA recombination and repair, peptidoglycan, and fatty acid metabolism (De Maayer et al., 2014; Baraúna et al., 2017). Proteins regulating all these functions were differentially regulated in *Iodobacter* sp. PCH194 upon low-temperature stress. The roles of the proteins in these categories are well-established in many cold-loving bacteria, such as *Planococcus halocryophilus* (Mykytczuk et al., 2013), *Sphingopyxis alaskensis* (Ting et al., 2010), and *Psychrobacter* sp. (Koh et al., 2017).

Chaperones and proteases play an important role in the cold adaptation of bacteria. *Iodobacter* sp. PCH194 chaperone system responded to low-temperature stress by increasing the expression of DnaJ, while the expression of DnaK did not show much change. DnaJ is known to interact with unfolded proteins and prevent their aggregation (Han and Christen, 2004). Besides, it also acts as Hsp40 and interacts with Hsp70 heat shock proteins (Hennessy et al., 2005). An interesting observation during the cold stress response of *Iodobacter* sp. PCH194 was the abundance of RNase E and RNase Z at 0°C. Low-temperature

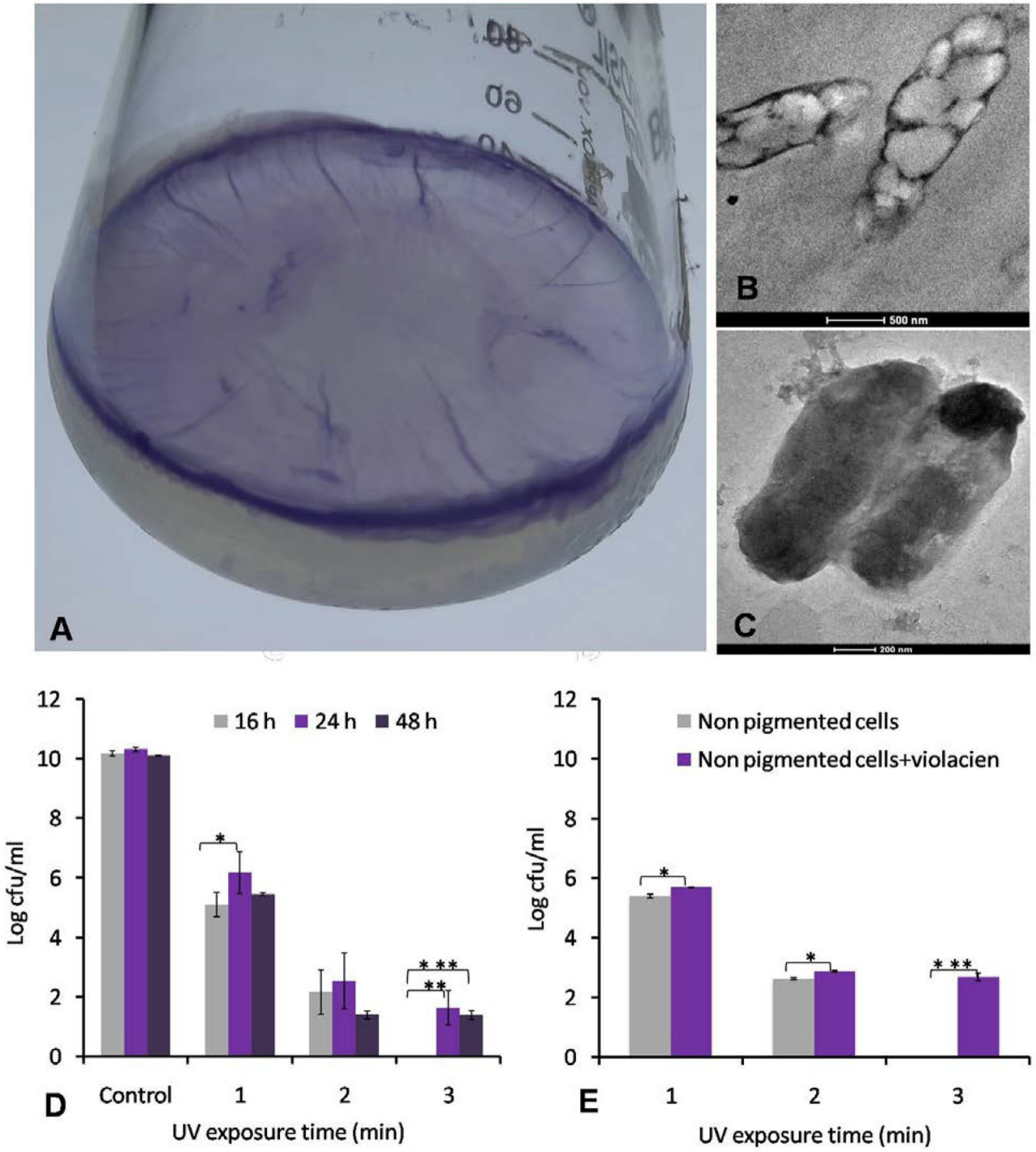

FIGURE 5 | Formation of violate biofilm by *Iodobacter* sp. PCH194 and UV protective role of violacein pigment. **(A)** Formation of violet-colored mat on the surface of medium when growing at 4°C under static conditions, **(B)** TEM image of ultrathin sections of cells showing the presence of PHA granules, **(C)** morphology of bacterial cells showing the presence of a sheath around the cell, **(D)** effect of UV irradiance to cells of *Iodobacter* sp. PCH194 harvested at different growth phases, *viz.*, non-pigmented cells of the initial log phase and pigmented cells of exponential log phase and stationary phase (expressing violacein pigment 43–50 and 41–45 μg/ml/OD_{460}), and **(E)** effect of violacein (100 μg/ml) addition to UV tolerance of non-pigmented cells. The level of significance was expressed as a *P*-value as *≤ 0.05, **≤0.01, and ***≤0.001.

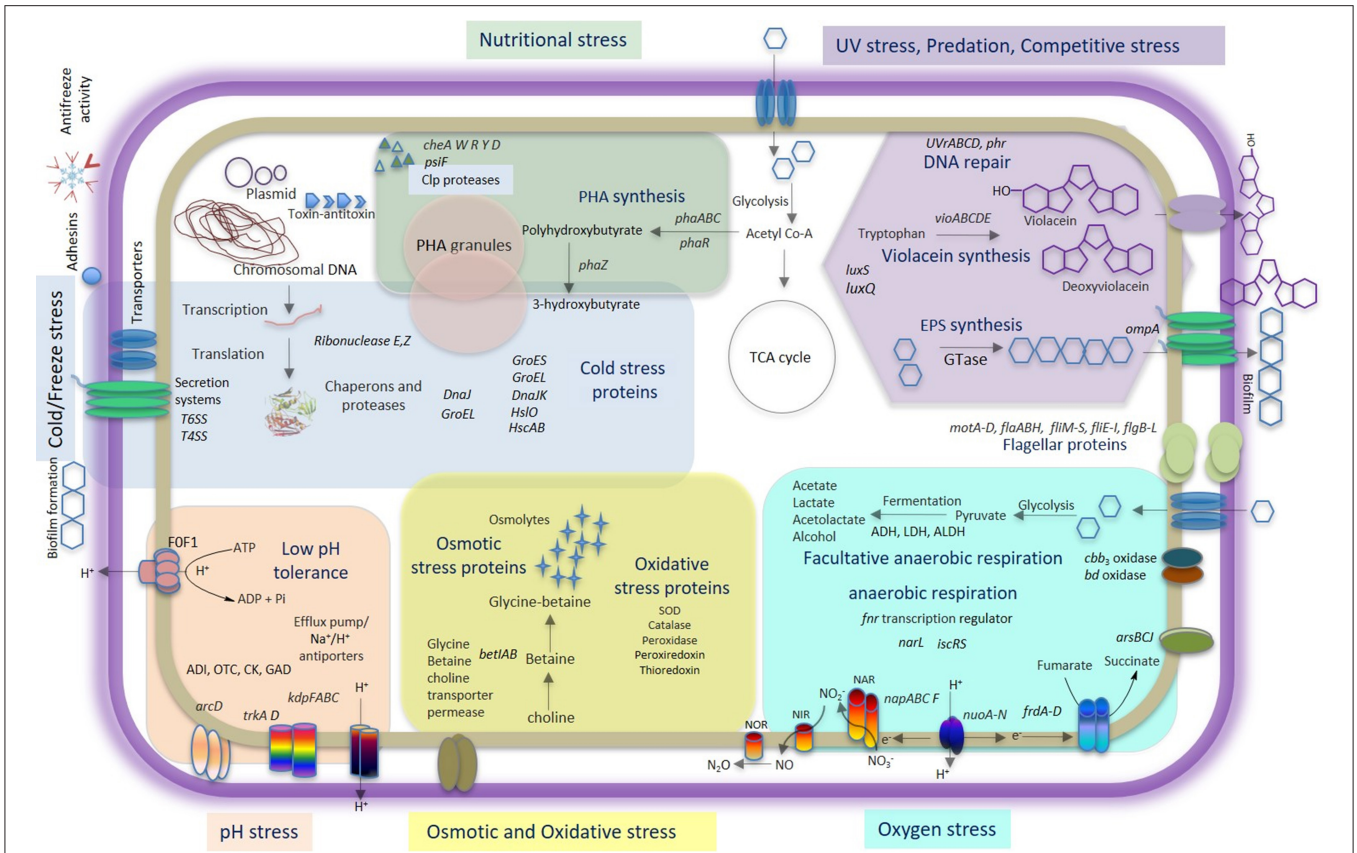

FIGURE 6 | Comprehensive model of *Iodobacter* sp. PCH194 adaptive strategies. The model is based on genomic, proteomic, and physiological data showing multiple strategies of *Iodobacter* sp. PCH194 to adapt to the predominantly frozen kettle lake environment in the high-altitude Himalayas.

stress triggers the RNase to maintain the optimum transcript levels. DEAD-box helicases are associated with RNase E-based degradosomes under cold shock conditions to degrade structured RNAs (Prud'homme-Genereux et al., 2004; Barria et al., 2013). Furthermore, the stress response regulator *rpoS* is known to be degraded by RNase E and RNase III (Basineni et al., 2009). The RNA polymerase sigma factor RpoD responsible for transcription of constitutive genes was detected in Himalayan *Iodobacter* while growing at 4°C, but RpoS was not found at cold or freeze stress. This might be because of *rpoS* degradation by upregulated expression of RNase E. Therefore, RNases seem to play an important role in the cold adaptation of *Iodobacter* sp. PCH194. In addition, upregulated T4SS and phage tail proteins closely resembling T6SS (Pukatzki et al., 2007) play a role in communication with their population, competing with others, and interacting with the environment (Russell et al., 2014).

Various organisms produce antifreeze proteins to cope up with the freezing conditions. During freezing, smaller crystals are formed in huge numbers. Their formation does not damage cells. However, large crystals harm cells during a process called recrystallization. During recrystallization, the smaller ice crystals grow by absorbing water and merging smaller ice crystals into larger ones. Antifreeze proteins (AFP) bind to ice crystals and prevent their growth during recrystallization, which results in an increased number of smaller ice crystals. Hence, AFP mitigate the damage caused to the cells. AFP are known to act extracellularly, for example, in plant apoplast space (Gupta and Deswal, 2012), while they operate in the periplasm and as adhesins in bacteria (Gilbert et al., 2005). The upregulation of adhesins in *Iodobacter* at 0°C indicated that they might play a role in freeze protection similar to MpAFP from the Antarctic bacterium *Marinomonas primoryensis* (Gilbert et al., 2005; Guo et al., 2017). The presence of IRI activity in *Iodobacter* sp. PCH194 validated the antifreeze proteins as one of the survival strategies to cope with the freezing climate of the Himalayan kettle lake. Bacterial AFP protect the cells from frost damage by inhibiting ice crystal growth during recrystallization. This study reports antifreeze activity in a Himalayan bacterium for the first time. Furthermore, antifreeze activity without cold acclimation indicates that the activity is constitutively inherited in PCH194 to cope with a frequent drop in daily temperature in the kettle lake.

Kettle lakes have frequent changes in physicochemical environments (Reverey et al., 2018); thus, nutritional fluctuation is inevitable. The presence of genes for chemotaxis and flagellar assembly in the bacterium suggested its ability to sense chemical and nutritional change and swim using flagella (Bren and Eisenbach, 2000). *I. fluviatilis*, *I. limnosediminis*, and *Iodobacter* sp. 7MAnt showed polar and lateral flagella (Logan,

1989; Su et al., 2013; Atalah et al., 2020). PHA synthesis to store carbon is a central strategy of many microbes in response to environmental and nutritional stress (Obruca et al., 2018; Kumar et al., 2020b). *Iodobacter* sp. PCH194 can synthesize and utilize PHA as a carbon reserve, evident from the genome analysis showing a complete set of genes for PHA synthesis (*phaABC*) and PHA depolymerization (*phaZ*). Accordingly, physiological experiments with various carbon/nitrogen ratios and environmental conditions revealed that the bacterium could synthesize PHB in the kettle lake environment. This has suggested the central role of PHB for *Iodobacter* sp. survival in the kettle lake. Apart from its role as a carbon reserve, PHA provides resistance to bacterial cells against multiple environmental stresses, including cold, freezing, oxidative, osmotic, and UV (Slaninova et al., 2018; Sedlacek et al., 2019; Obruca et al., 2020). Thus, PHA metabolism is one of the key metabolic strategies of *Iodobacter* sp. PCH194 to counter the multiple stresses in the Himalayan kettle lake.

Since the high-altitude Himalaya receives high amounts of UV irradiation (Singh and Singh, 2004), the inhabitant microflora must have adaptive strategies to deal with it. Consistently, *Iodobacter* sp. PCH194 possesses genes for the excinuclease system and deoxyribodipyrimidine photolyase to repair UV-induced DNA damage, as explained in the high-altitude bacterium *Acinetobacter* sp. Ver3 (Kurth et al., 2015). Additionally, PCH194 synthesizes violacein pigment as a UV protectant. The physiological experiment showed that violet-pigmented bacterium cells are more tolerant to UV (**Figure 5D**) than non-pigmented cells, demonstrating better survival upon adding methanol-extracted violacein pigment (**Figure 5E**). A literature survey supports the photoprotective role of violacein for *Janthinobacterium* spp. under UVB and UVC exposure (Abboud and Arment, 2013; Mojib et al., 2013). *Iodobacter* sp. PCH194 forms a violet microbial mat containing violacein at the surface of the medium. The phenomenon can be explained because violacein biosynthesis requires O_2, which would be higher on the surface than in sediments. Apart from UV tolerance, violacein production and biofilm formation may be responsible for protecting the bacterium from other environmental stresses, similar to *Janthinobacterium lividum* DSM1522 (Pantanella et al., 2007). Violacein is also known as a defense against bacterivorous nanoflagellates and other planktonic community members (Matz et al., 2004; Deines et al., 2009; Batista et al., 2017) and has a strong antibacterial effect against gram-positive bacteria (Kumar et al., 2021). Violacein synthesis also served as a mechanism of interspecies interaction in *Chromobacterium violaceum* (Lozano et al., 2020). Thus, violacein production and biofilm formation constitute essential survival strategies of Himalayan *Iodobacter* spp. against abiotic and biotic stresses in its high-altitude lake habitat.

Many genomic traits of *Iodobacter* sp. PCH194 (**Table 2**) that were not experimentally validated might play important roles in survival under different environmental stresses. For instance, *Iodobacter* sp. PCH194 possesses genes encoding high-affinity terminal oxidases, suggesting its ability to harvest O_2 at low concentrations for respiration (Morris and Schmidt, 2013). Genes encoding for periplasmic nitrate reductases, fumarate reductases, and transcriptional regulator (FNR) suggested that Himalayan *Iodobacter* can use nitrate or fumarate as a terminal electron acceptor under complete or near anaerobic conditions (Stewart et al., 2002). FNR is reported to act as an oxygen sensor and a molecular switch between aerobic and anaerobic respiration (Reinhart et al., 2008). Thus, *Iodobacter* has the genetic machinery for living under low oxygen concentrations and adapting to oxic-anoxic fluctuations at the sediment–water interface of the kettle lake. The various efflux pumps, porter and antiporters, and enzymes for amino acid-dependent acid tolerance might provide a survival advantage under acidic conditions (Guan and Liu, 2020). Furthermore, the toxin-antitoxin (TA) system encoded in this bacterium's chromosomal and plasmid DNA might play a crucial role in cell persistence, biofilm formation, tolerance to antibiotics, and other environmental stresses, as observed in many microbes (Page and Peti, 2016). The presence of plasmids and genes for conjugal transfer indicates the exchange of genomic information. Studies have demonstrated plasmids' adaptive, defensive, and metabolic roles in psychrophilic and psychrotolerant bacteria (Dziewit and Bartosik, 2014; Ciok et al., 2018).

CONCLUSION

The high-altitude Himalaya imposes numerous stresses on its bacterial communities. Therefore, it is vital to understand bacterial adaptation to the extreme environments of the Himalayas. The bacterium *Iodobacter* sp. PCH194 possesses multiple genomic and metabolic traits, which might enable its survival under cold and freezing temperatures, nutrient fluctuations, and high UV irradiation (**Figure 6**). Survival at subzero temperatures was further supported by antifreeze activity of the cell extract and a differential proteome response to cold and freezing conditions. PHB synthesis under different physicochemical conditions supports adaptation to fluctuating substrate and nutrient availability. Violacein pigment protects against UV radiation. The genomic and metabolic traits found in *Iodobacter* sp. PCH194 explain its survival under challenging high-altitude conditions and provide opportunities for exploring biotechnological applications and microbial community interactions.

DATA AVAILABILITY STATEMENT

The datasets presented in this study can be found in online repositories. The names of the repository/repositories and accession number(s) can be found in the article/**Supplementary Material**.

AUTHOR CONTRIBUTIONS

DS conceived the study. VK, VT, and DS did the field trip and sampling. VK, PK, and DS designed the study and analyzed the data and wrote and finalized the manuscript. VK performed microbial, genomic, and physiological

experiments. PK performed proteomic and AFP experiments. VT and SuK assisted in genomic and physiological experiments, respectively. SaK did scientific discussion and research support. All authors reviewed and approved the final manuscript.

FUNDING

The study was funded by Science and Engineering Research Board (SERB), Department of Science and Technology (DST), Government of India under the scheme of National Post-Doctoral Fellowship by Grant Nos. PDF/2016/000508 and PDF/2016/003805, Scheme for Young Scientist and Technologist (SYST) Grant No. SP/YO/2019/1261. The study was generously funded to DS by the Council of Scientific and Industrial Research (CSIR), New Delhi, India with a Grant No. MLP0143 under the Niche Creating Project scheme.

ACKNOWLEDGMENTS

The authors duly acknowledge the technical assistance provided by Mr. Mohit Swarnkar for whole-genome sequencing, Dr. Vishal Acharya for genome assembly, Dr. Robin Joshi for MALDI-TOF-TOF, and UHPLC-Q-TOF-IMS analysis, Dr. Rimpy Dhiman for ultramicrotomy, and Dr. Avnesh Kumari for TEM analysis. In addition, the authors duly acknowledge handling editor Andreas Teske and reviewers for their critical comments and suggestions on the manuscript. The manuscript represents the CSIR-IHBT communication number 4840.

SUPPLEMENTARY MATERIAL

The Supplementary Material for this article can be found online at: https://www.frontiersin.org/articles/10.3389/fmicb.2022.881873/full#supplementary-material

REFERENCES

Abboud, A. N., and Arment, A. (2013). The protective effects of the violacein pigment against UV-C irradiation in *Chromobacterium violaceum*. *Ohio J. Sci.* 111, 28–32. Available online at: http://hdl.handle.net/1811/53721

Atalah, J., Blamey, L., Munoz-Ibacache, S., Gutierrez, F., Urzua, M., Encinas, M. N., et al. (2020). Isolation and characterization of violacein from an Antarctic *Iodobacter*: a non-pathogenic psychrotolerant microorganism. *Extremophiles* 24, 43–52. doi: 10.1007/s00792-019-01111-w

Aziz, R. K., Bartels, D., Best, A. A., DeJongh, M., Disz, T., Edward, R. A., et al. (2008). The RAST Server: rapid annotations using subsystems technology. *BMC Genomics* 9, 75. doi: 10.1186/1471-2164-9-75

Baraúna, R. A., Freitas, D. Y., Pinheiro, J. C., Folador, A. R., and Silva, A. (2017). A proteomic perspective on the bacterial adaptation to cold: integrating OMICs data of the psychrotrophic bacterium *Exiguobacterium antarcticum* B7. *Proteomes* 5, 9. doi: 10.3390/proteomes5010009

Barria, C., Malecki, M., and Arraiano, C. M. (2013). Bacterial adaptation to cold. *Microbiology* 159, 2437–2443. doi: 10.1099/mic.0.052209-0

Basineni, S. R., Madhugiri, R., Kolmsee, T., Hengge, R., and Klug, G. (2009). The influence of Hfq and ribonucleases on the stability of the small non-coding RNA OxyS and its target rpoS in *E. coli* is growth phase dependent. *RNA Biol.* 6, 584–594. doi: 10.4161/rna.6.5.10082

Batista, A. H. M., Moreira, A. C. D., de Carvalho, R. M., Sales, G. W. P., Nogueira, P. C. N., Grangeiro, T. B., et al. (2017). Antimicrobial effects of violacein against planktonic cells and biofilms of *Staphylococcus aureus*. *Molecules* 22, 1534. doi: 10.3390/molecules22101534

Bolch, T., Kulkarni, A., Kääb, A., Huggel, C., Paul, F., Cogley, J. G., et al. (2012). The state and fate of Himalayan glaciers. *Science* 336, 310–314. doi: 10.1126/science.1215828

Bren, A., and Eisenbach, M. (2000). How signals are heard during bacterial chemotaxis: protein-protein interactions in sensory signal propagation. *J. Bacteriol.* 182, 6865–6873. doi: 10.1128/JB.182.24.6865-6873.2000

Chin, C. S., Alexander, D. H., Marks, P., Klammer, A. A., Drake, J., Heiner, C., et al. (2013). Nonhybrid, finished microbial genome assemblies from long-read SMRT sequencing data. *Nat. Methods* 10, 563–569. doi: 10.1038/nmeth.2474

Ciok, A., Budzik, K., Zdanowski, M. K., Gawor, J., Grzesiak, J., Decewicz, P., et al. (2018). Plasmids of psychrotolerant *Polaromonas* spp. isolated from Arctic and Antarctic glaciers–diversity and role in adaptation to polar environments. *Front. Microbiol.* 9, 1285. doi: 10.3389/fmicb.2018.01285

Corti, G., Cocco, S., Basili, M., Cioci, C., Warburton, J., and Agnelli, A. (2012). Soil formation in kettle holes from high altitudes in central Apennines, Italy. *Geoderma* 170, 280–294. doi: 10.1016/j.geoderma.2011.10.016

De Maayer, P., Anderson, D., Cary, C., and Cowan, D. A. (2014). Some like it cold: understanding the survival strategies of psychrophiles. *EMBO Rep.* 15, 508–517. doi: 10.1002/embr.201338170

Deines, P., Matz, C., and Jürgens, K. (2009). Toxicity of violacein-producing bacteria fed to bacterivorous freshwater plankton. *Limnol. Oceanogr.* 54, 1343–1352. doi: 10.4319/lo.2009.54.4.1343

Dhakar, K., and Pandey, A. (2020). Microbial ecology from the Himalayan cryosphere perspective. *Microorganisms* 8, 257. doi: 10.3390/microorganisms8020257

Dziewit, L., and Bartosik, D. (2014). Plasmids of psychrophilic and psychrotolerant bacteria and their role in adaptation to cold environments. *Front. Microbiol.* 5, 596. doi: 10.3389/fmicb.2014.00596

Gilbert, J. A., Davies, P. L., and Laybourn-Parry, J. (2005). A hyperactive. Ca2+ dependent antifreeze protein in an Antarctic bacterium. *FEMS Microbiol. Lett.* 245, 67–72. doi: 10.1016/j.femsle.2005.02.022

Goordial, J., Raymond-Bouchard, I., Zolotarov, Y., de Bethencourt, L., Ronholm, J., Shapiro, N., et al. (2016). Cold adaptive traits revealed by comparative genomic analysis of the eurypsychrophile *Rhodococcus* sp. JG3 isolated from high elevation McMurdo Dry Valley permafrost, Antarctica. *FEMS Microbiol. Ecol.* 92, 154. doi: 10.1093/femsec/fiv154

Goris, J., Konstantinidis, K. T., Klappenbach, J. A., Coenye, T., Vandamme, P., and Tiedje, J. M. (2007). DNA-DNA hybridization values and their relationship to whole-genome sequence similarities. *Int. J. Syst. Evol. Microbiol.* 57, 81–91. doi: 10.1099/ijs.0.64483-0

Guan, N., and Liu, L. (2020). Microbial response to acid stress: mechanisms and applications. *Appl. Microbiol. Biotechnol.* 104, 51–65. doi: 10.1007/s00253-019-10226-1

Guo, S., Stevens, C. A., Vance, T. D. R., Olijve, L. L. C., Graham, L. A., Campbell, R. L., et al. (2017). Structure of a 1.5-MDa adhesin that binds its Antarctic bacterium to diatoms and ice. *Sci. Adv.* 3, e1701440. doi: 10.1126/sciadv.1701440

Gupta, R., and Deswal, R. (2012). Low temperature stress modulated secretome analysis and purification of antifreeze protein from *Hippophae rhamnoides*, a Himalayan wonder plant. *Proteome Res.* 11, 2684–2696. doi: 10.1021/pr200944z

Han, W., and Christen, P. (2004). cis-Effect of DnaJ on DnaK in ternary complexes with chimeric DnaK/DnaJ-binding peptides. *FEBS Lett.* 563, 146–150. doi: 10.1016/S0014-5793(04)00290-X

Hennessy, F., Nicoll, W. S., Zimmermann, R., Cheetham, M. E., and Blatch, G. L. (2005). Not all J domains are created equal: implications for the specificity of Hsp40-Hsp70 interactions. *Protein Sci.* 14, 1697–1709. doi: 10.1110/ps.051406805

Hotaling, S., Hood, E., and Hamilton, T. L. (2017). Microbial ecology of mountain glacier ecosystems: biodiversity, ecological connections and

implications of a warming climate. *Environ. Microbiol.* 19, 2935–2948. doi: 10.1111/1462-2920.13766

Kashyap, P., Kumar, S., and Singh, D. (2020). Performance of antifreeze protein HrCHI4 from *Hippophae rhamnoides* in improving the structure and freshness of green beans upon cryopreservation. *Food Chem.* 320, 126599. doi: 10.1016/j.foodchem.2020.126599

Knight, C. A., and Duman, J. G. (1986). Inhibition of the recrystallization of ice by insect thermal hysteresis proteins: a possible cryoprotective role. *Cryobiology* 23, 256–262. doi: 10.1016/0011-2240(86)90051-9

Koh, H. Y., Park, H., Lee, J. H., Han, S. J., Sohn, Y. C., and Lee, S. G. (2017). Proteomic and transcriptomic investigations on cold-responsive properties of the psychrophilic Antarctic bacterium *Psychrobacter* sp. PAMC 21119 at subzero temperatures. *Environ. Microbiol.* 19, 628–644. doi: 10.1111/1462-2920.13578

Kumar, V., Darnal, S., Kumar, S., Kumar, S., and Singh, D. (2021). Bioprocess for co-production of polyhydroxybutyrate and violacein using Himalayan bacterium *Iodobacter* sp. PCH194. *Bioresour. Technol.* 319, 124235. doi: 10.1016/j.biortech.2020.124235

Kumar, V., Kumar, S., Darnal, S., Patial, V., Singh, A., Thakur, V., et al. (2019). Optimized chromogenic dyes-based identification and quantitative evaluation of bacterial l-asparaginase with low/no glutaminase activity bioprospected from pristine niches in Indian trans-Himalaya. *3 Biotech* 9, 275. doi: 10.1007/s13205-019-1810-9

Kumar, V., Kumar, S., and Singh, D. (2020b). Microbial polyhydroxyalkanoates from extreme niches: bioprospection status, opportunities and challenges. *Int. J. Biol. Macromol.* 147, 1255–1267. doi: 10.1016/j.ijbiomac.2019.09.253

Kumar, V., Kumar, S., and Singh, D. (2022). Metagenomic insights into Himalayan glacial and kettle lake sediments revealed microbial community structure, function, and stress adaptation strategies. *Extremophiles* 26, 3. doi: 10.1007/s00792-021-01252-x

Kumar, V., Thakur, V., Ambika, K. S., and Singh, D. (2018). Bioplastic reservoir of diverse bacterial communities revealed along altitude gradient of Pangi-Chamba trans-Himalayan region. *FEMS Microbiol. Lett.* 365, fny144. doi: 10.1093/femsle/fny144

Kumar, V., Thakur, V., Ambika, K. V., Kumar, R., and Singh, S. (2020a). Genomic insights revealed physiological diversity and industrial potential for *Glaciimonas* sp. PCH181 isolated from Satrundi glacier in Pangi-Chamba Himalaya. *Genomics* 112, 637–646. doi: 10.1016/j.ygeno.2019.04.016

Kurth, D., Belfiore, C., Gorriti, M. F., Cortez, N., Farias, M. E., and Albarracín, V. H. (2015). Genomic and proteomic evidences unravel the UV-resistome of the poly-extremophile *Acinetobacter* sp. Ver3. *Front. Microbiol.* 6, 328. doi: 10.3389/fmicb.2015.00328

Leblanc, C., Sarcos, A. C., Comeau, A. M., and Krisch, H. M. (2009). Isolation and genomic characterization of the first phage infecting *Iodobacteria*: φPLPE, a myovirus having a novel set of features. *Environ. Microbiol. Rep.* 1, 499–509. doi: 10.1111/j.1758-2229.2009.00055.x

Logan, N. A. (1989). Numerical taxonomy of violet-pigmented, Gram-negative bacteria and description of *Iodobacter fluviatile* gen. nov., comb. nov. *Int. J. Syst. Bacteriol.* 39, 450–456. doi: 10.1099/00207713-39-4-450

Lozano, G. L., Guan, C., Cao, Y., Borlee, B. R., Broderick, N. A., Stabb, E. V., et al. (2020). A chemical counterpunch: *Chromobacterium violaceum* ATCC31532 produces violacein in response to translation-inhibiting antibiotics. *mBio* 11, e00948–e00920. doi: 10.1128/mBio.00948-20

Matz, C., Deines, P., Boenigk, J., Arndt, H., Eberl, L., Kjelleberg, S., et al. (2004). Impact of violacein-producing bacteria on survival and feeding of bacterivorous nanoflagellates. *Appl. Environ. Microbiol.* 70, 1593–1599. doi: 10.1128/AEM.70.3.1593-1599.2004

Maurer, M., Schaefer, J. M., Rupper, S., and Corley, A. (2019). Acceleration of ice loss across the Himalayas over the past 40 years. *Sci. Adv.* 5, 7266. doi: 10.1126/sciadv.aav7266

Meier-Kolthoff, J. P., Auch, A. F., Klenk, H. P., and Göker, M. (2013). Genome sequence-based species delimitation with confidence intervals and improved distance functions. *BMC Bioinform.* 14, 60. doi: 10.1186/1471-2105-14-60

Meier-Kolthoff, J. P., and Göker, M. (2019). TYGS is an automated high-throughput platform for state-of-the-art genome-based taxonomy. *Nat. Commun.* 10, 2182. doi: 10.1038/s41467-019-10210-3

Mojib, N., Farhoomand, A., Andersen, D. T., and Bej, A. K. (2013). UV and cold tolerance of a pigment-producing Antarctic *Janthinobacterium* sp. Ant5-2. *Extremophiles* 17, 367–378. doi: 10.1007/s00792-013-0525-9

Morris, R., and Schmidt, T. (2013). Shallow breathing: bacterial life at low O2. *Nat. Rev. Microbiol.* 11, 205–212. doi: 10.1038/nrmicro2970

Mykytczuk, N., Foote, S., Omelon, C., Southam, G., Greer, C. W., and Whyte, L. G. (2013). Bacterial growth at−15 °C; molecular insights from the permafrost bacterium *Planococcus halocryophilus* Or1. *ISME J.* 7, 1211–1226. doi: 10.1038/ismej.2013.8

Obruca, S., Sedlacek, P., Koller, M., Kucera, D., and Pernicova, I. (2018). Involvement of polyhydroxyalkanoates in stress resistance of microbial cells: biotechnological consequences and applications. *Biotechnol. Adv.* 36, 856–870. doi: 10.1016/j.biotechadv.2017.12.006

Obruca, S., Sedlacek, P., Slaninova, E., Fritz, I., Daffert, C., Meixner, K., et al. (2020). Novel unexpected functions of PHA granules. *Appl. Microbiol. Biotechnol.* 104, 4795–4810. doi: 10.1007/s00253-020-10568-1

Page, R., and Peti, W. (2016). Toxin–antitoxin systems in bacterial growth arrest and persistence. *Nat. Chem. Biol.* 12, 208–214. doi: 10.1038/nchembio.2044

Pantanella, F., Berlutti, F., Passariello, C., Sarli, S., Morea, C., and Schippa, S. (2007). Violacein and biofilm production in *Janthinobacterium lividum*. *J. Appl. Microbiol.* 102, 992–999. doi: 10.1111/j.1365-2672.2006.03155.x

Polissi, A., De Laurentis, W., Zangrossi, S., Briani, F., Longhi, V., Pesole, G., et al. (2003). Changes in *Escherichia coli* transcriptome during acclimatization at low temperature. *Res. Microbiol.* 154, 573–580. doi: 10.1016/S0923-2508(03)00167-0

Prud'homme-Genereux, A., Beran, R. K., Iost, I., Ramey, C. S., Mackie, G. A., and Simons, R. W. (2004). Physical and functional interactions among RNase E, polynucleotide phosphorylase and the cold-shock protein, CsdA: evidence for a 'cold shock degradosome'. *Mol. Microbiol.* 54, 1409–1421. doi: 10.1111/j.1365-2958.2004.04360.x

Pukatzki, S., Ma, A. T., Revel, A. T., Sturtevant, D., and Mekalanos, J. J. (2007). Type VI secretion system translocates a phage tail spike-like protein into target cells where it cross-links actin. *PNAS* 104, 15508–15513. doi: 10.1073/pnas.0706532104

Reinhart, F., Achebach, S., Koch, T., and Unden, G. (2008). Reduced apo-fumarate nitrate reductase regulator (ApoFNR) as the major form of FNR in aerobically growing *Escherichia coli*. *J. Bacteriol.* 190, 879–886. doi: 10.1128/JB.01374-07

Reverey, F., Ganzert, L., Lischeid, G., Ulrich, A., Premke, K., and Grossart, H. P. (2018). Dry-wet cycles of kettle hole sediments leave a microbial and biogeochemical legacy. *Sci. Total Environ.* 627, 985–996. doi: 10.1016/j.scitotenv.2018.01.220

Reverey, F., Grossart, H. P., Premke, K., and Lischeid, G. (2016). Carbon and nutrient cycling in kettle hole sediments depending on hydrological dynamics: a review. *Hydrobiologia* 775, 1–20. doi: 10.1007/s10750-016-2715-9

Russell, A. B., Peterson, S. B., and Mougous, J. D. (2014). Type VI secretion system effectors: poisons with a purpose. *Nat. Rev. Microbiol.* 12, 137–148. doi: 10.1038/nrmicro3185

Sandoval, A. E., Arias-Barrau, M., Arcos, G., Naharro, G., Olivera, E. R., and Luengo, J. M. (2007). Genetic and ultrastructural analysis of different mutants of *Pseudomonas putida* affected in the poly-3-hydroxy-n-alkanoate gene cluster. *Environ. Microbiol.* 9, 737–751. doi: 10.1111/j.1462-2920.2006.01196.x

Sedlacek, P., Slaninova, E., Koller, M., Nebesarova, J., Marova, I., Krzyzanek, V., et al. (2019). PHA granules help bacterial cells to preserve cell integrity when exposed to sudden osmotic imbalances. *New Biotechnol.* 49, 129–136. doi: 10.1016/j.nbt.2018.10.005

Sharma, S., Ray, S., Moiyadi, A., Sridhar, E., and Srivastava, S. (2014). Quantitative proteomic analysis of meningiomas for the identification of surrogate protein markers. *Sci. Rep.* 4, 7140. doi: 10.1038/srep07140

Singh, S., and Singh, R. (2004). High-altitude clear-sky direct solar ultraviolet irradiance at Leh and Henle in the western Himalayas: observations and model calculations. *J. Geophys. Res.* 109, D19201. doi: 10.1029/2004JD004854

Slaninova, E., Sedlacek, P., Mravec, F., Mullerova, L., Samek, O., Koller, M., et al. (2018). Light scattering on PHA granules protects bacterial cells against the harmful effects of UV radiation. *Appl. Microbiol. Biotechnol.* 102, 1923–1931. doi: 10.1007/s00253-018-8760-8

Stewart, V., Lu, Y., and Darwin, A. J. (2002). Periplasmic nitrate reductase (NapABC enzyme) supports anaerobic respiration by *Escherichia coli* K-12. *J. Bacteriol.* 184, 1314–1323. doi: 10.1128/JB.184.5.1314-1323.2002

Stres, B., Sul, W. J., Murovec, B., and Tiedje, J. M. (2013). Recently deglaciated high-altitude soils of the Himalaya: Diverse environments, heterogenous bacterial communities and long-range dust inputs from the upper troposphere. *PLoS ONE* 8, e76440. doi: 10.1371/journal.pone.0076440

Su, W., Zhou, Z., Jiang, F., Chang, X. L., Liu, Y., Wang, S., et al. (2013). *Iodobacter limnosediminis* sp. nov., isolated from Arctic lake sediment. *Int. J. Syst. Evol. Microbiol*. 63, 1464–1470. doi: 10.1099/ijs.0.039982-0

Tatusova, T. M., DiCuccio, A., Badretdin, V., Chetvernin, V., Nawrocki, E. P., Zaslavsky, L., et al. (2016). NCBI prokaryotic genome annotation pipeline. *Nucleic Acid Res*. 44, 6614–6624. doi: 10.1093/nar/gkw569

Thakur, V., Kumar, V., Kumar, S., and Singh, D. (2018). Diverse culturable bacterial communities with cellulolytic potential revealed from pristine habitat in Indian trans-Himalaya. *Can. J. Microbiol.* 28, 1–11. doi: 10.1139/cjm-2017-0754

Ting, L., Williams, T. J., Cowley, M. J., Lauro, F. M., Guilhaus, M., Raftery, M. J., et al. (2010). Cold adaptation in the marine bacterium *Sphingopyxis alaskensis* assessed using quantitative proteomics. *Environ. Microbiol*. 12, 2658–2676. doi: 10.1111/j.1462-2920.2010.02235.x

Conflict of Interest: The authors declare that the research was conducted in the absence of any commercial or financial relationships that could be construed as a potential conflict of interest.

frontiers | Frontiers in Microbiology

TYPE Original Research
PUBLISHED 14 September 2022
DOI 10.3389/fmicb.2022.876044

OPEN ACCESS

EDITED BY
Andreas Teske,
University of North Carolina at Chapel Hill,
United States

REVIEWED BY
Maliheh Mehrshad,
Academy of Sciences of the
Czech Republic, Czechia
Stefan M. Sievert,
Woods Hole Oceanographic Institution,
United States

*CORRESPONDENCE
Craig L. Moyer
cmoyer@wwu.edu

SPECIALTY SECTION
This article was submitted to
Extreme Microbiology,
a section of the journal
Frontiers in Microbiology

RECEIVED 15 February 2022
ACCEPTED 09 August 2022
PUBLISHED 14 September 2022

CITATION
Stromecki A, Murray L, Fullerton H and
Moyer CL (2022) Unexpected diversity
found within benthic microbial mats at
hydrothermal springs in Crater Lake,
Oregon.
Front. Microbiol. 13:876044.
doi: 10.3389/fmicb.2022.876044

Unexpected diversity found within benthic microbial mats at hydrothermal springs in Crater Lake, Oregon

Amanda Stromecki[1], Laura Murray[1], Heather Fullerton[2] and Craig L. Moyer[1]*

[1]Department of Biology, Western Washington University, Bellingham, WA, United States, [2]Department of Biology, College of Charleston, Charleston, SC, United States

Crater Lake, Oregon is an oligotrophic freshwater caldera lake fed by thermally and chemically enriched hydrothermal springs. These vents distinguish Crater Lake from other freshwater systems and provide a unique ecosystem for study. This study examines the community structure of benthic microbial mats occurring with Crater Lake hydrothermal springs. Small subunit rRNA gene amplicon sequencing from eight bacterial mats was used to assess community structure. These revealed a relatively homogeneous, yet diverse bacterial community. High alpha diversity and low beta diversity indicate that these communities are likely fueled by homogeneous hydrothermal fluids. An examination of autotrophic taxa abundance indicates the potential importance of iron and sulfur inputs to the primary productivity of these mats. Chemoautotrophic potential within the mats was dominated by iron oxidation from *Gallionella* and *Mariprofundus* and by sulfur oxidation from *Sulfuricurvum* and *Thiobacillus* with an additional contribution of nitrite oxidation from *Nitrospira*. Metagenomic analysis showed that *cbbM* genes were identified as *Gallionella* and that *aclB* genes were identified as *Nitrospira*, further supporting these taxa as autotrophic drivers of the community. The detection of several taxa containing *arsC* and *nirK* genes suggests that arsenic detoxification and denitrification processes are likely co-occurring in addition to at least two modes of carbon fixation. These data link the importance of the detected autotrophic metabolisms driven by fluids derived from benthic hydrothermal springs to Crater Lake's entire lentic ecosystem.

KEYWORDS

hydrothermal springs, community structure, microbial mats, chemoautotrophs, Crater Lake

Introduction

Crater Lake is an ultra-oligotrophic freshwater caldera lake in south-central Oregon at the crest of the Cascade Mountain range. It formed in the crater of Mount Mazama left behind after a volcanic eruption approximately 7,000 years ago, yet volcanic activity has taken place as recently as 4,000 years ago (Bacon et al., 2002). Crater Lake is known for its

exceptionally clear water and deep basin; it is the ninth deepest lake in the world with a maximum depth of 594 meters (Collier et al., 1991; Bacon et al., 2002). Due to its clarity, Crater Lake receives significant ultraviolent light penetrance that limits the dissolved organic carbon and creates nutrient-poor conditions (Urbach et al., 2001). Although highly oxygenated, its primary productivity is also limited by nitrogen and trace metals (McManus et al., 1992; Groeger, 2007). The relatively small catchment area of the lake has no surface outlet and is fed primarily by rain and snowmelt, receiving minimal anthropogenic or allochthonous input of water (Page et al., 2004; Urbach et al., 2007). Due to these conditions, Crater Lake shares many similarities with oxygenated, oligotrophic ocean waters.

Crater Lake also resembles a marine system due to deep active hydrothermal springs fed by dense, enriched fluids that lie in the bottom of the lake. However, the thermally and chemically enriched hydrothermal springs distinguish Crater Lake from other freshwater systems and provide a unique ecosystem for study. These hydrothermal fluids are slightly elevated in temperature compared to the surrounding lake water, creating an inverse temperature gradient (McManus et al., 1996). The hydrothermal springs are also enriched in dissolved CO_2 compared to bulk lake water (Collier et al., 1991). In addition, the springs contain elevated concentrations of dissolved iron, sulfur, and manganese ions, bringing critical nutrients to the oligotrophic environment (Collier et al., 1991). These vent-derived chemicals provide bioavailable nutrients that benthic microorganisms may utilize; therefore, hydrothermal input to Crater Lake is crucial for primary productivity (Urbach et al., 2001, 2007).

Previous research on the hydrothermal springs at the bottom of Crater Lake was conducted by researchers from Oregon State University using the research submersible Deep Rover (Drake et al., 1990). Surveys of the hydrothermal venting sites led to the discovery of benthic pools that formed in depressions in the lake floor and filled with chemically enriched hydrothermal fluids. Two primary pool locations were identified: Llao's Bath in the south-central region of the lake, and Palisades Point Pools in the north-east basin (Collier et al., 1991). At both locations, dense microbial mats lined the pool margins and outlets (Dymond et al., 1989), suggesting the bacterial communities rely on these dense, nutrient-rich fluids emanating from the hydrothermal springs.

The benthic microbial mats that surround the pools and hydrothermal venting sites were hypothesized to be driven by chemoautotrophic bacteria (Dymond et al., 1989). Because chemoautotrophs obtain energy from inorganic chemicals such as those provided by hydrothermal vent fluids, they function as primary producers in environments lacking light or organic carbon (Nakagawa and Takai, 2008; McNichol et al., 2018). Crater Lake benthic microbial mats appeared to take advantage of the gradient among reduced forms of iron, sulfur, and manganese where hydrothermal fluids interact with the oxygenated freshwater lake (Dymond et al., 1989; Collier et al., 1991). These reduced ions provide an abundant energy source for chemoautotrophs that in turn produce organic carbon compounds utilized by other trophic levels, supporting diverse microbial communities (e.g., Sievert and Vetriani, 2012; Hager et al., 2017).

Cellular morphology was initially used to characterize these benthic microbial mat communities in Crater Lake, revealing a predominantly ubiquitous sheathed morphotype composition. Researchers used scanning electron microscopy to describe sheath-forming bacteria and identified the genera *Gallionella* and *Leptothrix* (Dymond et al., 1989). *Gallionella* and *Leptothrix* are found in freshwater environments and are capable of oxidizing iron for energy (Emerson et al., 2010). *Leptothrix* has also been shown to oxidize manganese ions (Eggerichs et al., 2020). Elevated levels of ferrous iron and manganese were detected at these mat sites (Dymond et al., 1989), supporting the hypothesis of mat communities dominated by iron-oxidizing chemoautotrophs (Bennett et al., 2014). Both are good candidates for functioning as primary producers within these microbial mats; however, many other genera also form sheaths and therefore microscopy is insufficient to accurately resolve mat community structure and diversity.

The Zetaproteobacteria are another more recently discovered class of iron-oxidizing bacteria capable of forming sheath-rich mat matrices (Emerson et al., 2007). Zetaproteobacteria habitat preferences have been best described in the submarine volcano Lō'ihi Seamount where hydrothermal fluids rich in CO_2 and iron and low in sulfide support dense mat communities (Glazer and Rouzel, 2009; Fullerton et al., 2017). Zetaproteobacteria have also been found in diffuse flow sites within high-temperature chimneys, the marine subsurface, brackish coastal environments, and CO_2-rich terrestrial springs. Among these disparate environments, the shared habitat conditions for Zetaproteobacteria are brackish to hypersaline water, a supply of reduced iron, and micro-oxic conditions (McAllister et al., 2019). These conditions are present in the benthic hydrothermal springs found in Crater Lake, making Zetaproteobacteria an ideal candidate for an autotrophic, sheath-forming iron-oxidizer driving the primary production of these mat communities.

Since previous studies of the benthic microbial mats relied solely on morphology, further analysis is necessary to identify which genera of sheath-forming lithoautotrophs are present and to understand the community structure differences across the various mat locations. Amplicon sequencing targeting the small subunit (SSU) rRNA gene has been shown to be an efficacious tool to accurately identify community structure and diversity (Caporaso et al., 2012; Hugerth and Andersson, 2017). SSU rRNA gene amplicon sequencing can therefore be used to reveal the diversity within the microbial mats from hydrothermal springs and hypersaline pools in Crater Lake and to identify putative lithoautotrophs. These data can be interrogated to determine which operational taxonomic units (OTUs) are present in high abundances within the communities, revealing which OTUs are playing major ecological roles in these mats. Since the SSU rRNA gene is widely used, our resulting analyses can then be compared to previously described ecosystems dominated by other lithoautotrophs such as *Gallionella*, *Leptothrix,* and *Zetaproteobacteria* (Johnson et al., 2012;

Hager et al., 2017). From this taxonomic information, we can infer the metabolic requirements of the microbial mats by identifying the autotrophs present in high abundances to determine if the communities are driven by iron oxidation. This can then be supported by shotgun metagenomics to verify that the autotrophic pathways are present in the taxa identified by SSU rRNA gene sequencing. These results will allow for insights into the potential for enhanced diversity of benthic microbial mats at hydrothermal springs in Crater Lake whose autotrophic members may affect crucial nutrients introduced to this oligotrophic ecosystem. These findings reveal patterns in mat community complexity and diversity at a stable, homogeneous hydrothermal system that can be compared to the episodic, heterogeneous conditions found at other hydrothermal vent ecosystems.

Materials and methods

Sample collection and location descriptions

Microbial mat and adjacent mat fluid collection occurred in the south-central and north-east regions of Crater Lake during 16 HOV Deep Rover dives in August 1989. Samples were collected from two primary areas: seven from Llao's Bath/Brain Mat complex in the south-central and one from Palisades Point Pools in the north-east regions of Crater Lake. Sample names, sites, and map locations along with geochemical profiles of respective mat and pool fluids are described in Table 1. These samples were collected, and chemical analyses were done by Collier et al. (1991) during a detailed study of hydrothermal activity at the bottom of the lake. A 50 kHz echo sounder was used to determine the depths of mats and pools. Mat temperatures were collected using a temperature probe attached to the wrist mechanism of *Deep Rover's* mechanical arm that was inserted into bacterial mat features. Water temperatures were collected using conductivity, temperature, and depth or "CTD" instrument carried on the submersible. Bacterial mat samples were collected using either push cores or Go-Flo bottles to collect mats and fluids with a minimum of lake water admixture (Dymond et al., 1989; Collier et al., 1991). Processed samples were stored at −80°C until extraction. Samples were named using the *Deep Rover* Dive number (216 to 230) followed by sample number (e.g., 216S1).

DNA extractions

DNA extractions were performed on mat and pool fluid samples using the FastDNA Spin Kit for Soil (MP Biomedicals, Irvine, CA) protocol, which was followed according to the manufacturer's instructions. Lysis was performed with two rounds of bead beating for 45 s at a setting of 5.5 using the FastPrep instrument with samples being placed on ice between runs. DNA was eluted in 100 µl of 1.0 mm Tris pH 8.0. Total DNA was quantified with a Qubit 2.0 fluorometer using the dsDNA HS kit (Thermo Fisher Scientific, Waltham, MA).

SSU rRNA gene PCR amplification and clone library analysis

Each sample was then processed within weeks of gDNA extraction, where bacterial SSU rRNA genes were amplified from the gDNA using the 68F forward primer (5' TdNA dNAC ATG CAA GTC GdKdK CG 3′) and the 1492R reverse primer (5' dKGdP TAC CTT GTT ACG ACT T 3′), where dK is a purine analog, dP is a pyrimidine analog, and dN is an equal mixture of dK and dP (Glen Research, Sterling, VA). Five replicate PCRs were performed using ~50 ng of gDNA template, 5 U of Taq polymerase, 2.5 mm $MgCl_2$, 200 µm each dNTPs, 1 µm (each) forward and reverse primers, and molecular-grade water to a total volume of 50 µl. The following conditions were used for the amplification process: an initial 8-min hot start at 95°C, followed by 25 to 30 cycles of denaturation (94°C for 1 min), annealing (58°C for 90 s), and elongation (72°C for 3 min). This was followed by a final elongation step at 72°C for 7 min. Amplicons were sized by 1% agarose gel electrophoresis against a 1-kb ladder. Negative controls were maintained throughout. The five replicate PCR mixtures were pooled, concentrated, and desalted. The desalted PCR amplicons were then cloned with a Topo-TA cloning kit following the manufacturer's instructions (Thermo Fisher Scientific). All putative clones were streaked for isolation, and the inserts were assayed for correct size using PCR with M13F and M13R primers prior to sequencing (Moyer, 2001).

SSU amplicon sequencing and analysis

For all samples, the V3-V4 variable regions of the SSU rRNA gene were amplified *via* polymerase chain reaction (PCR) from all samples using bacterial primers 340F-CCTACGGGNGG CWGCAG and 784R-GGACTACHVGGGTATCTAATCC (Klindworth et al., 2013) with Illumina compatible adaptors. Triplicate PCRs were performed in 25 µl reactions with 2X KAPA HiFi HotStart ReadyMix (Kapa Biosystems, Wilmington, MA), 0.1 mm forward/reverse primers, and 25 ng template DNA. The following PCR conditions were used: 3 min at 95°C; 25 cycles of 30 s at 95°C, 30 s at 55°C, and 30 s at 72°C; a final elongation of 5 min at 72°C; and a hold at 4°C. PCR products were pooled and purified using Agencourt AMPure XP beads (Beckman Coulter, Brea, CA). Adapters with unique index combinations were added to each sample in a 50 µl PCR using 2X KAPA HiFi HotStart ReadyMix with the following conditions: 3 min at 95°C; 8 cycles of 30 s at 95°C, 30 s at 55°C, and 30 s at 72°C; a final elongation of 5 min at 72°C; and a hold at 4°C. Products were again purified with AMPure XP beads. Libraries were quantified with a Qubit 2.0 fluorometer. Sequencing was performed on an Illumina MiSeq generating 2 × 300 bp using paired-end reads.

TABLE 1 Description of sample locations and geochemical profiles of mats and pool fluids. Data from Collier et al., 1991.

Sample	Site	Map location	T_{max} (°C)*	Depth (m)	pH	CO_2 mM	O_2 µM	SO_4 mM	Fe nM	Mn nM	NO_3 µM
216S1†	Brain Mat	Llao's Bath & Brain Mat Complex	4.54	463	7.13	1.26	nd	0.31	380	3.9	1.17
223S1	Llao's Bath	Llao's Bath & Brain Mat Complex	4.52	467	6.27	3.00	228.2	0.25	18	1,680	1.44
226S1	Llao's Bath	Llao's Bath & Brain Mat Complex	10.2	448	nd	4.96	nd	0.69	41	12,300	0.59
226S2	Near Llao's Bath	Llao's Bath & Brain Mat Complex	10.2	448	7.26	0.69	292.6	0.11	nd	nd	1.91
226S3‡	Near Llao's Bath	Llao's Bath & Brain Mat Complex	10.2	448	7.59	nd	nd	0.55	30,421	15,272	2.96
230S1	Brain Mat	Llao's Bath & Brain Mat Complex	5.98	443	7.23	4.95	17.7	0.55	254	25,200	0.61
230S3	Llao's Bath Milky Pool Mat	Llao's Bath & Brain Mat Complex	5.98	443	7.14	0.78	279.2	0.15	nd	nd	2.55
228S3	Palisades Point Pool Mat	Palisades Point Pools	9.68	554	7.97	2.70	nd	nd	42	38	1.57
Crater Lake Bottom Water	Composite	Deep Lake	3.6	429	6.95	0.64	295	0.10	0.2	3.0	1.39

*Ambient temperature = 3.6°C.
†Metagenomic analysis.
‡SSU rRNA clone library analysis.

Amplicon sequence reads were quality checked using FastQC (Andrews, 2010). Amplicons were then processed using the mothur software package (Schloss et al., 2009; Kozich et al., 2013). After forming contigs from the paired-end reads, any sequences shorter than 420 bp, longer than 470 bp, or with ambiguous base calls were eliminated from further processing. Reads were aligned to the SILVA v138.1 SSU reference database. Any sequences with a homopolymer greater than 8 bases were also eliminated. Reads were pre-clustered with the pre-cluster command with a threshold of four-nucleotide differences. Chimeras were removed with UCHIME (Edgar et al., 2011). Sequences were binned into OTUs based on 97% sequence similarity, and OTUs were classified to the genus level using RDP training set v18 (Wang et al., 2007).

OTU bins at the level of 97% sequence similarity as determined with mothur were used in all downstream analyses. Reads were randomly subsampled to the number of reads in the least sequenced sample (54,068 contigs) for calculation of Good's coverage, Abundance-based Coverage Estimator (ACE) richness (Kim et al., 2017), Chao-1 richness (Chao, 1984), and inverse Simpson diversity (Simpson, 1949) with the summary.single command. Non-metric multidimensional scaling in three dimensions was used to assess beta diversity among samples. Abundant OTUs were determined by selecting OTUs with >1% of the total reads/sample in at least one sample, and OTUs with >2% of the total reads/sample in at least one sample (Supplementary Table 1). Abundant autotrophic OTUs were determined by selecting OTUs with autotrophic metabolic potential that comprised >0.5% of the total reads/sample in at least one sample. The ggplot2 package (Wickham et al., 2016) in R (version 3.6.1) was used to visualize OTU taxon-abundance data. Rarefaction curves were calculated using mothur based on the number of observed OTUs per sample and 1000 iterations, and the ggplot2 package in R was used to visualize these data.

Further analysis of OTUs classified to the genus *Mariprofundus* were further assessed using the program *ZetaHunter* (McAllister et al., 2018). *ZetaHunter* assigns Zetaproteobacteria sequences to canonical Zetaproteobacterial OTUs (Zeta OTUs) in the SILVA v123 SSU reference database. Zetaproteobacteria reads across all eight mat communities with an abundance >10 reads were isolated, identified, and assessed using *ZetaHunter* to further classify these Zeta OTUs (Supplementary Table 2).

Metagenomic sequencing, assembly, and analysis

For sample 216S1, gDNA was further cleaned and concentrated using an Aurora System (Boreal Genomics, Vancouver, BC) prior to metagenomic sequencing. Libraries were prepared with the Nextera DNA library kit (Illumina, San Diego, CA) for Illumina sequencing with 2 × 300 bp paired-end reads. Sequenced reads were quality checked using FastQC (Andrews, 2010) and quality control was performed with Trimmomatic (Bolger et al., 2014).

The quality filtered metagenomic reads were assembled into contigs using the program MegaHIT (Li et al., 2015). Genes were predicted using the program Prodigal (Hyatt et al., 2010). A homology search for both COG and KEGG was then run on the predicted genes using Diamond (Buchfink et al., 2021). Each ORF was then functionally and taxonomically assigned using SqueezeMeta (Tamames and Puente-Sánchez, 2019). Contigs without any gene predictions were analyzed by BlastX with the Diamond sequence aligner for ORF identification. Gene abundances were calculated using STAMP (Parks et al., 2014), then relative abundance was calculated by taking the raw read counts for each orf, dividing it by the total reads in the sample, and multiplying by 100. Coverage values (bases mapped/ORF length) and normalized RPKM values were calculated using SqueezeMeta pipeline scripts.

The results of the pipeline were imported into R, version 3.6.1 using the SQMtools R package, version 0.7.0 (Puente-Sánchez

et al., 2020). This package was then used to visualize the taxonomy of the contigs and plot the functional profile of the genes in the samples with KEGG, COG, and PFAM annotations. The taxa with major autotrophy indicator genes were then extracted and plotted using ggplot2.

Results

Location descriptions and site geochemistry

Llao's Bath and Brain Mat Complex lies in the south-central area of the lake (Figure 1). It is in an area of low relief and is surrounded by sediment on three sides, while a rounded rocky outcrop projects upward from the northwestern edge of the pool. The pool margin is rimmed with a bacterial mat 10 to 20 cm thick. A gentle slope rises from the western edge of the pool that contains an extensive area also covered by bacterial mats. Due to the convoluted morphology of these mats (Figure 2A), this area was termed the "brain mat" and is spatially associated within a few meters of Llao's Bath (Figure 2B).

Palisades Point Pools occur in the north-east side of the lake near the terrestrial feature Palisades Point and north-east of the north-central underwater cinder cone Merriam Cone (Figure 1). Many small pools were observed in this area which extends approximately 50 m across by 100 m long and lies in a sedimented area of low relief at the base of the lake's caldera wall. A unique feature of this pool is the stream-like projections or rills that extend from the upslope region with dendritic patterns that indicate downstream flow (Figure 2C). Bacterial mats line the sides of this pool and occur along the rills much like the mats located along the margins of Llao's Bath. According to geochemical analyses conducted by Collier et al. (1991), mats and pool fluids were enriched in CO_2, SO_4, Fe, Mn, and NO_3 compared to bulk lake water, which are consistent with fluids of hydrothermal origin (Table 1). While the bulk lake water is near saturation in respect to dissolved oxygen, dissolved oxygen concentrations decreased with depth. This may be impacted by the introduction of anoxic hydrothermal fluids and reduced inorganic ions such as Fe and Mn (Collier et al., 1991). Among sample sites, sample 226S3 from near Llao's Bath had the highest Fe concentration of 30.4 mm (Table 1). In addition to the notable enrichments in iron, several samples also exhibited elevated Mn concentrations.

Community structure and diversity

An initial clone library of nearly full-length SSU genes was constructed from sample 226S3 (e.g., from the Llao's Bath and Brain Mat Complex area) that yielded a total of 76 clones, of these 45 clones were detected at least twice (i.e., not singletons) and comprised 16 operational taxonomic units (OTUs), which were then chosen to be fully sequenced. Of these OTUs, 40% were identified as putative chemoautotrophs, with most of these identified as iron-oxidizing bacteria and were represented by three OTUs belonging to the genus *Gallionella*. Three other OTUs were identified as being represented by the genus *Sulfuricurvum, Nitrosomonas,* and *Nitrospira*, putative sulfur-oxidizing, ammonia-oxidizing, and nitrite-oxidizing bacteria (or possibly complete nitrification), respectively.

Amplicon sequencing was done from seven Llao's Bath and Brain Mat Complex and one Palisades Point Pool bacterial mat samples. In total 6,646,366 raw, paired-end sequences covering the V3-V4 regions of the SSU rRNA gene were generated. Quality filtering in mothur (Schloss et al., 2009), resulted in 4,167,607 sequences were then analyzed for a more detailed examination of bacterial mat community structure and diversity. At a 97% sequence similarity cutoff, 67,668 OTUs were generated, of which 55 were abundant with >1% of the total reads in at least one sample.

The highest number of observed OTUs, as determined by 97% sequence similarity, occurred in community 226S2 from the Llao's Bath/Brain Mat Complex (Supplementary Table 1). The 226S2 community had proportionally higher richness and diversity estimates. Rarefaction analysis corroborated these alpha diversity estimates and revealed higher overall diversity in the 226S2 community from Llao's Bath relative to the remaining seven communities sampled (Supplementary Figure 1). In contrast, rarefaction analysis revealed lower than average overall diversity in the 226S1 and the 226S3 communities, both from the Llao's Bath area. These findings were corroborated by Inverse Simpson diversity estimates, which revealed the lowest richness and diversity in these two communities (Supplementary Table 1).

Although many samples had elevated Fe and Mn concentrations, the bacterial community structure was revealed to be similar across all eight samples that were examined. Non-metric multidimensional scaling in three dimensions revealed even distributions among all communities with no obvious clustering, indicating a low differential in beta diversity (data not shown). The majority of reads from all communities were from the Proteobacteria (NB, recently reclassified as the Pseudomonadota phylum; Oren and Garrity, 2021), at the phylum level (Figure 3A). The Proteobacteria phylum was dominated at the class level by the Betaproteobacteria, Alphaproteobacteria, Gammaproteobacteria, and Deltaproteobacteria (Figure 3B; NB, recently reclassified into four novel phylum-level lineages; Waite et al., 2020). In addition, a large proportion of reads were in the category of unclassified Bacteria with an average and standard deviation across all samples of 19.2%. Other abundant phyla include *Acidobacteria*, *Actinobacteria*, *Bacteroidetes*, *Candidatus Saccharibacteria*, *Chloroflexi, Gemmatimonadetes, Ignavibacteriae, Latescibacteria*, *Parcubacteria*, *Planctomycetes*, and *Verrucomicrobia*.

Betaproteobacteria represented the dominant Proteobacteria class with a maximum value of 13.0% of the community 226S3 from near Llao's Bath, which also exhibited the highest measured iron concentrations (Table 1). The majority of the Betaproteobacteria were from the genera *Gallionella* as well as *Rhodoferax,*

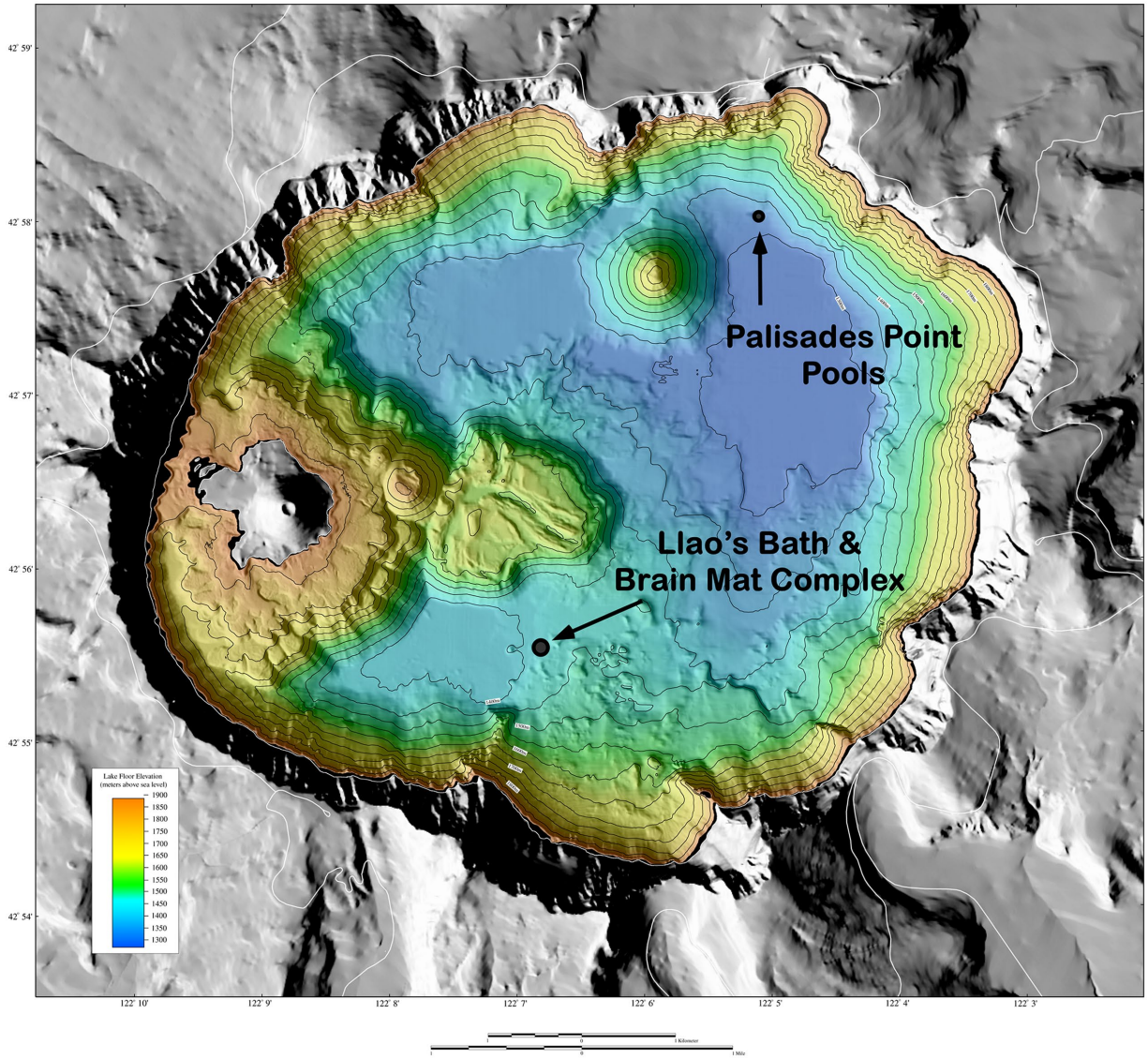

FIGURE 1
Shaded relief of surrounds and bathymetric map of the floor of Crater Lake, Oregon. Surrounding terrain from USGS 10m digital elevation model (DEM). DEM illuminated from 225°azimuth, 45°elevation. Colored region is the lake floor (±1m resolution), whereas the gray region is the surrounding land. The distance across the width of the lake is approximately 9km (5.6miles). The reds and yellows show the shallower depths of the lake, whereas the greens and blues show the deeper depths. Adapted from Bacon et al., 2002.

Undibacterium, and an unclassified genus. Next in abundance were the Alphaproteobacteria that had a maximum relative abundance of 10.9% of the Palisades Point Pools community, 228S3. The Alphaproteobacteria were dominated by the genera *Novosphingobium* and *Rhodoferax*. The maximum relative abundance of Gammaproteobacteria also occurred at Palisades Point Pools, comprising 8.8% of the community. The majority of these belonged to the genera *Thiobacillus* as well as *Xanthomonadaceae, Alteromonadales, Silanimonas,* and an unclassified genus. Deltaproteobacteria were the next most abundant class represented by the genera *Geobacter*, *Desulfobacteraceae*, and an unclassified genus with a maximum value of 8.2% from 226S2 near Llao's Bath. This unclassified Deltaproteobacteria genus represented the most abundant OTU across all eight communities with an average relative abundance of 1.9%.

Variability in community structure was revealed within the less abundant Proteobacteria classes Zetaproteobacteria and Epsilonproteobacteria (NB, recently reclassified as the Campylobacterota phylum; Waite et al., 2017). Community 228S3 from Palisades Point Pools contained the highest relative abundance of Campylobacterota at 1.6% (Figure 3A). This abundance was greater than the average relative abundance for Campylobacterota of 0.06% for the other seven communities. The majority of these were identified from the genus *Sulfuricurvum* that comprised 1.4% of the 228S3 community. Community 226S1 from Llao's Bath contained the highest relative abundance of Zetaproteobacteria,

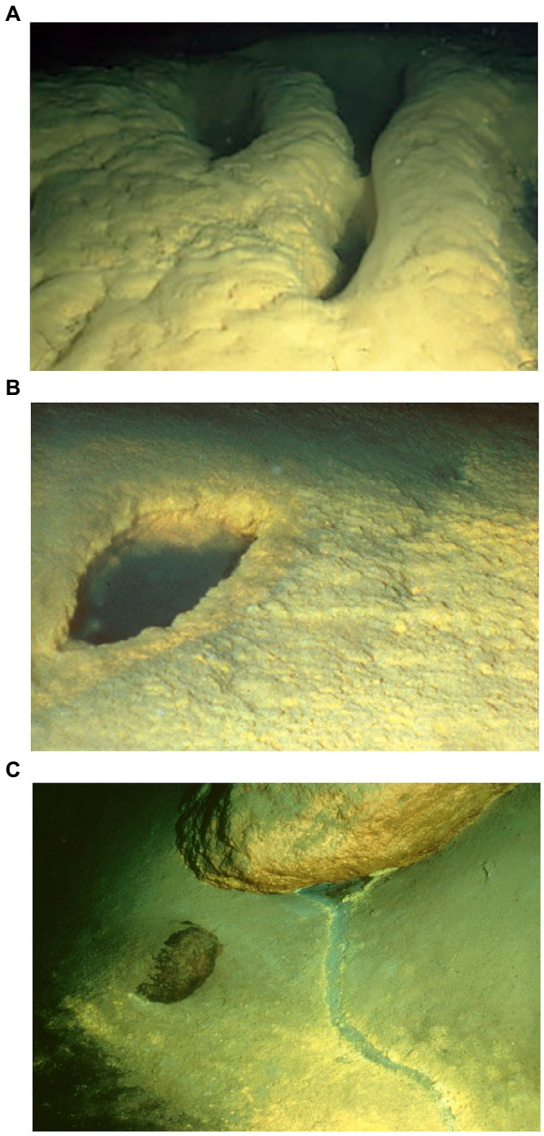

FIGURE 2
Representative photos of bacterial mat collection sites: **(A)** "Brain mat" bacterial growth west of Llao's Bath within the Llao's Bath/ Brain Mat complex; **(B)** Llao's Bath brine pool with surrounding bacterial mat; **(C)** A rill within the Palisades Point area. This channel or rill flows downhill from its origin under the boulder (upper part of the photo). Each photo field of view is approximately three meters across. Images courtesy of Collier et al., 1991.

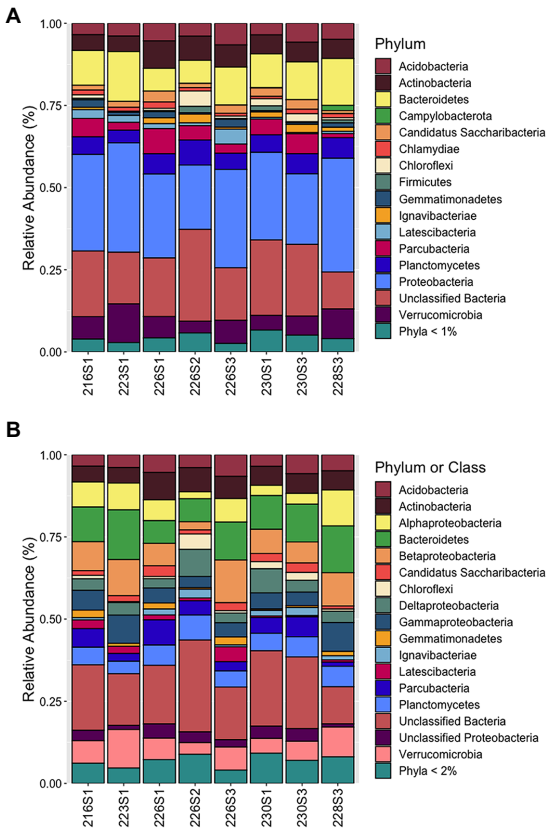

FIGURE 3
Community structure of eight benthic microbial mats from hydrothermal springs in Crater Lake, Oregon, at various taxonomic levels: **(A)** Community structure of abundant taxa representing >1% total reads per sample in at least one sample at the phylum level. Phyla <1% included as separate taxon; **(B)** Community structure of abundant taxa representing >2% total reads per sample in at least one sample at the phylum level with Proteobacteria shown at the class level.

represented by the single genus *Mariprofundus*, at 0.53% compared to an average relative abundance of 0.02% for the remaining seven communities (Figure 3B).

Autotroph diversity

Putative autotrophic taxa were characterized by OTUs belonging to five genera comprising >0.5% total reads per community that were detected in at least one community (Figure 4). The genus *Gallionella* was the most abundant putatively autotrophic taxa across all eight communities. Community 226S3 collected near Llao's Bath contained the highest abundance of reads from two *Gallionella* OTUs comprising a combined relative abundance of 3.4% of the total bacterial community. Across all eight communities, the average relative abundance of *Gallionella was* 0.75% of the bacterial community. The next most abundant autotrophic taxon was represented by the genus *Nitrospira,* which had a more consistent distribution across all eight communities, comprising an average relative abundance of 0.73%. The maximum relative abundance of *Nitrospira* occurred in the 216S1 community from Brain Mat comprising 1.0% of the total. Community 228S3 from Palisades Point Pools contained the highest abundance of an autotrophic *Sulfuricurvum* OTU. *Sulfuricurvum* was present in a relative abundance of 1.4% in the Palisades Point Pools community compared with an average relative abundance of 0.04% in the other seven communities. The genus *Mariprofundus* represented the fourth most abundant autotrophic taxa detected in the Crater Lake bacterial communities. *Mariprofundus* comprised an average relative abundance of 0.08% across all eight communities, with a maximum abundance of 0.53% found in community 226S1 from Llao's Bath.

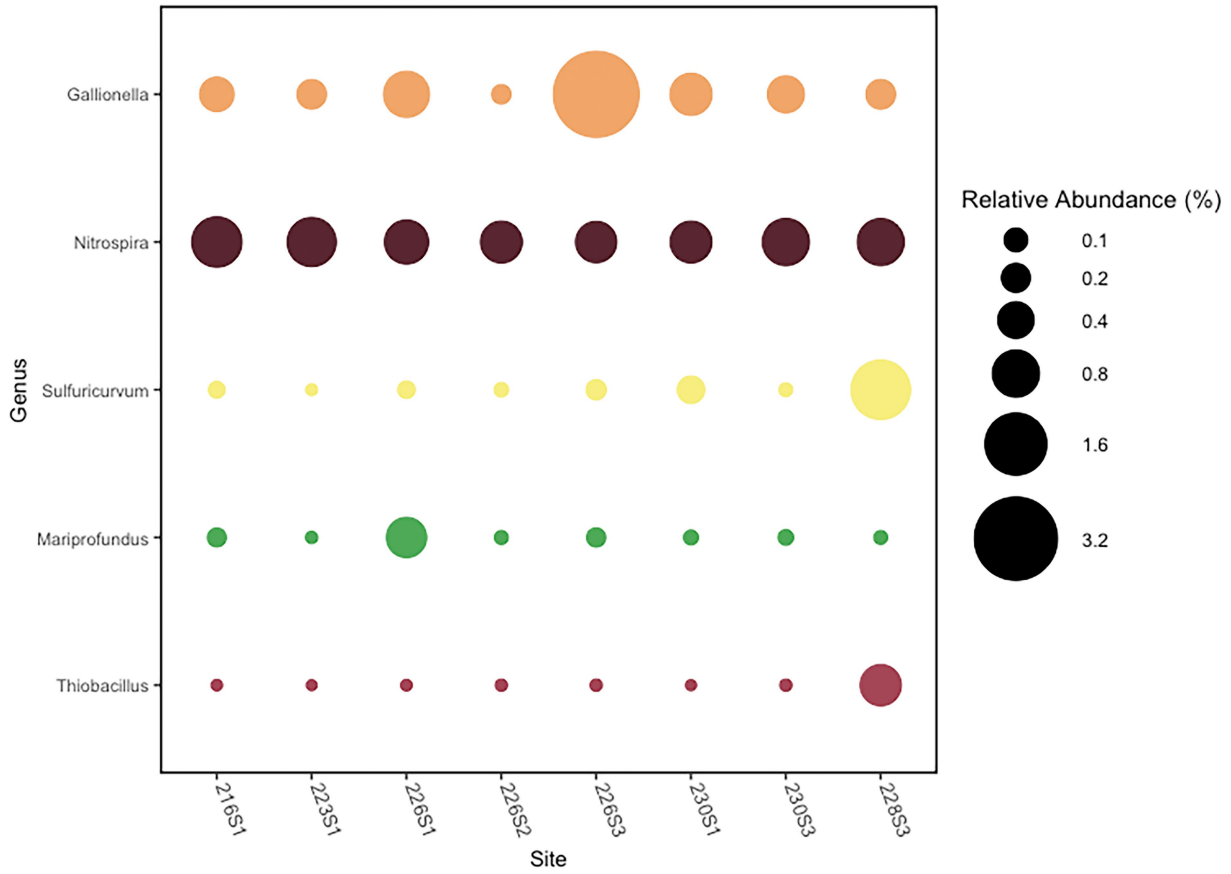

FIGURE 4
Relative abundance of putative chemoautotrophic genera with a maximum abundance >0.5% of reads in at least one sample.

Finally, the autotrophic genus *Thiobacillus* comprised an average relative abundance of 0.07% of the eight bacterial communities. The maximum relative abundance of *Thiobacillus* occurred in the Palisades Point Pools community at 0.56% (Figure 4).

Sequence reads determined as representing the genus *Mariprofundus* were further processed using the program *ZetaHunter* to provide finer scale OTU classification (McAllister et al., 2018). *ZetaHunter* assigned reads to eight previously characterized Zeta OTUs and one newly described New Zeta OTU 1; however, 452 reads (~0.01%) were unable to be classified representing novel Zetaproteobacteria phylotypes (Supplementary Table 2). The majority of reads were assigned to either Zeta OTU 2 or Zeta OTU 6. The average relative abundance of Zetaproteobacteria in the Crater Lake bacterial communities was ~0.08%. Zeta OTU 2 and Zeta OTU 6 each comprised a relative abundance of ~0.02% of the pooled Crater Lake community, respectively.

Metabolic potential of the Crater Lake bacterial mat community

The metagenomic sequencing of sample 216S1 resulted in 26,096,482 total reads that were assembled into 319,555 contigs. From these contigs, there were 616 SSU rRNA genes identified. Of which, 196 were taxonomically assigned; one-third of those being unclassified Bacteria. The next most abundant taxa were Betaproteobacteria and Planctomycetes, with seven contigs assigned to each class. Of the top 15 most abundant KEGG functional genes assigned to contigs, six were involved in cellular transport. The most abundant KEGG functional gene was determined to be a serine/threonine protein kinase with approximately 800 reads per million total reads (Supplementary Figure 2).

To better understand nutrient cycling and primary productivity, the abundance of specific genes was further investigated (Figure 5). Two genes of interest were *aclB* and *cbbM*, which are key for the reductive TCA cycle and the reductive pentose phosphate cycle, respectively. Within this microbial mat, genes encoding *cbbM* were more abundant than *aclB*, suggesting primary production *via* reductive pentose phosphate cycle is the dominant autotrophic pathway. The high oxygen Form I of RubisCO was not identified within this metagenome.

Additionally, abundance of genes for the nitrogen and sulfur cycle was analyzed. Key genes of the nitrogen cycle, *amoA* (ammonia monooxygenase), *nirK* (nitrite reductase), and *nifH* (nitrogenase) had variable abundances. Ammonia monooxygenase was identified in the bacterial phylum Nitrospirota and in the class Nitrospira. However, *amoA* was also detected in the archaeal

unclassified Thaumarchaeota at relatively high abundances. Nitrite reductase genes were identified across most of the major classes of autotrophic organisms and in the archaeal class Nitrososphaeria, whereas nitrogenase was only identified in three taxa at minimal levels. Genes involved in the sulfur cycle were more taxonomically restricted in comparison to nitrite reductase. The Betaproteobacteria contained genes encoding *dsrAB* and *soxAB*, suggesting both dissimilatory sulfate reduction and sulfur oxidation were important in respiratory pathways. Additionally, both the oxidative and reductive forms of *dsrAB* were found to be present. Betaproteobacteria, a taxon found to be most prevalent with SSU rRNA analysis, had nearly all the investigated functional genes except for *aclB* and *nifH*. Arsenic detoxification gene *arsC* (arsenate reductase) was identified in only a few taxa and was most abundant within the Alphaproteobacteria (Figure 5).

Discussion

A generally homogeneous bacterial community

Compared to other hydrothermal vent fields, the bacterial mats found in the basin of Crater Lake generally represent an unexpectedly homogeneous overarching community with a relatively large number of observed OTUs and a community structure characterized by relatively high species richness and alpha diversity. The low beta diversity and low spatial variability among sites were surprising given the highly dynamic and variable nature of microbial communities at other hydrothermal sites, even communities in extremely close proximity (Davis and Moyer, 2008; Sheik et al., 2015). In addition, the high alpha diversity observed in the mats is

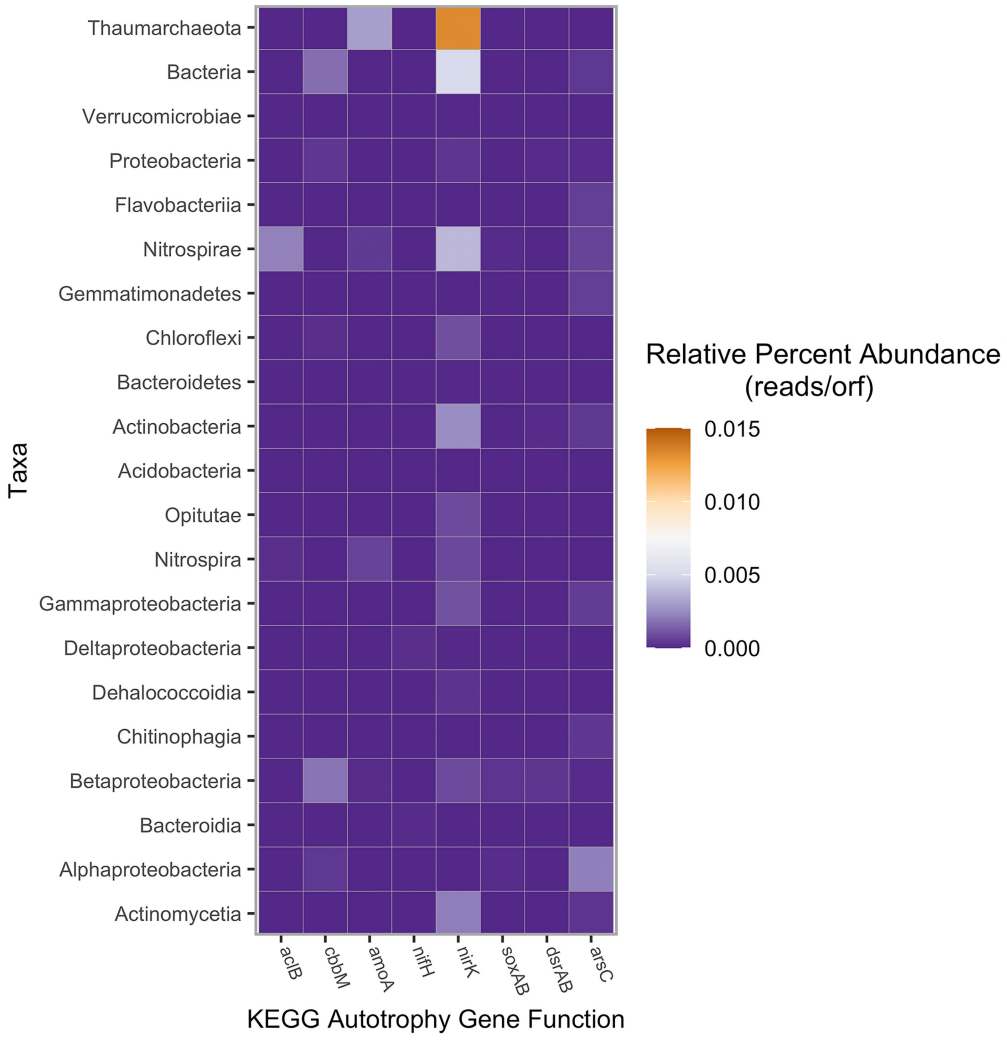

FIGURE 5
Autotrophy gene abundance based on assigned taxa, measured in percent of raw reads per total number of reads in the sample. KEGG gene abundance was calculated using SqueezeMeta with a lowest abundance threshold of 1.25×10^{-5} reads per ORF (Tamames and Puente-Sánchez, 2019). Taxa represented by super-taxa (e.g., Thaumarchaeota, Bacteria, etc.) were each the unclassified residual reads not included in the sub-taxa (either phyla or class) listed below, respectively.

surprising given the extreme oligotrophic nature of Crater Lake that often supports lower microbial diversity when compared to eutrophic lake systems (Newton and McLellan, 2015). This observed low spatial variability starkly contrasts with other hydrothermal vent ecosystems where heterogeneous vent effluent and episodic vent fluid composition, temperature, and flow rate results in distinctly different mat communities across small spatial scales (Nakagawa and Takai, 2008). For example, in the Mariana Arc and back-arc systems, hydrothermal vent microbial community structure has been shown to be extremely diverse even within a vent field (Emerson and Moyer, 2010). Another example of iron-dominated heterogeneous vent effluent leading to high bacterial community variability within a vent field occurs at Lō'ihi Seamount (Duchinski et al., 2019). The high beta diversity within these vent sites is linked to heterogeneous vent effluent providing variable geochemical species for microbial metabolic use (Hager et al., 2017); however, like Crater Lake springs, these vent fluids are enriched in reduced sulfur and iron compounds. The conditions at deep-sea hydrothermal vents are most likely distinctly different from the Crater Lake benthic microbial mats, where more variable hydrothermal fluid flow combined with higher heat flux results in geochemistry that is more temporally and spatially heterogeneous.

Selected diversity metrics from the Mariana Arc and back-arc and Lō'ihi Seamount hydrothermal ecosystems highlight the high alpha diversity and low beta diversity observed among Crater Lake bacterial mat communities (Supplementary Table 3). The high OTU richness (Chao 1 richness) and OTU evenness (Inverse Simpson diversity) at all eight sites is surprising given the extremely oligotrophic nature of Crater Lake, restricting diverse metabolic potential and ecological niches. In additional to diversity measures, the low beta diversity found among the mats can also be demonstrated by comparing abundant OTUs. Of the 55 dominant OTUs comprising >1% of the total reads in at least one sample, 54 OTUs were cosmopolitan across all eight sites. In contrast, across 22 bacterial mat communities from four vent fields in the Mariana Arc and back-arc, 162 OTUs were abundant with >1% of the total reads in at least one sample. Of these 162 OTUs, only 30 were cosmopolitan taxa across all mats (Hager et al., 2017). The ubiquitous and abundant OTUs detected across all eight sites indicate an exceptionally homogeneous bacterial mat community spanning the hydrothermal springs of Crater Lake. It is possible that the lower diversity observed in mat communities 226S1 and 226S3 revealed by rarefaction analysis (Supplementary Figure 1) may be attributed to these samples being taken from older, lower biomass mats instead of being from distinct, less diverse communities.

Gallionella

Among the taxa identifiable to genus level by both clone library and amplicon sequencing analysis, *Gallionella* were found to be the most abundant autotrophic genus within the Crater Lake bacterial mat community. However, there were many unclassified groups within the community that may also have contributed to mat primary production. The putative iron and manganese-oxidizing *Gallionella* produce twisted sheaths of precipitated iron hydroxides because of their metabolic processes that likely form the bacterial mat matrices at Crater Lake hydrothermal springs (Figure 2). *Gallionella* comprised an average relative abundance of 0.75% of the mat communities. A maximum relative abundance of 3.4% occurred at the site containing the highest concentration of iron, 226S3, indicating that this bacterial mat community is likely driven by iron oxidation by *Gallionella* over sulfur oxidation. In addition, high observed concentrations of manganese in all mat sites except 216S1 further support the conclusion that these iron and manganese-rich mats are driven by autotrophic *Gallionella*. These data corroborate the findings of Dymond et al. (1989), that *Gallionella* comprise a dominant proportion of the Crater Lake bacterial mat communities. However, no bacteria from the genus *Leptothrix* were detected in this study. *Leptothrix* growth is co-limited by calcium and magnesium; therefore, it is probable that the concentrations of these minerals were too high to support the growth of *Leptothrix* (Eggerichs et al., 2020). Zetaproteobacteria is another sheath-forming iron oxidizer (Emerson et al., 2007) that may have been misidentified as *Leptothrix*.

Zetaproteobacteria

The genus *Mariprofundus* from the class Zetaproteobacteria represented a small proportion of the Crater Lake bacterial mats with an average of 0.08% of the community but functions as an iron oxidizer that may contribute to the matrix of these mats (Emerson and Moyer, 2002; McAllister et al., 2011). The relative abundance of Zetaproteobacteria ranged from a minimum of 0.001% in sample 223S1 to a maximum of 0.53% in sample 226S1. The Crater Lake metagenome was constructed from sample 216S1, which had 0.04% of Zetaproteobacteria; however, no evidence of carbon fixation by Zetaproteobacteria was identified, which could be attributed to their low relative abundance.

Zetaproteobacteria are typically found in marine or brackish iron-rich environments and have only recently been found in terrestrial and coastal ecosystems (McAllister et al., 2019); therefore, detecting Zetaproteobacteria in the ultra-oligotrophic freshwater system at Crater Lake is a novel finding that expands their observed range. In addition, finding Zetaproteobacteria in a community with abundant *Gallionella* is also noteworthy. A highly significant correlation between relative abundances of *Mariprofundus* and *Gallionella* has been observed in marine hydrothermal iron mat communities (Vander Roost et al., 2017); therefore, finding these two taxa co-occurring in benthic mats at Crater Lake provides further evidence of their co-colonization of hydrothermal iron mats.

Fine-scale characterization of Zetaproteobacteria was conducted by using *ZetaHunter*, which assigns Zetaproteobacterial reads to canonical Zeta OTUs. The majority of Zetaproteobacteria detected in the Crater Lake community were assigned to either Zeta OTU 2 or Zeta OTU 6 (Supplementary Table 2). Zeta OTU 2 has been shown to be globally distributed and is often the most abundant Zeta OTU found in iron-dominated hydrothermal systems (McAllister et al., 2011; Duchinski et al., 2019). Zeta OTU

6 has also been found in lower abundances in hydrothermal iron mats although its distribution is generally more prevalent in coastal sediments and mineral weathering incubations. The discovery of Zetaproteobacteria at Crater Lake further expands the role of iron-oxidizing Zetaproteobacteria in freshwater iron-rich ecosystems and contributes to the understanding of Zetaproteobacteria habitat and niche preference.

Other notable autotrophs

In addition to iron oxidization by *Gallionella* and *Mariprofundus*, other reduced inorganic compounds may provide key nutrients to autotrophic taxa. The second most abundant autotrophic taxon found across all eight bacterial communities is from the genus *Nitrospira* belonging to the phylum Nitrospirota. The metagenomic data indicates that the Crater Lake *Nitrospira* have genes for nitrite reductase, indicating their potential role in denitrification. Because nitrite can be fatal to fish and other vertebrates, the presence of denitrification by *Nitrospira* is critically important in marine and freshwater ecosystems. Some members of the genus *Nitrospira* are capable of complete nitrification by oxidizing ammonia and nitrite into nitrate; these organisms are known as complete ammonia oxidizers or "comammox." The low allochthonous input, highly oligotrophic conditions present in Crater Lake, and the aggregation of benthic bacterial communities into microbial mats suggest that these abundant *Nitrospira* may be comammox (Daims et al., 2015). It has also recently been shown that when Fe(II) and nitrate are present in freshwater oligotrophic ecosystems that the presence of *Gallionella* enhances nitrate-reducing microbial assemblages (Jakus et al., 2021).

Another putative autotrophic sulfur-oxidizer within the mat community was represented by the genus *Thiobacillus*. The highest abundance of *Thiobacillus* comprising 0.56% of the bacterial community occurred at Palisades Point Pool, providing further evidence that this community is driven by the inclusion of sulfur oxidation as a source of primary production. One member of this genus, *Thiobacillus denitrificans*, has been shown to oxidize ferrous sulfide in the presence of nitrate (Straub et al., 1996; Hedrich et al., 2011). The detection of *Thiobacillus* and *Nitrospira*, particularly in the higher relative abundances observed in the Palisades Point Pool community, may provide the support that comammox *Nitrospira* are producing nitrate and driving ferrous sulfide oxidation by *Thiobacillus*. In addition, metagenomic analysis reveals the highest abundance of genes involved in sulfur oxidation, *soxAB*, belong to the Betaproteobacteria, providing further support that sulfur oxidation by *Thiobacillus* could be a significant source of primary production in Crater Lake mat communities. A relatively high abundance of Campylobacterota (formerly known as Epsilonproteobacteria) dominated by the genus *Sulfuricurvum* was also observed across all eight bacterial mats and was also most highly enriched at Palisades Point Pool comprising ~1.4% of the community. *Sulfuricurvum* spp. are chemolithoautotrophs which oxidize sulfur and fix carbon *via* the rTCA cycle, which allows them to be early colonizers of hydrothermal systems (Handley et al., 2014; Waite et al., 2017). The elevated relative abundance of *Sulfuricurvum* present in community 228S3 provides additional support that Palisades Point Pool mat community is the most reliant on sulfur of all the communities that were investigated. However, in the metagenomic sample, no *aclB* genes were associated with the Campylobacterota.

Sulfur and iron fuel dominant autotrophs

The spring-derived fluids showed elevated levels of CO_2, iron, and manganese and low levels of oxygen, which support the chemosynthetic microbial mat. The putative autotrophic taxa identified in notable abundances >0.5% of the total mat community in at least one community reveal the importance of iron and sulfur to the microbial mats. Four out of five abundant autotrophic taxa are chemoautotrophs that can utilize iron or sulfur oxidation reactions for energy, while the fifth taxon can use nitrite oxidation. Abundant autotroph diversity is largely homogeneous with respect to spatial distribution, yet slight variability in autotroph diversity may be attributed to slight variability in observed geochemistry among the mat sites. Previous work has suggested the importance of reduced iron as an energy source to these benthic mat communities; however, this is the first time that the contribution of reduced sulfur to the energy demand of the Crater Lake microbial mats has been suggested. This is also especially notable as normally sulfur-oxidizing bacteria occur at higher *in situ* temperatures, as the maximum temperature differential measured across these microbial communities reaches only just over 6°C above ambient.

The presence of autotrophy genes within the metagenome of the Crater Lake microbial mat confirms the prevalence of chemoautotrophs. Not only were similar taxa found to have these genes indicative of autotrophy, but these genes were present in relatively high abundance. Additionally, the most abundant taxa from the metagenomic analysis were found to have genes for autotrophic lifestyles. The identification of the form II RubisCO to the exclusion of form I indicates adaptation to low oxygen concentrations (Tabita et al., 2008; Böhnke and Perner, 2017). Crater Lake bottom water had elevated levels of oxygen in comparison to what was measured at the microbial mats (Table 1).

Further evidence for the importance of sulfur oxidation to the productivity of the Crater Lake mat community is seen in the abundance of both the dissimilatory sulfur reductase (*dsrAB*) and sulfur oxidase (*soxAB*). The most abundant gene involved in sulfur metabolism is the dissimilatory sulfur reductase gene *dsrAB*, followed closely by the sulfur oxidation gene *soxAB*, both identified in the highest abundances as Betaproteobacteria. The co-occurrence of *dsrAB* and *soxAB* genes in Betaproteobacteria is likely due to these sulfur-oxidizing autotrophs utilizing both sets of genes in the oxidative direction; some sulfur-oxidizing bacteria have been found to express both *dsrAB* and sox*AB* genes (Müller et al., 2015; Watanabe et al., 2019). In the active crater volcano lake

El Chichón, genes involved in oxidative and reductive sulfur metabolisms were found in high abundances in sediment microbial communities, indicating that sulfur cycling is critical in other crater lake benthos (Peña-Ocaña et al., 2022).

In addition to the Betaproteobacteria, other taxa were found to contain genes for sulfur metabolism. Another taxon with abundant *dsrA* is the Actinobacteria. Actinobacteria are one of the few microbial taxa with the capacity to reduce sulfite to sulfide using the dissimilatory sulfite reductase pathway (Anantharaman et al., 2018). Other taxa identified with abundant sulfur metabolizing genes include Gammaproteobacteria and Acidobacteria (*dsrB*), Alphaproteobacteria (*soxA*, *soxB*), and Nitrospirota (*soxB*). Detecting sulfur-oxidizing *soxB* genes in Nitrospirota may indicate that these organisms are oxidizing reduced sulfur compounds to fuel nitrite reduction. Previous studies have shown sulfate concentrations below 0.4 mm in freshwater oligotrophic lakes (Holmer and Storkholm, 2001). Samples from Crater Lake range from 0.11 to 0.69 mm. At Picard and Von Damm Vents, both of which have higher temperature fluids than Crater Lake, *dsrAB* and *soxA* were detected in metagenomes and metatranscriptomes (Galambos et al., 2019). At the low-temperature vents of Lō'ihi Seamount, sulfide is not abundant in the vent fluids (Glazer and Rouzel, 2009); however, many sulfur-oxidizing bacteria have been identified in the microbial mats (Fullerton et al., 2017). Therefore, it is likely these elevated sulfate values are the result of sulfur oxidation as indicated by metagenomic analyses in comparison to other well-studied hydrothermal vents.

In addition to sulfur cycling, genes for nitrogen cycling were identified to be abundant within the putative autotrophs. Nitrate concentrations ranged from 0.6 to 3.0 µm, a majority of which were elevated in comparison to Crater Lake bottom water. Other hydrothermal vents show low levels of *nifH*, similar to what is seen in the Crater Lake metagenome (Jesser et al., 2015; Anantharaman et al., 2016). Surprisingly, the two most abundant taxa with *nirK* and *amoA* were identified to be archaea. However, other vent systems have identified Thaumarchaeota *amoA* as abundant, such as in the hydrothermal vent plume of Guaymas Basin (Lesniewski et al., 2012). From the Crater Lake metagenome, less than 2% of reads were identified as archaeal, which is in line with other iron-dominated and low-temperature hydrothermal vent systems, such as Lō'ihi Seamount (Davis and Moyer, 2008). However, within the metagenome, the Thaumarchaeota showed relatively high abundance for these two genes. It is unknown if these archaeal taxa are contributing to primary production, since no genes from the 3-hydroxypropionate/4-hydroxybutyrate cycle were identified (Hügler and Sievert, 2011).

Conclusion

This study reveals the microbial biodiversity of hydrothermal microbial mat communities at the bottom of Crater Lake, Oregon. SSU rRNA gene amplicon sequencing from eight bacterial mats revealed a relatively homogeneous, yet diverse mat community. High alpha diversity in terms of richness and low beta diversity or variability among bacterial mats indicates that these communities are likely fueled by more homogeneous hydrothermal fluids than might have been predicted by the instantaneously collected, microbially relevant geochemical data. The examination of autotrophic taxa abundance revealed the potential importance of iron and sulfur inputs from benthic hydrothermal springs to the primary productivity of these mats. This is further supported by metagenomic analysis showing a potential for carbon fixation by both the rTCA and RPP cycles. Chemoautotrophic potential within the mats was dominated by iron oxidation from *Gallionella* and *Mariprofundus* and by sulfur oxidation from *Sulfuricurvum* and *Thiobacillus* with an additional contribution of nitrite oxidation from *Nitrospira*. These bacterial mat community structure data link the importance of the detected chemoautotrophic metabolisms driven by fluids derived from benthic hydrothermal springs to Crater Lake's entire lentic ecosystem.

Data availability statement

The datasets presented in this study can be found in online repositories. The names of the repository/repositories and accession number(s) can be found at: https://www.ncbi.nlm.nih.gov/genbank/, OM194204 through OM194219 https://www.ncbi.nlm.nih.gov/, SRA BioProject PRJNA792592.

Author contributions

CM and HF conceived, designed, and supervised the analysis of the experiments. AS, LM, HF, and CM wrote the manuscript. AS conducted SSU amplicon sequencing analysis. LM conducted metagenomic sequence analysis. All authors contributed to the article and approved the submitted version.

Funding

This work was funded in part by Western Washington University's Office of Research and Sponsored Programs to CM, AS, and LM and by the Biology Alumni Student Research Fellowship to AS and LM, and by the Fraser Family Endowment summer research fund to AS. Funds were also provided by the Fouts Foundation for the Enhancement of Student Research Experiences to CM and the College of Charleston Department of Biology Research and Development fund to HF.

Acknowledgments

We wish to thank Professor David Karl for providing the samples used in this study. We also thank WWU undergraduate researcher Mike Phelps for helping with the construction and analysis of the SSU rRNA gene clone library.

Conflict of interest

The authors declare that the research was conducted in the absence of any commercial or financial relationships that could be construed as a potential conflict of interest.

Publisher's note

All claims expressed in this article are solely those of the authors and do not necessarily represent those of their affiliated organizations, or those of the publisher, the editors and the reviewers. Any product that may be evaluated in this article, or claim that may be made by its manufacturer, is not guaranteed or endorsed by the publisher.

Supplementary material

The Supplementary material for this article can be found online at: https://www.frontiersin.org/articles/10.3389/fmicb.2022.876044/full#supplementary-material

References

Anantharaman, K., Breier, J. A., and Dick, G. J. (2016). Metagenomic resolution of microbial functions in deep-sea hydrothermal plumes across the eastern Lau spreading center. *ISME J.* 10, 225–239. doi: 10.1038/ismej.2015.81

Anantharaman, K., Hausmann, B., Jungbluth, S. P., Kantor, R. S., Lavy, A., Warren, L. A., et al. (2018). Expanded diversity of microbial groups that shape the dissimilatory sulfur cycle. *ISME J.* 12, 1715–1728. doi: 10.1038/s41396-018-0078-0

Andrews, S. (2010). FastQC: A quality control tool for high throughput sequence data. Available at: http://www.bioinformatics.babraham.ac.uk/projects/fastqc

Bacon, C. R., Gardner, J. V., Mayer, L. A., Buktenica, M. W., Dartnell, P., Ramsey, D. W., et al. (2002). Morphology, volcanism, and mass wasting in crater Lake, Oregon. *Geol. Soc. Am. Bull.* 114, 675–692. doi: 10.1130/0016-7606

Bennett, S. A., Toner, B. M., Barco, R., and Edwards, K. J. (2014). Carbon adsorption onto Fe oxyhydroxide stalks produced by a lithotrophic iron-oxidizing bacteria. *Geobiology* 12, 146–156. doi: 10.1111/gbi.12074

Böhnke, S., and Perner, M. (2017). Unraveling RubisCO form I and form II regulation in an uncultured organism from a deep-sea hydrothermal vent via metagenomic and mutagenesis studies. *Front. Microbiol.* 8:1303. doi: 10.3389/fmicb.2017.01303

Bolger, A. M., Lohse, M., and Usadel, B. (2014). Trimmomatic: a flexible trimmer for Illumina sequence data. *Bioinformatics* 30, 2114–2120. doi: 10.1093/bioinformatics/btu170

Buchfink, B., Reuter, K., and Drost, H. G. (2021). Sensitive protein alignments at tree-of-life scale using DIAMOND. *Nat. Methods* 18, 366–368. doi: 10.1038/s41592-021-01101-x

Caporaso, J. G., Lauber, C. L., Walters, W. A., Berg-Lyons, D., Huntley, J., Fierer, N., et al. (2012). Ultra-high-throughput microbial community analysis on the Illumina HiSeq and MiSeq platforms. *ISME J.* 6, 1621–1624. doi: 10.1038/ismej.2012.8

Chao, A. (1984). Nonparametric estimation of the number of classes in a population. *Scand. J. Stat.* 20, 572–579. doi: 10.1214/aoms/1177729949

Collier, R. W., Dymond, J., and McManus, J. (1991). Studies of hydrothermal processes in crater Lake. *OR. OSU College of Oceanography Report* 90:317.

Daims, H., Lebedeva, E. V., Pjevac, P., Han, P., Herbold, C., Albertsen, M., et al. (2015). Complete nitrification by *Nitrospira* bacteria. *Nature* 528, 504–509. doi: 10.1038/nature16461

Davis, R. E., and Moyer, C. L. (2008). Extreme spatial and temporal variability of hydrothermal microbial mat communities along the Mariana Island arc and southern Mariana back-arc system. *J. Geophys. Res. Solid Earth* 113:B8. doi: 10.1029/2007JB005413

Drake, E. T., Collier, R., Dymond, J., and Larson, G. L. (1990). *Crater Lake: An Ecosystems Study*. San Francisco: American Association for the Advancement of Science Pacific Division.

Duchinski, K., Moyer, C. L., Hager, K., and Fullerton, H. (2019). Fine-scale biogeography and the inference of ecological interactions among neutrophilic iron-oxidizing *Zetaproteobacteria* as determined by a rule-based microbial network. *Front. Microbiol.* 10:2389. doi: 10.3389/fmicb.2019.02389

Dymond, J., Collier, R. W., and Watwood, M. E. (1989). Bacterial mats from crater Lake, Oregon and their relationship to possible deep-lake hydrothermal venting. *Nature* 342, 673–675. doi: 10.1038/342673a0

Edgar, R. C., Haas, B. J., Clemente, J. C., Quince, C., and Knight, R. (2011). UCHIME improves sensitivity and speed of chimera detection. *Bioinformatics* 27, 2194–2200. doi: 10.1093/bioinformatics/btr381

Eggerichs, T., Wiegand, M., Neumann, K., Opel, O., Thronicker, O., and Szewzyk, U. (2020). Growth of iron-oxidizing bacteria *Gallionella ferruginea* and *Leptothrix cholodnii* in oligotrophic environments: Ca, mg, and C as limiting factors and *G. ferruginea* necromass as C-source. *Geomicrobiol J.* 37, 190–199. doi: 10.1080/01490451.2019.1686667

Emerson, D., Fleming, E. J., and McBeth, J. M. (2010). Iron-oxidizing bacteria: an environmental and genomic perspective. *Annu. Rev. Microbiol.* 64, 561–583. doi: 10.1146/annurev.micro.112408.134208

Emerson, D., and Moyer, C. L. (2002). Neutrophilic Fe-oxidizing bacteria are abundant at the Loihi seamount hydrothermal vents and play a major role in Fe oxide deposition. *Appl. Environ. Microbiol.* 68, 3085–3093. doi: 10.1128/AEM.68.6.3085-3093.2002

Emerson, D., and Moyer, C. L. (2010). Microbiology of seamounts: common patterns observed in community structure. *Oceanography* 23, 148–163. doi: 10.5670/oceanog.2010.67

Emerson, D., Rentz, J. A., Lilburn, T. G., Davis, R. E., Aldrich, H., Chan, C., et al. (2007). A novel lineage of proteobacteria involved in formation of marine Fe-oxidizing microbial mat communities. *PLoS One* 2:e667. doi: 10.1371/journal.pone.0000667

Fullerton, H., Hager, K. W., McAllister, S. M., and Moyer, C. L. (2017). Hidden diversity revealed by genome-resolved metagenomics of iron-oxidizing microbial mats from Lō'ihi seamount, Hawai'i. *ISME J.* 11, 1900–1914. doi: 10.1038/ismej.2017.40

Galambos, D., Anderson, R. E., Reveillaud, J., and Huber, J. A. (2019). Genome-resolved metagenomics and metatranscriptomics reveal niche differentiation in functionally redundant microbial communities at deep-sea hydrothermal vents. *Environ. Microbiol.* 21, 4395–4410. doi: 10.1111/1462-2920.14806

Glazer, B. T., and Rouzel, O. J. (2009). Redox speciation and distribution within diverse iron-dominated microbial habitats at Loihi seamount. *Geomicrobiol J.* 26, 606–622. doi: 10.1080/01490450903263392

Groeger, A. W. (2007). Nutrient limitation in crater Lake, Oregon. *Hydrobiologia* 574, 205–216. doi: 10.1007/s10750-006-0353-3

Hager, K. W., Fullerton, H., Butterfield, D. A., and Moyer, C. L. (2017). Community structure of lithotrophically-driven hydrothermal microbial mats from the Mariana arc and back-arc. *Front. Microbiol.* 8:1578. doi: 10.3389/fmicb.2017.01578

Handley, K. M., Bartels, D., O'Loughlin, E. J., Williams, K. H., Trimble, W. L., Skinner, K., et al. (2014). The complete genome sequence for putative H_2-and S-oxidizer Candidatus *Sulfuricurvum* sp., assembled *de novo* from an aquifer-derived metagenome. *Environ. Microbiol.* 16, 3443–3462. doi: 10.1111/1462-2920.12453

Hedrich, S., Schlömann, M., and Johnson, D. B. (2011). The iron-oxidizing proteobacteria. *Microbiology* 157, 1551–1564. doi: 10.1099/mic.0.045344-0

Holmer, M., and Storkholm, P. (2001). Sulphate reduction and Sulphur cycling in lake sediments: a review. *Freshw. Biol.* 46, 431–451. doi: 10.1046/j.1365-2427.2001.00687.x

Hugerth, L. W., and Andersson, A. F. (2017). Analysing microbial community composition through amplicon sequencing: from sampling to hypothesis testing. *Front. Microbiol.* 8:1561. doi: 10.3389/fmicb.2017.01561

Hügler, M., and Sievert, S. M. (2011). Beyond the Calvin cycle: autotrophic carbon fixation in the ocean. *Annu. Rev. Mar. Sci.* 3, 261–289. doi: 10.1146/annurev-marine-120709-142712

Hyatt, D., Chen, G. L., LoCascio, P. F., Land, M. L., Larimer, F. W., and Hauser, L. J. (2010). Prodigal: prokaryotic gene recognition and translation initiation site identification. *BMC Bioinfo.* 11:119. doi: 10.1186/1471-2105-11-119

Jakus, N., Blackwell, N., Straub, D., Kappler, A., and Kleindienst, S. (2021). Presence of Fe (II) and nitrate shapes aquifer-originating communities leading to an autotrophic enrichment dominated by an Fe (II)-oxidizing *Gallionellaceae* sp. *FEMS Microbiol. Ecol.* 97:fiab145. doi: 10.1093/femsec/fiab145

Jesser, K. J., Fullerton, H., Hager, K. W., and Moyer, C. L. (2015). Quantitative PCR analysis of functional genes in iron-rich microbial mats at an active hydrothermal vent system (Lō'ihi seamount, Hawai'i). *Appl. Environ. Microbiol.* 81, 2976–2984. doi: 10.1128/AEM.03608-14

Johnson, K. W., Carmichael, M. J., McDonald, W., Rose, N., Pitchford, J., Windelspecht, M., et al. (2012). Increased abundance of *Gallionella* spp., *Leptothrix* spp. and total bacteria in response to enhanced Mn and Fe concentrations in a disturbed southern Appalachian high elevation wetland. *Geomicrobiol J.* 29, 124–138. doi: 10.1080/01490451.2011.558557

Kim, B. R., Shin, J., Guevarra, R. B., Lee, J. H., Kim, D. W., Seol, K. H., et al. (2017). Deciphering diversity indices for a better understanding of microbial communities. *J. Microbiol. Biotechnol.* 27, 2089–2093. doi: 10.4014/jmb.1709.09027

Klindworth, A., Pruesse, E., Schweer, T., Peplies, J., Quast, C., Horn, M., et al. (2013). Evaluation of general 16S ribosomal RNA gene PCR primers for classical and next- generation sequencing-based diversity studies. *Nucleic Acids Res.* 41:e1. doi: 10.1093/nar/gks808

Kozich, J. J., Westcott, S. L., Baxter, N. T., Highlander, S. K., and Schloss, P. D. (2013). Development of a dual-index sequencing strategy and curation pipeline for analyzing amplicon sequence data on the MiSeq Illumina sequencing platform. *Appl. Environ. Microbiol.* 79, 5112–5120. doi: 10.1128/AEM.01043-13

Lesniewski, R. A., Jain, S., Anantharaman, K., Schloss, P. D., and Dick, G. J. (2012). The metatranscriptome of a deep-sea hydrothermal plume is dominated by water column methanotrophs and lithotrophs. *ISME J.* 6, 2257–2268. doi: 10.1038/ismej.2012.63

Li, D., Liu, C. M., Luo, R., Sadakane, K., and Lam, T. W. (2015). MEGAHIT: an ultra-fast single-node solution for large and complex metagenomics assembly via succinct de Bruijn graph. *Bioinformatics* 31, 1674–1676. doi: 10.1093/bioinformatics/btv033

McAllister, S. M., Davis, R. E., McBeth, J. M., Tebo, B. M., Emerson, D., and Moyer, C. L. (2011). Biodiversity and emerging biogeography of the neutrophilic iron-oxidizing *Zetaproteobacteria*. *Appl. Environ. Microbiol.* 77, 5445–5457. doi: 10.1128/AEM.00533-11

McAllister, S. M., Moore, R. M., and Chan, C. S. (2018). ZetaHunter, a reproducible taxonomic classification tool for tracking the ecology of the *Zetaproteobacteria* and other poorly resolved taxa. *Microbiol. Resour. Announc.* 7, e0932–e0918. doi: 10.1128/MRA.00932-18

McAllister, S. M., Moore, R. M., Gartman, A., Luther, G. W., Emerson, D., and Chan, C. S. (2019). Marine Fe-oxidizing Zetaproteobacteria: historical, ecological, and genomic perspectives. *FEMS Microbiol. Ecol.* 95:fiz015. doi: 10.1093/femsec/fiz015

McManus, J., Collier, R. W., Chen, C. T. A., and Dymond, J. (1992). Physical properties of crater Lake, Oregon: A method for the determination of a conductivity- and temperature-dependent expression for salinity. *Limnol. Oceanogr.* 37, 41–53. doi: 10.4319/lo.1992.37.1.0041

McManus, J., Collier, R., Dymond, J., Wheat, C. G., and Larson, G. L. (1996). Spatial and temporal distribution of dissolved oxygen in crater Lake, Oregon. *Limnol. Oceanogr.* 41, 722–731. doi: 10.4319/lo.1996.41.4.0722

McNichol, J., Stryhanyuk, H., Sylva, S. P., Thomas, F., Musat, N., Seewald, J. S., et al. (2018). Primary productivity below the seafloor at deep-sea hot springs. *Proc. Natl. Acad. Sci.* 115, 6756–6761. doi: 10.1073/pnas.1804351115

Moyer, C. L. (2001). Molecular phylogeny: applications and implications for marine microbiology. *Methods Microbiol.* 30, 375–394. doi: 10.1016/S0580-9517(01)30054-5

Müller, A. L., Kjeldsen, K. U., Rattei, T., Pester, M., and Loy, A. (2015). Phylogenetic and environmental diversity of DsrAB-type dissimilatory (bi) sulfite reductases. *ISME J.* 9, 1152–1165. doi: 10.1038/ismej.2014.208

Nakagawa, S., and Takai, K. (2008). Deep-sea vent chemoautotrophs: diversity, biochemistry and ecological significance. *FEMS Microbiol. Ecol.* 65, 1–14. doi: 10.1111/j.1574-6941.2008.00502.x

Newton, R. J., and McLellan, S. L. (2015). A unique assemblage of cosmopolitan freshwater bacteria and higher community diversity differentiate an urbanized estuary from oligotrophic Lake Michigan. *Front. Microbiol.* 6:1028. doi: 10.3389/fmicb.2015.01028

Oren, A., and Garrity, G. M. (2021). Valid publication of the names of forty-two phyla of prokaryotes. *Int. J. Syst. Evol. Microbiol.* 71:005056. doi: 10.1099/ijsem.0.005056

Page, K. A., Connon, S. A., and Giovannoni, S. J. (2004). Representative freshwater bacterioplankton isolated from crater Lake, Oregon. *Appl. Environ. Microbiol.* 70, 6542–6550. doi: 10.1128/AEM.70.11.6542

Parks, D. H., Tyson, G. W., Hugenholtz, P., and Beiko, R. G. (2014). STAMP: statistical analysis of taxonomic and functional profiles. *Bioinformatics* 30, 3123–3124. doi: 10.1093/bioinformatics/btu494

Peña-Ocaña, B. A., Ovando-Ovando, C. I., Puente-Sánchez, F., Tamames, J., Servín-Garcidueñas, L. E., González-Toril, E., et al. (2022). Metagenomic and metabolic analyses of poly-extreme microbiome from an active crater volcano lake. *Environ. Res.* 203:111862. doi: 10.1016/j.envres.2021.111862

Puente-Sánchez, F., García-García, N., and Tamames, J. (2020). SQMtools: automated processing and visual analysis of 'omics data with R and anvi'o. *BMC bioinfo.* 21:358. doi: 10.1186/s12859-020-03703-2

Schloss, P. D., Westcott, S. L., Ryabin, T., Hall, J. R., Hartmann, M., Hollister, E. B., et al. (2009). Introducing mothur: open-source, platform-independent, community-supported software for describing and comparing microbial communities. *Appl. Environ. Microbiol.* 75, 7537–7541. doi: 10.1128/AEM.01541-09

Sheik, C. S., Anantharaman, K., Breier, J. A., Sylvan, J. B., Edwards, K. J., and Dick, G. J. (2015). Spatially resolved sampling reveals dynamic microbial communities in rising hydrothermal plumes across a back-arc basin. *ISME J.* 9, 1434–1445. doi: 10.1038/ismej.2014.228

Sievert, S. M., and Vetriani, C. (2012). Chemoautotrophy at deep-sea vents: past, present, and future. *Oceanography* 25, 218–233. doi: 10.5670/oceanog.2012.21

Simpson, E. H. (1949). Measurement of diversity. *Nature* 163:688. doi: 10.1038/163688a0

Straub, K. L., Benz, M., Schink, B., and Widdel, F. (1996). Anaerobic, nitrate-dependent microbial oxidation of ferrous iron. *Appl. Environ. Microbiol.* 62, 1458–1460. doi: 10.1128/aem.62.4.1458-1460.1996

Tabita, F. R., Satagopan, S., Hanson, T. E., Kreel, N. E., and Scott, S. S. (2008). Distinct form I, II, III, and IV Rubisco proteins from the three kingdoms of life provide clues about Rubisco evolution and structure/function relationships. *J. Exp. Bot.* 59, 1515–1524. doi: 10.1093/jxb/erm361

Tamames, J., and Puente-Sánchez, F. (2019). SqueezeMeta, a highly portable, fully automatic metagenomic analysis pipeline. *Front. Microbiol.* 9:3349. doi: 10.3389/fmicb.2018.03349

Urbach, E., Vergin, K. L., Larson, G. L., and Giovannoni, S. J. (2007). Bacterioplankton communities of crater Lake, OR: dynamic changes with euphotic zone food web structure and stable deep water populations. *Hydrobiologia* 574, 161–177. doi: 10.1007/s10750-006-0351-5

Urbach, E., Vergin, K. L., Young, L., Morse, A., Larson, G. L., and Giovannoni, S. J. (2001). Unusual bacterioplankton community structure in ultra-oligotrophic crater Lake. *Limnol. Oceanogr.* 46, 557–572. doi: 10.4319/lo.2001.46.3.0557

Vander Roost, J., Thorseth, I. H., and Dahle, H. (2017). Microbial analysis of *Zetaproteobacteria* and co-colonizers of iron mats in the Troll Wall vent field, Arctic Mid-Ocean Ridge. *PLoS ONE* 12:e0185008. doi: 10.137/journal.pone.0185008

Waite, D. W., Chuvochina, M., Pelikan, C., Parks, D. H., Yilmaz, P., Wagner, M., et al. (2020). Proposal to reclassify the proteobacterial classes *Deltaproteobacteria* and *Oligoflexia*, and the phylum *Thermodesulfobacteria* into four phyla reflecting major functional capabilities. *Int. J. Syst. Evol. Microbiol.* 70, 5972–6016. doi: 10.1099/ijsem.0.004213

Waite, D. W., Vanwonterghem, I., Rinke, C., Parks, D. H., Zhang, Y., Takai, K., et al. (2017). Comparative genomic analysis of the class Epsilonproteobacteria and proposed reclassification to *Epsilonbacteraeota* (phyl. Nov.). *Front. Microbiol.* 8:682. doi: 10.3389/fmicb.2017.00682

Wang, Q., Garrity, G. M., Tiedje, J. M., and Cole, J. R. (2007). Naïve Bayesian classifier for rapid assignment of rRNA sequences into the new bacterial taxonomy. *Appl. Environ. Microbiol.* 73, 5261–5267. doi: 10.1128/AEM.00062-07

Watanabe, T., Kojima, H., Umezawa, K., Hori, C., Takasuka, T. E., Kato, Y., et al. (2019). Genomes of neutrophilic sulfur-oxidizing chemolithoautotrophs representing 9 proteobacterial species from 8 genera. *Front. Microbiol.* 10:316. doi: 10.3389/fmicb.2019.00316

Wickham, H., Navarro, D., and Pedersen, T. L. (2016). *n2: elegant Graphics for data Analysis*. New York: Springer-Verlag.

Frontiers in Microbiology

Explores the habitable world and the potential of microbial life

The largest and most cited microbiology journal which advances our understanding of the role microbes play in addressing global challenges such as healthcare, food security, and climate change.

Discover the latest Research Topics

See more →

Frontiers

Avenue du Tribunal-Fédéral 34
1005 Lausanne, Switzerland
frontiersin.org

Contact us

+41 (0)21 510 17 00
frontiersin.org/about/contact